Characterising novel Antibody-Drug Conjugate targets for ovarian cancer: Implications for patient stratification and precision medicine

Alice Luther

Submitted to Swansea University in fulfilment of the requirements for the degree of Doctor of Philosophy

Swansea University

Swansea University Medical School

2021

Summary

Ovarian cancer (OC) is the 6th most common cancer in females and accounts for 5% of all female cancer deaths in the UK. OC presents with ambiguous symptoms often leading to a late diagnosis. Only 42.6% of women diagnosed with OC will survive for five years or more with many not responding to current treatments. Platinum-based drugs are the most widely used chemotherapy drugs in ovarian carcinoma, but their efficacy is not satisfactory. Bevacizumab and PARP inhibitors are the only targeted therapies currently approved for the treatment of this disease. Still, most patients will still recur and unfortunately succumb to this disease, thus new and more effective treatments and diagnosis methods are urgently needed. Antibody-Drug Conjugates (ADCs) are a group of targeted therapeutic molecules that have proved efficacious as therapeutic options for the treatment of various cancers such as Acute Myeloid Leukaemia and Hodgkin Lymphoma. Currently there is not an ADC approved for the treatment of ovarian cancer. ADCs couple the targeting activity of a monoclonal antibody with the cytotoxic activity of a potent small molecule drug to selectively destroy malignant cells while leaving the healthy cells unaffected. The discovery of novel ADC targets for the treatment of OC is crucial in combatting the poor prognosis associated with late-stage ovarian cancer. The late-stage diagnosis of OC is significantly associated with a reduced chance of survival. Confirmation of OC diagnosis is achieved through histological examination of biopsy tissue taken at surgery. This current diagnosis process is not appropriate for the high-throughput screening needed for the early detection of OC that could be offered if minimally invasive high-throughput liquid biopsy diagnostic tests are developed for OC.

Objectives

- To identify and characterise transmembrane proteins as potential ADC targets
- To confirm the genetic stability of the antibody epitope DNA coding sequence in the Receptor for Advanced Glycation End products (RAGE) and the lead candidate ADC target
- To explore whether soluble RAGE (sRAGE) levels could serve as OC biomarker with diagnostic value using an Enzyme Linked Immunosorbent Assay (ELISA) liquid biopsy pipeline

Methodology

This study used western blots, immuno-fluorescent microscopy, internalisation assays by pH reactive dye, Illumina Next Generation Sequencing and Enzyme-Linked Immunosorbent assay. 2D cultured cells and protein were derived from primary patient biopsies. Eight immortalised ovarian cancer cell lines were used (See section 2.2.1.1).

Results

Immunofluorescent microscopy, immunoblotting and internalisation assay data in both ovarian cancer cell lines and cells derived from primary ovarian cancer patient biopsies revealed Tetraspanin 6 (TSPAN6) as the lead candidate target for novel ADC development. Not a lot is known about TSPAN6 function however it has been reported to mediate signal transduction events that play a role in the regulation of cell development, activation, growth, and motility. Three targets showed localisation to the cell membrane in ovarian cancer cells. Two targets (PCSK4 and TSPAN6), plus RAGE, showed antibody-internalisation capacity and translocation to the lysosomal compartment in cancer cells demonstrating their suitability as ADC targets. RAGE and TSPAN6 showed genetic stability by Illumina Next Generation Sequencing deep amplicon variant analysis. A novel TSPAN6 60 kDa immunoreactive protein band was identified in protein derived from a 3D primary tissue source and it significantly stratified OC from non-cancer patients. The ELISA technique was successful in detecting sRAGE in patient serum, however soluble serum RAGE levels did not exhibit a potential diagnostic value for OC disease in the clinical OC specimens analysed.

Conclusions

This thesis identified TSPAN6 as a novel ADC target for OC. In addition, both TSPAN6 and RAGE epitopes are highly conserved in humans, suggesting their promising therapeutic value for the development of immunotherapies. Nevertheless, levels of soluble serum RAGE are not indicators of an OC diagnosis.

DECLARATION

This work has not previously been accepted in substance for any degree and is not being concurrently submitted in candidature for any degree.

Signed …........ ████████ .... (candidate)

Date …................15.12.2020...

STATEMENT 1

This thesis is the result of my own investigations, except where otherwise stated. Where correction services have been used, the extent and nature of the correction is clearly marked in a footnote(s).

Other sources are acknowledged by footnotes giving explicit references. A bibliography is appended.

Signed …........... ████████ .... (candidate)

Date …................15.12.2020..

STATEMENT 2

I hereby give consent for my thesis, if accepted, to be available for photocopying and for inter-library loans **after expiry of a bar on access approved by the Swansea University.**

Signed …........ ████████ .... (candidate)

Date …..................15.12.2020..

Contents

Acknowledgments

There are many people I would like to thank for their endless encouragement, help and support during my PhD studies.

Firstly, I would like to thank my supervisor Dr. Ricardo Del Sol who has helped me get through the last four years with support, humour, and patience. I would also like to thank Prof. Deya Gonzalez for her incredible guidance and for supporting me with kindness and confidence. Prof. Steve Conlan and Dr. Lewis Francis have both given up their time to help me over the last 4 years with consistent encouragement and humour. Great thanks to Dr. Gareth Healey for his constant support, kindness and understanding. Thanks also to our kind and dedicated clinician Dr. Lavinia Margarit, the HCRW research nurses and the gynaecological oncology nursed for their efforts on patient recruitment and consent for the study. Also, a huge thank you to the patients who have kindly donated samples to be a part of this research study.

I would like to thank Life Sciences Research Network Wales and Swansea University for funding my research project and giving me the opportunity to undertake my PhD. I would like to thank all my friends and colleagues in the Centre of Nano Health and the Reproductive Biology and Gynaecological Oncology Group at Swansea University who have given me the best PhD experience I could ask for.

Special thanks go to my dear friends Anne, Kadie, Lily and Tiffany. I absolutely could not have gotten this far without your support, generosity, and kindness.

Finally, my family deserve the biggest thanks of all. I would like to dedicate my thesis to my continually supportive parents Dorothy and Martin and to the memory of my exceptional Nan Mary Davey. From the day I was born you have encouraged me to be the best version of myself, to push harder and reach higher. I would not be the person I am today without your unconditional love, support, and reassurance. I wish for my Nan to see the result of all her constant kindness and support, and I want her to know I couldn't have done any of it without her love.

Figure List

Tables list

ABBREVIATIONS

AA	AMINO ACIDS
AB	ANTIBODY
ACS	AMERICAN CANCER SOCIETY
AD	ALZHEIMER DISEASE
ADAM10	A DISINTEGRIN AND METALLOPROTEINASE DOMAIN-CONTAINING PROTEIN 10
ADC	ANTIBODY-DRUG CONJUGATE
ADCC	ANTIBODY-DEPENDENT CELLULAR CYTOTOXICITY
AGES	ADVANCED GLYCATION END PRODUCTS
AML	ACUTE MYELOID LEUKAEMIA
Aβ	BETA AMYLOID
BC	BREAST CANCER
BCMA	B-CELL MATURATION ANTIGEN
BMI	BODY MASS INDEX
BP	BASE PAIR
BRCA1/2	BREAST CANCER 1/2 GENE
BSA	BOVINE SERUM ALBUMIN
CA125	CANCER ANTIGEN 125
CCP	CLATHRIN-COATED PITS
CEACAM8	CARCINOEMBRYONIC ANTIGEN-RELATED CELL ADHESION MOLECULE 8
CEL	NƐ-CARBOXYETHYLLYSINE
CML	NƐ-CARBOXYMETHYLLYSINE
CVD	CARDIOVASCULAR DISEASE
DAR	DRUG/DYE TO ANTIBODY RATIO
DMSO	DIMETHYL SULFOXIDE
DN-RAGE	DOUBLE NEGATIVE RECEPTOR FOR ADVANCED GLYCATION END PRODUCTS
DNA	DEOXYRIBONUCLEIC ACID
EC	ENDOMETRIAL CANCER
ELISA	ENZYME-LINKED IMMUNOSORBENT ASSAY
EMA	EUROPEAN MEDICINES AGENCY
ESRAGE	ENDOGENOUSLY SECRETED RECEPTOR FOR ADVANCED GLYCATION END PRODUCTS
FAB	FRAGMENT ANTIGEN BINDING
FBS	FOETAL BOVINE SERUM
FC	FRAGMENT CRYSTALLISABLE
FDA	FOOD AND DRUG ADMINISTRATION
FLRAGE	FULL LENGTH RECEPTOR FOR ADVANCED GLYCATION END PRODUCTS

GAPDH	GLYCERALDEHYDE 3-PHOSPHATE DEHYDROGENASE
HBOC	HEREDITARY BREAST AND OVARIAN CANCER SYNDROME
HE4	HUMAN EPIDIDYMIS PROTEIN 4
HER-2	HUMAN EPIDERMAL GROWTH FACTOR RECEPTOR 2
HGSOC	HIGH GRADE SEROUS OVARIAN CANCER
HMGB1	HIGH MOBILITY GROUP BOX 1
HNPCC	HEREDITARY NONPOLYPOSIS COLORECTAL CANCER
HRT	HORMONE REPLACEMENT THERAPY
IHC	IMMUNOHISTOCHEMISTRY
IL-10	INTERLEUKIN-10
IL-6	INTERLEUKIN-6
IVF	*IN VITRO* FERTILISATION
JNK	C-JUN N-TERMINAL KINASE
µM	MICRO MOLAR
M	MOLAR
MAB	MONOCLONAL ANTIBODY
MHC	MAJOR HISTOCOMPATIBILITY COMPLEX
MM	MINI MOLAR
MMAE	MONOMETHYL AURISTATIN E
MMAF	MONOMETHYL AURISTATIN F
MS	MASS SPECTROSCOPY
MVBS	MULTIVESICULAR BODIES
ML	MILLI LITRE
NF-KB	NUCLEAR FACTOR KB
NHS	NATIONAL HEALTH SERVICE
NK	NATURAL KILLER
OC	OVARIAN CANCER
PBD	PYRROLOBENZODIAZEPINE
PBS	PHOSPHATE BUFFERED SALINE
PCOS	POLYCYSTIC OVARY SYNDROME
PCSK4	PROPROTEIN CONVERTASE SUBTILISIN/KEXIN TYPE 4
PFA	PARAFORMALDEHYDE
PID	PELVIC INFLAMMATORY DISEASE
PIEZO2	PIEZO TYPE MECHANOSENSITIVE ION CHANNEL COMPONENT 2
PM	POST-MENOPAUSAL
PMA	PHORBOL 12-MYRISTATE 13-ACETATE
PMB	POST-MENOPAUSAL BLEEDING

PRR	PATTERN RECOGNITION RECEPTOR
RAGE	RECEPTOR FOR ADVANCED GLYCATION END PRODUCTS
RBGO	REPRODUCTIVE BIOLOGY AND GYNAECOLOGICAL ONCOLOGY GROUP
RIP	REGULATED INTRAMEMBRANE PROTEOLYSIS
RMI	RISK OF MALIGNANCY INDEX
ROMA	RISK OF MALIGNANCY ALGORITHM
RT	ROOM TEMPERATURE
SLC39A10	SOLUTE CARRIER FAMILY 39 MEMBER 10
SNP	SINGLE NUCLEOTIDE POLYMORPHISM
SRAGE	SOLUBLE RECEPTOR FOR ADVANCED GLYCATION END PRODUCTS
SUSD2	SUSHI DOMAIN CONTAINING
TAMS	TUMOUR ASSOCIATED MACROPHAGES
TEMS	TETRASPANIN ENRICHED MICRODOMAINS
TLR9	TOLL-LIKE RECEPTOR 9
TNF	TUMOUR NECROSIS FACTOR
TSPAN6	TETRASPANIN 6
UK	UNITED KINGDOM
UTR	UNTRANSLATED REGION
VEGF	VASCULAR ENDOTHELIAL GROWTH FACTOR
WHO	WORLD HEALTH ORGANISATION

Chapter 1: Introduction

1.1 Introduction to the thesis

The following flow diagram introduces the thesis and provides the main research highlights

of each chapter in more detail

Selection of putative targets for ovarian cancer

Six novel ADC targets, TSPAN6, PCSK4, PIEZO2, SLC39A10, CEACAM8 and SUSD2 are introduced and analysed by western blot and immunofluorescent microscopy. In the western blot, only TSPAN6 showed a clean specific band at the expected size in ovarian cancer cell lines TOV-112D and SKOV-3. No significant difference was observed in TSPAN6 expression between eight ovarian cancer cell lines of various subtypes. TSPAN6 expression was more abundant in TOV-21G when compared to a panel of various healthy tissues. TSPAN6 showed the clearest localisation to the membrane by fluorescent immuno-microscopy. PCSK4 and PIEZO2 also showed acceptable expression and localisation to the membrane. However, SLC39A10, CEACAM8 and SUSD2 did not, therefore they were not further explored beyond this point.

Expression of putative ADC targets in primary samples derived from patient ovarian tissue biopsies

TSPAN6, PCSK4 and PIEZO2 showed expression on the plasma membrane in 2D cultured cells derived from patient biopsies. This clear, but variable between pathologies, expression and localisation to the membrane is a prerequisite for the next stage of analysis. In western blot analysis, TSPAN6 displayed expression in protein extracted from 2D cells derived from patient tissue biopsies however no significant difference was observed in TSPAN6 abundance between non-cancer and ovarian cancer. However, this chapter identified a novel 60 kDa band which does show a significant difference.

Assessment of putative ADC target antibody internalisation by receptor mediated endocytosis in 2D cultured cells

Time point analysis revealed 4 hours to be the optimal time to incubate the pH reactive Antibody-Dye conjugate with 2D cells to observe the most fluorescent signal. TSPAN6 internalisation was highest in OVCAR-3 cell line (High Grade Serous subtype). Higher TSPAN6 internalisation was observed in 2D cells derived from a High-Grade Serous subtype when compared to non-cancer cells. PSCK4 internalisation was observed to be statistically less abundant between cell line UACC (Serous) and the other cell lines. Additionally, PCSK4 internalisation was significantly different between non-cancer and cancer 2D cells derived from patient biopsies. RAGE (brought in to replace PIEZO2) internalisation varied between cell lines and internalisation was significant higher in cancer 2D cells derived from patient biopsies when compared to non-cancer. RAGE showed the biggest significant difference out of all three targets.

Deep amplicon variant analysis of TSPAN6 and RAGE antibody epitope DNA coding sequence by Illumina Next Generation Sequencing

The TSPAN6 and RAGE antibody binding epitope DNA coding sequence showed extremely high levels of conservation between 96 patients.

Soluble RAGE as a biomarker for stratification of ovarian cancer patients

A significantly lower abundance of sRAGE is expressed in the serum of ovarian cancer patients when compared to non-cancer. Overall, sRAGE is not powerful enough alone to stratify or diagnose ovarian cancer patients.

1.2 Female reproductive system

The female reproductive system produces, transports and sustains egg cells to develop offspring. It comprises of the uterus, ovaries, uterine tubes and the vagina. In addition, it produces and controls various hormones to regulate the menstrual cycle. A representation of the female reproductive system can be seen in **Figure 1-1**.

1 - Stomach
2 - Omentum
3 - Intestines
4 - Pancreas
5 - Ovary
6 - Falopian tube
7 - Uterus
8 - Bladder
9 - Rectum/bowel
10 - Cervix
11 - Vagina
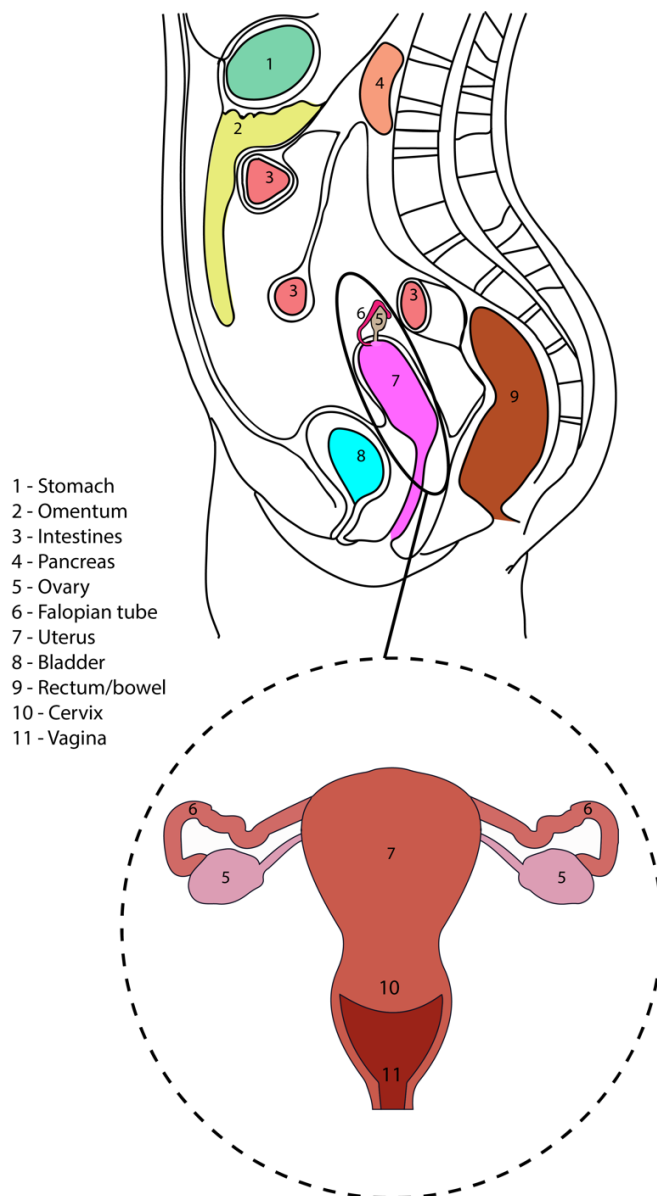
Figure 1-1 – The female reproductive system

The female reproductive system consists of the uterus, ovaries and fallopian tubes. The system works together to produce oocytes (eggs) for fertilisation and embryonic growth in the uterus. Various hormones are produced to regulate the menstrual cycle and pregnancy within the female reproductive system (image drawn by myself using Adobe Illustrator 2019).

The ovaries are organs that develop oocytes (female gametes or eggs) and produce reproductive hormones. The surface of the ovary is covered with a layer of ovarian mesothelium (epithelium) and after puberty this becomes progressively scarred from rupturing of ovarian follicles during ovulation (1). The uterine tubes (fallopian tubes) transport the oocyte from the ovary to the uterine cavity and fertilisation happens at this site. The uterine cavity (womb) is a hollow, thick walled, pear shaped muscular organ which adapts as the foetus grows and provides the power needed to expel during childbirth (2).

The initial development of the ovary begins with undifferentiated germ cells becoming segregated and migrating towards the genital ridges (bilateral thickenings of coelomic epithelium) (3). Proliferation of this coelomic epithelium and its underlying mesenchyme occur in the second stage, followed by the division of the ovary into a peripheral cortex (outside) and central medulla (stromal inside) in stage 3. The final stage consists of the development of the cortex and the shrinkage of the medulla (4).

1.3 Structure and function of adult ovaries

The adult ovary is a highly organised composition of germ cells and somatic cells. The interaction of these cells form oocyte containing follicles, dictate ovulation and form the endocrine structure that forms the ovarian follicle after ovulation for the establishment and maintenance of pregnancy (2). Traditionally, all OC subtypes were thought to arise in the ovarian surface epithelium (5) however, precursor lesions were found in the fallopian tube in women at high risk of OC who underwent salpingo-oophorectomy (6). Malignant OC cells are commonly found on the mesothelial cell layer lining the ovarian surface (ovarian coelomic epithelium) however this is not necessarily the cell of origin (7). Malignant germ cell tumours of the ovary account for approximately 2-3% of all OCs and a very rare subtype arising from the primitive germ cells of the embryonic gonad (8). They have been shown to be more common in the second and third decade of life (9) and the survival rates in the last 30 years have improved dramatically (10) potentially due to aggressive surgical staging and combination therapy. Mesenchymal stem cells are a critical component of the ovarian tumour microenvironment. Mesenchymal stem cells are distinctly different from carcinoma-associated mesenchymal stem cells with unique expression profiles and protumourgenic functions. As with other OC subtypes, the origin of carcinoma-associated mesenchymal stem cells remain unknown, however it has been shown that normal mesenchymal stem cells can be induced by OC to become carcinoma-associated mesenchymal stem cells (11). Overall, there are different regions within the ovary that OC has been shown to

develop (coelomic epithelium, germ cells and mesenchyme) each contributing to the unique OC subtype.

1.4 Gynaecological malignancies

Whilst some tumours of the female reproductive system are benign, such as fibroids (myomas) and cysts, others are metastatic and potentially deadly in nature (12). Gynaecological cancers can be described as any cancer that begins in the female reproductive system. Ovarian cancer is discussed in more detail below as the focus of this thesis.

1.4.1 Ovarian cancer

Ovarian cancer (OC) begins in the ovaries, is the second most common cancer in women and is the leading cause of cancer death in women (13). Known for its ambiguous symptoms and late diagnosis (14), OC will be the main focus of this thesis. The most common cancer in women is breast cancer (15) however, breast cancer has already received much research attention and already has a human epidermal growth factor receptor 2 (HER2) targeting ADC approved for the treatment of triple negative breast cancer; Ado-Trastuzumab emtansine (T-DM1) (16).

OC can be classified by the origin and development of the diseased tissue. The classification system segregates OC types by their derivation from coelomic epithelium, germs cells and mesenchyme. Epithelial OC is by far the most prevalent subtype with over 85% of all OCs being epithelial in classification and these epithelial OCs can be further sub-categorised into serous cystadenocarcinoma (accounting for almost half of epithelial OCs), mucinous cystadenocarcinoma, endometrioid carcinoma, undifferentiated carcinoma and clear cell carcinoma. Mucinous, endometrioid and undifferentiated carcinomas account for approximately 15% of epithelial OCs, with clear cell accounting for only 6% (17). Mucinous OC is a rare distinct subtype of epithelial OC with a distinct natural history, molecular profile, chemo-sensitivity and prognosis (18). It is thought to make up approximately 3% of epithelial OCs (19). Endometrioid OC is another uncommon subtype of epithelial OC with its own unique histology and pathogenesis. Little is known about this OC subtype therefore its treatment is often grouped with that of high-grade epithelial OCs. Endometrioid presents at an earlier stage and a younger age unlike high grade OCs. In addition they are commonly associated with endometriosis with a unique molecular profile (20). About 5% of ovarian carcinomas are so poorly differentiated and difficult to classify that they are known as undifferentiated. In a lot of cases these types of tumour spread widely beyond the ovary and have the worst prognosis of all the epithelial OC subtypes (21). Clear cell OC is another rare subtype of epithelial OC with higher prevalence at a

younger age and a link to endometriosis. Prognosis when caught early is good and the main difference in prognosis has been linked to chemoresistance (22). The high grade serous (HGS) subtype is reported to be the most aggressive of the OC subtypes with the other subtypes (endometriosis, clear cell, mucinous and undifferentiated) still being described as clinically aggressive (23). A least aggressive subtype is not reported however generally speaking, the earlier the OC is diagnosed, the earlier the stage, the chance of a good prognosis from a lesser aggressive OC is commonly reported. A summary of the histopathological classification of ovarian tumours can be seen in **Figure 1-2**.

1. Serous tumors
   (1) Benign
       1. Cystadenoma and papillary cystadenoma
       2. Surface papilloma
       3 Adenofibroma and cystadenofibroma
   (2) Of borderline malignancy (of low malignant potential)
       1. Cystic tumor and papillary cystic tumor
       2. Surface papillary tumor
       3. Adenofibroma and cystadenofibroma
   (3) Malignant
       1. Adenocarcinoma, papillary adenocarcinoma, and papillary cystadenocarcinoma
       2. Surface papillary adenocarcinoma
       3. Adenocarcinofibroma and cystadenocarcinofibroma (malignant adenofibroma and cystadenofibroma)
2. Mucinous tumors, endocervical-like and intestinal types
   (1) Benign
       1. Cystadenoma
       2. Adenofibroma and cystadenofibroma
   (2) Of borderline malignancy (of low malignant potential)
       1. Cystic tumor
       2. Adenofibroma and cystadenofibroma
   (3) Malignant
       1. Adenocarcinoma and cystadenocarcinoma
       2. Adenocarcinofibroma and cystadenocarcinofibroma (malignant adenofibroma and cystadenofibroma)
3. Endometrioid tumors
   (1) Benign
       1. Cystadenoma
       2. Cystadenoma with squamous differentiation
       3. Adenofibroma and cystadenofibroma
       4. Adenofibroma and cystadenofibroma with squamous differentiation
   (2) Of borderline malignancy (of low malignant potential)
       1. Cystic tumor
       2. Cystic tumor with with squamous differentiation
       3. Adenofibroma and cystadenofibroma
       4. Adenofibroma and cystadenofibroma with squamous differentiation
   (3) Malignant
       1. Adenocarcinoma and cystadenocarcinoma
       2. Adenocarcinoma and cystadenocarcinoma with squamous differentiation
       3. Adenocarcinofibroma and cystadenocarcinofibroma (malignant adenofibroma and cystadenofibroma)
       4. Adenocarcinofibroma and cystadenocarcinofibroma with squamous differentiation (malignant adenofibroma and cystadenofibroma
          with squamous differentiation)
   (4) Epithelial-stromal and stromal
       1. Adenosarcoma, homologous and heterologous
       2. Mesodermal (mullerian) mixed tumor (carcinosarcoma), homologous and heterologous
       3. Stromal sarcoma
4. Clear cell tumors
   (1) Benign
       1. Cystadenoma
       2. Adenofibroma and cystadenofibroma
   (2) Of borderline malignancy (of low malignant potential)
       1. Cystic tumor
       2. Adenofibroma and cystadenofibroma
   (3) Malignant
       1. Adenocarcinoma
       2. Adenocarcinofibroma and cystadenocarcinofibroma (malignant adenofibroma and cystadenofibroma)
5. Transitional cell tumors
   (1) Brenner tumor
   (2) Brenner tumor of borderline malignancy (proliferating)
   (3) Malignant Brenner tumor
   (4) Transitional cell carcinoma (non-Brenner type)
6. Squamous cell tumors
7. Mixed epithelial tumors (specific types)
   (1) Benign
   (2) Of borderline malignancy (of low malignant potential)
   (3) Malignancy
8. Undifferentiated carcinoma

Figure 1-2 – Histopathological classification of ovarian tumours

The Figure above shows the classification of ovarian tumours as described by the World Health Organisation. The Figure above was taken from 'Histological classification of OC' by T. Kaku et al (24).

						Cell of Origin
Epithelial (~90%)	Sex-cord stromal		Germ cell		Mixed-cell type	

| (68%–71%) | (9%–11%) | (12%–13%) | (3%) | Brenner (1%) | histologies (6%) † | Subtypes |

| Low-grade serous carcinoma (LGSC) * | High-grade serous carcinoma (HGSC) * | *Traditionally, well differentiated (low-grade) serous tumors were thought to progress to moderately and, ultimately, poorly differentiated (high-grade) serous carcinomas; †Mixed epithelial histologies is no longer included in the 2014 WHO classifications of ovarian cancer. |

C

| Serous | Endometrioid | Mucinous | Clear cell |

Figure 1-3 – The classification of OC subtypes
(A) Cell of origin (B) Subtypes of epithelial OCs (25) (C) The histological and surgical images of serous, endometrioid, mucinous and clear cell OC. Images taken from Webpathology (26)

OC can be classified into various subtypes as shown in **Figure 1-3** with epithelial serous OC being the most common (25). Each subtype has its own histological and surgical morphology as can be seen in **Figure 1-3-C**.

1.4.1.1 Incidence and epidemiology of OC

There are around 7400 new OC cases estimated in the UK every year using data collected from 2015-2017. OC is the 6th most common cancer among females and accounts for 4% of all new cancer cases in females in the UK (27). The incidence rates are highest for women ages 75-79 years of age and each year 28% of all new OC cases are diagnosed in females 75 years of age and over (28). Almost 6 in 10 cases of OC are diagnosed at a late stage (stage 3 or later) and the incidence of OC has remained stable since the 1990s (27). There are around 4100 deaths from OC in the UK every year and in the UK, OC is the 6th most common cause of cancer death (27). OC accounts for 5% of all cancer deaths and mortality rates from OC are highest in women ages 85-89 (27). Since the 1970s, OC mortality rates have decreased by 21% and over the last decade OC mortality rates have decreased by 17% (27). This shows that although the number of new cases of OC are remaining steady, the deaths relating to it are decreasing which indicates more effective treatment intervention in the last decade. From data collected in 2013-2017, 71.7% of women with OC survived for 1 year or more and 42.6% of women survived for 5 years or more (27). Survival is highest in women diagnosed aged under 40 where 9/10 women who are diagnosed aged 15-39 survive for more than 5 years. This is compared to only a fifth of women surviving longer than 5 years if they are diagnosed at age 80 or over (29). Overall, this demonstrates that although OC mortality rates have been improved in the last decade, more emphasis needs to be placed on an early diagnosis for the maximum chance of recovery and the development of new treatments that improve disease outcome.

1.4.1.2 Pathogenesis of OC

OC is difficult to confidently classify and stage at the time of diagnosis due to most ovarian carcinomas originating from cells which are not typically observed in the ovary but are linked to ovarian development. Some are have a clear histological subtype with clear origin whilst others (dependant on the stage and level of metastasis) are much harder to confidently classify (30). The origin of ovarian tumours is still unknown due to the tumour cell histology and the immunophenotype that differ from normal ovarian cells (31). Primary ovarian tumours and subsequent metastases grow massively in the ovary but not on the fallopian tube mucosa because the ovarian stroma is known to stimulate the growth and invasion of cancer cells whereas the fallopian tube stroma inhibits this progression (32). The ovarian microenvironment including the fallopian tube and the peritoneum play important roles in cancer initiation, progression, growth and invasion (**Figure 1-4**).
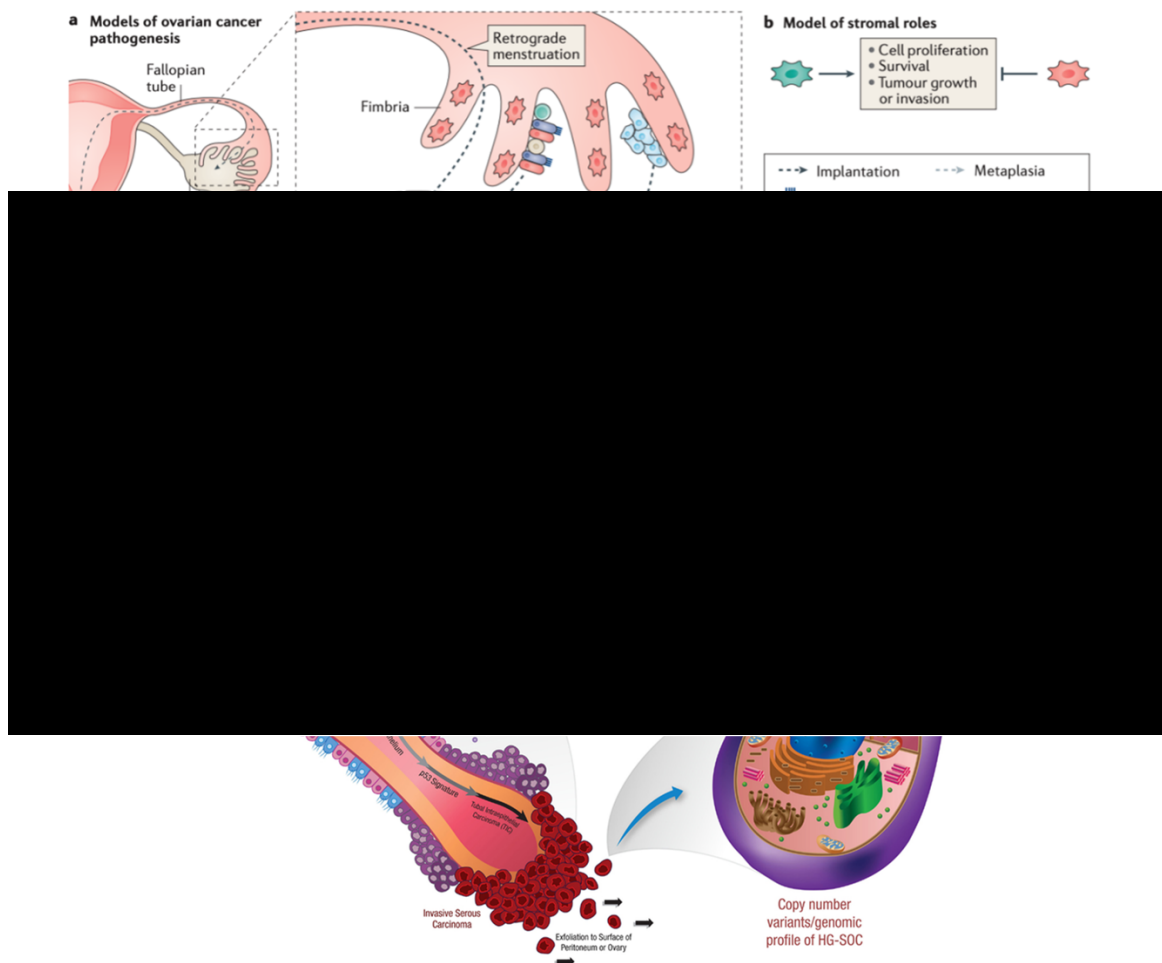
Figure 1-4 – The pathogenesis of OC microenvironment and early-stage lesions to OC

(a) Primary and metastatic OCs grown in the ovary but not the fallopian tube mucosa due to the ovarian stroma stimulating cancer cell growth and invasion and fallopian tube stroma inhibiting this growth and invasion. Advanced OC commonly metastasises to other peritoneal areas such as the omentum, endometrium, fallopian tubes and sigmoid colon (33) HGSC: High Grade Serous Cancer. SBT: Serous Borderline tumour. LCSC: Low Grade Serous Carcinoma. CCC: Clear Cell Carcinoma. EC: Endometrioid Carcinoma. EMO: Ovarian Endometriosis. CIC: Cortical inclusion cysts. (b) HGSOCs are generated first in the fallopian tube fimbria which progress to implant to the ovary. Some HGSOCs are caused by the TP53 mutation. Other HGSOCs present with a tumour that is developed from tubal-type cortical inclusion cysts which are developed by epithelium implantation of fimbria or by metaplasia of ovarian surface epithelium. A serous borderline tumour and Low-grade serous carcinoma are originated by large tubal cortical inclusion cysts, caused by Ras gene and BRAF mutation. Ovarian endometriosis is raised by retrograde menstruation and metaplasia. Ovarian endometriosis is further developed into clear cell carcinoma or endometrioid carcinoma. Dashed lines display the processes or origin of cells (metaplasia or implantation, retrograde menstruation). Solid lines display the progression of tumour cells. Image from Karnezis et al, 2017 (34). (c) HGSOC early tumour development from initial pre-cancerous lesion in the fallopian tube. TP53 gene mutations are an early event in the pathogenesis of HGSOC in secretory cells which appear to be benign. The acquisition of a preneoplastic lesion phenotype and proliferative capacity results in the formation of a serous tubal intraepithelial carcinoma (STIC). Invasive HGSOC develops when the basement membrane is invaded, and early lesions disseminate to the ovary and/or peritoneal cavity (35).

A large proportion of HGSOCs are reported to initially generate in the fallopian tube fimbria which go on to implant on the ovary. HGSOCs are typically reported to present with mutations in the tumour suppressor gene *TP53* (36). In other cases, the HGSOC tumour has been reported to originate from the intra-ovarian tubal epithelium known as tubal-type cortical inclusion cysts (37). The precursor lesions of HGSOCs are serous tubal intraepithelial carcinoma in the FTE (Fallopian Tube Epithelium) of women who have *BRCA1/2* mutations. Tubal cortical inclusion cysts are generated either by epithelium implantation of fimbria or by metaplasia of ovarian surface epithelium to a tubal phenotype (34).

Serous borderline tumours and low grade serous carcinomas originate from large tubal cortical inclusion cysts, reported to be caused by *RAS* and *BRAF* genetic mutations that facilitate ovarian carcinogenesis (37).

Ovarian clear cell and endometrioid carcinoma can develop from endometriosis due to its inflammatory nature (**Figure 1-3**). Ovarian endometriosis has been reported to originate from menstruation and metaplasia (38). The relationship between OC and endometriosis has been well studied with both diseases having causal links to infertility, early menarche, late menopause and nulliparity (39). Endometriosis is characterised by inflammatory processes such as an imbalance in cytokines including Interleukin-1, Interleukin-6, and Interleukin-8 (40). These imbalances are reported to induce the immunomodulatory tumour necrosis factor alpha which stimulates cytokine in ovarian malignancy (41). Inflammation and intrinsic anomalies cause several stimulatory signals and therefore, progressive transcriptional changes are induced which leads to sustained proliferation and the mutations in ovarian endometrioid cells (42). This results in the phosphate and tensin homolog tumour suppressor gene (*PTEN*) as an ovarian endometroid carcinoma gene mutation (41). The expression of oncogenic *KRAS* and the deletion of *PTEN* tumour suppressor gene within the ovarian surface epithelium has been demonstrated in a research study in murine tumours and in the tumour xenografts of human ovarian surface epithelium (43). The deletion of *PTEN* and oncogenic activation of *KRAS* has been previously shown to increase the endometriotic precursor lesions, which further initiate the invasive endometrioid ovarian carcinogenesis (44). Clear cell OC and endometrioid OC are ovarian epithelial carcinoma subtypes that originate from endometriosis or adenofibroma (34).

1.4.1.3 Risk factors for OC

There are several risk factors associated with OC as described by The American Cancer Society (45), the National Health Service NHS (46) and the Centre for Disease Control (47), with the risk of developing OC increasing with age. OC is much less common in women under the age of 40

with most ovarian cancers being diagnosed in women after the menopause. It is unclear if diet affects the risk of developing OC (45), but some studies have shown a reduced rate of OC in women who ate a diet lower in fat and higher in vegetables (48), whereas another study disagreed with this and showed no significant correlation (48). It is generally agreed that more research is needed in this area (49).

Diet does have associations with obesity and obesity has been identified as an unclear risk factor for OC in multiple sources. Obesity has been linked to a slightly higher risk of cancer in general (50)however, the current information linking obesity to OC is unclear, and somewhat conflicting. It is suggested that obese women, with a BMI of over 30, may have a higher risk of developing OC but not necessarily a higher risk of the more aggressive subtypes (51). Obesity may also negatively affect the overall survival of women with OC (45). A study by Leitzmann *et al* in 2009 (52) reported data that suggested obesity is associated with enhanced OC risk through a hormonal mechanism. However, a systematic review looked at 43 papers and found a limited, inconsistent association between OC and obesity (53). Thus overall, it is unclear if obesity is a risk factor for developing OC.

The risk of developing OC has also been linked to older age at first birth (54). It is reported that women who have their first birth at age 35 or over, or never have a pregnancy to full term, have an increased risk of epithelial OC. It is suggested that the hormonal modifications induced by the first term pregnancy at different ages seem to result in similar consequences in the progression of carcinogenesis in the ovary and also in the breast (55). Pregnancy and breast feeding have also been linked to a reduced risk of OC. Studies also show that breastfeeding may lower this risk even further (56).

It is reported that women using estrogen alone or with progesterone after menopause as a hormone therapy, have an increased risk of developing OC when compared to women who never used hormones (57, 58). This association is widely agreed upon in studies and meta-analysis data.

Many studies have investigated the association between OC and the use of Talc and conclusions have been mixed (59-62). It has been suggested that powder may cause cancer in the ovaries if the powder particles were to travel through the vagina, uterus, and fallopian tubes to the ovary. Some studies reported a slightly increased risk where other studies reported no increase at all (59-62).

Using fertility treatment with *in vitro* fertilisation (IVF) has been reported to increase the risk of certain subtypes of OC such as borderline tumours, also known as tumours of low malignant potential. There have also been studies (63, 64) showing no association between fertility

treatment and OC. This suggests the link is largely unclear with minimal evidence to support the association.

Research has shown that women with endometriosis may be more likely to develop OC (65-67). It is thought that the inflammatory nature of endometriosis may increase the likelihood of mutations leading to cancer, but the mechanisms that lead to the malignant transformation of endometriosis needs more research.

Some factors have been reported to decrease the risk of OC. Less frequent ovulation as a result of using contraceptives, such as the pill, have a lower risk of OC. The risk is reported to be lower the longer the contraception is used, and the low risk continues for many years after the contraception is stopped. Other types of birth control such as tubal ligation and intrauterine devices have also been associated with a lower risk of OC. Additionally, a hysterectomy (the removal of the uterus without the removal of the ovaries) has also been reported to reduce the risk of OC by about a third (68, 69).

1.4.1.4 Inherited OC

Having a family history of OC, breast cancer or colorectal cancer can significantly increase the risk of OC in an individual. The risk increases further if multiple relatives have OC, breast cancer or colorectal cancer (70). Up to 25% of OCs are part of family cancer syndromes or inherited cancers due to the inheritance of mutations in certain genes (71).

Hereditary breast and ovarian cancer syndrome (HBOC) are caused by inherited mutations in the BReast CAncer (*BRCA*) 1 and 2 genes. The diagnosis of a *BRCA1* or *BRCA2* HBOC is established by the identification of a heterozygous germline pathogenic variant in *BRCA1* or *BRCA2* gene. The exact risk of cancer depends on if the *BRCA1* or *BRCA2* gene is mutated (72). *BRCA1* encodes a protein which acts as a tumour suppressor, it is recruited to DNA damage sites and has an important role in DNA end resection, the G2/M checkpoint and the s-phase checkpoint (73). The protein encoded by *BRCA1* also repairs DNA during replication and is involved in homologous recombination (74). These various functions support the role of *BRCA1* in regulating cell proliferation. *BRCA2* encodes a protein that is involved in DNA damage repair, specifically homologous recombination (75). If a mutation is identified in the *BRCA1* or *BRCA2* gene, then several surgical interventions can be considered depending on the stage of the tumour. Generally, PARP inhibitors are given to metastatic patients with *BRCA1/2* mutations. A bilateral mastectomy can reduce the risk of breast cancer, while an oophorectomy, a hysterectomy or a total abdominal hysterectomy can reduce the risk of OC. In some cases, preventative chemotherapy (tamoxifen) is administered (76).

Hereditary nonpolyposis colorectal cancer (HNPCC), also known as Lynch syndrome, is a genetic disease of autosomal dominant inheritance. It occurs when a gene in the DNA mismatch repair system is mutated and results in a significantly increased risk of OC, endometrial cancer and colorectal cancer. Women with this disease have about a 10% chance of developing OC and about 1% of all patients with OC have been previously diagnosed with Lynch syndrome (77).

Peutz-Jeghers syndrome is a rare genetic syndrome where polyps develop in the stomach and intestines during the teenage years. Individuals with this syndrome have a significantly increased risk of cancers, particularly of the digestive tract. Women who have this syndrome have an increased risk of developing OC, including epithelial OC and a stromal tumour called sex chord tumour with annular tubules (78). The gene mutated in this syndrome is *STK11*. *STK11* is a gene encoding a protein kinase which acts as a tumour suppressor by regulating cell growth (79).

MUTYH-associated polyposis is a condition where the *MUTYH* gene is mutated, resulting in polyps on the colon and small intestine. This syndrome has a high risk for colon cancer and other cancers such as cancer of the bladder or ovary. *MUTYH* gene encodes a protein which is involved in DNA repair mechanisms and a mutation here prevents errors in the DNA from being corrected. This leads to an accumulation of mutations and potentially progression to cancer (80).

There are significant and numerous links between breast cancer and OC (72). Many of the risk factors associated with either cancer also commonly increase the risk of the other. The risk of OC after breast cancer is highest in women with a family history of cancer. This includes the associated risks with mutations in the *BRCA1* and *BRCA2* genes and hereditary breast cancer and ovarian cancer syndrome (81).

1.4.1.5 Symptoms, signs and early detection

Due to the nonspecific nature of OC signs and symptoms, early detection is difficult. The common signs of OC are feeling bloated, feeling full quickly and/or loss of appetite, pain or discomfort in the lower stomach and/or back, needing to pass urine more often or more urgently, changes in bowel habits, pain during sex, weight gain or weight loss and unexplained or extreme tiredness (82). However, by the time symptoms such as abdominal swelling and pain occur the disease is often in a later stage. Currently the only confirmatory method of diagnosing OC before treatment is by cytology from surgery that is as minimally invasive as possible (83). Often it is a difficult decision to recommend an invasive surgical procedure with such ambiguous symptoms. An early detection method is desperately needed to avoid difficult medical decisions and to ensure as many women as possible can be screened for OC in a minimally invasive, high throughput manner.

A report from NHS UK (84) described the refinement of the existing diagnostic CA125 blood serum marker in OC. This development built on research by Menon U in 2005 where the Risk of OC Algorithm (ROCA) was used to assess OC prevalence in high risk (post-menopausal) women (85). The hypothesis was that OC mortality could be reduced by regular biomarker blood tests. Two screening trials were undertaken where women had CA125 measured annually. Before progressing to larger trials, the statistical analysis of serial CA125 levels showed that each woman had her own baseline CA125 level. In the case of OC, CA125 rose rapidly following a change point. This method could improve early detection if women were tested for the presence of a change point (86). Using data from these trials a statistical method was developed to quantify the probability a change point had occurred. The latest development describes further where 46,237 women ages 50 years or older had annual ROCA screening. Women who were determined at normal risk continued to have annual ROCA screening. Women who were at intermediate risk had their CA125 serum levels checked every 12 weeks. Finally, women who were at an elevated risk had a CA125 test repeated every 6 weeks and had a transvaginal ultrasound. In this study the ROCA algorithm accurately predicted 86% of women with OC and ruled out almost 100% of those who were cancer free (87).

In August 2017, the cost effectiveness of an NHS OC screening programme was assessed using data from the UK Collaborative Trial of OC Screening (88). Considering costs from blood tests and analysis, transvaginal ultrasounds and resulting surgical procedures versus the mortality benefits and patient health outcome. Data concluded that this strategy rapidly approaches the threshold for cost effectiveness. This will be reassessed and if the mortality benefit increases then this method could be recommended for use by the NHS on health grounds, as well as economic grounds (88).

1.4.1.6 Current diagnosis methods

1.4.2 Algorithms for the detection of ovarian cancer

Due to biomarkers on their own not always being sensitive enough to indicate OC, algorithms have been developed for use in addition to a biomarker. Algorithms use multiple indicators to generate an arbitrary number to indicate malignancy. This number is placed on that algorithms scale to indicate the likelihood of malignancy.

1.4.2.1 Risk of Malignancy Index (RMI)

In 1990, Jacobs *et al* introduced the Risk of Malignancy Index (RMI) (89). RMI takes into account CA125 serum levels, ultrasound findings and menopausal status. The RMI score indicates the risk of the individual having OC where an score of over 200 is the cut-off point to discriminate

between benign and malignant tumours (90). RMI used the formula RMI= U x M x CA125 where U is ultrasound score (U=0 if ultrasound score = 0, U=1 if ultrasound score =1 and U=3 if ultrasound score is 2-5), M= menopausal status (M=1 for premenopausal women and M=3 for postmenopausal women). An RMI score of over 200 has been shown to have a strong association with a high risk of malignancy with a sensitivity of 85.4% and a specificity of 96.9%. However, a study in 2010 demonstrated that the ultrasound on its own actually has superior sensitivity (91) when compared to RMI. The data was confirmed by a subsequent study in 2016 (92). Due to the specificity for OC being quite high using RMI, the threshold for malignancy could be increased to 250 to increase the sensitivity.

Since the introduction of the RMI algorithm in 1990, several modifications have been made to try and improve the sensitivity and specificity. Chopra *et al* used 100 patients and changed the maximum values of U and M to 4 rather than 3. This increased the sensitivity and specificity to 96.7% and 84% respectively (93). Overall, the RMI algorithm does have some use for the diagnosis of OC and modifications have made it more sensitive and specific, however it does not appear to be the most reliable method for the detection of OC when compared to other methods such as the use of ultrasound scan alone (94).

1.4.2.2 Risk of Ovarian Malignancy Algorithm (ROMA)

In 2009, another algorithm for the diagnosis of OC was published. Moore proposed the Risk of Ovarian Malignancy Algorithm (ROMA) where HE4 and CA125 serum levels were associated with menopausal status (95). The algorithm uses two indexes, one each for pre-menopausal and post-menopausal. The appropriate index is then used in an equation to determine the predicted probability expressed as a percentage.

The ROMA algorithm has been used in meta-analysis studies (96) (97), where it was reported to have less specificity when compared to HE4 levels, but a better correlation with CA125 levels. Other meta-analysis studies showed ROMA was more sensitive than HE4 but less specific when compared to HE4 (98). Overall, the measurement of both CA125 and HE4 appears to be the best diagnostic tool for OC thus far, the inclusion of age in ROMA could be a valuable contribution to the diagnosis of OC (99).

1.4.2.3 Current treatment methods

The current treatment method depends on the type of OC diagnosed and often, diagnosis, removal of the tumour and staging of the tumour happen all within the same surgery. Standardly, surgical intervention is followed by chemotherapy or (rarely) radiotherapy. Epithelial stage 1 cancers are often treated with surgery alone, stage 2, 3 and 4 epithelial OCs

are commonly treated with a combination of surgical debulking and chemotherapy. More recently, targeted therapies are being offered to women with a BRCA mutation and in some cases radiation therapy. A germ cell or stromal OC is often treated with a combination of surgical debulking and chemotherapy and a borderline tumour is often treated with surgery only (100).

1.4.2.3.1 Surgery

Surgical debulking of the tumour is often the first option with OC treatment. The risk of surgery often includes infertility, and a fertility specialist can be consulted if the individual is pre-menopause. A general anaesthetic is applied and either a laparoscopy or a laparotomy will be carried out. A laparoscopy is a minimally invasive surgery with 3-4 small cuts being made in the abdomen, whereas a laparotomy is a long vertical cut from the belly button to the bikini line. A laparoscopy is often used to investigate a suspicious mass where a laparotomy is commonly used in advanced cancers to debulk the malignant tissue (101).

A total hysterectomy and bilateral salpingo-oophorectomy are the removal of the uterus, the cervix, the fallopian tubes and the ovaries. Most women with OC will have this surgery (102). Unilateral salpingo-oophorectomy is usually carried out if the cancer is found early enough and is only in one ovary. Additionally, young women who still wish to have children may opt for this surgical procedure to remove only one ovary and fallopian tube (103). An omentectomy is the removal of part of the omentum, a sheet of fatty tissue attached to the stomach and bowel. OC often spreads to the omentum and it is often removed during surgery (104). Cancer cells can spread from the ovaries to nearby lymph nodes. In this case, a lymphadenectomy (or lymph node dissection) will be carried out to control the spread of malignant cells (105). It is also possible that cancer from the ovaries can spread to the bowel. In cases such as this a colectomy will be carried out where some of the bowel is removed (106). In other cases where the cancer has spread to other organs within the abdomen, these tissues such as the liver, diaphragm, bladder and spleen may also be removed if it is safe to do so (107).

1.4.2.3.2 Chemotherapy

Chemotherapy is commonly used in combination with surgery in later stage cancers. Chemotherapeutic agents are anti-cancer cytotoxic drugs that aim to destroy malignant cells. Chemotherapy works with the cell cycle to target cells at different phases of the cell cycle. Each new cell goes through the cell cycle to become a fully functioning mature cell. Malignant cells can be characterised by their ability to form new cells faster than non-cancer cells, this means they are a better target for chemotherapeutic agents (108). Chemotherapy however, cannot differentiate and target malignant cells from healthy cells. For this reason, chemotherapy often

affects other fast dividing cells such as hair follicles, nails, the mouth, the digestive tract and bone marrow leading to side effects such as hair loss, nausea and a compromised immune system (109). Chemotherapy can be given systemically *via* an intravenous drip in cycles or directly into the abdominal cavity. During intraperitoneal chemotherapy, drugs are administered directly to the space between the abdominal organs and the abdominal wall *via* a tube that is put in place during surgery and is removed once the course of chemotherapy ends. Intraperitoneal chemotherapy is not commonly used in the UK or the USA, instead, chemotherapy by intravenous drip is the standard way to deliver the drugs (107). The chemotherapy drug carboplatin is often used on its own or with paclitaxel. Other drugs used include cisplatin, docetaxel, etoposide, gemcitabine, liposomal doxorubicin and topotecan (110).

1.4.2.3.3 Radiation therapy

Radiation therapy, or radiotherapy, uses x-rays to damage cancer cells. The radiation is directed at the specific area of cancer with the aim to reduce the growth of the mass. Radiotherapy is rarely used in OC but it can be used in conjunction with chemotherapy or on its own. Radiotherapy for OC is given over the whole abdominal area which can affect the bladder and bowels (111). Common side effects include tiredness, diarrhoea, needing to pass urine more often, burning when urine is passed (cystitis) and a minor burn to the skin surrounding the treatment area. Radiation can be used as part of palliative treatment which helps to improve the patients quality of life by managing cancer symptoms and pain without trying to cure the cancer (107).

1.4.2.3.4 Targeted therapy

Targeted therapies are able to differentiate healthy cells from malignant cells and deliver the cytotoxic payload directly to the malignant cells. This increases the effectiveness and decreases the side effects to the patient. Targeted therapies are an up-and-coming treatment for OC and can be used on their own or after chemotherapy has not been successful. Targeted antibody-based therapies relies on the action of a specific monoclonal antibody which recognises and binds to a carefully selected protein present on the malignant cells but not on the healthy cells. This allows the therapy to affect the malignant cells, while leaving the healthy cells largely unaffected. A common targeted therapy used in the treatment of OC is with DNA damage repair alteration by the administration of small molecule poly ADP ribose polymerase (PARP) inhibitor, such as Olaparib (112). PARPs are proteins that are involved in damaged cells repair. Olaparib

inhibits the actions of PARP in cancer cells with a mutation in the *BRCA* gene causing the malignant cells to die due to the inability for DNA damage to be repaired *via* homologous recombination. Olaparib is only used in patients with *BRCA* and can be used after having chemotherapy. Olaparib is also used for the treatment of *BRCA* positive breast cancer (113). Formerly Olaparib was only available for eligible patents as part of clinical trials, however most recently in 2019 due to the survival benefit to patients with OC, the National Institute for Health and Care Excellence have approved Olaparib for use on the NHS (114).

Bevacizumab (Avastin®) is another common targeted therapy used for the treatment of OC. Bevacizumab targets vascular endothelial growth factor (VEGF) (115). VEGF is a protein that enables angiogenesis in malignant cells. Using Bevacizumab to inhibit VEGF reduces the supply of oxygen and nutrients that the tumour gains through a healthy blood supply. This treatment aims to shrink and stop the tumour from growing. Bevacizumab is not available as an NHS treatment but there are other ways to enable treatment with Bevacizumab, such as private health care and clinical trials (116). Bevacizumab has shown a survival advantage in OC patients in a progression-free survival advantage of 2.4 months, an overall survival benefit of 8 months in patients with high risk of progression and a less than 10-point difference in quality of life between the two groups (117)

1.4.2.4 Staging

The staging of OC recognises that it is not a homogenous disease but a group of diseases, each with a different biological behaviour and morphology. Approximately 90% of ovarian tumours are malignant epithelial carcinomas and can be further subcategorised into high-grade serous, endometrioid, clear cell, mucinous and low-grade serous carcinomas by histopathology, immunohistochemistry and molecular genetic analysis, as can be seen in **Figure 1-2** and Figure **1-3**.

The process of staging is an agreed consensus by the FIGO Committee and all the relevant gynaecological oncology organisations around the world. **Table 1-1** shows the current TNM and FIGO classifications for staging OC (118-121).

Table 1-1 - TNM and FIGO Classifications for Ovarian Cancer

Primary tumour (T)		
TNM	*FIGO*	
TX		Primary tumour cannot be assessed
T0		No evidence of primary tumour
T1	I	Tumour limited to the ovaries (one or both)
T1a	IA	Tumour limited to one ovary; capsule intact, no tumour on ovarian surface; no malignant cells in ascites or peritoneal washings
T1b	IB	Tumour limited to both ovaries; capsules intact, no tumour on ovarian surface; no malignant cells in ascites or peritoneal washings
T1c	IC	Tumour limited to one or both ovaries with any of the subcategories below (IC1-3)
T1c1	IC1	Surgical spill
T1c2	IC2	Capsule ruptured before surgery or tumour on ovarian or fallopian tube surface
T1c3	IC3	Malignant cells in ascites or peritoneal washings
T2	II	Tumour involves one or both ovaries with pelvic extension below pelvic brim
T2a	IIA	Extension and/or implants on the uterus and/or tube(s)

N1b	IIIAIii	Metastasis more than 10 mm in greatest dimension
Distant metastasis (M)		
TNM	*FIGO*	
M0		No distant metastasis
M1	IV	Distant metastasis including cytology-positive pleural effusion; liver or splenic parenchymal involvement; extra-abdominal organ involvement including inguinal lymph nodes; transmural intestinal involvement
M1a	IVA	Pleural effusion with positive cytology
M1b	IVB	Liver or splenic parenchymal metastases; metastases to extra-abdominal organs (including inguinal lymph nodes and lymph nodes outside the abdominal cavity); transmural involvement of intestine

The table above has been taken from Grabosch's article on Medscape (118-122)

1.4.3 Endometrial cancer

Endometrial cancer (EC) begins in the endometrium (the lining of the uterus) and is the most common cancer of the female reproductive system. It is also referred to as uterine cancer and womb cancer. 1 in 36 women will be diagnosed with EC in their lifetime and there are around 9300 new cases of EC each year in the UK equating to approximately 26 new cases every day. Among females in the UK, EC is the most common gynaecological cancer, the 4th most common cancer and it accounts for 5% of new cancer cases in women. Incidence rates are highest for women ages 75-79 and around a fifth of ECs are diagnosed at a late stage. Incidence rates have increased by 57% since the early 90's and again by 19% in the last decade however they are projected to fall by 7% between 2014 and 2035. EC is not associated with deprivation and is equally common between White, Asian and Black females (123). In the United States there will be an estimated 61,889 new cases of and 12,160 deaths from EC in 2019 (124). This is similar to the 2018 predictions where 63,230 new cases were expected and 11,350 deaths were predicted (125). There are around 2,300 deaths in the UK associated with EC each year equating to more than 6 each day. EC is the 8th most common cause of cancer death in females in the UK and accounts for 3% of all cancer deaths in females in the UK. Mortality rates associated with EC are highest in females over the age of 90. Since the 1970's EC mortality rates remained reasonably stable, however in the last decade mortality rates have risen by 23%. Mortality rates are predicted to rise further by 19% by 2035 (123). Survival rates of EC are highest in women under the age of 39 and when diagnosed at its earliest stage. 78% of women in the UK survive for ten years or more and EC survival is improving and has increased in the last 40 years in the UK. Risk of EC depends on many factors such as age, genetics and exposure to risk factors such as radiation (126).

The current approach to diagnosing EC is the 'two week wait' where the patient is made an appointment as a matter of urgency within two weeks as a result of a visit to their GP. The current treatment method is most commonly major surgical resection (80% of patients), radiotherapy (21% of patients) and chemotherapy (16% of patients) (123). Patients will commonly receive surgery plus chemotherapy or radiotherapy (127).

Although surgery is commonly the primary treatment for early stage, late stage and high-risk EC cases alike, a select group of patients have an increased risk of recurrence. In these cases, adjuvant therapy (a therapy given in addition to the primary treatment) is necessary to improve the prognosis for these patients. Adjuvant therapy could be followed up with chemotherapy, radiotherapy or a combination of the two. The type of adjuvant therapy administered is patient

specific and the treatment decision is largely influenced by cancer stage, age and other factors (128) (129).

Lymph node involvement is considered a critical factor in determining the prognosis and the response to therapy in EC. Staging cancer correctly is important as patients with a stage 3 EC, treated with chemotherapy, have a survival advantage, whereas this is not true for patients with locally advanced disease (130). On top of that, complete staging lymphadenectomies have been associated with morbidity that can negatively impact the quality of life. Therefore, criteria has been explored to define patients that have a low enough risk to safely bypass the lymphadenectomy (131). Kang *et al* explored predicting which patients could safely bypass the lymphadenectomy where there was endometrioid histology, no evidence of deep invasion or enlarged lymph nodes and a pre-operative CA125 of less than 35 units/mL (132). Of patients who have a reoccurrence of their EC two thirds are in the stage I and II subgroup. These individuals could benefit from a more aggressive adjuvant therapy to prevent relapse (133, 134).

1.4.4 Cervical cancer

Cervical cancer is the third most common malignancy in women and historically provides a first-class illustration of the benefit of early detection *via* a non-invasive approach. The Pap smear is recognised medically as being discovered by George Papanicolaou (135) and the implementation of this revelation *via* the introduction of the cervical cancer screening program in 1949, where women received annual Pap smears (136), demonstrated the power of high throughput screening. A recent evaluation shows that since the late 1970s cervical cancer mortality rates have fallen by 72% and is predicted to fall another 7% between 2014 and 2035. Moreover the jump from a 74% survival rate in 1971-1972 to 83% in 1980-1981 is the largest improvement seen in the last 50 years potentially linked to the advances in early detection (137).

1.4.5 Breast cancer

Breast cancer is the most commonly occurring malignant disease in women and usually presents as a painless movable mass in the area of the breast (13). Breast cancer has strong links to OC in terms of risk factors, genetic mutations in *BRCA1* and *BRCA2* and links to an increased risk of one cancer after suffering the other (81). Breast cancer is the most common cancer in the UK, accounting for 15% of all new cancer cases (15). According to CRUK statistics in 2017 breast cancer represents 30% of all female cancer incidences. Breast cancer is more common in older people and incidence increases with age. Breast cancer is the 4th most common cause of cancer death in females the UK, and accounts for 7% of cancer deaths in 2017 (138). The risk factors for

breast cancer are similar to that of OC. Genetic *BRCA1/2* mutations, a high body mass index (BMI), first birth at an age greater than 30 or nulliparity, early menarche, family history, late menopause and post-menopausal hormone therapy use are all common risk factors for breast cancer and OC. Four breast cancer subtypes have been identified: Luminal A, Luminal B, HER-2 positive and triple negative (basal) breast cancer (139). Each subtype is associated with a specific histology and prognosis. Breast cancer is also classified by its anatomical origin (lobular or ductal), its hormone receptivity and expression of human epidermal growth factor receptor 2 (HER-2) (140). The hormone receptivity is in regard to the presence or absence of estrogen and progesterone receptor expression in the malignant cells. Triple negative breast cancer refers to breast cancers that do not express the estrogen receptor, progesterone receptor or HER-2 (141). Triple negative breast cancers are more likely to be diagnosed at a younger age but at a later stage (142). In addition, triple negative breast cancers are more likely to be a higher grade and therefore a more aggressive cancer compared to other subtypes (143).

Breast cancers are commonly diagnosed by mammogram imaging and confirmed by a biopsy obtained using a core needle biopsy, excisional biopsy, stereotactic biopsy or an MRI guided biopsy (144). Treatment options include surgery, chemotherapy and radiotherapy. Surgical treatment can involve a lumpectomy, mastectomy or bilateral mastectomy. Adjuvant therapy is often used after surgery and can include endocrine blockers, anthracycline and taxane based chemotherapy or monoclonal antibody therapy depending on histology, HER-2 status and hormone receptor status (145). The chemotherapeutic drug chosen also depends on subtype and the presence of metastatic disease. Common chemotherapeutic agents include doxorubicin, cyclophosphamide, and paclitaxel. Side effects are variable and can include significant nausea, vomiting, diarrhoea and fatigue. Radiation therapy is commonly used before or after tumour removal surgery (146).

1.5 Other gynaecologic conditions

1.5.1 Polycystic Ovaries

Polycystic ovary syndrome (PCOS) is metabolic endocrine disease that is heterogenous in nature. Its signs and symptoms include abdominal pain, difficulty getting pregnant, irregular menstruation, excess hair growth on the body, thinning hair on the head, weight gain and oily acne prone skin. It is categorised by symptoms of androgen excess and dysfunction of the ovary (as described above) (147). The aetiology of PCOS is multifactorial and complex with evidence suggesting that it is influenced by epigenetics and environmental factors such as diet and

lifestyle. PCOS is frequently associated with obesity, insulin resistance and metabolic disorders (148).

Diagnosis of PCOS is carried out by clinical imaging, monitoring hormone levels and ovulation and potentially a laparotomy or laparoscopy. Initially, women presenting with PCOS symptoms must immediately be examined for an androgen-secreting neoplasm by clinical imaging. Difficulty can occur with differentiating PCOS from similar disorders such as idiopathic hyperandrogenism (149).

Treatment of PCOS depends on the symptoms presented. Usually, lifestyle recommendations are initially suggested and those with mild symptoms may improve without further treatment. No drugs are currently approved for the treatment of PCOS but the contraceptive pill is often prescribed to ensure hormone levels remain within normal limits (150).

Due to the inflammatory nature of PCOS several studies investigate the relationship it has with gynaecological malignancies, in particular OC. Jiao *et al* explored the relationship between PCOS patients with irregular menstruation and malignancy, concluding that irregular menstruation carried an increased risk of OC (151). Ding *et al* carried out a population-based cohort study in Taiwan where 8,155 patients with PCOS were compared to 32,620 individuals who did not have PCOS. Overall, they showed a significant association between PCOS and endometrial cancer suggesting they could be related. In the study by Ding *et al* and Harris *et al* there was no such association found between PCOS and OC (152, 153).

1.5.2 Endometriosis

Endometriosis is a disease characterised by endometrial tissue being present outside of the uterine cavity causing chronic pelvic pain and potentially interfertility. Endometriosis affects 10-15% of all women of a reproductive age and 70% of women with chronic pelvic pain (154). Symptoms in women include intermenstrual bleeding, painful periods, painful intercourse, painful defecation, and painful urination (155). Pain in the pelvic area may be present early in life before menstruation begins and can often be asymptomatic and remain undiagnosed until investigation for infertility (154). An increased risk for endometriosis is associated with early age menarche (156-160), shorter menstrual cycle length (159-163), taller height (156, 164) and alcohol use (165-167).

Endometriosis has been associated with a malignant potential and large studies have found OC to develop in 5-10% of endometriosis cases (168, 169). However, there is still some uncertainty surrounding neoplasms associated with endometriosis. Some have suggested that they may have distinct histologic entities (170), which can result in clinical and prognostic differences in

endometriosis and subsequent OC diagnosis. It has been reported that up to 19% of epithelial OC were associated with endometriosis (171).

1.5.3 Pelvic inflammatory disease

Pelvic Inflammatory Disease (PID) is an infection of the upper genital tract, including the uterus, fallopian tubes and ovaries. PID is a common condition although it is not certain how many women are affected in the UK due to the condition often going undiagnosed or being mistaken for another diagnosis (172). Many of these gynaecological conditions, including OC, have similar symptoms including pelvic pain, pain during intercourse, pain when urinating, bleeding between periods and painful periods. Women with PID, unlike in other conditions, can experience an unusual vaginal discharge (173). Complications of PID can include infertility, ectopic pregnancy and chronic pelvic pain. Recent findings suggest that the rates of unfavourable outcomes in women with PID are high and largely affect the young minority. Sexually transmitted diseases can increase the risk of PID and improving national screening can improve quicker treatment for a better long term prognosis (174).

Inflammation has been linked to cancer and therefore ovarian carcinogenesis. However, studies linking PID to OC are few and inconsistent. Data from 13 case-controlled studies were pooled (175) from the Ovarian Cancer Association Consortium including 9,162 women with OC tumours, 2,354 women with borderline tumours and 14,736 control patients. A history of PID was associated with an increase in borderline tumours with a 95% confidence interval. Women with at least 2 episodes of PID were reported to have a two-fold increased risk of borderline ovarian cancer tumours.

1.6 Inflammation and cancer

Inflammation is a biological response of the immune system that can be triggered by pathogens, damaged cells and toxic compounds. Inflammation can lead to pain, tissue damage or disease (176). Inflammation caused by infectious agents, non-infectious agents and cell damage can all cause the activation of inflammatory signalling pathways such as the NF-kB, MAPK and JAK-STAT pathways (177, 178). The purpose of inflammation is to remove the offending stimuli and initiate the healing process. Inflamed tissue is characterised by redness, swelling, heat and pain. On a microcirculatory level vascular permeability changes, leukocytes are recruited and accumulate, and inflammatory mediators are released. In response to the injury of tissue, a chemical signalling cascade is activated which stimulates responses aimed at healing the affected tissues. Factors such as histamine, chemokines and cytokines are triggered by the oligomerisation of pattern recognition receptors which recruit leukocyte chemotaxis from the general circulation

to the site of damage (179). The activated leukocytes produce cytokines that induce the inflammatory response. All types of inflammation share a common mechanism of cell surface pattern receptors recognising detrimental stimuli, inflammatory pathway activation, the release of inflammatory markers, and the recruitment of inflammatory cells (176). Inflammation is significantly associated with the development and progression of most cancers. The cancer-associated inflammation cells are stable genetically and are therefore not subjected to emerging drug resistance (180). For this reason, targeting inflammation is viewed as a popular strategy for cancer prevention and treatment. Inflammation occurring independently of a tumour can be caused by infection, autoimmune diseases, obesity, smoking, asbestos exposure and excessive alcohol consumption (181). As well as inflammation, these factors also increase cancer risk. On the other hand, inflammation intrinsic to cancer or inflammation as a result of cancer can be activated by mutations initiated by cancer and can support the recruitment and activation of inflammatory cells. Both types of inflammation can result in immunosuppression providing the ideal environment for tumour development and progression (180).

Tumour necrosis factor (TNF) is a proinflammatory cytokine which is secreted by inflammatory cells that may be involved in inflammation associated cancer progression. TNF activates the nuclear factor kB (NF-kB) and c-Jun N-terminal kinase (JNK) pathways (182). NF-kB and JNK work synergistically together to balance cell survival and anti-apoptosis with cell death. This indicates that TNF can support or work against tumour progression and development (183). There is some evidence that inflammatory cytokines and chemokines may contribute to cancer progression. Several cytokines and chemokines can be induced by hypoxia (184). This is a significant physiological difference between tumour and normal tissue. Cytokines derived from tumour cells, such as Fas ligand, VEGF and transforming growth factor-h have been reported to supress the immune response to tumours (185). Interleukin-6 (IL-6) is a pleiotropic inflammatory cytokine that is released by normal cells as well as in multiple tumour types such as OC, breast and colorectal cancer. IL-6 has also been reported to be involved in tumour apoptosis, growth, proliferation, migration, invasion, angiogenesis and metastasis (186). Interleukin-10 (IL-10) is a cytokine inhibitor involved in tumour growth. IL-10 inhibits cytokine production by T helper cells and is produced by almost all leukocytes and many tumour cells, including those from breast, colon and ovarian cancer (187). IL-10 is integral to the suppression of tumour promoting inflammation mediators and therefore aids tumour growth and metastasis (187).

A host of leukocytes in the tumour environment and surrounding stroma are characteristic of an inflammatory tumour microenvironment. Tumour Associated Macrophages (TAMs) make up a large proportion of the cells that infiltrate the tumour microenvironment. TAMs derive from

monocytic precursors and are directed to the tumour by chemokines. Tumour cells also produce cytokines that prolong the survival of TAMs. TAMs both work for and against tumour development and progression by killing tumour cells, activating tissue destructive reactions while also stimulating tumour cell proliferation, promoting angiogenesis and encouraging invasion and metastasis (188).

Dendritic cells play important roles in the activation of immunity and the maintenance of tolerance which provides a link between adaptive and innate immunity. Tumour associated dendritic cells commonly have an immature phenotype that does not have the ability to stimulate T-cells for the immune response against foreign particles. The immaturity of the tumour associated dendritic cells may reflect the absence of signals instructing the cells to mature, decreased migration of mature cells to the lymph nodes or the presence of maturation inhibitors (189).

Cytokines are mainly released from immune cells such as monocytes, macrophages and lymphocytes. Pro and anti-inflammatory cytokines promote and inhibit inflammation depending on the cytokine and its function. For example, IL6 is sourced mainly from macrpphages and has a pro inflammatory function as well as being involved in differentiation and cytokine production. Whereas IL10 is an antiinflammation cytokine and inhibits the production of inflammatory cytokines (190). Inflammation plays a critical role in tumour growth and it is now generally accepted that an inflammatory tumour microenvironment is an essential component of all tumours (191). Chronic inflammation can contribute to the induction of oncogenic mutations, genomic instability, early tumour promotion and angiogenesis. Tumour associated inflammation is linked to tumour development by the enhancement of angiogenesis, metastatic spread and local immunosuppression (192).

Overall, inflammation is well known to be a hallmark of cancer (193) and has been reported to associate with tumours and induce the development and progression of cancer (180). Although inflammation is known in a variety of benign conditions, it is a common factor in almost all cancers and the pain, swelling and certain markers can be used as an indicator for further investigation in cancer diagnosis.

1.7 Receptor for Advanced Glycation End products (RAGE)

The receptor for advanced glycation end products (RAGE) is a multiligand protein of the immunoglobulin superfamily, expressed on the membrane of multiple cells and is implicated in the immune-inflammatory response (Uniprot-RAGE_HUMAN- Q15109). RAGE was first described as a receptor for the products of nonenzymatic glycation and oxidation of proteins, advanced glycation end products (AGEs) (194). Glycation is the non-enzymatic reaction between

reducing sugars, such as glucose, and proteins, lipids or nucleic acids (195). Section 1.7.8.1 below discusses AGEs in more detail. RAGE is a type 1 cell surface transmembrane receptor and pattern recognition receptor (PRR) and has a multi domain structure that gives it the ability to bind a variety of ligands (see section 1.7.8). RAGE is implicated in a range of diseases and signalling pathways such as diabetes, acute and chronic inflammation in atherosclerosis and complications of diabetes. This is expanded upon later in this section. The AGE/RAGE signalling pathway regulates the production and expression of TNF-alpha, oxidative stress and endothelial dysfunction in type 2 diabetes (196) (see section 1.7.7 for more detail). In diabetes, poor glycaemic control reduces sRAGE levels, in association with enhanced oxidative stress and endothelial dysfunction (197). RAGE generates proinflammatory mediators by interacting with S100A12 on the endothelium, mononuclear phagocytes and lymphocytes. RAGE has also been documented to interact with S100B to play a role in myocyte apoptosis by activating ERK1/2 and p53/TP53 signalling (198). RAGE has also been implicated in neurological disorders by binding amyloid beta peptide. This contributes to the translocation of amyloid beta peptide across the cell membrane to the intracellular space in cortical neurons (199).

RAGE has been extensively studied by members of the Reproductive Biology and Gynaecological Oncology group at Swansea University Medical School for its use as an Antibody-Drug Conjugate (ADC) and biomarker in gynaecological malignancies (200-202). RAGE is described here as an example of a known strong ADC target with implications for the treatment of OC and patient stratification. The data presented in this thesis is novel as the directly visualised internalisation of a RAGE antibody conjugated to a pH reactive dye uses a new RAGE antibody clone. In addition, the sRAGE ELISA has not been performed with this patient sample cohort before.

1.7.1 RAGE gene (AGER)

RAGE is a 42 kilodalton protein encoded by the AGER gene present on chromosome 6 (location 6p21.32) and is found on the Major Histocompatibility Complex (MHC) locus and is comprised of a 1.7-kb 5' flanking region and 11 exons with 10 introns (see **Figure 1-5**). The total length of the gene is about 1,400 base pairs and the *AGER* gene overlaps with the *Pre-B-cell leukemia transcription factor 2* (*PBX2)* gene in the MHC locus (203). *PBX2* is a transcriptional activator that binds the sequence 5'-ATCAATCAA-3' and activates transcription of PF4 in complex with MEIS1 (204). The *AGER* promotor is located in the 5' flanking region and contains binding sites for a variety of transcription factors to regulate its expression.
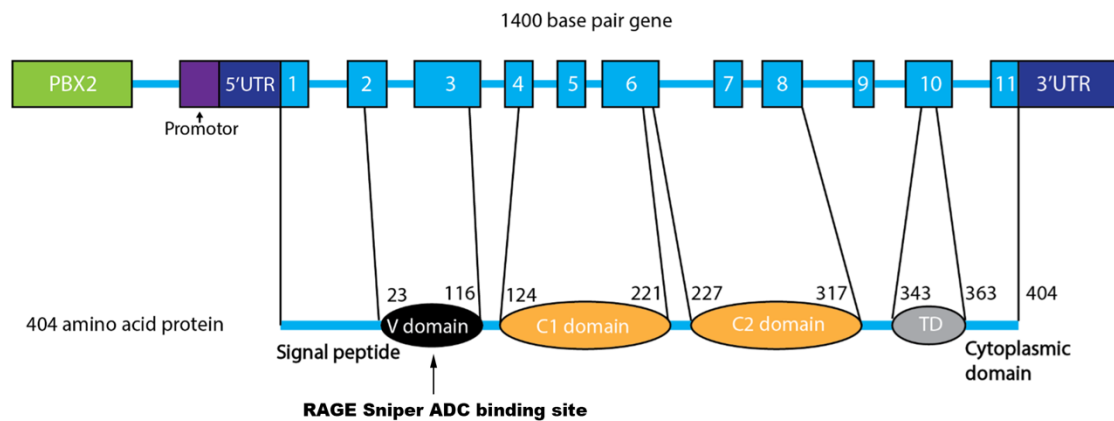
Figure 1-5 – Schematic of AGER gene

The RAGE protein is encoded by the AGER gene on chromosome 6 (location 6p21.32) and is approximately 1400 base pairs long. AGER contains 11 exons and 10 introns with the promotor located close to the 5'UTR. The promotor has a large variety of binding sites for transcription factors such as NF-kB. The V domain refers to the variable region responsible for ligand binding. The C domains refer to constant domains that specify effector functions and such as Fc receptor binding (205).

1.7.2 RAGE protein structure

RAGE is a 404 amino acid long transmembrane protein with a molecular weight of around 42 kDa (199). It is comprised of the signal peptide, three extracellular domains (the V domain, C1, C2 domain) a single transmembrane region and a short intracellular region. The V domain has two N-glycosylation sites and is responsible for almost all of the ligand binding such as High Mobility Group Box 1 (HMGB1), AGEs, S100 proteins and Amyloid-β oligomers (206). The C domains are thought to stabilise the V domains during ligand binding (207) and the cytoplasmic tail is considered essential for intracellular signalling (206).

1.7.3 RAGE isoforms

There are three major isoforms of RAGE that are generated by alternative splicing which can be described as full-length RAGE, N-truncated RAGE and secretory RAGE. All of these isotypes include the V-type and C-type domains and therefore bind RAGE ligands in the same way (207). These isoforms, specifically the secreted isoform, can produce a decoy effect for RAGE ligands. This prevents binding to the full-length RAGE and therefore down-regulates RAGE signalling pathways (208). Additionally, there is a fourth soluble RAGE variant, produced by protein cleavage. These isoforms can be seen in detail in **Figure 1-6** below.
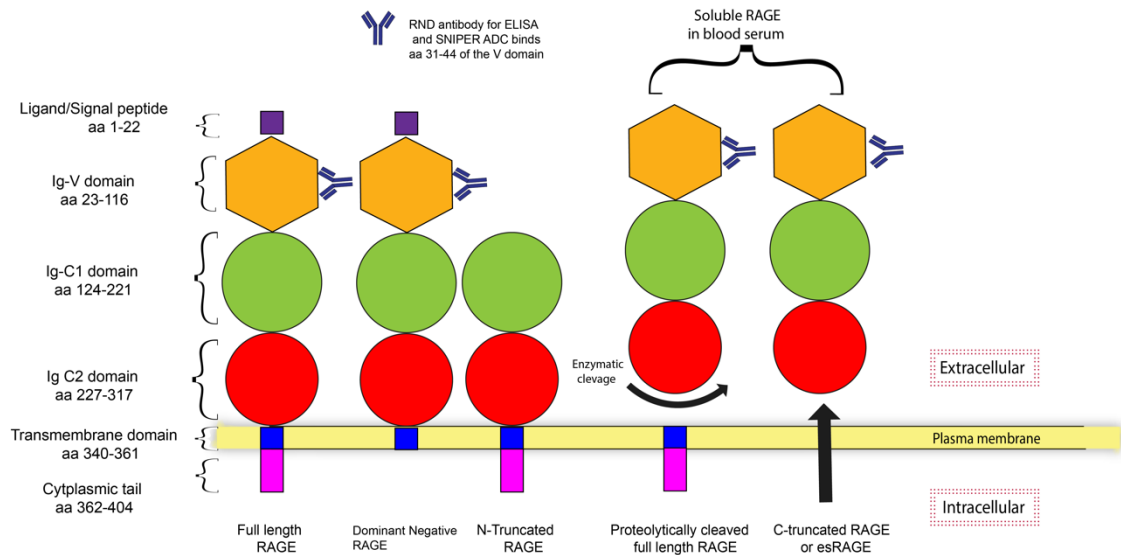
Figure 1-6 – Isoforms of the RAGE protein

RAGE exists as various isomers including full length RAGE, N-truncated RAGE, cleaved soluble RAGE and C truncated endogenously secreted soluble RAGE. Image inspired by Tekabe et al (209).

Soluble RAGE, both alternatively spliced and endogenously secreted, contain the V-type and C-type regions as the full-length RAGE but characteristically lacks the transmembrane region. As result, these soluble RAGE proteins are free to circulate in the extracellular space and allowed to interact with RAGE ligands before they have the chance to interact with full-length RAGE and activate signalling pathways. Soluble RAGE can alter the generation and maturation of potential full-length RAGE ligands. An example of this is sRAGE and beta amyloid (Aβ). Aβ is a small 40-42 amino acid protein that undergoes aggregation which is associated with fibrillization and oligomerization of the protein (210, 211). This aggregation of Aβ and its insoluble plaques is associated with Alzheimer's Disease. Full-length RAGE is believed to bind highly crosslinked and aggregated Aβ. Recent studies have shown that sRAGE is able to bind Aβ in the earlier stages of aggregation and this binding can also prevent the generation of insoluble Aβ structures by reducing Aβ aggregation. Due to this, sRAGE can down-regulate full-length RAGE activation by altering the Aβ before it can interact (207).

sRAGE is found to be highly expressed in the brain and is localised to the neuronal cytoplasm (212). Two forms of sRAGE are expressed in the brain and *AGER* gene isoform that encodes sRAGE is approximately 3-fold higher than other forms of RAGE in the brain. This suggests that neurons might retain sRAGE to release as a decoy upon encountering stimuli such as AGEs or Aβ. This highlights the importance of RAGE activation and the potential therapeutic role of sRAGE in suppressing its activation (213, 214).

Dominant negative RAGE is almost identical to full-length RAGE but lacks the short intracellular domain. Dominant negative RAGE is the least understood of all the RAGE isoforms. It still has the ability to bind RAGE ligands but does not activate signalling pathways due to the missing intracellular domain. This suggests a binding competition between itself and full-length RAGE (215, 216).

The N-truncated form of RAGE, as shown in **Figure 1-6**, lacks the N-terminal signal sequence and the first V-type domain. This isoform of RAGE is incapable of binding most RAGE ligands, such as AGEs, due to the lack of the V-domain. The expression of this isoform has been reported to be similar to that of full-length RAGE but its function remains unclear (217). It has been suggested that N-truncated RAGE is involved in angiogenic regulation that is independent of the full-length RAGE signalling pathway (218). This isoform lacks the binding site for the antibody used in previous experiments carried out by Swansea University and therefore is not expected to compete or influence ADC binding in any way.

1.7.4 Polymorphisms of RAGE

Polymorphisms have been described in the *AGER* and have been linked to various diseases and pathologies (219). A single nucleotide polymorphism (SNP) is one of the most common polymorphisms and usually results in a slightly altered protein. This is in comparison to some larger mutations which cause frame shifts and the protein is not transcribed or cannot function at all (220). The polymorphisms described by Gonzalez *et al* (219) have been reported within introns, exons and gene regulatory regions. These mutations can affect not only if the protein is transcribed but also the binding affinity of, in this case, RAGE to its ligands (203, 221). Summarised by Gonzalez *et al* (219) the most commonly studied RAGE polymorphisms and their disease risk association is described in **Table 1-2**.

Table 1-2 – Table of common AGER polymorphisms and their associated pathologies

AGER polymorphism	Associated pathology
-374T/A	Nephropathy, retinopathy, proteinuria, cardiovascular disease in diabetic patients. Coronary artery disease, ischemic heart disease, prevalence of restenosis coronary after stent implantation. Multiple sclerosis. Chronic fatigue syndrome.
63 base pair deletion (-407 to -345)	Diabetic neuropathy
2184A/G	Diabetic neuropathy. Higher mortality rate from vascular diseases in haemodialysis patients. Microvascular dermatoses and risk for plaque psoriasis.
1704G/T	Influence on the development of chronic periodontitis. Microvascular dermatoses.
G82S	Amplified inflammatory response. Microvascular dermatoses, skin microangiopathy, diabetic retinopathy, advanced neuropathy and psoriasis vulgaris in diabetic patients. Increased risk of gastric cancer. Increased risk of Alzheimer's Disease. Coronary artery disease.
-429T/C	Retinopathy in type 2 diabetes. Mortality rate in haemodialysis patients. Risk of ischemic heart disease.
-1152C/A	Duration of diabetes before onset of nephropathy.
-388T/A	Non-small cell lung cancer development.

Zhang *et al* (222) identified *AGER* polymorphisms and the associated risks of developing epithelial OC. The study involved 190 patients over the age of 40 who had been diagnosed with epithelial OC, and 210 healthy control subjects. Four SNPs polymorphisms were determined in the patients, 82G/S, -374T/A, -429C/T and 1704G/T. It was found that the frequency of the 82G/S polymorphism was associated significantly with epithelial OC, whereas the other three polymorphisms were not significantly associated. This suggests that the 82G/S polymorphism could be used to diagnose or identify a risk of epithelial OC and stratify patients for earlier treatment. However, there is no literature to suggest the 82G/S polymorphism is associated with OC stage.

It was reported that some alleles in the central major histocompatibility complex (MHC) region class 3, can modify the risk of cancer development. An SNP (-429T/C) in the RAGE gene, known to be in the MHC region, was identified in 183 patients with colorectal cancer and at first no significant association was observed. However, when three or four locus haplotypes consisting of known constituents in the 8.1 ancestral haplotype were considered, marked differences were observed. The frequency of the RAGE polymorphism was significantly increased among cancer patients when compared to non-cancer patients. These findings were consistent with similar results seen in OC, which indicate that carriers of the 8.1 ancestral haplotype have an increased risk for some cancers (223).

1.7.5 Post translational modifications

Heizmann *et al* summarise the main posttranslational modifications of RAGE (224) as phosphorylation, disulphide bonds, proteolysis of full length RAGE and glycosylation. RAGE is glycosylated in two places, in the V-type domain region at amino acid position 25 and 81. It has been reported that RAGE, carbonylated glycans and S100A8/A9 play essential roles in tumour-stromal interactions, leading to inflammation-associated carcinogenesis as a result of a significant impact of RAGE ligand binding and signalling from glycosylation (225). Wei *et al* (226) report that RAGE forms dimer-based oligomers as a result of disulphide bonds from cystines 259 and 301 within the C2 domain. This dimerization takes place in the endoplasmic reticulum and RAGE proteins that are not able to dimerise, due to mutations, are unstable and subjected to endoplasmic reticulum degradation. This suggests that the disulphide bond mediated dimerization of RAGE is a critical step for RAGE biogenesis and without this, RAGE does not reach the cell surface.

1.7.6 Proteolysis of RAGE

Various gene splice isoforms of RAGE have been detected and classified by analysing *AGER* cDNA from human tissue and cells. This identification suggested some differences in the way that soluble RAGE may be formed (227). **Figure 1-6** shows sRAGE by proteolytic cleavage as one of the known isoforms of full-length RAGE. In addition, some receptor proteins that present a similar topology as RAGE such as Notch, APP, Receptor protein-tyrosine kinase (ErbB-4) or Leucine-responsive regulatory protein (LRP), undergo regulated intramembrane proteolysis (RIP) which is catalysed by metalloproteinases such as A disintegrin and metalloproteinase with thrombospondin motifs (ADAMs) and the γ-secretase (228). Galichet *et al* report that RAGE is also a substrate of RIP leading to the production of sRAGE into the extracellular space and

cytoplasm (229). It is also shown that calcium is an essential regulator of this RAGE processing, and the production of RAGE intracellular domains promotes apoptosis.

This type of ectodomain shedding, mediated by various metalloproteinases, is an essential and normal physiological function but can sometimes be aberrantly regulated in various diseases where altered expression of metalloproteinases are found. It is suggested that RAGE is cleaved specifically by ADAM10 to produce sRAGE (230) and can be induced with phorbol 12-myristate 13-acetate (PMA) and calcium ionophores in a PKCα/β1-dependant manor. Since ADAM10 is part of the degradome and is involved in the breakdown of the extracellular matrix to enable cell migration (231). However, RAGE has not been shown to play a role in cell motility and extracellular matrix remodelling. It is reported that RAGE ectodomain shedding is an integral function and could be a target for designing novel therapies for use in RAGE associated diseases such as diabetes and Alzheimer's Disease (232).

1.7.7 RAGE activity and cellular signalling

A large variety of signalling pathways are activated when RAGE undergoes ligand binding. MAPK and PI3K/AKT or NADPH oxidase, RAC-1, CDC42 are activated which results in the activation of transcription factors such as STAT-3, AP-1, Sp-1 and NF-κB to stimulate the production of genes involved in inflammation, cell proliferation and migration (233-235). When NF-κB is activated by RAGE dependent signalling, this, in turn, increases RAGE expression as part of a positive feedback loop. This creates an increasingly pro-inflammatory environment (236). **Figure 1-7** shows a schematic of the signalling pathways controlled by RAGE activation by its various ligands. These signalling pathways lead to the increased expression of RAGE by Glo-1/AGEs, apoptosis by p53/Bax, cell proliferation by reactive oxygen species/Src/JAK/STAT3/Pim1 and inflammation by various pathways such as Cdc42/Rac-1-MKK6-p38 and PKCβII-JNK-Egr-1 (237).

Figure 1-7 – Cellular signalling pathways controlled by RAGE activation

The schematic above (taken from Xie J, Méndez JD, Méndez-Valenzuela V, Aguilar-Hernández MM. Cellular signalling of the receptor for advanced glycation end products (RAGE). Cell Signal. 2013 (237)) shows examples of the most common cellular signalling pathways as a result of RAGE activation. The schematic is not exhaustive as there are a very large number of signalling cascades affected by RAGE activation. Common signalling pathways shown include the RAGE positive feedback loop mediated by NF-κB, Glo-1 and AGEs, inflammation mediated by several pathways such as by Src, cdc42, MKK6 and p38MAPK and autophagy by CaMKKβ and AMPK.

The pathways shown in **Figure 1-7** can all have implications in cancer if a normal function is inhibited. If cells fail to go through apoptosis then mutations can be replicated and a necrotic environment can be produced as a result of unexpected cell death. Tumour cells are often characterised by their aberrantly fast proliferation and inflammation is a known hallmark of cancer. These consequences indicate RAGE is the common denominator in cancer associated signalling pathways and it worthy of a full investigation.

1.7.8 RAGE ligands

The identification of RAGE ligands is essential for elucidating the biological repercussions of RAGE/ligand binding and potential diagnostics and therapies for various RAGE associated pathologies. RAGE is known to be a multiligand pattern recognition receptor however it is currently unclear why RAGE has so many associated ligands (238).

1.7.8.1 Advanced Glycation End products (AGEs)

Advanced Glycation End products (AGEs) were the first RAGE ligands to be described (239). AGEs are a heterogenous group of molecules that are produced as a result of condensation and oxidative processes between sugars and proteins or peptides (240). The stages of AGE formation from a non-enzymatic process can be seen in **Figure 1-8**. In the first step towards AGE production, sugars react *via* their aldehyde functional group with an amine or guanidine group from lysine or arginine residues on proteins or peptides. This process of glycation is non-specific and non-enzymatic and affects many proteins in a healthy individual. However, increased levels of protein glycation are reported in diabetic patients and in aging individuals (241). This glycation produces a Schiff base in a reversible manner. Once formed, the Schiff base rearranges into a more stable Amadori product, which occurs as cyclic forms in equilibrium for more stability. Glucose-derived Amadori products react with themselves or with primary amines, such as a lysine, to form AGEs (242). This transformation increases the overall negative surface charge of a protein by carboxymethylation of the amino and guanidine groups of lysine and arginine residues. Due to this negative surface charge, AGEs go onto bind any RAGE isoform with a V domain with a high affinity, triggering the initiation of a pro-inflammatory signalling cascade (243). Nε-carboxymethyllysine (CML) and pentosidine, and glucosepane and crossline are common AGEs formed through the oxidative and non-oxidative pathways respectively. CML and Nε-carboxyethyllysine (CEL) are the most abundant AGEs and are well documented ligands to the V-type domain of RAGE (244).
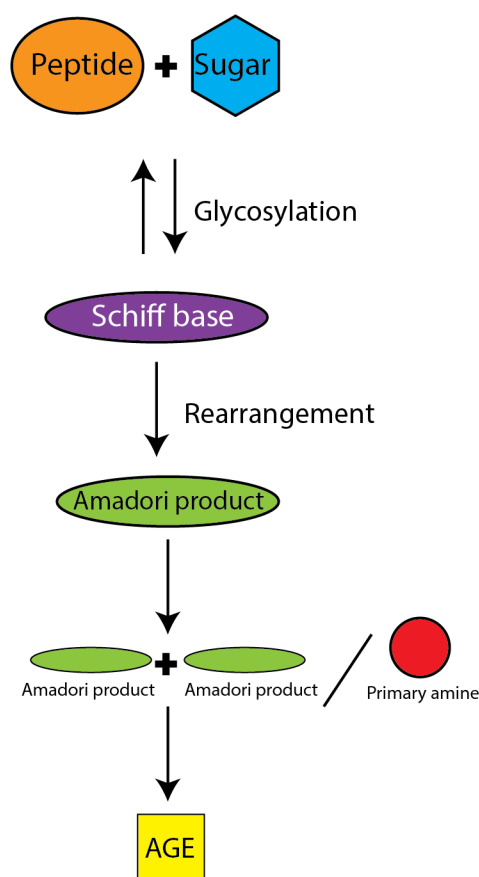
Figure 1-8 – Production of AGEs from non-enzymatic glycation of proteins

AGEs are produced in a non-enzymatic glycosylation of peptides or proteins by a sugar in a reversible reaction to produce a Schiff base. The Schiff base rearranges to form a more stable cyclic Amadori product which goes on to react with itself or other primary amines to produce AGEs. Image inspired by Cepas et al (245).

1.7.8.2 S100 proteins

The S100 family of proteins in humans consists of more than 25 members which vary in expression pattern, binding properties and oligomeric states. S100 proteins are small acidic proteins that are made up of two different calcium-binding EF hands connected by a flexible loop. The majority of S100 proteins form homodimers but many have the ability to form heterodimers and higher order oligomers (246-248). The S100 family of proteins is known to be diverse with a wide variety of functions, expression patterns and distribution in the cell. Looking at sequence homology, several sub-groups of S100 proteins have been identified. These sub-groups differ in the cellular processes they are involved in and therefore their function. S100 proteins are generally localised to the cytoplasm where they function as calcium sensors (249). Other family members (S100A7, S100A12, S100A8/A9, and S100B) display cytokine-like properties in the extracellular space (250). Additionally, some S100 proteins can perform both of these properties by functioning first as an intracellular calcium sensor and then, after

secretion, go on to perform cytokine-like functions. A conformational change in S100 proteins occurs as a result of calcium binding, which changes the distribution of surface charge and the accessibility of the hydrophobic residues. The extracellular space is high in calcium concentration therefore S100 proteins are permanently loaded with calcium. This calcium binding is essential for the interaction between S100 proteins and RAGE. Specifically, the oligomeric assemblies of the S100 proteins are considered crucial for their cytokine functions (251). Specific S100 proteins that are known to interact with RAGE include S100B, S100P, S100A1, S100A2, S100A4, S100A5, S100A6, S100A7, S100A8/A9, S100A12 and S100A13. Each of these S100 family members have different binding affinities for RAGE and can range widely from a dissociation constant in the nanomolar range to the micromolar range. S100B can interact with RAGE to promote a concentration-dependent neuronal survival and axon growth (252). S100A7, S100A8/A9 and S100A12 act in the well documented pro-inflammatory pathways from their interaction with RAGE. S100A2 and S100A4 have been associated with cell growth and differentiation with another subgroup consisting of S100A5, S100A6 and S100P promoting tumour growth (243, 252).

Almost all S100 proteins are RAGE ligands with the exception of S100G, S100Z, S100A16, S100A14, S100A10, S100A5, S100A3 and S100A2 (206). It is the V-type domain of the RAGE protein which recognises all the binding S100 proteins with the exception of S100A12 and S100A6 which bind in the C1 and C2-type domains respectively (253).

S100 is used as a biomarker for melanoma, however, also labels T-cells and dendritic cells (254) and RAGE signalling is also deregulated in melanoma (255). There is no literature to suggest s100 protein expression correlates to RAGE activity however S100 proteins are upregulated in tumours and contribute to tumour progression (256).

1.7.8.3 High Mobility Group Box 1 (HMGB1)

The High Mobility Group Box 1 (HMGB1) protein was initially reported as a nuclear DNA-binding protein (257). More recently, HMGB1 protein has been shown to exhibit an extracellular regulatory function to act as a pro-inflammatory activator (258). HMGB1 is comprised of three main domains; Two N-terminal domains involved in DNA binding, and a C-terminal region that is made up of acidic amino acid residues that directly bind RAGE. Furthermore, DNA-bound HMGB1 is reported to bind with RAGE and Toll-like receptor 9 (TLR9), which forms a HMGB1-RAGE-TLR9 complex that activates autoreactive B-cells (259, 260).

HMGB1 is also known as amphoterin and is reported to be located within the cytoplasm, but can be released into the extracellular space by the stimulation of cytokines or by post-translational modification when cell damage is detected (224). The binding of RAGE to HMGB1

in the V-type domain has been reported to promote the activation of NF-κB which establishes a positive feedback loop for the expression of RAGE on the surface which upregulates signalling pathways in migration, maturation, invasion, inflammation, angiogenesis and proliferation. These consequences can be linked to various pathologies such as cancer, diabetes and neurodegenerative diseases (261).

1.7.8.4 Amyloid β (Aβ)

A well-documented hallmark of Alzheimer's Disease is the extracellular accumulation of insoluble aggregates of the Aβ peptide. The Aβ peptide is produced when the amyloid precursor protein is cleaved. There are two Aβ peptides described, one with 40 amino acids and the other with 42 amino acids. Both forms consist of mainly acidic and hydrophobic residues and are prone to aggregation as amyloid fibrils. Amyloid fibrils build up to produce the amyloid plaques seen in the brains of Alzheimer's Disease patients (262).

RAGE binds Aβ to mediate cellular perturbation with implications to Alzheimer's Disease. RAGE interacts with Aβ in neurons, microglia and vascular cells to accelerate and amplify negative effects on neuronal and synaptic function. RAGE dependent signalling is reported to be involved in Aβ-mediated amyloid pathology and cognitive dysfunction observed in an Alzheimer's disease mouse model. The blockage of RAGE is reported to significantly constrict neuronal and synaptic injury (263). Aβ aggregates are recognised by the V-type domain of RAGE and interact to induce inflammation, oxidative stress and the transport of Aβ across the blood brain barrier, to allow the accumulation of Aβ aggregates leading to amyloid fibrils and amyloid plaques in the brain for the progression of Alzheimer's Disease (264).

1.7.9 RAGE in human health and disease

The following sections discuss RAGE in homeostasis, Alzheimer's Disease, cardiovascular disease, diabetes. Inflammation and cancer.

1.7.9.1 RAGE and homeostasis

As mentioned above, RAGE is expressed at a low basal level in the majority of healthy adult tissues. Due to this widespread, conserved expression it is suspected that RAGE has a physiological function to maintain homeostasis. It is suggested that RAGE plays a role in tissue repair and remodelling due to its involvement in inflammation. The higher expression of RAGE in the lung suggests that it may have a beneficial role in maintaining homeostasis in the lung or protecting the lungs from fibrosis following injury (265-267). RAGE is also implicated in

homeostasis in the central nervous system due to its affinity to HMGB1 protein. This is demonstrated where higher levels of RAGE are present in the central nervous system during embryogenesis. Additionally, RAGE has been reported as vital for the plasticity and regeneration of the peripheral nervous system (265, 268, 269).

1.7.9.2 RAGE and Alzheimer's Disease

Alzheimer's is the most common cause of dementia world-wide. Its prevalence continues to grow as the population as a whole has a longer life span. Alzheimer's Disease is a neurodegenerative disease that is characterised by the deposition of β-amyloid plaques and the neurofibrillary tangles of hyperphosphorylated tau. The diagnosis is based on clinical presentation and fluid and imaging biomarkers. Currently treatment is limited to symptomatic therapy, although many trials are in progress for the treatment of Alzheimer's disease (270). There are a vast number of publications associating RAGE to Alzheimer's disease. As discussed above in section 1.7.8.4, RAGE has the ability to bind to Aβ which can alter cell behaviour and its toxicity. It has been reported that increased expression of full-length RAGE contributes to the rise in Aβ, and therefore amyloid plaques, seen in the brains of Alzheimer's disease patients. This suggests that while Alzheimer's disease remains complex and RAGE signalling is not the only contributing factor, RAGE does play a key role in the development and progression of Alzheimer's disease (271, 272).

1.7.9.3 RAGE and cardiovascular disease

Cardiovascular disease (CVD) is known as a leading cause of death globally. The top two leading causes of CVD death include ischemic heart disease and stroke. It is predicted that by 2030 22.2 million people will die annually from CVDs (273). RAGE has been reported to be expressed in the heart and has been thought to reduce heart function. Activation of RAGE is known to stimulate inflammation and oxidative stress and the circulating levels of AGEs are increased. This increase in AGEs accelerate atherosclerosis which has been suggested to cause cardiovascular problems (274).

1.7.9.4 RAGE and diabetes

Diabetes Mellitus is a group of metabolic diseases that are categorized by hyperglycaemia as a result of defects in insulin secretion and/or insulin action. The chronic hyperglycaemia in diabetes is associated with long-term damage leading to dysfunction and failure of many organs including the eyes, kidneys, nerves, heart and blood vessels. Long term complications of diabetes include retinopathy with a potential for the loss of vision; neuropathy leading to renal

failure; peripheral neuropathy with a risk for foot ulcers, amputations, and Charcot joints; and autonomic neuropathy causing gastrointestinal, genitourinary and cardiovascular symptoms and sexual dysfunction. Diabetes can be further subcategorised into type 1, type 2, gestational and other specific types. Type 1 diabetes accounts for 5-10% of those with diabetes and is also known as juvenile-onset diabetes as a result of cellular-mediated autoimmune destruction of the β-cells of the pancreas. Type 2 diabetes accounts for 90-95% of all cases of diabetes and is also known as non-insulin dependent diabetes or adult-onset diabetes. This type encompasses adults who have acquired an insulin resistance and is often associated with diet and obesity. Gestational diabetes was for a long time defined as any degree of glucose intolerance with onset or first recognition during pregnancy. Most cases are resolved upon delivery. After deliberation it is now recommended that high-risk women who have diabetes at their initial prenatal visit receive a diagnosis of overt, not gestational, diabetes. Other specific types of diabetes include those with genetic defects causing β- cell dysfunction or insulin action, diseases of the exocrine pancreas, endocrinopathies, drug or chemical induced diabetes, diabetes as a result of infections, uncommon forms of immune-mediated diabetes and other genetic syndromes associated with diabetes such as Down syndrome or Turner syndrome (275).

AGEs are reported to be involved in a number of complications as a result of diabetes. AGEs can facilitate the loss of pericytes, which is a histological characteristic of diabetic neuropathy. AGEs also bind RAGE on the surface of pericytes and endothelial cells to act on micro vessels. AGEs are well known to contribute to the development and progression of atherosclerosis and atherosclerotic plaques which results in CVDs such as a heart attack or stroke being the primary cause of morbidity and mortality in diabetic patients. RAGE has been shown to be over expressed in these plaques and diabetic patients in general (276).

1.7.9.5 RAGE, inflammation and cancer

RAGE has been linked to the development and progression of various cancers by promoting inflammation in the tumour microenvironment (219). RAGE has been reported to be over-expressed in a large number of cancers including gastric, pancreatic, melanoma, colorectal, prostrate and breast (277). As described previously, RAGE is also expressed on the surface of many cell types involved in the development and progression of tumours. These cells are found within the tumour microenvironment and include malignant cells, leukocytes, fibroblasts, endothelial cells, myeloid cells, myeloid-derived suppressor cells and lymphocytes (278). RAGE activates several pro-inflammatory mediators through binding with a variety of RAGE ligands. NF-κB, cytokines and MAPKs are all upregulated as a result of RAGE activation and contribute to the development and progression of cancer by maintaining a pro-inflammatory environment.

Pro-inflammatory cytokines such as TNFα, IL-1 and IL-6 are released and RAGE ligands and RAGE itself activate endothelial and myeloid cells to recruit more myeloid cells to the tumour microenvironment. This has been reported to inhibit T and NK cells which results in a weakened antitumour immunity due to a T-cell tolerance. In addition, the proliferation and survival of cancer cells *via* autocrine and paracrine feedback loops are engaged by RAGE binding to its ligands.

RAGE is most extensively documented to activate NF-Kβ transcription factor which is known to have implications in inflammation and the regulation of RAGE expression (279). Angiogenesis markers such as VEGF and MMP-2 have been reported to be upregulated with RAGE activation. This can aid the development and progression of tumours by increasing capillary formation and blood supply leading to a more established tumour with increased survival. RAGE activation has been repeatedly reported to support tumour growth, survival and invasiveness (276, 280).

In a healthy individual, RAGE is found to be expressed on cells of the endothelium, smooth muscle cells, neural cells, mononuclear cells and cardiac myocytes (239). RAGE is expressed on these cells at a low basal level but becomes more highly expressed during embryonic development (281). RAGE is expressed at a constant rate in alveolar type 1 epithelial cells in the lung. This expression is more constant when compared to the low basal expression of RAGE on other cells such as smooth muscle or neural cells (282). RAGE has also been shown to be expressed in the pulmonary endothelium, bronchial and vascular smooth muscle, alveolar macrophages, leiomyocytes and the visceral pleural surface in the lung (281). It was further reported that RAGE was expressed in bronchiolar epithelia, alveolar type 2 cells and macrophages (283).

In lung cancer RAGE expression has shown to be reduced suggesting it may play a tumour suppressive role in the in the lung (284). Loss of RAGE or reduced expression has been theorised to contribute to the loss of cell polarisation and differentiation (285) which therefore leads to an impaired functioning of lung epithelium by disrupting cell homeostasis and increasing the migratory and invasive behaviour and oncogenic transformation (286, 287). In the lung, RAGE has been reported to contribute to the redox regulation in alveolar epithelial cells and RAGE knockdown significantly reduces the key regulators of redox signalling. Redox regulation is key for cellular signalling and a disruption in this process can lead to oxidative stress and the production of reactive oxygen species. Reactive oxygen species in the lung are thought to contribute to lung pathologies such as lung cancer. Reactive oxygen species can also affect the responsiveness to therapeutic intervention (288-291). In contrast Mei-Chih Chen indicate that RAGE plays an oncogenic role in the lung (292). RAGE is reported to be expressed in normal lung

and appears to be down regulated in human lung cancer and the down regulation of RAGE has thought the be positively correlated with lung tumour growth and invasiveness (293). However, it has been reported that abundant expression of RAGE and its ligand S100A6 in lung tumour tissue which suggests a positive role of RAGE-mediated signals in lung cancer development (294). Additionally, Taguchi at al. indicate that RAGE-amphoterin signalling blockade decreases the growth and metastasis of lung tumours (295). Therefore, the role of RAGE in lung cancer progression is still unclear and further insights into the effects and mechanisms being the expression of RAGE in lung cancer is required (292).

1.7.9.6 RAGE in ovarian cancer

RAGE has been investigated in OC in a number of publications; however, this specific area of RAGE involvement remains understudied. RAGE has been shown to be overexpressed in OC in a study by Rahimi *et al* (296). *AGER* gene expression levels were analysed by real time quantitative PCR and immunohistochemistry techniques. A significantly higher expression of *AGER* was observed in OC patients when compared to non-cancerous tissues. There was also a significant association between RAGE protein and tumour size, depth of stromal invasion, lymphovascular invasion and stage of cancer. This suggested that RAGE overexpression could be a useful biomarker to predict tumour development and progression.

The RAGE ligand S100B has been reported to mediate the stemness of OC stem-like cells by inhibiting p53. S100B has been involved in the progression of many cancers. OC is known to be driven by cancer-like stem cells involved in tumorigenesis, metastasis, chemo-resistance and relapse. S100B upregulation is associated with more advanced tumours and is correlated with increased expression of stem cell markers such as CD133, Nangog and Oct4. S100B was reported to be preferentially expressed on CD133 positive ovarian cancer stem-like cells derived from OC cell lines and from primary tumours of patients. In addition, knockdown of S100B supressed the *in vitro* self-renewal and *in vivo* tumorgenicity of OC stem-like cells and their expression of stem cell markers was reduced. Ectopic expression of S100B gave non-cancer stem-like cells stemness in both *in vitro* and *in vivo* experiments. It was reported that this mechanism was not dependent on the binding of S100B to RAGE but rather through the intracellular regulation through the inhibition of p53 expression and phosphorylation (297).

RAGE has further been reported to potentially regulate the final destiny of the ovarian cell populations prior to and during folliculogenesis, possibly controlling the metastatic potential of OC. RAGE and IGF-1 protein expression pattern were analysed by immunohistochemistry in a variety of foetal, adult and OC ovaries. OC cells were strongly positive for RAGE and IGF-1 (298). In a study investigating embryo quality in assisted reproduction, high intrafollicular

concentrations of sRAGE were shown to be associated with poor embryo development following ovarian stimulation of intracytoplasmic sperm injection (299). A study by Rai *et al* (300) identified novel roles of RAGE as a conduit for lysophosphatidic acid signalling and suggested that targeting the interaction between lysophosphatidic acid and RAGE could provide a therapeutic strategy for targeting oncogenic pathways in OC. Polymorphisms in AGER are discussed in more detail in section 1.7.4.

The Human Protein Pathology Atlas (301) reports RAGE (AGER) expression in 12 patients, as can be seen in Table 1-3, and the tissue based map of the human proteome (302) shows RAGE expression in healthy human ovary localised to the plasma membrane with some cytoplasm localisation. From this, 50% (6/12) of the patients present with a serous subtype (the most commonly occurring subtype of epithelial OC) (303). All three of the subtypes in Table 1-3 show expression of RAGE with some differences between patients. Only one out of the twelve patients with OC do not show any staining. The average age of the patients being 60 years old is also consistent with the literature where most OC patients are diagnosed late in life (304). The data in the table below suggest RAGE could be a target of interest to explore in terms of diagnosis and treatment of OC. Cell type was not specified however cellular location where expression was seen it was localised to the cytoplasm and plasma membrane. Follow up work is needed to confirm this using larger data sets (including clinicopathological feature correlations).

Table 1-3 – The Human Protein Atlas Immunohistochemistry scoring of RAGE in 12 OC patients

Pathology	Age	Stain	Intensity of stain	Location	Percentage quantity of stain
Serous	59	None	None	None	None
Serous	79	Low	Weak	Cytoplasm/ membrane	<25%
Serous	44	Low	Weak	Cytoplasm/ membrane	25-75%
Serous	57	Medium	Moderate	Cytoplasm/ membrane	25-75%
Serous	56	Low	Weak	Cytoplasm/ membrane	>75%
Mucinous	37	Medium	Moderate	Cytoplasm/ membrane	>75%
Mucinous	80	Low	Weak	Cytoplasm/ membrane	>75%
Endometrioid	62	Medium	Strong	Cytoplasm/ membrane	>75%
Endometrioid	51	Medium	Moderate	Cytoplasm/ membrane	>75%
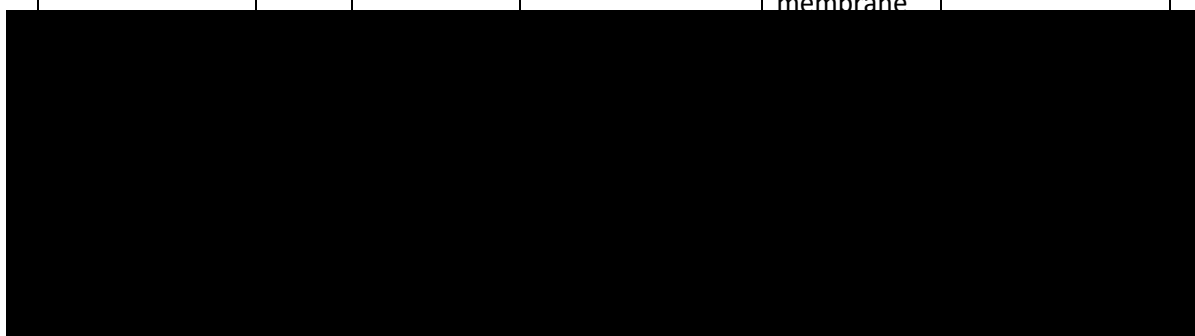
The table above shows the immunohistochemistry scoring of 12 patients in The Human Protein Atlas database. The Information is available from www.proteinatlas.org/ENSG00000204305-AGER/pathology/tissue/ovarian+cancer#ihc (2019) (301).

The metalloproteinase ADAM10 can cleave full length RAGE to produce sRAGE (305). At present no link between sRAGE and metastatic disease has been reported, however full-length RAGE has been reported to have oncogenic and tumorigenic roles (292) and been linked to a poor prognosis in some cancers including gastric cancer (306). This association could be important when considering the utility of RAGE ADCs for a particular stage of disease progression, such as

primary or metastatic. If sRAGE or full-length RAGE expression is altered in cancer, then the utility of the RAGE ADC could be affected.

1.7.10 RAGE as a biomarker for disease

The information on RAGE, detailed in the above sections, result in the RAGE protein being worthy of investigation in gynaecological malignancies. RAGE has already been extensively researched by team members at Swansea University Medical School, however its use as a biomarker has not yet been reported. Full-length RAGE has been associated with many cancer types, including OC (296). Therefore, there is rationale for the investigation of sRAGE in OC and non-cancer patients with implications for diagnosis, monitoring prognosis, monitoring patient treatment and patient stratification.

Multiple studies have used ELISA to evaluate the use of sRAGE as a cancer biomarker including the assessment of sRAGE in colorectal cancer (307-309), haematological malignancies (310), lung cancer (311, 312), melanoma (313), pancreatic cancer (314-316) and breast cancer (317). Pre-diagnostic sRAGE concentrations were reported to be inversely correlated with colorectal cancer risk in men but not women (307), while sRAGE was additionally reported to be inversely correlated with BMI, suggesting an association to obesity-related colorectal cancer (308). Higher pre-diagnostic levels of sRAGE were additionally reported to be inversely associated with a lower risk of colorectal cancer in male smokers (309). An ELISA using 73 bone marrow samples from various haematologic cancer patients reported that no significant difference was observed between the haematologic malignancy and control groups (310). sRAGE levels were observed to be significantly decreased in the plasma of lung cancer patients (311, 312), suggesting its use as a diagnostic biomarker in lung cancer. In malignant melanoma diminished levels of sRAGE have been reported to increase the chances of a poor survival rate suggesting the use of sRAGE as biomarker in melanoma (313). In pancreatic cancer, sRAGE levels have been reported to show prognostic relevance in pancreatic cancer patients undergoing chemotherapy (314, 315) and have been shown to be decreased in the serum of patients with pancreatic cancer when compared to patients with diabetes and those with no described pathology (316). Finally, in breast cancer a significantly higher abundance of sRAGE was detected prior to radiation therapy but after radiation the abundance did not significantly change.

1.8 Antibody-Drug Conjugates

Antibody-Drug Conjugates (ADCs) (**Figure 1-9**) are a specifically designed therapeutic molecule for the treatment of various cancers. ADCs combine the specificity of a tumour targeting monoclonal antibody and the cytotoxic activity of a potent small molecule drug. The antibody

acts as a targeting agent to deliver its toxic payload directly into the tumour cells. This specificity aims to reduce any off-target toxicity acting on non-malignant cells (318).
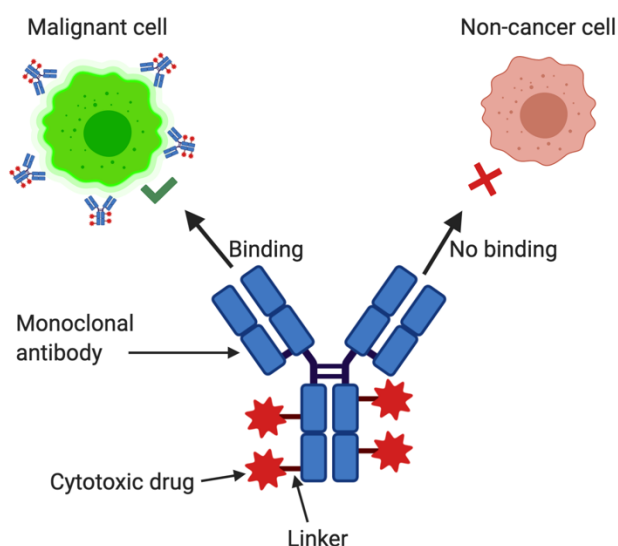
Figure 1-9 – Schematic of an Antibody-Drug Conjugate (ADC) (318)

An Antibody-Drug Conjugate is a therapeutic molecule made up of a monoclonal antibody (shown in blue) and a potent, cytotoxic small molecule drug (red star). The cytotoxic drug is joined to the monoclonal antibody by a short linker. ADCs are designed to use the monoclonal antibody to specifically target the malignant tumour cells and leave the non-cancer cells unaffected.

Current treatment methods for cancer that are non-specific for cancer cells can have unpleasant side effects with a less efficacious therapeutic effect, owing to off target toxicity (319). For this reason, more specific, potent alternative therapies are currently being investigated. For ADCs to have the maximum therapeutic effect they need to bind to their target cell, internalise into the cell and finally, release its toxic payload into the malignant cell. ADCs can therefore overcome some of the issues associated with other nanomedicines based on synthetic nanomaterials such as cellular internalisation, clearance, sterically hindering of binding to the epitopes and failing to release into targeted cells (320). ADCs were first reported in experimental analysis in the mid 1960's (321) and have, in recent years, become a successful cancer therapy with the introduction of several ADCs to the market, approved for their use in cancer patients.

1.8.1 ADC mechanism of action

Treatment with an ADC results in the death of the malignant cell it binds to. This mechanism of action (**Figure 1-10**) begins with the monoclonal antibody portion of the ADC binging specifically to its cancer marker protein on the surface of a malignant cell. Upon binding the ADC-antigen complex is internalised into the cell where it is degraded by lysosomal activity and the cytotoxin

(such as auristatins or doxorubicin) is released to either disrupt microtubule formation thereby preventing cell division, or by causing DNA strand breakage which in both cases leads to cell death (apoptosis) (322).
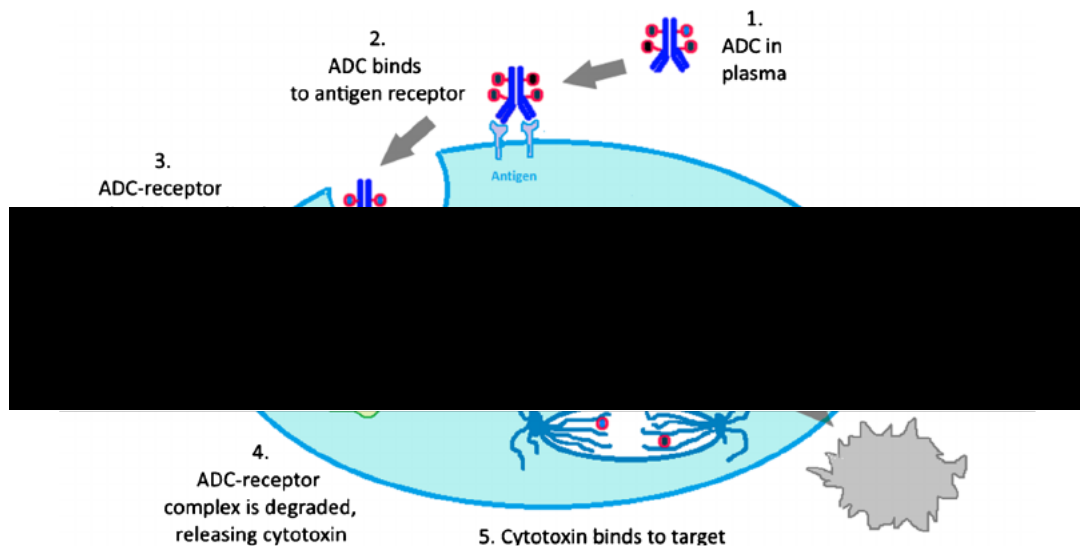
Figure 1-10 – Mechanism of action of ADCs

(1) The ADC is circulated systemically in the plasma. (2) The ADC binds to its cancer specific marker. (3) The ADC-antigen complex is internalised by receptor mediated endocytosis. (4) The ADC-antigen complex is degraded by the lysosomes which releases the cytotoxin. (5) The cytotoxin binds to its target leading to microtubule disruption or DNA strand breakage. (6) Apoptosis of the malignant cell. Image taken from Jain et al 2015 (322).

1.8.2 Tumour markers in ADC development

The tumour marker protein selected to stratify malignant cells from non-cancer cells is arguably the most critical part of the ADC. Without it, the ADC would have no specificity and the drug would behave in the same manner as systemic chemotherapy with no specific internalisation. A tumour marker must have a high relative level of expression when compared to non-cancer cells, it must not shed into circulation and it must internalise into the cell. Tumour markers must also be membrane bound with an extracellular domain for the purpose of antibody binding. It could be valuable for tumour markers to be genetically well conserved across the population to allow for maximum therapeutic effect in a wide variety of individuals (318).

1.8.3 Monoclonal antibodies

The structure of a monoclonal antibody can be seen in **Figure 1-11** (323). The Fc (Fragment crystallizable) region is at the base of the antibody and consists of two heavy chains. The function of the Fc region is to bind to specific proteins to ensure each antibody generates an appropriate immune response for any given antigen. The Fc region also binds to various cell Fc receptors and

other immune molecules to mediate different physiological effects such as cell lysis and degranulation of mast cells, basophils and eosinophils (324).

The Fab region (Fragment antigen binding) is comprised of one constant and one variable domain from each heavy and light chain of the antibody. The antigen binding site (paratope) is shaped at the amino terminal at the top end of the antibody by the variable domains from each light and heavy chain. The variable region of the antibody (Fv region) consists of three variable loops, three on each of the variable light and variable heavy and is responsible for the specific binding properties of the antibodies to a specific antigen. These loops are referred to as the complementarity determining regions (CDRs) (325). In ADC development, once an appropriate tumour marker has been chosen, it is the synthesis of this region of the antibody that is paramount for optimal specific binding to malignant cells.

The heavy chain is sub-categorised into mammalian Ig $\alpha/\delta/\varepsilon/\gamma/\mu$. The type of heavy chain determines the class of the antibody and these chains are found in IgA, IgD, IgE, IgG and IgM antibodies. Each heavy chain has two regions, as can be seen in **Figure 1-11**. The lower region is the constant domain (Fc) and the upper region (Fab) is the variable region. The constant region is part of the Fc region and is the same in all antibodies of the same isotype. Heavy chains λ, α and δ have three Ig domains in their constant region with a hinge region for flexibility. Heavy chains μ and ε have four Ig domains in their constant region (326). It is the variable region of the heavy chain that is responsible for specific antigen binding due to the antibody being produced by unique B-cells. The variable region of each heavy chain is around 110 amino acids long and is composed of a single Ig domain (327).
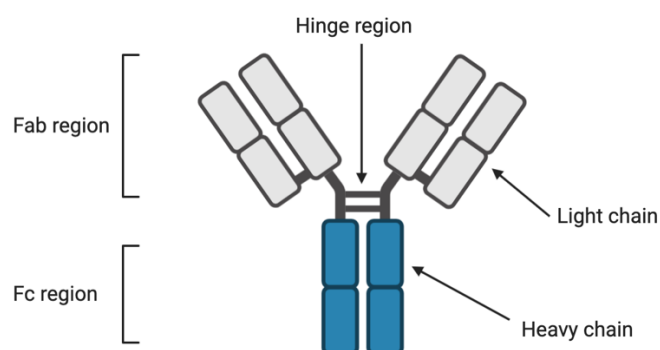
Figure 1-11 – Structure of a monoclonal antibody (327)

The schematic above shows the regions of an antibody. The antibody can be split into two main regions, the Fragment Antigen Binding (Fab) and the Fragment Crystallizable (Fc). These regions are comprised of a heavy and a light chain held together by a hinge region.

The light chain can be sub-categorized into lambda (λ) and kappa (κ) light chains. The light chain is the shorter chain found in the Fab region of the antibody. The light chain consists of one constant and one variable Ig domain with a total length of approximately 211-217 amino acids. The two light chains in an antibody are always identical within that one antibody and are either λ or κ. The variable domain of the light chain contributes to its unique binding specificity that is crucial for ADC development (325).

Monoclonal antibodies have been used in therapeutics for their anti-tumour activity and Fc-mediated immunological reaction blocks the tumour cell signalling by targeting a certain antigen on the tumour cell surface. Antibody-dependent cellular cytotoxicity (ADCC) occurs when antibodies bind to tumour cells and the Fc region binds Fc receptors on the surface of immune effector cells. This engagement stimulates the recruitment of adaptor proteins and the activation of immune effector cells. It is presumed that the cells recruited for this purpose are Natural Killer (NK), macrophages, and neutrophil cells. The antigen specified by the monoclonal antibody is exclusively present on tumour cells and, unlike ADCs which have a cytotoxic agent attached, recruit NK cells using the Fc region to destroy the malignant cell (328). It has been reported that three different processes can be activated through Fc binding; ADCC, activation of complement dependent cytotoxicity (CDC) and the induction of adaptive immunity (329).

The complement system is a part of the immune system that is paramount for protection against pathogenic microorganisms and damaged cells. Monoclonal antibody therapies use CDC to destroy tumour cells (330). The interaction between the Fc region of a monoclonal antibody and a C1 complex leads to the formation of a membrane attack complex that functions to cause cell death (331).

1.8.4 Potent ADC cytotoxic drugs

The small molecule cytotoxic drug attached to ADCs are responsible for eliminating the malignant cell the ADC has specifically bound to. The cytotoxic payload must be highly super-toxic, low immunogenic, stable during preparation, storage and circulation and amenable to modification (318). Due to its structure, the antibody can only carry a limited number of cytotoxic molecules therefore the drug must be super-toxic in order to have the maximum effect on the tumour cell (332). When injected into a tumour, only 0.003-0.08% per gram of the initial dose of ADC is taken up by the cells (333, 334). Additionally, poor internalisation activity and low expression of the tumour marker may again work against sufficient delivery of the payload into malignant cells. This again highlights why a super-cytotoxic drug is critical due to the challenges faced before the drug can take its action within the cell. It has been reported that a cytotoxic drug of this calibre should have an IC50 of approximately 10nM or less (333-336). Drugs such as

this are likely to be chemical anti-cancer chemotherapeutic drugs that are too potent to be used systemically in chemotherapy and are less immunogenic than glycol/peptide cytotoxic agents when circulating in the blood.

Current cytotoxic drugs can be split into two categories, those which affect DNA synthesis and those which affect cell division to block mitosis (337, 338). Auristatins are the most commonly used drugs in ADC design and bind to tubulin to inhibit microtubule assembly and polymerisation (339). Maytansinoids derivatives, pyrrolobenzodiaze-pine, camptothecin analogues, n-acetyl-γ-calicheamicin, duocarmycin and doxorubicin are among other common cytotoxic payloads for ADCs. In addition to being 100-10000 times more potent than systemic chemotherapeutic drugs, some drugs that modulate DNA have specific effects on cancerous cells because they divide more rapidly than non-cancer cells (340). Examples of common cytotoxic drugs and their mechanism of action can be seen in **Table 1-4**.

Table 1-4 – Common cytotoxic drugs for ADCs and their mechanisms of action

Cytotoxic Drug	Mechanism of action
Auristatins	Tubulin inhibitor
Maytansines	
Calicheamicins	DNA damage inducers
Duocarymycins	
Doxorubicin	
PBD dimers	

The table above shows the most common cytotoxic drugs used in ADC development and their mechanism of action (318).

Due to the purpose of an ADC being specific to malignant cells and leaving non-cancer cells unaffected, it is essential that the cytotoxic payload is stable. Unstable drugs can be converted to undesirable drugs during preparation and/or storage. This means that drug solubility in an aqueous solution is another highly important consideration. With the monoclonal antibody being a protein, its conjugation to the payload must be carried out in an aqueous solution with minimal organic solvents. If a cytotoxic drug is highly hydrophobic then this could change the biological properties of the antibody which could result in hydrophobic aggregation of the antibody during conjugation or storage (340, 341). The hydrophilicity of the drug can also have an impact on the cell membrane permeability of the ADC or its metabolites. The ability of the payload to form a hydrophobic metabolite after cleavage within the cell could be considered preferable due to metabolites with increased hydrophobic properties having a better capacity for blood clearance and safety (341). According to reports by Azvolinsky *et al* 95-99% of ADC

molecules are metabolised before they have the chance to bind to tumour cells (332). This raises serious safety considerations concerning off target toxicity and therefore the use of cytotoxic drugs with well-characterised metabolite profiles can be useful in enhancing the safety of ADCs. The cytotoxic payload conjugated to the antibody should have a dominant functional group suitable for joining the two together. If such a group does not exist on the drug then the drug must be amenable to modification (342, 343). Heterogeneity of antigen expression and the copy number also need to be taken into consideration when choosing a cytotoxic drug. If the target antigen is highly expressed, then a drug with a lower potency could be used with increased safety. In general, payloads that stimulate the bystander effect in cancer cells are more suitable for ADC design (336, 344, 345).

1.8.5 Linkers

The chemical linker which joins the antibody to its cytotoxic payload is a crucial part of ADC formulation and success. It must have a conjugation site, a well-defined drug-antibody ratio (DAR), homogeneity, chemical stability, a cleavable/non-cleavable site, a smart cleavage mechanism and site specific conjugation (318). The most commonly used residues on the antibody for conjugation to a cytotoxic payload are interchain disulphide bridges and surface exposed lysine's. In theory, the linkage of the drug to the surface-exposed lysine's of an antibody occurs after the reduction of around 40 lysine residues on both the heavy and the light chain of the antibody. This results in the ability to conjugate 0-8 cytotoxic payload linkages per antibody (346, 347). A conjugation method using available cysteines after the reduction of four interchain disulphide bonds make eight exposed sulfhydryl groups. It is this that allows the conjugation of 0-8 molecules to the antibody (336). It is possible to reduce only two of the four interchain disulphide bonds of the cysteine residues with mild reduction conditions. However, this process is not easily done accurately and often a variety of cystines may be reduced from 0-4 resulting in a heterogenous mixture of ADCs (336, 347).

To overcome some of the challenges associated with conjugating *via* reduction, some site-specific conjugation methods have been developed. In these methods, defined conjugation sites are identified, and a known number of payloads are attached. Four reported methods include conjugation through engineered cysteine residues (THIOMAB technology), reengineered antibodies with the ability to incorporate with unnatural amino acids, site-specific enzyme-mediated conjugation to a genetically engineered antibody and chemoenzymatic site direct conjugation (318). The linker chemistry used in the current ADCs on the market can be seen below in **Table 1-5**. ADC linkers have the possibility to change antibody conformation, which could mean the antibody does not behave in the same way or even bind to its target at all after

linkage to the drug (343). Protein structure, including that of antibodies, can be checked using protein crystallography (348). Additionally, antibodies can be re-validated after the conjugation to check the same behaviour is observed by immunohistochemistry and quantitative immunofluorescence (349).

Table 1-5 – Current ADCs linker chemistry

ADC	Linker
Belantamab mafodotin (BLENREP)	A non-cleavable maleimidocaproyl (mc) linker (350)
Sacituzumab govitecan (TRODELVY)	Site specific – SN-38 is covalently linked to hRS7 *via* a hydrolysable CL2A linker (351)
Trastuzumab deruxtecan (Enhertu)	Site specific enzymatically cleavable tetrapeptide based linker (352)
Enfortumab vedotin (Padcev)	Protease cleavable maleimidocaproyl-valyl-citrullinyl-p-aminobenzyloxycarbonyl linker (353)
Polatuzumab vedotin (Polivy)	Engineered cysteines (THIOMABs). Protease-cleavable peptide linker (valine-citrulline) (354)
Gemtuzumab ozogamicin (Mylotarg)	Bifunctional 4-(4-acetylphenoxy) butanoic acid (AcBut) moiety to surface-exposed lysines of the antibody through an amide bond. Acyl hydrazone linkage with N-acetyl-γ-calicheamicin dimethyl hydrazide (355)
Inotuzumab ozogamicin (BESPONSA)	Covalently linked *via* an acid-labile 4-(4′-acetylphenoxy) butanoic acid (acetyl butyrate) linker (356)
Ado-trastuzumab emtansine (Kadcyla)	Modification of lysines on trastuzumab with succinimidyl 4-(N-maleimidomethyl) cyclohexane-1-carboxylate linker and subsequent reaction with sulfhydryl of the DM1 drug (357)
Brentuximab vedotin (Adcetris)	Protease-sensitive dipeptide linker, citrulline-valine linker (358)

The table above details the linker chemistry of ADCs currently on the market in 2020

1.8.6 Mechanisms of ADC internalisation

The success of ADC therapy is equally governed by a number of essential characteristics. One of these essential characteristics is the internalisation of the ADC into the cell after binding to its tumour marker. The knowledge of endocytosis and endosomal trafficking has improved vastly in recent years, and as a result these pathways can be efficiently exploited to improve the efficacy of ADC therapy (359). Cells are regularly internalising proteins and their cell surface receptors into the cell by various endocytosis pathways. Internalised receptors are then incorporated into endosomes where they are guided through recycling or degradation pathways (359). For ADCs to be successful, they must be successfully delivered to the lysosome for effective release of the cytotoxic payload to the cell *via* degradation (360). Molecules can be internalised into the cell after binding to their surface receptor by clathrin-independent mechanisms such as phagocytosis, micropinocytosis and caveolin-dependent endocytosis or by clathrin dependent mechanisms such as receptor mediated endocytosis. Clathrin-dependent receptor mediated endocytosis is the best characterised and most predominant method for the internalisation of cell surface receptors and their ligands (361, 362). The main different methods of internalisation are shown below in **Figure 1-12**.
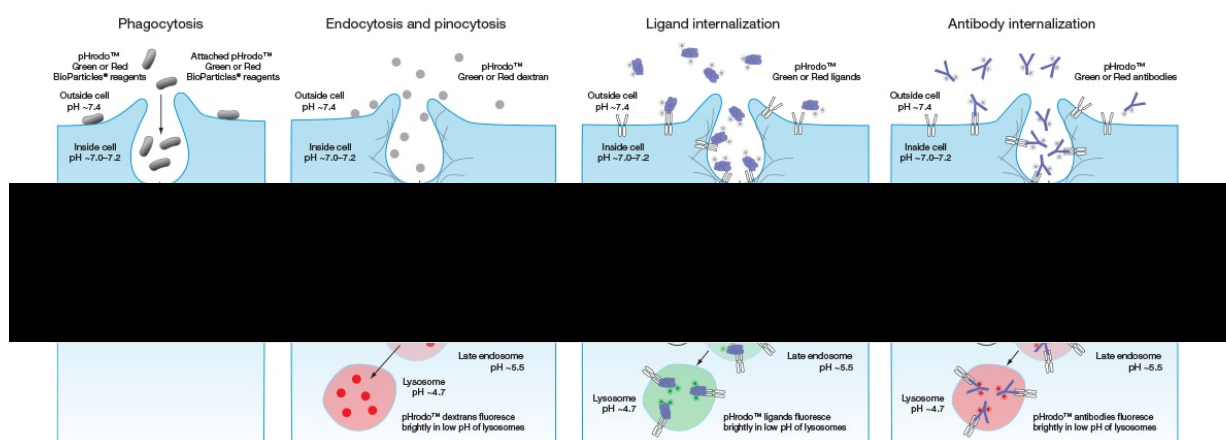
Figure 1-12 – Methods of internalisation (Image from Thermo Fisher Scientific (363))

54

Table 1-6 – Mechanism of internalisation of ADCs

ADC	Mechanism of internalisation
Gemtuzumab ozogamicin (Mylotarg)	Pinocytosis, Receptor-mediated endocytosis
Inotuzumab ozogamicin (BESPONSA)	Receptor-mediated endocytosis
Ado-trastuzumab emtansine (Kadcyla)	Receptor-mediated endocytosis
Brentuximab vedotin (Adcetris)	Clathrin-mediated endocytosis

The table above shows the internalisation mechanisms for ADCs Mylotarg, BESPONSA, Kadcyla and Adcetris (364)

1.8.6.1 Clathrin-dependent endocytosis

Clathrin-dependent endocytosis is one pathway by which ADCs bind to their receptor and are internalised into the cell, before being trafficked to the lysosomes for degradation. Clathrin-dependent endocytosis begins with the recruitment of adapter proteins, accessory proteins and a clathrin polymeric lattice to phosphatidylinositol-4,5-bisphosphate-enriched plasma membrane regions (365). The clathrin adapters, most commonly adaptor complex 2, select the ADC to be internalised. Once this selection process is complete, clathrin moves from the cytoplasm to adapter protein-enriched regions of the membrane. The accumulation of clathrin causes polymerisation which results in membrane displacement and the formation of budding vesicles on the cell surface, called clathrin-coated pits (CCP) (366). Dynamin, a GTPase, plays a part in the freeing of the budding vesical from the plasma membrane and its release into the cell. After single vesicles are created, they fuse with each other in the cytoplasm to produce early endosomes. Endosomes function to regulate the intracellular distribution of internalised proteins. Endosomes classically send their cargo through two different pathways; One pathway is characterised by the recycling of the receptor back to the cell surface (367) and the other pathways is through endo-lysosomal degradation (368). In the degradation route, the internalised cargo is retained in a maturing endosome until it is delivered to the lysosome. Late endosomes are also known as multivesicular bodies (MVBs) and their formation is characterised by an increase in luminal acidification, movement to the perinuclear space and the formation of intraluminal vesicles (369-371).

1.8.6.2 Caveolae-mediated endocytosis

Caveolar endocytosis is a clathrin-independent endocytic process and is known to be a pathway of ADC internalisation (364). During caveolar endocytosis, a bulb shaped invagination is formed, driven by membrane proteins called caveolins and cavins. Recent publications have shown that caveolae are endocytic carriers where previously they had been shown as highly immobile and

non-endocytic (372, 373). In caveolar endocytosis, caveolae bud off from the plasma membrane and the majority of these buds reach the early endosome while a minority fuse back to the plasma membrane. These early endosomes, as described above, either recycle back to the plasma membrane or mature into a late endosome which is trafficked to the lysosomes. The budding of caveolae is mediated by dynamin whereas EHD2 negatively regulates caveolar endocytosis (374, 375).

1.8.6.3 Pinocytosis

Pinocytosis is another method of molecules being internalised into the cell; however, it is less commonly used by ADCs. Pinocytosis is a continuous process in the majority of cells and is a non-specific method of internalisation. Pinocytosis involves the movement of a large number of small molecules through a fluid. Once inside the cell, the small molecules form vesicles that fuse with early endosomes for recycling or degradation. The presence of the molecule to be taken up is the initiator for the process (376).

1.8.7 Safety considerations for ADCs (on and off target toxicity)

The toxicity of an ADC can be subcategorised into 'on target' and 'off target' toxicity. Toxicity as a result of the tumour specific target is 'on target' and toxicity that occurs independently of the target is known as 'off target'. Target induced toxicity is accomplished by, in the case of ADCs, finding an antibody which only internalises when it binds to a specific tumour marker. Other forms of 'on target' target toxicity include chemotherapeutic drugs, which only affect proliferating cells. Although, this type of toxicity is known to affect fast dividing cells such as hair follicles and stomach endothelial cells, and whilst considered 'on target' can result in unpleasant side effects. Off target toxicity is one of the main reason's ADCs do not make it through clinical trials. Off target toxicity can be driven by non-specific Fc binding and subsequent internalisation, pinocytosis driven off target toxicity by non-specific endocytosis and bystander toxicity, where cytotoxic drugs are recycled back to the plasma membrane and are internalised by near-by cells. Bystander toxicity is not necessarily a disadvantage. Although it is considered 'off target', its highly likely that near-by cells are also malignant and therefore benefit from being destroyed. The bystander effect will only target cells in the immediate environment (377).

1.8.8 ADC development process

This thesis focuses on the selection process of the tumour marker used to guide the ADC to malignant cells. This preliminary ADC development process characterises the targets to ensure they are minimally expressed on healthy non-cancer tissue, comparatively highly expressed on

the surface of malignant cells, have the ability to internalise into the cell and be trafficked to the lysosomes and are genetically stable or easily stratified to ensure patient specific treatment. Other considerations before ADC synthesis include a limited degree of shedding by the target and novel target opportunity (no filed patents) (318).

Following the target identification, the antibody is generated by mice hybridoma or phage display techniques to generate sufficient quantities of the antibody. The antibody is characterised by confirming its high affinity binding to the human antigen, its specificity for the antigen, its ability to bind homologues and its genetic stability. The conjugation then takes place where the conditions are optimised for low aggregation, high monomeric content, a consistent drug to antibody ratio, high yield and no loss of binding affinity. Pre-clinical trial requirements include cytotoxicity testing *in vitro*, pharmokinetic analysis, *in vivo* tumour efficacy in human tumour models and finally *in vivo* toxicology in animal models. Finally, human clinical trials phase I, II and III are undertaken before application for market approval (378).

1.8.9 ADCs currently on the market

The ADC market is a rapidly changing environment. After successful clinical trials, ADCs can apply for approval from the United States Food and Drug Administration (FDA) or the European Medicines Agency (EMA). The Antibody Society (379) have a regularly updated list of antibody therapeutics approved or in regulatory review in the EU or US (380). This database identifies, at the time of writing, there are eight ADCs approved for use by the FDA, of which six are approved by the EMA and an additional ADC is currently under review by the FDA. Each ADC is discussed in more detail below. Interesting, ADCs historically focus on haematological malignancies and breast cancer predominantly (see sections below). ADCs against haematological malignancies are common due to surgery not being an option in cancers of the blood. Treatment must be systemic to effectively reach all the malignant cells throughout the body (381). Additionally, breast cancer receives a lot of research attention due to it being the most common cancer in the UK (138). Furthermore, the discovery of HER2 as a breast cancer biomarker was found early resulting in a clear an easy ADC target choice (382). Other cancers provide more of a challenge as the biomarker discovery process is on-going.

1.8.9.1 Gemtuzumab ozogamicin (Mylotarg)

Mylotarg was the first ADC to be approved by the FDA to the US market in 2010 for the treatment of Acute Myeloid Leukaemia (AML) however, it was subsequently recalled and removed from the market shortly after due to subsequent clinical trials failing to verify clinical benefit and demonstration of safety concerns. In September 2017, the US FDA announced the

re-approval of Mylotarg to the market. Mylotarg is a CD33 targeting ADC for the treatment of newly diagnosed and relapsed/refractory AML. The introduction of Mylotarg provided much needed relief for the therapy of AML, which since 1973 has remained the same with no advancements towards therapeutics (383).

AML is a heterogenous disease affecting hematopoietic stem and progenitor cells. It is characterised by the impaired proliferation, differentiation and self-renewal of these cells. AML can also be characterised by chromosome aberrations such as translocations, deletions, inversion, monosomies and trisomies (384). Treatment of AML is often ineffective due to these complex heterogenous properties. In comparison to other cancers, the relapse rate remains high and the 5-year overall survival rate remains low at 40%. This survival rate becomes even lower for older patients who have a 5-year survival rate of less than 25% (385, 386).

Mylotarg is a CD33 targeting ADC that is made up of hP67.6 monoclonal antibody covalently linked to the cytotoxic agent N-acetyl γ calicheamicin (387). CD33 is a ubiquitous marker in AML patients which presents as a potent target for immunotherapies against AML. CD33 is present on AML blasts in 90% of patients and is a 67 kDa transmembrane cell surface glycoprotein. CD33 is a prominent member of the sialic acid-binding immunoglobulin-like lectic family and has a high expression in cells undergoing myeloid differentiation. CD33 is believed to inhibit cellular signalling through the recruitment of the Src homology 2 domain containing protein tyrosine phosphatases SHP-1 and SHP-2 after phosphorylation of tyrosine residues in the immune-receptor tyrosine-based inhibitory motif domain on the cytoplasmic tail (388, 389). Mylotarg therapeutic action begins with the internalisation of the ADC after the antibody has bound to the IgV domain of CD33 present on the membrane of malignant cells. The ADC is trafficked to the lysosomes by mature endosomes where the calicheamicin is cleaved from the ADC-CD33 complex and enters the nucleus where it initiated single and double stranded DNA breaks causing apoptosis (387, 390).

The current standard of care for the treatment of AML remains intensive 3 + 7 (DNR/AraC) induction chemotherapy and in cases of remission, this is usually followed by two to four courses of consolidation therapy or transplant in patients eligible (391).

Calicheamicin is a potent anti-tumour drug that forms the cancer killing part of the Mylotarg ADC. Once inside the lysosomes, the acidic atmosphere hydrolyses the disulphide bond joining calicheamicin to the acidic labile linker which releases the drug into the cell (387). When free, calicheamicin accumulates in the nucleus where it recognises 3'-5' sites (AGGA, TCCT, TCCA) by its oligosaccharide moiety. Double stranded DNA breaks are induced at these points which leads to overall cytotoxic effects (392).

1.8.9.2 Brentuximab vedotin (Adcetris)

Brentuximab vedotin (Adcetris) is a CD30 targeting ADC made by Seattle Genetics for the treatment of Hodgkin lymphoma. It consists of an anti-CD30 monoclonal antibody conjugated using a protease cleavable linker to an anti-microtubule agent monomethyl auristatin E (MMAE). Once internalised and processed by the lysosomes, released MMAE binds to tubulin which leads to cell cycle arrest and apoptosis. Adcetris was approved by the FDA in 2011 and by the EMA in 2012 for the treatment of relapsed/refractory Hodgkin lymphoma, systemic anaplastic large cell lymphoma or primary cutaneous CD30-positive lymphoproliferative disorders (358). Each Adcetris molecule carries an average of 5 MMAE molecules (393) and is internalised by clathrin mediated endocytosis (364). Adcetris is linked *via* a citrulline-valine linker which is highly stable in plasma. The dipeptide bond is readily cleaved by lysosomal enzymes for selective therapeutic effects. This results in higher efficacy and lower toxicity when compared to other ADCs which are less stable in plasma (393). Adcetris can also cause selective apoptosis by antibody dependent cellular phagocytosis or by directly affecting the tumour cell signalling by binding CD30. In addition, Adcetris can also have therapeutic affect by the off-target bystander effect, where MMAE molecules are recycled out of the cell to be up taken by nearby cells causing the death of cells in the surrounding area (394). In preclinical evaluation, Adcetris was shown to induce cell death in CD30 positive cells *in vitro* with an IC_{50} of <10ng/ml while being over 300-fold less active on CD30 negative cells, indicating high specificity and low off target toxicity. When used in a Hodgkin lymphoma xenograft model, the anti-tumour activity was improved when Adcetris was used in conjunction with other chemotherapeutic agents such as gemcitabine and the combination of adriamycin, bleomycin, vinblastine, and dacarbazine (395, 396). Treatment using Adcetris involves a dose of 1.8 mg/kg every three weeks where the half-life for the ADC is considered 4-6 days. Peak blood concentrations were achieved by the end of each treatment session compared to a 1-3 day delay when using the free drug alone (397, 398). Overall, Adcetris is considered an effective treatment for relapsed/refractory Hodgkin lymphoma, systemic anaplastic large cell lymphoma or primary cutaneous CD30-positive lymphoproliferative disorders and is the longest standing ADC on the market after the removal of Mylotarg.

1.8.9.3 Ado-trastuzumab emtansine (Kadcyla)

Ado-trastuzumab emtansine (Kadcyla) is a HER2 targeting ADC for the treatment of HER2 positive breast cancer (399). Kadcyla received FDA approval in 2012, and was soon after approved by the EMA in 2013 (380). Approximately a quarter of all breast cancers are HER2

positive due to an amplification of the HER2 gene in malignant cells. This has been associated with more aggressive breast cancers and a poorer prognosis when compared to non-HER2 positive breast cancers (400). The monoclonal antibody therapy trastuzumab has been shown to reduce tumour size in approximately 25% of patients and due to this is often combined with chemotherapy to increase its effects (401, 402). Kadcyla takes the specificity of this monoclonal antibody therapy and combines it with the potent cytotoxic drug emtansine to destroy malignant cells by binding to tubulin and causing cell cycle arrest and subsequent apoptosis. Kadcyla is the first ADC directed at a solid tumour and was approved by the FDA only 5 years after its first publication in 2008 (403). Kadcyla links the monoclonal antibody trastuzumab *via* a stable thioether linker to emtansine molecules. Emtansine is a derivative of maytansine and has anti-tumour properties by binding tubulin in the nucleus, preventing the assembly of microtubules by promoting depolymerisation and inhibiting polymerisation (404).

1.8.9.4 Inotuzumab ozogamicin (BESPONSA)

Inotuzumab ozogamicin (BESPONSA) is a CD22 targeting monoclonal antibody conjugated to the potent cytotoxic molecule calicheamicin for the treatment of relapsed/refractory B-cell precursor acute lymphoblastic leukaemia (405-408). CD22 is a surface antigen present on over 90% of the B-cell blasts present in patients with B-cell acute lymphoblastic leukaemia. The ADC is internalised and trafficked to the lysosomes where the calicheamicin is released and binds to double stranded DNA causing double stranded DNA breaks and subsequently apoptosis (409, 410). In 2012, BESPONSA was approved by the FDA and the EMA in 2017 for the treatment of acute lymphoblastic leukaemia (380).

1.8.9.5 Polatuzumab vedotin (Polivy)

Since the approval of BESPONSA in 2017, the number of ADCs being approved has picked up considerably. In 2019, Polatuzumab vedotin (Polivy) was approved by the FDA and later in 2020 by the EMA for the treatment of diffuse large B-cell lymphoma (380). Polivy is an ADC targeting CD79b and was developed by Grenetech/Roche using a proprietary technology designed by Seattle Genetics for the treatment of diffuse large B-cell lymphoma. Polivy is conditionally approved to be used in conjunction with bendamustine and rituximab in patients who have received at least two prior therapies. Polivy is an ADC comprising of an anti-CD79b monoclonal antibody conjugated to MMAE through engineered cystines (THIOMABS) by a protease-cleavable peptide valine–citrulline linker, where it is highly stable in plasma and easily released under lysosomal conditions. Approximately 3.5 MMAE molecules are present on each ADC molecule and upon internalisation and trafficking to the lysosomes, MMAE is released where it

binds tubulin and inhibits its polymerisation which causes cell cycle G2/M phase arrest and subsequently malignant cell apoptosis (354).

1.8.9.6 Enfortumab vedotin (Padcev)

In 2019, Enfortumab vedotin (Padcev) was approved by the US FDA for the treatment of urothelial cancer. At the time of writing it has not yet been submitted for approval by the EMA for use in Europe (380). Padcev is an ADC produced by Seattle Genetics and Astellas Pharma targeting Nectin-4 for patients with urothelial cancer who have previously received and progressed on a programmed death receptor 1 or programmed death ligand 1 inhibitor and a platinum-based chemotherapy. Padcev comprises of an aniti-Nectin-4 monoclonal antibody conjugated to MMAE *via* a protease-cleavable maleimidocaproyl-valyl-citrullinyl-p-aminobenzyloxycarbonyl linker. The conjugation takes place on cystines residues that comprise of interchain disulphide bonds on the antibody to yield a drug to antibody ratio of approximately 3.8. Padcev is the first ADC designed to treat urothelial cancer and targets Nectin-4 (Poliovirus Receptor-related 4; PVRL4) which is a transmembrane protein highly expressed on the surface of cells in the bladder. After internalisation and trafficking to the lysosomes, Padcev releases MMAE due to proteases present in the lysosomes and travels to the nucleus where it binds tubulin and inhibits its polymerisation which causes cell cycle G2/M phase arrest and subsequently malignant cell apoptosis (411).

1.8.9.7 Trastuzumab deruxtecan (Enhertu)

Trastuzumab deruxtecan (Enhertu) is an ADC developed by Daiichi Sankyo and AstraZeneca for the treatment of adult patients with unresectable or metastatic HER2-positive breast cancer who have received two or more prior anti-HER2 based treatments. Enhertu was approved by the US FDA in 2019 and, at the time of writing, it has not yet been submitted for approval by the EMA for use in Europe (380). Enhertu is an ADC comprised of an anti-HER2 monoclonal antibody, a cleavable tetrapeptide based linker and a small molecule cytotoxic topoisomerase I inhibitor. Enhertu was approved under the FDAs Accelerated Approval based on its tumour response rate and the duration of the response. The approval was based on the results of a clinical trial where the ADC was dosed at 5.4mg/kg in patients with HER2-positive breast cancer. The results confirmed an objective response rate of 60.3% including a 4.3% complete response rate and a 56% partial response rate. The median duration of the response was 14.8 months. Once internalised and released, the cytotoxic topoisomerase I inhibitor prevents the repair of double stranded DNA breaks in the nucleus and results in apoptosis of the malignant cell (352).

1.8.9.8 Belantamab mafodotin (BLENREP)

Belantamab mafodotin (BLENREP) is an ADC developed by GlaxoSmithKline and Seattle Genetics for the treatment of relapsed/refractory multiple myeloma and other advanced hematologic malignancies expressing B-cell maturation antigen (BCMA). It was approved by the US FDA and EMA in 2020 (380). BLENREP comprises of a monoclonal antibody targeting Tumour Necrosis Factor receptor super family member 17 (BCMA/CD269) conjugated using a non-cleavable maleimidocaproyl linker to cytotoxic drug Monomethyl Auristatin F (MMAF). There is an average of 4 MMAF molecules attached *via* cystine residues onto the monoclonal antibody. MMAF is a tubulin polymerise inhibiter and after BLENREP has been internalised and trafficked to the lysosomes and degraded, MMAF travels to the nucleus where it binds tubulin and inhibits its polymerisation which causes cell cycle G2/M phase arrest and subsequently malignant cell apoptosis (350).

1.8.9.9 Loncastuximab tesirine (In review)

At the time of writing, Loncastuximab tesirine is in review for approval by the FDA and has not yet been submitted for approval by the EMA (380). Loncastuximab tesirine is an ADC targeting CD19 conjugated to a small molecule potent pyrrolobenzodiazepine (PBD) dimer cytotoxin for the treatment of elapsed or refractory diffuse large B-cell lymphoma. The cytotoxic payload is designed to bind irreversibly to DNA to create highly potent inter-strand cross links which block DNA strand separation and therefore DNA replication. This disruption results in apoptosis of the malignant cell (412).

1.8.10 ADCs for gynaecological malignancies

There are currently no FDA or EMA approved ADCs for the treatment of any gynaecological malignancy such as OC, however several are in clinical trials. Mirvetuximab Soravtansine is an ADC in clinical development targeting folate receptor alpha (FRa) for platinum resistant, folate receptor alpha positive epithelial ovarian cancer. FRa binds folic acid and its derivatives which is important in foetal development and is a popular anti-cancer target due to its over expression in many cancers such as ovarian, breast, renal, lung, colorectal, and brain. As of 2019, Mirvetuximab Soravtansine has completed phase III clinical trials but has yet to be submitted for approval. Additional ADCs are reported to be in clinical development for the target NaPiB2, Trop2, mesothelin, or MUC16 (413). NaPiB2 is transmembrane, sodium dependant phosphate transporter that is overexpressed in ovarian cancer cells, and is also expressed in normal breast and lung tissue (413). Trop2 is a membrane bound tumour associated calcium signal transducer-2 and was initially discovered as a transducer of an intracellular calcium signal (414). Mesothelin

is a cell surface glycoprotein present on mesothelial cells and is upregulated in a variety of cancers including OC (415). Muc16 (also known as CA125) functions as a component of the ocular surface, respiratory tract and the female reproductive tract epithelia. Its glycosylation creates a hydrophilic environment which acts as a lubricant (416).

Anti-NaPi2b antibody-drug conjugate lifastuzumab vedotin (DNIB0600A) is an ADC for the treatment of platinum resistant OC. At the time of writing lifastuzumab vedotin is in phase II clinical trials (NCT01991210). Lifastuzumab vedotin is an ADC targeting NaPi2b and is conjugated to a potent antimitotic agent, MMAE (417, 418). Lifastuzumab vedotin, in its phase Ia, trials was also considered as a treatment for patients with Non-Small-Cell Lung Cancer (419). A1mcMMAF is an antibody-drug conjugate targeting cells expressing the tumour-associated antigen 5T4 for the treatment of epithelial OC. It is currently being investigated for its therapeutic benefit in combination with routine chemotherapeutic drugs (420). ADC DMOT4039A is an ADC targeting mesothelin and comprises of a monoclonal antibody conjugated to MMAE for the treatment of platinum resistant OC. DMOT4039A published a phase I clinical trial in 2016 but has not yet been further reported (421).

In Swansea University Medical Schools Reproductive Biology and Gynaecological Oncology (RBGO) group the transmembrane protein RAGE has been extensively characterised for its use as an ADC in gynaecological malignancies. An ADC targeting RAGE has been produced and is currently still undergoing pre-clinical analysis by RBGO group members (200-202).

1.9 Research aims

The purpose of this thesis is to characterise novel Antibody-Drug Conjugate targets for ovarian cancer using a pipeline already in place from the development of the RAGE ADC. The characterisation of the novel targets will be discussed, and the implications for patient stratification, improved diagnostics, treatment and therapeutic intervention outcome monitoring.

The aims of this study are:

- To explore the protein expression levels of six novel potential ADC targets in ovarian cancer cell lines, using western blot.
- To characterise the sub-cellular location of six novel ADC targets in 2D cultures of ovarian cancer cell lines using immunofluorescence microscopy.
- To determine the sub-cellular location of selected novel ADC targets in 2D primary cultured cells derived from patient tissue biopsies, using immunofluorescence microscopy.

- To determine the capacity of selected ADC targets to mediate antibody internalisation in primary and established ovarian cancer cells grown as 2D cultures, using immunofluorescence microscopy.

- To determine the genetic stability and patient stratification potential of the epitope coding sequence for both RAGE and a selected novel ADC target, using Illumina amplicon sequencing.

- To explore the potential of soluble RAGE as a liquid biopsy biomarker for early diagnosis of ovarian cancer.

Chapter 2: Materials and methods

2.1 Patient recruitment and samples

Ovarian serum and primary cells were obtained from patients recruited to the 'Identifying ovarian and blood biomarkers for ovarian pathologies' project (REC reference: 15/WA/0065). Long term storage of serum was at -80°C, unless serum was known to be required within 4 weeks where it was then stored at -20°C. All patients for this project were recruited from Swansea Bay University Health Board (formerly known as Abertawe Bro Morgannwg University). Trust Hospital and ethical approval was obtained from the Local Research Ethics Committee at Swansea Bay University Health Board. Formal written consent was obtained from all the patients at the time of recruitment into the study.

2.1.1 Patient Grouping

Blood samples and tissue biopsies were obtained by clinicians and research nurses at Swansea Bay University Health Board before serum and 2D cells respectively were harvested by members of the Reproductive Biology and Gynaecological Oncology team. 116 patients were grouped for serum analysis by ELISA as can be seen in **Table 2-1** below. One of the difficulties of grouping the data included the way in which the data was classified or in some cases (as shown in table 2-1) not recorded. For example, some patients have a cancer stage recoded and others do not. The table below shows that out of all patients 52% were postmenopausal, only 5% were premenopausal and 43% were not documented either way. This patient grouping is analysed further in section 7.2.1. Overall **Table 2-1** shows that most patients are postmenopausal. A full list of all patients and their data is provided by accessing the following link:
 https://drive.google.com/file/d/1wFjwhbEtMm1gT9TbXoesfWAwDt-soa_M/view?usp=sharing.

Table 2-1 - Number of patients recruited in each group

Group	Number of patients	Percentage Postmenopausal	Percentage Premenopausal	Percentage menopausal stage not recorded
No cancer	26	42% (11/26)	23% (6/26)	35% (9/26)
OC (Ovarian cancer)	81	53% (43/81)	0% (0/81)	47% (38/81)
Other cancer	3	100% (3/3)	0% (0/3)	0% (0/3)
Undocumented	6	50% (3/6)	0% (0/6)	50% (3/6)
Total	116	52% (60/116)	5% (6/116)	43% (50/116)

OC stage	Number of patients	Percentage Postmenopausal	Percentage Premenopausal	Percentage menopausal stage not recorded
Unspecified mass	34	76% (26/34)	0% (0/34)	24% (8/34)
Stage 1	9	33% (3/9)	0% (0/9)	67% (6/9)
Stage 2	3	67% (2/3)	0% (0/3)	33% (1/3)
Stage 3	17	29% (5/17)	0% (0/17)	71% (12/17)
Stage 4	16	44% (7/16)	0% (0/16)	56% (9/16)
Endometrioid	1	0% (0/1)	0% (0/1)	100% (1/1)
Clear cell	1	0% (0/1)	0% (0/1)	100% (1/1)
Total	81	53% (43/81)	0/81	47% (38/81)

The pathologies of patients, allowing them to be grouped as in **Table 2-1**, were obtained from patients attending general gynaecology clinics or gynaecology oncology clinics in ABMU. These patients were both pre- and post-menopausal that had presented to primary care or emergency services with symptoms suggesting ovarian pathology. Symptoms included pelvic pain, abdominal bloating, weight loss and a change in bowel habit.

Clinical imaging such as ultrasound, computerised tomography (CT) scan or Magnetic Resonance Imaging (MRI) scan was used to identify any ovarian masses. If masses were present, then levels of tumour markers Cancer Antigen 125 (CA125/Mucin16) and Carcinoembryonic antigen (CEA) in the blood were determined by staff at Swansea Bay University Health Board. If necessary patients would undergo primary surgery or Interval Debulking Surgery (IDS) following 4-6 cycles of chemotherapy (422). All patients were recruited because they were determined to need primary surgery. Those who did not need surgery were not approached to participate in the study.

Surgery can include unilateral salpingo-oophorectomy (Surgical removal of one ovary and one fallopian tube), bilateral salpingo-oophorectomy (Surgical removal of both ovaries and both fallopian tubes), total hysterectomy (Surgical removal of the uterus, including the cervix), omentectomy (Surgical removal of part or all of the omentum, a fold of fatty tissue inside the

abdomen), bowel resection (Surgical removal of part of the small or large intestine), diaphragm surgery (Surgical removal of part of the diaphragm), appendix surgery (Surgical removal of the appendix) and/or lymph node dissection (Surgical removal of multiple lymph nodes in the abdominal cavity) (423).

A biopsy is taken during one of the treatment surgeries mentioned above and patients receive a diagnosis after this has been carried out. Diagnosis is noted on their ovarian pathology biomarker study proforma which is delivered with the blood and biopsy samples. This proforma data is anonymised using a numbering system (OV###) before being disclosed towards this PhD project.

The non-cancer group contains patients undergoing surgery for benign gynaecological conditions such as fibroids or cysts and patients undergoing risk reduction surgery due to the presence of a **Br**east **Ca**ncer (BRCA) gene mutation. Those with a family history of breast and OC, due to a mutation in the BRCA 1 or 2 gene, can choose to have their ovaries and fallopian tubes removed to greatly reduce their risk of breast or ovarian cancer. BRCA 1 and 2 act as tumour suppressors and when operating correctly control cell proliferation and apoptosis, however if mutated can lose their function and allow uncontrolled proliferation to occur resulting in a mass (424).

Serum was harvested as described in section 2.1.2 and biopsy tissue was processed to extract primary stromal and epithelial cells as described in section 2.1.3.

2.1.2 Serum harvest

Blood collection was carried out by a clinician or nurse from Swansea Bay University Health Board. Blood serum harvest is carried out at room temperature on an open top bench. Blood is collected from patients recruited to the above studies at the time of surgery by clinicians at Singleton Hospital or Morriston Hospital. Full written consent is obtained. Blood is collected in a gold topped BD Vacutainer™ with acrylic gel in the tube to separate the serum from the cellular components. This prevents contamination of the serum and enables a short centrifuge time for separation. Routine analytes such as potassium and glucose are still stable after a week of storage in these tubes at 2-8°C. Despite this when received the blood tubes are centrifuged the same day, as soon as possible, at 1300 g for 10 minutes. In addition, the tube contains silica particles to act as a clot activator to ensure that as soon as the blood enters the tube, it is coagulated right away. Once centrifuged the serum is aliquoted 300 ul into each 1.5 ml microcentrifuge tube. The majority of serum tubes are stored at -80 for long term storage and two aliquots are stored at -20 for short term storage.

2.1.3 Isolation of primary ovarian cells from a biopsy

Tissue biopsies are taken by a clinician from Swansea Bay University Health Board before the biopsy is couriered to the Reproductive Biology and Gynaecological Oncology Group (RBGO) for the process described below. Members of the RBGO team process the ovarian tissue biopsies to develop these primary cell lines.

Isolating cells from a primary patient biopsy is carried out inside a class II laminar flow biosafety cabinet. Patient ovarian biopsies arrive from Singleton or Morriston hospital in Dulbecco's Modified Eagle Medium: Nutrient Mixer F-12 (DMEM/F12 Gibco, Thermo Fisher Scientific 11320033) with no additional supplements in a 30 ml universal tube (Star Lab E1412-3010). In brief, small pieces are cut and set aside for DNA extraction, RNA extraction and protein extraction. The ovarian (often both left and right) biopsies are then digested to extract epithelial cells from the outer layer of the ovary and stromal cells from the inside of the ovary using collagenase type 1A from Clostridium histolyticum (Sigma-Aldrich, Merck C2674). Initially, the epithelial side is identified by looking for a curved, smooth surface that is whiter in appearance. Identification can present its own challenges, depending on the size of the biopsy it can be easy or impossible. Collagenase powder (Sigma Aldrich C0130) is added to pre-warmed primary ovarian cell media (See section 2.2.2) with no additives to make a final concentration of 2 mg/ml. This is then filtered through a 0.22 syringe filter and warmed to 37°C before use. Upon arrival, the patient samples are kept at 4°C before they are ready to be processed. Processing happens as soon as possible after the sample is received within at least 24 hours. The tissue biopsy is rinsed until clean in PBS (GIBCO 10010-015) before being placed into a petri dish for cutting. The biopsy is representatively cut in half, with half being reserved for cell extraction and the other half being cut into a further three pieces for DNA, RNA and protein extraction. The epithelial side is placed facing 800-1000 µl of collagenase in a 6 well tissue culture plate. This is incubated at 37°C for 30 minutes with manual agitation every 5-10 minutes. After 30 minutes a scalpel is used to gently scrape the epithelial side to help the cells detach before the rest of the ovary is transferred to the next well for stromal cell digestion. The collagenase containing epithelial cells is collected into a 15 ml tube and the well is washed to collect any left behind epithelial cells. The tube is centrifuged at 300 g to pellet the cells and after discarding the supernatant the pellet is resuspended in 2 ml of fresh primary ovarian biopsy media and plated in a clean well. The stromal digestion is carried out after the epithelial digest using the left-over ovary tissue. The remaining tissue is chopped finely using a scalpel and approximately 2 ml of warm collagenase is added. This is incubated for 30 minutes at 37°C with manual agitation or more chopping every 5-10 minutes depending on the size and texture of the biopsy. The collagenase containing the

digested ovary is recovered in a 15 ml tube and the well is washed twice with media to ensure minimal cells have been left behind. This mixture is centrifuged at 300 g for 7 minutes and the supernatant is transferred to a new tube (not discarded) and the pellet (containing ovary tissue) is plated in a 6 well tissue culture plate. The saved supernatant is then centrifuged at 300 g for 7 minutes and the pellet plated. The supernatant is not discarded again but transferred to a new tube. This process is repeated until the supernatant is clear. The pellets are all plated together in one well and the stromal and the epithelial cells are incubated in a tissue culture incubator set at 37°C, 5% CO_2 in a humid environment. These samples are left to attach and grow for 3-5 days before following the procedure in section 2.2.2 to grow to 80-100% confluency in a T75 flask. Once confluency has been reached cells are cleaved from the flask using trypsin (GIBCO 25300-062) as in section 2.2.1.2.3 and stored in liquid nitrogen in Foetal Bovine Serum (FBS) with 10% Dimethyl sulfoxide to prevent crystallisation and disruption of the cells (425).

2.2 Tissue Culture

All tissue culture techniques are carried out inside a class II laminar flow biosafety cabinet to create an aseptic environment necessary for cell culture experiments.

2.2.1 Introduction to ovarian cancer cell lines

2.2.1.1 Ovarian cancer cell media

Eight ovarian cancer cell lines are described below (426) along with the manufactures recommended growth medium. All cells were grown inside an incubator with a 37°C and 5% CO_2 environment.

IOC (427) (Sourced from ABM, catalogue number: T1074)

- Pre-malignant. Fast growing
- Prigrow I medium (AMB TM001)
- 10% FBS (Gibco 10500-064), Thermo Fisher Scientific)
- 1% Penicillin Streptomycin (Pen Strep/PS) (GIBCO 15140-122)

TOV112D (endometrioid) (Sourced from ATCC, catalogue number: CRL-11730) and TOV 21G (clear cell) (Sourced from ATCC, catalogue number: CRL-11731)

- Medium growing speed. Sometimes contain vesicles and detach
- 1:1 MCDB 105 (Sigma M6395-1L) with final concentration of 1.5 g/l of Na_2CO_3 (17ml in 1L) and Medium 199 with final concentration of 2.2 g/L of Na_2CO_3 (13ml in 500ml) (Sigma S8761 500 ml). Filter before use.
- 15% FBS (75 ml in 500ml)

- 1% Penicillin Streptomycin (Pen Strep/PS)
- (Primary Ovarian cells same media just 20% FBS)

UACC-1598 (Poorly differentiated papillary serous grade 4) (Sourced from ATCC, catalogue number: CRL-3128) and **UWB1-289** (Papillary serous epithelial like) (Sourced from ATCC, catalogue number: CRL-2945)

- Can be sensitive. Easily become over confluent and detach
- DMEM/F12/50/50 1x (corning 10-103-CV)
- 10% FBS
- 1% Penicillin Streptomycin (Pen Strep/PS)

SKOV 3 (Sourced from ATCC, catalogue number: 91091004)

- Grade 1-2 serous from ascites. Fast growing
- McCoy's 5A Medium 1x (Thermo Fisher Scientific 16600082)
- 10% FBS
- 1% Penicillin Streptomycin (Pen Strep/PS)

COV 644 (Sourced from Public Health England, catalogue number: 07071908)

- Mucinous. Slow to medium growth speed. Hardy once established
- DMEM 1x (corning 10-013-CV)
- 15% FBS
- 1% Penicillin Streptomycin (Pen Strep/PS)

OVCAR 3 (Kindly donated from colleagues at Swansea University ILS1)

- High Grade Serous. Slow growing. Can be difficult to get going. But hardy once established
- RPMI 1640 (corning 15-040-CV)
- 20% FBS
- 1% Penicillin Streptomycin (Pen Strep/PS)
- 0.01 mg/ml bovine insulin (500ul in 500ml) (Sigma 19278 5ml)

2.2.1.2 General cell culture

All cell culture is carried out in an aseptic environment inside a class II laminar flow biosafety cabinet. Different cells require different media (see section 2.2.1.1) and can vary in their hardiness, behaviour and requirements. For example, SKOV-3 cells are fast growing, hardy and can grow when cells are at a low density, whereas OVCAR-3 are slower growing and prefer to be seeded at a higher density. The following section describes generic cell culture techniques including raising from liquid nitrogen, passaging and freezing down for liquid nitrogen storage.

2.2.1.2.1 Raising from liquid nitrogen storage

Cells are stored in liquid nitrogen for long term storage in a 2 ml cryogenic *vial*. The correct media is warmed to 37°C in a water bath, materials are gathered in the biosafety cabinet and everything is sprayed with 70% ethanol before defrosting the *vial* for the minimum amount of time (approximately 1 minute) in a 37°C water bath.

Once defrosted the contents of the tube are added to a 30 ml universal tube with clean media. The cryogenic *vial* is washed with media twice to ensure no cells are left behind. The cells suspended in media are centrifuged at 300 g for 2 minutes and the supernatant is discarded. The pellet is resuspended (ensuring a homogenous solution as far as possible) in fresh warm media and transferred to a flask. The size of the flask is chosen based on how many cells there are however usually this is a T25. If the flask is too big and the cells to few then the cells will have difficulty growing or may not grow at all. The flask is labelled with the person's name, the date, the contents and the passage number before placing it in a humid incubator at 37°C and a 5% CO_2 atmosphere. When the cells reach confluency 80-100% the cells are either used in their intended experiment or split as detailed in section 2.2.1.2.2 or frozen down again as in section 2.2.1.2.3.

2.2.1.2.2 Passaging/Splitting

Once cells are 80-100% they need to transferred to a larger flask or maintained in the same size flask. Materials should be gathered, media, PBS should be pre-warmed to 37°C and everything should be sprayed with 70% ethanol before beginning.

The current media in the flask is discarded and the surface the cells are growing on is gently washed twice with warm PBS. Enough trypsin is added to the cells to cover (500 μl -3 depending on flask size). The flask is placed at 37°C for a maximum of 5 minutes. Incubation times longer than 5 minutes can dehydrate and have a detrimental effect on the cells. After this incubation, the flask is manually agitated by clapping the flask to your hand. A microscope is used to check all the cells have detached. Media is added to the flask containing the trypsin and cells and the pipette is used to draw solution up and squirt onto the surface where the cells grew to help dislodge any remaining cells. This is done several times before the solution is transferred to a clean 30 ml universal tube. The tube is centrifuged at 300 g for 2 minutes, the supernatant is discarded and the pellet (see section 2.2.1.2.3) is ready to be resuspended in clean media and added to a new flask. If moving to a larger flask size then all the cells are transferred. If the intention is for one flask to become two, then the resuspended cells are divided equally between

the flasks. If the cells are being maintained in the same size flasks then some cells should be discarded (or frozen down – see section 2.2.1.2.3) and the remaining cells transferred to a clean flask of the same size. All flasks make are incubated until 80-100% at 37°C and 5% CO2.

2.2.1.2.3 Freezing down cells for storage at -80°C

Cells were trypsinised as described in section 2.2.1.2.2 up to (*). The cell pellet was resuspended in FBS with 10% DMSO and 1ml aliquoted into cryogenic *vial*s and quickly moved to a Mr Freeze isopropanol storage container at -80°C. After 24h the *vial*s are moved to liquid nitrogen storage where they can be raised for use in experiments are detailed in section 2.2.1.2.1.

2.2.2 Culture of primary cells

Primary patient cell culture is largely the same as the cell culture techniques described in this section with some small extra considerations. Primary patient cells are obtained using the methods described in section 2.1.3 and when culturing work is always carried out in separate space to the culture of non-primary cells. Primary cells are healthier and more reliable when they are seeded at a higher density, therefore before splitting primary cells should be left until they are 100% confluent. Finally, primary cells derived from patient tissue all behave in different ways. There is a huge variety in growth speed, morphology etc between cells deriving from different patients. Media is 1:1 MCDB 105 (Sigma M6395-1L) with final concentration of 1.5 g/l of Na_2CO_3 (17ml in 1L) and Medium 199 with final concentration of 2.2 g/L of Na_2CO_3 (13ml in 500ml), 20% FBS and 1% antibiotic. The passage number of primary cells is important to consider. Cells derived from a primary biopsy are frozen down as soon as possible as it is advantageous to keep the passage number low (below 9) to avoid mutations as a result of over passaging (428).

2.2.3 Introduction to other cell lines

The Human Embryonic Kidney 293T (HEK293T) (Kindly donated by colleagues at Swansea University ILS1 lab) is used in this project as a cell type that was not related to female reproductive tissues. HEK293T is cultured in the same media as the UACC and UWB1 cell lines (see section 2.2.1.1). They are very fast growing to the point they can overgrow very easily. They are morphologically very small round cells that detach very easily and can peel off in a large layer if they overgrow. These HEK293T cells were used in the basal expression (localisation) immunofluorescence experiments and were not included in the following internalisation experiments.

2.3 Isolation and quantification of protein

Protein was extracted from is grown to 80-100% confluency. The flask is removed from the incubator and the protein extraction is carried out on an open bench top.

The current media is discarded and the surface the cells are growing on is washed gently twice with PBS. All PBS is discarded and the flask is positioned so any remaining PBS can drain into one corner. This PBS is removed and Radioimmunoprecipitation assay buffer (RIPA) buffer (50 mM Tris-HCL-pH 8.0, 150 mM NaCl, 1% Nonidet P-40 (NP-40), 0.5% sodium deoxycholate, 0.1% sodium dodecyl sulphate (SDS), 1nM sodium orthovanadate, 1mM NaF) with Holt™ protease (Thermo Fisher, catalogue number: 78442) inhibitor 100x to a final concentration of 1x is added. All the PVS must be removed because PBS will cause the final volume to be higher and the sample more dilute. With the RIPA/Holt™ added, the cell scraper is used to manually dislodge the cells. The surface should be scraped thoroughly, and everything pushed into one corner. As before the flask is positioned so everything can drain into one corner. The mixture is then transferred to a microcentrifuge tube and left on ice for 30 minutes with pulse vortexing every 5 minutes. After 30 minutes the tube is centrifuged at 4°C for 10 minutes at top speed. The supernatant is collected carefully, without disturbing the pellet, and transferred to a clean, labelled microcentrifuge tube. The protein is then be stored at -20°C for the short term, stored at -80°C for long term or quantified before storage. Freeze-thaw cycles should be avoided.

Protein quantification

Protein is quantified using the BioRad DC assay (Kit II 5000112). The BSA (Pan Biotech P061391050) standards are made up to the range the protein concentration is expected to fall in. In this case eight BSA protein standard were made (0, 0.5, 1, 1.5, 2, 2.5, 5, 10 mg/ml) in RIPA buffer. RIPA buffer is the cell lysis buffer used to extract protein from cells, therefore this same buffer is used to dilute the protein standards. 5 µl of each standard/sample are plates in duplicate and 25 µl of reagent A' is added to each well. A' is made by adding 20 µl of reagent S per 1 ml of reagent A. 200 µl of reagent B (light sensitive) is added to each well and the plate is protected from light and left with gentle agitation for 15 minutes. After 15 minutes the wells should have turned from yellow to blue. Bubbles should be popped with a small needle. Any wells that are not properly mixed (green colour) should be manually mixed with a pipette without contaminating other wells. The plate must be read within 30 minutes. The plate is read at 750 nm on a FLUOstar Omega plate reader (BMG Labtech). Raw data is interpreted by the MARS software (BMG Labtech) to give a standard curve. The r max of the standard curve should be as close to 1 as possible to indicate the standards are correct. The mars wizard is used to

create a 4-parameter fit curve to which all the samples are compared against. The standards should be accurate for the quantification of the samples to be reliable.

2.4 Western blot

Quantified protein is run on an SDS page gel to separate protein by size before probing with the antibody of interest to determine protein expression of the target protein in the given protein sample.

2.4.1 Western blot buffers

Running buffer 10x (Tis/Glycine/SDS 10x) 250Mm Tris (pH 8.3), 1.92M Glycine, 1% (w/v) SDS – store on bench (rt)

30.3g Tris Base (Melford T60040-5000.0)

144.1g Glycine (Melford G36050-5000.0)

100mL 10% (w/v) SDS or 50mL 20% (w/v) SDS (Severn Biotech 20-4002-10)

ddH2O to 1L

pH 8.3

Running Buffer 1x- 25mM Tris (pH 8.3), 192mM Glycine, 0.1% (w/v) SDS

100mL Tris/Glycine/SDS 10x

900mL ddH2O

Wash buffer 10x (TBS 10x) 200mM Tris (pH 7.6), 1.37M NaCl – store on bench (rt)

24.2g Tris Base

80.1g NaCl (Sigma Aldrich S7653 1kg)

ddH2O to 1L

HCl to pH 7.6 (adjust pH dropwise)

Wash Buffer 1x (TBS/T 1x)- 20mM Tris (pH 7.6), 125mM NaCl, 0.1% (v/v) Tween20

100mL TBS 10x (pH 7.6)

1mL Tween20 (Sigma Aldrich P1379-25ML)

ddH2O to 1L

BSA Blocking Buffer – 20mM Tris (pH 7.6), 137mM NaCl, 5% (w/v) BSA, 0.1% (v/v) Tween20 – store at 4°C

12.5g BSA (Pan Biotech P061391050)

TBS/T to 250mL

*Non-fat milk can be substituted here if needed

Stripping Buffer- 200mM Glycine (pH 2.2), 0.1% (w/v) SDS, 1% (v/v) Tween20

3.8g Glycine

2.5mL 10% (w/v) SDS

2.5mL 10% (v/v) Tween20

ddH2O to 250mL

HCl to pH 2.2

2.4.2 Western blot protocol

Quantified protein is prepared by transferring the correct volume for 30 µg into a PCR tube. The proteins are all made up to the same volume using RIPA buffer to ensure uniform running on the gel. Laemmli buffer (BioRad 1610747) -2-mercaptoethanol mixture is prepared by adding 100 µl of 2-mercaptoethanol per 900 µl of laemmli and added to a final concentration of 1x to the protein samples. The samples are then heated using a hot plate or PCR machine to 95°C for 5 minutes. Whilst this short incubation is occurring the western blotting cassette (Mini Trans-Blot Cell and PowerPac Basic Power Supply BioRad 1703989) is assembled. The precast gel (BioRad, 4–20% Mini-PROTEAN® TGX™ Precast Protein Gels, 10-well, 50 µl #4561094) is prepared by removing the green strip from the bottom of the gel and being inserted into the cassette. The middle of the cassette is filled with running buffer and some time is allowed to ensure no leakage. The comb is removed carefully ensuring the delicate wells are not damaged and 3 µl of precision plus dual protein ladder (BioRad, #1610374) is added to the first lane followed by the samples. The powerpack is set at 120 v for 30 minutes and the gel front should run to the black line at the bottom of the gel before stopping. The gel must not overrun.

When the gel has finished running it is removed from its plastic case and placed in a Trans-Blot Turbo Midi 0.2 µm Nitrocellulose Transfer Pack. The package is placed inside the Trans-Blot Turbo machine and run on the programme for 1 mini TGX gel. The protein has transferred to a membrane and this membrane is quickly submerged in blocking buffer (BSA or Milk) to prevent it from drying out from the heat remaining from the transfer process. The membrane is blocked for 1 hour at room temperate on a plate rocker with gentle rocking. After 1 hour the blocking buffer is replaced by the primary antibody diluted in the blocking buffer. Antibody dilution is antibody dependent. The membrane in the primary antibody is incubated either at room temperature for 1 hour or overnight at 4°C.

After incubation with the primary antibody, the antibody solution is discarded, and the membrane is washed in wash buffer 1x (TBS/T 1X) with strong agitation for 30 minutes with fresh wash buffer every 5-10 minutes. During this time the appropriate species of secondary antibody labelled with horse radish peroxidase (HRP) is diluted in blocking buffer 1/2000. The membrane is incubated with the secondary antibody for 1 hour at room temperature with gentle rocking before the wash process is repeated to remove any unbound antibodies. The

membrane is incubated with Clarity™ Western ECL Substrate (BioRad UK 1705060) for 1 minute before using the BioRad ChemiDoc™ Imaging system with Image Lab software (BioRad UK) to visualise the membrane.

The membrane is then stripped of all antibody using stripping buffer and the process above is repeated with Glyceraldehyde 3-phosphate dehydrogenase (GAPDH) as the primary antibody. GAPDH is commonly used as a 'housekeeping' gene both here in western blot and in qPCR because the GAPDH gene is stably expressed at high levels in many tissues and cells. In this context, because of the stability GAPDH has between different tissues and cells, GAPDH is used as a loading control to confirm the same amount of protein has been loaded into each well. This allows for errors in protein quantification and loading errors.

The Software Image Lab (BioRad version 6.0.1) was used to quantify the bands and a ratio of target band: GAPDH was taken to normalise the protein samples. SPSS (version 26.0.0.0) was used to compile graphs and perform statistical analysis.

2.5 Confocal microscopy

The confocal configurations were set up for detecting a Texas Red™ fluorophore. Texas Red™ has an excitation max of 596 nm and an emission max of 615 nm. The 594 laser on the confocal microscope was used and the wavelengths adjusted to ensure minimal cross over with the 488 laser. The 488 laser was picking up Wheat Germ Agglutinin (WGA), Alexa Fluor™ 488 Conjugate (Thermo Fisher Scientific W11261) as a membrane control stain with an excitation/emission maxima of 495/519 nm. WGA lectin binds to sialic acid and N-acetylglucosaminyl residues. Both the Texas Red™ and the WGA configurations were adjusted to make sure they did not cross talk with the DAPI nuclei stain Hoechst 33342, Trihydrochloride, Trihydrate - 10 mg/mL Solution in Water (Thermo Fisher - H3570).

2.5.1 Basal expression assay

The basal expression assay visualises where in the cell the target protein is located. Cells are plated in 8-well Chambered Coverglass w/ non-removable wells (Thermo Fisher UL 155411PK) in the amounts shown in **Table 2-2** and left to grow for 48 hours to reach 80-100% confluency.

Table 2-2 – Number of cells plated in one well of an 8-well Chambered Coverglass

Cell type	Number of cells plates per well
IOC	10,000
TOV21G	15,000
TOV112D	15,000
UACC	15,000
UWB1	15,000
SKOV-3	15,000
COV-664	30,000
OVCAR	30,000
Primary patient cells	30,000
HEK 293T	10,000

Cells are cleaved from the flask and centrifuged to a pellet as in section 2.2.1.2.2. Cells are counted by pipetting 10 µl of fully homogenised cells in media onto a Cell Counting Slide for TC10™/TC20™ Cell Counter (BioRad – 1450011) and read using a TC20 cell counter (BioRad). A media solution containing the correct number of cells is made from the 'stock' solution of counted cells and plated in the well of the 8-well Chambered Coverglass slide. The cells are incubated in a 37°C 5% CO_2 environment for 48 hours. After checking the cells are attached and healthy the cells are prepared for the basal expression assay. The live cells are stained with WGA first to give the clearest results. The WGA is diluted 1/700 in PBS and incubated with the cells for 5 minutes at 4°C. This short incubation time at this low temperature on live cells prevents the WGA from entering the cell and staining the cytoplasm as much as possible while still staining the membrane. This allows for a clearer visualisation of the membrane under the confocal microscope. Immediately after WGA, the cells are gently washed once with PBS before incubating with 5% paraformaldehyde (PFA) for 20 minutes at room temperature. This fixes the cells, freezing them in time so they can remain the same for observation under the confocal microscope. Fixation preserves the cells by preventing autolysis and putrefaction while also freeing any biochemical processes. This allows observation at a fixed moment in time. After this step, the PFA is removed and Triton X-100 0.1% is added for 5 minutes at 4°C. Triton X-100 is a detergent used for permeabilising the cells membrane. This makes small holes in the membrane which antibodies can pass through to attach to their target. After permeabilising, the cells are washed gently once with PBS before 3% BSA is added for 1 hour at room temperature. The BSA acts as a blocker and binds to any available proteins. After 1 hour the blocking buffer is removed and the primary antibody is added and incubated overnight at 4°C. The primary antibody of interest is diluted in a blocking buffer. The dilution is antibody-dependent as per the manufacturer's direction. The following day the primary antibody is removed and the cells are washed gently 4x with PBS to remove any unbound antibody. The secondary antibody (diluted

in blocking buffer) is then added to the cells for 1 hour at room temperature. The secondary antibody is species specific and is attached to a Texas Red™ fluorophore to allow visualisation. After 1 hour the secondary antibody is removed and the cells are washed gently 4x with PBS to remove any unbound secondary antibody. The cells are incubated with a nuclei stain Hoechst for 5 mins. Hoechst is diluted 1/4000 in PBS and removed after incubation and replaced by PBS only to increase clarity under the confocal microscope. The cells are taken to the confocal microscope where they are viewed using the appropriate laser. Photographs are taken using the Zeiss Zen software.

2.5.2 Indirect internalisation assay

Indirect internalisation aims to show if the antibody is being internalised into the cell by live cells. This is an indirect method as after the internalisation has taken place, the cells are fixed, permeabilised and a secondary antibody is used to visualise those antibodies which have internalised. The target antibody does not itself fluoresce.

The cells are plated and grown as above in section 2.5.1. Once the cells are 80-100% confluent they are incubated with the primary target antibody at 50 µg/ml for 30 minutes on ice and then a further incubation of 1-24 hours at 37°C 5% CO2 environment. The initial 30 minutes on ice allows the antibodies to find their receptor (the target antibody) to allow for a more intense, uniform internalisation when the cells are moved to 37°C. After internalisation incubation the cells are fixed and permeabilised using the method described above in section 2.5.1 with PFA and Triton X-100. The cells are then incubated with the appropriate Texas Red™ secondary antibody for 1 hour at room temperature before being washed gently 4x with PBS. The cells are incubated with 1/4000 diluted Hoechst for 5 minutes at room temperature before the Hoechst is replaced by PBS and the cells are viewed on the confocal microscope and photographed using the Zeiss Zen software.

2.5.3 Internalisation assay using pH reactive amine dye

Internalisation using a pH reactive dye is a direct method of visualising internalisation because the antibody itself is conjugated to a pH reactive fluorescent dye. Two methods are available for conjugating the antibody to the pH reactive dye, on bead conjugation and in solution conjugation.

2.5.3.1 On bead conjugation

Promega pH reactive amine dye (G9841) is conjugated to the primary antibody using Promega Magne® Protein A magnetic beads (G8781) and a magnetic separation stand (Promega- Z5342).

Table 2-3 - Buffers and solutions for pH reactive amine dye

Buffer name	Buffer purpose	Buffer composition
Amine conjugation buffer (10mM sodium bicarbonate buffer)	To prepare the beads for addition of amine dye to provide optimal conjugation conditions	0.084g sodium bicarbonate dissolved in deionised water. - pH adjusted to 8.5 - Volume adjusted to 100ml
Antibody bind buffer (10mM phosphate buffer)	To equilibrate the beads ready for the addition of antibody and to wash away any unbound material	0.0378g sodium phosphate, monobasic, monohydrate 0.195g sodium phosphate, dibasic, heptahydrate - Dissolved in deionised water, adjusted to pH7 - Final volume made to 100ml with deionised water
Elution buffer (50mM glycine-HCL)	Acidic solution (below pH 3) to elute antibody from beads	0.118g glycine - Dissolved in deionised water - pH adjusted to 2.7 with 37% HCL - Final volume adjusted to 50ml with deionised water
Neutralisation buffer (2M tris buffer)	To neutralise the acidic elution buffer for safe addition to live cells	0.472g trizma base 2.54g trizma hydrochloride - Dissolved in deionised water - pH adjusted to pH 7.5 - Final volume adjusted to 10ml with deionised water

A total of 100 μg of antibody is conjugated to 50 μl of protein A magnetic bead slurry for 60 minutes at room temperature using a wheel end over end mixer.

50 μl of the beads are washed/equilibrated in a 1.5 ml microcentrifuge tube with 250 μl of antibody bind buffer. This is placed in the magnetic stand and the buffer discarded. 1 ml of a sample containing 100 μg of antibody is added and the bead/antibody solution is mixed on a wheel end over end mixer for 60 minutes at room temperature. The supernatant is removed using the magnetic stand and the beads are washed with 250 μl of antibody bind buffer and then amine conjugation buffer. All buffer is removed from the beads and 100 ul of amine

conjugation buffer is added. The amine pH reactive dye is prepared fresh by reconstituting to 10 mg/ml by adding 25 µl of 1:1 DMSO:water mix to 0.25 mg of dye. 1.2 µl of this dye is added to the beads and this is mixed at room temperature for 60 minutes. The tube is placed on the magnetic stand and the supernatant removed. The beads are washed with antibody bind buffer twice, with the buffer completely removed after each wash. Finally, the antibody is eluted in 100 µl elution buffer (pH 2.7) and quickly neutralised with 5 µl of neutralisation buffer. The concentration and DAR are calculated using the methods described below in section 2.5.3.3.

2.5.3.2 In solution conjugation

A buffer exchange is carried out initially to remove any storage buffer such as sodium azide from the antibody solution. The buffer exchange is carried out using a Zeba™ columns from Pierce, Cat.# 87766 or similar. The pH dye is prepared fresh as described in the above section 2.5.3.1 and 1.2 µl is added per 100 µg of antibody. The antibody and pH dye are incubated together using an end over end mixer for 60 minutes and the unconjugated dye is removed by another desalting column. The concentration and DAR are calculated using the methods described below in section 2.5.3.3.

2.5.3.3 Quantification of conjugated antibody

The antibody concentration in mg/ml was calculated by taking two readings using a nanodrop at 280 nm and 532 nm. The following equation was used:

$$\text{Antibody Concentration (mg/ml)} = \frac{A_{280} - (A_{532} \times 0.256)}{1.4}$$

The Dye to Antibody ratio (DAR) was calculated by the following equation:

$$\text{Dye-to-Antibody Ratio (DAR)} = \frac{(A_{532} \times 150{,}000)}{\text{Ab Concentration (mg/ml)} \times 75{,}000}$$

Where:

Molecular weight of antibody = 150,000 Da

Extinction coefficient of pHAb Reactive Dye = 75,000

Correction factor for pHAb Reactive Dye = 0.256

The DAR shows how many pHAb Reactive Dye molecules are attached to 1 antibody and the concentration allows the addition of the correct dilution of antibody uniformly across all experiments.

The pH response of the conjugated antibody can be measured to ensure the fluorescent properties have been retained throughout the conjugation process. Antibody conjugated to a pHAb Dye should have an increased fluorescence in an acidic environment. The antibody-pHAb Dye fluorescence response was measured at pH 4 and pH 8 by adding 1 µl of antibody-pHAb Dye to 100 µl of either 100 mM citrate buffer or to 100 µl of 100 mM phosphate buffer. The response is read on a fluorescence reader at Ex 532 nm/Em 569 nm. The fold increase in fluorescence is calculated by using the following equation:

$$\text{Fold increase} = \frac{\text{Fluorescence of antibody-pHAb (pH 4)} - \text{Fluorescence of blank wells (pH 4)}}{\text{Fluorescence of antibody-pHAb (pH 8)} - \text{Fluorescence of blank wells (pH 8)}}$$

2.5.3.4 Internalisation using antibody-pHAb Dye

2D cells were grown in replicates of 5 in a LabTek 8 well chambered cover glass slide (Thermo Fisher UK 155411PK) and incubated with the TSPAN6, RAGE HA9, PCSK4 and IgG antibody-dye conjugates for 30 minutes on ice. After this initial incubation period to allow the antibodies to bind to the membrane, the cells were placed at 37°C for 4 hours. Antibody-dye conjugates then internalised more uniformly this way with a better chance of seeing more intense fluorescence. The incubations were staggered to allow imaging with the confocal microscope to take place in quick succession whilst still ensuring each well had the same 4 hours of incubation. After incubation, the antibody-dye conjugate was removed from the cells and the cells were stained with DAPI (Hoechst) for 5 mins before removal of DAPI and addition of PBS to image the cells. The cells are taken directly to the confocal for viewing. No fixation or permeabilization is carried out. Photographs are taken using the Zeiss Zen software.

Image analysis was performed using CP open-source software (McQuin *et al*., 2018). LSM files, containing two image channels were uploaded to CP. DAPI DNA stained images were assigned to the DNA image set and TexasRed internalization images were assigned to the 'internalization' image set. To identify individual nuclei within each image of the DNA image set the following steps were performed. Firstly, a median filter was applied to remove background noise using the CP 'Smooth' module. The filter diameter was set to five pixels. Secondly, nuclei regions were identified by applying an intensity threshold to the image using the CP 'IdentifyPrimaryObjects' module. Intensity thresholds for each image were automatically calculated using the minimum

cross entropy algorithm. Individual nuclei were identified by connected pixels in the thresholded image. The number of nuclei present in each image was calculated using the CP 'MeasureObjectIntensity' module. To quantify antibody internalization, first a median filter was applied to images in the internalization image set to remove background noise, using the CP smooth module. Then regions of high stain intensity above the background were identified in the same way as nuclei, applying an intensity threshold using CP 'IdentifyPrimaryObjects'. Finally, the stain intensity of the image was calculated as the sum of the pixel intensities in all high stain intensity regions. Copies of the original images with the segmentation outlines super imposed were saved to disk, to allow manual inspection of the segmentation. Images with poor segmentation results in either the DAPI or TexasRed channels were removed.

2.6 DNA extraction and quantification

DNA extraction from primary patient tissue biopsies was carried out using the Qiagen DNeasy Blood & Tissue Kits 69504. The extraction was carried out as per the manufacturer's instructions included in the protocol. The tissue was chopped as small as possible before buffer 180 ul ALT (a lysis buffer) was added to the tissue sample with 20 ul proteinase K and incubated with strong agitation at 56°C for at least 2 hours until completely lysed. The proteinase K is a protease that digests, in this case, nucleases that can attack and digest the nucleic acids present in DNA. 200 ul of ethanol and 200 ul of buffer AL are added and the solution is run through a spin column by adding and centrifuging at 6000 x g for 1 minute. The column membrane is then washed twice with two different buffers AW1 and AW2 by adding, centrifuging at 6000 x g for 1 minute and discarding the flow through. The spin column is transferred to a fresh labelled microcentrifuge tube before 50 ul of elution buffer is added, incubated for 1 minute at room temperature and centrifuged at 6000 x g to retrieve the eluted DNA.

2.6.1 PCR primer design

Primers were designed for the RAGE and TSPAN6 antibody epitope DNA coding sequence using Primer Blast (429). The DNA sequence chosen included the epitope and the flanking sequence which resulted in a total of 300-400 bases being used to design the primers. The minimum product size was set to 250 bases and the 'Genomes for selected organisms' database was selected. The organism was set to Homosapiens and the search was carried out. The search returned 10 suggested primer pairs and the primers were chosen based on a product size of

approximately 350 base pair and based on the lack of any possible off target products that were of a similar size to the band of interest.

The primers used in the following analysis are as follows in . The primers described below contain the adapter sequences: 5'- CTGTCTCTTATACACATCT -3'

Table 2-4 – Primers used for RAGE and TSPAN6 antibody epitope DNA coding sequence amplification

RAGE forward primer	5'-TCGTCGGCAGCGTCAGATGTGTATAA GAGACAGTTCCCTTCCTACCCCTCTACC-3' (54)
RAGE reverse primer	3'-GTCTCGTGGGCTCGGAGATGTGTATA AGAGACAGGCAGGGCCTAAACAGTGCAA-5' (55)
TSPAN6 forward primer	5'-TCGTCGGCAGCGTCAGATGTGTATAA GAGACAGTTATTTTCTGGATCACTGGCGT-3' (55)
TSPAN6 reverse primer	3'-GTCTCGTGGGCTCGGAGATGTGTATA AGAGACAGGAAAACAAATCCTACGATGGCA-5' (56)

2.6.2 PCR optimisation

DNA was extracted from SKOV-3 cells using the Qiagen DNeasy Blood and Tissue DNA extraction column-based kit (catalogue number: 69504). SKOV3 cells were grown as 2D monolayers and DNA extracted and used it as a template for PCR amplification reaction, using a four-temperature gradient and Qiagen HotStartaq (Catalogue number: 203443). The PCR conditions can be seen in .

Table 2-5 – PCR conditions for annealing temperature optimisation

Step	Temperature	Time	Cycles
Initial heat activation	95°C	15	1
Denature	94°C	30 seconds	
Anneal	70°C, 62°C, 53°C and 50°C	1 min	
Extension	72°C	1 min	35
Final extension	72°C	10 min	1

Eight reactions were set up in total. Four with the RAGE primers at the four different temperatures and four with the TSPAN6 primers at the four different temperatures. The aim was to see which temperature amplified the DNA most effectively. **Figure 2-1** shows the eight reactions run on a 1% agarose gel by gel electrophoresis. It can be seen that annealing temperatures 70°C and 62°C did not produce a band compared to 50°C and 53°C which produced a single band at the expected size.
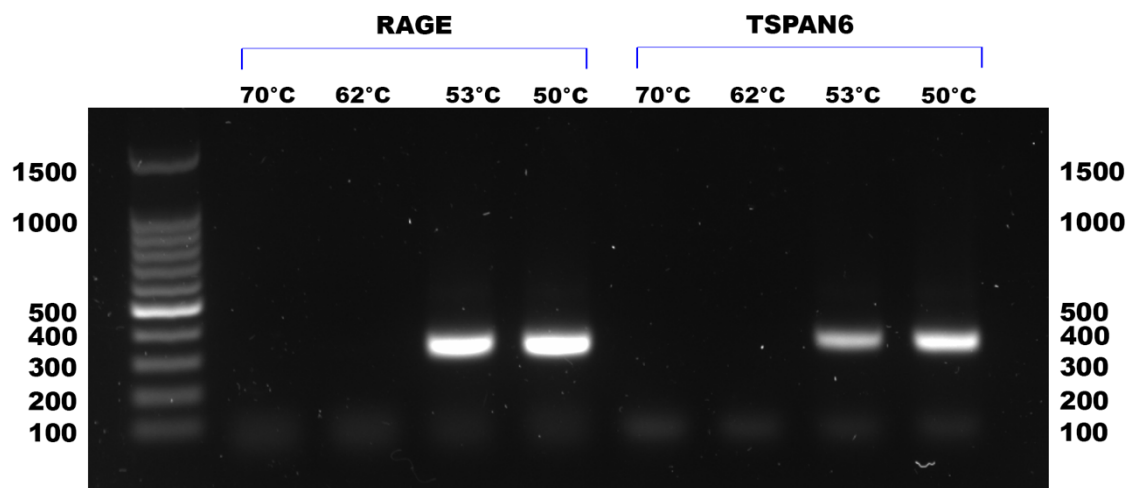
Figure 2-1 – Agarose gel electrophoresis of RAGE and TSPAN6 annealing temperature optimisation PCR products

To ensure the PCR product was the intended sequence, the PCR products were purified using sodium acetate and sent for Sanger sequencing (LGC). As expected, the 70°C and 62°C did not produce a read for either TSPAN6 or RAGE and the 50°C and 53°C aligned with the TSPAN6/RAGE reference sequence.

Therefore, the annealing temperature of 50°C was chosen for the final PCR amplification due to being the most intense band on the gel and its correct alignment to the reference sequences for both targets.

2.6.3 PCR amplification

The DNA was extracted from 95 patient biopsies and from the 2D cultured cells of one OC cell line (SKOV-3) using the Qiagen DNeasy Blood and Tissue DNA extraction column-based kit (catalogue number: 69504). 95 patients plus one cell line were chosen to comply with the 96 well plate format for the following experiments. The 95 patients included all non-cancer patients, any patients of rare subtypes (such as endometrioid or clear cell OC) and a representative cohort of patients with various OC pathologies.

The DNA coding sequence for both the RAGE and the TSPAN6 antibody epitope was amplified in 96 DNA samples by PCR using the conditions described in **Table 2-6**.

Table 2-6 – PCR conditions for amplification of 96 DNA samples for NGS analysis

Table 2-6 – PCR conditions for amplification of 96 DNA samples for NGS analysis

Step	Temperature	Time	Cycles
Initial heat activation	95°C	15	1
Denature	94°C	30 seconds	
Anneal	50°C	1 min	
Extension	72°C	1 min	35
Final extension	72°C	10 min	1

The amplified DNA was run using agarose gel electrophoresis to check the amplification had been performed correctly. A 1% agarose gel was made using TAE (40 mM Tris-acetate, 1 mM EDTA). 1 µl of a random selection of wells was added to the gels with 6x loading buffer. The gel was run until the bands could be seen clearly and the gel was photographed using BioRad ChemiDoc™ Imaging system with Image Lab software (BioRad UK).

A small selection of the amplified DNA was run on a gel to confirm successful amplification as can be seen in **Figure 2-2**. A band of varying intensity can be seen in all the randomly selected samples across the gel. This indicates that the DNA templates were successfully amplified in these samples and therefore requirements were met for the progression to NGS.
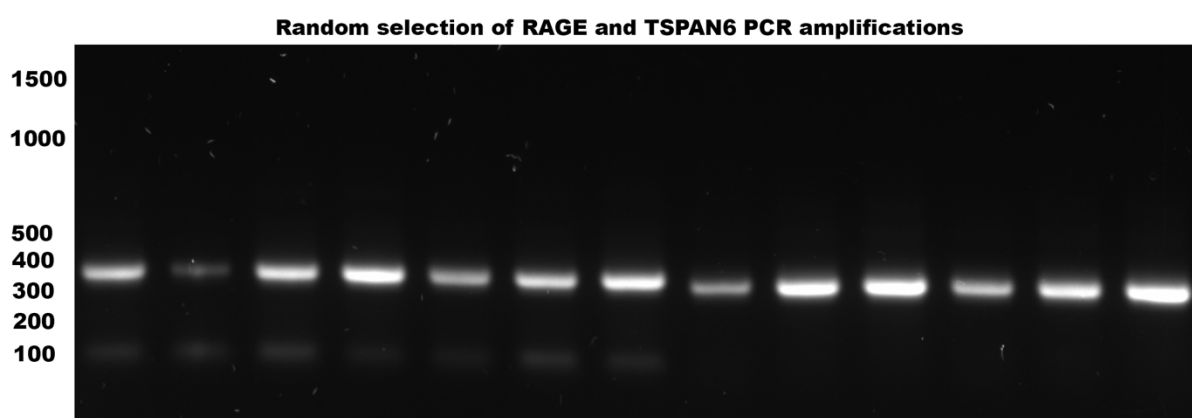
Figure 2-2 - Agarose gel electrophoresis of randomly selected RAGE and TSPAN6 PCR products

The gel above shows a random selection of PCR products from the RAGE and TSPAN6 PCR amplification. A random selection of amplified product from different areas of the plate were separated by size on a 1% agarose gel. A single band was observed at the expected size between 300 and 400 base pairs. This suggests that the PCR amplification was successful, and the requirements were met for the progression to NGS.

2.6.4 Deep amplicon variant analysis

The amplified DNA was sent to Swansea University Sequencing facility for NGS analysis on all samples. The resulting data reads were subjected to a quality control process where any reads of poor quality were removed.

The reads to be analysed were returned using a server on a virtual machine (Host: 137.44.59.134. Username: ubuntu) due to the large size of the files. The data was analysed on an iMac (macOS Catalina version 10.15.6) using Terminal. The server was accessed, and basic command line and Unix commands were used to carry out deep amplicon variant analysis on the reads obtained from NGS analysis. Files were retrieved from the server using FileZilla Client (version 3.48.1). The RAGE analysis and TSPAN6 analysis was carried out separately, one after the other, with all the RAGE and TSPAN6 reads and files having their own separate folder on the server.

2.6.4.1 Quality filtering

Before alignment to the reference sequence, adapter and quality filtering was carried out to maximise the quality of the reads. The tool 'Sickle' takes as input the paired end reads looking for the forward read and the reverse read. It uses Sanger based phred scores and outputs the reads as forward and the paired reverse read. This process was streamlined by creating a list of files that needed filtering and using a "for loop". The list file was created by listing all the samples that contained the syntax R1 or R2. The sample name is separated from the rest of the read name by an underscore (_), therefore the files can be listed using the *ls* command but instead of writing to the screen the output can be piped into another command. That other command is the *cut* command, where the underscore is used to break apart the file name and take only the first field. The command used to carry this out was - *ls -1 *R1*.fastq.gz | cut -d_ -f1.* This can be outputted to a file using the command *ls -1 *R1*.fastq.gz | cut -d_ -f1 > samples.txt.*

Initial primer overhangs (described in Chapter 2) were added to the initial primer design in order for additional adapters to be added as part of NGS sequencing protocol to allow the binding of the DNA to the flow cell on the Illumina platform. For analysis, these sequences need to be removed. The tool *scythe* was used to accomplish this task. The sequence adapter was disclosed to the scythe tool using the command *>nextera CTGTCTCTTATACACATCT.* A new file containing the adapter sequence was created using the tool *nano*. The copied nextera sequence was pasted into the text editor *nano* and saved as a text file.

The files could then be processed using a "for loop" and the command *vi qual_filt.sh.* This command takes the names from the list of files created earlier. The shell script command *sh*

qual_filt.sh is run and then sickle creates outputs for each of the reads that have had the adapter sequence trimmed off.

2.6.4.2 Read alignment

The processed reads needed to be aligned to a reference sequence. This alignment helps make sure the reads are properly aligned and that off target reads can be filtered out easily and it can help with the annotation process should any variant sights be found so that the effect of this variant can be predicted. The work was carried out inside a tmux window from this point onwards to prevent any internet connection problems killing the running commands. BWA, Samtools and bcftools were used to align reads against the reference, identify possible variant positions and finally to call variant positions.

The first stage was to index the reference sequence using the command *bwa index -p gr38 Hsapiens_GRCh38_chr6.fa.* This is the indexing of the RAGE reference sequence. The TSPAN6 reference sequence had a different file name but used the same command.

Another "for loop" script was created to align the reads against the indexed reference sequence. The command *vi mem_aln.sh* was used first followed by *sh mem_aln.sh* for all the samples. The inputs loop through and a BAM file is created for each sample. Now the reads are aligned and sorted against the reference sequence the alignments need to be indexed to speed up random access to the file. This was achieved by running the command *sh indexing.sh*.

2.6.4.3 Variant Calling

Mutations were detected within the amplicon data first by using "bcftools mpileup" to generate a pileup process which calculates genotype likelihoods at each genomic position using coverage information. This was followed by "bcftools call" to call the variants. This variant detection is carried out twice. First, using a method that outputs all alternative allele frequencies that pass all the filters for being a variant, these are often extremely low frequencies. Secondly a method was used that reports variants in a stricter manner where only true variants are called. The command *sh complete_pileup.sh* was used to output two VCF files for each sample, one multi-allelic and the other stricter.

2.7 Sanger sequencing

The amplified DNA from section 0 was prepared for Sanger Sequencing by LGC group ltd. The sequencing package chosen was Ready2Run by LCG and the samples were prepared as follows:

- In 1.5 ml microcentrifuge tubes

- Appropriately labelled

- 10 µl of plasmid DNA at 10 ng/ µl concentration

- 2 µl of each primer at 5 µM ≙ 5 pmol / µL concentration

- Total volume 14 µl

2.8 Next Generation Sequencing

Next Generation Illumina Sequencing was performed by Matthew Hitchings at Swansea University. More detailed information on Next Generation Sequencing data analysis methods can be found in chapter 6 section 0.

2.9 ELISA

A sandwich ELISA was performed using the serum described in the section 2.1.2. Human RAGE (Receptor for Advanced Glycation End products) Quantikine ELISA kit (R&D systems SRG00) was used to quantify the natural and recombinant RAGE present in the blood serum of patients recruited to the 'Identifying ovarian and blood biomarkers for ovarian pathologies' study, as can be seen in **Figure 2-3**. A monoclonal antibody, specific for the extracellular domain of RAGE, was precoated onto a microplate. Samples (serum), standards and controls were added to the wells and any RAGE present was bound by the immobilized antibody. After washing away any unbound substances, a polyclonal antibody conjugated to an enzyme was added to the wells. Any unbound substances were washed away and a substrate solution was added to the wells. Colour development is proportional to the amount of RAGE bound in the first step. The colour development was stopped and the colour intensity measured using a FLUOstar Omega plate reader (BMG Labtech) at 450 nm. Raw data is interpreted by the MARS software (BMG Labtech) and a 4-parameter fit is used by the MARS software to calculate a standard curve and subsequently the concentration of RAGE in the samples in pg/ml.
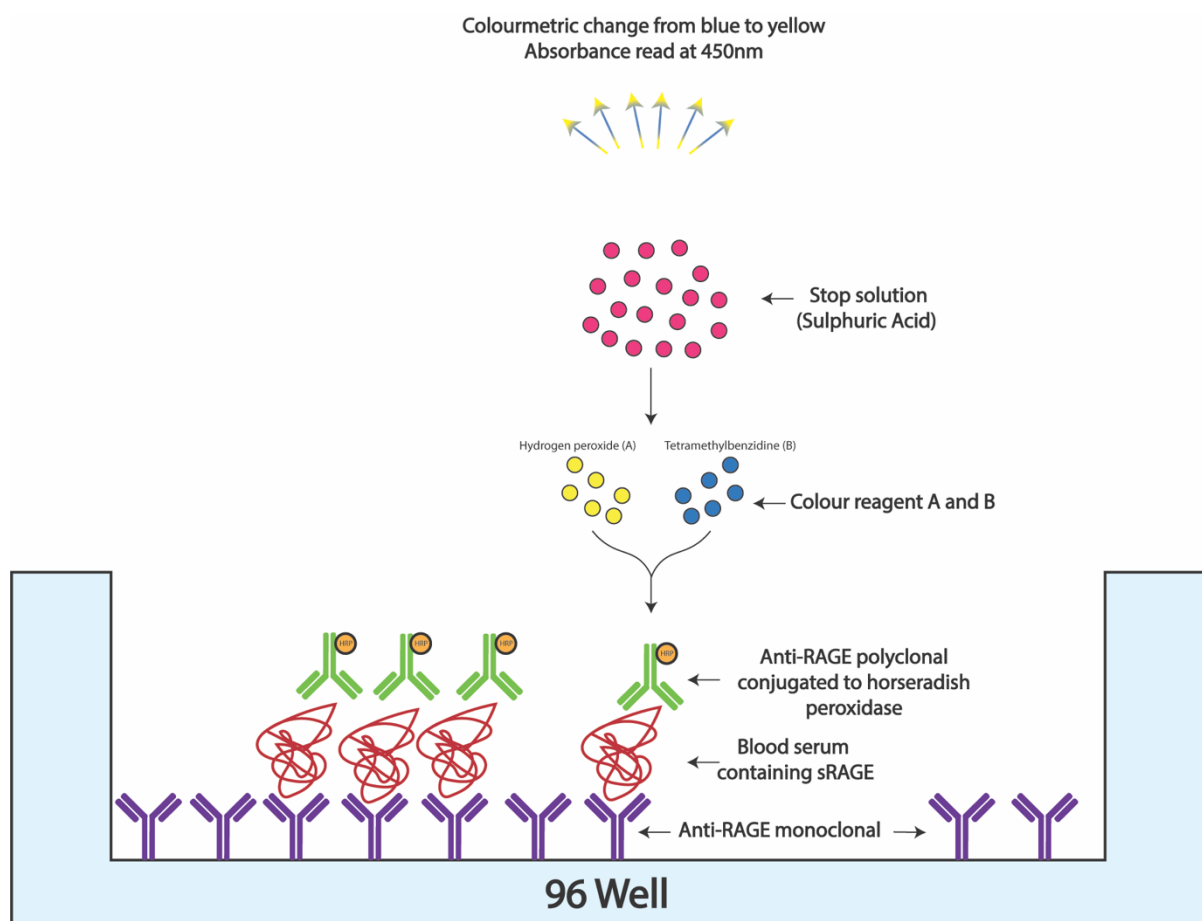
Figure 2-3 Schematic of the ELISA method (Image inspired by Immuno Assay Methods 2012 (430))

Human RAGE standards were prepared by serial dilution (5000, 2500, 1250, 625, 313, 156 and 78 pg/ml) from a 50,000 pg/ml stock in Calibrator Diluent RD6-10 containing sodium azide. Here Calibrator Diluent RD6-10 on its own served as the blank (0 pg/ml) standard.

Excess microplate strips were removed from the plate frame and stored at -4°C in preparation for the next ELISA. To the wells to be used 100 µl of assay diluent RD1-60 was added, followed by 50 µl of either sample (serum), standard or control. This plate was covered with an adhesive strip and left to incubate at room temperature for 2 hours. After the incubation, each well was aspirated and washed with 400 µl of wash buffer for a total of 4 washes. Following washing, 200 µl of Human RAGE conjugate (polyclonal antibody conjugated to Horse Radish Peroxidase specific for human RAGE) was added and the plate was sealed and left for another 2-hour incubation at room temperature. The plate was aspirated and washed 4 times as described previously and 200 µl of substrate solution is added to each well. The substrate solution is a 1:1 mixture of Colour Reagent A and Colour Reagent B provided in the kit. This is freshly prepared just before adding to the plate and light sensitive. The plate was incubated for 30 minutes at

room temperature, protected from light by aluminium foil. Finally, 50 μl of an acidic stop solution was added to each well and a colour change from blue to yellow was observed. The optical density of each well was read within 30 minutes using a FLUOstar Omega plate reader (BMG Labtech) at 450 nm. Wavelength corrected was set to 540 nm to correct for optical imperfections in the plate. The amount of RAGE in pg/ml was calculated by taking an average of the repeated measures, subtracting the blank and 540 nm value and creating a standard curve using the MARS Data Analysis Software (BMG Labtech) to generate a four-parameter logistic curve fit. Data was grouped and statistically analysed using SPSS version 26.0.0.0 statistical analysis software using a Mann Whitney U test or a T test. Normality was determined using the Kolmogorov-Smirnov test.

2.10 Statistical analysis

Statistical analysis and graph construction were carried out using SPSS version 26.0.0.0 analysis software. The data was assessed for normality using the Kolmogorov-Smirnov test. If $p = <0.05$ then the data was considered not normal and a Mann Whitney U test or a one-way ANOVA was performed. If the data was considered normal then a T test or Kruskal Wallis test was performed. In graphs generated using SPSS, outliers are indicated with a circle ° and far outliers, also described as extreme outliers are indicated with a star * (431). SPSS defines what is considered as an outlier or a far out/extreme outlier in the Exploratory Data Analysis (EDA) framework by John Tukey (432).

Chapter 3: Selection of putative ADC targets for ovarian cancer

3.1 Introduction

The discovery of novel targets for Antibody-Drug Conjugates (ADCs) development is essential for the development of efficacious targeted therapies for cancers with poor prognosis including ovarian cancer (OC). ADCs combine the specificity of a monoclonal antibody with the potent cytotoxicity of a chemotherapeutic agent. The advantages ADCs are hoped to provide are a reduction in toxicity, increased tumour selectivity, improved potency resulting in a faster recovery and fewer side effects for the patient. This has many benefits, beginning with a better prognosis, quality of life less stress for the patient. Additionally, this would have increased economic benefits for the UK and beyond as if patients recover faster, have fewer side effects and don't relapse then this will cost less in terms of treatment. This could result in more time and money being available for current patients and more money being available to improve what is already in place for many diseases.

ADCs achieve these advantages by being tumour specific. ADCs should bind and deliver their toxic payload to only the cancer cells – leaving the healthy cells unaffected. This is possible by discovering a unique cell surface fingerprint on tumour cells and designing an antibody against it. Once the antibody has been characterised and fully investigated it is linked to a potent cytotoxic chemotherapeutic agent. This ADC molecule then goes through many stages before it can reach the clinic, including cytotoxicity assays, animal models and finally clinical trials.

This project is at the very beginning of this pipeline to develop new ADC molecules. The discovery of the monoclonal antibody targets is an integral part of the whole process. The target chosen is the guide to the tumour cell, influencing tumour specificity, off target toxicity and the amount of drug that eventually reaches the tumour cell.

The aims of this chapter are to use available in silico data to identify novel cancer -enriched cell surface proteins, perform a literature search to confirm the novelty of the target and previously described functions and finally provisionally screen these protein targets to determine if they are worthy of further exploration as potential drug targets, markers of disease a state or for use in patient stratification.

Initially, six novel candidate targets were identified and published data supported their novelty. Subsequent screening using western blot and immuno-fluorescent (IF) imaging confirm protein expression levels, and that they resided on the surface of OC cells specifically.

3.2 In-silico identification of six novel ADC targets

Six targets were identified using a mathematical algorithm designed and used by Dr Yasmin Friedmann (Swansea University) to interrogate the human proteome for membrane bound proteins. These proteins were then assessed in databases such as UNIPROT, Ensembl, Human Protein Atlas, REACTOME and Market Report. The output was a comprehensive spreadsheet with details of the proteins found on the databases. The output was then manually assessed by Dr Garcia Parra and Prof Gonzalez and narrowed down to the six targets investigated in this thesis. The selection of these targets, in particular, were chosen by ordering them first by the proteins expressed least in healthy female reproductive tissue followed by those which were expressed highest in malignant female tissues.

To fulfil the criteria the targets had to be:

- Highly expressed in OC

- Minimally expressed in healthy ovary

- Present on the cell surface plasma membrane

This list was manually narrowed down to six targets using the following criteria:

- No patents on the protein

- Commercial antibodies available

- Highest expression in OC

- Lowest expression in healthy ovary

This initial in-silico analysis was carried out prior to commencement of this project and the summary of these findings can be found by accessing this link: https://drive.google.com/file/d/1tvGShGwrOFsbnLKXJCu469mmS3iVjy-C/view?usp=sharing. In relation to a protein being highly expressed in OC; this was in relation to expression in normal female reproductive tissue and the expression levels were determined by looking at the immunohistochemistry results (high medium, low staining) on the human protein atlas. At the beginning of this project the names of the 6 targets were provided as a starting point.

In order to be an effective ADC target, the protein and its chosen antibody must also have the ability to:

- Internalise into the cell by receptor mediated endocytosis

- Traffic to the lysosome for digestion and release of cytotoxic payload

The Human Protein Atlas (THPA) tissue, pathology and Human Cell Atlas (301, 302, 433) was used to explore these six targets in more detail. The subcellular map located all of these targets on the plasma membrane, the tissue map indicated low expression in healthy ovary and the pathology atlas indicated high expression in OC as can be seen in **Figure 3-1**.

Figure 3-1 below shows immunohistochemistry images from patients with the three subtypes of OC – serous (the most common), mucinous and endometrioid. Each subtype includes staining for each of the six novel targets plus a well-established target within the Swansea University Reproductive Biology and Gynaecological Oncology (RBGO) group for comparison highlighted in the green box. **Figure 3-1** shows that all targets are minimally expressed in healthy ovary and have varying expressions in each of the three OC subtypes. The target TSPAN6, although at this stage does not show any difference from the other targets, is highlighted in a pink box as it becomes important as the project progresses. The images shown in **Figure 3-1** from the human protein atlas may not have been confirmed by a pathologist as the human protein atlas does not specify either way. Therefore, this could be considered a limitation of the data.
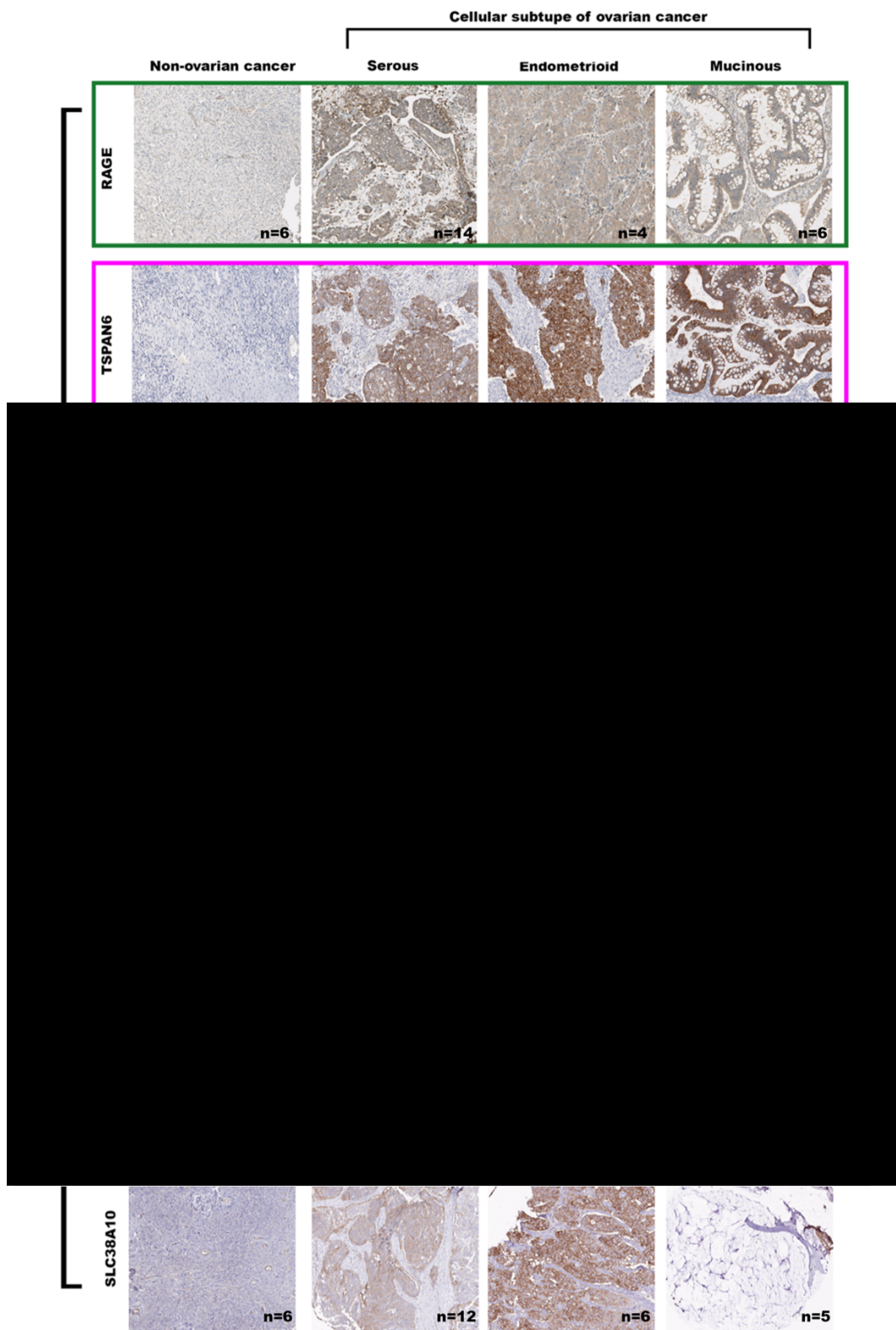
Figure 3-1 Immunohistochemistry staining of ovarian cancer subtypes from Human Protein Atlas (301, 434).

Immunohistochemistry images are taken from THPA (301, 434) showing the six targets and their varying expression in the three OC subtypes. A well-established target within the Swansea University Reproductive Biology and Gynaecological Oncology group is included, highlighted in green, for comparison.

3.2.1 Analysis of published data on target's properties and suitability for ADC targeting

After *in silico* analysis of the target expression levels by IHC on THPA, a literature search was performed to substantiate the novelty of the 6 selected targets and their known expression and function. PubMed database was used to search for the known expression and function of each of the targets, using known target names as the search terms. The sequences for all targets were obtained from UniProt (199) and added to software TOPCONS (435) for topology predictions that are described in the schematic figures produced for each target below.

3.2.1.1 Proprotein convertase subtilisin/kexin type 4 (PCSK4)

PCSK4 is a large 755 amino acid long transmembrane protein with one transmembrane domain and a large extracellular domain as can be seen in **Figure 3-2**. PCSK4 belongs to a family of subtilisin-like proprotein convertases, which include proteases that process protein and peptide precursors trafficking through the secretory pathway. The PCSK4 gene encodes one of the seven basic amino acid specific members which cleave their substrates at single or paired basic residues. PCSK4 is expressed only in the testis, placenta and ovary and it plays a vital role in fertilisation, fetoplacental growth and embryonic development. Additionally, in female fertility, PCSK4 has been reported to be involved in the regulation of trophoblast migration and placental development. It is speculated this could be due to proteolytical processing and activation of proteins such as pro-insulin-like growth factor II (199, 436).

PCSK4 is a relatively under-researched protein with less than 40 publications on PubMed. Much of the current literature around PCSK4 points to male infertility (437-439), mammalian fertility (440, 441), one paper linking to endometrial carcinoma (442) and papers linking to placental development (443).

A review on the subtilisin/kexin like proprotein convertase (PCSK) protease family (444) summarises that proteins in this family cleave and therefore convert proproteins to their biologically active forms, therefore contributing to overall health and homeostasis. Its logical to then suspect that altered PCSK4 gene and protein expression could contribute to human health and disease. PCSK4 is similar to its first 4 family members in that they all process their substrates at a motif (amino acid sequence (K/R)-(X)n-(K/R), where n is 0, 2, 4 or 6 and X any amino acid) made from paired basic amino acid residues (444). This characteristic, common to the first 7 PCSK family members, results in some degree of biological redundancy *in vitro* and therefore substrates that are shared between these first 7 family members. Target molecules known to interact with PCSKs (and by extension PCSK4) include, adhesion molecules such as integrins,

enzymes such as ADAM9, hormones such as insulin, glucagon and endothelin, cytokines, receptors, serum proteins, extracellular matrix components and lastly infectious agents such as HIV and Ebola (445). As the phenotypes of the Knock-out mice are investigated its clear a common theme is fertility and embryonic/foetal development. Specifically, PCSK4 Knock-out mice show impaired fertility (446). Compared to other family members PCSK4 is less researched and less understood. There are no large gene association studies showing any polymorphisms linked to human health and disease. Its speculated that this is due to a restricted expression profile and biological function. Several publications support this review and the data available on UNIPROT and GeneCards that PCSK4 is limited in expression to testicular and ovarian cells (437, 447-449). This information supports exploration into this target as a potential ADC drug target or disease marker.

The commercially available antibody for PCSK4 (Sigma Aldrich UK SAB2103722) recognises and binds the extracellular domain of PCSK4 (**Figure 3-2**) suggesting its potential to evaluate the internalisation capacity of PCSK4. Additionally, the protein is large (755 amino-acids) and there is evidence to suggest that larger proteins do not internalise as efficiently as smaller ones (450).
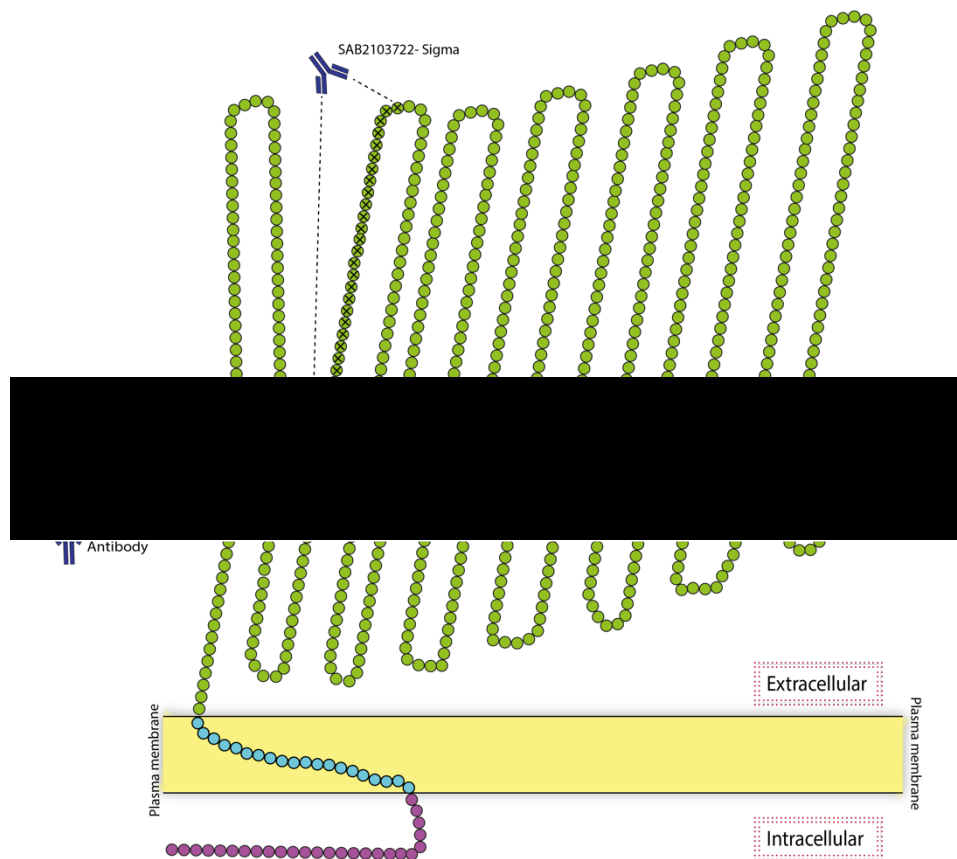
Figure 3-2 – Protein schematic of PCSK4

A predicted topology schematic of PCSK4 predicted by TOPCONS online topology predictor (435) using the human PCSK4 reference Q6UW60 sequence from the UNIPROT database (199). The schematic shows the antibody binding epitope and the size of the protein (755 amino-acids).

3.2.1.2 Piezo-type mechanosensitive ion channel component 2

PIEZO2 (UniProt - Q9H5I5 PIEZ2_HUMAN) is a component of a mechanosensitive channel required for rapidly adapting mechanically activated currents (199). It has been somewhat well researched so far with over 180 publications on PubMed. As can be seen in **Figure 3-3** below, compared to the other targets it is a very large protein (2752 amino-acids (199)) and contains over 30 transmembrane regions. Although the function is speculative, PIEZO2 is likely to act as part of mechanically activated cation channels. These various channels connect mechanical forces to biological signals (436).

The function of PIEZO2 and its family members are varied amongst the publications on PubMed. In a literature search 45 publications reported approximately 15 functions of PIEZO2. Approximately 25% of these publications report PIEZO2 to be involved in mechanically activating cation channels to initiate the sensation of touch. It is reported that PIEZO2 is expressed in a subset of sensory neurons of the dorsal root ganglion and cutaneous mechanoreceptors. For

example, Renade *et al* (451) showed that mice lacking PIEZO2 in both sensory neurons and Merkel cells exhibited a profound loss of touch sensation. They also localise PIEZO2 to the peripheral endings of a broad range of low-thresh hold mechanoreceptors that innervate both hairy and glabrous skin [21].

The next most commonly reported function was reported in approximately 13% of the 45 publications. PIEZO2 is reported to be correlated with distal arthrogryposis. Distal arthrogryposis is a group of hereditary disorders characterised by joint deformities that restrict movement in the hands and feet (452). A study of a two-generation family (453) showed a novel heterozygous mutation of PIEZO2. PIEZO2 is reported to function as a mechanosensitive ion channel which, when malfunctions, provides a pleiotropic effect on joints, ocular muscles, lung function and bone development. Interestingly, two members of this family had a restrictive lung disease which is another parallel to PIEZO2 function in two other papers (454, 455).
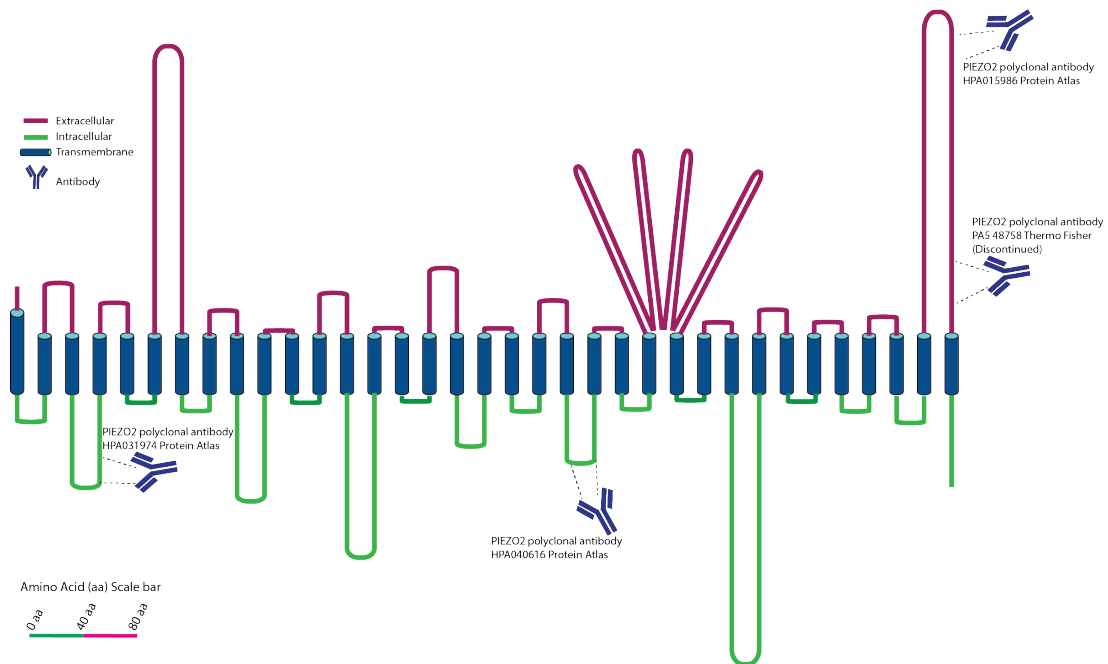
Figure 3-3 – Protein schematic of PIEZO2

PIEZO2 is a large transmembrane protein that has over 30 transmembrane regions. This figure shows a scaled schematic of PIEZO2 using TOPCONS online topology predictor (435). Several antibodies are shown here including the three antibodies used by THPA (302) and the polyclonal antibody against PIEZO2 used in the following experiments. Two THPA antibodies target intracellular epitopes and as such were not suitable for the long-term goal of an ADC targeted therapy. The third antibody used by THPA was not validated in western blot or immunofluorescence, only in IHC, therefore the polyclonal from Thermo Fisher was used.

Huang *et al* (456) reports that the PIEZO channels are stretch activated channels that are involved in wound sealing and cell proliferation. Next-generation sequencing of lung cancer patients indicates that PIEZO functions are implicated in lung cancer development. The authors demonstrated that the mRNA expression of PIEZO1 and PEIZO2 isoforms was clearly decreased in non-small cell lung cancer tissue. PIEZO1 often deleted whereas mutations in PIEZO2 were frequently observed. A higher mRNA expression of PIEZO channels as a whole was correlated with a better overall survival for non-small cell lung cancer patients, particularly with patients with lung adenocarcinoma but not with lung squamous cell carcinoma. The prognostic role of PIEZO channels seemed to be more sensitive in both female patients and patients at earlier cancer stages. Finally, knock down of PIEZO2 in non-small cell lung cancer cells promoted cell migration *in vitro* and tumour growth *in vivo*.

PIEZO2 has been reported to be involved in cancer in only 5 papers including the one discussed above (456) (457) (458) (459) (460). Yang *et al* (457) report PIEZO2 to be a novel regulator of tumour angiogenesis and hyperpermeability. Angiogenesis is important for invasive tumour growth and metastasis. In their paper, Yang *et al* show that PIEZO2 knockdown lead to a decreased glioma angiogenesis and reduced vascular hyperpermeability *in vivo* and *in vitro*. PIEZO2 was found to be highly expressed on the surface on glioma tumour endothelial cells and its knockdown suppressed angiogenesis and vascular leakage. Although in a very different part of the body – this is the opposite of the decreased mRNA expression found in non-small cell lung cancer by Huang *et al* (456).

Another study by Cheng *et al* (458) suggests promotor hypermethylation of PIEZO2 is a risk factor and a potential clinical biomarker for laryngeal squamous cell carcinoma (LSCC). In 99 LSCC patients specimens a quantitative methylation-specific polymerase chain reaction (PCR) was used to measure methylation levels. Their results showed a significantly higher level of PIEZO2 promoter methylation in LSCC patients compared to normal tissues. They also found methylation levels were significantly associated with gender, differentiation, tumour stage, lymph node metastasis and clinical stage.

Both PIEZO1 and PIEZO2 was shown to have increased expression in human and mouse bladder carcinoma (459). Etem *et al* used histopathological evaluation, reverse transcriptase-PCR and immunohistochemistry to explore the expression of the PIEZO1 and PIEZO2 genes and protein in mice and humans (456). There was a significant increase of both PIEZO1 and PIEZO2 in both cancer groups compared to the control group. PIEZO1 expression was significantly increased at tumour size, stage and grade where as PIEZO2 expression was increased in high grade tumours

in human subjects. This study supported the observations previously published by Yang and colleagues concluding that varied PIEZO1/2 expression may contribute to the carcinogenesis of bladder cancer by causing proliferative changes and angiogenesis, (457). Thus, supporting the notion that PIEZO2 may serve as a prognostic indicator for disease progression and response to treatment.

Finally, in a study by Lou *et al* (460) the role of PIEZO2 in breast cancer was explored. Breast cancer was selected due to its high expression of PIEZO2 which is consistent with what is seen for PIEZO2 in THPA (302). They identified a decrease in expression of PIEZO2 when compared to normal controls which is not consistent with what is shown on THPA for breast cancer pathology tissue expression levels (301). This conflicting data could be due to the small sample size or lack of validation on THPA. This suggests that more work needs to be carried out in this area for a better insight. They additionally reported a positive correlation of PIEZO2 and human epidermal growth factor 2 (HER2), Nottingham Prognostic Index (NPI) score, Scarff-Bloom Richardson (SBR) grade, basal like and triple negative status. Overall, unlike the other reports discussed above, decreased expression of PIEZO2 may be used as a prognostic marker for breast cancer. With breast cancer showing strong links to OC (461) the association reported in this study, in particular, supports the investigation of PIEZO2 in OC.

Overall, from the literature there are no publications linking PIEZO2 to any gynaecological malignancy. This along with the protein expression levels on THPA (301, 302) indicate PIEZO2 could be a novel ADC target for OC.

THPA summarise PIEZO2 is mostly found in the brain on the plasma membrane, nucleoplasm, vesicles as well as the cytosol. Information regarding function and a gene mutation in PIEZO2 leading to distal arthrogryposis are consistent with the literature (433).

In the body overall on THPA tissue database (302) the mRNA expression of *PIEZO2* gene does not match the PIEZO2 protein expression. As supported in the literature regarding function, PIEZO2 RNA expression is highest in the brain and the lung (454). For instance, protein expression is highest in endocrine tissues, gastrointestinal tract, liver and gallbladder, pancreas and female reproductive tissues, yet mRNA expression is low. Of the female reproductive tissues, PIEZO2 protein is most highly expressed in the breast, placenta and ovary. However, this data from THPA is based on the best estimate of the true protein expression from knowledge-based annotation. Therefore, when looking at using antibodies in primary patient samples this may not be the case. THPA used three antibodies (shown in **Figure 3-3**) to perform immunohistochemistry on 8 primary patient samples and detected none-low expression in ovarian stromal cells and a medium expression in follicle cells. This indicates PIEZO2 expression

in a healthy ovary is very low (**Figure 3-1**). In contrast, when looking at what cancers have a higher expression of PIEZO2, the results on THPA vary depending on which of three antibodies are used. This highlights the huge variability of antibodies even against the same target protein and some of this variability could be due to non-specific binding. PIEZO2 is expressed in 75-100% of patients, considering all antibodies, and it is highly expressed in all OC subtypes (**Figure 3-1**). Images from antibody HPA040616 are shown as a representative example in **Figure 3-1**.

3.2.1.3 Carcinoembryonic antigen-related cell adhesion molecule 8

CEACAM8 (UniProt - P31997 CEAM8_HUMAN) is a cell surface glycoprotein involved in cell adhesion in a calcium-independent manner. CEACAM8 mediates heterophilic cell adhesion with other carcinoembryonic antigen related cell adhesion molecules (199). CEACAM8 is a comparatively small cell surface protein at 349 amino-acids long and is associated with the membrane by Glycosylphosphatidylinositol (GPI) linkage (**Figure 1-4**), a type of posttranslational modification of proteins that involves adding a glycolipid. GPI is found most commonly in eukaryotes and in humans there are over 150 types of GPI anchored proteins including CEACAM8 and other cell surface proteins (462, 463).

According to the THPA data, CEACAM8 is enriched in the bone marrow and the placenta as well as on the surface and intracellular compartment of neutrophils and non-classical monocytes. The protein expression profile shows no detection in all body tissues apart from the bone marrow, their RNA expression is also at its highest. RNA expression is second highest in the placenta but this does not extend to protein expression. CEACAM8 protein is not detected in any non-diseased female tissues (302) as is displayed in **Figure 3-1**. Looking further in CEACAM8 and its association with different pathologies, THPA states that antibody staining data by immunohistochemistry is not consistent with the RNA expression data and therefore could be disregarded due to off target binding. CEACAM8 was detected in some (4 out of 7) cases of OC (301) however it was mainly seen in lung and colorectal cancer patients. CEACAM8 was also detected in higher instances in breast and cervical cancer. It is important to note the small sample size used for THPA experiments for this target, as well as potentially a poor antibody with off-target binding. These factors limit the interpretation of the findings. This antibody (Santa Cruz 59875) has been used by Okda *et al* to evaluate the possible role of indomethacin and vitamin D as a preventative as well as a therapeutic operator for colon cancer growth induced by dimethylhydrazine (DMH) in male Albino rats (464), however this was only for use in western blot not IHC. Overall, this antibody requires more validation.

The CEACAM family, in general, is well reported on PubMed with over 240 publications but when narrowed down to specifically CEACAM8 the number of publications is reduced, but only to 170.

These publications most commonly refer to CEACAM8 in conjunction with neutrophils. Neutrophils are a type of white blood cell that act first as part of the immune system, protecting the human body from infectious agents and are often associated with blood-related cancers, viral infections, sepsis, B12 deficiency and chemotherapy (465).
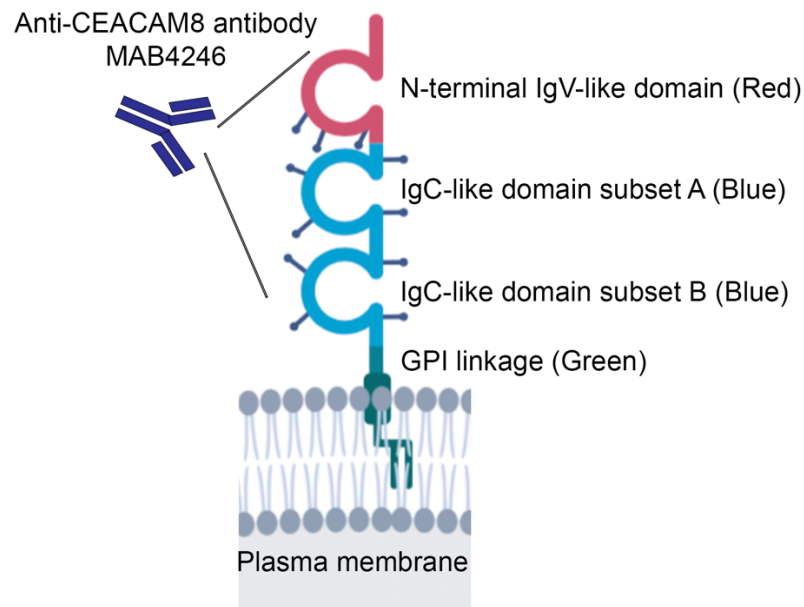
Figure 3-4 - Protein schematic of CEACAM8 (Image inspired by Tchoupa et al (466)

CEACAM8 is a cell adhesion molecule with no transmembrane domain and an association to the plasma membrane commonly of neutrophils by GPI linkage. CEACAM8 has 3 domains, as shown above, and interacts most commonly with CEACAM6. The polyclonal antibody against CEACAM8 in this project is shown above binding to CEACAM8 but the multi-epitope specificity for this antibody has not been published. CEACAM8 can also exist as a soluble form in the cytosol when it is not anchored to the membrane by GPI linkage.

Ribon *et al* shows that extracellular chromatin can trigger the release of soluble CEACAM8 upon activation of neutrophils (467). An increased concentration of extracellular chromatin can be found in many of the conditions associated with neutrophils such as cancer and sepsis. Specifically, polymorphonuclear neutrophils express CEACAM8 on the plasma membrane and secrete a soluble CEACAM8 when activated. The study showed that chromatin fragments induce neo-synthesis of soluble CEACAM8 and (after neutrophil activation) secretion of soluble CEACAM8, with a higher concentration of soluble CEACAM8 in the syno*vial* fluid of patients with rheumatoid arthritis. The presence of a soluble isomer, as well as its secretion upon neutrophil activation during a diseased state, does make CEACAM8 an interesting target for human disease as a prognostic and response to treatment indicator.

Singer *et al* (468) report that CEACAM8 interacts with CEACAM1 to inhibit the TLR2-triggered immune responses. CEACAM8 is expressed on the membrane of and also in the cytosol of human granulocytes which release soluble CEACAM8 in response to the invasion of bacterial DNA. In this study, it was demonstrated that recombinant CEACAM8-Fc binding to CEACAM1 reduced the inflammatory response, thus suggesting a mechanism by which granulocytes reduce the pro-inflammatory immune response by secreting CEACAM8 and supporting CEACAM8 overexpression in inflammatory conditions. With inflammation being a hallmark of cancer including gynaecological cancers, this study indicates CEACAM8 is worthy of investigation as a potential ADC target.

A high expression of CEACAM8 mRNA is reported in Acute Lymphoblastic Leukaemia's (ALL) in a publication by Lasa *et al* (469). To determine the expression of CEACAM8 in leukemic blast cells a qPCR was performed in 135 patients. When compared to non-diseased granulocytes CEACAM8 (and CEACAM6) were shown to be overexpressed.

CEACAM8 is also reported to be involved in cell adhesion. Kuroki *et al* (470) investigated and compared the structural requirements for the heterophilic adhesion between CEACAM6 and CEACAM8 at the amino-acid level. By using homologue-scanning mutagenesis they discovered that the location of the sequences critical for adhesion is overlapped and highly similar to the residues previously shown as essential for the binding of CEACAM antigens to Opa proteins of pathogenic Neisseriae. Opa proteins are variable outer membrane proteins expressed in Neisseria gonorrhoeae and Neisseria meningitides that mediate the interaction of these pathogens with human cells (471).

An additional study (472) supports the specific heterophilic adhesion between CEACAM8 and CEACAM6. Oikawa *et al* show that the N-domain alone is sufficient for this specific binding and other domains are not required.

Overall, from the literature, CEACAM8 is reported to be involved in human health and disease – especially surrounding activated neutrophils from response to infection. The literature suggests that this target may be useful in blood cancers diagnostics or treatment and no references to OC or other gynaecological malignancies have been made as yet. This gap in the literature coupled with the protein expression analysis in THPA do support the further investigation of CEACAM8 as a novel ADC target in OC.

3.2.1.4 Sushi domain-containing protein 2 (SUSD2)

SUSD2 is a novel and under researched target with just over 50 publications mentioning it on PubMed. Only 13 papers on PubMed have reported on SUSD2 specifically. Together with this

gap in the literature and the protein expression reported on THPA, it shows a potential for SUSD2 exploration in OC.

SUSD2 is a large 822 amino-acid protein with one transmembrane domain, a short intracellular domain and one large extracellular domain which accounts for most of its size (**Figure 3-5**). Similar to previously mentioned larger targets, a large protein may internalise less effectively (450).
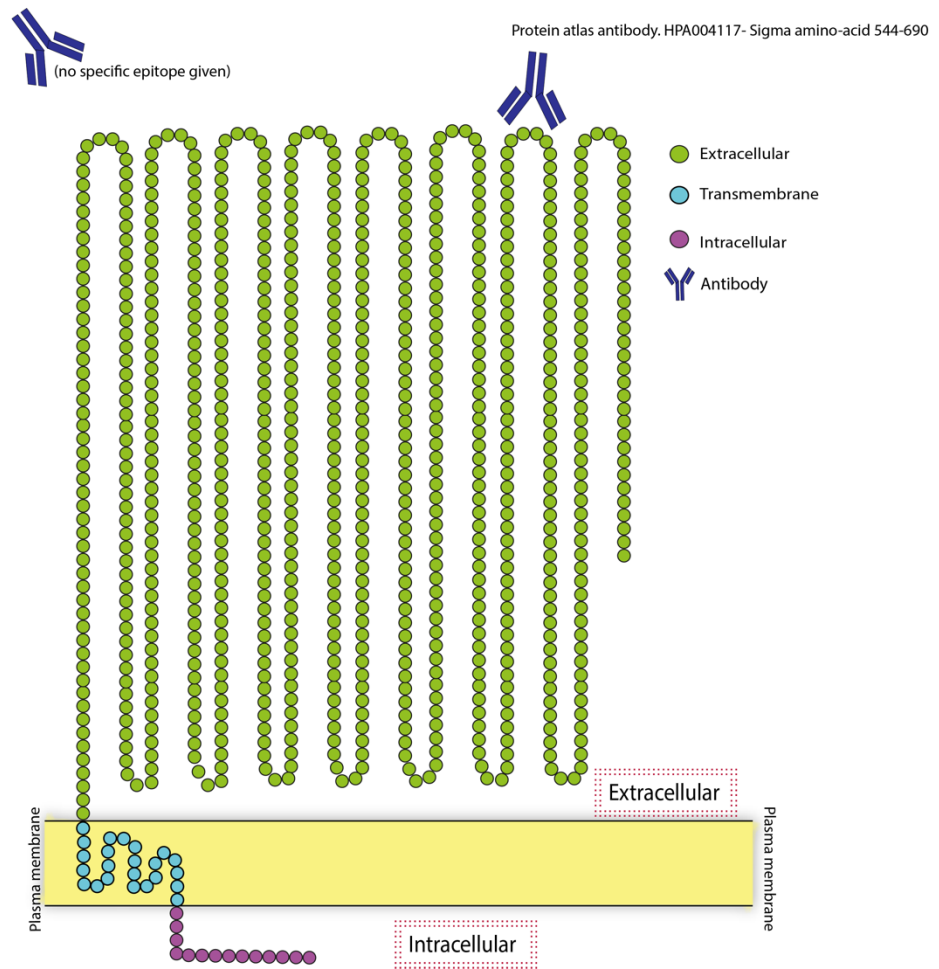
Figure 3-5 - Protein schematic of SUSD2

SUSD2 schematic as predicted using the sequence from UniProt SUSD2 (Q9UGT4 SUSD2_HUMAN) (199) and using online topology predictor from TOPCONS (435). The antibody used in this project did not disclose an epitope however it is in the extracellular region. The antibody used by THPA is a polyclonal antibody (Sigma UK) spanning amino-acids 544-690. THPA antibody is verified for use in IHC whereas the antibody used in this project is a monoclonal and is verified for use in western blot and IHC.

THPA reports SUSD2 being present most commonly on the plasma membrane and also in the cytoplasm (433). In terms of protein expression on non-diseased tissue they found the antibody staining to be mainly consistent with the RNA expression data and although is pending external verification it has been awarded an enhanced reliability score. In comparison to CEACAM8 this IHC data can be considered a lot more reliable. SUSD2 protein is reported to be expressed in varying amounts in most tissues of the body with the exception of the blood and the eye. The two highest tissues in SUSD2 expression are the lung and kidney/urinary bladder tissues. Female tissues express SUSD2 in much the same levels as the other tissues in the body- about half that of lung and kidney. Out of the female tissues, the ovary, cervix and vagina are the lowest expressing with fallopian tube, endometrium, placenta and breast being higher but still only classed as a low-medium expression (302). Looking at the expression of SUSD2 in various cancerous tissues it can be seen that strong membranous and cytoplasmic staining can be seen in the IHC for testicular cancer and OC. SUSD2 is present in most of the cancer tissue such as thyroid, stomach, melanoma and pancreatic cancer however these show weak staining in IHC. For comparison 6 out of 11 patients stained medium-high for SUSD2 in OC patients whereas only 2 out of 12 show medium-high expression in liver cancer. As mentioned before, a small sample size was used in THPA experiments.

Several online databases (199, 301, 302, 433, 436) agree that SUSD2 could be a cytokine receptor for C10ORF99 and together they could function as a tumour suppressor with a growth inhibitory effect on colon cancer cells involving G1 cell cycle arrest (473). C10ORF99 (chromosome 10m open reading frame 99) function remains largely unknown but it has been identified as a novel human antimicrobial peptide (474) as well as a colon cancer tumour growth inhibitor (473). Additionally, it is reported that SUSD2 may play a role in breast tumorigenesis (475) and given the link between breast and ovarian cancers (461) this supports SUSD2 might be worth investigating in OC.

From the literature it is clear there are several studies linking SUSD2 expression to lung, breast, ovarian and endometrial cancers. Loss of SUSD2 expression correlated with a poor prognosis for patients with lung adenocarcinoma who had undergone surgical resection (476).

SUSD2 was reported in three publications to be implicated in breast cancer. Firstly, it has been reported that cleavage of SUSD2 requires the glycine-aspartic acid-proline-histidine (GDPH) amino acid sequence and inter-fragment disulphide bonds in order to present galectin-1 on the surface of breast cancer cells (477). This identification provides a potential therapeutic tool for inhibiting the combined tumorigenic function of SUSD2 and galectin-1 in breast cancer.

Hultgren *et al* (478) presents that the recruitment of tumour assisted macrophages is promoted by SUSD2 by increased levels of Monocyte Chemoattractant Protein-1 (MCP-1) in breast cancer. Due to SUSD2 playing a role in recruiting macrophages to the tumour microenvironment of breast cancer, inhibiting the function of SUSD2 could be an effective therapy for patients with breast cancer.

As mentioned previously SUSD2 has been reported to play multiple roles in breast tumorigenesis (475). A breast cancer cDNA library was created that was enriched for genes that encode membrane bound proteins and secreted proteins. SUSD2 showed minimal staining in IHC of normal breast tissue and increased staining on breast cancer tissues. Supporting the paper described above (477), this paper (475) reports SUSD2 interacting with galectin-1. Galectin-1 is a small secreted protein that is synthesised by tumour cells and promoted tumour invasion, evasion, angiogenesis and metastasis. Watson *et al* reported that the presence of galectin-1 on the surface of cells was dependent on the presence of SUSD2. Phenotype assays show that SUSD2 increased the invasion of breast cancer cells and contributes to an immune evasion pathway. Four papers report SUSD2 involvement in gynaecological malignancies. Three report in HGSOC (479-481) and one report in endometrial cancer cells (482). A recent study reports how SUSD2 inhibits platelet activation (479). Platelets play an important role in haemostasis which affects tumour survival and metastasis. Platelets aggregate around tumours and bind to cancer cells; this prevents them from being detected by the immune system and often leads to an increased number of platelets in the blood (thrombocytosis). In ovarian cancer patients, one-third present with thrombocytosis and this is correlated with a shorter survival. In HGSOC SUSD2 is expressed on endothelial cells and influence platelet activity which could inhibit metastasis in HGSOC. This study co-cultured OC cell lines and SUSD2 knockdown cell lines with labelled platelets to quantify platelet binding. It was found that platelet activation and binding to HGSOC was inversely correlated with the presence of SUSD2. Thus, suggesting SUSD2 potential use for diagnostic and prognostic monitoring and potential as a therapeutic target for HGSOC.

In a contrasting study, Xu *et al* found that SUSD2 promotes cancer metastasis (480). The paper suggests that SUSD2 is elevated in HGSOC and regulates the Notch3 pathway, which when activated is associated with poor progression of OC, tumour invasion, metastasis and chemoresistance in HGSOC. High expression of SUSD2 was also reported to positively correlate with worse overall survival, early recurrence and lymph node metastasis. When SUSD2 was silenced in aggressive OC cells *in vitro* and *in vivo*, epithelial-mesenchymal transition (EMT) and the metastatic properties of tumour cells was inhibited. Exploring further it was shown that

SUSD2 could cause cisplatin resistance in OC, potentially by enhancing autophagy. This suggests a potential new therapeutic target for HGSOC.

The third studying linking SUSD2 to HGSOC (481) is in agreement with SUSD2 expression in HGSOC correlating with increased survival. This study performed IHC analysis to show SUSD2 is present in several types of epithelial OC with the strongest staining in HGSOC. A high-density tissue microarray using HGSOC samples was staining for SUSD2 and patients with tumours that had a significantly lower percentage of SUSD2 staining cells had a shorter survival compared to patients with more extensive staining. To explore further, knock-down cell lines of SUSD2 were created and a wound healing assay revealed that the knock-down cell lines migrated significantly faster. Further qPCR analysis and western blotting showed an inverse relationship between SUSD2 and well characterized mesenchymal proteins suggesting that the higher the SUSD2 expression the less expression of proteins that promote making and repairing connective tissues, blood vessels and lymphatic tissues. In addition, spheroids from the SUSD2 knock-down cell lines displayed an increased mesothelial clearance ability when compared with cells expressing SUSD2, suggesting a role for SUSD2 in the inhibition of metastasis by mesothelial clearance. A correlation of SUSD2 in HGSOC of this nature can have implications for diagnosis, prognosis, response to treatment, a more personalised treatment plan and potential therapeutic target.

A recent study support the above observations but focused on SUSD2 role in endometrial cancer (482). Zhang *et al* report that the downregulation of SUSD2 causes cell senescence and cell death in endometrial cancer cells. Cancer cells, in late stage endometrial cancer, migrate to other parts of the peritoneal cavity and implant cancer spheroids to neighbouring organs. It is agreed that SUSD2 mediates metastasis by its influence on cell adhesion and migrations. *SUSD2* mRNA was quantified by qRTPCR in human endometrial cancer cells and the proportion of SUSD2 positive cells was quantified using FACS and western blotting (482). Treatment of these cells with transforming growth factor beta significantly decreased the amount of SUSD2 transcribed and the percentage of SUSD2 positive cells whereas silencing of SUSD2 with siRNA caused cell death by activation of SMAD2/3. Its suggested that SUSD2 counteracts senescence and cell death and could be considered for a drug target in human endometrial cancers.

Of the targets discussed so far, SUSD2 is the only protein to have been reported to have its expression correlated with HGSOC in two publications (481, 483). Although this lessens the novel aspect of SUSD2 in OC, the protein remains largely under researched and the few papers which have been published support the promising investigation of this target in OC.

3.2.1.5 Zinc Transporter ZIP10 (also referred to as SLC39A10)

The gene SLC39A10 translates to a protein most commonly referred to as Zinc transporter ZIP10 (UniProtKB – Q9ULF5. S39AA_HUMAN). It is most commonly recognised as a zinc-influx transporter and high expression levels have been correlated with invasiveness in several breast cancer cell lines (484).

This gene/protein has several names with Zinc transporter ZIP10 being the recommended name for the protein. Other names include solute carrier family 39 member 10 (SLC39A10), Zrt and Irt-like protein 10 and simply ZIP10. The gene is most commonly referred to as *SLC39A10* but is also known as *KIAA1265* and *ZIP10* (199).

ZIP10 is a large 831 amino-acid long protein that traverses the plasma membrane 6 times (**Figure 3-6**). It has three small and one large extracellular domain and two small and one large intracellular domain. Like other large proteins, its size might influence its internalisation efficiency.

THPA displays this protein as SLC39A10 and summarises its functions as a zinc transporter. Zinc is an essential ligand for hundreds of enzymes and it is known to be involved in protein, nucleic acid, carbohydrate and lipid metabolism as well as being involved in vital homeostasis functions such as the control of gene expression, growth, development and differentiation (485).

In tissue expression on THPA, the antibody staining is pending external verification but is thought to be largely reliable as it is mainly consistent with the RNA expression data. The protein expression data reveals that ZIP10 protein is expressed in most bodily tissues. The highest expression is in the endocrine tissue, lung, male tissues and female tissues. None of these tissues have a high expression, only a medium, and of the female tissues it is expressed most highly in the endometrium, the fallopian tubes and the placenta. Interestingly, it was not detected in the ovary at all despite expression in other female tissues. Expression was not detected at all in three primary ovarian samples using two anti-ZIP10 antibodies (302). According to the THPA, ZIP10 localises to the nucleoplasm, cytosol and plasma membrane (433).
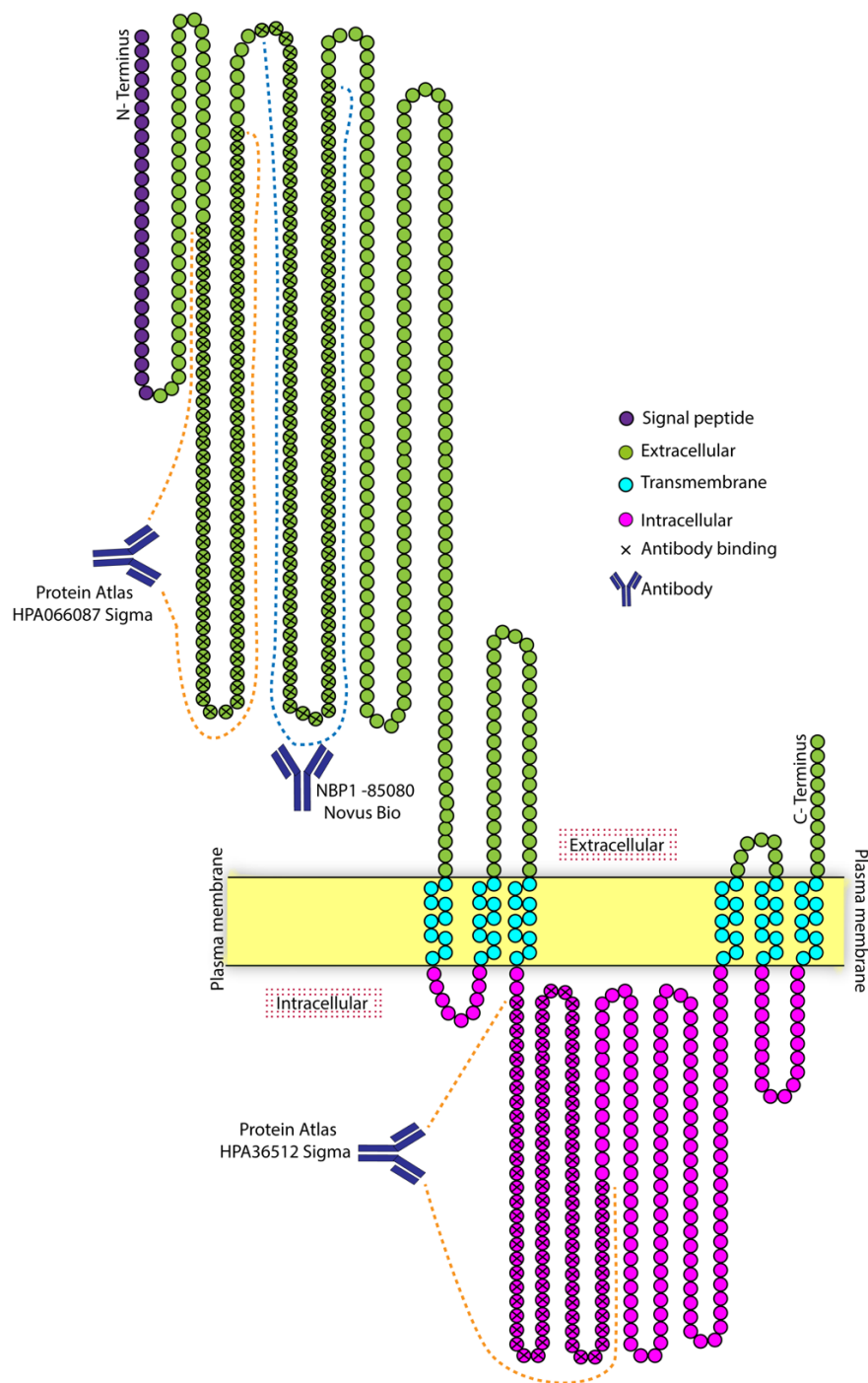
Figure 3-6 – Protein schematic of ZIP10 (SLC39A10)

The schematic above is a scaled (one circle is equal to one amino-acid) representation of the protein ZIP10 (also known as SLC39A10). The schematic shows a large protein with several antibodies binding. THPA used two antibodies to obtain protein expression data and one can be seen here binding to the large intracellular region and the other binding to the large extracellular region. The intracellular binding antibody was not appropriate for novel ADC target exploration therefore the other extracellular antibody (verified for use in western blot) and an additional polyclonal from Novus Bio was used in this project. Image inspired by Uniprot sequence entered into Topcons topology predictor (435).

THPA recognises that ZIP10 is expressed in 100% of patients with thyroid cancer and breast cancer and in approximately 75% of patients with lung, pancreatic, urothelial and OC. This data reflects the use of Sigma antibody HPA036512 (which can be seen binding in **Figure 3-6**). Upon staining with the second antibody used by THPA (HPA036513 as seen in **Figure 3-6**) the expression data changes dramatically. Expression is detected in low amounts in minimal patients and medium-high expression is only seen in patients with urothelial cancer, cervical cancer and skin cancer.

The two antibodies used here are Prestige Antibodies® that are highly characterised and extensively validated by tissue array, protein array and validated for many common uses such as IHC, IF and western blot. If both of these antibodies are extensively validated, then the very different staining intensity seen by the two different antibodies is a cause for concern.

In the literature, ZIP10 is not well researched. As with all the novel targets chosen so far, it is mentioned infrequency in publications and a lot of uncertainty and contradictions occur. When searched using the search term "SLC39A10" mentioned anywhere in the publication only 29 papers are found, with most of them being gene analysis studies. Using the search term ZIP10 mentioned anywhere in the publication there are 47 returns with some overlapping with the SLC39A10 search.

There are a variety of pathways and medical conditions reported to be associated with ZIP10. However almost none are backed up with agreeing publications. The one exception is activity surrounding the skin, epithelial cells and epidermal layer. Bin *et al* (486), in addition to their publication detailing how ZIP10 epigenetically regulates human epidermal homeostasis also sent a letter to the editor reinforcing the involvement of ZIP10 in contact dermatitis (487). It is reported that the skin is the first organ to manifest the responses to a zinc deficiency and suggests that ZIP10 and the resulting zinc levels in the body contribute to the epigenetic maintenance of human epidermal homeostasis. Adult human skin was stained for ZIP10 and histone acetyltransferase (HAT) activity was measured by treating human keratinocytes with ZIP10 siRNAs. The data showed that ZIP10 is predominantly expressed in the interfollicular epidermis, epidermal appendages and hair follicles. When ZIP10 is depleted, epidermal malformations are seen as a result of the downregulation of the enzyme HAT. Bioinformatic analysis for gene sets regulated by the knock down of SLC39A10 (ZIP10 gene) and HAT inhibition it was shown that ZIP10 and HATS are closely linked together with the regulation of genes in epidermal homeostasis.

An additional study published in Proceedings of the National Academy of Sciences of the United States of America (PNAS) is in agreement with the above study, reporting that ZIP10 is required

for epidermal development and epithelial homeostasis (486). ZIP10 was highly expressed in the outer root sheath of hair follicles and plays an important role in epidermal development. ZIP10 marked epidermal progenitor cells and removal of ZIP10 resulted in significant epidermal hypoplasia and the downregulation of the transactivation of p63, a vital regulator of epidermal progenitor cell proliferation and differentiation. ZIP10 and p63 are overexpressed and work together during epidermal development, where ZIP10 mediates zinc influx which in turn promotes p63 transactivation.

ZIP10 can exist as a heteromer with ZIP6. This interaction can control Neural Cell Adhesion Molecule 1 (NCAM1) phosphorylation and integration of NCAM1, a cell adhesion protein, into focal adhesion complexes during epithelial-to-mesenchymal transition (488). The heteromer is reported to mediate phosphorylation of NCAM1 by using the histidine-rich cytoplasmic loops within the heteromer to bind the kinase GSK3.

Although ZIP10 hasn't been reported in any gynaecological cancers, it has been referred to in renal cell cancer (489), breast cancer (484), the development of mammalian oocyte to egg (490) and spermatogenesis (491). As with the other targets discussed above and papers relating to them, it is vital to note that most of the functions and associations are reported in usually only one or two research papers.

In one such paper (489), homeostasis of zinc is described as being regulated by its transporter ZIP10. Fifty-seven renal cell cancer samples and their corresponding normal renal tissue was analysed using real time PCR to assess for ZIP10 gene (SLC39A10) expression. Significantly higher expression of ZIP10 mRNA was noticed in high grade clear cell renal cancer tissue when compared to a lower grade 1 or 2. Additionally a significant correlation was observed between ZIP10 mRNA and the aggressiveness of the cancer. Although only reported in this one paper this shows some promise as a potential biomarker of disease state and a target for novel treatment strategies in aggressive renal cancer.

In addition, ZIP10 and ZIP6 have been associated with the transition of mammalian oocytes to eggs. A rapid zinc influx has been associated with this transition and rather than using a transcriptionally based mechanism of zinc regulation the mammalian oocyte controls zinc uptake by ZIP6 and ZIP10. Disruption of these zinc transporters resulted in cell cycle arrest and this established a model of zinc insufficiency during the oocyte to egg transition (490).

As mentioned before, breast cancer and ovarian cancer share strong genetic links (461). One study (484) reported how zinc and its transporter ZIP10 are involved in the invasiveness of breast cancer cells, which may be an interesting observation to substantiate its use as a novel target. Zinc deficiency has been reported in the literature to be linked to several human maladies

including stunted growth, delayed wound healing, skin problems, brain development disorders and impaired immunity. Zinc is also important for cell replication, nucleic acid metabolism, tissue repair and growth and therefore tumour growth. Additionally, reports of zincs involvement in cancer development are common and therefore it is logical to find similar publications involving its transporter (492-498). Clinical samples were analysed for ZIP10 mRNA expression and the data suggested that ZIP10 was significantly associated with metastasis of breast cancer to the lymph node. The expression of ZIP10 mRNA was higher in invasive and metastatic breast cancer cell lines. In vitro cell migration assays showed the depletion of ZIP10 reduced the migratory activity of invasive metastatic breast cancer cell lines (484).

Further involvement with ZIP10 in the human reproductive system is described in a male infertility publication (491). Again, zinc and its regulation by ZIP10 play a vital role in spermatogenesis, sperm *via*bility and motility. A zinc deficiency can severely compromise male fertility by altering these processes. Several ZIP proteins were identified using IHC in mice. ZIP5 was reported to move zinc into Sertoli cells with this process being made greatly more effective by XIP10 and ZIP8. The expression of ZIP6 8 and 10 was located mainly in round spermatids with ZIP8 and 10 expression lessening during maturation where ZIP1 and 6 were discovered to be expressed in mature spermatids. Finally, ZIP14 was found to be expressed in undifferentiated spermatogonia and Leydig cells. Zinc deficient mice had a smaller number of terminal deoxynucleotidyl transferase dUTP nick end labelling-positive cells, altered seminiferous tubule structure and reduced ZIP10 and ZIP6. This suggests zinc and ZIP10, with other zinc transporters, to be associated with infertility in men – although further research is needed to strengthen this theory based on a single set of results.

Overall, ZIP10 is reported to be involved mainly in the homeostasis of the skin with some links to reproductive development in embryonic development, cell migration, oocyte to egg transition and spermatogenesis. In cancer, ZIP10 is mentioned infrequently however an association has been reported in renal cancer and more importantly, in this context, breast cancer.

3.2.1.6 Tetraspanin-6 (TSPAN6)

TSPAN6 (UniProtKB - O43657 TSN6_HUMAN) (also referred to as A15 homolog, Putative NF-kappa-B-activating protein 321, T245 protein, Tetraspanin TM4-D, Transmembrane 4 Superfamily Member 6 and TM4SF6) is a novel membrane protein that has been scarcely studied according to the low number of publications mentioning this target. It was first identified in 1998 as TM4SF6, a member of the tetraspanin super family of proteins, by Kenji Meada *et al* in Japan (499).

TSPAN6 is a comparatively small 245 amino-acid long transmembrane protein that has one large and one small extracellular domain, four transmembrane domains and three small intracellular domains (**Figure 3-7**). As smaller proteins have been reported to internalised more effectively (450) TSPAN6 shows some promise in this area as a novel ADC target.

3.2.1.6.1 The tetraspanin family

The tetraspanin family as a whole have been more heavily researched to elucidate their role in eukaryotes. They are ubiquitous among eukaryotes (500) and topology predictions (435) suggest all tetraspanins commonly have two extracellular domains, one large and one small and three short intracellular regions. Tetraspanins exhibit homotypic and heterotypic interactions to form a novel microdomain called a Tetraspanin Enriched Microdomain (TEM). These TEMs regulate the position of transmembrane receptors such as integrins. This results in the regulation of signalling pathways and the regulation of biosynthetic maturation.

As a large family, tetraspanins have diverse functions including cell mobility, adhesion, proliferation and activation. They also play a role in metastasis and viral infection (501). They are conserved among species and are thought to have the characteristics mentioned above due to their ability to associate with one another and a small selection of other proteins to form complexes that act as scaffolds to jointly perform the biochemical functions above.

Several studies show the expression of certain tetraspanins influence cancer and its progression (502-504). Altering tetraspanins in tumour cell lines has also shown to affect cell growth, morphology, invasion and metastasis (505).
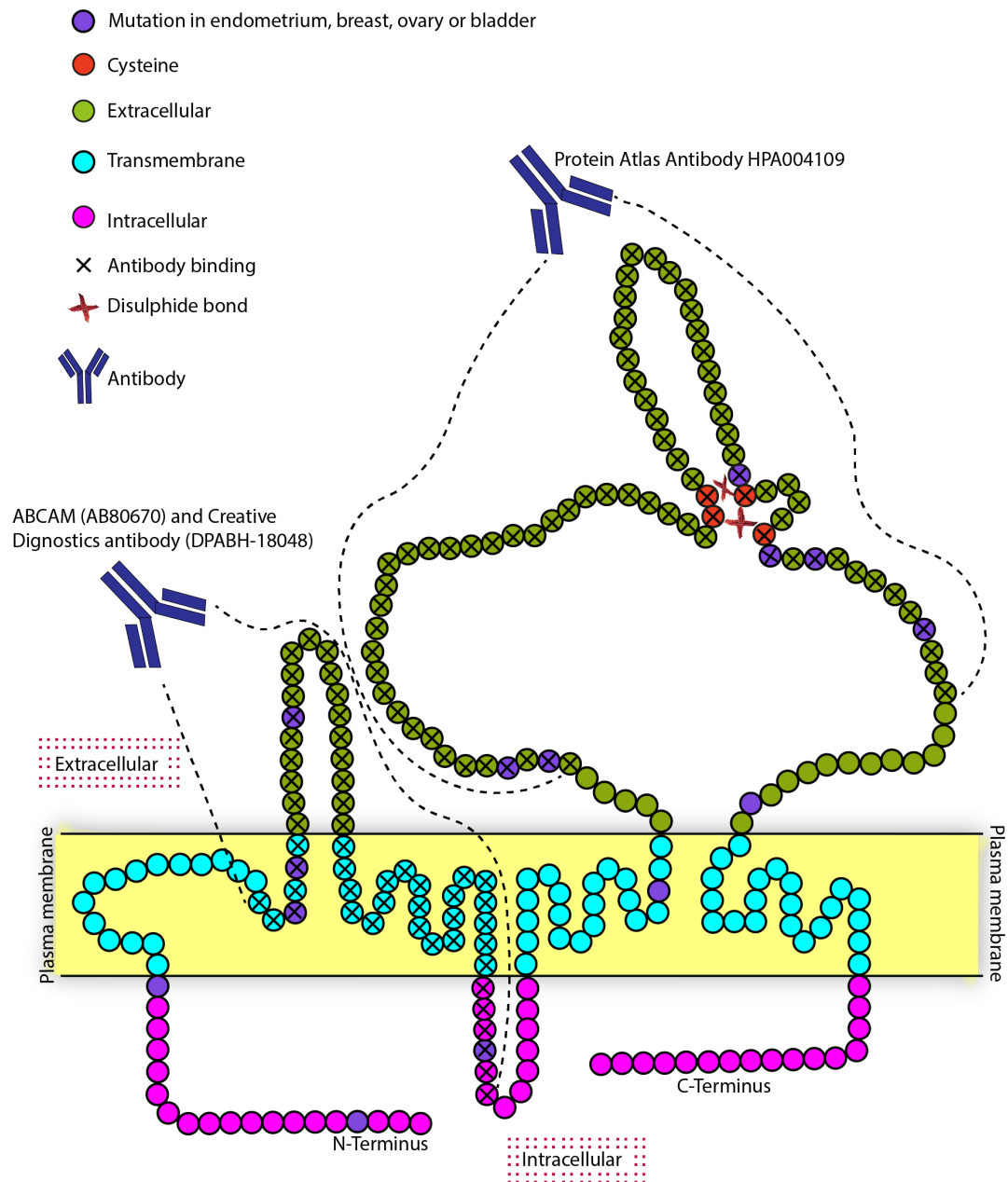
Figure 3-7 – Schematic of TSPAN6 protein

TSPAN6 is shown here as a predicted topology schematic (435). The antibodies used here both bind the two different extracellular domains. THPA antibody shown is not suitable for western blot as can be seen in Figure 3-16 therefore an additional antibody was chosen (ABCAM AB80670) and due to discontinuation was replaced by Creative Diagnostics antibody (DPBH-18048). Here on this schematic cysteine residues and their disulphide bonds are shown, which are thought to be involved in the binding of TSPAN6 to itself and other family members. Some mutations in the amino-acid sequence are shown here and represented as purple circles.

To date, there are 33 members of the tetraspanin family of proteins that are expressed variably around the body on the plasma membrane. TSPAN6 shares a 20-30% sequence homology with its other 33 family members (506). Their function as a receptor, both individually and as a family, is largely unknown. It is known that they are organised and interact laterally with other tetraspanin family members and other membrane proteins as well as forming homodimers (507).

In the context of these lateral complexes of tetraspanins and other membrane proteins, Tetraspanin Enriched Microdomains (TEMS) or Tetraspanin webs, this family of proteins have strong influences in cell adhesion, migration, invasion, signalling, cell-cell fusion, infection by cancer causing viruses, morphology and survival (508). TEMs have been reported by Spoden *et al* (509) as a clathrin and caveolin independent invasion route for viral pathogens such as HPV16. Specifically, the tetraspanins CD63 and CD51 have shown a close association with virions and viral entry was inhibited by treatment of cells with siRNA or tetraspanin specific antibodies. These characteristics all have links to cancer progression, marking the tetraspanin family of proteins as worthy of investigation in human health and disease (510).

Further studies link tetraspanins to metastasis (511-513), epithelial malignancies (514), immune responses (515), tumour progression and targeting (516-519). Some specific tetraspanins have been investigated in cancer more than others. For example, CD9 could have an oncogenic function in an ovarian cancer cell line (520), TSPAN8 has been investigated and suggested as a promising potential therapeutic target in epithelial ovarian cancers (EOC) (521) and TSPAN1 has been reported to increase the invasiveness of cervical cancer cells (522).

Angiogenesis is the formation of blood vessels in the tumour environment enabling it to grow and sustain itself. Tetraspanins have been reported to enhance tumour growth by facilitating angiogenesis (523).

3.2.1.6.2 TSPAN6 gene, protein isoforms and homologues

The gene encoding TSPAN6 is found on the X chromosome at location Xq22.1 and is known to have 9 exons. TSPAN6 is known to have 5 transcript variants which are a result of alternative splicing (524) (525). Table 3-1 shows the five recognised variants of TSPAN6 that result in 4 isomers of the TSPAN6 protein. Variant 1 is the longest and is considered the canonical sequence. All variants are N-truncated (isomer B) with isomer C, encoded by variant 4, additionally missing an exon resulting in a C-truncated protein. Finally, variant 5 encodes isomer D which lacks a whole in frame exon resulting in a missing portion in the 3' coding region. **Figure 3-8** shows the alignment of the four different protein variants the genetic isomers (**Table 3-1**) translate to. Isoform A is the longest and considered the canonical sequence and arises from

transcript variant 1. **Figure 3-8** (below) demonstrates the antibody targeting TSPAN6 is unique to the full-length sequence and does not bind the other three protein isomers.

Table 3-1 – Isoforms of TSPAN6 (From Uniprot)

Variant	Description	Isoform encoded	Uniprot reference
1	The longest variant. Considered the **canonical sequence**	A	O43657
2	Differs in its **5' UTR and uses a downstream in-frame start codon**, compared to variant 1	B	A0A024RCI0
3	Differs in its 5' UTR, **lacks a portion of the 5' coding region**, and uses a downstream in-frame start codon, compared to variant 1	B	A0A024RCI0
4	Differs in its 5' UTR, lacks a portion of the 5' coding region, uses a downstream in-frame start codon, **and lacks an exon that results in an alternate 3' coding region**, compared to variant 1.	C	A0A087WZU5
5	Differs in its 5' UTR, lacks a portion of the 5' coding region, uses a downstream in-frame start codon, **and lacks an alternate in-frame exon in the 3' coding region**, compared to variant 1.	D	A0A087WYV6

Figure 3-8 below shows the alignment of the protein isomers the five gene variants make. These variants are observed in other species (mouse, Rhesus Monkey, Bovine) as well as humans suggesting their conservation and potential biological importance.

	Amino Acids	KDa
TSPAN6_ISOFORM_A	129	14.9
TSPAN6_ISOFORM_B	245	27.5
TSPAN6_ISOFORM_C	157	17.8
TSPAN6_ISOFORM_D	137	15.6

```
                                                              Antibody epitope
TSPAN6_ISOFORM_A  MASPSRRLQTKPVITCFKSVLLIYTFIFWITGVILLAVGIWGKVSLENYFSLLNEKATNV   60
TSPAN6_ISOFORM_B  ------------------------------------------------------------   0
TSPAN6_ISOFORM_C  ------------------------------------------------------------   0
TSPAN6_ISOFORM_D  ------------------------------------------------------------   0


                     Antibody epitope
TSPAN6_ISOFORM_A  PFVLIATGTVIILLGTFGCFATCRASAWMLKLYAMFLTLVFLVELVAAIVGFVFRHEIKN  120
TSPAN6_ISOFORM_B  --------------------------MLKLYAMFLTLVFLVELVAAIVGFVFRHEIKN   32
TSPAN6_ISOFORM_C  --------------------------MLKLYAMFLTLVFLVELVAAIVGFVFRHEIKN   32
TSPAN6_ISOFORM_D  --------------------------MLKLYAMFLTLVFLVELVAAIVGFVFRHEIKN   32
                                            ********************************

TSPAN6_ISOFORM_A  SFKNNYEKALKQYNSTGDYRSHAVDKIQNTLHCCGVTDYRDWTDTNYYSEKGFPKSCCKL  180
TSPAN6_ISOFORM_B  SFKNNYEKALKQYNSTGDYRSHAVDKIQNTLHCCGVTDYRDWTDTNYYSEKGFPKSCCKL   92
TSPAN6_ISOFORM_C  SFKNNYEKALKQYNSTGDYRSHAVDKIQNTLHCCGVTDYRDWTDTNYYSEKGFPKSCCKL   92
TSPAN6_ISOFORM_D  SFKNNYEKALKQYNSTGDYRSHAVDKIQNTLHCCGVTDYRDWTDTNYYSEKGFPKSCCKL   92
                  ***********************************************************

TSPAN6_ISOFORM_A  EDCTPQRDADKVNNEGCFIKVMTIIESEMGVVAGISFGVACFQLIGIFLAYCLSRAITNN  240
TSPAN6_ISOFORM_B  EDCTPQRDADKVNNEGCFIKVMTIIESEMGVVAGISFGVACFQLIGIFLAYCLSRAITNN  152
TSPAN6_ISOFORM_C  EDCTPQRDADKVNNEGCFIKVMTIIESEMGVVAGISFGVACFQDI---------------  137
TSPAN6_ISOFORM_D  EDCTPQRDADKVNNE---------------------------LIGIFLAYCLSRAITNN  124
                  ***************                           *

TSPAN6_ISOFORM_A  QYEIV
TSPAN6_ISOFORM_B  QYEIV          Denoting conserved sequence (*), conservative mutations (:),
TSPAN6_ISOFORM_C  -----       semi-conservative mutations (.), and non-conservative mutations ( ).
TSPAN6_ISOFORM_D  QYEIV
```

Figure 3-8 - Alignment of the 4 reported TSPAN6 isomers

Isomer A is the full-length protein and as the longest, it is widely considered the canonical sequence. This demonstrates that the antibody used in this project binds to an epitope unique to the full-length isomer A in comparison to the other 3 isomers. Alignment carried out by Clustal Omega online Multiple Sequence Alignment (526). Denoting conserved sequence (*), conservative mutations (:), semi-conservative mutations (.), and non-conservative mutations ( ).

TSPAN6 has been documented to interact with several proteins as can be seen in Table 3-2 below. Specifically, Wang *et al* (527) concluded that TSPAN6 interacts with mitochondrial antiviral signalling (MAVS) in a ubiquitination-dependent manner to negatively regulate the retinoic acid-inducible gene I-like receptors (RLR) pathway. Both a positive and negative regulation of this pathway is important for the antiviral immune response. Specifically, TSPAN6 was shown to negatively regulate the pathway by affecting the formation of MAVS-cantered signalosome (527). When TSPAN6 is overexpressed RLR-mediated activation of the IFN-stimulated response element, NF-kB and IFN-B promoters was impaired. Alternately, when TSPAN6 expression knocked down the pathway was enhanced. As the RLR pathway was activated, TSPAN6 went through Lys-63-linked ubiquitination. This promoted its association with MAVS and interfered with downstream molecules such as TNF Receptor Associated Factor 3 (TRAF3), MITA and Interferon Regulatory Factor 3 (IRF3) from associating with MAVS. The

ubiquitination of TSPAN6 was shown to be crucial for its subsequent association to MAVS. If the RLR pathway is positively regulated inflammatory cytokines will be induced along with type 1 interferons (IFNs). In a normal healthy state this pathway is how a viral infection is detected and subsequently how it is combatted (528). If TSPAN6 is over expressed in OC then this pathway could be inhibited leading to inflammation as a well-known hallmark of cancer (529).

Table 3-2 – Table of TSPAN6 interactions
Proteins are known to interact with TSPAN6 (530-532). Proteins highlighted in yellow have been reported by Wang et al (527) and describe the function of this interaction. Proteins that are not highlighted have simply been shown to interact with TSPAN6 by Affinity Capture Mass Spectroscopy, Two-hybrid and Affinity Capture-Western with no knowledge available on the function of this interaction.

Interactant name	Interactant full name	Uniprot/BioGRID reference number	PubMed reference ID
CHD3	Chromodomain helicase DNA binding protein 3	Q12873	PMID: 16169070
LRIF1	Ligand dependent nuclear receptor interacting factor 1	Q5T3J3	PMID: 16169070
ASIC4	Acid sensing ion channel subunit family member 4	BioGRID:120693	PMID: 28514442
CDS1	Cdp-diacylglycerol synthase 1	BioGRID:107471	PMID: 28514442
CHD3	Chromodomain helicase DNA binding protein 3	BioGRID:107532	PMID: 16169070
CLEC5A	C-type lectin domain containing 5a	BioGRID:117135	PMID: 28514442,26186194
DDX58	Dexd/h-box helicase 58	BioGRID:117121	PMID: 22908223
EVA1C	Eva-1 homolog c	BioGRID:121863	PMID: 28514442,26186194
GPR141	G protein-coupled receptor 141	BioGRID:131689	PMID: 28514442
IFIH1	Interferon induced with helicase c domain 1	BioGRID:122082	PMID: 22908223
LRIF1	Ligand dependent nuclear receptor interacting factor 1	BioGRID:120905	PMID: 16169070
LRRTM1	Leucine rich repeat transmembrane neuronal 1	BioGRID:131480	PMID: 28514442
LYPD4	Ly6/plaur domain containing 4	BioGRID:127081	PMID: 28514442
MAVS	Mitochondrial antiviral signalling protein	BioGRID:121570	PMID: 22908223
NSG2	Neuronal vesicle trafficking associated 2	BioGRID:119640	PMID: 21900206
SERPINA12	Serpin family a member 12	BioGRID:126901	PMID: 28514442
STING1	Stimulator of interferon response cgamp interactor 1	BioGRID:130988	PMID: 22908223

TMEM185A	Transmembrane protein 185a	BioGRID:124133	PMID: 28514442,26186194
TMEM30B	Transmembrane protein 30b	BioGRID:127780	PMID: 28514442
TNFRSF17	Tnf receptor superfamily member 17	BioGRID:107080	PMID: 28514442
VNN2	Vanin 2	BioGRID:114394	PMID: 28514442

3.2.1.6.3 TSPAN6 homologs

A sequence alignment using Clustal Omega online Multiple Sequence Alignment (526) was performed to identify TSPAN6 conservation among species (**Table 3-3**). TSPAN6 can be seen to be approximately 89% conserved between the 7 species below, suggesting TSPAN6 has an important biological role (533). Additionally, high conservation has the advantageous option of using any of the species below for future in-vivo experiments.

Table 3-3 – TSPAN6 homologs

Human TSPAN6 shares 89% homology with Mouse, Chimpanzee, Rhesus Monkey, Rat, Sumatran Orangutan and Bovine (cow). The polyclonal antibodies used in this project is marked in green and can be seen to be very stable (96%) between species. Denoting conserved sequence (*), conservative mutations (:), semi-conservative mutations (.), and non-conservative mutations ( ).

```
                                                Antibody epitope
TSPAN6_Human       MASPSRRLQTKPVITCFKSVLLIYTFIFWITGVILLAVGIWGKVSLENYFSLLNEKATNV   60
TSPAN6_Mouse       MASPSRRLQTKPVITCLKSVLLIYTFIFWITGVILLAVGIWGKVSLENYFSLLNEKATNV   60
TSPAN6_Chimpanzee  MASPSRRLQTKPVITCFKSVLLIYTFIFWITGVILLAVGIWGKVSLENYFSLLNEKATNV   60
TSPAN6_Rhesus      MASPSRRLQTKPVITCFKSVLLIYTFIFWITGVILLAVGIWGKVSLENYFSLLNEKATNV   60
TSPAN6_Rat         MASPSRRLQTKPVITCFKSVLLIYTFIFWITGVILLAVGIWGKVSLENYFSLLNEKATNV   60
TSPAN6_Sumatran    MASPSRRLQTKPVITCFKSVLLIYTFIFWITGVILLAVGIWGKVSLENYFSLLNEKATNV   60
TSPAN6_Bovine      MASPSRRLQTKPVITCFKSVLLIYTFIFWITGVILLAVGIWGKVSLENYFSLLNEKATNV   60
                   ***************:********************************************

                                Antibody epitope
TSPAN6_Human       PFVLIATGTVIILLGTFGCFATCRASAWMLKLYAMFLTLVFLVELVAAIVGFVFRHEIKN  120
TSPAN6_Mouse       PFVLIGTGTVIILLGTFGCFATCRTSAWMLKLYAMFLTLIFLVELVAAIVGFVFRHEIKN  120
TSPAN6_Chimpanzee  PFVLIATGTVIILLGTFGCFATCRASAWMLKLYAMFLTLVFLVELVAAIVGFVFRHEIKN  120
TSPAN6_Rhesus      PFVLIGTGTVIILLGTFGCFATCRASAWMLKLYAMFLTLIFLVELVAAIVGFVFRHEIKN  120
TSPAN6_Rat         PFVLIGTGTVIILLGTFGCFATCRASAWMLKLYAMFLTLIFLVELVAAIVGFVFRHEIKN  120
TSPAN6_Sumatran    PFVLIATGTVIILLGTFGCFATCRASAWMLKLYAMFLTLIFLVELVAAIVGFVFRHEIKN  120
TSPAN6_Bovine      PFVLIGTGTVIILLGTFGCFATCRASAWMLKLYAMFLTLIFLVELVAAIIGFVFRHEIKN  120
                   *****.*****************::***************.*********:**********


TSPAN6_Human       SFKNNYEKALKQYNSTGDYRSHAVDKIQNTLHCCGVTDYRDWTDTNYYSEKGFPKSCCKL  180
TSPAN6_Mouse       SFKSNYENALKEYNSTGDYRSEAVDKIQSTLHCCGVTNYGDWKGTNYYSETGFPKSCCKL  180
TSPAN6_Chimpanzee  SFKNNYEKALKQYNSTGDYRSHAVDKIQNTLHCCGVTDYRDWTDTNYYSEKGFPKSCCKL  180
TSPAN6_Rhesus      SFKNNYEKALKQYNSTGDYRSHAVDKIQSTLHCCGVTDYRDWTNTNYYSEKGFPKSCCKR  180
TSPAN6_Rat         SFKSNYENALKEYNSTRDYRSEAVDKIQSTLHCCGVTNYRDWKGTNYYSETGFPKSCCKL  180
TSPAN6_Sumatran    SFKNNYEKALKQYNSTGDYRSHAVDKIQNTLHCCGVTDYRDWTDTNYYSEKGFPKSCCKL  180
TSPAN6_Bovine      SLKNNYEKALKQYNATGDYRSDAVDKIQSMLHCCGVTNYRDWKDTNYYSEKGFPESCCKL  180
                   *:*.***:***:**:* ****.******. *******:* **..*******.***:****


TSPAN6_Human       EDCTPQRDADKVNNEGCFIKVMTIIESEMGVVAGISFGVACFQLIGIFLAYCLSRAITNN  240
TSPAN6_Mouse       EGCYPQRDADKVNEEGCFIKVMTTIESEMGVVAGISFGVACFQLIGIFLAYCLSRAITNN  240
TSPAN6_Chimpanzee  EDCTPQRDADKVNNEGCFIKVMTIIESEMGVVAGISFGVACFQLIGIFLAYCLSRAITNN  240
TSPAN6_Rhesus      EDCTPQRDADKVNNEGCFIKVMTIIESEMGVVAGISFGVACFQLIGIFLAYCLSRAITNN  240
TSPAN6_Rat         EGCYPQRDADKVNEEGCFIKVMTTIESEMGVVAGISFGVACFQLIGIFLAYCLSRAITNN  240
TSPAN6_Sumatran    EDCTPQRDADKVNNEGCFIKVMTIIESEMGVVAGISFGVACFQLIGIFLAYCLSRAITNN  240
TSPAN6_Bovine      EDCSPQRDADKVNNEGCFIMVMTIIESEMGVVAGISFGVACFQLIGIFLAYCLSRAITNN  240
                   *.* ********:***** *** **************************************


TSPAN6_Human       QYEIV   245
TSPAN6_Mouse       QYEIV   245
TSPAN6_Chimpanzee  QYEIV   245
TSPAN6_Rhesus      QYEIV   245
TSPAN6_Rat         QYEIV   245
TSPAN6_Sumatran    QYEIV   245
TSPAN6_Bovine      QYEIV   245
                   *****
```

3.2.1.6.4 TSPAN6 expression

THPA antibody used in the IHC experiments has been approved for reliability by THPA due to the antibody staining mainly agreeing with the RNA expression data. The antibody was still pending external verification at the time the experiments reported in this thesis took place and has subsequently been verified by THPA. THPA approved the cellular location of TSPAN6 to both intracellular at cell junctions and the membrane (433).

Protein expression in normal tissue is highest in the lung, proximal digestive tract, kidney, urinary and bladder, male tissues, female tissues, skin and bone marrow and lymphoid tissues.

Although the expression is high in female tissues, including the vagina, fallopian tube, endometrium, cervix, placenta and breast- it was not detected at all in the ovary (302).

In cancers, it was detected in all cancers apart from glioma, lymphoma and thyroid cancer. Although the highest expressing cancers were lung cancer, stomach cancer, pancreatic cancer, prostate cancer, cervical cancer, endometrial cancer, ovarian cancer and skin cancer. The most notable and relevant here is ovarian cancer as it has gone from having no detected expression in healthy ovarian tissue to 11 out of 11 patients showing medium-high expression in various ovarian cancer subtypes as shown in **Figure 3-1**.

3.2.1.6.5 TSPAN6 function

The precise function of TSPAN6 is largely unknown and there are minimal papers published on its function. Only 10 papers mention tetraspanin-6 or TSPAN6 anywhere in the paper and one is the paper where it was originally reported (499).

TSPAN6 has been reported to negatively regulate exosome production (534). Tetraspanins as a family have been reported in relation to exosomes somewhat extensively in the literature (535, 536), however a paper by Ghossoub *et al* published in PNAS is the only publication to mention TSPAN6 specifically in this area (534). Exosomes are small extracellular vesicles that originate from inside the cell and contain representative proteins and DNA fragments from their cell of origin. They have been linked cell to cell signalling in human homeostasis and human disease. Exosomes highly express tetraspanins and syndecans (SDCs) and it is shown that TSPAN6 and SDC4 associate with one another to govern exosome biology (534). TSPAN6 binds tightly with SDC4 to regulate its processing and trafficking. In addition, this complex is responsible for the binding of TSPAN6 to syntenin and therefore the lysosomal degradation of the SDC4-syntenin complex. Additionally, TSPAN6 was shown to inhibit the shedding of the SDC4 ectodomain, mirroring the effects of matrix metalloproteinase inhibitors. Important physical and functional interconnections between TSPAN6 and SDC4 were also shown to contribute to the production of exosomes, which have been linked to cancer in the literature (537). These observations suggest a role for TSPAN6 in cancer progression through stimulation of cancer derived exosomes.

One paper by Wang *et al* indicates that TSPAN6 negatively regulates immune signalling as a result of ubiquitination. An impaired immune response leads to type 1 IFNs and inflammatory cytokines not being produced and thereby causing autoimmune and inflammatory related diseases (527). With inflammation being a well-documented hallmark of cancer (529), this association with inflammation may be an explanation of the overexpression of TSPAN6 in the malignant ovary. In support, the overexpression of TSPAN6 has been shown to impair Retinoic

Acid-inducible Gene 1-like Receptor (RLR) mediated immune signalling by undergoing Lys-63-linked ubiquitination, which promoted its association with mitochondrial antiviral signalling (MAVS) in response to TSPAN6 overexpression (527). TSPAN6 associates with MAVS resulting in the interference in the formation of the MAVS signalosome and impedes downstream signalling. TSPAN6 inhibits RIG-I-, MDA5- and MAVS dependant IFN-B promotor activity and MAVS-dependant NF-kB and ISRE promotor activity. This indicates TSPAN6 likely acts at the level of MAVS (538).

TSPAN6 has been correlated with Alzheimer's Disease (AD). Specifically down regulating TSPAN6 in primary neuronal cultures reduced amyloid beta (the main component of extra neuronal plaques characteristic of AD) production significantly (539). The association of TSPAN6 with exosome release and the lysosomal degradation of amyloid precursor protein fragments has also been reported by Guix *et al* (540). Tetraspanins with altered expression in AD brains were identified and it was reported that TSPAN6 was increased in AD brains and this over expression had the unexpected effect of increasing amyloid precursor proteins C-terminal fragments and Aβ levels at the same time. TSPAN6 slows down the degradation of amyloid precursor proteins C-terminal fragments by influencing autophagosome-lysosomal fusion. As in other publications described above, TSPAN6 is also shown to interact with syntenin which increases the secretion of exosomes that contain amyloid precursor proteins C-terminal fragments (534).

Further reports of TSPAN6 involvement in brain function are reported by Salas *et al* (541) where TSPAN6 was described to regulate hippocampal synaptic transmission and long term plasticity. Deletions of TSPAN6 were reported in patients with Epilepsy Female-restricted with Mental Retardation (EFMR). This investigation was prompted by the similarity of TSPAN6 to TSPAN7, which is associated with X-linked intellectual disability by playing a role in synapse development and AMPAR trafficking. This suggests that both of these proteins are vital for cognition. Knock down of TSPAN6 in mice show an enhanced basal synaptic transmission and impaired long-term potentiation (541). TSPAN6 is shown to affect the postsynaptic rather than the presynaptic terminal as suggested by a normal paired-pulse facilitation response. In contrast, knock out mice showed no changes in spine morphology or postsynaptic markers, normal locomotor behaviour and no defects in memory tests.

Overall, a review of the literature indicates that TSPAN6 is not associated with any type of cancer. has a link to AD and has involvement with exosomes which could explain its altered expression in ovarian cancers. The lack of publications makes this target in particular the most novel of all six targets and coupled with THPA IHC (**Figure 3-1**) the most promising for novel ADC target discovery.

3.2.1.7 Summary of *in-silico* findings for the six ADC candidates

In summary the *in-silico* findings suggest all targets are promising to explore as potential novel ADC targets. All the targets are under published in the literature suggesting an opening for novel research. From what little is published, some links to various cancers have been suggested however not in the case of gynaecological malignancies.

As can be seen in **Figure 3-1**, all targets are over-expressed in the main OC subtypes whilst remaining minimally expressed in the healthy ovary. Unfortunately, the IHC images do not have a high enough magnification to see in more detail if the proteins are present on the plasma membrane of epithelial ovarian cells. However, each target protein is confirmed as being present on the membrane (and also the cytoplasm) in the cell atlas section of THPA (433).

3.3 Expression levels of six novel targets in ovarian cancer cell lines by western blot

After *in silico* investigation, ovarian cancer cell lines representative of serous and endometrioid ovarian cancers, the most common OC subtypes, were investigated for the expression levels of the six targets discussed above by western blot. Commercially available antibodies were chosen based on their validated use for immunoblotting with a preference of selecting monoclonal antibodies when possible instead of polyclonal antibodies. All antibodies were preselected based on their specificity for epitopes found in the extracellular domain of the targets.

3.3.1 Expression levels of PCSK4 in ovarian cancer cell lines by immunoblot

In order to determine PCSK4 expression levels in ovarian cancer, SKOV-3 and TOV-112D cell lines representing the serous and endometrioid OC subtypes were grown to confluency and protein extracts made as described in Chapter 2. The antibody selected for immunoblot was tested using 5% BSA, 5% fat free milk and using PBS-T instead of TBS-T the clearest blot is shown below in **Figure 3-9** (5% BSA in TBS-T).

The data sheet for this antibody showed a clean band at 82 kDa and no other bands on the gel using PBS-T and antibody at 1μg/mL on OVCAR-3 cell lysate. OVCAR-3 is an ovarian cancer cell line of HGSOC subtype used further on in this project and was used to test this antibody however the multiple bands still remained under our experimental conditions. Although PCSK4

expression could not be characterised using this antibody in these cell lines, the target PCSK4 and this antibody (for continuity) would be used further in the project to explore PCSK4 expression and localisation in 2D cells using IF.
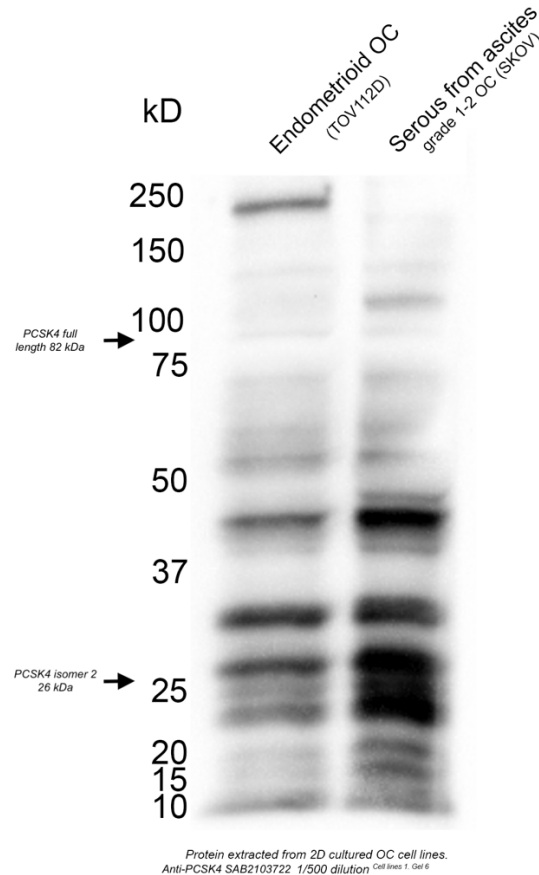
Figure 3-9 – Expression of PCSK4 in ovarian cancer cell lines by immunoblot

The polyclonal antibody from Sigma UK (SAB2103722) was chosen to investigate PCSK4 in a western blot on two different OC cell lines SKOV-3 and TOV-112D. The protein was extracted from 2D cultured cells and the antibody was diluted 1/500 in TBS-T. PCSK4 is a 82 kDa protein with an isomer at 26 kDa (199). Although some bands can be seen at the expected sizes there are too many other bands on the rest of the gel to confidently show PCSK4 expression using this antibody.

3.3.2 Expression levels of PIEZO2 in ovarian cancer cell lines by immunoblot

In order to determine PIEZO2 expression levels in ovarian cancer, SKOV-3 and TOV-112D cell lines representing the serous and endometrioid OC subtypes were grown to confluency and protein extracts made as described in Chapter 2.

Figure 3-10 shows the western blot when the two OC cell lines were analysed in western blot using Thermo Fisher anti-PIEZO2 polyclonal antibody PA5-48758. PIEZO2 is a very large protein

with an expected band size of 318 kDa. Apart from being off the scale of the ladder used for western blotting, all of the western blots shown on the data sheets for various PIEZO2 antibodies show instead, a band at approximately 95 kDa and commonly an additional band at approximately 70 kDa. There are several reasons for this difference. Migration on the western blot is affected by several factors so that the band size observed is different to what is expected. Post-translational modifications such as phosphorylation and glycosylation can increase the size of the protein. Post-translational cleavage can make the protein smaller. Some proteins are synthesised as pro-proteins which are then cleaved to their active form. Splice variants create different isoforms of the proteins from the same gene and the relative charge of amino-acids (charged vs not-charged can affect the size of the band. Finally, as is the case in the below Figure 3-14, multimers can exist of the protein resulting in dimers and other higher order multimers. In this case, the observed band is smaller than the expected band. This means it is likely to be post-translational cleavage, a splice variant or a difference due to the relative charge (542).
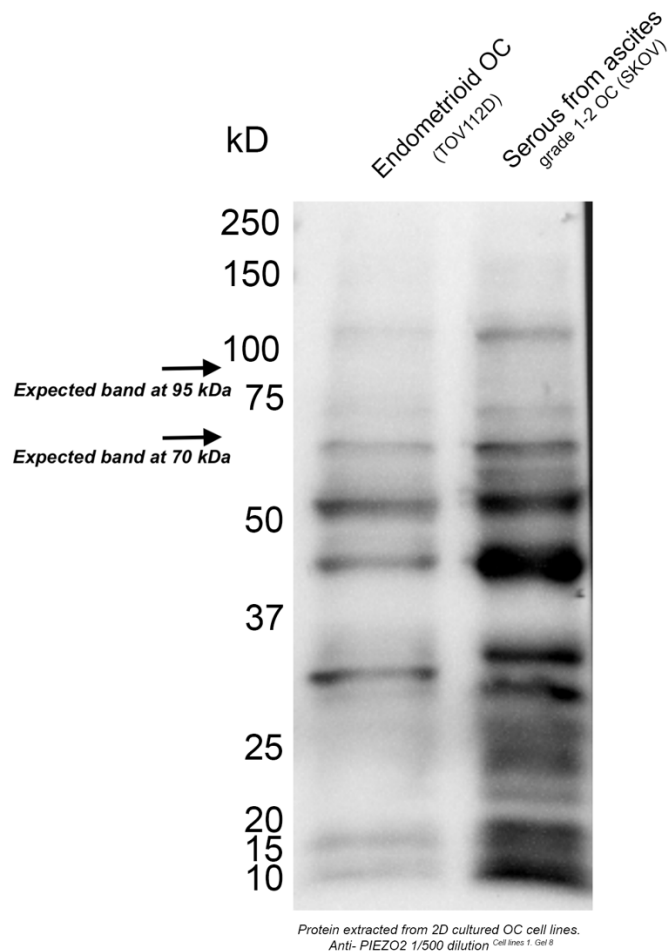
Figure 3-10 –PIEZO2 expression in two OC cell lines by immunoblot

A western blot on two OC cell lines SKOV-3 and TOV-1112D incubated with polyclonal anti-PIEZO2 antibody PA5 48758 (Thermo Fisher UK). The western was performed according to manufactures recommendations (5% BSA in TBS-T) and was incubated with the primary antibody at a 1/500 dilution. Expected band sizes are indicated by the arrows. A band is not clearly seen at 95 kDa. A band can be seen around the 70 kDa mark however many other unidentifiable bands make it not possible to use this antibody on these proteins to interpret PIEZO2 expression.

There are 4 PIEZO2 isomers produced by alternative splicing (199) as shown in **Table 3-4** below.

Table 3-4 – Isomers of PIEZO2 (199)

Isomer	UniProt reference	Length (Amino-Acids)	Size (kDa)	Identifying feature
1	Q9H5I5-1	2752	318	Canonical sequence
2	Q9H5I5-2	2689	311	Missing 2387-2449
3	Q9H5I5-3	709	80	Missing 1-2043
4	Q9H5I5-4	2777	320	831-831: R → SHAKVNGRVYLIINSIKKKLPIHQNE

The expected 80 or 95 KDa band may be produced by this third isomer highlighted yellow in the table above. Yang *et al* (457) do show a western blot showing PIEZO2 at 80 kDa – backing up what is stated on the expected band data sheets for various PIEZO2 antibodies. The antibody used by this group was from Abcam therefore in the future it may be worth testing different antibodies against this target. However, it is not commented on as to why the band seen is so different to the predicted molecular weight of PIEZO2. It is not mentioned in the literature and widely accepted that the expected band size for PIEZO2 is 80 kDa (543).

Overall, it was not possible to determine the expression of PIEZO2 using the antibody PA5-48758. It is possible another antibody could work better in western blot but they must meet the specification of binding extracellularly. Many available antibodies bind intracellularly and are suitable for western blot however an intracellular epitope would not be suitable for an ADC target.

3.3.3 Expression levels of CEACAM8 in ovarian cancer cell lines by immunoblot

In order to determine CEACAM8 expression levels in ovarian cancer, SKOV-3 and TOV-112D cell lines representing the serous and endometrioid OC subtypes were grown to confluency and protein extracts made as described in Chapter 2. **Figure 3-11** below shows the western blot from incubating two OC cell lines SKOV-3 and TOV-112D with anti-CEACAM8 monoclonal antibody MAB4246 from R and D Systems UK.
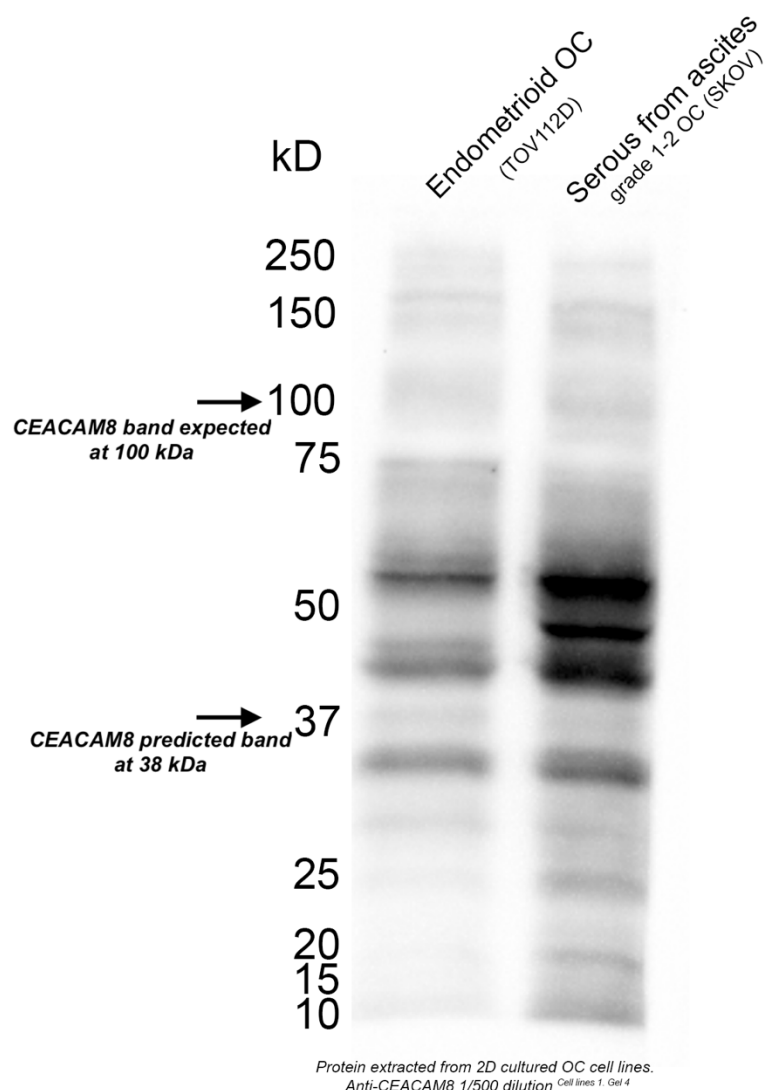
Figure 3-11 – CEACAM8 expression in two OC cell lines by immunoblot

Initial experiments conducted to assess target expression on protein lysates extracted from the OC cell lines SKOV-3 and TOV-112D, grown as 2D monolayers, using the monoclonal antibody MAB4246. The experiment was carried out as per manufactures guidelines (5% BSA in TBS-T) and used a 1/500 antibody dilution. Arrows indicate where bands are predicted and expected. Several unidentified bands make it not possible to confirm the specificity of this antibody for CEACAM8 expression in these cell lines.

A monoclonal antibody was preferred above polyclonal antibodies due to the long-term goal of synthesising a monoclonal for future ADC targeted therapy. R and D did not reveal the epitope of the anti-CEACAM8 antibody and reported a band at 100 kDa representing CEACAM8. However, due to CEACAM8 being a cell adhesion molecule with a very small membrane embedded region this did not pose a problem as the majority of the protein domains were extracellular. Similar to PIEZO2 the size in kDa of CEACAM8 did not match the band size shown by western blot.

There are no recorded isomers for CEACAM8 that could explain this large size however CEACAM8 is known to associate with CEACAM1 and CEACAM6 (468, 470). Specifically, CEACAM1 is a 56 kDa protein and added to the 38 kDa of CECAM8 this could account for a band at 94 kDa which is near the expected 100 kDa. The interaction between CEAMCA8 and CEACAM6 would yield a band at 75 kDa which is too small to account for the band expected. However, the bonds between homodimers and heterodimers are reported to be hydrogen bonds and it is expected that these bonds would break from the addition of a reducing agent and the denaturing as part of the western blot preparation. The literature supports that CEACAM8 exists mainly as a monomer in solution and the heterodimerisation with CEACAM6 to be a weak interaction using bonds such as hydrogen or van der wall forces (544). Overall, from the literature, it is unlikely that CEACAM8 binding to another family member or forming a higher order multimer is responsible for the band seen to represent CEACAM8 at 100 kDa.

It is more likely that CEACAM8 has undergone glycosylation. Eleven glycosylation sites were discovered on CEACAM8 (545) but whether this amount of glycosylation is enough to see a shift from 38 kDa to 100 kDa is unknown.

Overall, it appears CEACAM8 undergoes some kind of post translational modification to appear as a band at 100 kDa rather than the expected 38 kDa. However, the western blot in reality has too many unidentifiable bands to be able to confidently discuss the expression of CEACAM8 using this antibody on these cell lines.

3.3.4 Expression levels of SUSD2 in ovarian cancer cell lines by immunoblot

In order to determine SUSD2 expression levels in ovarian cancer, SKOV-3 and TOV-112D cell lines representing the serous and endometrioid OC subtypes were grown to confluency and protein extracts made as described in Chapter 2.

**Figure 3-12** shows the western blot from incubating two OC cell lines SKOV-3 and TOV-112D with anti-SUSD2 monoclonal antibody MAB9056 from R and D Systems UK. SUSD2 is a 90 kDa protein however similar to CEACAM8 and PIEZO2 does not appear as a band on the western blot at the expected size. Instead, SUSD2 is reported to be present as two bands on the data sheet for MAB9056 at approximately 110 and 60 kDa. Similarly, antibodies from Abcam UK (ab168162 and ab182147) show bands at 110 and 60 kDa and 90 and 50 kDa respectively. It is important that these antibodies from different companies agree with each other and also important to notice the slight differences in expected band size even between antibodies from the same company.

SUSD2 does not have any reported isomers and very few predicted glycosylation sites (199, 545). SUSD2 has 3 predicted N-linked glycosylation sites and it has been reported that each glycosylation site adds 2.5 kDa to the molecule (546). This would see an increase in molecular weight only by 7.5 kDa.

SUSD2 is not reported in the literature to exist as a homodimer or another higher order multimers.

In **Figure 3-12** the bands for TOV-112D are clearer on the gel than the SKOV-3. There are two clear bands at approximately 65 and 80 kDa which is not far from the expected 50-60 and 90-110 kDa shown on the antibody data sheets. There are some background faint bands seen however the two bands around the correct size are the clearest and darkest. It is possible that with optimisation these faint bands could disappear. For the SKOV-3, the band at 60 kDa is present but there are many other darker unidentifiable bands. Some of these even match the faint bands on the TOV-112D lane. This calls into question the many unidentified bands in both lanes and suggests this antibody coupled with this protein lysate is not suitable for assessing the protein expression of SUSD2 by western blot.

Figure 3-12 –SUSD2 expression in two OC cell lines by immunoblot

Initial experiments conducted to assess target expression on protein lysates extracted from the OC cell lines SKOV-3 and TOV-112D, grown as 2D monolayers, using the monoclonal antibody MAB9056. The experiment was carried out as per manufactures guidelines (5% BSA in TBS-T) and used a 1/500 antibody dilution. Arrows indicate where bands are predicted and expected. Several unidentified bands make it not possible to confirm the specificity of this antibody for CEACAM8 expression in these cell lines.

3.3.5 Expression levels of ZIP10 in ovarian cancer cell lines by immunoblot

In order to determine ZIP10 expression levels in ovarian cancer, SKOV-3 and TOV-112D cell lines representing the serous and endometrioid OC subtypes were grown to confluency and protein extracts made as described in Chapter 2. Immunoblots were performed using protein lysate from TOV-112D and SKOV3 OC cell lines and (**Figure 3-13**) the anti-ZIP10 antibody NBP1 85080 (Novus Bio UK).

Figure 3-13 –ZIP10 expression in two OC cell lines by immunoblot

Initial experiments conducted to assess target expression on protein lysates extracted from the OC cell lines SKOV-3 and TOV-112D, grown as 2D monolayers, using the polyclonal antibody NBP1 85080. Experiment was carried out as per manufactures guidelines (5% BSA in TBS-T) and used a 1/500 antibody dilution. Arrows indicate where bands are predicted and expected. No band can be seen at the expected band size of 94 kDa on either cell lines indicated by an arrow. ZIP10 has a second isomer at 42 kDa which could be producing the band shown by an arrow at just under 50 kDa. Several unidentified bands make it not possible to confirm specificity of this antibody for ZIP10 expression in these cell lines.

ZIP10 is a 94 kDa protein and at the time of purchasing the antibody was verified in western blot but has since been revised to only suitable for IHC. The expected band is at 94 kDa and other antibodies available currently such as ab83947 from Abcam do show a band at 94 kDa but also at approximately 50 kDa. In **Figure 3-13** below no band can be seen in either cell line however, ZIP10 does have an isomer at 42 kDa which could be responsible for the band just under the 50 kDa marker. The bands seen below the 50 kDa marker could be small broken pieces of ZIP10

from denaturing protein due to protease activity, sub-optimal storage temperature or freeze-thaw cycles. It is also just as likely that these bands are due to non-specific binding and an antibody performing poorly in western blot.

3.3.6 Expression levels of TSPAN6 in ovarian cancer cell lines by immunoblot

In order to determine TSPAN6 expression levels in ovarian cancer, SKOV-3 and TOV-112D cell lines representing the serous and endometrioid OC subtypes were grown to confluency and protein extracts made as described in Chapter 2.

A comparison between the initial TSPAN6 antibody and a clone obtained from another supplier was made to determine the best antibody to progress the validation of this target (**Figure 1-19**). The polyclonal ABNH0007105 was originally purchased from VWR UK as an antibody validated in western blot and tested in our experimental conditions (**Figure 3-14A**). No clear band could be seen at the 27 kDa TSPAN6 monomer, some bands were seen around the 54 kDa of the homodimer and several non-specific immunoreactive bands were also observed. This result suggests this antibody is not suitable for further development given the unspecific pattern of expression observed for the target. Upon revisiting the VWR website the antibody ABNH0007105 had since been changed to not validated in western blot but was now only validated in Enzyme Linked Immunosorbent Assay (ELISA). At this stage a new antibody against TSPAN6 was sought out. The initial screening planned to involve screening by western blot, therefore the ideal TSPAN6 antibody needed to fulfil the following criteria: suitable and validated for western blot experiments, a monoclonal antibody where possible and most importantly with an epitope within the extracellular domain of TSPAN6.

A band is identified in **Figure 3-14B** at 15 KDa that is present in endometroid OC but not in serous grade 1-2 OC. This band is also visible later in chapter 4, **Figure 4-13** and is likely to be protein degradation due to the antibody epitope not targeting the TSPAN6 isoform at 15 KDa. The band could also be non-specific binding, however (as discussed later in chapter 4) the band is shown to be more intense in the tissue extracts which have been through a rough extraction process which makes protein degradation likely.
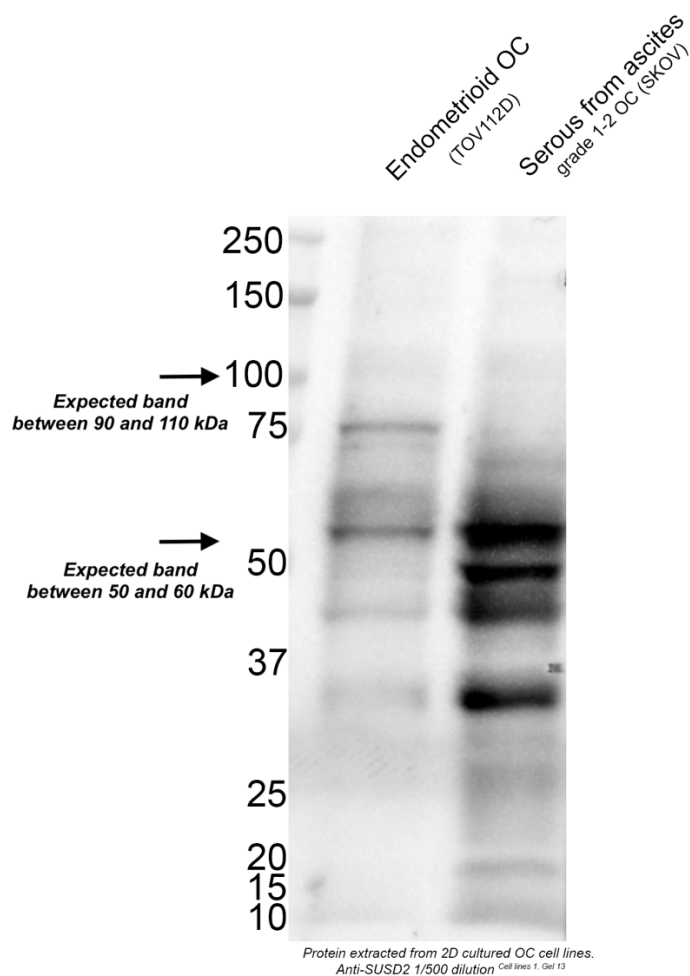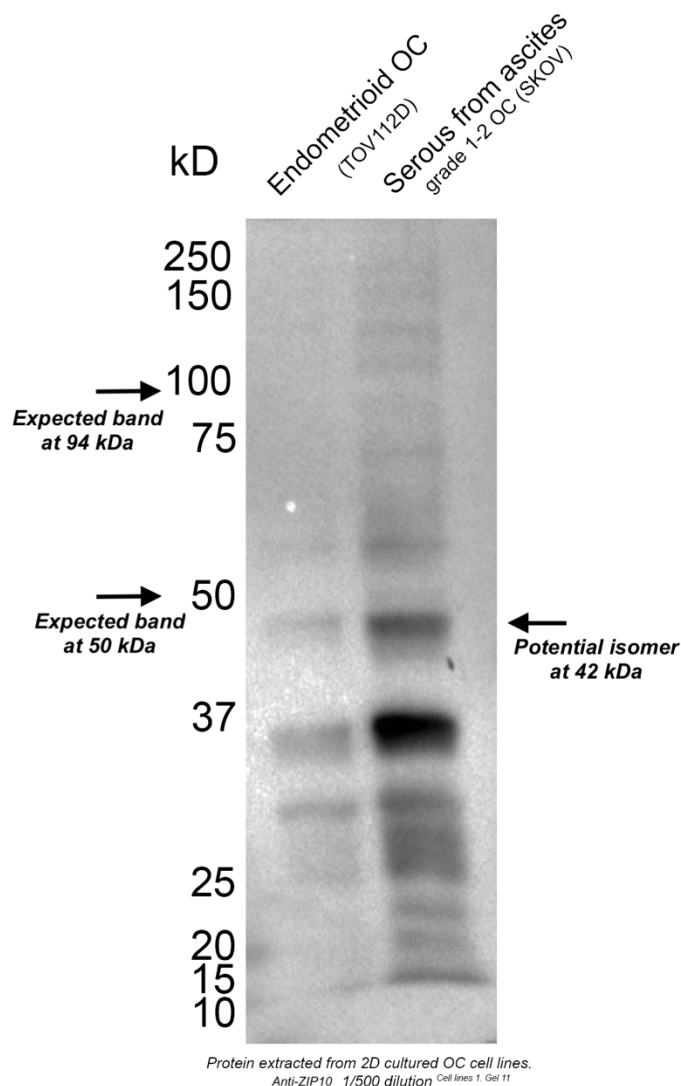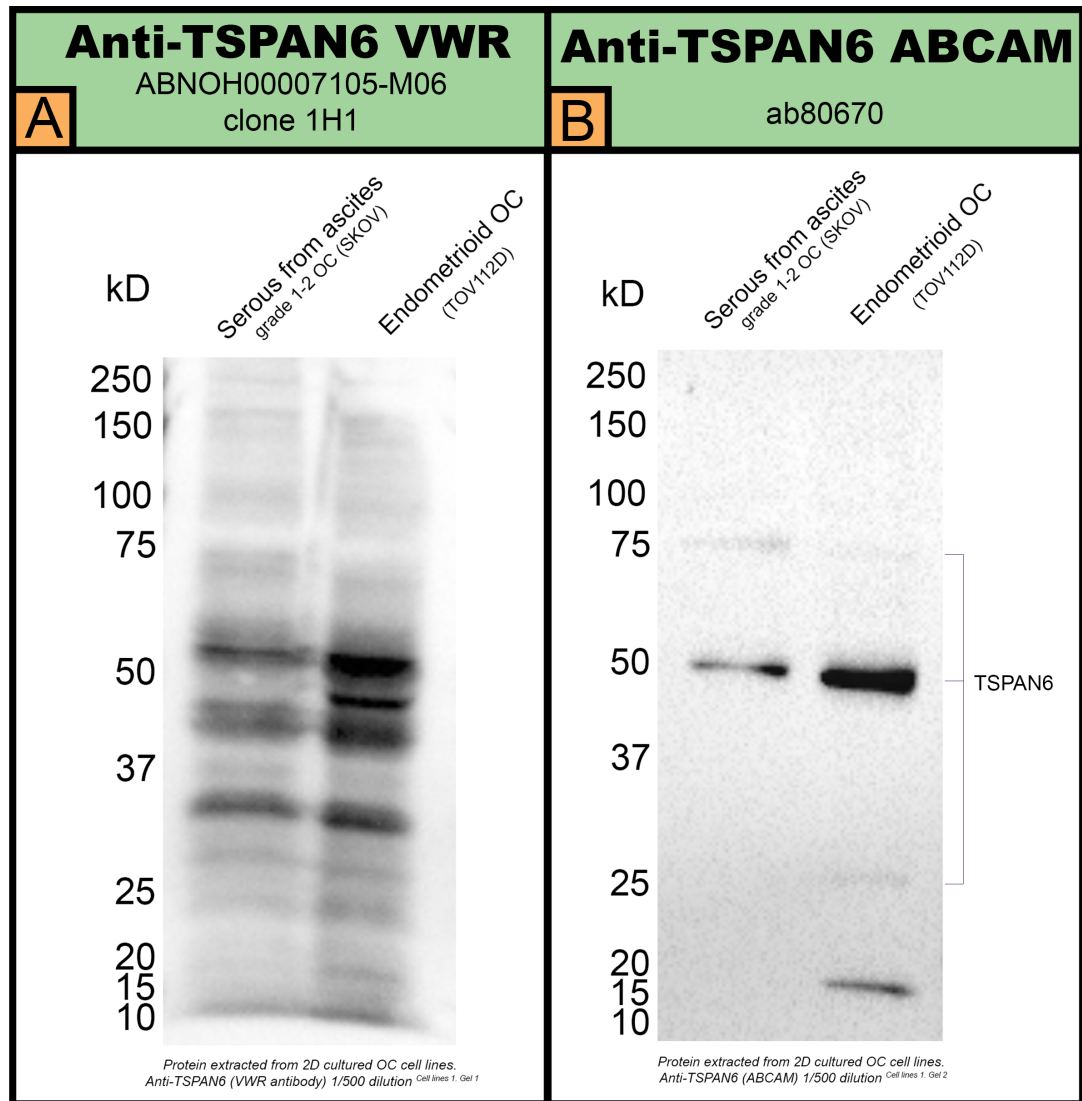
Figure 3-14 –TSPAN6 expression in two OC cell lines by immunoblot

Initial experiments conducted to assess target expression on protein lysates extracted from the OC cell lines SKOV-3 and TOV-112D, grown as 2D monolayers, using the polyclonal antibody ABNOH00007105 (A) and Abcam UK AB80670 (B). The experiment was carried out as per manufactures guidelines (5% BSA in TBS-T) and used a 1/500 antibody dilution. (A) Several unidentified bands make it not possible to confirm the specificity of this antibody for TSPAN6. (B) TSPAN6 expression can be seen as either a monomer (27 kDa) a homodimer (54 kDa) and a homotrimer (81 kDa). Specific bands (in B) make it possible to confirm the specificity of the ABCAM antibody for TSPAN6 expression in these cell lines.

There were no monoclonal antibodies against TSPAN6 that fulfilled the other two requirements therefore a polyclonal antibody from Abcam UK (AB80670) was purchased. When a western was carried out according to manufactures guidelines (5% non-fat dry milk in 0.05% PBS-T) it produced the blot shown above in **Figure 3-14B**. Clear bands could be seen at the monomer, homodimer and trimer band – 27, 54 and 81 kDa respectively. TSPAN6 is known to exist as homodimer and homotrimer that has been described in the literature as covalently bonded, as

it was not broken by denaturing at 95°C or reducing with β-mercaptoethanol (547). Patent WO2013/113696 characterises the band they presumed to be the homodimer in their western blot membranes. Here, two antibodies targeting the N-terminus and the C-terminus and both antibodies yielded both the monomer and homodimer band. The same two bands are also still visible when lysates of HEK cells overexpressing TSPAN6-GFP (Green Fluorescent Protein) are incubated with an anti-GFP antibody. Furthermore, the presumed dimer band was not shown to be destroyed by a strong detergent (1% SDS), high temperature (95°C and the presence of a reducing agent β-mercaptoethanol. TSPAN6 was also shown by western blot to be expressed in mouse brain and during human development. Indicating a possible important function during development. It is possible that an antibody binding the larger extracellular loop (the one in this project binds to the smaller extracellular loop) could prevent the dimerization of TSPAN6. Looking at the predicted topology in **Figure 3-7** which supports that an antibody binding the regions where a disulphide bridge could form could prevent a dimer from forming (539).

Further evidence of TSPAN6 and other tetraspanin family members forming homodimers is reported in a paper by Kovalenko *et al* (548). Kovalenko and colleagues described that tetraspanins associate extensively with each other and other transmembrane and near membrane proteins, and the resulting homodimers are fundamental units within larger tetraspanin complexes. Spontaneous crossing-linking *via* intermolecular disulphide bonds, the use of a cysteine-reactive covalent cross-linking agent, the use of an amino-reactive covalent cross-linking agent and the use of covalent cross-linking *via* direct intermolecular disulphide bridging between unpalmitoylated membrane-proximal cysteine residues was used to show tetraspanins have a tendency to homodimerize (549). Homodimers were constructed from newly synthesised proteins in the Golgi and most importantly these homodimers were seen on the surface of the cell in the tetraspanin webs or TEMS. Homodimers were shown to be the most common complex but evidence of higher order complexes such as homotrimers, homotetramers and higher were seen at a lower level.

Overall, from the results in **Figure 3-14** it was decided that the Abcam 80670 antibody would be used to continue the investigation of TSPAN6 as a novel ADC target. Additionally, the existence of higher order homodimers was reported in several places in the literature supporting the conclusion that the additional bands seen in **Figure 3-14B** are indeed likely to be higher level complexes covalently bonded together due to the cysteines and disulphide bonds in the large extracellular region of TSPAN6.

3.3.7 Screening of ZIP10 and TSPAN6 levels in different ovarian cancer subtypes by immunoblot

Protein was extracted from more OC cell lines and from primary patient 2D cells as a non-cancer control to determine the expression of ZIP10 and TSPAN6 protein in different ovarian cancer subtypes. The non-cancer 'healthy' primary patient samples were not considered true healthy controls; They were donated by patients who have had cause for concern to have a biopsy taken, risk reduction surgery due to a BRCA mutation or a hysterectomy. Samples are classed as non-cancer so long as no cancer diagnosis is given by the pathologist. This includes benign masses, benign simple cysts and normal ovaries.

Before beginning the second more extensive stage of western blotting with TSPAN6, it was found that THPA antibody against ZIP10 recognised the extracellular domain of the protein. Although the suitability of this antibody for western blot experiments was unknown, it was purchased to assess ZIP10 expression using other commercially available resources with the aim to obtain a specific pattern for ZIP10 expression in OC cell lines.

Analysis of ZIP10 expression on eight OC cell lines grown as 2D cell monolayers was performed using the THPA anti-ZIP10 antibody HPA066087 (**Figure 3-15)**. Unfortunately, the overall result was no clearer than the previous preliminary immunoblot using the NBP1 85080 antibody (**Figure 3-13**). Interestingly, the non-cancer primary patient protein was clearer than the cancer cell lines, supporting the literature and THPA that there is a lower expression of ZIP10 in the healthy ovary. There are still a lot of unidentifiable bands but there was a band seen at the approximate 94 kDa band on all samples and the band that could be the 42 kDa isomer was again present.
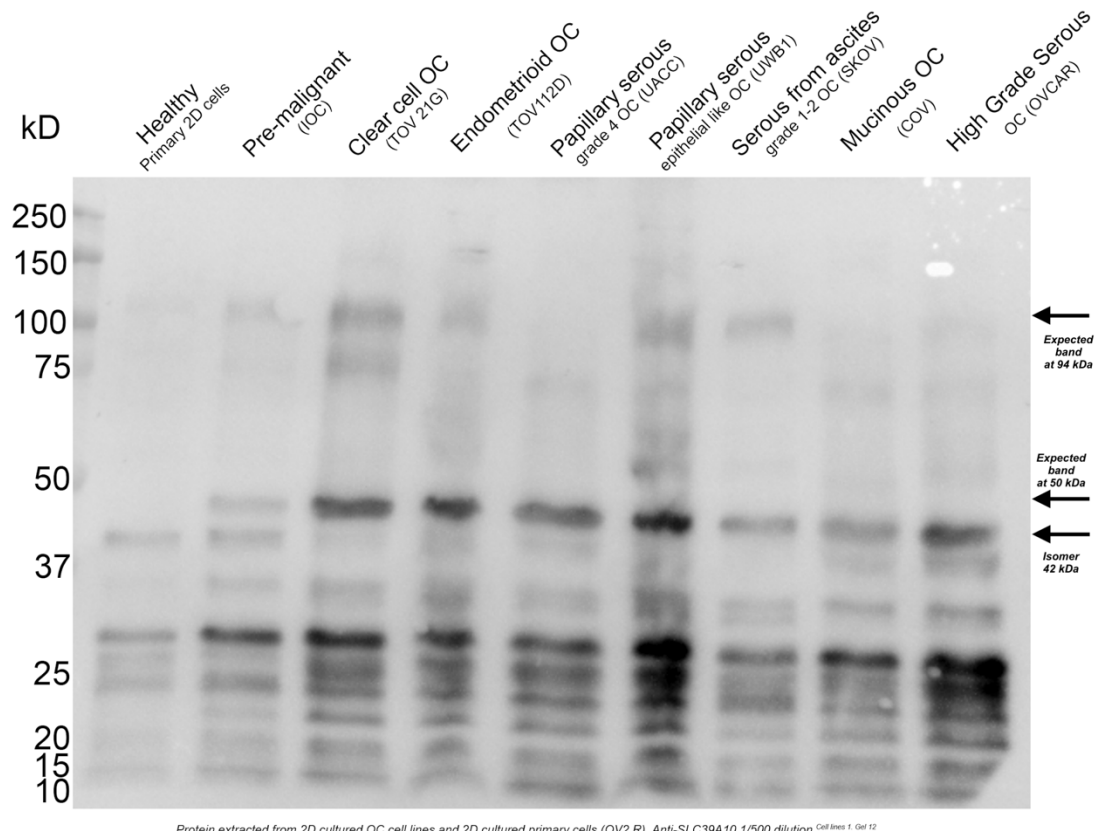
Figure 3-15 –ZIP10 expression in nine OC cell lines by immunoblot

Western blot showing healthy protein extracted from primary patient ovary and eight ovarian cancer cell lines. The antibody used was the extracellularly binding antibody used on THPA HPA066087. There is a band on all samples at the expected 94 kDa and at the size of the 42 kDa isomer. However multiple unidentifiable bands result in the decision that this antibody on these samples is not suitable for quantifying ZIP10 expression in ovarian cancer tissue.

In conclusion, none of the antibodies tested were suitable for specific detection and quantification of ZIP10 expression in OC cell lines. Therefore, ZIP10 target was not further evaluated in subsequent immunoblot experiments.

The purpose of these preliminary experiments was to determine the best targets in terms of ovarian cancer expression. Overall, from these initial *in vitro* quantification expression experiments, TSPAN6 was the only target where expression in OC cell lines could be determined with confidence. Therefore, it was concluded that ZIP10, PIEZO2, SUSD2, CEACAM8 and PCSK4 were not going to be carried forward in more extensive analysis by western blot.

TSPAN6 was the only target to be used from this point onwards in further western blots using more OC cell lines of different subtypes, protein extracted from primary patient cells, protein extracted from primary patient tissue and commercial healthy protein lysate from different areas of the body.

Figure 3-16 below, shows the Abcam anti-TSPAN6 antibody ab80607 used on a western blot with eight OC cell lines protein lysates and one non-cancer primary protein lysate extracted from a primary 2D cultured monolayer derived from a 'healthy' patient biopsy. It's clear the presumed dimer band is still visible, and the predicted band of the monomer is visible at the expected size of 27 kDa. Some additional bands can be seen around 15 kDa and these are presumed to be small fragments of denatured TSPAN6. There are two small predicted isomers of TSPAN6 (Uniprot O43657) (199) that could explain the small bands, however these haven't been verified and remain only a prediction. Here the differences in expression of TSPAN6 between the cell lines become noticeable. This was a single western blot membrane therefore no statistical analysis could be done at this stage. The SKOV-3 homotrimer band at approximately 80 KDa is not present on the blot in **Figure 3-16**, however it was observed in **Figure 3-14**. This is likely a reproducibility issue common with western blots as lysates were harvested from wells of the same confluency and passage number.

Quantification of the TSPAN6 monomer and dimer bands seen in **Figure 3-16** was performed (**Figure 3-17**). Looking at the axis of the two graphs the fainter expression of the monomer band (**Figure 3-17A**) is reflected in this quantification by a smaller normalised intensity compared to the dimer (**Figure 3-17B**). Although the graphs do not mirror each other by having the same trend, it was decided that the presumed dimer band would be used to quantify the expression of TSPAN6 in these cell lysates. TSPAN6 exists in the human body as a part of the tetraspanin webs, more often associating with itself and other family members than being alone. If the monomer band is added to the dimer band then the trend shown in the dimer graph does not change as the monomer is so weakly expressed in comparison. For this reason, the dimer band will be used to quantify expression.
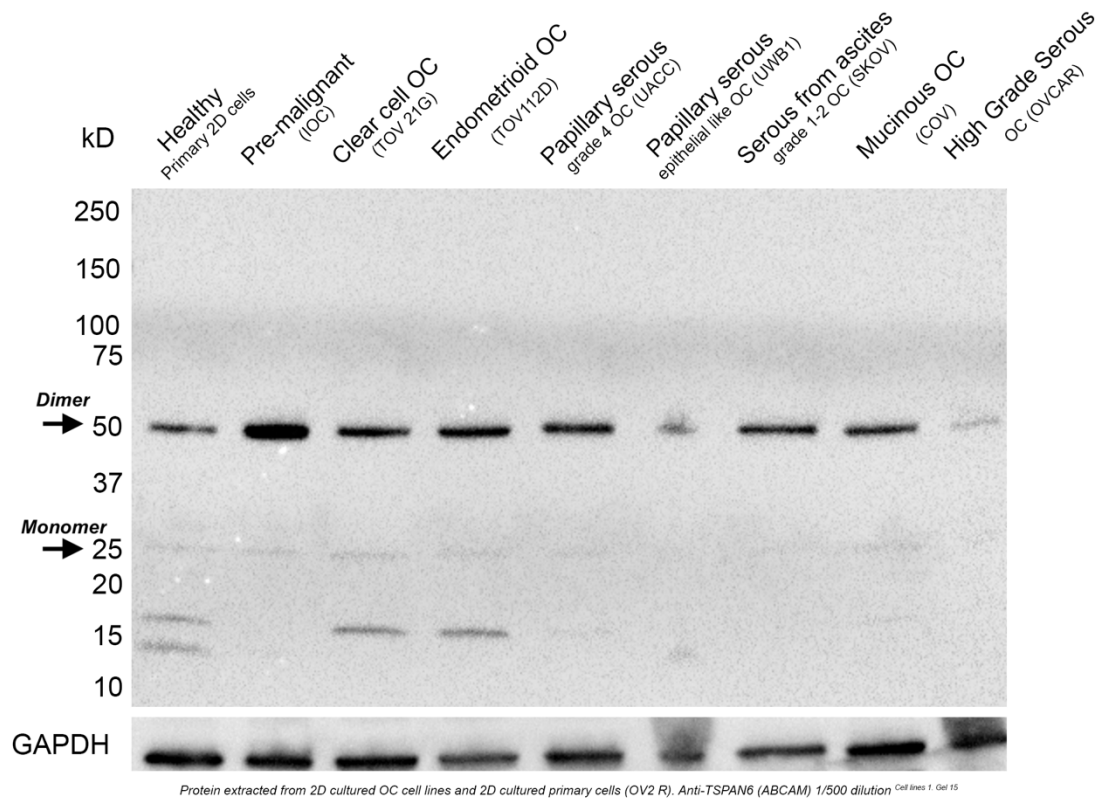
Figure 3-16 - TSPAN6 antibody ab80607 in western blot on all OC cell lines and non-cancer primary cells

The western blot with TSPAN6 antibody ab80607 in eight OC cell lines shows the expression of TSPAN6 dimer in all cell lysates and the monomer in some but not all cell lines. This western was performed as a single experiment with the intention to perform three replicates for statistical analysis. Initially, it can be seen that the bands are clear in all protein lysates using this antibody, TSPAN6 is expressed in all cell lines in varying intensities and some cell lines show smaller fragment bands. GAPDH was used to normalise this data and the band can be seen at the bottom.
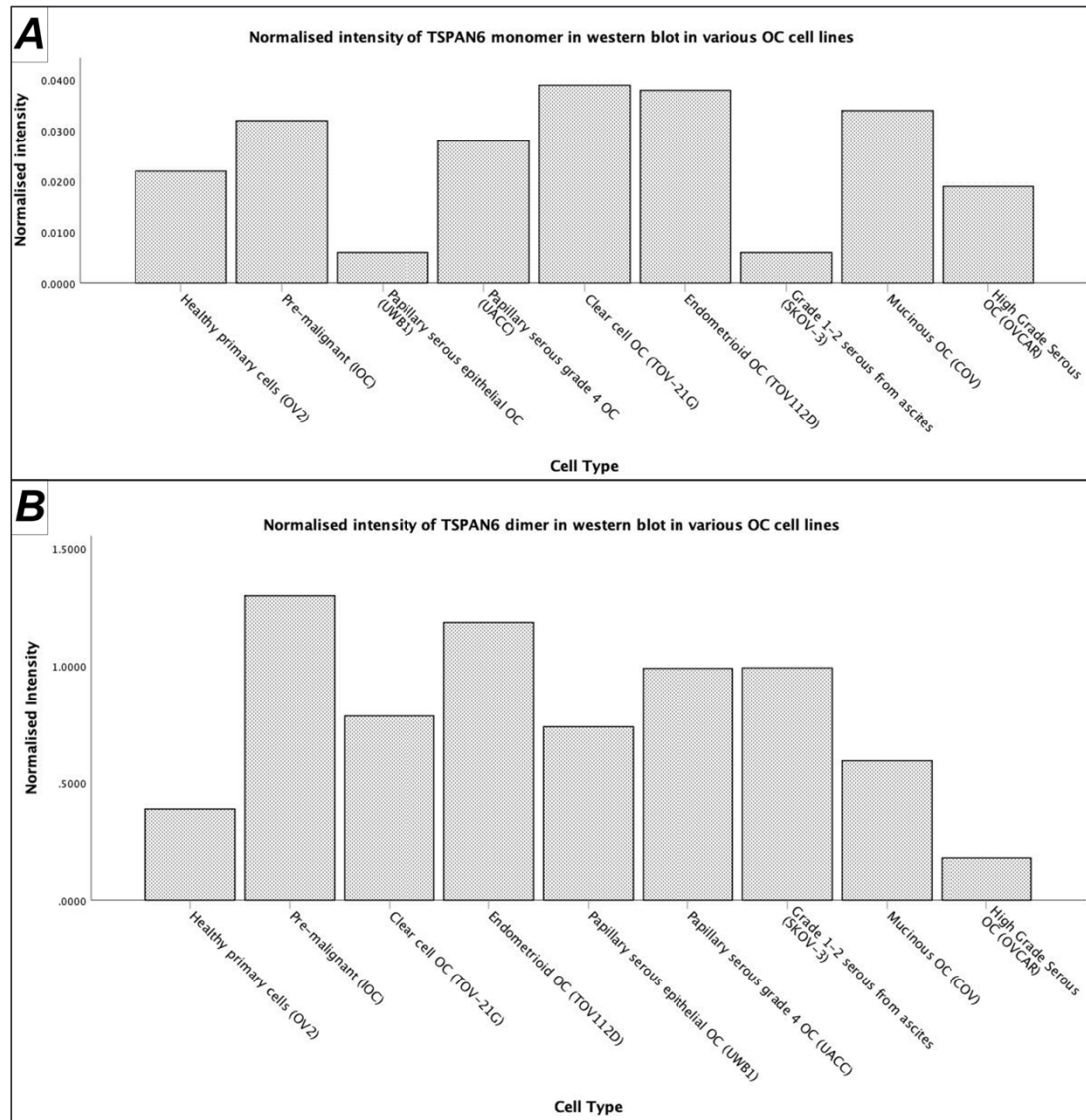
Figure 3-17 – Quantification of TSPAN6 antibody ab80607 in a western blot on all OC cell lines and non-cancer primary cells

Bar graphs showing the normalised intensity quantification of the monomer and dimer band from the western blot seen in Figure 3-16. Graph A shows the monomer and B the dimer. No statistical analysis was performed as only one experiment was performed with the intention to perform further replicates. From this quantification it can be seen that the monomer band is much less expressed than the dimer and taking both into account does not change the trend of the dimer. As TSPAN6 exists more prevalently as a dimer in the human body, it was decided the dimer band would be used for future quantification of expression.

At this stage Abcam discontinued the TSPAN6 ab80607 antibody. An alternative antibody with the same epitope was chosen from Creative Diagnostics (USA). The western using Creative Diagnostics DPABH-18048 was shown to behave the same way in western blot as can be seen in **Figure 3-18** below. The antibody produces a western blot so alike to the ab80607 antibody that even the cell lines that do not appear to produce a monomer band using ab80607 (IOC, UACC,

UWB1) also do not present a monomer band on the Creative Diagnostics DPABH-18048 western. Therefore, anti-TSPAN6 antibody Creative Diagnostics DPABH-18048 was used in all future experiments from this point onwards.

Figure 3-18 is a representative example of three biological replicates performed of this western blot using the new DPABH-18048 antibody. Due to the former antibody being discontinued, replicates were not possible for the previous antibody. In this experiment each cell line was grown three separate times and three protein extractions per cell line were carried out to create biological replicates. As with the former antibody, TSPAN6 is shown to be expressed in all cell lines in both dimer and monomer form. GAPDH was stained as a housekeeper gene for loading control normalisation in the quantification. Interestingly, the smaller 15 KDa band is not visible here in **Figure 3-18** and could be explained by western blot reproducibly issues.

This figure also shows the first appearance of a band not seen in cell lines, but only in the healthy tissue protein extract. The presence of this band is discussed further in this chapter and the following chapter.

Protein extracted from 2D cultured cell lines and purchased from Novus Bio. Anti-TSPAN6 DPABH-18048 1/500 dilution ^{Gel 2}
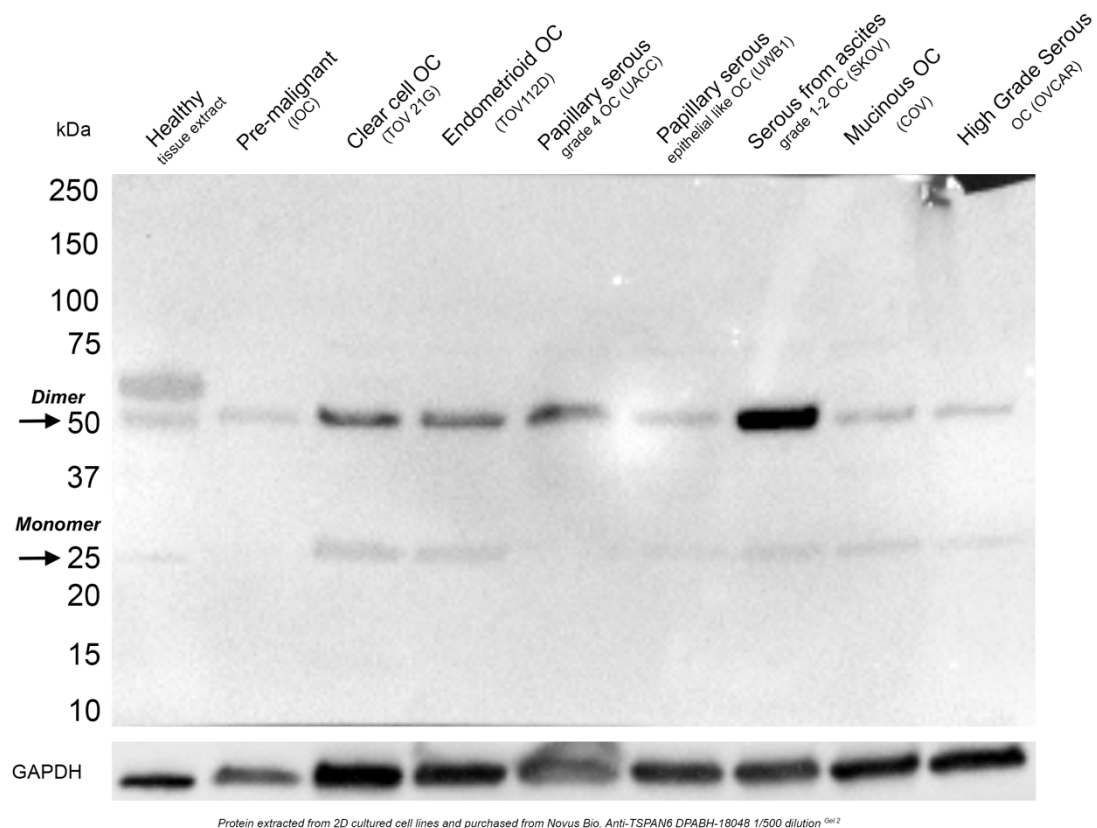
Figure 3-18 – Western using Creative Diagnostics DPABH-18048

A western blot using anti-TSPAN6 Creative Diagnostics DPABH-18048 polyclonal antibody. The purpose of this western was to confirm this antibody behaved in the same way as the former antibody. This antibody displayed almost identical bands to the former antibody, including the absence of the monomer band in the same cell lines (IOC, UWB1, UACC). This gel differs from Figure 3-16 in that a commercially available protein lysate from healthy ovary tissue was obtained (Novus Bio NB820-59243) and used in this gel instead of a protein lysate from the primary patient cell. This resulted in the first appearance of the additional band at approximately 60 kDa.

In **Figure 3-19** below, the boxplot for the above western (**Figure 3-18**) can be seen. The box plot combines the band intensity from three biological replicates of the same samples. The bands from each of the three gels were quantified using Image Lab™ Version 6.0.1 build 34 standard edition ©2017 Bio Rad laboratories, Inc. Each gel was quantified separately before transferring to IMB© SPSS© version 26.0.0.0 for statistical analysis. A Kolmogorov-Smirnov test showed the data to be not normally distributed with a p value < 0.05. To reveal any significant differences between all the samples, a Kruskal Wallis test was carried out. If the data had been normally distributed a One-way Anova would have been carried out. The Kruskal Wallis test revealed no significant differences between any of the samples. To explore further, the lowest mean (the healthy tissue extract) and the highest mean (cell line UACC) were compared in a Mann Whitney U test which again showed no significant difference with p=0.200. Although no significance

146

difference was shown the quantification does support THPA by showing less expression in the healthy ovary when compared to OC cell lines. The differences in expression between the OC cell lines could also prove valuable in future experiments if more replicates revealed a significant difference. The sample size here was comparatively small to those in the literature and only three biological replicates were carried out.
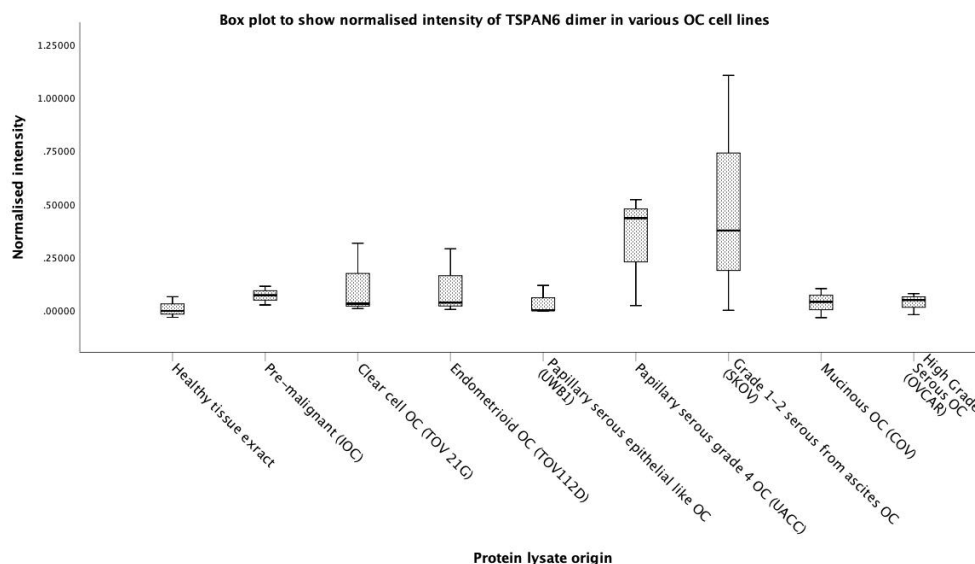
Figure 3-19 – Box plot of the quantification of TSPAN6 in various OC cell lines using Creative Diagnostics DPABH-18048 polyclonal antibody

This boxplot was produced from three biological replicates of eight OC cell lines. The data is not normally distributed p= <0.05 by Kolmogorov-Smirnov test. There was no significant difference between any of the samples (Kruskal Wallis test p=0.6). The box plot does show that the healthy ovary tissue lysate does have the lowest expression when compared to the OC subtypes, although not statistically significantly lower. OC subtype Papillary serous grade 4 (UACC) and grade 1-2 serous from ascites (SKOV-3) were noticeably higher than the other OC subtypes, although not significantly higher.

3.3.8 Differential expression of TSPAN6 in healthy tissue versus ovarian cancer cells by immunoblot.

One of the properties of an ideal ADC target is its low expression in healthy cells compared to cancer cells. It was then decided to explore the expression levels of TSPAN6 in healthy tissue given the promising results on target expression observed in ovarian cancer cells. **Figure 3-20** below shows the antibody anti-TSPAN6 DPABH-18048 in a western blot on healthy tissue purchased from Novus Bio UK. Healthy ovary (NB820-59243), uterus (NB820-59274), breast (NB820-59203), lung (NB820-59239), spleen (NB820-59259), brain (NB820-59177), liver (NB820-59232) and lymph node (NB820-59242) were analysed in this western blot. In addition, the OC cell line TOV-112D is shown for comparison. Initial observations are that TSPAN6 is present in

all healthy tissues however considerably less so than the OC cell line and the healthy protein lysates extracted from tissue all show the presence of the 60 kDa band just as the healthy ovary protein lysate did in **Figure 3-18**. This will be explored in the following chapter, where western blot analysis is carried out on protein extracted from primary patient tissue as there may be a connection between this 60 kDa band and protein extracted from tissue rather than 2D cells and interestingly the healthy brain tissue lysate is the only one that doesn't express this band.
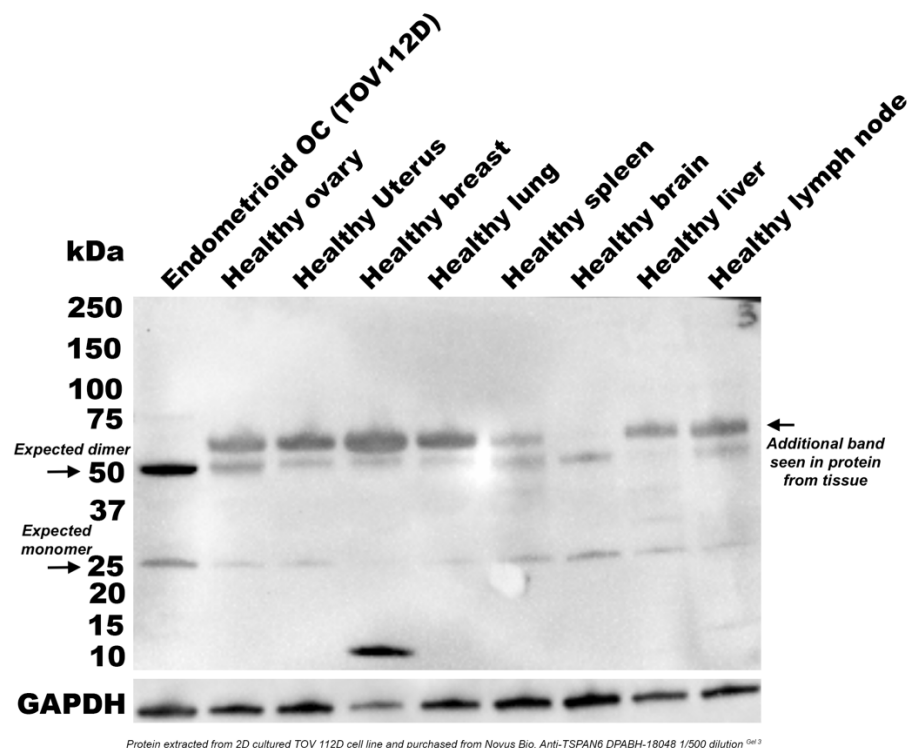
Figure 3-20 – TSPAN6 western for healthy protein extracted from the tissue

A western blot showing a lower intensity of TSPAN6 in healthy tissue protein extracts purchased from Novus Bio UK. GAPDH can be seen at the bottom as a loading control to normalise by for quantification. It can be seen that TSPAN6 is present in all healthy tissue samples and the 60 kDa band is present in all of the healthy protein from tissue although much less so in the healthy brain.
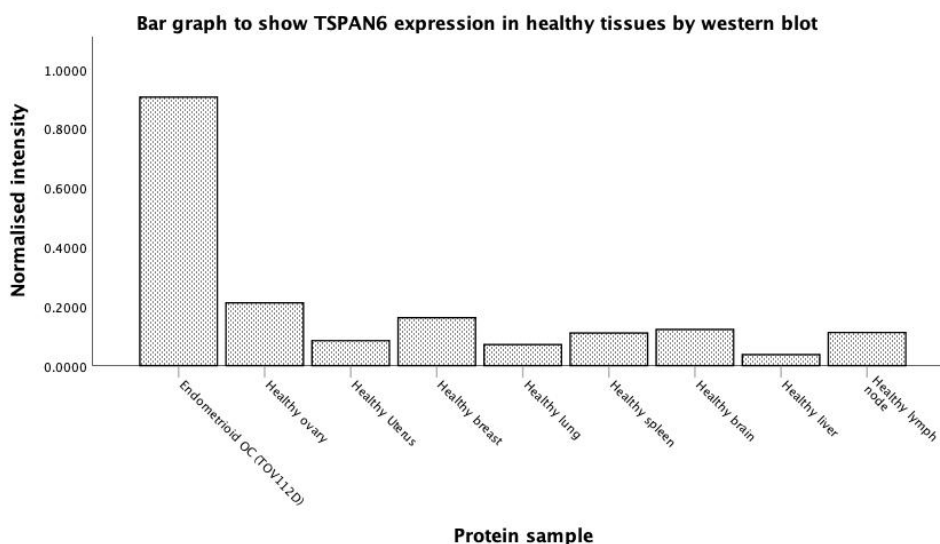
Figure 3-21 – Quantification of TSPAN6 western blot using antibody DPABH-18048 on healthy protein lysates from tissue.

Bar graph showing quantification of the TSPAN6 immunoblot of Figure 1-20. This was a single experiment and so no statistical analysis was carried out. The Intensity in OC cell line TOV-112D is considerably higher than in the various healthy tissues from around the body.

The quantification of the preliminary investigation of TSPAN6 expression in various healthy tissues was also performed (Figure **3-21**). The intensity of the immunoreactive bands was quantified using Image Lab™ Version 6.0.1 software (BioRad Laboratories, Inc). As shown in **Figure 1-21**, the OC cell line TOV-112D reported higher TSPAN6 expression levels than the various healthy tissues analysed. Whilst healthy ovary has the highest expression compared to the other tissues the expression on all of them is comparatively low when compared to TOV-112D. The liver shows the least intense expression of the TSPAN6 dimer, closely followed by the lung and the uterus.

In regard to an ADC target, off target expression in other healthy tissues around the body is not ideal. However, it is dependent on the delivery method as to how much of a problem this poses. Due to TSPAN6 being expressed in various tissues around the body a systemic ADC treatment may produce off target toxicity. If the ADC is administered locally to the ovary only, then off target toxicity is potentially less of a problem.

Overall, TSPAN6 expression in various OC cell lines and healthy protein lysates could be clearly determined using polyclonal antibody anti-TSPAN6 DPABH-18048 in western blot analysis. Although no statistical significance was seen between the various OC subtypes, further replicates could uncover a significant difference.

3.4 Target characterisation by immunofluorescence (IF)

TSPAN6 was the only target out of all six targets explored that showed potential for development as ADC target based on expression level measured by immunoblot. However, it was decided to assess all the antibodies by immunofluorescence to assess the membrane location of the targets as predicted by the literature and THPA and to inform future development, beyond the scope of this project, of better antibodies suitable for both applications.

Hence, antibodies were tested to confirm target expression in 2D cultured OC cell by immunofluorescence. An appropriate secondary antibody labelled with a Texas Red fluorophore (Santa Cruz UK anti-rabbit sc-2780 and anti-mouse sc-2781) was also used and the HEK 293T cells were used as cell line not linked to female tissues. In all of the IF figures below, Hoechst stain was used to detect the nuclei (in blue), Wheat Germ Agglutinin (Thermo Fisher Scientific UK W11261) was used to stain the membrane (in green) and Texas Red fluorophore signal indicated the presence of the target proteins (red).

As shown in **Figure 3-22**, TSPAN6 antibody binds to 2D cultured cells from eight OC cell lines, non-cancerous primary cells and the immortalised HEK 293T cell lines. TSPAN6 staining was localised to the plasma membrane in all cell samples assessed. In particular, TSPAN6 is strongly localised to the membrane in IOC, TOV-112D, OVCAR, non-cancer primary and HEK-293T. WGA and TSPAN6 staining don't appear to co-localise. Where a yellow signal should have been seen in the case of co-localisation the red and green staining are shown separately. This could be due to occupying slightly difference places on the plasma membrane.

Figure 3-23 shows the cellular location of PCSK4 in the various cell types. There is a lot of variation in the expression and localisation of PCSK4. Expression is seen in all cell types with the exception of TOV-112D and HEK-293T. Clear membrane localisation is seen in IOC and SKOV. Variation in behaviour between different cell types is encouraging as it indicates that PCSK4 could be used to stratify patients. The antibody used here is the same antibody used in the western blot experiments, and therefore non-specific binding is possible. However, in contrast here, the localisation is shown to be specifically localised to the plasma membrane as opposed to an abundance of general fluorescent signal. This suggests more specificity than in the western blot experiments. Differences could be due to antibodies performing differently in different applications due to antibody epitope availability.

The expression and location of PIEZO2 can be seen in **Figure 3-24**. Expression of PIEZO2 was seen in all cell types. In particular, PIEZO2 was located to the membrane mostly in HEK-293T, OVCAR, TOV-112D and IOC cells. Overall, there did seem to be a more intense cytoplasmic

location of PIEZO2 with some membrane localisation seen. COV cells seem to show diffuse cytoplasmic staining of PIEZO2. As long as there is expression on the plasma membrane as well, the cytoplasmic expression of PIEZO2 is not a problem for a potential ADC target. The antibody in this experiment is the same as the one used in the western blot experiments therefore, as discussed above with PCSK4, non-specific binding is possible.

When looking closely at the colocalization of WGA and target expression, it can be seen these don't always colocalize directly. The rationale behind using the WGA stain was to visualize the membrane and ensure it wasn't damaged by the fixation process. The green on the WGA should colocalize with the red of the target stain to produce a yellow colour if the two do colocalize. This can be seen to be the case in a small number of images such as in PCSK4 in the IOC cell line, however this is not seen in general overall. The target stain does appear to be following the membrane (such as in TSPAN6 in the IOC cell line) but not directly colocalizing with the WGA. This could be due to the stains occupying slightly different positions on the membrane. WGA binds to N-acetyl-D-glucosamine and Sialic acid present on the plasma membrane which means there is the potential to be occupying a slightly different space on the plasma membrane.

Overall, these IF experiments demonstrate membrane location and overexpression in cancer cells for these three targets. Hence it was decided to progress them further along the characterisation pipeline – protein expression in primary patient derived samples.
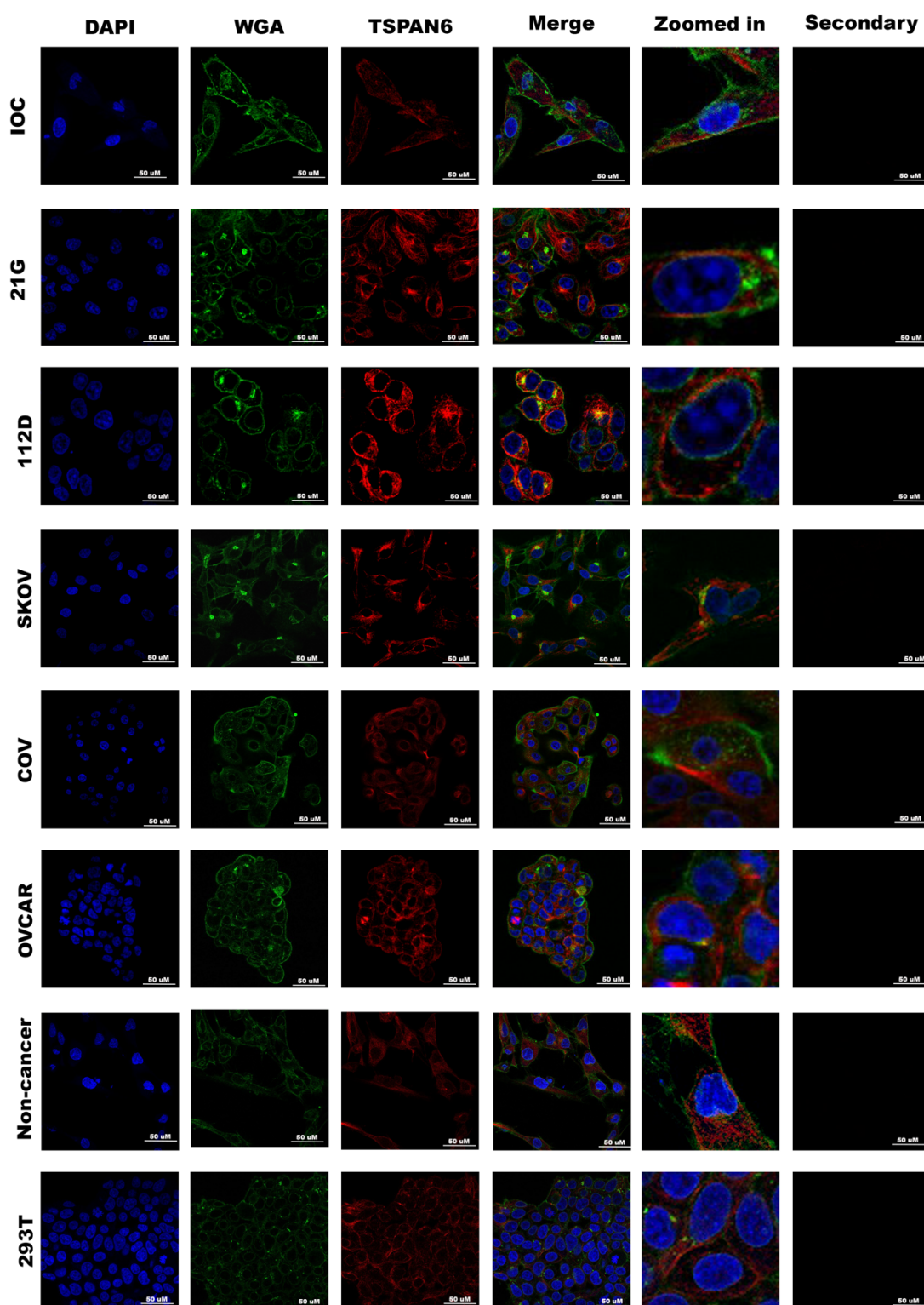
Figure 3-22 – Localisation of TSPAN6 in 2D ovarian cancer cell lines in vitro

Representative images of TSPAN6 IF revealed TSPAN6 in all cell types and localisation to the plasma membrane is seen most clearly in HEK-293T, non-cancer primary, OVCAR, COV, SKOV, TOV112D, TOV21G and IOC cell lines. WGA = green, TSPAN6 = red, co-localised = yellow. Magnification = x40, scale bar = 50 μM (n = 3 fields of view). 'Zoomed in' refers to a zoomed in and cropped version of the x40 image.
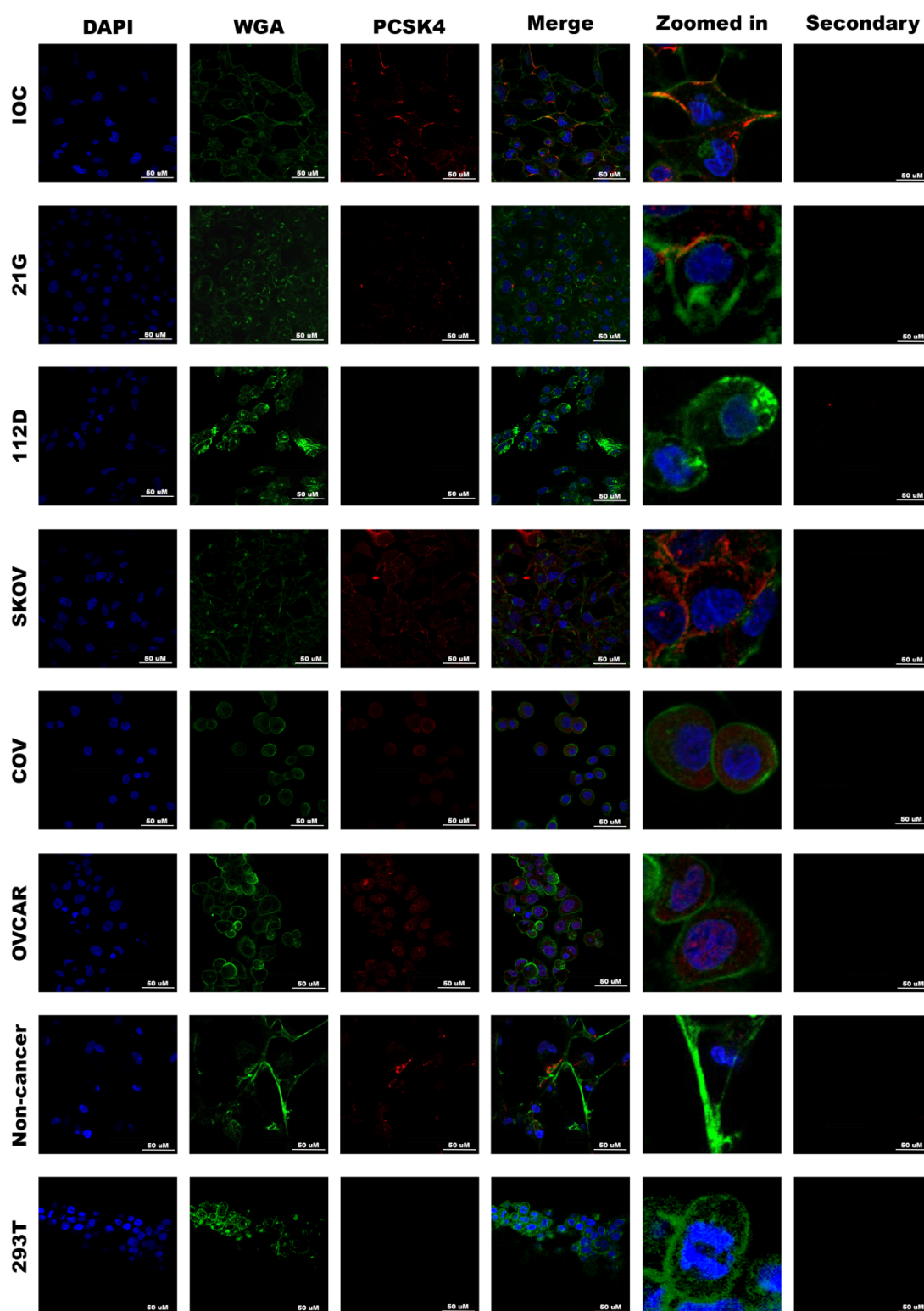
Figure 3-23 – Localisation of PCSK4 in 2D ovarian cancer cell lines in vitro

Representative images of PCSK4 IF revealed PCSK4 in all cell types except HEK-294T and TOV-112D and localisation to the plasma membrane. Localisation to the membrane is seen most clearly in SKOV, TOV-21G and IOC cell lines. WGA = green, PCSK4 = red, co-localised = yellow. Magnification = x40, scale bar = 50 μM (n = 3 fields of view). 'Zoomed in' refers to a zoomed in and cropped version of the x40 image.
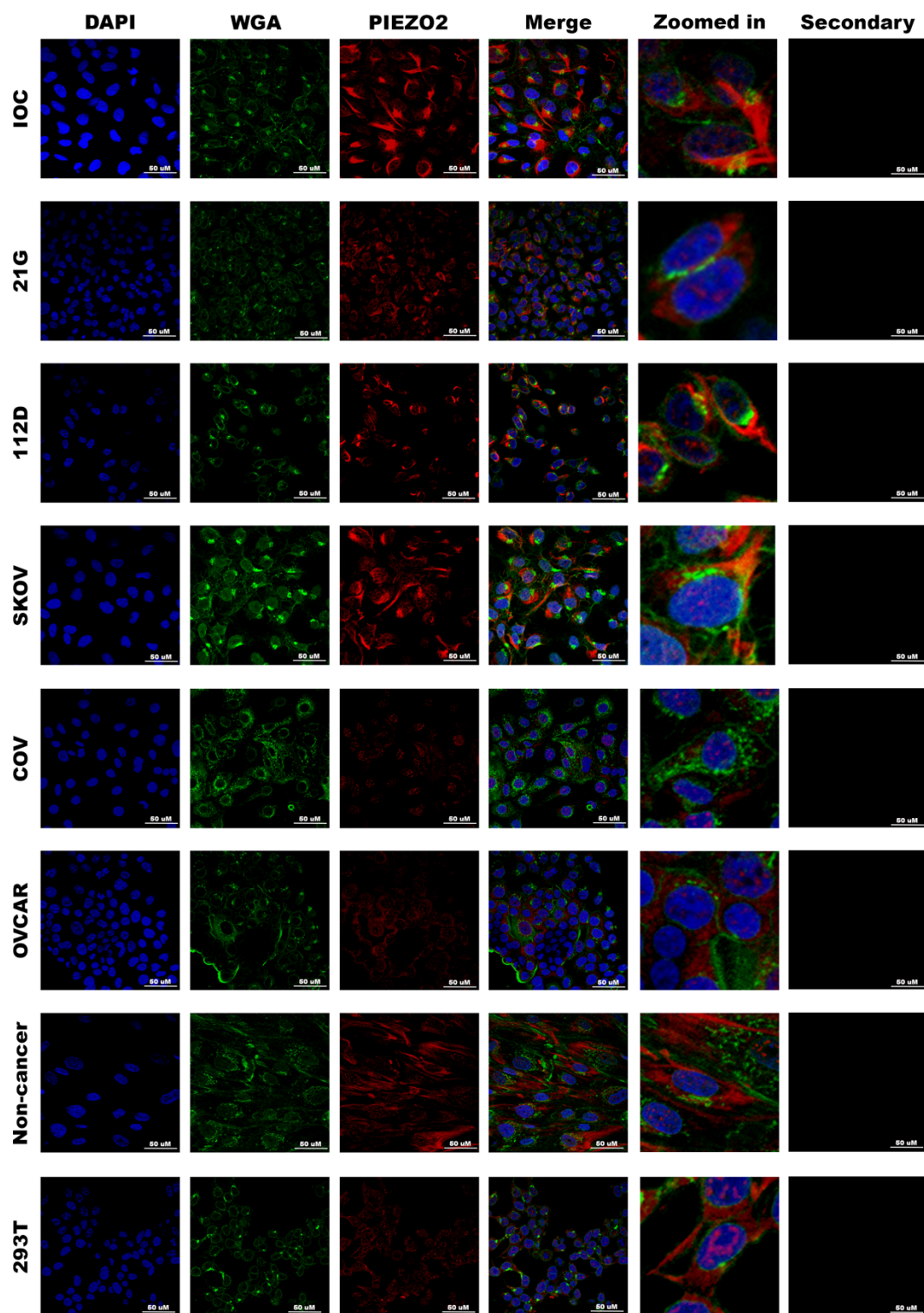
Figure 3-24 – Localisation of PIEZO2 in 2D ovarian cancer cell lines in vitro

Representative images of PIEZO2 IF revealed PIEZO2 in all cell types and on the plasma membrane, however some show more intense cytoplasmic location. Localisation to the membrane is seen most clearly in HEK-293T, OVCAR, TOV-112D and IOC cell lines. WGA = green, PIEZO2 = red, co-localised = yellow. Magnification = x40, scale bar = 50 μM (n = 3 fields of view). 'Zoomed in' refers to a zoomed in and cropped version of the x40 image.

Figure 3-25 to **Figure 3-27** display the expression and localisation of the remaining targets CEACAM8, SUSD2 and ZIP10 by IF. IF to detect CEACAM8 (**Figure 3-25**) expression in IOC, TOV-112D, TOV-21G and SKOV-3 revealed weak and cytoplasmic staining. Some membrane localisation can be seen on the non-cancer primary patient cells which is an undesirable characteristic for a potential ADC target. SUSD2 (**Figure 3-26**) shows very weak cytoplasmic staining in all cell types and no membrane localisation can be seen. Finally, ZIP10 (**Figure 3-27**) shows almost no expression in any of the cell types. Some very weak expression can be seen however this is also located in the cytoplasm and no membrane localisation can be seen in **Figure 3-27**. These experiments further confirm CEACAM8, SUSD2 and ZIP10 have either limited expression or overwhelming cytoplasmic localisation and hence these targets were not selected to progress further along the characterisation pipeline. The antibodies used in **Figure 3-25** – **Figure 3-27** are the same ones used in the western blots, therefore non-specific binding is possible. However, in **Figure 3-25** – **Figure 3-27** no localisation to the membrane is displayed and fluorescent signal is weak. This is not consistent with the abundance of non-specific binding seen in the western blots when using these same antibodies. This again highlights the differences seen in antibodies performance when they are used in different applications potentially due to antibody epitope availability from different protein conformations.
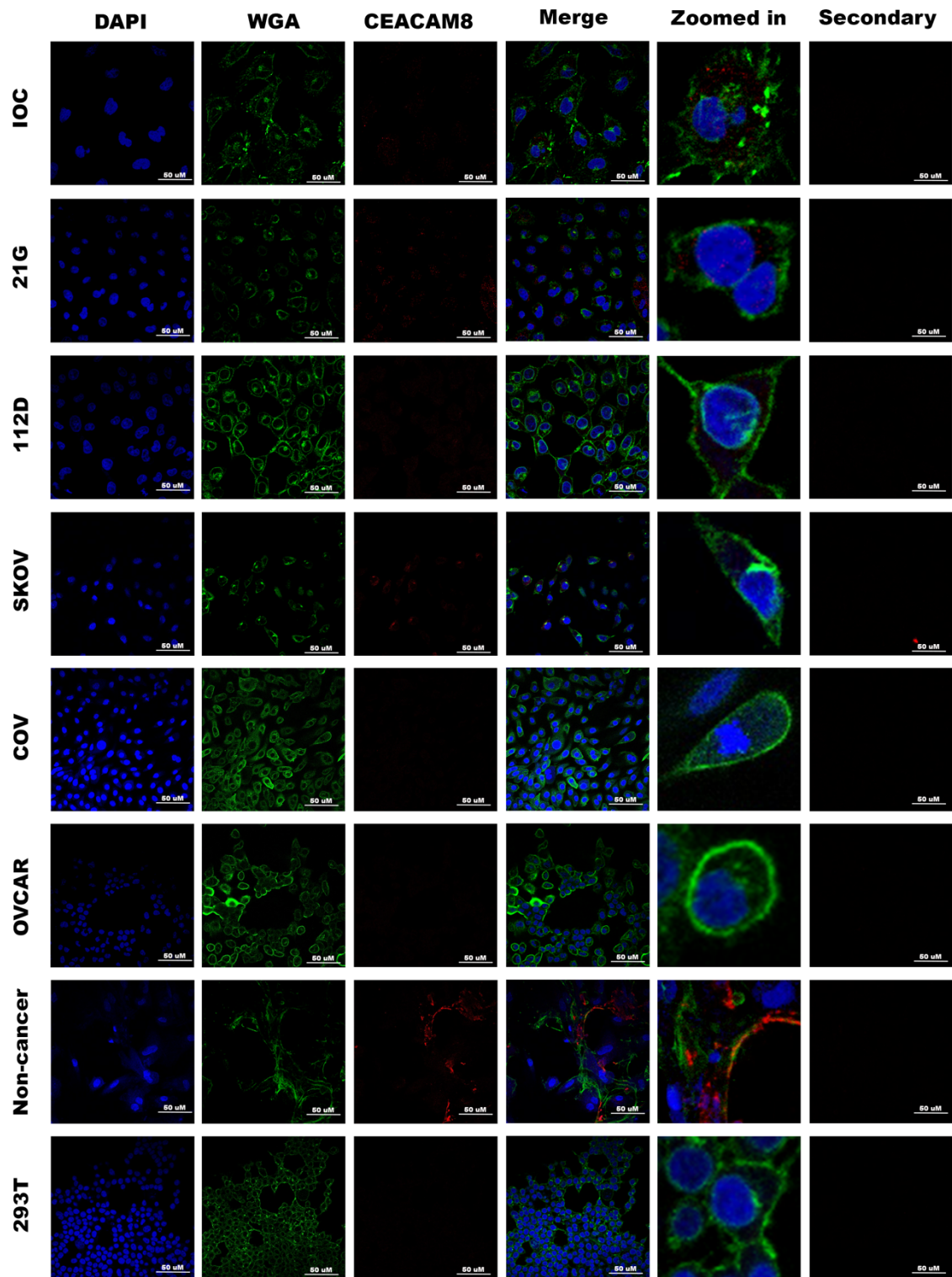
Figure 3-25 – Localisation of CEACAM8 in 2D ovarian cancer cell lines in vitro

Representative images of CEACAM8 IF revealed CEACAM8 only in non-cancer primary patient cells, SKOV-3 TOV-21G and IOC cell line. WGA = green, TSPAN6 = red, co-localised = yellow. Magnification = x40, scale bar = 50 μM (n = 3 fields of view). 'Zoomed in' refers to a zoomed in and cropped version of the x40 image.
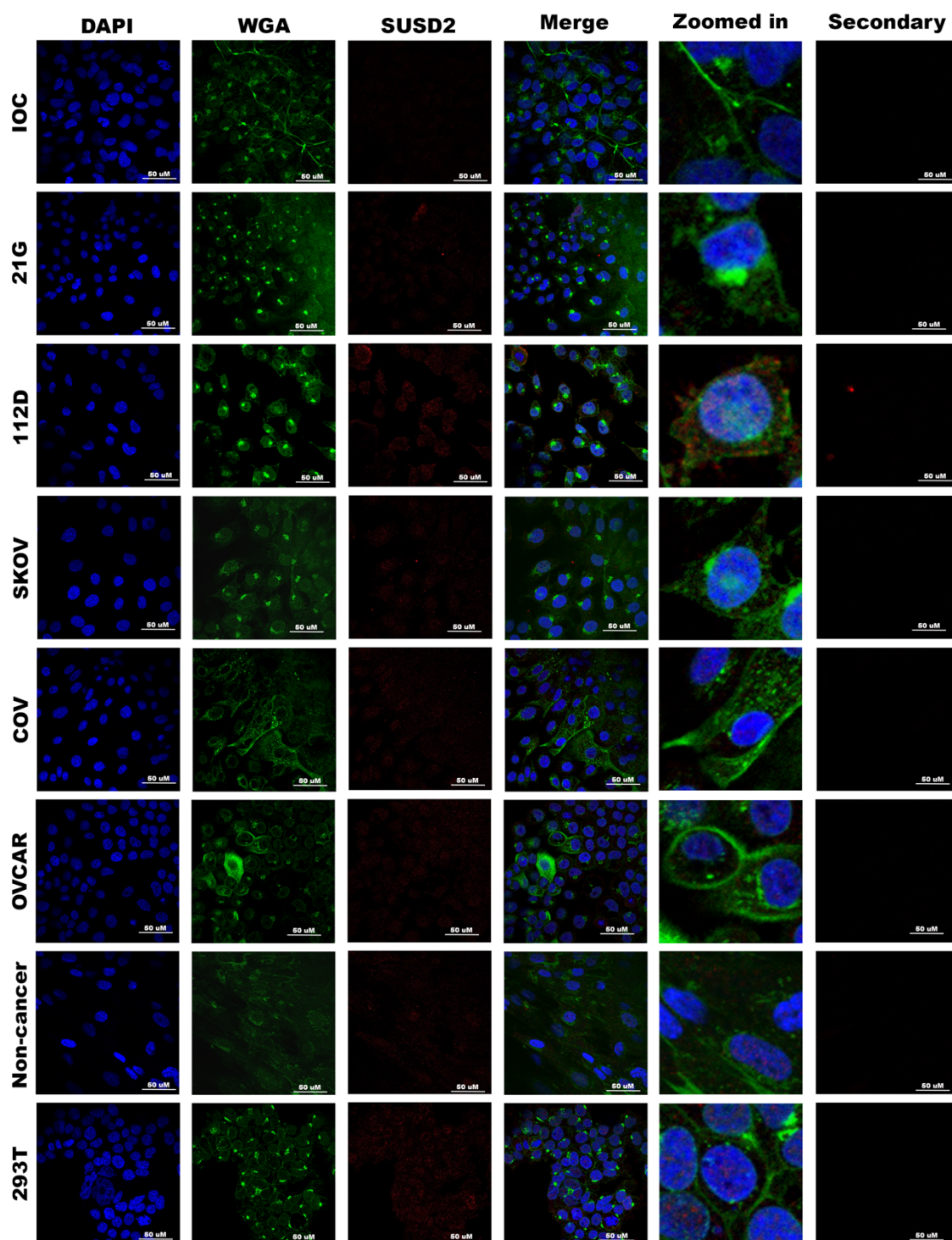
Figure 3-26 – Localisation of SUSD2 in 2D ovarian cancer cell lines in vitro

Representative images of SUSD2 IF revealed SUSD2 only very weakly in all cell types. Localisation to the plasma membrane is not seen clearly. WGA = green, SUSD2 = red, co-localised = yellow. Magnification = x40, scale bar = 50 µM (n = 3 fields of view). 'Zoomed in' refers to a zoomed in and cropped version of the x40 image.
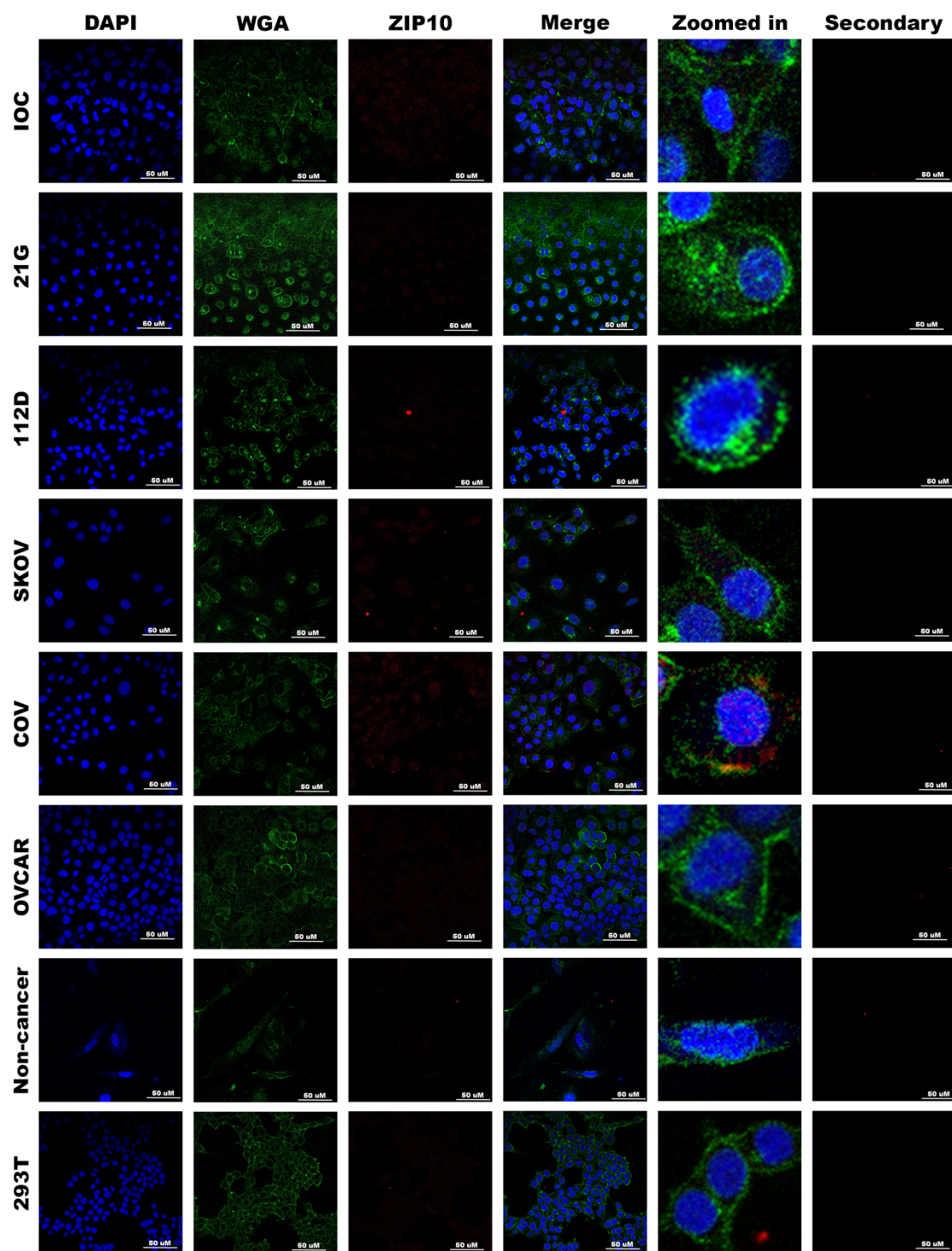
Figure 3-27 – Localisation of ZIP10 in 2D ovarian cancer cell lines in vitro

Representative images of ZIP10 IF revealed ZIP10 only very weakly in COV, SKOV-3, TOV-21G and IOC cell lines. Localisation to the plasma membrane is not seen clearly. WGA = green, ZIP10 = red, co-localised = yellow. Magnification = x40, scale bar = 50 μM (n = 3 fields of view). 'Zoomed in' refers to a zoomed in and cropped version of the x40 image.

This IF analysis was carried out using antibodies that showed evidence of non-specific binding by western blot. The decision to continue with the IF experiments despite the negative western blot results was made due to different antibodies behaving different in different applications. Just because the antibodies were inappropriate for use in western blot did not mean they would be poor in IF. The proteins are presented in a 3D conformation in IF compared to the linear conformation the proteins in western blot. This different protein conformation could allow for differences in antibody binding behaviour. This does, however, highlight a limitation of this project in the great need for antibody validation in this ADC target identification process. This could be carried out by generating a knockout cell line; however, it is unclear at what point this should be carried out. The generation of a knockout cell line is costly and time consuming and is not immediately appropriate in the high through put identification of novel targets as this would be better carried out when one target is being focused on. However, it could be argued that antibody specificity and validation need to be carried out early on to avoid wasting time on non-specific antibodies. Further work is clearly needed in this instance with a larger sample size to avoid over interpretation of the data.

3.5 Summary

In conclusion, this chapter has introduced six potential novel ADC targets. They were chosen due to minimal expression in healthy ovary and a higher expression in OC by IHC on THPA. All of the targets looked promising to different degrees in the literature, although as they are such novel targets there were minimal publications about these targets in particular, which in itself is advantageous in terms of patents, publications and proprietary technology.

The first stage of screening was the analysis of protein expression levels by western blot. Preliminarily, only two cell lines (TOV-112D and SKOV-3) were used and only TSPAN6 produced a suitable expression pattern for ADC development. The TSPAN6 antibody was used in a western blot with eight OC cell lines and one non-cancer control. At this stage, before any replicates could be done, the company discontinued the antibody and it was replaced by an antibody from a different company but with the same epitope. The replacement antibody produced the same bands on the western blot as the first antibody and was subsequently used for the rest of the project. When performed in triplicate there was no significant difference seen in TSPAN6 expression between various OC cell lines and a non-cancer primary patient sample. In addition, expression levels of TSPAN6 were elevated in OC cell line TOV-21G compared to expression in various healthy tissues further suggesting its suitability as target for ADC development.

All targets and their antibodies were further evaluated by immunofluorescence. TSPAN6 showed the clearest localisation to the membrane with PCSK4 and PIEZO2 also showing acceptable expression and localisation to the membrane. CEACAM8, SUSD2 and SLC39A10 did not show satisfactory expression or localisation to the membrane and therefore they were not further explored in this project. Although the IF was performed using antibodies which showed non-specific binding in western blot, this project was more centred around developing a pipeline for potential ADC target discovery and characterisation. Another project could have focused on one target and explored multiple antibodies against it whereas this project explored a pipeline for the characterisation of several targets.

The following chapters explore the TSPAN6, PCSK4 and PIEZO2 expression and localisation of these three targets in primary patient cells to identify a lead candidate target for ADC development.

Chapter 4: Expression of putative ADC targets in primary samples derived from patient ovarian tissue biopsies

4.1 Introduction

ADC-targets have been described as tumour associated-antigens because most antigens expressed in tumours, are expressed in a certain degree in healthy tissues (329, 550). For instance, the HER2 receptor targeted by Kadcyla® ADC, is abundantly expressed in breast cancer cells but it is also expressed in the skin, heart and on epithelial cells in the gastrointestinal, respiratory, reproductive and urinary tracts (551). In addition, an optimal target needs to be homogeneously expressed at the cell membrane of all cancer cells (552). Another important feature of ADC targets, is their antibody internalisation capabilities allowing the efficient release and activation of the cytotoxic payload inside the cell (552).

In the previous chapter, a literature review of six potential ADC targets was used as a basis to further evaluate the expression and location of these targets using a panel of ovarian cancer cell lines and commercially available antibodies. Immortalised cell lines offer a very valuable model of disease for preliminary experiments; however, it is important to use human primary cells to replicate key findings in clinically relevant specimens and to further validate results. Immortalised cell lines are invaluable due to being diverse, readily commercially available and immortal. They are also easy to compare to data generated by other researchers. TSPAN6 was the only target to have both specific binding, as determined by western blotting, and membrane localisation determined by immunofluorescence. Although both PIEZO2 and PCSK4 proteins were expressed in ovarian cancer cell lines, the quality of the immunoblots was poor, but the immunofluorescence images obtained confirmed target expression and location at the cell membrane.

Therefore, this chapter explores the expression of novel ADC targets TSPAN6, PCSK4 and PIEZO2 in patient biopsy samples to validate previously obtained results in patient's samples, identify significant differences between groups or patients and determine if the targets are suitable for further development along the ADC characterisation pipeline. Ultimately, this will increase the potential translation of the targets as druggable options for ADC development based on results more relevant to human physiology. Additionally, any variation identified between patients could open up the possibility to stratify patients in the future with implications for a more accurate personalised diagnosis and therapeutic strategy. The number of patients recruited to the ovarian biomarker study has the advantage of a large and diverse cohort of patient samples with a range of pathologies to introduce diversity into the assays.

Patient biopsies were processed and utilised in three different ways for experimental analysis in this chapter. Firstly, 2D primary cell cultures derived from patient ovarian cells were cultured for use in basal expression assays using immunofluorescent microscopy. Secondly, total protein

was extracted from these 2D primary cell cultures and additionally from a matching paired piece of ovarian tissue biopsy for use in western blot analysis.

4.2 Cellular location of TSPAN6, PIEZO2 and PCSK4 protein in 2D primary cell cultures derived from patient biopsies

Basal expression and subsequent cellular location of each target was assessed in 2D primary cell cultures derived from four non-cancer patients, four patients with High Grade Serous (HGS) OC pathology and one patient with endometrioid OC pathology. Target proteins must be present on the plasma membrane of OC cells for the ADC to bind and have a successful therapeutic effect (318). The expression of TSPAN6, PIEZO2 and PCSK4 has been visualised on the plasma membrane of commercially available immortalised OC cell lines – this section addresses if that expression and localisation to the plasma membrane extends to 2D primary cell cultures and total protein derived from patient biopsies. 2D cells derived from patient biopsies were plated and incubated with the target antibody and subsequently the appropriate species of antibody conjugated to a Texas Red® fluorophore before fixation with paraformaldehyde, permeabilization with triton X and viewing on the confocal microscope as described in materials and methods Chapter 2.

Patients were selected based on their clinical history and diagnosis from an anonymised database hosted by the RBGO group under ethical approval (LREC Wales 6). Each patient was chosen carefully to ensure they did not have any additional comorbidities including diabetes. Additional low frequency medical issues, not seen commonly in the dataset, will introduce more variables into the data set which should be avoided where possible. In particular, diabetes has been linked to inflammation (553, 554), which has been shown to be a hall mark of cancer (529). Patients were also chosen based upon a confirmatory diagnosis or HGS or non-cancer. The pathologies of the patients the samples were derived from are shown in more detail is shown below in **Table 4-1**.

Table 4-1 – Pathologies of patients from which 2D primary cell cultures were derived

Patient number	Pathology
OV7	Ovarian cyst – No cancer
OV29	Risk reduction surgery familial MSH6 gene mutation – No cancer
OV82	No ovarian pathology – control
OV73	No ovarian pathology – control
OV12	HGS stage 4- OC
OV57	HGS stage 3c- OC
OV86	HGS stage 3c-OC
OV75	HGS-OC
OV106	Clear cell-OC

The table above shows the corresponding pathologies of the samples used in the immuno-fluorescent analysis. Specifically, OV29 had no described ovarian pathology or cancer diagnosis but did have a familial mutation in a DNA mismatch repair gene MSH6. This has been associated with Lynch syndrome and a significantly increased chance of developing a gynaecological malignancy (555, 556). For this reason, the patient will have had the ovaries removed as a precaution.

Figure 4-1 below shows the visual images obtained from incubating the TSPAN6 antibody with 2D primary cell cultures derived from patient biopsies of various pathologies. The cell nuclei are shown in blue (Hoechst), the cell plasma membrane in green (Wheat Germ Agglutinin-WGA-Thermo Fisher W11261) and the TSPAN6 antibody in red (Texas Red® secondary antibody). The antibody used here is the same as used previously (Creative Diagnostic (USA) DPABH 18048). Initial observation of the nucleus and the plasma membrane revealed that the 2D primary cells derived from patient biopsies are larger than that of the cell lines and, like all cell types, have a different morphology. Instead of being rounded, the primary cells are longer and more fibrous. Primary cells could be validated as true ovarian stromal cells by outsourcing to a company who would confirm the presence surface markers specific for ovarian stromal cells, however this is not yet done as standard. The intensity was not quantified as the aim was to simply show where the protein was located in the cell. However, there are variations in intensity observed between patients. Each patient derived 2D cells image in **Figure 4-1** below, is a representative example of several fields of view taken from the single well in which those patient cells were grown. Differences in cell morphology and intensity of TSPAN6 can be seen between patients of the same pathology.
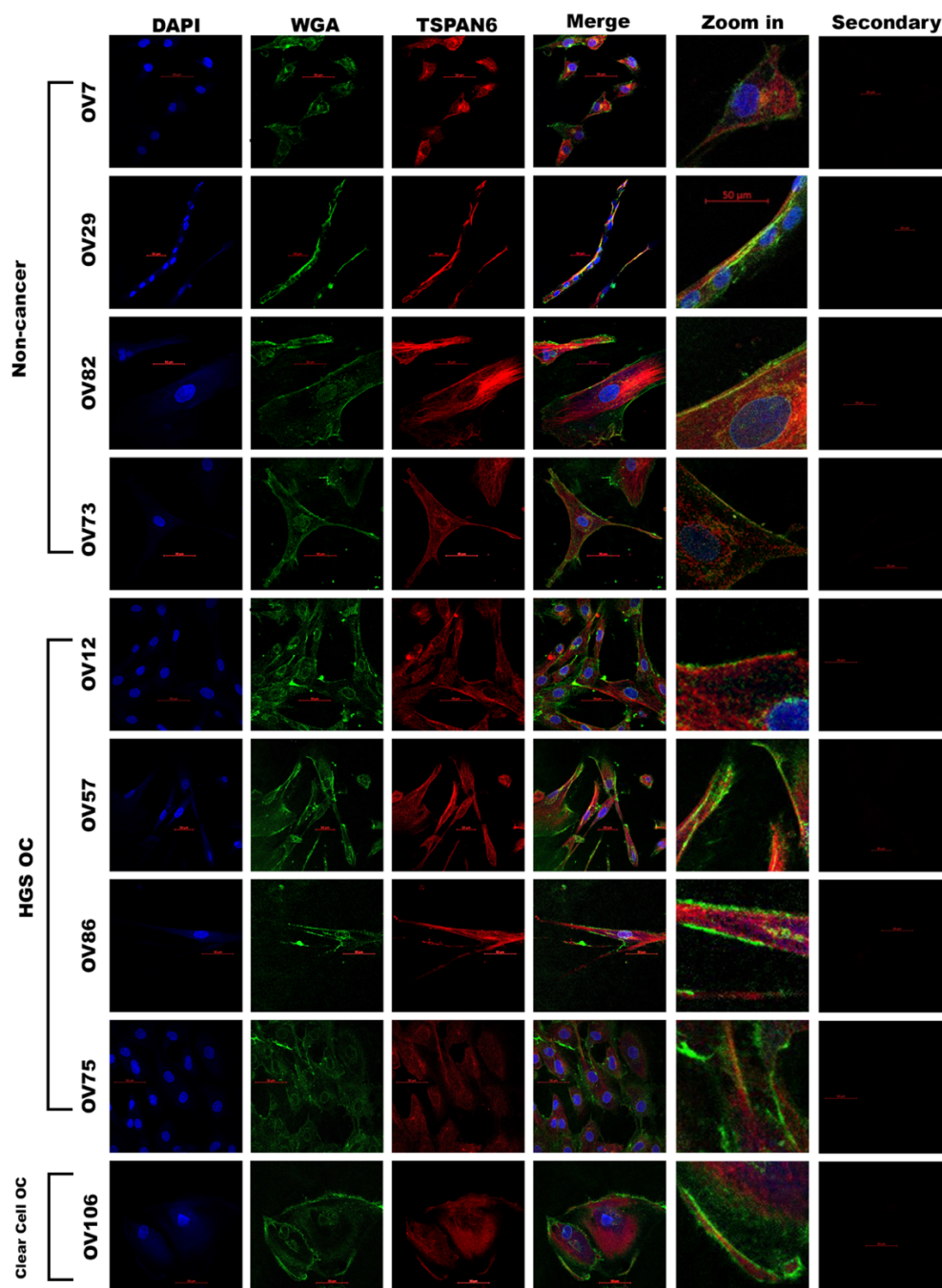
Figure 4-1 – Cellular location of TSPAN6 protein in primary cells by immunofluorescence Ovarian biopsies collected from consented patients diagnosed with various pathologies were used to isolated ovarian epithelial cells and grown them as 2D monolayers.

Confocal images showing the cellular location of TSPAN6 in the 2D patient derived primary cell cultures. TSPAN6 staining can be observed at the plasma membrane of all cells with variations on the levels of TSPAN6 within the patient's samples. The secondary only control was performed in the same way as the target protein wells but cells were only incubated with the secondary antibody (last column). This shows no non-specific binding from the secondary antibody. The 50 μM scale bar is shown in red across the images. Overall, this figure shows TSPAN6 present on both cancer and non-cancer cells and the specificity of the primary antibody staining as no background staining signal was obtained from incubations with the secondary antibody.

All images were taken using the same configuration and gain on the confocal microscope and differences such as a higher intensity of TSPAN6 can be seen in non-cancer OV82 compared to non-cancer OV73, despite both patients being reported as non-cancer with no described ovarian pathologies. This highlights the extent of the variation between patients, even within the same groups. It is not possible to comment confidently on which patient derived 2D cells have the highest expression without quantification, however, it was possible to confirm that TSPAN6 protein is expressed in ovarian primary cells grown as 2D monolayers. It can be seen that TSPAN6 is present on the plasma membrane of all types of the ovarian cell shown in Figure **4-1**. TSPAN6 is also present in the cytoplasm in all the cell types, but its confirmed membrane location is key to assess the possibility of receptor mediated internalisation to occur. On the membrane, TSPAN6 forms higher order complexes with itself and other scaffolding proteins to contribute to cell development, activation, growth and motility. TSPAN6 has not reported function in the cytoplasm. Due to this result and the positive immunoblot data previously obtained using cell lines (Figures in chapter 3), TSPAN6 was selected for subsequent evaluation on patient derived protein extracts by western blot in section 4.3.

Figure 4-2 below shows the cellular location of target PCSK4 in fixed 2D primary cell cultures derived from patient biopsies. PCSK4 staining was observed on the plasma membrane of all cell types shown in **Figure 4-2**; validating the cellular location of PCSK4 in 2D primary cell cultures derived from patient biopsies. A higher cytoplasmic expression of PCSK4 can be observed in the non-cancer samples, although at this point this increase in expression appears to be marginal, however quantitation is needed to confirm if a statistical significance exists between cancer and non-cancer. The secondary only control image shows no detectable fluorescence suggesting there is no off-target binding by the secondary antibody. Variation can be seen between patients of the same pathology, once again highlighting the amount of variation observed between different patients. Due to PCSK4 showing clear localisation to the plasma membrane in commercially available immortalised cell lines and primary 2D cultured cells derived from patient biopsies – PCSK4 was selected as a target to assess its receptor mediated internalisation capacity in subsequent experiments. In **Figure 4-2**, WGA staining is not clearly labelling the plasma membrane particularly in OV82 and OV7. As cells were healthy and confluent this could be explained by differences seen between patient samples even of the same pathology due to individual patient differences.
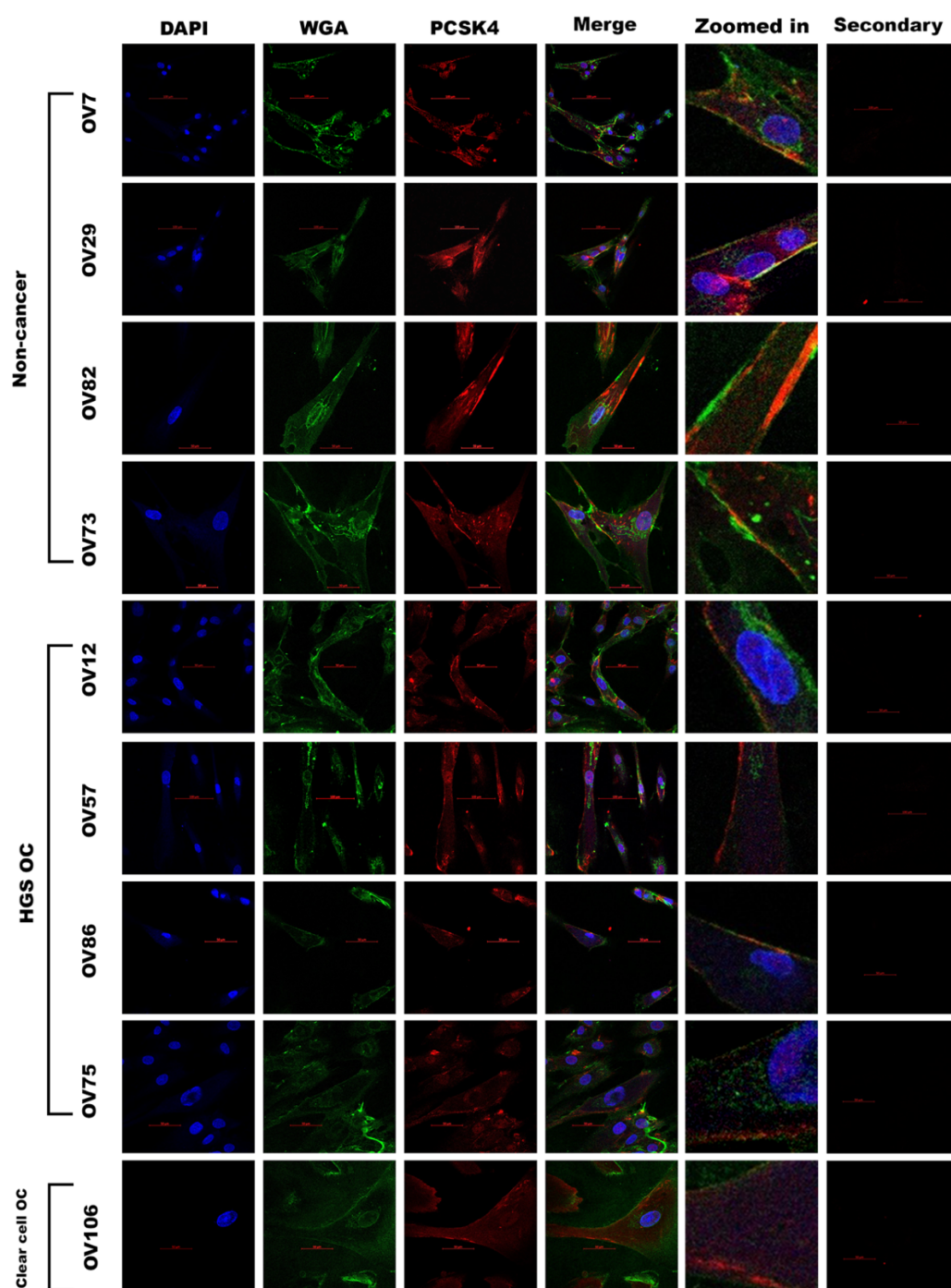
Figure 4-2 – Cellular location of PCSK4 protein in 2D primary cell cultures derived from patient biopsies of various pathologies by immuno-fluorescent microscopy

Confocal images showing the cellular location of target PCSK4 in 2D primary cell cultures derived from patient biopsies of various pathologies. Variation can be seen between patients of the same pathology and PCSK4 can be seen on the plasma membrane of all cell types. The secondary only control was performed in the same way as the target protein wells but the only antibody added was the secondary. This shows no non-specific binding from the secondary antibody. The 50 µM scale bar is shown in red across the images. Overall, this figure shows PCSK4 present in both cancer and non-cancer cells and no non-specific binding from the secondary antibody

Next, the expression and location of PIEZO2 protein was assessed in primary OC cell lines *in vitro*, as before (**Figure 4-3**). In comparison to TSPAN6 (**Figure 4-1**) and PSCK4 (**Figure 4-2**), overexpression of PIEZO2 at the plasma membrane is less defined in primary patient 2D cells. PIEZO2 expression appears to be reduced at the plasma membrane with additional expression in the cytoplasm. Additionally, the differences between patients and pathologies appear less pronounced for PIEZO2 staining in OC cells (**Figure 4-3**). Overall, PIEZO2 appears on both the plasma membrane and in the cytoplasm of 2D primary cell cultures derived from patient biopsies of various pathologies donated by both non-cancer and ovarian cancer patients with HGS and Clear cell subtypes assessed. Due to this localisation, PIEZO2 could be potentially still able to mediate antibody internalisation and hence it was selected together with TSAPN6 and PSCK4 for evaluation in the subsequent internalisation experiments. IF staining shows target antibodies in **Figures 4-1 – 4-3** are expressed in both non-cancer and cancerous cell lines derived from patient biopsies. This could indicate the targets are not successful in targeting only malignant cells. However, an ADC against these targets would be used locally in the ovary and only on cancer patients.
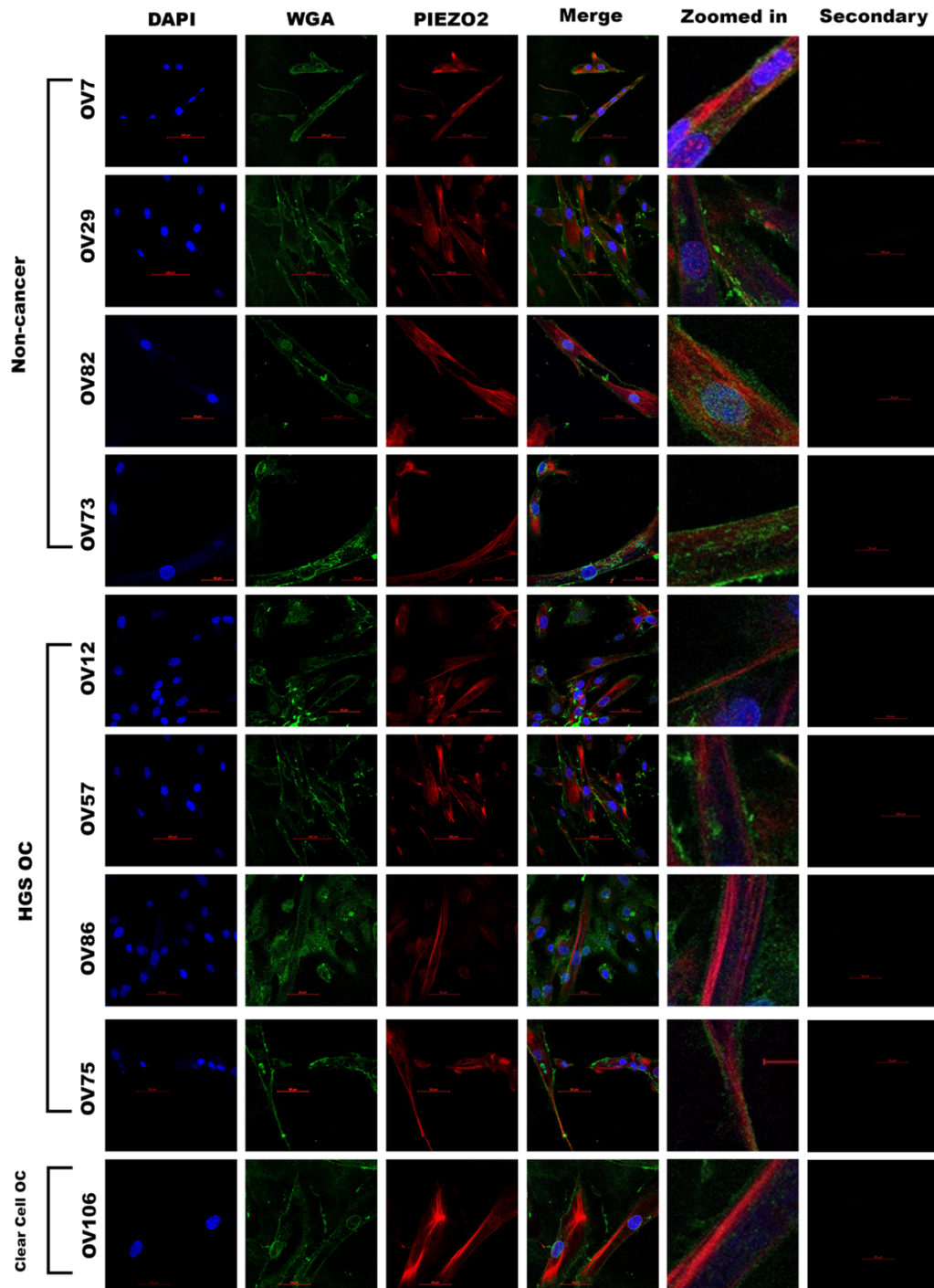
Figure 4-3 - Cellular location of PIEZO2 protein in 2D primary cell cultures derived from patient biopsies of various pathologies by immuno-fluorescent microscopy

Confocal images showing the cellular location of target PIEZO2 in 2D primary cell cultures derived from patient biopsies of various pathologies. Variation is less apparent between patients of the same pathology. PIEZO2 can be seen on the plasma membrane and in the cytoplasm of all cell types. The secondary only control was performed in the same way as the target protein wells but the only antibody added was the secondary. This shows no non-specific binding from the secondary antibody. The 50 µM scale bar is shown in red across the images. Overall, this figure shows PIEZO2 present on both cancer and non-cancer cells and no non-specific binding from the secondary antibody

4.3 The abundance of TSPAN6 protein by western blot in total protein lysates derived from patient biopsies

Previously, expression of TSPAN6 protein was confirmed in protein extracts obtained from OC cell lines, its membrane location validated on OC cell lines and primary cells grown as 2D monolayers hence, it was important to validate the immunoblot results by investigating the expression of TSPAN6 in total protein extracts obtained from patient biopsies. Total protein was extracted from two different patient derived sources. Firstly, the protein was extracted from 2D cultured primary cells isolated from patient biopsies. Primary ovarian cell cultures were grown to 100% confluency before protein was extracted and quantified for use in western blot. Secondly, the protein was extracted directly from ovarian tissue biopsies before being quantified and used in western blot. This allowed a direct comparison between the expression of TSPAN6 in protein derived from the same patient but from different sources. There are advantages and disadvantages to working with 2D primary cells compared to a tissue sample. Once isolated from patient tissue, 2D primary cells can produce more protein overall in their lifespan and they have a wider variety of uses in other assays. Tissue biopsies generate a lower amount of protein and can only be used for one purpose and cannot grow. However, tissues biopsies do have the advantage of being from a source closer to real life. 2D cells, once established, can be hardy and easy to work with, easy to maintain and they have the ability to grow over their lifespan. For this reason, 2D cells are often chosen over single patient tissue biopsies. The advantage of using the RBGO Ovarian Biopsy Biomarker bank of samples is that when an ovarian tissue biopsy is processed, 2D cells are isolated for primary cell culture and in addition three paired single pieces of tissue are set aside specifically for protein, DNA and RNA extraction. When the biopsy piece is big enough to allow this, the need to choose the best use for the tissue biopsy is eliminated and direct comparisons can be made between 2D primary cells, DNA, protein and RNA derived from the same patient. In this case, the piece of tissue designated for protein extraction was used and compared against total protein from the matched 2D primary cells.

Overall, the purpose of extending the analysis to total protein derived from patient tissue biopsies is to explore if TSPAN6 is also expressed in samples closer to the clinical setting and to see if the trends seen so far remain the same. This will provide more evidence for the suitability of TSPAN6 as a novel ADC therapeutic target and insights into biomarker potential. All western blots were performed using the antibody from Creative Diagnostic (USA) DPABH 18048. The protein expression was normalised by additionally probing for GAPDH and image analysis was carried out using Image Lab (BioRad UK) and statistical analysis was carried out using SPSS version 26.0.0.0.

4.3.1 The abundance of TSPAN6 protein in total protein lysate extracted from 2D cultured primary cells derived from patient biopsies by western blot

The pathology of patients from which samples were derived and used in the following analysis, can be seen in more detail in Table 4-2 below. TOV-112D was included as a comparison as it had previously shown specific bands for TSPAN6 by western blot. The non-OC control samples were recruited specifically as 'normal controls' with no described ovarian pathology. However, it is important to keep in mind that the reason for which the patient came to be recruited for the study is not disclosed. There is the option they could have been recruited from hysterectomy surgery due to no longer wanting children and/or due to reproductive system related symptoms such as heavy bleeding or pelvic pain. At the same time, they could have had no symptoms at all and the patient opted for a hysterectomy voluntarily. Another option is they could have another non-ovarian gynaecological symptom that was not recorded at the time of biopsy collection. Overall, it cannot be assumed that the non-OC patients are totally disease free, it can only be confirmed that they are non-cancer patients.

Table 4-2 – Pathologies of patients from which 2D primary cell cultures were derived

Sample name/patient ID	Pathology
TOV 112D	Immortalised endometrioid OC cell line
OV7	Non-OC control (presence of benign ovarian cyst)
OV69	Non-OC control
OV73	Non-OC control
OV82	Non-OC control
OV12	OC HGS stage 4
OV57	OC HGS stage 3C
OV75	OC HGS
OV86	OC HGS stage 3C

Analysis of TSPAN6 expression levels on the samples described in **Table 4-2** was performed by immunoblot (**Figure 4-4**). In this experiment, the TOV-112 2D cell line protein lysate was used as a positive control comparison, on the same experiment together with the 4 non-OC protein lysates and 4 HGSOC protein lysates extracted from 2D primary cultured cells derived from patient biopsies (**Table 4-2**). The immunoblot shows specific bands for TSPAN6 as the appearance of the monomer and homodimer as described in the literature (539), and in accordance with previous data in immortalised cell lines (**Figure 3-14**). The abundance of the monomer and the homodimer between patients is shown to be variable with one non-OC patient showing considerably less abundance of the monomer compared to the other patients

(lane 5, **Figure 4-4**). Additionally, there is the appearance of a band at 75 kDa which due its size could be the homotrimer, however this has not been reported in the literature so far. Finally, in the protein run in lanes 6,7 and 8 on the gel (OC HGS stage 4, OC HGS stage 3 and OC HGS respectively) there is a very faint band above the dimer at around 60 kDa. This band has been seen previously in the western blot using commercially obtained healthy tissue lysates from tissue (**Figure 3-20**) but is not reported in the literature and is not seen in protein lysate extracted from 2D immortalised cell lines. This band could potentially be a post translationally modified dimer

Protein extracted from primary ovarian 2D cultured cells. Anti-TSPAN6 DPABH-18048 1/500 dilution Gel 1
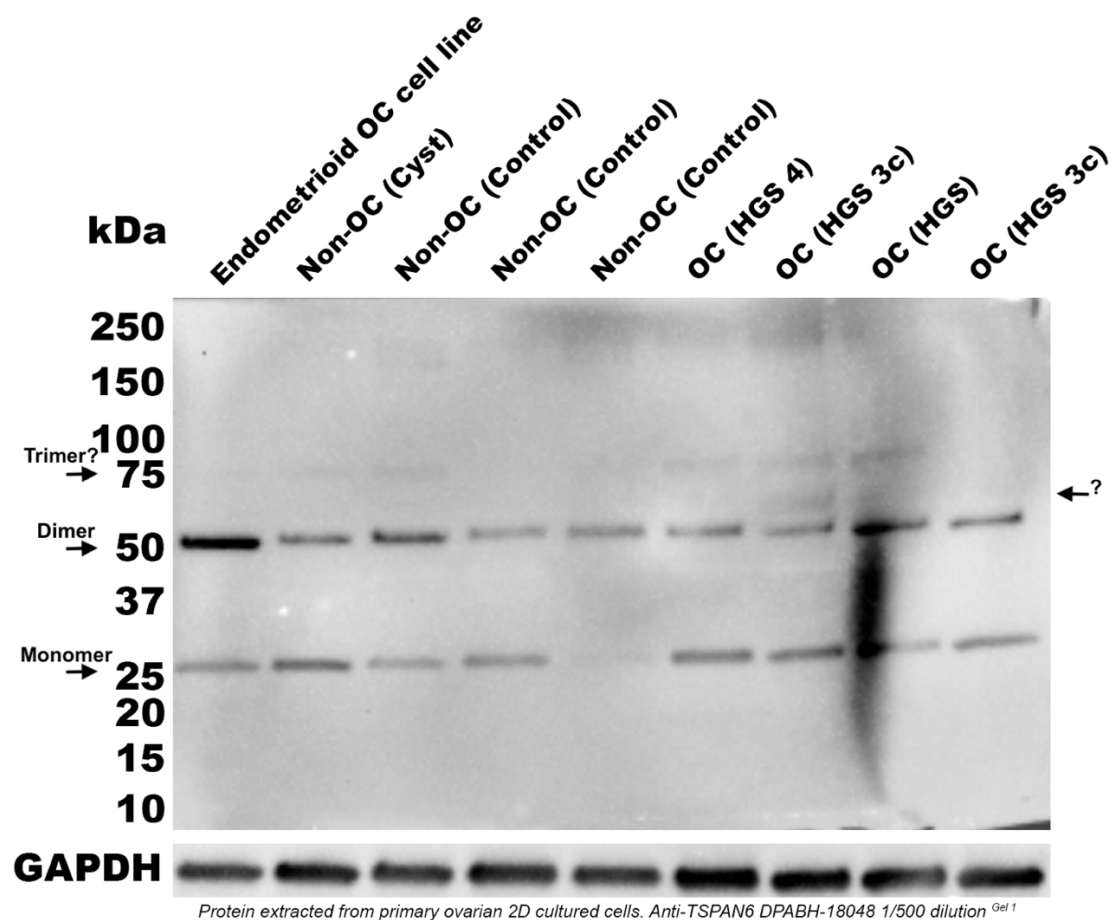
Figure 4-4 - Detection of TSPAN6 by Western blot in total protein extracted from 2D primary cultures derived from patient biopsies

In the above western blot, TSPAN6 protein was detected using the anti-TSPAN6 antibody DPBH-18048. Total protein was extracted from 2D cultured primary cells isolated from patient biopsies. The same membrane was then probed for target GAPDH, shown at the bottom of the figure, for a loading normalisation control. The TSPAN6 homodimer can be clearly seen at 50 kDa along with the monomer at 25 kDa. There is also the hint of a band at 75 kDa that based upon its size could be a TSPAN6 homotrimer. Additionally, there is a very faint band seen just above the homodimer at around 60 kDa on only two samples (marked with a question mark). GAPDH appears largely stable over the samples and there is a level of variation seen in the expression of TSPAN6 between patients. N=1

Figure 4-5 below shows the quantification and subsequent statistical analysis of the western blot shown above in **Figure 4-4**. This graph represents the total TSPAN6 expressed and includes the monomer and the dimer. The abundance of TSPAN6 in each group was comparable, and not statistically significant (HGS 0.2, Non-OC 0.21 (+/- SD). Independent samples T-test p value= 0.6 n=4. In this case the p value was >0.05 therefore no statistically significant difference is indicated. The alternative non-parametric test, the Mann Whitney U test, also showed no statistically significant difference with a p value of 0.8.

Relative to the immunofluorescent images seen in **Figure 4-1**, there could be some parallels drawn between the abundance of TSPAN6 observed on the western blot shown in **Figure 4-5**. In **Figure 4-1**, there is a higher intensity of TSPAN6 protein in some of the non-cancer cells (OV82, OV29 and OV7). Likewise, the abundance of TSPAN6 protein in some non-OC (non-OC-Cyst and Non-OC control) is higher (lane 2 and 3 **Figure 4-4**) than that of HGS , albeit not statistically significant.

Figure 4-5 - Quantification of TSPAN6 protein (monomer and dimer) abundance in total protein extracted from 2D cultured primary cells isolated from HGSOC and non-cancer patient biopsies by western blot

The box plot shows densitometry analysis of TSPAN6 expression normalised to GAPDH and there is no significant difference between the total TSPAN6 abundance in HGSOC patients (n=4) when compared to non-OC patients (n=4). The data was shown to be normally distributed by one sample Kolmogorov-Smirnov test for normality with p=0.2. An independent samples T-Test showed no significant difference with a p=0.6. Additionally, a non-parametric Mann Whitney test also revealed no significant difference with p=0.8. Overall, the total TSPAN6 abundance cannot statistically significantly stratify the 8 patients by HGSOC or non-cancer.

The abundance of TSPAN6 monomeric and heteromeric forms was also quantified to assess differential expression between groups that could lead to patient stratification. **Figure 4-6** below begins to break down the abundance of TSPAN6 protein by looking at the abundance of the monomer band specifically. Densitometry analysis of the monomer band revealed that there was no statistically significant difference in the TSPAN6 monomer, although a trend was observed for slightly higher expression in the HGSOC patient-derived cells, relative to the non-cancerous ovarian patient-derived cells.

Quantification of TSPAN6 monomer isoform protein abundance in total protein extracted from 2D cultured primary cells isolated from HGSOC and non–cancer patient biopsies by western blot
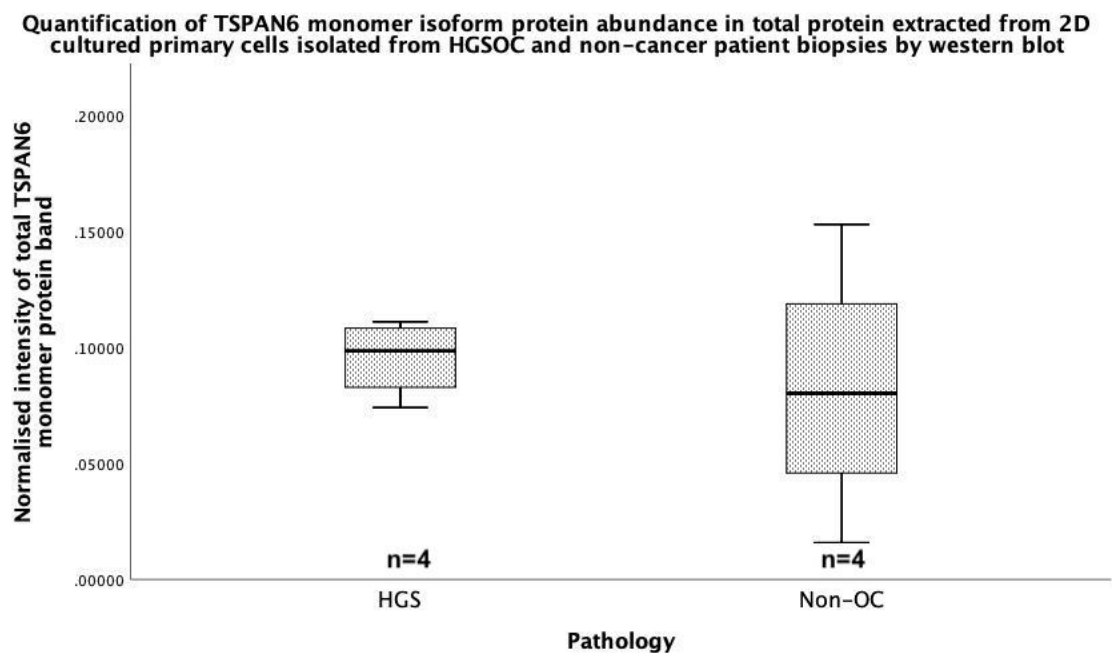
Figure 4-6 - Quantification of TSPAN6 monomer isoform protein abundance in total protein extracted from 2D cultured primary cells isolated from HGSOC and non-cancer patient biopsies by western blot

The box plot above shows there is no significant difference between the abundance of TSPAN6 monomer in HGSOC patients (n=4) when compared to non-OC patients (n=4). The data was shown to be normally distributed by one sample Kolmogorov-Smirnov test for normality with p=0.2. An independent samples T-Test showed no significant difference with a p=0.6. Additionally, a non-parametric Mann Whitney test also revealed no significant difference with p=0.6. Overall, the abundance of TSPAN6 monomer cannot statistically significantly stratify the 8 patients by HGSOC or non-cancer.

Looking at the dimeric forms of TSPAN6 specifically, in **Figure 4-7**, the opposite is observed in comparison to the monomer. Normality analysis using the Kolmogorov-Smirnov test indicates the data is normally distributed (p=0.2). For the TSPAN6 dimer, data revealed a marked increased abundance in the non-OC patient group, however, this increase was not statistically significant (independent t-test p-value (p=0.3). Overall, these findings suggest two observations could each other out resulting in a non- significant difference when assessing the overall

abundance of total TSPAN6. Further work with additional samples is needed to determine if TSPAN6 protein levels correlate with OC.
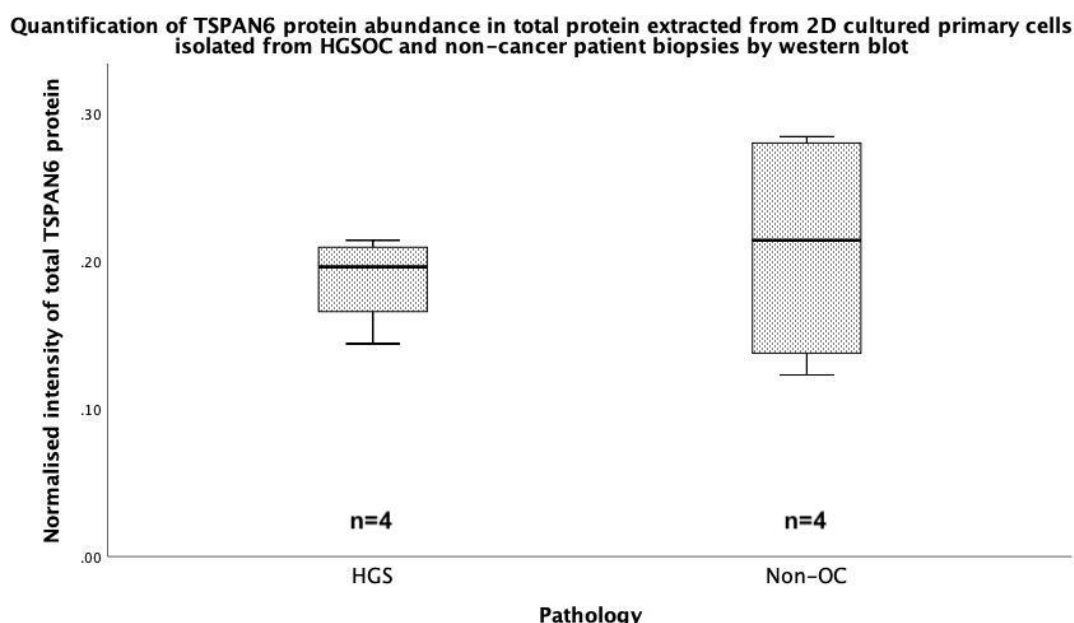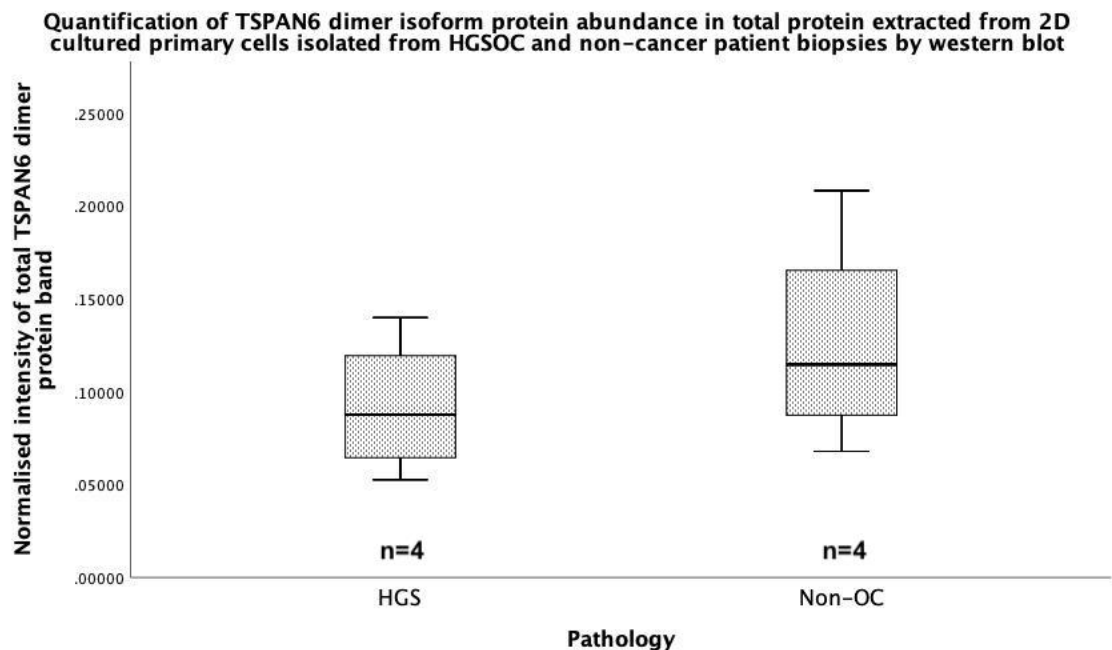

Figure 4-7 - Quantification of TSPAN6 dimer isoform protein abundance in total protein extracted from 2D cultured primary cells isolated from HGSOC and non-cancer patient biopsies by western blot

The box plot above shows there is no significant difference between the abundance of TSPAN6 dimer in HGSOC patients (n=4) when compared to non-OC patients (n=4). The data was shown to be normally distributed by one sample Kolmogorov-Smirnov test for normality with p=0.2. An independent samples T-Test showed no significant difference with a p=0.3. Additionally, a non-parametric Mann Whitney test also revealed no significant difference with p=0.4. Overall, the abundance of TSPAN6 dimer cannot statistically significantly stratify the 8 patients by HGSOC or non-cancer.

Overall, the abundance of TSPAN6 cannot stratify the 8 patients reported here into HGSOC or non-cancer. Stratification is also not possible when looking specifically at the individual isomers. However, it has been confirmed that TSPAN6 is expressed in patient derived cells – therefore it is worthwhile furthering the investigation into the abundance of TSPAN6 in total protein lysate extracted from patient tissue biopsies.

4.3.2 The abundance of TSPAN6 in total protein lysate extracted from patient tissue biopsies by western blot

Western blots using protein extracted directly from matched patient tissue biopsies are reported in this section. When each ovarian tissue biopsy, received from the hospital is processed, and the cells from the ovarian epithelial layer and stromal layer are extracted for cell culture, three small representative pieces of tissue are cut and set aside for protein, DNA and

RNA extraction. In this section the pieces set aside for protein extraction were digested with a lysis buffer, manually disrupted and put through freeze thaw cycles in the presence of protease inhibitors to extract total proteins from the tissues, as described in Materials and Methods Chapter 2. The proteins released from the disrupted cells were collected by centrifugation and quantified for use in western blot. Total protein extracts directly derived from tissue biopsies are generally considered to be more representative of the *in vivo* scenario compared to the proteins extracted from the 2D cultured cells, however they also include both the stromal and epithelial compartments of the tumour which need validating. The proteins present in 2D cultured cells could change depending on the environment, cell confluency, media and differences introduced by the person maintaining the cells. Previously it was shown that TSPAN6 was overexpressed in cancer cell lines (**Figure 3-16**) compared to healthy tissues. In addition, these 'healthy' protein extracts from different tissues purchased from Novus Biologicals were also directly extracted from tissue and showed very low expression of the monomeric isoform of TSPAN6, and low expression of an isoform that migrated at 60 KDa (**Figure 3-20**).

In total, 33 different patient samples were processed to obtain protein extracts directly from tissue as described above. **Figure 4-8** shows a preliminary comparison between the protein extracted from 2D cultured primary cells derived from patient biopsies and the matched protein extracted directly from the tissue biopsy of the same patient. It is observed that the monomer is present in all samples apart from protein extracted from the tissue of patient OV73 (**Figure 4-8**- lane 4) and the homodimer is only clearly seen in protein extracted from cells (**Figure 4-8**, lanes 1, 3, 5 and 7). For the matched protein samples extracted from tissue, there is either a less intense or non-existent homodimer band and instead, a band that have migrated at 60 kDa is observed. Additionally, a band at around 75 kDa is visible specifically on the protein extracted from 2D cultured primary cells for patients OV7 and OV73 (lane 1 and 3). Only patient OV73 shows a faint 60 kDa as well as the possible homotrimer band. Finally, an immunoreactive band at around 15 kDa is observed with strong intensity in protein extracts obtained directly from ovarian tissue biopsies. These differences, such as the 60 kDa band and the protein accumulation at 15 kDa, are discussed in more detail below where the full membranes and other protein extracts directly from tissue biopsies are shown. Overall, the appearance of an immunoreactive band at 60kDa instead of 50kDa homodimer band seems to be the biggest difference in expression profile between the 2D and 3D protein sources.
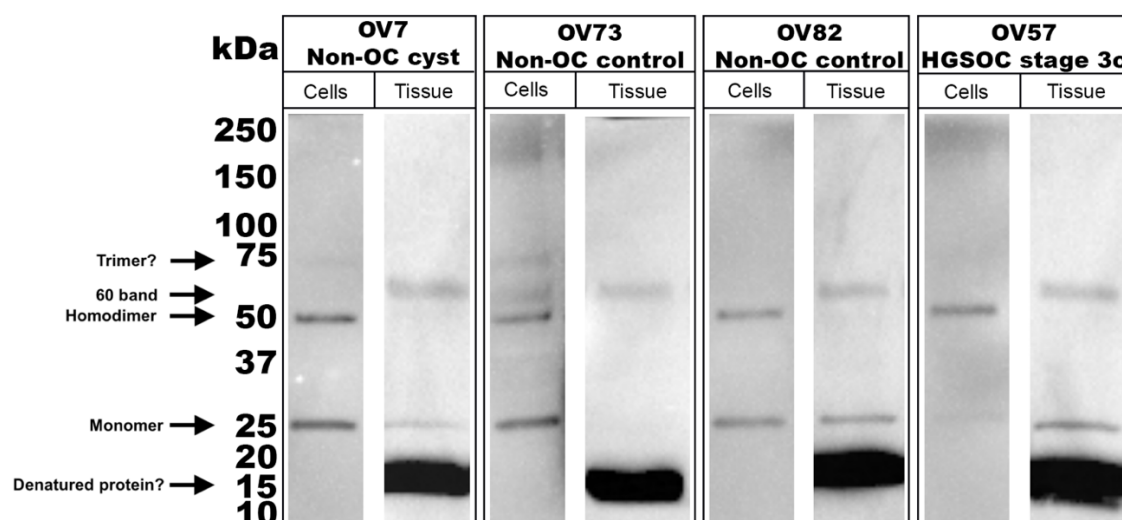
Figure 4-8 – Expression of TSPAN6 protein by western blot – a side by side comparison between paired protein extracted from 2D cultured primary cells derived from patient biopsies and protein extracted directly from patient tissue biopsies

A preliminary comparison between the protein extracted from 2D cultured primary cells derived from patient biopsies and the matched protein extracted directly from the tissue biopsy of the same patient. The TSPAN6 monomer band can be seen in all samples apart from patient OV73 protein from tissue. There is a large accumulation of protein detected at the bottom of the gel around 15 kDa only on the protein from tissue – this could be a denatured protein from the protein extraction process. The TSPAN6 homodimer is present in all protein samples from 2D cells but is replaced by a band at 60 kDa in protein from tissue. A band that could represent the TSPAN6 homotrimer can be seen in patient OV7 and patient OV73 protein extract from cells. OV73 protein from cells is the only samples to show a faint band at 60 kDa which is commonly observed in protein from tissue.

Next, protein samples directly extracted from 33 tissue biopsies were analysed for TSPAN6 expression by immunoblot. In this cohort, eight samples corresponded to patients that were given a non-cancer diagnosis. These samples were split over 4 western blot membranes with 2 non-cancer protein lysate extracts on each membrane for visual comparison (**Figure 4-9, Figure 4-10, Figure 4-11** and **Figure 4-12**). Overall, the main observations from the immunoblot data of these 33 patients were the presence of a previously undetected immunoreactive band above the dimer, and a highly abundant, smaller protein detected at the bottom of the immunoblot around 15 kDa, (observed before in **Figure 4-8**). In addition, poor GAPDH expression was observed in a small number of patients despite a similar amount of protein is loaded in the gels after protein quantification. The homodimer and monomer bands specific to TSPAN6 were also observed on all 4 gels.

Firstly- the additional immunoreactive band observed above the dimer band, between 50 and 75 kDa (hereafter referred to as the 60 kDa band), has been previously detected on protein lysate extracts from healthy tissue (Novus Biologicals) (Chapter 3 **Figure 3-20**). This band was

also observed very faintly in protein lysate extracted from 2D cultures primary cells derived from patient biopsies (**Figure 4-4**) and in the samples described **Figure 4-8** where the direct comparison of expression profiles is observed. Data from all these experiments indicate this 60kDa immunoreactive band only associated with protein samples extracted from cells grown in a 3D tissue configuration. The inclusion of the stromal compartment in the tissue lysate could be a contributing factor due to the presence of active and functioning TSPAN6. This suggests that in the 3D environment the protein being detected by the anti-TSPAN6 antibody is represented differently from what was observed in any 2D cell cultures. A post translational modification is likely occurring on the TSPAN6 dimer that results in a shift in the gel migration pattern of TSPAN6 dimers by 10 kDa larger than the others dimer observed in 2D configuration and therefore resulting in two bands close to one another. This theory is supported by the increasing intensity of the 60 kDa band at the expense of the intensity of the homodimer band (**Figure 4-9, Figure 4-10, Figure 4-11** and **Figure 4-12**). Different types of post translational modification would result in different size alterations to the protein. The most common types of post translational modification, discussed here, are N-linked glycosylation, phosphorylation, ubiquitination, and proteolytic cleavage. Consideration of the underlying cause for the 60 kDa band in tissue samples is also important in terms of functional consequence. Phosphorylation is reversible and principally in serine, threonine or tyrosine residues and is the most well studied of all the post translational modifications. The purpose of phosphorylation is to play critical roles in the cell cycle, growth, apoptosis, and the signal transduction pathway (557). This does not line up with the reported functions of TSPAN6 which suggests the 60 kDa band may not be a result of phosphorylation. Glycosylation is acknowledged as one of the most common post translational modifications and is reported to have significant effects on protein folding, conformation, distribution, stability, and activity. Glycosylation is known to encompass a diverse selection of sugar-moiety additions to proteins that range from simple to complex modifications (558). TSPAN6 is known to interact readily with itself and other scaffolding proteins to form tetraspanin webs, meaning protein folding, conformation and distribution is vital to TSPAN6 function. To assess what is truly happening here, site directed mutational analysis could uncover the importance of specific residues in protein structure and function. A larger sample size would greatly improve the reliability of the data, as well as considering the addition of other data sets to increase diversity.

Figure 4-9 - Detection of TSPAN6 by Western blot in total protein extracted from patient tissue biopsies

A TSPAN6 expression western blot showing eight (out of a total of 33) total protein extracts from patient tissue biopsies. This is gel one out of a total of 4 gels with a total of 33 protein extracts from patient tissue biopsies. On each gel the first two lanes show non-cancer patients and the following wells show patients of a HGSOC pathology. This gel shows some variability between the GAPDH loading control intensity band at the bottom of the gel suggesting that the protein quantification was inaccurate or the loading or preparing was inaccurate for lanes 4, 7 and 8. The samples on this gel and two samples in Figure 4-12 are the only example of this happening and due to the samples being quantified and prepared under uniform conditions using master mixes where possible – it is likely that these samples had a poor protein recovery and the quantification detected non-specific binding indicating more protein than there was in reality. This gel shows the dimer band (2) at approximately 50-54 kDa as expected from previous TSPAN6 westerns. The expression of the TSPAN6 dimer is varied between patients of different pathologies. The previously unseen band at around 60 kDa is present here (1) and appears to be a common in protein extracted from a 3D source. The monomer is seen variably between patients (3) and a large accumulation of TSPAN6 or TSPAN6 fragments can be seen at the bottom of the gel (4). Quantification and statistical analysis can be seen in Figure 4-14 to Figure 4-17

Protein extracted from primary ovarian tissue. Anti-TSPAN6 DPABH-18048 1/500 dilution [Gel 7]

Figure 4-10 - Detection of TSPAN6 by Western blot in total protein extracted from patient tissue biopsies

A TSPAN6 expression western blot showing eight (out of a total of 33) total protein extracts from patient tissue biopsies. This is gel two out of a total of 4 gels with a total of 33 protein extracts from patient tissue biopsies. On each gel, the first two lanes show non-cancer patients and the following wells show patients of a HGSOC pathology. This gel shows an empty well in the middle due to high volume in the neighbouring well. This gel shows a uniform GAPDH at the bottom of the gel suggesting an equal loading amount in μg of each protein. This gel shows the dimer band (2) at approximately 50-54 kDa, as expected from previous TSPAN6 westerns. The expression of the TSPAN6 dimer is varied between patients of different pathologies. The previously unseen band at around 60 kDa is present here (1) and appears to be common in protein extracted from a 3D source. The monomer is seen variably between patients (3) and a large accumulation of TSPAN6 or TSPAN6 fragments can be seen at the bottom of the gel (4). Quantification and statistical analysis can be seen in Figure 4-14 to Figure 4-17

Protein extracted from primary ovarian tissue. Anti-TSPAN6 DPABH-18048 1/500 dilution [Gel 8]

Figure 4-11 - Detection of TSPAN6 by Western blot in total protein extracted from patient tissue biopsies

A TSPAN6 expression western blot showing eight (out of a total of 33) total protein extracts from patient tissue biopsies. This is gel three out of a total of 4 gels with a total of 33 protein extracts from patient tissue biopsies. On each gel, the first two lanes show non-cancer patients and the following wells show patients of a HGSOC pathology. This gel shows a uniform GAPDH at the bottom of the gel suggesting an equal loading amount in μg of each protein. This gel shows the dimer band (2) at approximately 50-54 kDa, as expected from previous TSPAN6 westerns. The expression of the TSPAN6 dimer is varied between patients of different pathologies. The previously unseen band at around 60 kDa is present here (1) and appears to be common in protein extracted from a 3D source. The monomer is seen variably between patients (3) and a large accumulation of TSPAN6 or TSPAN6 fragments can be seen at the bottom of the gel (4). Quantification and statistical analysis can be seen in Figure 4-14 to Figure 4-17
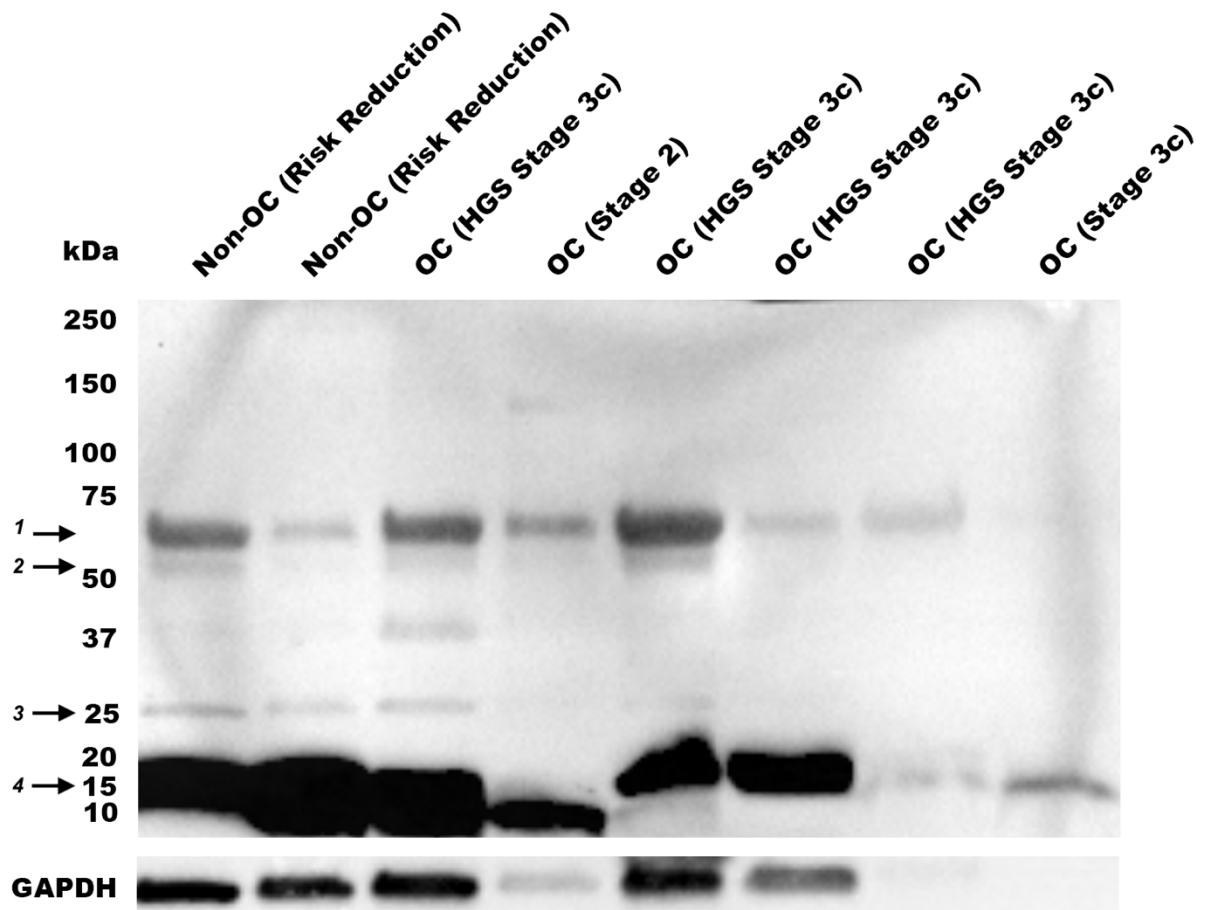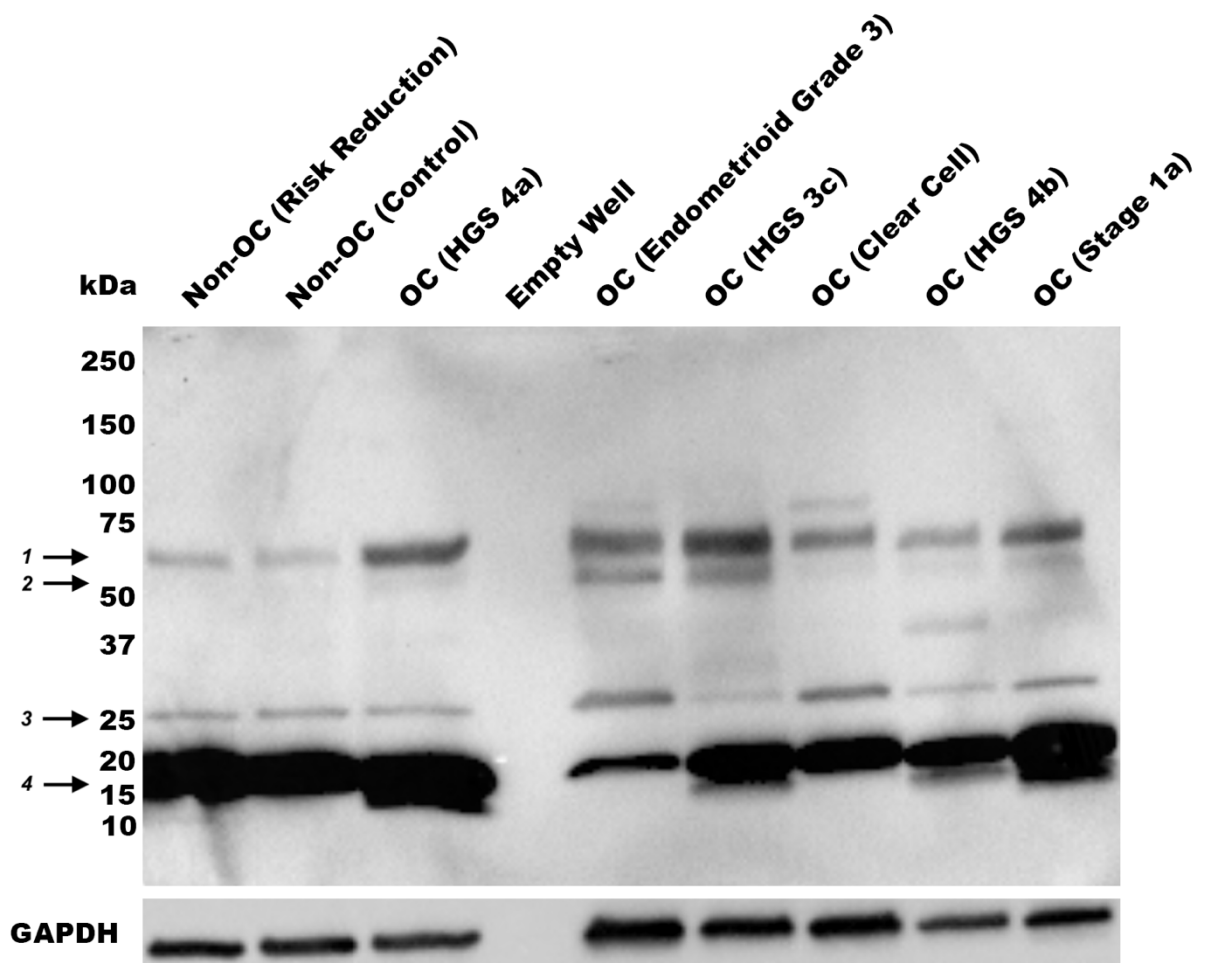
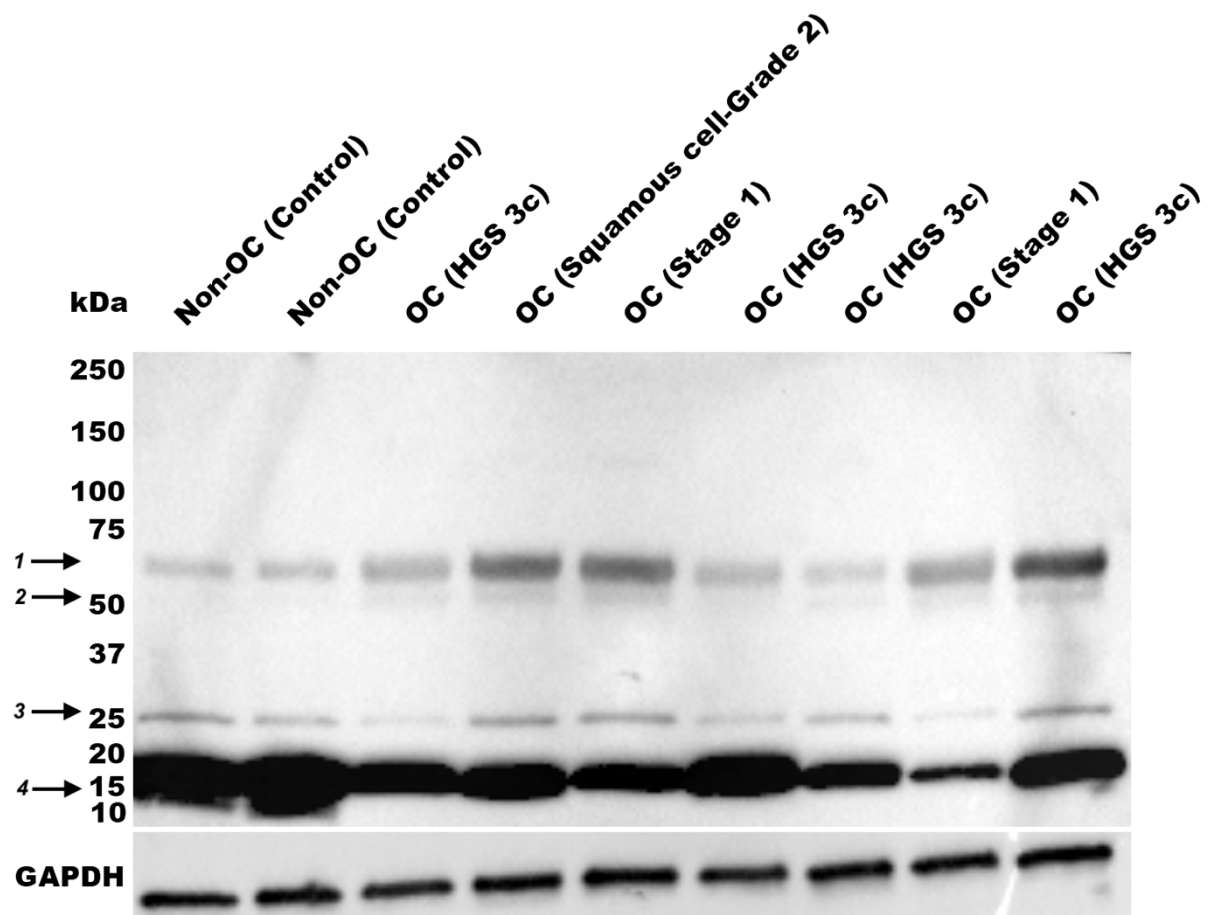*Figure 4-12 - Detection of TSPAN6 by Western blot in total protein extracted from patient tissue biopsies*

A TSPAN6 expression western blot showing eight (out of a total of 33) total protein extracts from patient tissue biopsies. This is gel four out of a total of 4 gels with a total of 33 protein extracts from patient tissue biopsies. On each gel, the first two lanes show non-cancer patients and the following wells show patients of a HGSOC pathology. This gel shows some variability between the GAPDH loading control intensity band at the bottom of the gel suggesting that the protein quantification was inaccurate or the loading or preparing was inaccurate for samples loaded on lanes 5 and 7. This gel shows the dimer band (2) at approximately 50-54 kDa as expected from previous TSPAN6 westerns. The expression of the TSPAN6 dimer is varied between patients of different pathologies. The previously unseen band at around 60 kDa is present here (1) and appears to be common in protein extracted from a 3D source. The monomer is seen variably between patients (3) and a large accumulation of TSPAN6 or TSPAN6 fragments can be seen at the bottom of the gel (4). Quantification and statistical analysis can be seen in Figure 4-14 to Figure 4-17

Figure 4-9 to **Figure 4-12** in total have an n=33. The western blots were not run in technical triplicates due to limited primary patient material. Instead, a higher number of individual patients (n=33) was used instead. n=8 non-cancer and n=25 OC.

N-linked glycosylation is the attachment of an oligosaccharide to a nitrogen atom of the amide nitrogen of asparagine residue of a protein. The addition of this oligosaccharide can alter the tertiary structure of the protein which in turn affects its function (559). Online predictions of

post translational modification sites can be found using online calculators such as ExPASy (UK). By using the tool 'FindMod tool' on ExPASy, a variety of low to high probability of different post translational modifications were predicted and added to a schematic (Figure **4-13**). There is only one N-linked glycosylation site that was marked as a high probability (marked as a yellow square on **Figure 4-13**) with phosphorylation being the most common type of post translational modification predicted on the TSPAN6 protein (**Figure 4-13**, marked as orange square. While N-linked glycosylation only adds around 2.5 kDa (546) and there could be more N-linked glycosylation sites than predicted, phosphorylation adds approximately 1 kDa (560). However, multiple phosphorylation sites are predicted with a high probability for TSPAN 6 protein (Figure **4-13**, orange squares).

It could be possible that in the protein extracts from tissue, multiple TSPAN6 phosphorylated isoforms are present. This could cause some of the standard homodimers to appear at 60 KDa rather than the expected 50 KDa. t is notable here that this extra band appears above the dimer band but not the monomer. This could suggest that the monomer is not functional and does not undergo post translational modification. The reports of tetraspanins in the literature include descriptions of them in Tetraspanin Micro Domains (TEMs) or tetraspanin webs (561). Suggesting that they do need to exist as a multimer to be functional although further work is needed to test this hypothesis.

It is reported that phosphorylated proteins can migrate slower on a gel (562) and this size difference is not always as simple as 1 kDa extra for each phosphate addition. The addition of a phosphate group can alter the tertiary structure of a protein such that it does not run true to the expected size on a western blot gel (563).

Post-translational modifications of TSPAN6

Figure 4-13 - Protein schematic showing post translational modifications predicted in TSPAN6

The above Figure shows the predicted post translation modifications in the TSPAN6 protein using the ExPASy (UK) online database. The antibody epitope is presented in green and the various modifications are represented by the coloured squares in the key. Only those modifications with a high probability of occurring are depicted in this Figure. Phosphorylation is the most common post translational modification with some cleavage sites that could explain small 15 kDa bands seen in the western from Figure 4-9 to Figure 4-12

The large amounts of protein detected by the TSPAN6 antibody on the bottom of the western blots in **Figure 4-9** to **Figure 4-12** indicate the detection of proteins that are approximately 15 kDa or smaller. There is an isomer of TSPAN6 at 15 kDa, seen on the UniProt database (199). However, this isomer would not be detected by the TSPAN6 antibody used due to epitope binding. Given the large accumulation of this small protein fragment, it suggests that it is more

likely to be a cleaved fragment of protein or denatured protein fragments from protein extraction or storage.

 It can be seen in **Figure 4-13** that there are predicted cleavage sites at amino acids 7, 9 and 140 – where TSPAN6 has the potential to be cleaved by proteolytic activity. The fragment produced by proteolytic cleavage at these sites would produce an approximate band at 15 kDa and could be produced from either the monomer or any multimer. This may be only happening in protein from a tissue lysate because these modifications are only occurring in a 3D environment in patient samples. It is agreed in the literature that post-translational modifications do occur in 2D cells (564, 565) and there are products available specifically to investigate post-translational modification using 2D cells (566). This leaves the possibility that more post-translational modifications, specifically the ones that could result in the additional 60 kDa band and the large accumulation of protein at 15 kDa, are happening in the tissue-derived protein. Being a more diverse and complex environment than a 2D cell culture, it would not be surprising that more complex protein modifications are taking place. However, the strong immunoreactive signal observed at 15kDa only in 3D extracts of OC suggest TSPAN6 may be involved in signalling pathway or protein complex only active in primary ovarian cells when grown in a 3D configuration. These bands differ from the extra band at 60 kDa because they are not present on all the protein gels from 3D sources. The abundant 15 kDa species is only seen on the breast healthy tissue protein lysate and not on the other tissues (**Figure 3-20**) suggesting either this band is tissue specific or appears as result of protein degradation.

Protein extraction from patient samples, involve manually disrupting the tissue with a TissueRuptor device in the presence of a lysis buffer and a protease inhibitor to first break open the cells and to protect the proteins from proteases inside the cell being released at the same time (2.4.2). The next stage to release protein from the tissue and cells was to repeatedly freeze thaw the solution using dry ice and a water bath before centrifuging at high speed to separate the supernatant containing the protein from the cell debris. This freeze/thaw cycle in particular could have caused protein degradation resulting in the large accumulation of small TSPAN6 protein fragments.

Interestingly, this 15 kDa immunoreactive band can also be detected (at a lesser intensity) in ovarian cancer cell lines grown as 2D monolayers (chapter 3, **Figure 3-16**-TOV 112D sample; TOV 21G and the primary non-cancer sample OV2 (risk reduction patient). However, the results for cell lines are not consistent given this band is not observed in the TOV 112D sample shown in **Figure 3-18** or **Figure 3-20**. Overall, there is a strong possibility of this band resulting from the

accumulation of denatured protein due to the disruption and freeze thaw cycles used in our protein extraction protocol.

It is worth mentioning an alternative explanation for these findings. It has been described that ubiquitination of TSPAN6 results in smaller immunoreactive bands for this protein. In addition, ubiquitinated TSPAN6 interacts with MAVS and disturbs the formation of the MAVS-centred signalosome resulting in negative regulation of the RLR signalling pathway by TSPAN6 (527). A growing number of studies show that the RLR signalling can be induced in tumour cells and non-tumour cells within the tumour microenvironment and support innate immune responses against tumour cells (567). For example, RIG-I activation in ovarian cancer cells enables NK-mediated tumour cell killing in culture (568). It is plausible that ubiquitinated TSPAN6 is promoting tumour development by inhibiting the RLR signalling in OC cells. In the case of a healthy ovary, it is also plausible TSPAN6 protects the ovarian cells from the attack of the immune system given ovarian activity increases local inflammatory processes during the ovarian cycle.

The bands representing TSPAN6 in **Figure 4-9** to **Figure 4-12**, were quantified using Image Lab (BioRad UK) software and normalised by the corresponding GAPDH band. This was achieved by dividing all the TSPAN6 bands by their corresponding GAPDH band to provide a normalised ratio value. For this analysis, those samples that did not show a GAPDH band were removed from the data set.

This quantification was done to inform the total expression of TSPAN6 in patient samples to explore patient stratification. Moreover, if a novel TSPAN6 ADC were to be applied to the ovary of an OC patient, the ADC would seek and bind to all the variants of TSPAN6 detected by the anti-TSPAN6 antibody. Therefore, for the westerns described above in **Figure 4-9** to **Figure 4-12**, the total TSPAN6 expression from all bands have been quantified and discussed here. Here, it is also worth mentioning that an ADC used *in vivo* would only bind to TSPAN6 associated with the plasma membrane and exposed on the cell surface. The total TSPAN6 expression for each sample was calculated by adding together the normalised intensity for each of the homodimer, the monomer and the 60 kDa band for each sample and using that total to calculate the average total TSPAN6 expression for each group. The large accumulation of protein at 15 kDa was not included, as it requires future clarification beyond this project. This is likely a degraded protein and it will not be considered representative of the TSPAN6 expression in this study.

The resulting graph shown in **Figure 4-14** shows a higher total expression of TSPAN6 in OC patients when compared to non-OC patients. A Kolmogorov-Smirnov Test found the data to be not normally distributed (p= 0.01) and therefore a non-parametric Mann Whitney test was used

to assess statistical significance between the two groups. A p value of 0.05 was obtained indicating total TSPAN6 expression is statistically significantly higher in OC tissue samples compared to non-cancer samples.

Figure 4-14 - Quantification of total TSPAN6 intensity in protein extracted from the patient tissue biopsy of OC vs non-OC patients

The box plot above shows the total expression intensity of TSPAN6 in the primary protein extracted from the tissue of 8 non-OC and 21 OC patients. The above box plot only quantifies all the bands including the dimer, the 60 kDa band and the monomer. From the 29 data points by Kolmogorov-Smirnov Test the data was considered not normally distributed (p=0.01). From this a non-parametric Mann Whitney revealed a statistically significant difference in the intensity of total TSPAN6 in OC and non-OC patients (p=0.05). Note the different markers for "out" values (small circle) and "far out" or as SPSS calls them "Extreme values" (marked with a star). SPSS uses a step of 1.5×IQR (Interquartile range).

Figure 4-15 shows a box plot of only the homodimer band intensity in protein extracted from patient tissue. Due to the homodimer being present and quantified in all previous western blots, this western blot can be directly compared to the others. So far, the TSPAN6 dimer has been variably statistically significantly different in various OC pathology cell lines and no statistically significant difference is seen in **Figure 4-15** where TSPAN6 homodimer intensity was compared between OC and non-OC patients. Although the p value was close to the cut off point for significance, technically there was no significant difference observed. Here in **Figure 4-15**, no significant difference between the intensity of the homodimer band between patients with OC

and those with no OC diagnosis was observed. The data was shown to be not normally distributed by Kolmogorov-Smirnov Test (p=0.0000013) and therefore a non-parametric Mann Whitney test was performed with a p value of 0.06. This shows that using the homodimer band only, patients could not be stratified into OC and non-OC.

Figure 4-15 - Quantification of TSPAN6 homodimer band intensity in protein extracted from the patient tissue biopsy of OC vs non-OC patients

The box plot above shows the expression intensity of the TSPAN6 homodimer in the primary protein extracted from the tissue of eight non-OC and 21 OC patients. The above box plot only quantifies the homodimer and from the 29 data points by Kolmogorov-Smirnov Test the data was considered not normally distributed (p=0.0000013). From this, a non-parametric Mann Whitney revealed no statistically significant difference in the intensity of TSPAN6 homodimer in OC and non-OC patients (p=0.06). Overall, this graph shows that there is no significant difference and therefore patients cannot be stratified using the TSPAN6 homodimer by western blot using this anti-TSPAN6 antibody.

TSPAN6 more commonly exists in its active form as a dimer or other higher order complexes rather than a monomer however here in the tissue the monomer is clearly present and could be a part of the total TSPAN6 expression on OC cells and can therefore aid the targeting of the cancer cells by a putative ADC. Although, in comparison to the dimer and the 60 kDa band, the expression of the monomer is very weak, the intensity between the two groups can be seen in **Figure 4-16**.
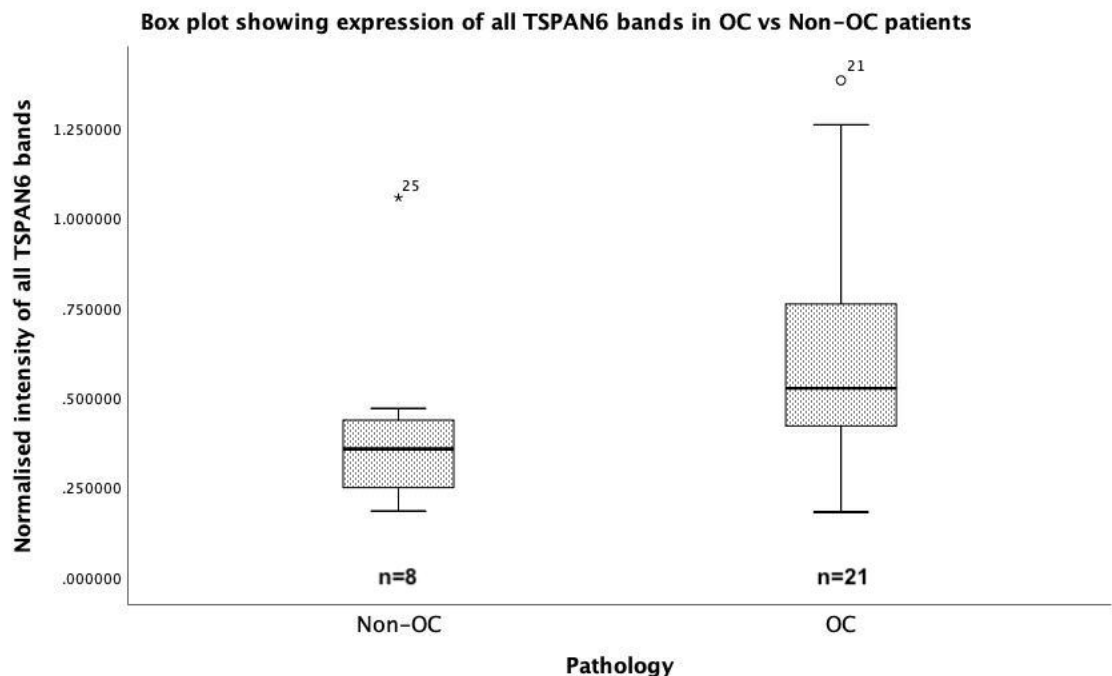
Figure 4-16 - Quantification of TSPAN6 monomer band intensity in protein extracted from the patient tissue biopsy of OC vs non-OC patients

The box plot above shows the expression intensity of the TSPAN6 monomer in the primary protein extracted from the tissue of 8 non-OC and 21 OC patients. The above box plot only quantifies the monomer and from the 29 data points by Kolmogorov-Smirnov Test the data was considered normally distributed (p=0.2). From this, a parametric T-Test revealed no statistically significant difference in the intensity of TSPAN6 homodimer in OC and non-OC patients (p=0.7). Overall, this graph shows that there is no significant difference in expression levels of the monomeric immunoreactive band recognised by the anti-TSPAN6 antibody.

The data points for the intensity of the monomer were analysed by Kolmogorov-Smirnov Test and found to be normally distributed (p=0.2). Therefore, a T-test was carried out to reveal no statistically significant difference with a p value of 0.7. This data suggests that the TSPAN6 monomer in protein extracted from 3D patient tissue is not suitable for stratifying patients and suggests the monomer alone would not be able to successfully guide the novel TSPAN6 ADC to the cancer cells for targeted therapy.

However, when looking at the immunoblot images in **Figure 4-9** to **Figure 4-12** the intensity of the homodimer seems to have diminished as a greater intensity of the 60 kDa band, only seen in protein extracted from a 3D source. This suggests that perhaps some of the 'active' TSPAN6 formerly shown as a homodimer has been modified so that the majority of the homodimers are now showing as a separate band of slightly higher molecular weight – suggesting this new band is still the homodimer. Due to this observation, the 60 kDa band will also be quantified and discussed in addition to the classic monomer and homodimer.

The band seen at 60 kDa has the potential to be the majority of the homodimer band with a post-translational modification as a result of the protein originating in a 3D environment. It is possible, from the literature, that this is not another separate isoform of TSPAN6 – simply a modified version of the homodimer that has been seen formerly. **Figure 4-17** shows the average of the intensity of the 60 kDa band from primary protein extracted from patient tissue in eight non-OC patients and 21 patients with OC. The data is shown to be not normally distributed by Kolmogorov-Smirnov Test (p=0.004) and there is a statistically significant difference between the two groups from a Mann Whitney test with a p value of 0.02. From this quantification, based on the information that this band is the modified homodimer, patients could be stratified using protein extracted from primary tissue. Additionally, as the expression here is higher in protein extracted from OC tissue, a novel TSPAN6 ADC has the potential to be more effective in OC tissue than in non-OC tissue. This TSPAN6 variant is expressed more abundantly in OC tissue which could have implications for diagnosis, but it has the potential to bind ADCs targeting TSPAN6 in primary human cancer ovarian cells, thus also conferring therapeutic potential. Therefore, future experiments are urgently needed to clarify if this band corresponds to a post-translationally modified TSPAN6 protein.
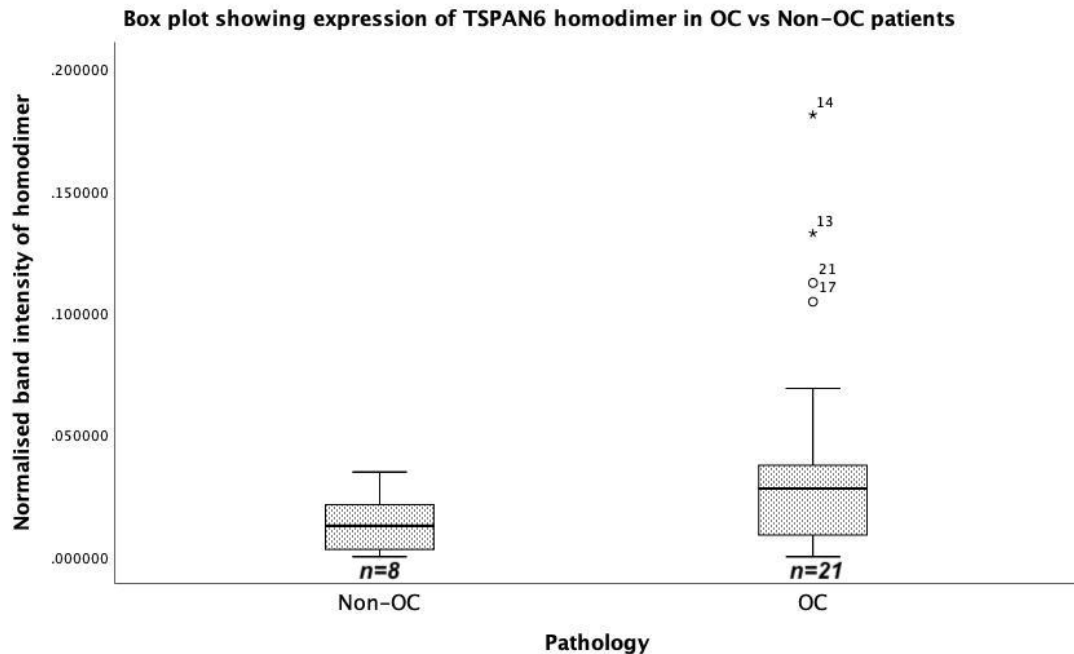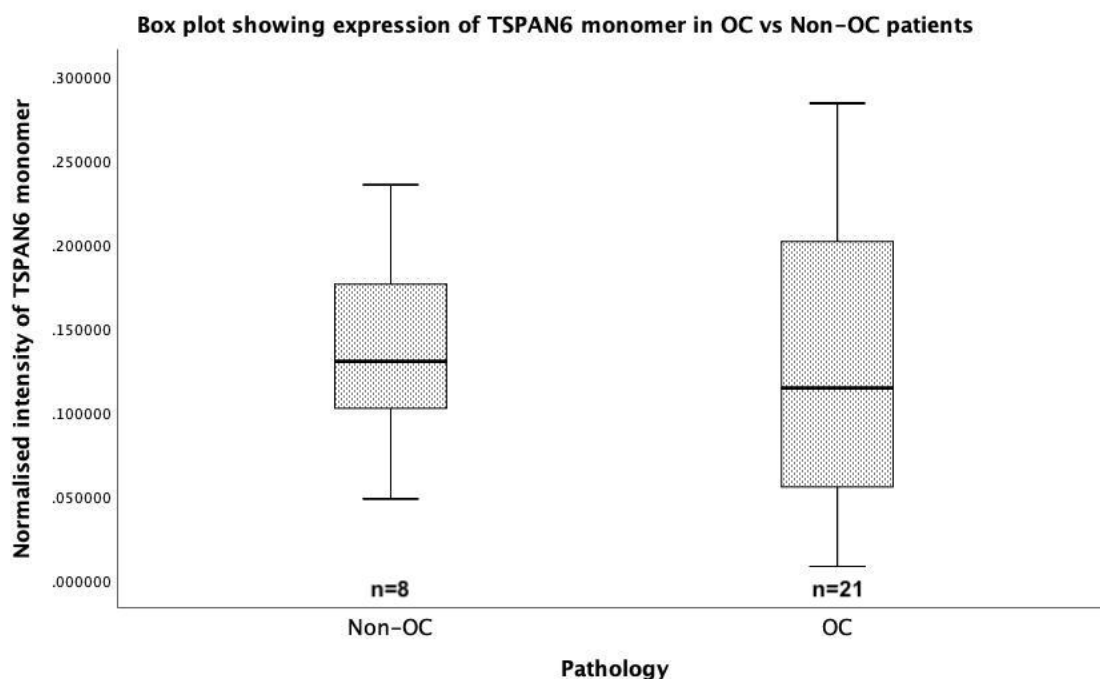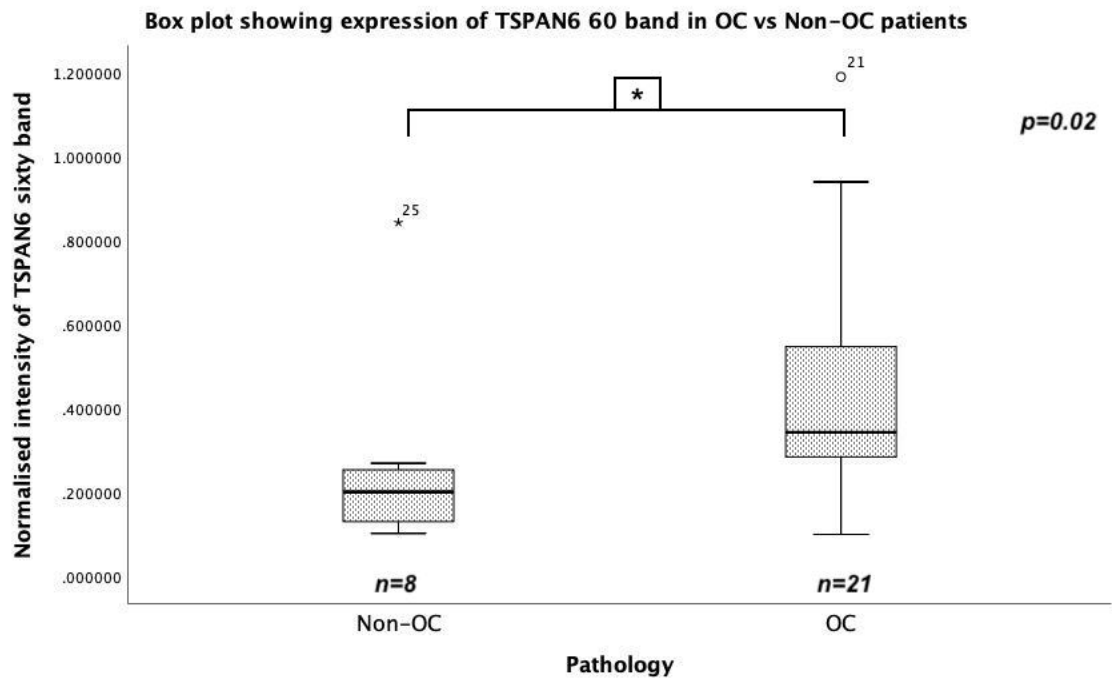
Figure 4-17 - Quantification of TSPAN6 60 kDa band intensity in protein extracted from the patient tissue biopsy of OC vs non-OC patients

The box plot above shows a significant difference (p=0.02) in the intensity of the 60 kDa band in the protein isolated from patient tissue in OC vs non-OC patients. The data was found to be not normally distributed by Kolmogorov-Smirnov Test (p=0.004) therefore a non-parametric Mann Whitney test was used. If the 60 kDa band is a modified version of the dimer then it can be said that OC and non-OC patients can be stratified by looking at this band in western blot. Additionally, an ADC using this TSPAN6 antibody would be more effective as a therapeutic if this binding is a reflection of the binding that would occur in primary human ovary in vivo.

Overall, the western blots above on protein lysate extracted from patient tissue biopsies have shown that total levels of TSPAN6 stratified HGSOC patients from non-OC patients, as well as the 60kDa immunoreactive band. The identification of an isomer capable of stratifying patients is crucial to the goals of more effective patient care by treatment and diagnosis.

4.4 Conclusions

Immunofluorescence examination of the three most promising targets from the previous chapter (TSPAN6, PCSK4 and PIEZO2) shows expression and localisation to the membrane variably for all three targets in 2D cultured cells derived from patient biopsies. This clear, but variable between pathologies, expression and localisation to the membrane is a prerequisite for the next stage of analysis. A limitation of this section is the lack of cell authentication by methods such as Short Tandem Repeat profiling. This process, ideally, would need to be done for each cell extraction and is vital to ensure primary cultures are the expected cell type, especially given the fibrous morphology observed. A representative light microscope phase contrast image of representative 2D cells derived from patient biopsies can be seen in **Appendix Figure 3**. It could be argued this needs to be addressed before any publications can be submitted. Additionally, all cell lines should be tested for mycoplasma before interpreting any results from cell cultures. The next stage of analysis as described below is an assessment and quantification of receptor mediated endocytosis internalisation of these targets into the cell and subsequent analysis of how effective and ADC using this target and antibody would be.

This chapter concludes the western blot section of the thesis. In the previous chapter, it was shown that the creative diagnostics (US) antibody DPABH 18048 can detect TSPAN6 clearly in western blot and that TSPAN6 expression varied between OC cell lines of different pathology. Furthermore, TSPAN6 was detected in healthy protein lysates from tissue purchased from Novus Bio (UK). In this chapter, no significant difference was observed between the intensity of the TSPAN6 dimer in protein extracted from 2D cells derived from patient biopsies with no OC diagnosis and those with an OC diagnosis. Looking further into the primary samples that were available. Protein was extracted directly from a 3D piece of tissue biopsy from ovaries with various pathologies including OC and non-OC. The results were more complex to analyse here as there was the appearance of an extra band just above the homodimer band (the 60 kDa band). As this band grew in intensity the intensity of the homodimer began to diminish, suggesting that this new band could be modified homodimer by a post translational modification such as phosphorylation or glycosylation. When taken individually, the intensity of the dimer and monomer did not show a statistically significant difference between the OC and the non-OC group. However, the 60 kDa band on its own did show a statistically significant difference. This suggests the 60 kDa band could be used to stratify patients into these two groups. Moreover, when comparing total levels of TSPAN6 by immunoblot a higher statistically significant level of total TSPAN6 was observed in OC samples compared to non-OC samples.

The immunoblots describe here, have proved useful as an extra characterisation step for antibody development, securing confidence that the anti-TSPAN6 antibody is indeed binding to TSPAN6, that this protein is present in cell lines, healthy protein from tissue, primary protein from 2D cells and primary protein from 3D tissue.

The next stage of exploration for these novel ADC targets is assessing to what extent they internalise into the cell and therefore the extent to which the toxic payload of an ADC would enter an OC cell using these target antibodies. This next chapter is a good indication of how effective a novel ADC would be with these targets.

Chapter 5: Assessment of putative ADC target antibody internalisation by receptor mediated endocytosis in 2D cultured cells

5.1 Introduction

This chapter further characterises the target proteins by assessing if they can mediate the internalisation of antibodies into the target cells and trafficking to the lysosomes. Receptor mediated endocytosis is the process by which circulating proteins (ligands) find and attach to their protein receptors on the surface of the cell and are subsequently brought into the cell (569). Receptor mediated endocytosis can support the nutritional needs of the cell by facilitating the internalisation of, for example, the ligands specific for galactose, mannose and LDL receptors (570). Some molecules such as transferrin and IgGs are recycled to the plasma membrane where they facilitate the transport of vital molecules such as iron (571). Often, ligands are modified upon entering the cells, for example by proteolysis for the removal of essential molecules. Receptor proteins are highly diverse but can be placed into 4 general categories. Receptors that recycle and traffic their ligands to the lysosomes, receptors that recycle but do not traffic their ligands to the lysosome, receptors that do not recycle and traffic their ligand to the lysosome and receptors that do not recycle and do not traffic their ligand to the lysosome (572). For an ADC, trafficking to the lysosomes is essential for the release of the cytotoxic payload and the recycling of the receptor back to the plasma membrane is inconsequential as the cell is expected to be destroyed.

The mechanism of action of ADCs showcases the importance of internalisation as a pathway to ensure the intracellular release of the cytotoxic payload (**Figure 5-1**).
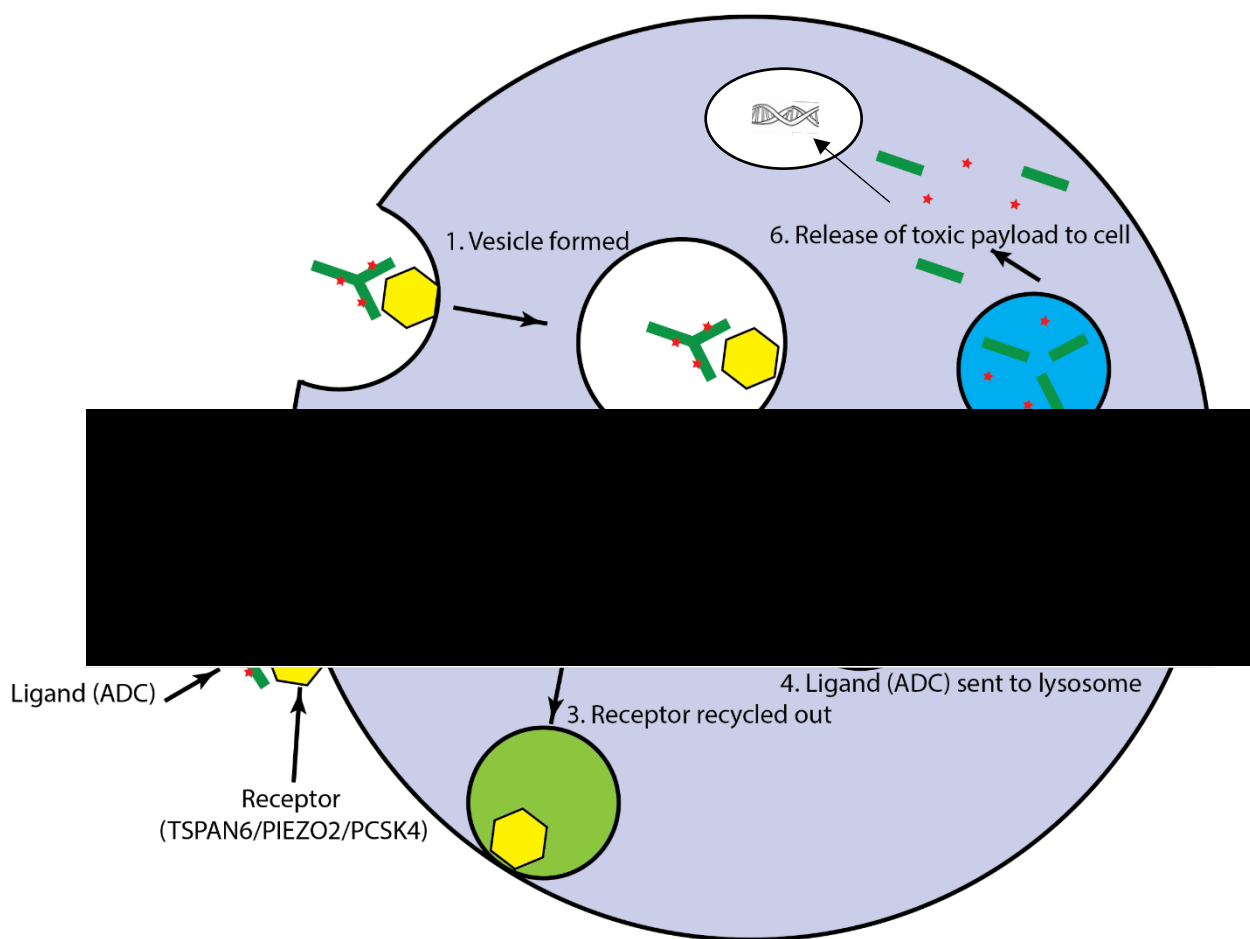
Figure 5-1 – Receptor mediated endocytosis mechanism of action (Kataoka et al (573))

ADCs mechanism of action. The ADC will be designed such as the monoclonal antibody will bind to and guide the ADC complex to the protein receptor. The binding will initiate the internalisation of the whole receptor-ligand complex into the cell (1) as an intracellular vesicle. The vesicle will fuse with an endosome (2) whereupon the receptor will be recycled out of the cell (3) and the ligand (in this case an ADC) will be trafficked to the lysosome (4). The lysosome will degrade the ligand (ADC) (5), where the active drug is released from the antibody to other compartments of the cell (6) where exerts its cytotoxic action, generally damaging DNA or microtubules and killing cancer cells.

Antibody internalization *via* receptor mediated endocytosis is a prerequisite for strong ADC efficacy because most of the toxic payloads function by disrupting important cellular pathways. Hence the initial antibody/receptor binding must initiate receptor meditated endocytosis for the toxic payload to be brought into the cell. Several factors can affect the efficiency of ADC internalisation. The binding affinity of the antibody to the target has been linked to an efficient uptake into the cells. The internalization kinetics is related to binding affinity, with high-affinity antibodies exhibited greater internalization potential comparing to low-affinity antibodies (336). It has been reported that different antibodies against the same target can show different rates of internalisation, potentially due to affinity (574). Logically, rapid internalisation could be favourable to reduce the likelihood of off-target toxicity and increase the safety and efficacy of

the ADC at the same time. There are different pathways by which the antibody can be internalised into the cell and each can have a different effect on ADC processing (575). For example, Clathrin-coated Pit-mediated receptor internalisation (576) has been reported to traffic the ligand (ADC) to the Golgi or endoplasmic reticulum instead of to the lysosomes. If this happens then the ADC is not processed in a way that can release the cytotoxic drug which impedes the effect of the ADC.

Having previously selected suitable targets from the in-silico database and identified antibodies targeting the extracellular domain of these targets (Chapter 3) as well as validated the differential expression of these targets in healthy versus cancer samples using best antibodies candidates (Chapter 4), then this chapter looks deeper into the internalisation capabilities of these antibodies/target pairs to determine suitable ADC candidates. For instance, a target can be highly expressed on the surface of the cell but have a low antibody internalisation rate. This means that to compensate, the ADC payload drug would have to be more potent to have the required therapeutic effect and the linker would need to be more stable to reduce systemic toxicity (575). With trafficking the lysosomes such a vital part of ADC success, this chapter uses a pH sensitive dye (Promega) which only reacts and becomes fluorescent when it is in the acidic environment of the lysosomes (577).

An additional ADC target, the Receptor for Advanced Glycation End Products (RAGE) will be introduced in this study, as a well characterised novel ADC target that has been heavily researched in the Reproductive Biology and Gynaecological Oncology (RBGO) group in Swansea University Medical School. RAGE was the first target developed through the pipeline described here for the new potential ADC targets described in this project. Being further ahead, RAGE has already been well characterised and validated *in vitro* and *in vivo* as a therapeutic target against endometrial cancer, with current validation experiments ongoing for its use against ovarian cancer (200, 201). Additionally, several new mouse IgG1 monoclonal antibody clones have been produced using hybridoma technology and are currently being screened by immuno-microscopy, western blot and immunohistochemistry to reveal lead candidate antibodies. The RAGE monoclonal antibody clone HA9 (Human) has shown evidence of clear specific binding in preliminary immunoblots and 2D cell immunofluorescent microscopy (not published, Gonzalez *et al*., personal communication). Therefore, it was chosen to be a part of this study for comparison with the new targets to inform development. In addition, it was decided to explore whether target internalisation was impeded if antibodies to TSPAN6 and RAGE were added to mimic a potential future ADC combination therapy approach.

Assessment and quantification of the target-antibody complex internalisation and trafficking to the lysosomes will be performed by quantifying the pH Dye fluorescent signal (Promega). The acidic pH of the lysosomes will be used to confirm the presence of the Ab-conjugated to pH Dye in this compartment given these pH reactive dyes have a dramatic increase in fluorescence as the pH becomes more acidic and a very low/non-existent fluorescence at a pH greater than 7. This chapter covers data resulting from three main experiments conducted to fulfil the following objectives:

- Evaluate the internalisation capacity of target/antibody-dye complex over time to determine the best internalisation time at 37°C using immunofluorescence time point assays
- Evaluate and quantify antibody internalisation abundance in cell lines and 2D cultured primary cells derived from patient ovarian tissue biopsies at a defined timepoint (selected above)
- Evaluate how targets abundance influence internalisation capacity using a competition assay between the lead target TSPAN6 and an established RBGO group ADC target: the Receptor for Advanced Glycation End products (RAGE)

5.2 Antibody-dye conjugations, antibody recovery and Dye to Antibody Ratios (DARs)
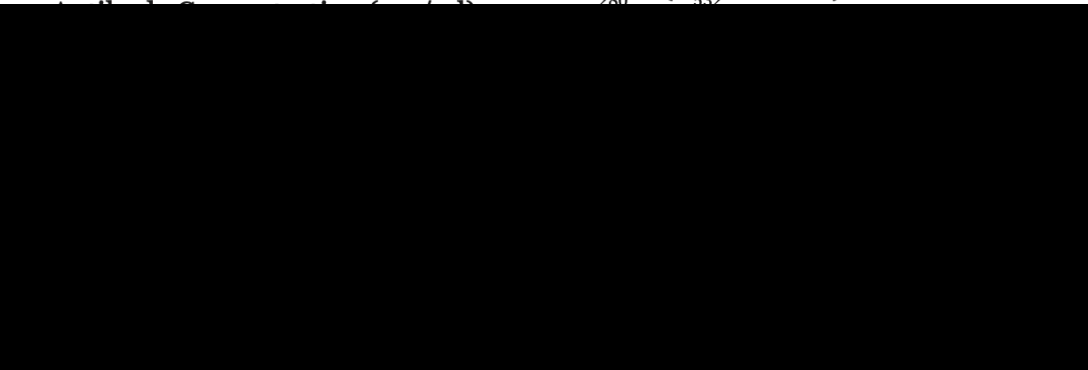
The amine pH reactive dye used here is a one-use solution that once reconstituted (directly before conjugation), is not recommended to be stored for future use. In addition, once the conjugation has taken place the fluorescence is reported to begin diminishing after 1-2 weeks. For these reasons, only four conjugations in total took place for the results reported here in this chapter (one for each of TSPAN6, PCSK4, RAGE and IgG isotype control) and the internalisation experiment was carried out as soon as possible after the conjugation. First the time points, then the internalisation in the cell lines and 2D cultured primary cells derived from patient ovarian tissue biopsies and lastly the competition assay. All of the internalisation assays shown here were carried out within 3 days of the initial conjugation.

In addition to the cost of the pH reactive dye, the antibody recovery after conjugation makes this process expensive. Often, a large proportion of the antibody is lost during the conjugation process. This is why six targets were narrowed down to 3 and why the preliminary characterisation from the previous chapters had to be in place before internalisation was to be attempted here. Recovery could range from 50-90%, with a good chance that 50% of the antibody would be lost and each conjugation is unique in terms of recovery and efficiency. This

was reflected in a different Dye to Antibody Ratio (DAR) for each individual conjugation. The DAR is a ratio of how many dye molecules had conjugated to one antibody molecule. It was reported that successful conjugations had a DAR between 3 and 6.

5.2.1 Dye to Antibody Ratios (DARs)

The DARs of each conjugation was calculated using the equations shown in **Figure 5-2** below. Due to each conjugation having different DARs, even when the concentration of antibody-dye conjugate added to each well was the same, the separate conjugations (individual targets targets) cannot be reliably compared to each other. Only wells using the same conjugated antibody (and therefore the same DAR) can be compared.

$$\text{Antibody Concentration (mg/ml)} = \frac{A_{280} - (A_{532} \times 0.256)}{}$$

Extinction coefficient of pHAb Reactive Dye = 75,000

Correction factor for pHAb Reactive Dye = 0.256

Figure 5-2 – Equations used to calculate the Dye to Antibody Ratio (DAR)

Equations for the calculation of the DAR from individual conjugates were taken from the Promega pH reactive dyes handbook (578)

Table 5-1 below shows the DARs for each of the conjugations. The success of the conjugation depends on the antibody, the isotype and the concentration of the starting solution. TSPAN6 had the lowest initial concentration (0.5 mg/ml), PCSK4 had a slightly higher concentration of 0.6 mg/ml and the RAGE clone and the IgG isotype had the highest concentrations at 1 mg/ml. Comparing TSPAN6 to PCSK4 although the starting concentration was similar, PCSK4 had the superior DAR and also the superior recovery. PCSK4 recovered 80-90% of antibody after conjugation where TSPAN6 only recovered 40-50%. Here a non-specific IgG antibody was conjugated as an IgG isotype control antibody and assessed along with the other targets to check for any non-specific binding and subsequent internalisation. The IgG results are not displayed in this chapter as they all reported no quantifiable or visible fluorescence on the confocal images (see Appendix 1).

Table 5-1 – Dye to Antibody Ratios calculated for each of the 4 antibody-dye conjugations

	DAR
TSPAN6	3.9
PCSK4	6.4
RAGE HA9	5.5
IgG Isotype	5.1

The pH response of the antibody-dye conjugates was immediately measured following successful conjugation and before adding to the cells. One μl of antibody-dye conjugate was added respectively to either 100 μl of 100 mM citrate buffer (pH 4) or 100 μl of 100 mM phosphate buffer (pH 8). The fluorescence was read on the FLUOstar Omega plate reader (BMG Labtech) at Ex 532/Em 560 nm. A fold increase of fluorescence was observed for all conjugations, therefore progression to the internalisation assays was permitted.

5.3 Timepoint assay

After obtaining antibody-dye conjugates suitable for assessing antibody-target mediated internalisation, optimisation experiments were conducted to select the optimal time to assess and visualise this process. The optimal time will show the highest intensity of fluorescence which allows for easier quantification, comparison and analysis. This assay is also a preliminary assessment of how rapidly the target/antibody-dye conjugate complex can internalise which can offer insights into the appropriateness of the target for ADC development. For each time point, the SKOV-3 cells were plated in triplicate; one for TSPAN6, one for RAGE and one negative control as cells only. SKOV-3 cells were chosen due to being a serous subtype, which is the most common subtype of OC. During this time point analysis, a non-cancerous cell line would have been beneficial to include, however due to a limited amount of antibody-dye conjugate and time restrictions just one cell line was chosen. The addition of the antibody-dye conjugate to the cells was staggered to ensure each time point was accurate and not held up by the visualisation of the previous time point.

At this stage, the six novel targets selected at the beginning of the study have been narrowed down to three: TSPAN6, PIEZO2 and PCSK4. However, the PIEZO2 antibody was discontinued by Thermo Fisher (UK) and the replacement used a different epitope sequence. Unlike previously with TSPAN6, no other PIEZO2 commercially available antibody had the same epitope and at this stage in the project it was decided not to continue with a completely new PIEZO2 antibody, hence PIEZO2 was not selected for further evaluation in our pipeline. The RAGE HA9 clone was brought in as a replacement of RBGO1 antibody targeting the same epitope, and to act as a

positive control of a target mediating antibody internalization (200, 201). For the optimisation experiments, TSPAN6 and RAGE only were chosen to preliminarily test the best incubation time for internalisation, so as not to waste antibody and pH reactive dye. SKOV-3 cells were chosen as they showed expression of the targets on the membrane in past experiments and for this preliminary and time sensitive experiment, SKOV-3 are a reliable robust cell line. Once the conjugation had been carried out the cells needed to be ready to avoid delay and loss of fluorescent properties. The aim was to find a mutually agreeable internalisation time that could be extended to all targets. Although each target will have a different internalisation rate and the targets could not be directly compared to one another (due to different DARs), keeping the incubation times the same allowed for some degree of comparison and reduced the number of variables and likelihood of potential mistakes in the assay procedure.

5.3.1 TSPAN6 timepoint

A visual representation of the internalisation time point assay with TSPAN6 antibody-dye conjugate is shown in **Figure 5-3**. TSPAN6 antibody-dye conjugate was added to live cells and, after 30 mins at 4°C, was allowed to internalise for 1, 2, 4, 6, 8 and 24 hours at 37°C before staining the nuclei with Hoechst and being taken directly to the confocal microscope for visualisation. The images shown below are representative images chosen to display out of a minimum of three fields of view taken randomly across the well. From a rapid internalisation perspective, it was encouraging to see internalisation from as early as 1 hour which increased till 4 hours. After 4 hours the fluorescent intensity decreased with considerably less signal detected at 24 hours. Overall, this figure shows that the TSPAN6 antibody-dye conjugate was successfully trafficked to an area of high pH, which is assumed to be the lysosomal compartment. The solution covering the cells was a mixture of PBS and DAPI, which was shown to not trigger red fluorescence. The cytoplasm of the cell is known to be pH 7-7.5 and the lowest pH (the most acidic) is agreed to be the lysosome at pH 4.5 (579). Based upon this knowledge and the purpose of the product validated by the company (Promega UK) (577), it is concluded that the fluorescence seen here does represent the TSPAN6 antibody-dye conjugate reaching the lysosomes.

Figure 5-3 – Abundance of pH reactive dye fluorescence indicating TSPAN6 antibody-dye conjugate internalisation by receptor mediated endocytosis into SKOV-3 cells at various time points

The figure above shows a representative field of view from the internalisation TSPAN6 antibody-dye conjugate into SKOV-3 cells at various internalisation time points. This figure shows the internalisation was visible at all time points with the most abundant internalisation seen at 4 hours and less than 4 hours. The scale bar can be seen at the bottom of each field in white and represents 20 μm.

Looking in more detail at the internalisation seen in **Figure 5-3**, the software CellProfiler (CP) was used to quantify the intensity of the fluorescent signal using a programme developed in house by Dr David James (RBGO postdoctoral bioinformatician researcher).

A spreadsheet was made with each image name followed by the normalised intensity of fluorescence that was calculated. The intensity was normalised by the number of cells counted in the field of view. The data points were compiled in SPSS statistical analysis software and the following graph and analysis was produced.

Figure 5-4 shows the box plot from the quantification of the intensity of fluorescence indicating internalisation of TSPAN6 antibody into SKOV-3 cells at various time points. SKOV-3 cell line was chosen for two main reasons. Firstly, SKOV-3 is a serous OC subtype which is the most common subtype of OC. Secondly, the SKOV-3 cell line is known to be easy to grow and hardy in the interest of this time sensitive experiment. In the future, it would be beneficial to include additional cell lines in this assessment, particularly a control non-OC cell line. The data was shown to be not normally distributed by Kolmogorov-Smirnov Test (p=5.0 x10^{-8}). Several statistical tests were performed to identify differences between time points. Firstly, due to the data being not normally distributed and there is more than two groups, the Kruskal-Wallis one-way analysis of variance was performed. The Kruskal-Wallis test is the non-parametric alternative to the one-way ANOVA, is considered an extension of the Mann-Whitney U test and is used to allow the determination of statistically significant differences between two or more groups. The Kruskal-Wallis test alone can only show a significant difference or not in the data set – it cannot show where or between what groups it is. The Kruskal-Wallis test showed a p value of 0.002, suggesting there was statistically significant differences between the groups. Therefore, a post-hoc test was carried out to find out exactly where this difference was. The pairwise comparisons of the different time points revealed mainly significant differences between the 4-hour time point and the other time points. This is represented on the boxplot shown in **Figure 5-4**.
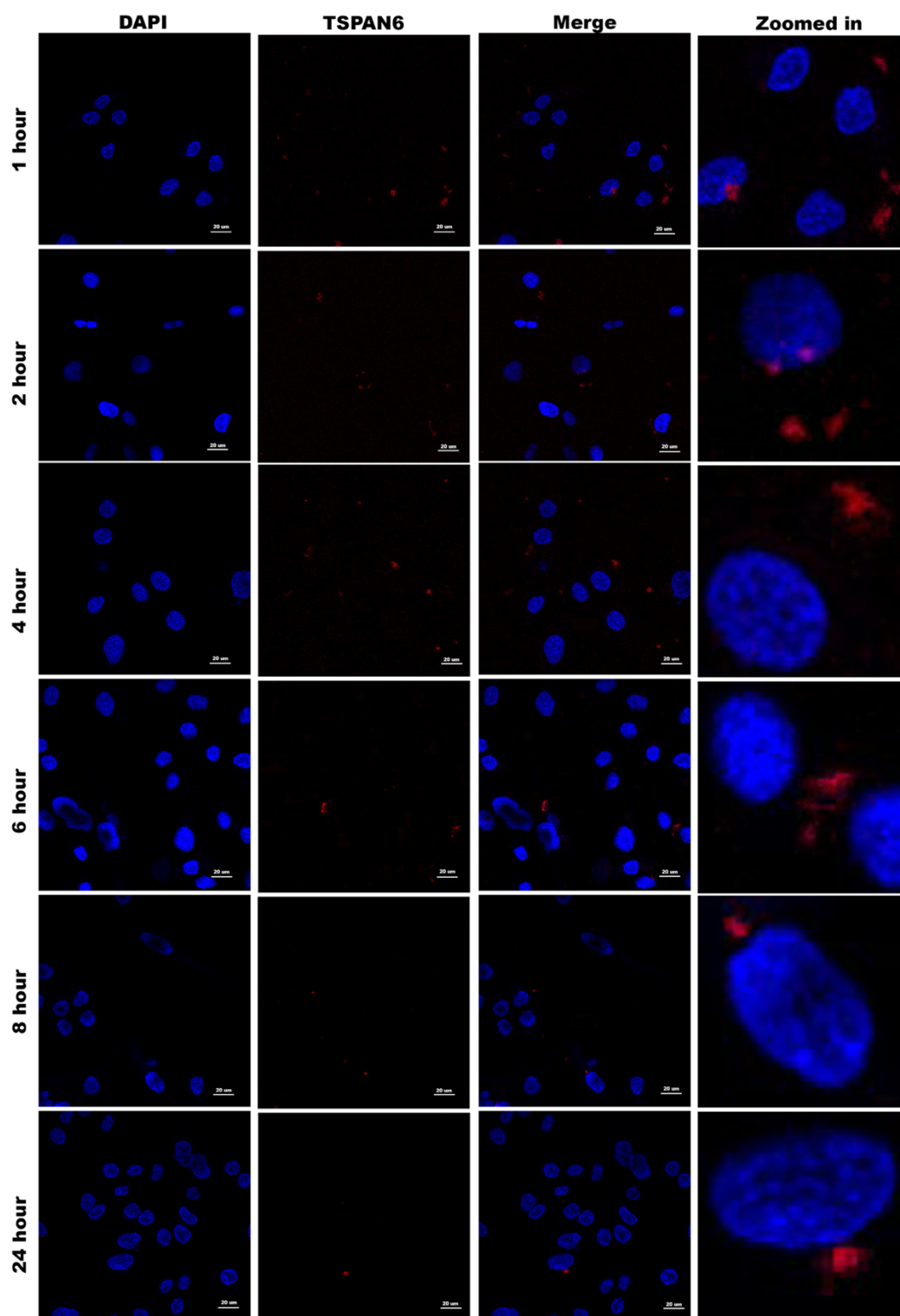
Figure 5-4 – Quantification of abundance of pH reactive dye fluorescence indicating TSPAN6 antibody-dye conjugate internalisation by receptor mediated endocytosis into SKOV-3 cells at various time points

The above boxplot shows the intensity of fluorescence indicative of internalisation of the TSPAN6 antibody-dye conjugate into SKOV-3 cells. The statistical analysis (Kruskal-Wallis followed by pairwise comparison and Mann-Whitney U) revealed a statistically significant difference between the 4-hour time point and all the other time points. This boxplot also shows internalisation becoming lower in the 24-hour time point, suggesting the antibody-dye conjugate may have been recycled out of the cell after around 24 hours. Overall, this boxplot shows that the optimal time to allow TSPAN6 antibody to internalise is 4 hours.

The pairwise comparison showed statistically significant differences between the 4-hour time point and the other time points. A follow up Mann-Whitney U test between the samples showed a significant difference between the 4-hour time point and all other time points with p values between 0.002 and 0.004.

From this analysis, for the TSPAN6 antibody, 4-hours was the optimal time to allow internalisation to provide the highest intensity of fluorescence.

The same assay was performed using the RAGE HA9 clone to assess the optimal length of time to allow RAGE HA9 to internalise. The visual representation of the data can be seen in **Figure 5-5** below. RAGE HA9 clone does internalise into 2D cultured SKOV-3 cells at all six time points to varying degrees (**Figure 5-5**). The images shown below are representative images chosen to display out of a minimum of three fields of view taken randomly across the well. It is observed that fluorescence is least intense at the 1-hour time point and the most intense at the 4 and 24-

hour time point. As in **Figure 5-4**, it is encouraging to see evidence of internalisation at such an early time point. This is a good sign for the rapid internalisation of RAGE HA9 clone and its success as an ADC. When compared to TSPAN6, the abundance of internalisation does seem to be less intense. This could be due to not being able to compare RAGE and TSPAN6 directly due to different conjugations and therefore different DARs. Additionally, this is the first time this RAGE clone has been evaluated in these cells and it is already known that different antibody clones, even against the same target, can differ in binding affinity and internalisation.

Figure 5-5 – Abundance of pH reactive dye fluorescence indicating RAGE (HA9) antibody-dye conjugate internalisation by receptor mediated endocytosis into SKOV-3 cells at various time points

This figure shows a representative image of internalisation from each time point using the RAGE HA9 antibody. SKOV-3 cells were incubated with the RAGE HA9 antibody conjugated to a pH reactive dye. The dye only fluoresces under acid conditions within the cell (the lysosomes) and therefore the red fluorescence is indicative of the amount of antibody-dye conjugate successfully internalised into the cell. This figure shows internalisation at all time points. The scale bar can be seen at the bottom of each field in white and represents 20 μm.

Figure 5-5 shows only the visual representation of one field of view taken within the well. Figure 5-6 shows the quantification, taking into account all the fields of view. It can be seen that there is actually very little difference between the intensity of internalisation at different time points. The highest intensity over all fields of view was seen at the 4-hour time point – although this was not statistically significantly different. The data was shown to be not normally distributed by One-Sample Kolmogorov-Smirnov Test with a p value of 1.2×10^{-15}. A Kruskal Wallis test showed a p value of 0.054 which is close to the significance value cut off point. This suggests that one of the mean ranks is almost significantly different from the others. When looking at the mean ranks it is shown that the 4-hour time point is the highest and most statistically different from the others. Although it is not statistically significantly different from the others this is in agreement with the TSPAN6 timepoint data, therefore 4 hours was chosen as the optimal time to leave the antibodies to internalise.
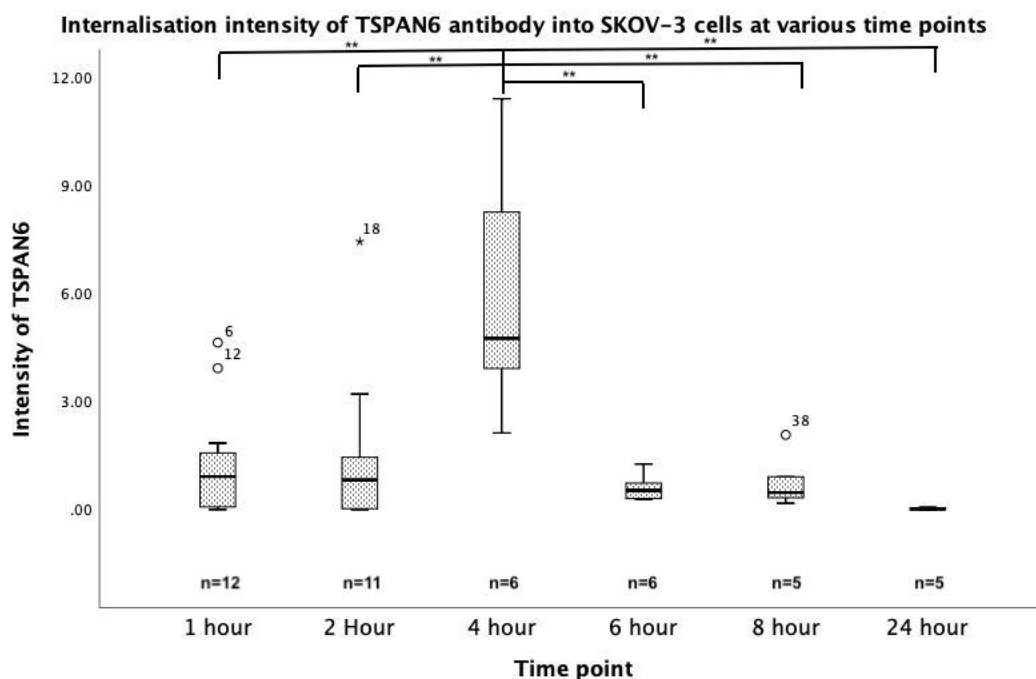

Figure 5-6 - Quantification of the abundance of pH reactive dye fluorescence indicating RAGE (HA9) antibody-dye conjugate internalisation by receptor mediated endocytosis into SKOV-3 cells at various time points

The above boxplot shows the intensity of fluorescence indicative of internalisation of the RAGE HA9 antibody-dye conjugate into SKOV-3 cells. The statistical analysis (Kruskal-Wallis followed by pairwise comparison and Mann-Whitney U) revealed no statistically significant difference between the time points. The data was shown to be not normally distributed by One-Sample Kolmogorov-Smirnov Test with a p value of 1.2×10^{-15}. A Kruskal Wallis test showed no significant difference with a p value of 0.054. The time point with the highest intensity was 4 hours therefore 4 hours was chosen as the incubation time for internalisation.

5.3.2 Internalisation assay with TSPAN6, RAGE HA9 and PCSK4

The timepoint assay revealed the most effective time to allow for internalisation was 4 hours. Therefore, subsequent experiments explore target mediated internalisation at this time point using 8 OC cell lines and 2D primary cell cultures derived from 4 patients (2 non-cancer and 2 HGSOC). Table 5-2 below shows the different subtypes relating to the 2D cells used in this section.

Table 5-2 – Pathology description of 2D cells used in internalisation assay

Cell name/Sample ID	Pathology
IOC	Pre-malignant OC
TOV 112D	Endometrioid OC
TOV 21G	Clear cell OC
UACC	Papillary Serous OC stage 4
UWB1	Papillary Serous OC stage 4 BRCA1 mutation
SKOV-3	OC stage 1-2
COV-664	Mucinous OC
OVCAR-3	HGSOC
OV73 (Patient derived)	Non-Cancer – Control- No described ovarian pathologies
OV29 (Patient derived)	Non-Cancer -Risk reduction surgery for MSH6 mutation
OV48 (Patient derived)	HGSOC stage 4
OV12 (Patient derived)	HGSOC stage 4

Comparisons can only be made between cells where the same antibody-dye conjugate was used. For example, the fluorescence of anti-TSPAN6-dye conjugate in IOC and OVCAR cells could be compared to each other. But fluorescence in IOC with two different antibody-dye conjugates could not be compared due to differences introduced by the individual conjugations and DARs. Differences in internalisation fluorescence signal for TSPAN6/antibody-dye conjugate complex were observed between the different cell types (**Figure 5-7**). The initial observation indicated evidence of internalisation in all cell types. Secondly, from the images, it can be seen a different pattern for each cell line representative of a different OC subtype. DAPI stains the cell nucleus and confirms the presence and uniform growth of cells in the well. It is important to note the rate of internalisation in the cell lines here and in the following figures. Here the internalisation after 4 hours is shown, however because the time point analysis was only done in SKOV-3 cells using TSPAN6 and RAGE the other targets and cell lines may internalise much earlier or later, which means this wouldn't have been captured in this experiment. Due to this, further time point analysis should be done with more cell lines and all the targets to increase data reliability.
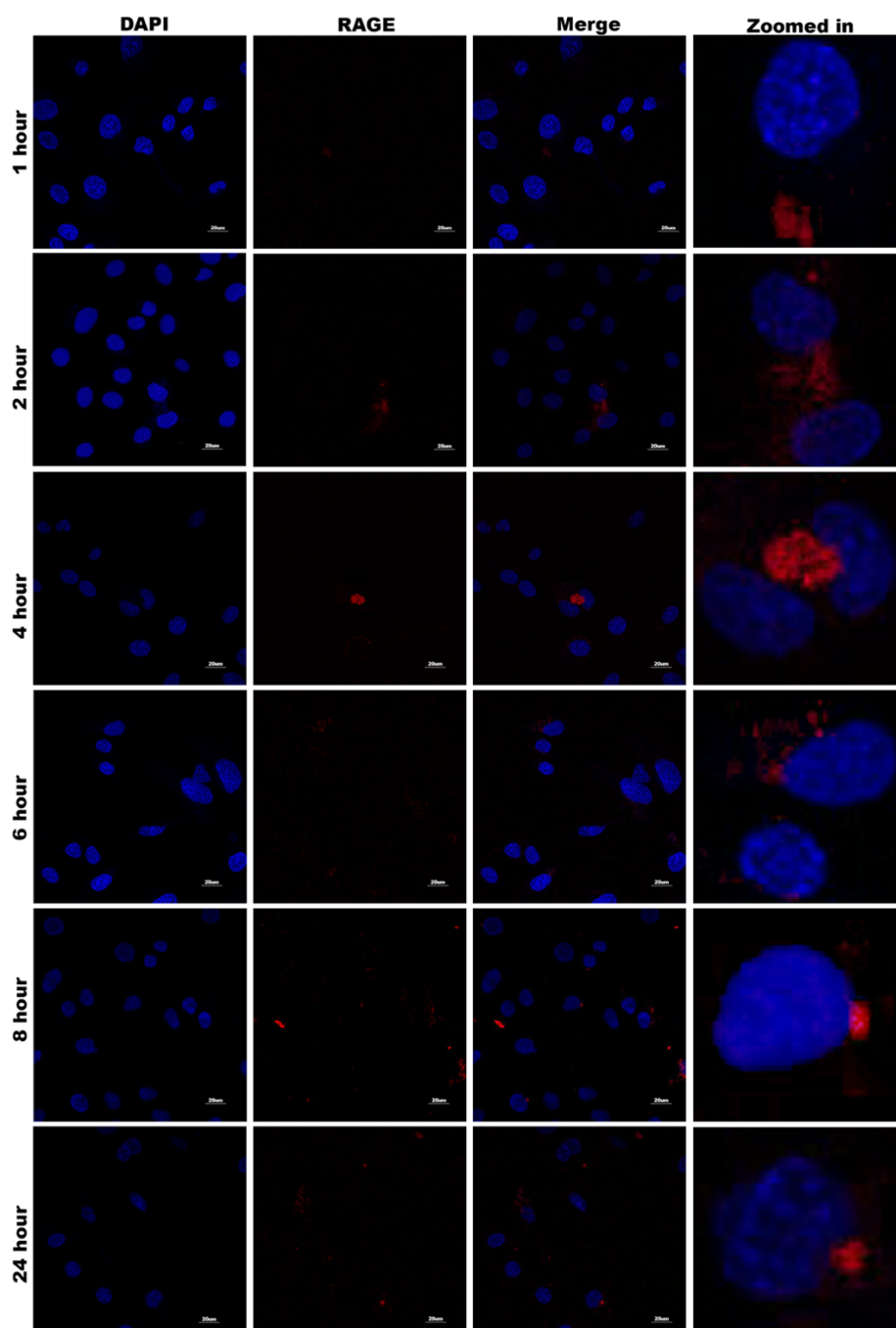
Figure 5-7 – Abundance of pH reactive dye fluorescence indicating TSPAN6 antibody-dye conjugate internalisation by receptor mediated endocytosis into various 2D cultured cells

Fluorescence indicating TSPAN6 antibody-dye conjugate internalisation into cells of various ovarian pathology and non-OC control cell lines (4 h time point). It is observed that fluorescence indicating internalisation is seen in all cell types. The amount of internalisation is variable depending on the cell type. Additionally, to display evidence of internalisation more clearly, the most intense and clearest field was chosen as the image to display in this figure out of all the fields of view replicates. For this reason, it is not possible to comment and compare the abundance of internalisation in this figure. This image simply shows the cells are uniformly distributed, indicating good health and the fluorescence indicating internalisation is visible in all cell types. Figure 5-8 shows the quantification for each cell line, taking into account all the fields of view replicates. Figure 5-9 shows the quantification for the internalisation of TSPAN6 into primary cells derived from patient biopsies.

Quantification of all the fields of view from the cells shown above in **Figure 5-7** was made and it is shown as a box plot (**Figure 5-8**). Here, it can be seen that receptor-mediated internalisation fluorescence signal in OVCAR-3 is statistically significantly higher than in all of the other cell lines (**Figure 5-8**). These results suggest that potentially patients with a HGSOC subtype could benefit the most, among all OC subtypes, from an ADC targeting TSPAN6 with this antibody. Previous data (Chapter 3) showed the expression of TSPAN6 on the plasma membrane of 2D cultured OVCAR-3 cells, supporting the internalisation seen here, however the fluorescence observed was not quantified. Furthermore, when TSPAN6 expression was analysed by immunoblot (Chapter 3), TSPAN6 did show expression in protein extracted from OVCAR-3 2D cultured cells, however OVCAR-3 did not express the most TSPAN6 when compared to the other 8 cell lines. This suggests that overall expression of TSPAN6 from immunofluorescent data and immunoblot (Chapter 3) is not correlated with the abundance of internalisation seen here in this data. The data was considered not normally distributed by one-Sample Kolmogorov-Smirnov Test with a p value of 0.000345. Therefore, a non-parametric Mann-Whitney test was used to assess for significant difference between the two groups. **Table 5-3** shows each individual p value by Mann Whitney test for significance in more detail.

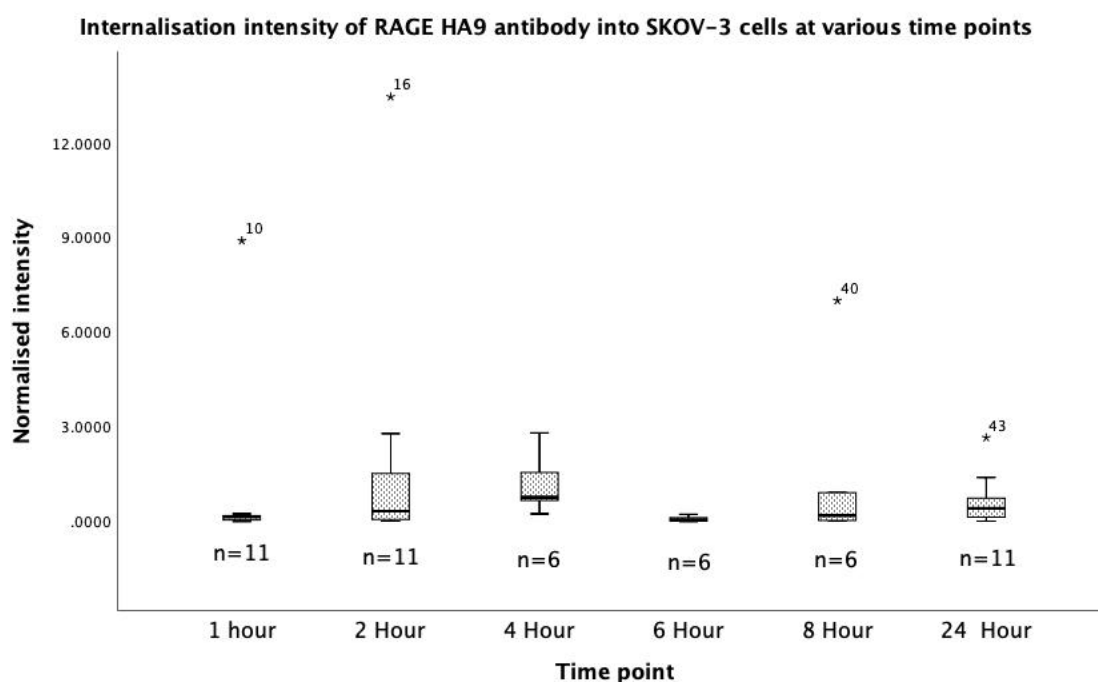*Figure 5-8 – Quantification of abundance of pH reactive dye fluorescence indicating TSPAN6 antibody-dye conjugate internalisation by receptor mediated endocytosis into various 2D cultured cell lines*

A boxplot showing the quantification of fluorescence of TSPAN6 antibody-dye conjugate indicating receptor mediated endocytosis into various cell types after 4 hours incubation. OVCAR-3 (HGSOC subtype) is statistically significantly different from all the other cell lines in its fluorescent intensity. Where *= <0.05 and **= <0.01. A breakdown of the p values by Man-Whitney can be seen in Table 5-3 below.

Table 5-3 – P-Values by Mann-Whitney test for significance of fluorescence values for TSPAN6 antibody-dye conjugate internalisation into various cell lines

	IOC	21G	112D	UWB1	UACC	SKOV	COV	OVCAR
IOC		0.724	0.755	0.286	0.662	0.413	0.190	0.016
21G			0.536	0.368	0.491	0.283	0.283	0.008
112D				0.927	0.836	0.927	0.230	0.073
UWB1					0.914	1.000	0.114	0.029
UACC						0.610	0.352	0.019
SKOV							0.200	0.029
COV								0.029
OVCAR								

211

Regarding the fluorescence indicative of internalisation from the 2D cultured primary cells derived from patient biopsies shown in **Figure 5-7**, quantification also indicates TSPAN6 binds and internalises antibodies into the cells (**Figure 5-9**). The boxplot shows the average value of fluorescence intensity taking into account all the replicate fields of view from the 2D cultured cells derived from 4 different patients – 2 HGSOC and 2 non-cancer as described above in Table 5-2. The data was found to be normally distributed by one-Sample Kolmogorov-Smirnov Test with a p value of 0.2, therefore, a T-test was used to compare means between the two groups. The T-test returned a p value of 0.012 – indicating statistically significantly higher fluorescence indicative of internalisation in HGSOC patient derived 2D cells. A significant result here means that there is statistically significantly more TSPAN6 antibody-dye conjugate being internalised into 2D cultured primary cells derived from the biopsies of HGSOC patients than patients with a non-OC diagnosis. This indicates an ADC using this TSPAN6 antibody could have internalised more effectively in HGSOC cells when compared to non-cancer cells expressing lower amounts of target. This could offer a therapeutic advantage in HGSOC patients. In previous data (Chapter 3), TSPAN6 expression by immunoblot was shown to be statistically significantly higher in OC patients versus non-cancer patients. Therefore, the statistically significantly higher indicated internalisation of TSPAN6-Ab dye complex into HGSOC cells derived from primary patient biopsies is in accordance with these previous observations.

Internalisation of TSPAN6 antibody into HGS-OC and non-cancer primary patient 2D cells

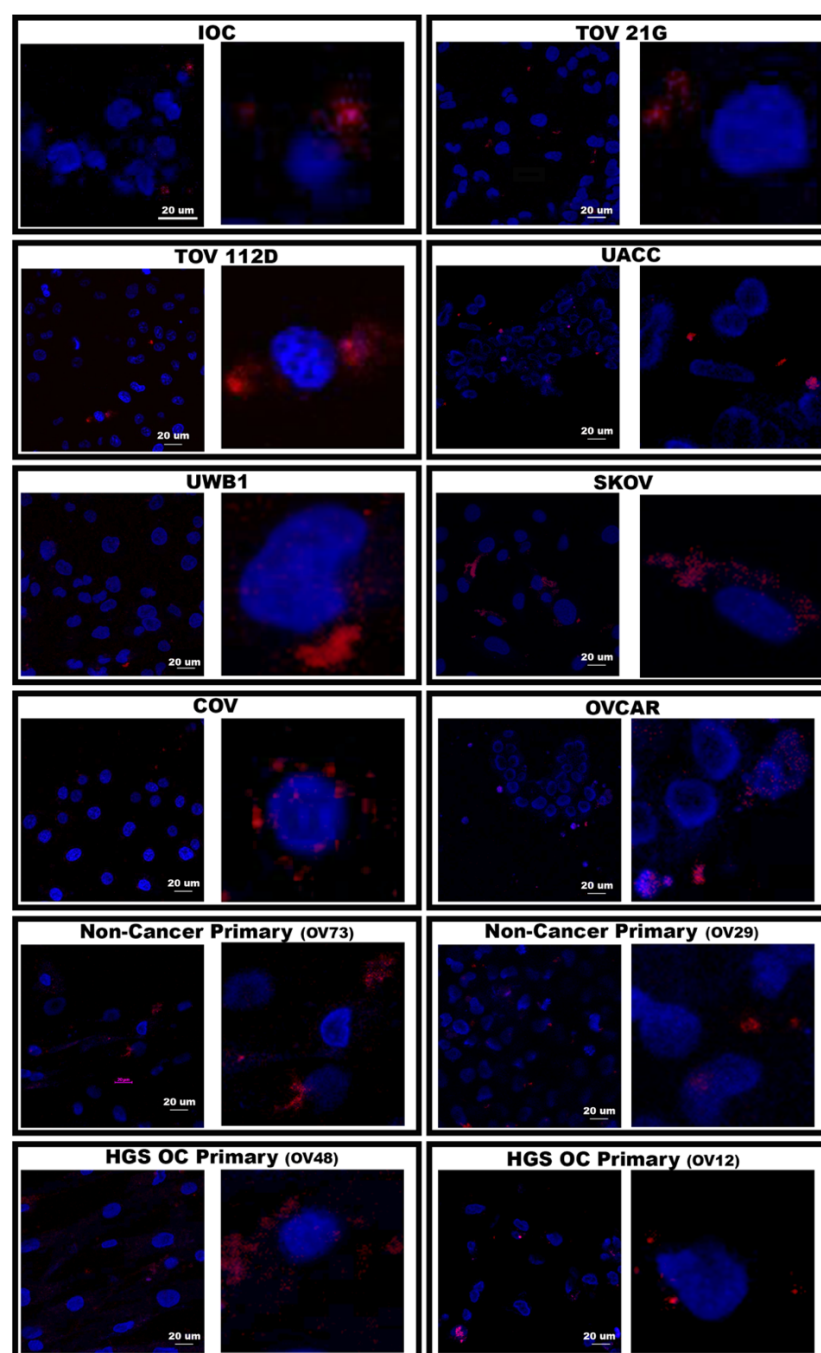*Figure 5-9 – Quantification of the abundance of pH reactive dye fluorescence indicating TSPAN6 antibody-dye conjugate internalisation by receptor mediated endocytosis into 2D primary cultured cells derived from HGSOC and non-cancer patients*

The box plot above compares fluorescence from all of the fields of view in 2D primary cultures cells derived from HGSOC (n=12) and non-cancer (n=11) patients. The data was found to be normally distributed by one-Sample Kolmogorov-Smirnov Test with a p value of 0.2 therefore a T-test was used to compare means between the two groups. The T-test returned a p value of 0.012 – indicating statistically significantly higher fluorescence indicative of internalisation in HGSOC patient derived 2D cells.

Next, the internalisation of the PCSK4 antibody-dye conjugate into various OC cell lines and patient samples grown as 2D monolayers was evaluated (**Figure 5-10**). Images show fluorescence, indicating successful internalisation and trafficking to the lysosomes, in every cell type in **Figure 5-10**. There is variation seen between cell types which is encouraging for future patient stratification using this target. The images seen are representative images of several fields of view taken to best represent internalisation.
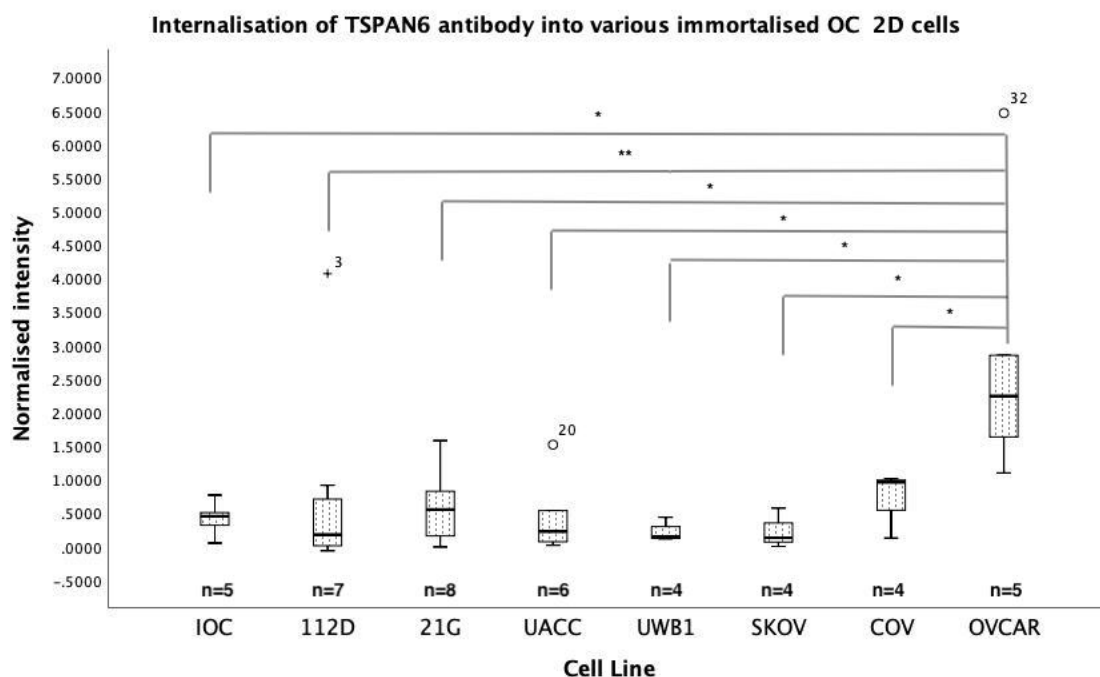
213

Figure 5-10 – Abundance of pH reactive dye fluorescence indicating PCSK4 antibody-dye conjugate internalisation by receptor mediated endocytosis into various 2D cultured cells

Fluorescence indicating PCSK4 antibody-dye conjugate internalisation into cells of various ovarian pathology. It is observed that fluorescence indicating internalisation is seen in all cell types. The amount of internalisation is variable depending on the cell type. Additionally, to display evidence of internalisation more clearly, the most intense and clearest field was chosen as the image to display in this Figure out of all the fields of view replicates. For this reason, it is not possible to comment and compare the abundance of internalisation in this figure. This image simply shows the cells are uniformly distributed, indicating good health and the fluorescence indicating internalisation is visible in all cell types. Figure 5-11 shows the quantification for each cell line, taking into account all the fields of view replicates. Figure 5-12 shows the quantification for the primary cells derived from patient biopsies.

214

Quantification analysis of the fluorescence signal observed when 2D OC cell lines of various OC subtype were allowed to internalise the PCSK4 antibody-dye conjugate for 4 hours revealed differences between groups (**Figure 5-11**). When compared to TSPAN6 and RAGE there is a greater level of variation between the cell lines here in **Figure 5-11**. A significant difference is observed between UACC (papillary serous OC) and 4 of the other cell lines, IOC, SKOV, COV and OVCAR. A one-Sample Kolmogorov-Smirnov Test showed the data to be not normally distributed with a p value of 0.011. A Kruskal Wallis non-parametric ANOVA revealed statistical differences between the groups with a p value of 0.008. Further post hoc testing revealed where these significant differences could be seen and are shown in **Table 5-4**.

Figure 5-11 – Quantification of abundance of pH reactive dye fluorescence indicating PCSK4 antibody-dye conjugate internalisation by receptor mediated endocytosis into various 2D cultured cells

A boxplot showing the quantification of fluorescence of PCSK4 antibody-dye conjugate indicating receptor mediated endocytosis into various cell types after 4 hours incubation. Cell line UACC is significantly different from other OC subtype cell lines. IOC (p=0.02), SKOV (p-0.02), COV (p=0.02) and OVCAR (p=0.02). A breakdown of the p values by Man-Whitney can be seen in Table 5-4 below.

Table 5-4 – Kruskal Wallis post hoc testing pairwise comparison p values of the fluorescence of PCSK4 antibody-dye conjugate indicating internalisation by receptor mediated endocytosis into various cell types

	IOC	21G	112D	UWB1	UACC	SKOV	COV	OVCAR
IOC		0.114	0.114	0.057	0.029	1.00	0.343	0.686
21G			0.886	0.486	0.200	0.057	0.114	0.057
112D				0.886	0.200	0.114	0.114	0.114
UWB1					0.200	0.114	0.114	0.057
UACC						0.029	0.029	0.029
SKOV							0.486	1.000
COV								0.486
OVCAR								

In previous data (Chapter 3), PCSK4 was observed to be expressed on the plasma membrane of all OC cell lines with the exception of TOV-112D, whereas here it is shown that TOV-112D does display low levels of internalisation. The fluorescence observed in chapter 3 was not quantified therefore it is assumed the membrane expression of TSPAN6 on TOV-112D 2D cells that allowed for the low levels of internalisation seen here, was not visible to the naked eye in the data presented in chapter 3.

Analysis of the internalisation capacity of the target expressed in primary cells derived from patient biopsies shown in **Figure 5-10**, indicates PCSK4 binds and internalises antibodies into the cells (**Figure 5-10**). Quantification analysis shown as boxplot representing the average value of fluorescent intensity taking into account all the replicate fields of view was performed (Figure **5-12**). A one-Sample Kolmogorov-Smirnov Test showed each group was not normally distributed, hence a Mann Whitney U test was conducted and statistically significant differences were observed between groups (p=0.029). This result indicates that PCSK4-mediated antibody internalisation is higher in HGSOC patient samples when compared to non-cancer patient samples.

Internalisation of PCSK4 antibody-dye conjugate into 2D cells derived from patients with HGSOC and no cancer diagnsis
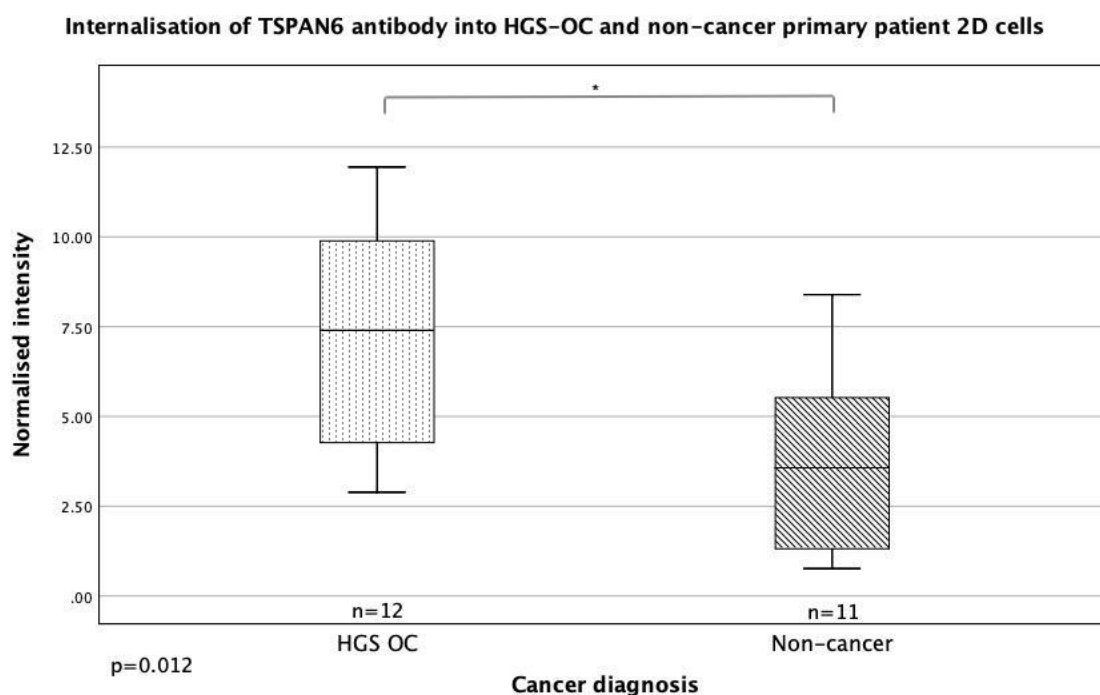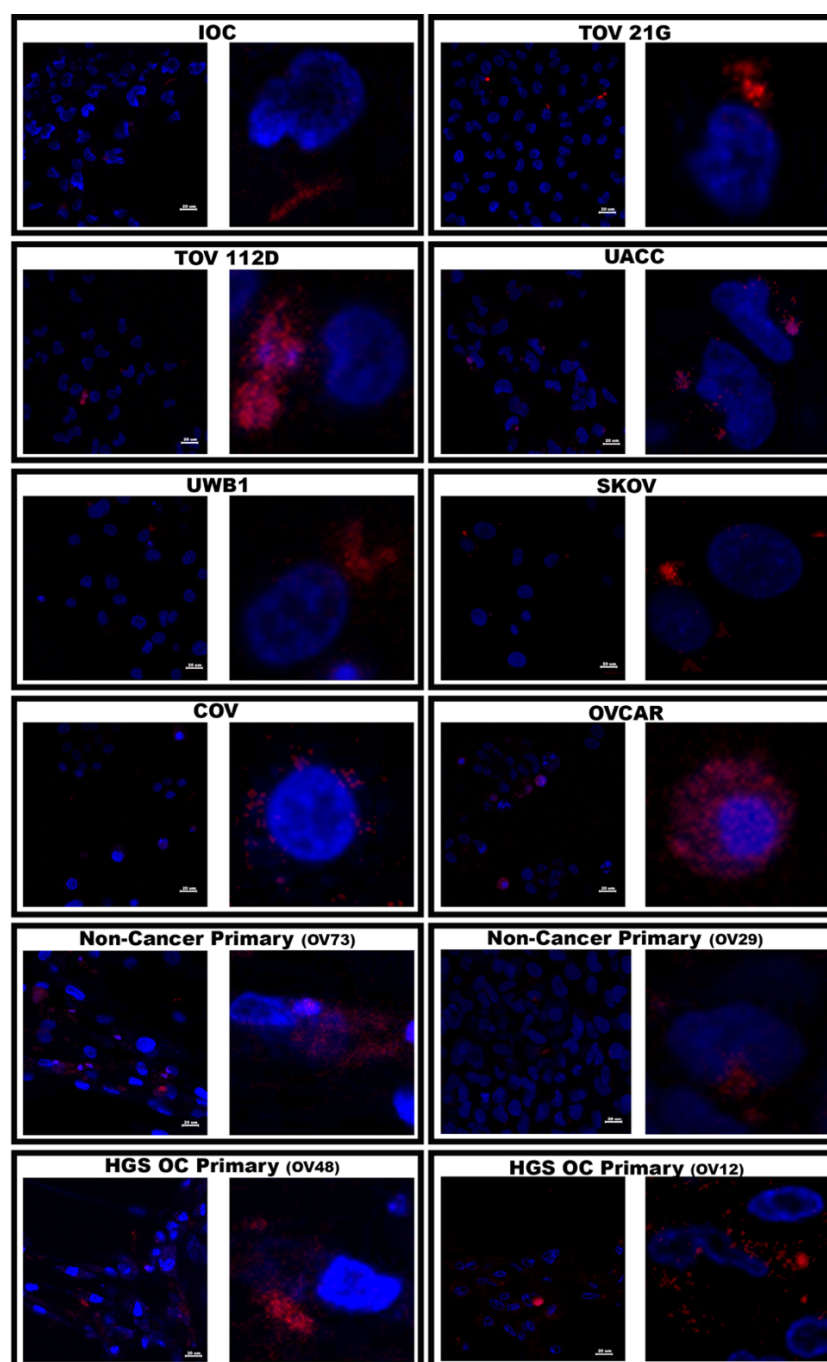
Figure 5-12 – Quantification of the abundance of pH reactive dye fluorescence indicating PCSK4 antibody-dye conjugate internalisation by receptor mediated endocytosis into 2D primary cultured cells derived from HGSOC and non-cancer patients

The box plot above compares fluorescence from all of the fields of view in 2D primary cultures cells derived from HGSOC (n=8) and non-cancer (n=8) patients. Mann Whitney test shows a significant difference with a p value of 0.02.

Finally, the ability of the RAGE HA9 clone to internalise antibodies was examined using the pH reactive dye internalisation assay (**Figure 5-13**). As before, the antibody-dye conjugate was incubated with the various cells for 30 minutes on ice before being placed to internalise at 37°C. Initially it is observed that fluorescence seen is variable between cell types. Most notably, TOV 112D and TOV 21G doesn't show any visible fluorescence whereas SKOV looks to have the most intense fluorescence observed in this figure. To display internalisation more clearly, the most intense and clearest field was chosen as the representative image to display in this figure out of all the fields of view replicates. Looking at the primary cells derived from patient tissue biopsies, there is more evidence of a wider spread of overall more fluorescence see in 2D cells derived from patients who had HGSOC cancer than those with no cancer. The quantification of this fluorescence can be seen in **Figure 5-14** and **Figure 5-15** below.
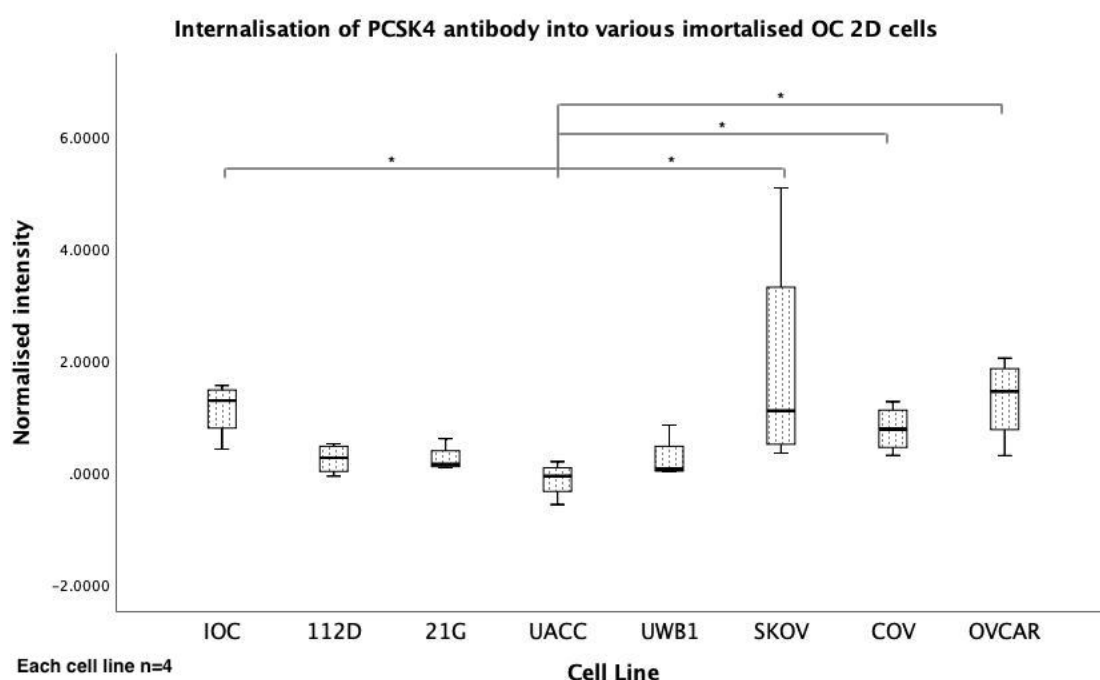
Figure 5-13 – Abundance of pH reactive dye fluorescence indicating RAGE antibody-dye conjugate internalisation by receptor mediated endocytosis into various 2D cultured cells

Fluorescence indicating RAGE (HA9) antibody-dye conjugate internalisation into cells of various ovarian pathology. It is observed that fluorescence indicating internalisation is not seen in all cell types. The amount of internalisation is variable depending on the cell type and TOV 112D and TOV 21G showed no visible fluorescence at all. Additionally, to display evidence of internalisation more clearly, the most intense and clearest field was chosen as the image to display in this figure out of all the fields of view replicates. For this reason, it is not possible to comment and compare the abundance of internalisation in this figure. This image simply shows the cells are uniformly distributed, indicating good health and the fluorescence indicating internalisation is visible variably amongst cell types. Figure 5-14 shows the quantification for each cell line, taking into account all the fields of view replicates. Figure 5-15 shows the quantification for the primary cells derived from patient biopsies.

Figure 5-14 shows a box plot quantifying fluorescence of RAGE HA9 antibody-dye conjugate indicating receptor mediated endocytosis into the eight OC cell lines. The quantification confirms that there was no detected quantifiable fluorescence in either TOV 112D or TOV 21G cell lines. The absence of fluorescence seen in TOV 112D and TOV 21G coupled with SKOV showing the highest fluorescence resulted in a statistically significant difference between SKOV and TOV112D and between SKOV and TOV21G. Overall, the data was shown to be not normally distributed by One-Sample Kolmogorov-Smirnov Test with a p value of 1.6×10^{-10}. A non-parametric ANOVA, the Kruskal Wallis test, showed there was statistically significant differences within the groups with a p value of 0.002. Finally, a pairwise comparison revealed the significant differences represented by a * in **Figure 5-14** between SKOV, TOV 112 and TOV 21G. By Kruskal Wallis test the RAGE internalisation showed the biggest statistical differences between groups of cell type when compared to TSPAN6 and PCSK4 and RAGE was the only target to show no detectable fluorescence in any cell lines.
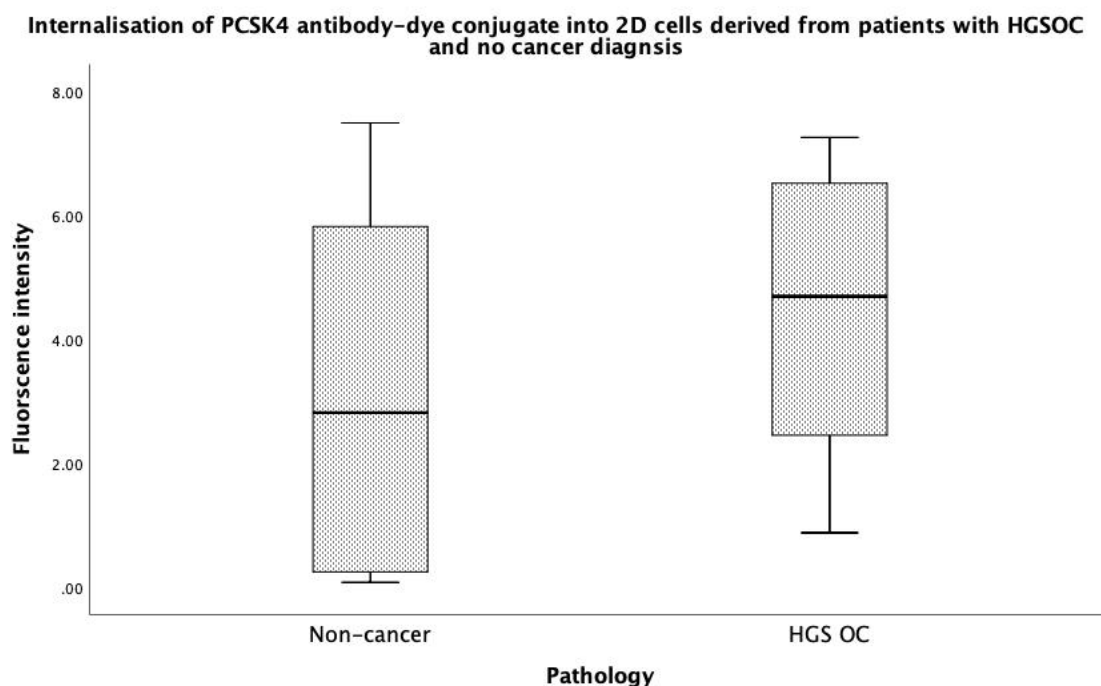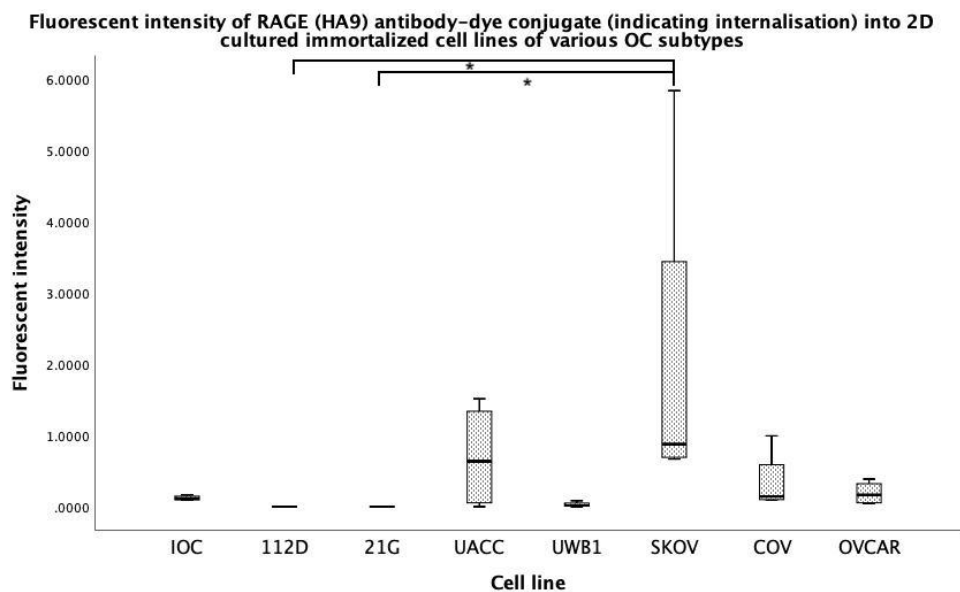

Figure 5-14 – Quantification of abundance of pH reactive dye fluorescence indicating RAGE antibody-dye conjugate internalisation by receptor mediated endocytosis into various 2D cultured cells

A boxplot showing the quantification of fluorescence indicating internalisation of RAGE HA9 antibody-dye conjugate by receptor mediated endocytosis into various cell types after 4 hours incubation. Fluorescence indicating internalisation is variably present in all cell lines apart from TOV 112D and TOV 21G where there was no detected fluorescence at all. The data was shown to be not normally distributed by One-Sample Kolmogorov-Smirnov Test with a p value of 1.6×10^{-10}. A Kruskal Wallis test revealed a significant difference within the groups with a p value of 0.002. A pairwise comparison showed the absence of fluorescence for TOV 112D and TOV 21G created a significant difference between these cell lines and the cell line with the highest fluorescence- SKOV-3.

In addition, **Figure 5-15** shows the quantification comparing the fluorescence (indicating internalisation) from HGSOC patients (n=7) and from non-cancer patients (n=8). A one-Sample Kolmogorov-Smirnov Test showed normally distributed data with a p value of 0.07. A T-test revealed a large significant difference with a p value of 0.000108. An outlier was removed from the HGSOC data set as it was over 4x bigger than all the other data points. Even with the outlier removed the significant difference remained substantial between the two groups. This result is not unexpected as RAGE has been studied within the RBGO group for several years and the target has already been validated as a strong ADC candidate ((200, 201)). The statistically significant difference seen in this result confirms that a higher level of RAGE internalisation in HGSOC patients could be used as a therapeutic advantage with a RAGE ADC potentially used as an effective treatment in these patients.

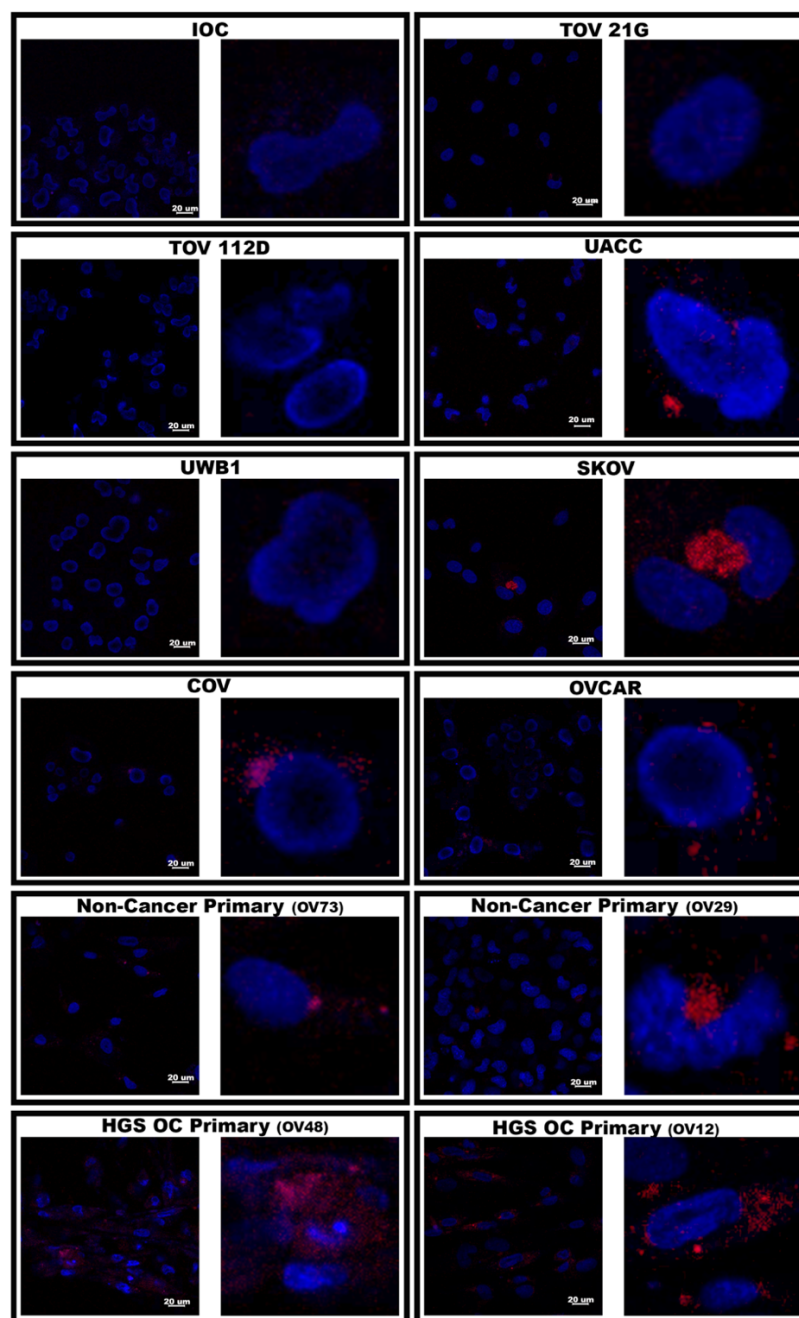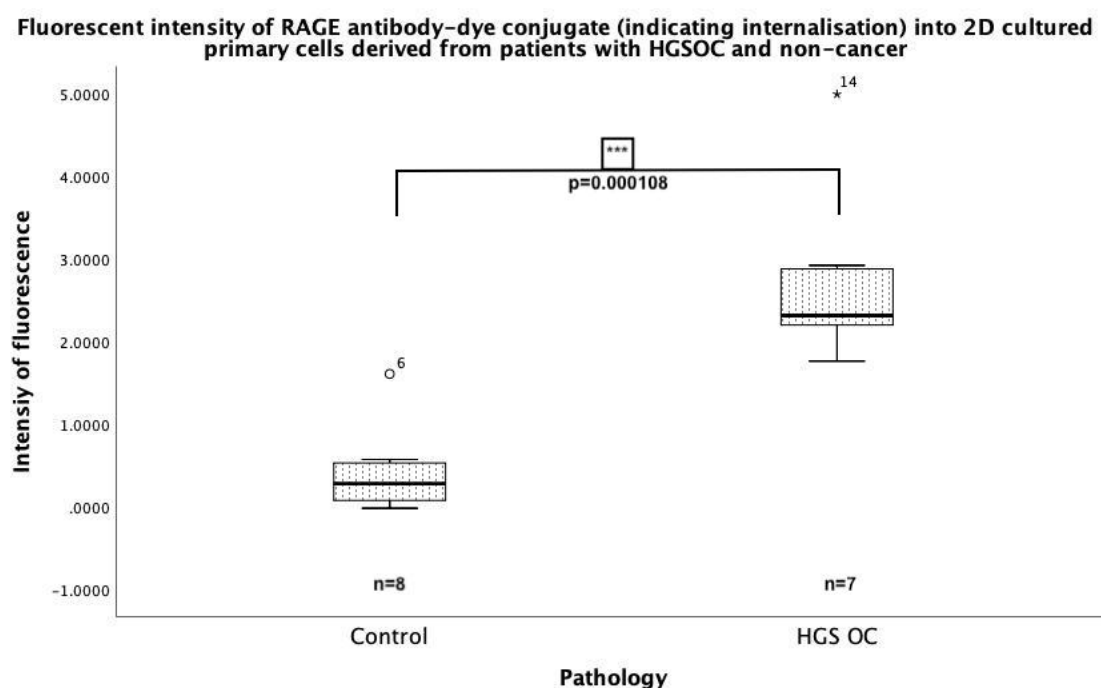*Figure 5-15 – Quantification of abundance of pH reactive dye fluorescence indicating RAGE antibody-dye conjugate internalisation by receptor mediated endocytosis into 2D primary cultured cells derived from HGSOC and non-cancer patients*

The box plot above compares RAGE HA9 fluorescence from all of the fields of view in 2D cultured primary cells derived from HGSOC (n=7) and non-cancer (n=8) patients. The data was found to be normally distributed by one-Sample Kolmogorov-Smirnov Test with a p value of 0.07. A T-test was used to compare means between the two groups and showed significant different with a p value of 0.000108. From the HGSOC data set an outlier was removed from the data set as it was over 4x bigger than all the other data points. Even with the large outlier removed the significant differences remained large between the two groups.

In addition to the internalisation assays completed with TSPAN6, PCSK4 and RAGE – an IgG isotype control was also used to ensure no non-specific internalisation was occurring. As described in section 5.2.1 and Table 5-1, the IgG isotype control was conjugated to the pH reactive dye along with the other antibodies for RAGE, PCSK4 and TSPAN6. The IgG antibody-dye conjugate was used in exactly the same way as described in section 5.3.2 above however, as expected, no fluorescence was visible or detected by quantification (Appendix 1).

5.3.3 Competition internalisation assay between TSPAN6 and RAGE HA9

The internalisation assays carried out in section 5.3.2 above, showed that TSPAN6 and RAGE showed the biggest statistically significant differences in internalisation using ovarian samples from patients diagnosed with HGSOC compared to those with no cancer diagnosis. For this reason, it was explored whether incubation with both antibodies in combination will impact the internalisation of pH-dye conjugated antibodies. It is possible that targets can stratify and mediate treatment of patients more effectively if they are used in conjunction with another therapy. The first step in that direction is to first understand if internalisation mediated by one target impacts the internalisation event mediated by another target. In simple terms, the idea is to assess whether there is competition between internalisation events mediated by different targets or not, paving the way for multi-ADC formulations that may prove to be more efficacious. This experiment assesses the fluorescence (indicative of internalisation) of RAGE and TSPAN6 whilst in the presence of the other target antibody. SKOV-3 cells were grown in replicates of 4. The following indicated what was added to each well containing SKOV-3 cells:

1. RAGE HA9 antibody-dye conjugate only
2. TSPAN6 antibody-dye conjugate only
3. RAGE HA9 antibody-dye conjugate in the presence of 2x excess of TSPAN6 antibody
4. TSPAN6 antibody-dye conjugate in the presence of 2x excess of RAGE HA9 antibody

As before, the cells were incubated on ice for 30 minutes before placing at 37°C for 4 hours to allow internalisation to occur. Visual representation of this competition to see how the presence of the other target antibody affected the internalisation of the antibody-dye conjugates is shown (**Figure 5-16**). The fluorescence signal was detected in all images, the scale bar can be seen at the bottom right of each image and DAPI (Hoechst) staining shows an even distribution of cells indicating healthy growth (**Figure 5-16**).
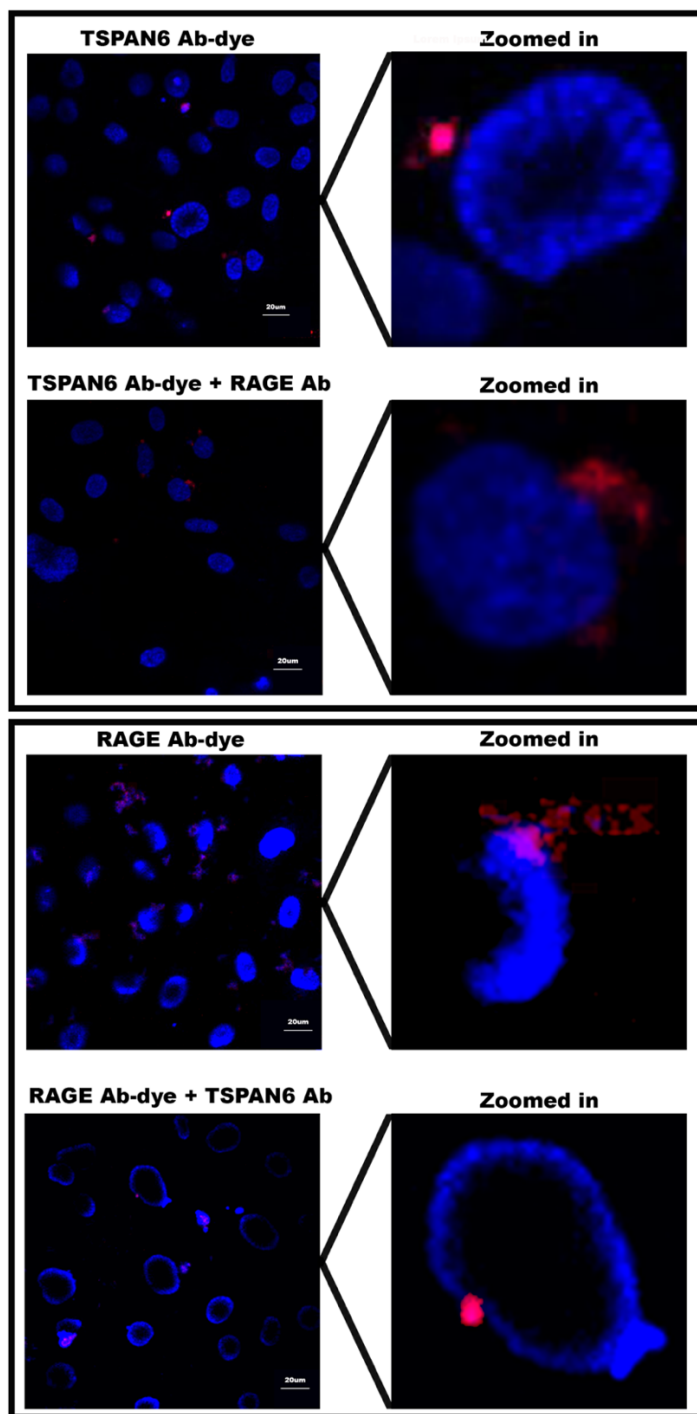
Figure 5-16 – Internalisation competition assay with RAGE HA9 and TSPAN6

The above figure shows the detected fluorescence when RAGE and TSPAN6 antibody-dye conjugates were allowed to internalise alone compared to in the presence of the other target antibody. The 'TSPAN6 Ab-dye' well had only the TSPAN6 antibody-dye conjugate present, the 'TSPAN6 Ab-dye + RAGE Ab' had the TSPAN6 antibody-dye conjugate in the presence of the RAGE HA9 antibody, the 'RAGE Ab-dye' had the RAGE HA9 antibody-dye conjugate only and finally the 'RAGE Ab-dye + TSPAN6 Ab' had the RAGE HA9 antibody-dye conjugate in the presence of the TSPAN6 antibody. Fluorescence is detected in all 4 wells and the quantification can be seen in Figure 5-17. A scale bar is shown in the bottom right corner of each image. Blue= DAPI, Red= dye. Internalisation time 4 hours. N values shown in 5-17.

The box plot in **Figure 5-17** shows the quantification taking into account all the fields of view from the assay represented in **Figure 5-16**. The purpose of quantification was to allow all replicates to be represented and to see if the presence of TSPAN6 Ab altered RAGE Ab internalisation and vice versa. A one-Sample Kolmogorov-Smirnov Test showed the data to be not normally distributed with a p value of 0.000323. Initially a Kruskal Wallis test did show significant differences detected in the group with a p value of 0.01, however in a pairwise comparison these differences were between the RAGE fluorescence and the TSPAN6 fluorescence (for example between RAGE only and TSPAN6 only) and the significance was no longer present once Bonferroni correction for multiple tests was applied. No significant difference was detected between 'RAGE Ab-dye' and 'RAGE Ab-dye + TSPAN6 Ab' and between 'TSPAN6 Ab-dye' and 'TSPAN6 Ab-dye + RAGE Ab'. An additional Mann Whitney test was performed to assess any significance and no significant difference was observed between 'RAGE Ab-dye' and 'RAGE Ab-dye + TSPAN6 Ab' with a p value of 0.6 and no significant difference between 'TSPAN6 Ab-dye' and 'TSPAN6 Ab-dye + RAGE Ab' with a p value of 1. This suggests that these two antibodies do not alter the internalisation of each other. Although they do not enhance the internalisation of each other it is encouraging that they do not inhibit each other's internalisation, suggesting these two antibodies could be used in combination with one another in the future to potentially produce an additive effect. Future work is needed to confirm this as this data only represents one setting and one time point. A limitation of the work here is that there is no true negative control. A knockout cell line would be a valuable addition to future work to confirm specific binding and validate any antibodies used.

In **Figure 5-17**, the whiskers on the box and whisker graph represent the range of the data points from the lowest point to the highest value. The range of the RAGE Ab-Dye values is the biggest, but it is unclear why the fluorescence is so variable here when compared to the others. This could influence the findings due to reproducibility.
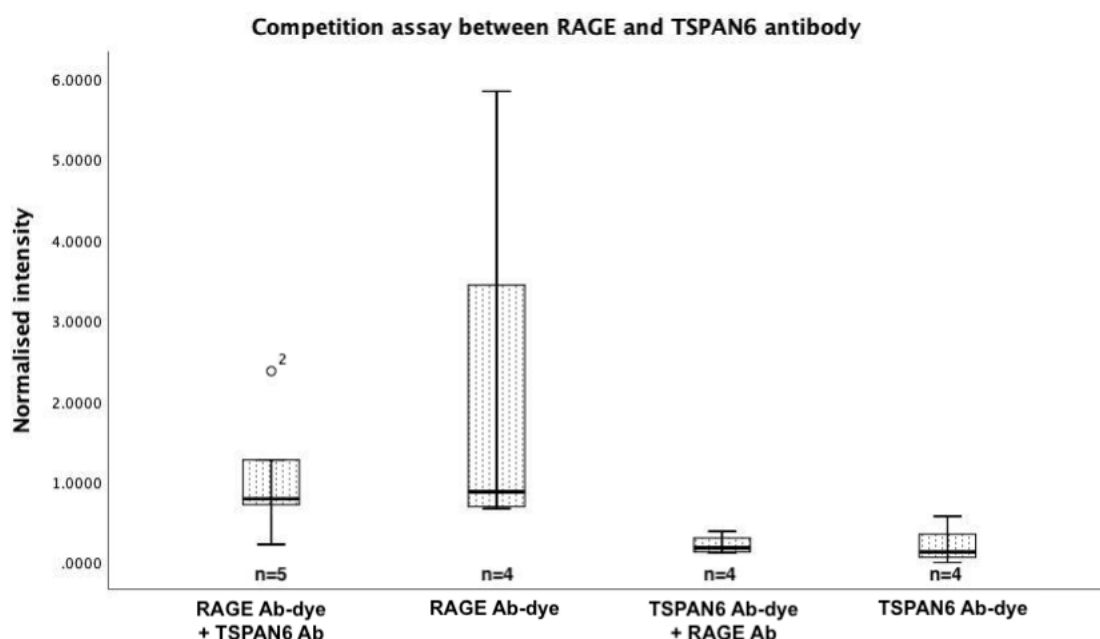
Figure 5-17 -Boxplot showing quantification of internalisation competition assay with RAGE HA9 and TSPAN6 antibody-dye conjugate

The boxplot above shows the quantification of the internalisation competition assay with RAGE HA9 and TSPAN6 antibody-dye conjugate. A one-Sample Kolmogorov-Smirnov Test showed the data to be not normally distributed with a p value of 0.000323. No significant difference was observed between the competition and the antibody-dye conjugate only wells by Kruskal Wallis followed by pairwise comparison. The pairwise comparison did detect a significant difference between RAGE and TSPAN6 however this cannot be compared as they are two different conjugations. Mann Whitney test also did not detect any significant difference in RAGE Ab-dye and RAGE Ab-dye + TSPAN6 Ab with a p value of 0.6 and no significant difference was detected between TSPAN6 Ab-dye and TSPAN6 Ab-dye + RAGE Ab with a p value of 1. This suggests that RAGE and TSPAN6 do not alter the internalisation of each other, opening up the possibility that could be used in conjunction with each other.

5.3.4 Conclusion

This chapter explored the internalisation of the target-antibody complexes by receptor mediated endocytosis. This internalisation event is crucial for the successful specific elimination of malignant cells displaying the target protein. TSPAN6 and PCSK4 protein-antibody internalisation was explored here in addition to the previously well-established RAGE ADC target. RAGE was included here as a comparison, as the protein has already been through the ADC characterisation pipeline. Additionally, the RAGE clone used here (HA9) was included, because while RAGE has been investigated in internalisation experiments before the HA9 clone was new and had not been explored in internalisation experiments. Unfortunately, the target PIEZO2 antibody was discontinued shortly before the internalisation experiments took place and

no suitable alternative was available. Therefore, PIEZO2 could not be included in the internalisation experiments.

The first experiment used TSPAN6 and RAGE to reveal that 4 hours was the optimal time to leave the antibody to internalise before viewing. The highest intensity of fluorescence was observed after 4 hours incubation when compared to 1, 2, 6, 8 and 24 hours. Therefore, in order to observe fluorescence most clearly the optimal internalisation incubation time was 4 hours.

The main TSPAN6 internalisation experiments showed that cell line OVCAR-3 had a statistically significantly higher fluorescence intensity indicating OVCAR-3 supported more internalisation when compared to the other cell lines. This does not correlate with previous data (chapter 3) where OVCAR-3 did not show the highest expression of TSPAN6 by immunoblot. This suggests that basal expression doesn't necessarily correlate with internalisation. The TSPAN6 protein more abundantly by immunoblot in other cell lines may not support internalisation. Due to this, internalisation rate is key when characterising novel ADC targets. Looking at the internalisation in 2D primary cultured cells derived from patient biopsies, cells derived from patients with a HGSOC pathology had a higher fluorescent intensity when compared to cells derived from patients with no cancer. This data correlates with previous data (chapter 4) where TSPAN6 expression was shown to be statistically significantly more abundant by immunoblot in OC when compared to non-cancer.

The main PCSK4 internalisation experiments showed some statistically significant differences between cell line UACC and several other cell lines. UACC showed statistically significant less fluorescent intensity than the other cell lines. Looking at the internalisation in 2D primary cultured cells derived from patient biopsies, cells derived from patients with a HGSOC pathology exhibited a statistically significantly different fluorescent intensity when compared to cells derived from patients with no cancer. This correlates with previous data (chapter 3 and 4) where PCSK4 was shown to be expressed on the plasma membrane of all 8 OC cell lines and on the membrane of 2D cells derived from patient biopsies. The confirmed expression observed on the plasma membrane (seen in chapter 3 and 4) translates to the internalisation of PCSK4 seen here in all 8 cell lines and the patient derived 2D cells. Future work is needed to determine the true specificity of the PCSK4 antibody.

RAGE internalisation behaved as expected with variation in the fluorescent intensity between cell lines. SKOV-3 cells were statistically significantly different from two other cell lines. RAGE showed the largest significant difference between 2D cultured primary cells derived from patient biopsies. Cells derived from patients with a HGSOC pathology were statistically

significantly higher in fluorescent intensity, when compared to cells derived from patients with no cancer diagnosis. This was the biggest significant difference seen out of all three targets.

Antibody internalisation is vital for ADC development as highlighted by the current ADCs which have received approval from the FDA and EMA. Kadcyla is a HER2 based ADC for the treatment of recurrent and refractory HER2-positive metastatic or locally advanced breast cancer previously treated with trastuzumab and a taxane and has been shown to be present in clathrin coated pits suggesting its intracellular trafficking could use this clathrin dependent pathway. This pathway would also a plausible pathway of internalisation for the targets reported here due to the same antibody dependant cellular toxicity (ADCC) displayed by Kadcyla. In addition, the bystander effect could also affect neighbouring cells whereby internalised and degraded drug can be recycled out of the cell leaving it free to exhibit toxic effects on nearby cells (580). The time point of highest observed internalisation here was chosen to be 4 hours. This internalisation time correlated with approved ADC Adcetris where the intracellular levels where shown to reach a plateau at 5 hours (581).

The intracellular trafficking of the ADC to the lysosome is vital as this is where the cytotoxic payload is released from the ADC complex and is free to travel to the nucleus where it can carry out its cytotoxic activity by creating double stranded DNA breaks or disrupting microtubule action whereby preventing cell division. If the ADC complex is not directed to the lysosome, the cytotoxic payload will not be released from the monoclonal antibody and it will remain attached, stable and unable to have its cytotoxic effects (580).

The final experiment used the two most promising ADC targets to investigate how they internalised in the presence of each other. Internalisation by fluorescent intensity was assessed when each target antibody was used alone and in the presence of the other antibody. This showed if the presence of the additional target antibody altered the internalisation of the other. Overall, it was shown the presence of RAGE antibody in addition to the TSPAN6 antibody-dye conjugate did not alter TSPAN6 internalisation. The opposite was also true when the presence of the TSPAN6 antibody in addition to the RAGE antibody-dye conjugate did not alter RAGE internalisation. This suggests these targets do not negatively impact each other and therefore could be used for a potential additive effect. The benefit of combining two ADCs to create a bispecific ADC with one arm targeting RAGE and the other TSPAN6 would be to increase the specificity of the ADC and increase the amount of drug reaching malignant cells. This increase in specificity could increase the risk of adverse side effects if the dose is not regulated. With this in mind, future tolerability studies are required.

The internalisation assay could be improved by using the time lapse of an instrument such as an Incucyte to image live cells in real time. This would allow for a deeper understanding of how the antibody-dye conjugate moves and where over 24 hours.

Overall, internalisation was detected by the fluorescence of the pH reactive dye in all targets variably in various 2D cell lines and primary 2D cell cultures derived from patient biopsies. Both TSPAN6 and RAGE internalisation was statistically significantly higher in 2D cultured primary cells derived from patient biopsies with ovarian cancer relative to non-cancerous primary lines. TSPAN6 remains the lead candidate target and RAGE remains a well-established, well researched target within the RBGO group. Therefore, both TSPAN6 and RAGE will progress to the final stage of analysis in this project where the DNA extracted from the tissue of 96 patient biopsies will be used in next generation sequencing to assess the DNA coding region stability of the antibody epitopes.

Chapter 6: Deep amplicon variant analysis of TSPAN6 and RAGE antibody epitope DNA coding sequence by Illumina Next Generation Sequencing

6.1 Introduction

The integrity of the genome is compromised in cancer cells, exhibiting genomic mutations in oncogenes and/or tumour suppressor genes (582). These cells are more likely to develop additional genetic faults, some of which may give rise to tumour-specific antigens which are those only found on the surface of tumour cells or tumour-associated antigens which are overexpressed on tumour cells, but also present on normal cells (583). Interestingly development of ADCs is based on the identification of both tumour-specific and tumour-associated antigens uniquely expressed in human cancers cells. These antigens are of great value as targets for large molecule, monoclonal antibody (mAb)-based therapy including ADCs and bi-specifics (584).

The ability of antibodies to bind to the extracellular region of these antigens often correlates to their efficacy as therapeutic agents. Furthermore, in the case of ADCs special consideration is also given to epitopes within the same target that promotes antibody-internalisation, a key feature of ADC mechanism of action (585). Previous research has shown that different epitopes promote different internalisation rates and binding affinities for the same protein (200). The binding of an antibody to an antigen is entirely dependent upon non-covalent interactions. Small changes in the antigen structure can profoundly affect the strength of the antibody–antigen interaction. Understanding the epitopes recognized by these antibodies provides insight into the organization of the antigen–antibody complexes at the cell surface, and opportunities to further engineer affinity and selectivity.

The intent of this study is to analyse the DNA sequence stability of the epitope coding sequence for two putative ADC targets in DNA extracted from patient tissue biopsies. This analysis will assess the conservation of the DNA coding sequence of the epitope between patients and will identify any low frequency mutations with implications for patient stratification and treatment efficacy with future potential TSPAN6 /RAGE ADCs.

DNA was extracted from patient tissue biopsies and the DNA coding sequence for the TSPAN6 and RAGE antibody epitope was amplified by high fidelity Polymerase Chain Reaction (PCR) using specifically designed primers. The amplified DNA was run on an agarose gel and sent for Sanger sequencing (LGC) to confirm successful amplification. The amplified DNA was used in Next Generation Sequencing (NGS) which was carried out by Dr Matthew Hitchings (Swansea University Sequencing Facility). Dr Hitchings performed quality control on the reads which removed any reads of poor quality. The sequence reads that were returned were analysed using a command line on a virtual machine. The resulting data analysis was reported and discussed in the context of known genetic polymorphisms in TSPAN6 and AGER (that encodes RAGE).

6.2 Results

6.2.1 Selection of targets for Next Generation Sequencing Analysis

As discussed above, the best point in the ADC development pipeline to carry out epitope sequencing analysis is still unknown. In this case, time and cost restraints resulted in choosing the most promising targets to sequence rather than sequencing them all. RAGE was chosen as it is further along the pipeline than the other targets included in this project, and TSPAN6 was chosen as overall it was identified to be the most promising novel target from western blots, cellular localisation and internalisation assays.

6.2.2 Identification and analysis of published known variants

There are genetic polymorphisms previously described and identified in the DNA coding region of the TSPAN6 epitope. Using the Ensembl online variation resources (release 101) (586), 79 SNPs were identified by the Genome Aggregation Database (587). A detailed report of these variations can be seen below in . The information in **Figure 6-1** was constructed using information from both the Ensembl database and the Genome Aggregation Database. The Genome Aggregation Database provided more detail into the consequences to the protein sequence as a result of the variant. Numerous variant types are identified in **Figure 6-1** below. Some elicited a change in the amino acid sequence (78%) while some are synonymous (22%).

TSPAN6 VARIANT TYPES
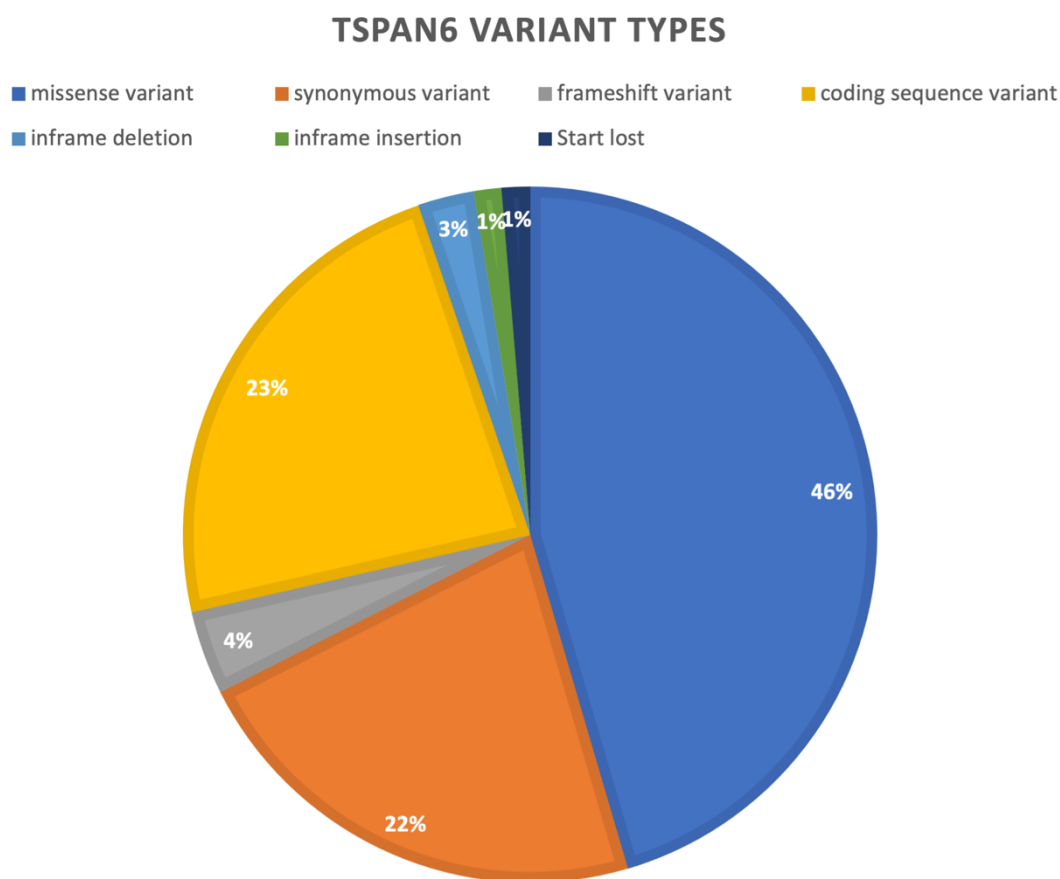
Figure 6-1 – Genetic variant types in TSPAN6 antibody epitope coding sequence

Using the same Ensembl (586) and Genome Aggregation Databases (587) any polymorphisms in the DNA coding sequence of the RAGE antibody epitope were also identified. There were considerably less polymorphisms identified in the RAGE sequence when compared to the TSPAN6 sequence. There were 21 polymorphisms identified in the RAGE sequence compared to the 79 identified in the TSPAN6 sequence. This suggests that the RAGE sequence is more genetically stable in theory than the TSPAN6 sequence.

RAGE VARIANT TYPES

■ missense variant   ■ synonymous variant   ■ frameshift variant   ■ coding sequence variant
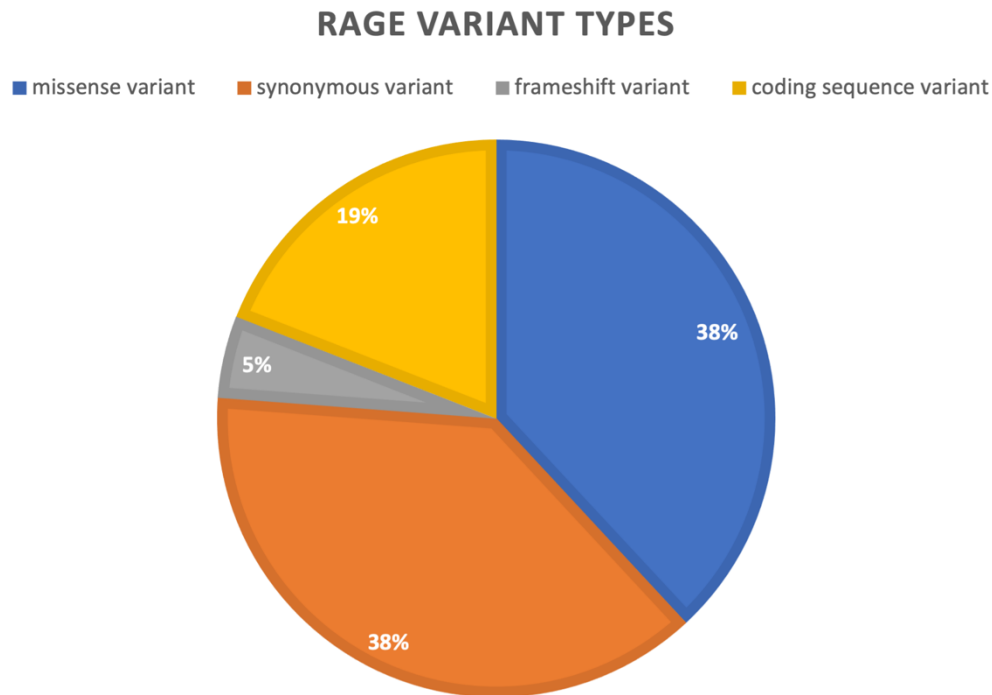
Figure 6-2 - Genetic variant types in RAGE antibody epitope coding sequence

6.2.2.1 Variant Counting

The main aim of the analysis was to assess the conservation of the DNA coding sequence corresponding to the epitope the antibody uses to bind the target protein. The simplest way to represent this is by calculating the number of bases that match the reference sequence. This frequency was calculated using the command *sh ref_freq.sh* followed by the command *sh names.sh*. These two commands together put together resulted in a text file that contains two columns, the base position in column 1 and the newly calculated and formatted frequency of reference bases at each position. The compilation of these statistics was finished using the command *sh combine_frequencies.sh*. Finally, the chart was generated using the command *R < RAGE_chart.R --no-save* for RAGE and *R < TSPAN6_chart.R --no-save* for TSPAN6. The output was a pdf of the frequency graphs shown below in **Figure 6-3** and **Figure 6-6**.

6.2.2.2 Deep amplicon variant analysis of TSPAN6

The graph in **Figure 6-3** below shows the frequency graph of variations in all the TSPAN6 reads when compared to the reference sequence. The dotted line represents the epitope sequence and the Y axis shows the percentage of reads that match the reference sequence. Each line across the graph represents each of the 96 samples sent for sequencing (95 from DNA extracted from patient tissue and 1 from DNA extracted from 2D SKOV-3 cells). The X axis of the graph is the nucleotide sequence and at each nucleotide, each sample has a percentage match plotted. It can be seen that all 96 samples match the reference sequence in >95% of reads.
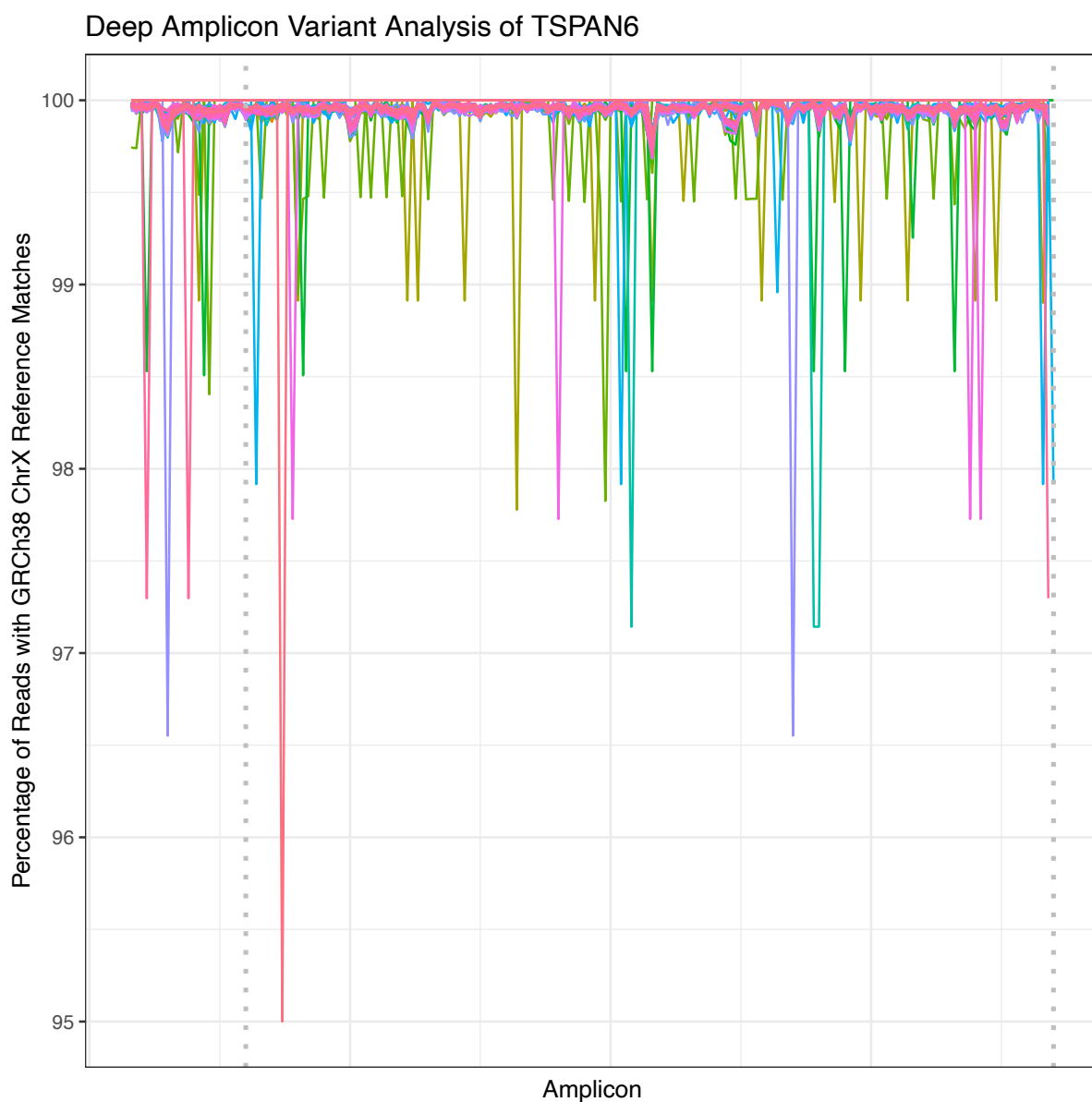
Figure 6-3 – Deep amplicon variant analysis of TSPAN6 antibody epitope DNA coding sequence with all samples

The above graph shows the deep amplicon variant analysis of the TSPAN6 antibody epitope DNA coding sequence in all 96 samples. The dotted lines indicate the TSPAN6 antibody epitope DNA coding sequence. Each coloured line going across the graph is one of the 96 samples. The DNA sequence runs along the X axis and the percentage reads that match the reference sequence can be seen on the Y axis. The graph shows that all samples match the reference sequence in 95% or higher of their reads- indicating no polymorphisms. The majority of samples are highly similar to each other with only 9 out of the 96 samples contributing to the variation shown by the multicoloured troughs in the epitope region. This graph indicates that the TSPAN6 antibody epitope DNA coding sequence is over 95% genetically stable in all 96 patients.

The first observation is that, with the exception of a few samples, the vast majority of samples match the reference sequence in over 99.6% of reads. There are only 9 samples out of 96 which contribute to the variation represented by the coloured troughs seen in **Figure 6-3**. OV15, OV23, OV30, OV42, OV56, OV70, OV82, OV97 and SKOV-3 all de*via*te more from the reference sequence than all the other samples. If these samples are taken away, then the remaining sequences are highly similar to one another as shown in **Figure 6-4**. Looking at these patients together, in more detail, they do not appear to have anything in common to explain why they are more variable than the others. OV30 is non-cancer risk reduction surgery, OV42 is malignant pelvic mass, OV56 is OC stage 2, OV70 is a pelvic mass, OV82 is a control patient with no described ovarian pathology and OV97 is an ovarian mass. There is no described patient information that link these patients.
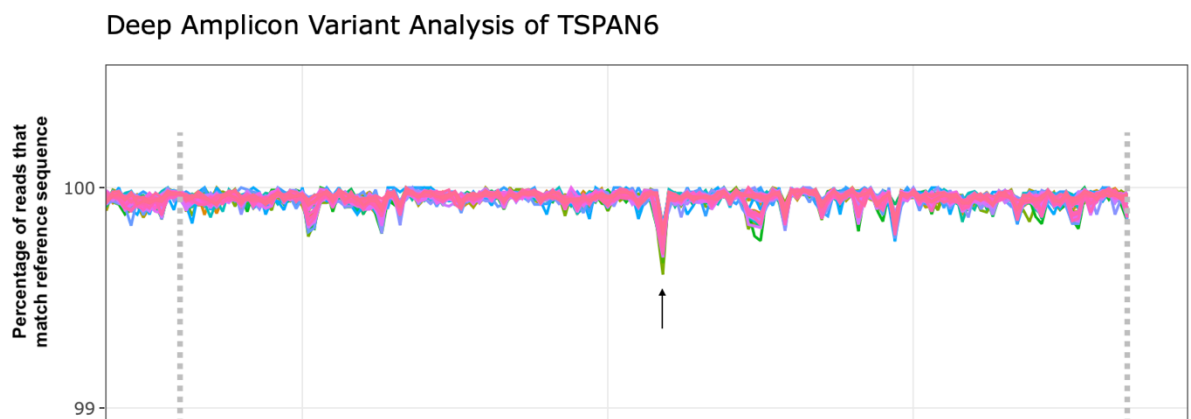
Figure 6-4 Deep amplicon variant analysis of TSPAN6 antibody epitope DNA coding sequence with 9 samples removed

The graph above shows the percentage of genetic stability when 9 samples are removed. This shows that only OV15, OV23, OV30, OV42, OV56, OV70, OV82, OV97 and SKOV-3 contribute to the mild variation seen in Figure 6-3. The removal of these samples shows the rest of the samples more clearly. There is a nucleotide at position 100635659 where all the samples display a noticeable drop in match percentage when compared to the rest of the sequence. However, a mutation present in 0.4% or less of reads does not constitute a pattern. The observation that most of the patients experience slightly more variation here could be a comment on the repetitive nature of that region of DNA.

All patients have approximately 0.2-0.5% of reads differing specifically at chromosome location 100635659 as indicated by an arrow in **Figure 6-4** and the flanking nucleotides 100635658 and 100635660. There are known polymorphisms around that area, a missense mutation (rs374431442) and another mutation that is reported to be involved in prostate cancer (COSV65957220 – deletion). Additionally, a polymorphism on this graph would show as a much

234

lower percentage of reads matching the reference sequence. With all of the samples matching the reference sequence by 95% or above, this does not indicate any polymorphisms in the data. The variations at certain chromosome locations seen in OV15, OV23, OV30, OV42, OV56, OV70, OV82, OV97 and SKOV-3 are not common between the samples. This is displayed in **Figure 6-5** where the green troughs are OV30 and the gold troughs are OV15. It can be seen that none of the variations are common to both samples at any percentage. This remains true when including all 9 variable samples on the graph – however, **Figure 6-5** shows only two samples to make it clearer to see.
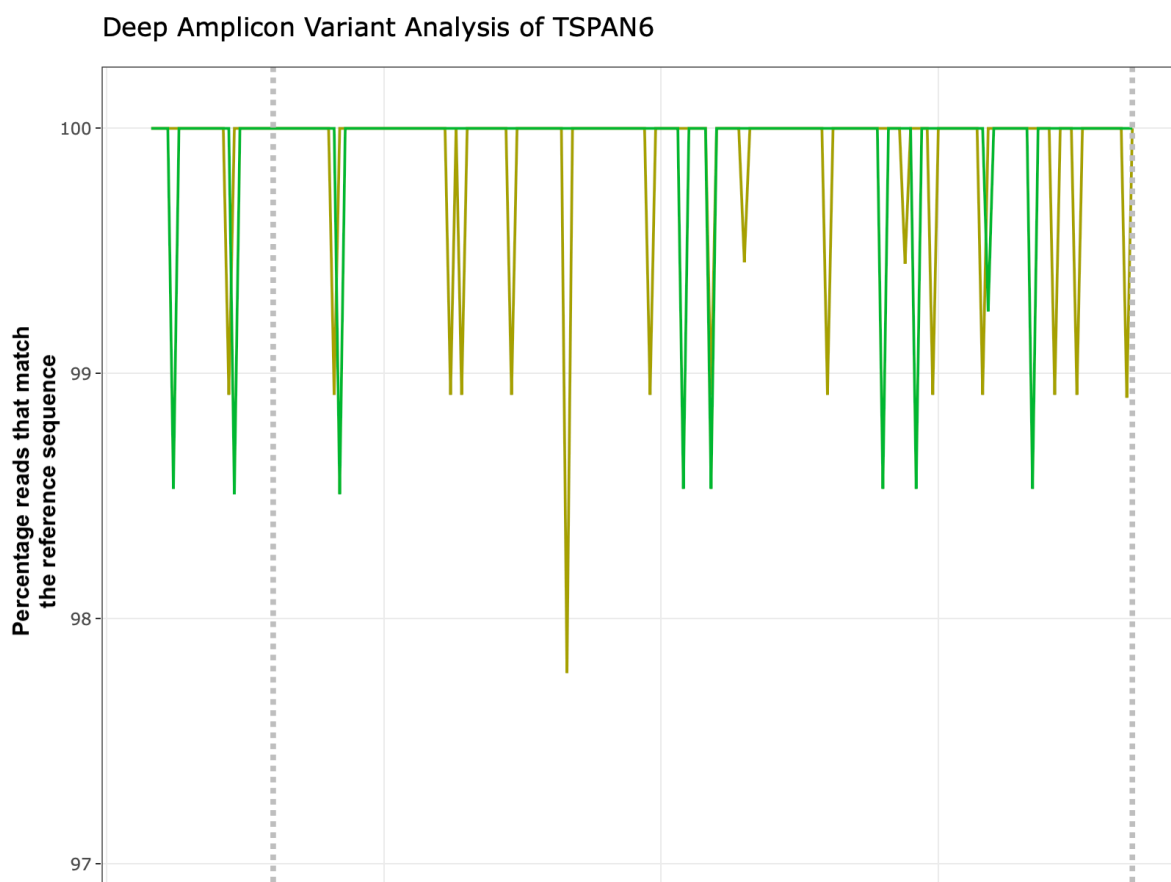
Figure 6-5 – Deep amplicon variant analysis of TSPAN6 antibody epitope DNA coding sequence comparing OV15 (gold) and OV30 (green)

The graph above shows two samples, OV15 (gold) and OV30 (green), that are more variable than the majority of the 96 samples. The graph above compared the variation seen in these samples to see if any common variation locations can be identified. It can be seen that none of the low frequency mutations seen in these two samples are common between the two. This is still true when adding in the other more variable samples (OV23, OV42, OV56, OV70, OV82, OV97 and SKOV-3). There are no common points in the variation seen in these samples.

6.2.2.3 Deep amplicon Variant Analysis of RAGE

Figure 6-6 shows the graph representing the deep amplicon variant analysis of RAGE. The dotted line represents the RAGE antibody epitope. As with the TSPAN6 deep variant analysis, each coloured line across the graph represents 1 or each of the 96 patients. The X axis represents the nucleotide sequence and the Y axis represent the percentage match to the reference sequence at each nucleotide point.

The initial observation is that there is a lot less variation seen in the RAGE epitope when compared to the TSPAN6 epitope in **Figure 6-3**. The RAGE epitope is shown to be highly conserved when 96 individual samples were subjected to deep amplicon variant analysis. This is consistent with the number of variants that were reported in the literature in and . TSPAN6 reported 79 variants in the literature whereas only 21 were reported in RAGE. The graph shows that the reads from all the samples match the reference sequence in the epitope region in 99.5% and higher of cases.

Deep Amplicon Variant Analysis of RAGE
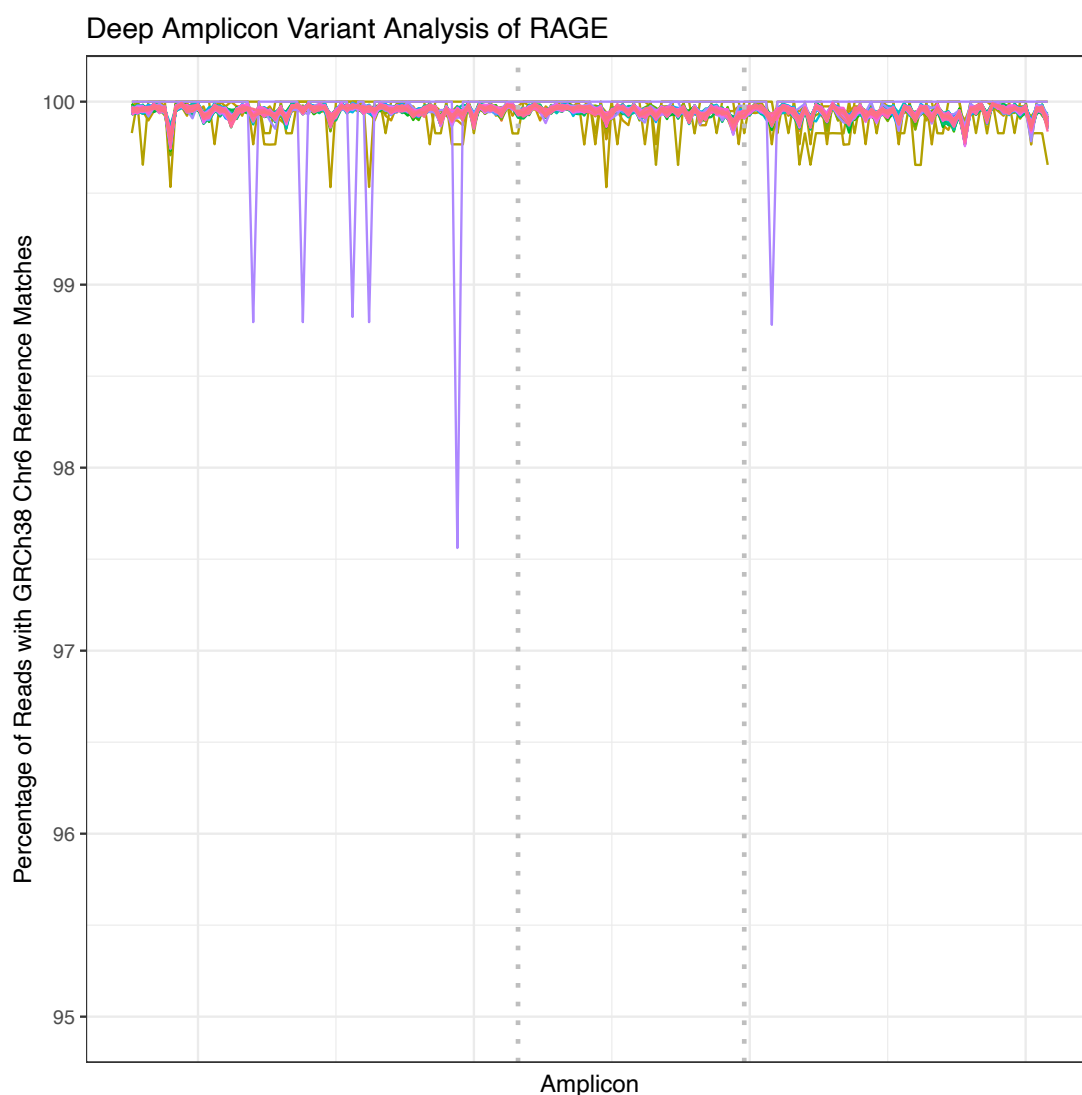
Figure 6-6 – Deep amplicon variant analysis of RAGE

The graph above shows that the RAGE antibody epitope DNA coding sequence is highly conserved between patients and within reads of the same patient. The epitope sequence is represented by the dotted line. The X axis (the amplicon) represents the nucleotide sequence and the Y axis represents the percentage of reads in each individual sample that match the reference sequence in that particular read. Each line across the graph represents one patient. The RAGE epitope is shown to match the reference sequence in over 99.5% of patient reads.

Figure 6-7 shows that three samples (OV120, OV121 and OV72) are responsible for the minor variation seen in in **Figure 6-6**. When these three samples are removed the percentage match goes up from 99.5% to 99.8%. Without these samples it can be seen that the rest of the samples are highly similar to each other and highly conserved to the reference sequence. There is nothing common between these three samples. OV120 and OV121 are both diagnosed as high-grade serous OC where as OV72 is an undiagnosed pelvic mass. These patients are not linked by another pathology, smoking, diabetes or cancer history.
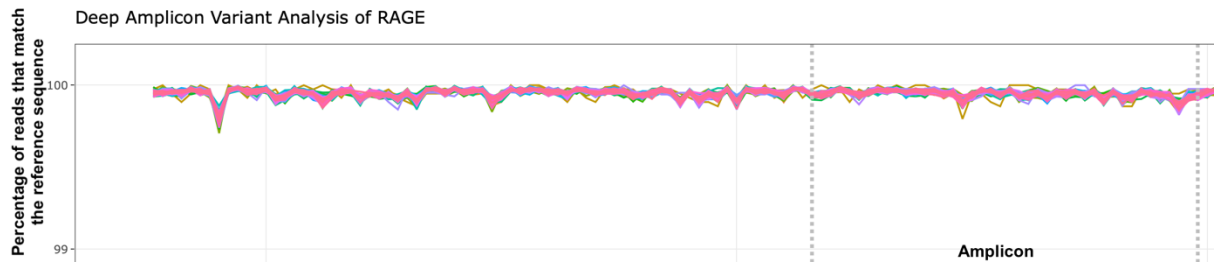
Figure 6-7 Deep Amplicon Variant Analysis of RAGE epitope DNA coding sequences with OV120, OV121 and OV72 samples removed

The graph above shows that three samples (OV120, OV121 and OV72) are responsible for most the minor variation in the RAGE epitope DNA coding sequence. When these samples are removed, the remaining 93 samples are highly similar to each other and match the reference sequence in 99.8% of cases and above.

The individual samples shown to be the most variable in the RAGE amplicon (with OV120, OV121 and OV72) are not the same samples that were the most variable in the TSPAN6 analysis. This suggests that it is not the particular patients that are more variable than others.

The PCR amplification carried out with Qiagen HotStar HiFidelity DNA Polymerase has an error rate of 2.3 x 10-6 (per base, per cycle), meaning, one error may occur every 4.5-5 x 10^5 bases (588). The error rate of Illumina NGS is reported to be 0.24% (589) which also explains the low-frequency mutations seen in the above graphs.

6.3 Conclusion

In the literature, papers reporting the characterisation of novel ADC targets do not describe exploring the variation in the DNA coding sequence of the antibody epitope. In terms of epitope conservation, the most common characterisation check is to align the amino acid sequence against other species rather than looking for variation in the DNA coding sequence between individual patients (590). This kind of analysis does have specific relevance to therapeutics as the therapy will potentially be administered to many individuals who may differ in their DNA sequence. Sequencing the epitope or the whole coding sequence from a target protein could provide an initial screening step for the identification of novel ADC targets. The question remains, when the sequencing should be performed. NGS itself can be expensive, therefore it could be argued that cheaper characterisation should be carried out to confirm the targets cellular location and expression. However, NGS is fast when compared to other techniques such as western blotting and immunofluorescent microscopy, therefore it could be argued there is no point in engaging in the time-consuming process of confirming cellular location and expression if the coding sequence is highly variable within the population or the patient cohort. Additionally, unless the whole target is to be sequenced, the antibody epitope needs to be

known. The cellular location and expression assays help to choose the best antibody and therefore guides which section of the gene to be sequenced.

With ADCs already present on the market, only Ado-trastuzumab emtansine (Kadcyla) mentioned any kind of NGS and that was to identify and confirm the HER2 mutation in patients for the trial (591), not the genetic stability of the ADC epitope DNA coding sequence between patients. Not all patients in the Kadcyla trial with HER2 mutations all responded to treatment. 46.2% of patients responded to treatment leaving 53.8% who did not respond. The main causes of ADC non-responders include mutations affecting binding and failure to internalise, resulting in no therapeutic effect.

The development of Gemtuzumab ozogamicin did involve sequencing as part of the characterisation process. Fultang *et al* carried-out RNA-sequencing of Monocytic and Granulocytic Myeloid-Derived Suppressor Cells (M-MDSC, G-MDSC) from cancer patients and identified the ADC target CD33 as a common surface marker but did not look at variation in the CD33 epitope between patients (592).

Some papers discuss deep sequencing of antibody epitopes (593) however the data displayed is not looking for low frequency mutations in patient samples. One study uses NGS for the genomic characterisation of ERBB2-Driven biliary cancer and its response to ADC Ado-Trastuzumab Emtansine. The study used NGS to identify ERBB2 mutations in biliary duct cancers (594). Another study modelled biological and genetic diversity in upper tract urothelial carcinomas with patient derived xenografts. NGS sequence analysis of a HER2 S310F-mutant patient derived xenograft suggest that a HER2 targeting ADC would have better efficacy when compared to HER2 kinase inhibitors (595). No other papers mentioned NGS together with ADCs. When looking at the use of NGS in general antibody epitope DNA coding region sequencing less than ten papers are available on PubMed. Layton *et al* adapted an Illumina high-throughput sequencing chip to display a high diversity of ribosomal translated proteins. They then carried out functional assays directly on these flow cells to demonstrate that both sequencing and protein assays can be performed on the platform. They discovered a "superFLAG" epitope variant when deep sequencing the epitope of the M2 anti-FLAG antibody (596). A study looking to improve epitope identification used Illumina NGS to sequence phage-display antigen-specific libraries. It was found that as well as the precise identification of the regions was possible, NGS could also significantly empower the analysis of antigen specific libraries due to the simultaneous processing of dozens of combinations in a short space of time (597).

Several papers use NGS on patient DNA to diagnose a specific disease by looking for a particular gene mutation that is not detected by Sanger Sequencing (598, 599). However, at this time no

papers describe using NGS for identifying low frequency mutations in the DNA coding sequence of an ADC epitope in a cohort of patients. This opens up a novel method for identifying potential ADC targets and patient stratification.

The genetic stability of the TSPAN6 and RAGE antibody epitope DNA coding sequence is highly stable between patients and within patient reads. RAGE is more conserved than TSPAN6, with TSPAN6 reporting a match to the reference sequence in over 95% of reads compared to RAGE reporting a match in over 99.5% of reads.

This has great implications for treatment with a RAGE or TSPAN6 targeting ADC. The high genetic stability of the two targets makes them both highly promising targets in terms of binding efficiency within and between patients. There are benefits of identifying more specific and stable epitopes, such as a reduced dose being needed which would therefore potentially minimise side effects. Additionally, it would quickly identify any patients which would not benefit from a RAGE/TSPAN6 ADC, which would allow more time to find a treatment that does work for the patient. A higher genetic stability also suggests that generally, most people would benefit from this type of treatment. Furthermore, a high conservation suggests the biological importance of both RAGE and TSPAN6, further validating its suitability as an ADC target.

NGS is, at the present, expensive, and not carried out as standard practice. Currently, it would not be reasonable to expect this to become routine for OC patients. However, in the coming years as methods improve and become more financially available, it is very possible, and would be very beneficial for NGS to be standard practice in the clinic.

The sequencing does not indicate any groups that patients can be stratified into based upon their sequencing data, as the sequence conservation is so high in all patients when compared to the reference sequence. This suggests that it is likely that a very high percentage of patients treated with a RAGE or TSPAN6 targeting ADC would successfully bind the ADC in a high percentage of cells during treatment. This would result in the maximum cytotoxic payload being delivered into the malignant cells for maximum efficiency of treatment.

There is room for discussion as to when this kind of deep amplicon sequencing should be carried out. If the ADC target epitope is not known to be genetically stable within the population then regardless of its cellular location, expression abundance and internalisation abundance, it will not be a good target (584). However, NGS is expensive and from a cost efficiency perspective it is arguably better to perform cheaper experiment first, such as western blot and immuno-fluorescent microscopy to narrow down the targets before more expensive experiments are undertaken such as assessment of internalisation with a pH conjugated dye and NGS.

Additionally, the literature can provide some indication of the genetic stability of the protein target, aiding in the initial selection process.

From this data, patients are unable to be stratified for diagnosis or treatment method based on any low frequency mutations or polymorphisms in the DNA coding sequence of the antibody epitope.

Overall, this data agrees with the literature that TSPAN6 and RAGE epitopes are both highly conserved proteins in the population. These results de-risk the TSPAN6 and RAGE ADC development pipelines, and probes the suitability of the targets in particular the epitopes explored that are conferring and strategic advantage for immunotherapy development.

Chapter 7: Soluble RAGE as a biomarker for stratification of ovarian cancer patients.

7.1 Introduction

There are around 7400 new OC cases diagnosed in the UK every year making OC the 6th most common cancer. OC is strongly related to age with the highest incidences being in older women over the age of 70. In the UK between 2015 and 2017, on average 28% of new cases of OC were diagnosed in females over 75 years of age. Age specific incidence rates rise steadily from 15-19 years of age and more steeply from age 35. In ages above 80 the incidence drops off sharply, suggesting if an individual is going to get OC then they are more likely to get diagnosed at around age 70 (600).

For OC, a higher percentage of women are diagnosed at late stage (stage 3 or 4) OC when compared to an early stage (stage 1 or 2) OC (601). A late-stage diagnosis is positively correlated with age where 77% of women 80 or above are diagnosed with a late-stage OC. This could be due to older people disregarding the symptoms, mobility issues, fear to go to the hospital, rather than age. Younger people tend to be more proactive in terms of health. In comparison, of those aged 60-79, 66% were diagnosed with a late-stage OC. Finally, of women aged 15-59 only 39% had a late stage OC diagnosis (304).

Overall, the statistics show that irrelevant of age, OC is not being diagnosed early enough – resulting in a more aggressive, less treatable cancer (602). It is clear a more effective early diagnostic tool is desperately required. If diagnosed and treated at an earlier stage, the tumour is also more likely to be less aggressive, more localised and less invasive in a younger woman resulting in a better prognosis and quality of life.

A high through-put, minimally invasive, sensitive and OC specific diagnostic test could dramatically benefit all women who do not yet know they have OC and to give peace of mind to the female population as a whole, who can eliminate the worry of finding out they have late-stage OC. This has already been achieved for cervical cancer, where a yearly vaginal smear test (Pap smear) can quickly and easily establish the presence of malignant cells resulting in a faster course of action (135, 136). This improved diagnostic tool highly likely contributed to the 74% decrease in mortality rate due to cervical cancer since the 1970's (137). In epithelial ovarian cancer 82% of patients have increased CA125 levels compared to 1.4% of healthy women (603). However, only 50% of OC patients with stage I disease have elevated CA125. CA125 has a greater ability to distinguish between post-menopausal and pre-menopausal with a sensitivity of 81% vs 60%, and specificity of 91% vs 73% ((604-606). Early-stage disease (I/IIa) has a 95% 5-year survival rate however 20% of ovarian cancer patients express little or no CA125 (603). The OVA-1 test was the first FDA approved blood test that evaluates ovarian mass for malignancy prior to planned surgery and evaluates the expression levels of the following biomarkers: CA-125 II,

transthyretin [prealbumin], apolipoprotein A1, b2-microglobulin, and transferrin. Currently, other serum markers are being investigated as a means of detecting early-stage disease.

This chapter aims to determine whether a soluble, free circulating, well-established ADC target protein, RAGE, could be used as a potential biomarker with high specificity and sensitivity in detecting early-stage ovarian cancer. TSPAN6 has not been assessed as a potential biomarker in this chapter because it has not been reported to exist as a soluble, free circulating isomer in the blood.

The Receptor for Advanced Glycation End products (RAGE) is a membrane bound protein implicated in inflammation (284, 607, 608) and various cancers (201, 609-611). RAGE is a protein already well-established as an ADC target for OC within the RBGO group and has been extensively researched by other members of the group (200-202). The abundance of full-length membrane bound RAGE has been indicated to be higher in OC in past data (301) and in Chapter 6 the abundance of RAGE internalised into the various 2D cultured cells was shown to be statistically significantly increased in HGSOC patients. RAGE is a particularly appropriate diagnostic target due to its existence as a cleaved or alternatively spliced soluble isoform, present in the blood. This enables levels of soluble RAGE (sRAGE) to be detected in the blood using assays such as an ELISA. Blood tests are simple, fast, high throughput and are minimally stressful for the patient. The key is to avoid difficult medical decisions surrounding a surgical diagnosis method by implementing a diagnostic test any one can have.

sRAGE will be used as an example to develop the ELISA technique as a pipeline for future protein biomarkers present in the blood serum, with implications for patient diagnosis, stratification and monitoring response to treatment using a high-throughput, minimally invasive diagnostic test. The purpose of stratifying patients using serum levels of sRAGE is to improve upon the diagnosis for OC already in place, both in terms of sensitivity and accuracy and to provide an early-stage diagnostic indicator.

7.2 Results

The following analysis aims to uncover if:

- serum levels of sRAGE are correlated with any patient metrics (described in section 7.2.1 below)
- serum levels of sRAGE can stratify OC patients from non-OC patients
- serum levels of sRAGE are correlated with CA125

Patients who are reported to be diabetic (n=16) were not included in the dataset due to evidence that sRAGE expression in the blood significantly correlates with diabetes (612).

7.2.1 Patient data

With each patient biopsy and blood sample, a patient data form was provided with answers to questions about age, parity, menopausal status, smoking status, history of cancer, diabetic status, CA125 levels, Risk of Malignancy Index (RMI) and other metrics.

Patient metrics are recorded on the patient data proforma by hospital staff at the time of surgery. Patient metrics reported are:

- Age

- BMI

- Diabetic status

- Cancer history

- Current ovarian pathology

- Current cancer status

- Parity

- Smoking status

- Menopausal status

- Endometriosis status

- Polycystic Ovary Syndrome (PCOS) status

- Previous ovarian pathologies

- Post-Menopausal Bleeding (PMB) status

- Hormone Replacement Therapy (HRT) status

- Serum CA125 levels

- Risk of Malignancy Index (RMI) value

Personal patient data such as name, date of birth and home address are anonymised by ovarian biomarker study staff before the above data is made available for use. Not all metrics are recorded on the forms and if the data has not been recorded, the field is left blank and that data point is not included in that particular analysis. When a blank field is left, no assumptions are made. For example, if the cancer history field is left blank then it is not assumed the patient has or does not have a history of cancer and the team contacted the RBGO associated clinician to confirm the diagnosis given by the pathologist. In this case, if looking at cancer history, any blank fields are left out of the analysis.

These patient metrics and subsequent follow up data, were used to allocate the patient to the most appropriate group for analysis as described in **Table 7-1**.

Table 7-1 displays the 129 patients have been split into 13 groups. The group with the highest number of patients is 'Cancer' (ovarian cancer) with 35 patients, followed by High Grade Serous Ovarian Cancer (HGSOC) with 30 patients. The groups with the lowest number of patients are clear cell and endometrioid OC. This reflects the literature describing serous, particularly HGS, as the most common type of OC (613).

Table 7-1 – Number of patients in each group

Group	Number of patients
Benign Mass	6
Borderline cancer	2
Cancer	35
Cancer clear cell	1
Cancer Endometrioid	1
Cancer HGS	30
Control	5
Endometriosis	5
Other Cancer	5
Ovarian cyst	11
Pelvic Mass	22
Risk reduction	6
Total	129

A benign mass is a mass that is confirmed as not capable of invading neighbouring tissue. Borderline cancers are ovarian tumours that are abnormal but not malignant and as for all samples their diagnosis is confirmed by the pathologist report. They were formally called tumours of low malignant potential (614). 'Cancer' is any ovarian cancer that is not specified as clear cell, endometrioid or high grade serous. These three OC subtypes have their own category.

Patients in the 'Control' group are any patients that specifically have no ovarian pathology described. Endometriosis is an inflammatory condition where cells from the endometrium grow outside of their usual location within the uterus including the pelvic cavity (615). Endometriosis patients are at risk of developing OC later in life and as such is included here in this study as at-risk group (66). The 'other cancers' group include patients who have another type of cancer not in the ovary. The ovarian cyst group includes patients with benign simple ovarian cysts. The pelvic mass group contains patients who have a benign pelvic mass. Patients in the risk reduction group were having surgery to remove their ovaries and/or their uterus due to a genetic mutation that predisposes them to a significantly higher chance of developing OC.

7.2.2 Normality of data

The 129 sRAGE values were subjected to a One-Sample Kolmogorov-Smirnov Test for normality. The p value returned was 0.000062, indicating not normally distributed data. A Kruskal Wallis test is used initially to detect significant differences between all groups and then, if significant differences are identified, a Mann Whitney U test is carried out to assess any significant difference between two specific groups.

7.2.3 Correlation of sRAGE to patient metrics

To explore the specificity of sRAGE as a diagnostic indicator for OC, it is important to discover if sRAGE correlates to any other patient metrics in this dataset including known risk OC factors. The following analysis looks at the abundance of sRAGE by each of the patient metrics described above in 7.2.1. It is important to note here than 14 additional samples were added to make the total number of samples 130. The patient samples added were simple healthy fertile patient serum from a parallel study, the endometrial biomarker study. These samples were chosen to increase the sample size and were age and menopausal status matched to the original 116 patients.

The risk of developing ovarian cancer increases with age and ovarian cancer is rare in women younger than 40. Most ovarian cancers develop after menopause with half of all OC diagnosed in women 60 years of age or older. Analysis of sRAGE and age at diagnosis was performed (**Figure 7-1**) to determine if the levels of sRAGE correlate with age in the Swansea patient dataset. A One-Sample Kolmogorov-Smirnov Test reports that the patient age data is not normally distributed with a p value of 0.033. A Spearman Rho correlation analysis between patient age and levels of sRAGE show no significant correlation with a p value of 0.69. This suggests that the age of the patient has no impact on their sRAGE levels in this dataset.

A scatter plot showing no significant correlation between patient age and serum sRAGE

R² Linear = 0.002

n=130

Spearman's Rho p = 0.69

y=1.09E3−1.95*x
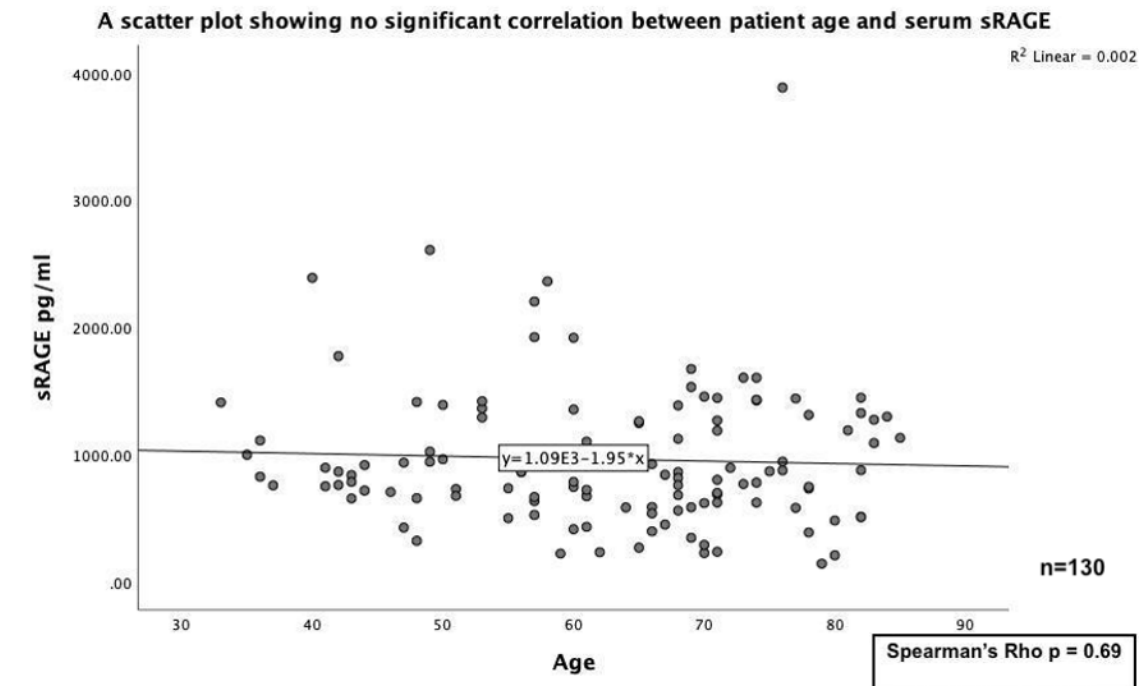
Figure 7-1 – Scatter plot showing no correlation between sRAGE serum levels and patient age at diagnosis (in years)

Analysis of sRAGE and Body Mass Index (BMI) at the time of diagnosis was made (**Figure 7-2**). The scatterplot and subsequent tests for correlation aim to reveal if the levels of sRAGE correlate with BMI in this dataset. A study published in 2014 found that women with a body mass index (BMI) above 28 seem to have a slightly higher risk of developing OC (616). BMI is a measurement that considers weight and height to aid in advising if a person's weight is healthy for their height. For adults, an ideal BMI is in the range of 18.5 to 24.9. A healthcare professional will use BMI along with other factors such as muscle mass and ethnicity to advise patients on the healthiest weight for them (617). In the scatter plot shown in **Figure 7-2**, patients with OC frequently have a BMI of 20-30, with a BMI of over 30 being less common. A Spearman Rho correlation analysis showed no significant correlation between patient BMI and their levels of sRAGE with a p value of 0.860. This suggests that the serum level of sRAGE does not correlate with BMI.

Scatter plot showing no significant correlation between sRAGE and Body Mass Index (BMI)

R^2 Linear = 0.002

y=1.12E3−3.4*x

n=130

Spearman's Rho p = 0.860
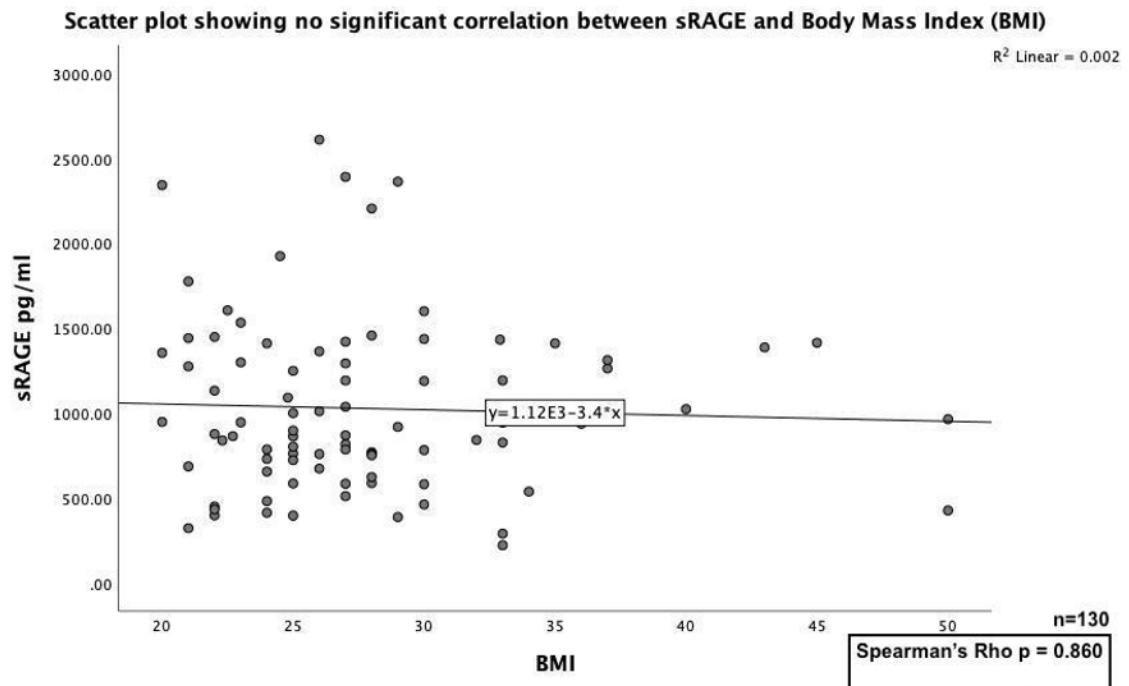
Figure 7-2 - Scatter plot showing no significant correlation between sRAGE (pg/ml) and Body Mass Index (BMI) at time of diagnosis (n=130)

Next, analysis of sRAGE serum level and cancer history at the time of diagnosis was undertaken (**Figure 7-3**). Out of the 130 patients reported in this dataset, 16 had a history of cancer, 73 had no history of cancer and 41 were undocumented either way. RAGE is documented to be upregulated in cancer (611), potentially from its involvement in inflammation as a known hallmark of cancer. **Figure 7-3** suggests that after having cancer in the past, the levels of sRAGE return to normal and are not significantly different from the levels in patients who have no past history of cancer. A Mann Whitney U test showed no statistically significant difference with a p value of 0.3. This suggests, in this dataset, having had cancer in the past does not correlate with altered sRAGE expression. However statistical power here is low, only 16 patients out of 130 have a history or cancer, this could affect the findings by not having a representative data set due to small samples size. Therefore, to further validate the findings further work is needed. The same is true in later graphs with low samples size. Regularly, a certain patient metric would not be recorded either way therefore it could not be included in the dataset which lowered the overall N number.

Box plot showing no significant difference in sRAGE levels between patients with and without cancer history

Mann Whitney U p=0.3
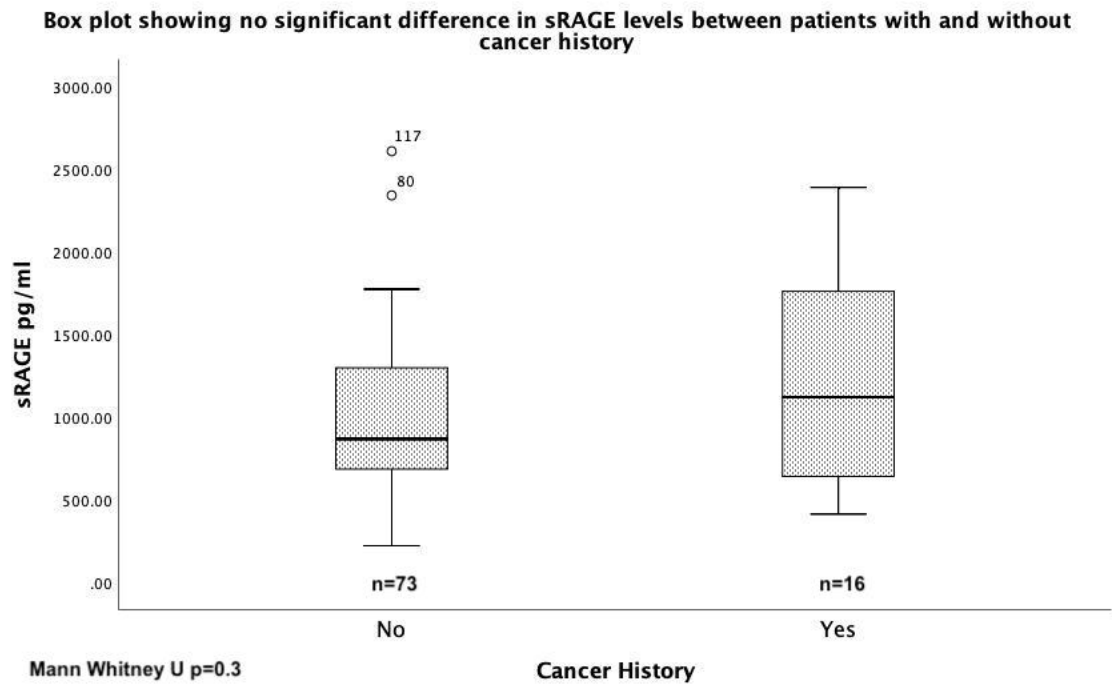
Figure 7-3 – Box plot showing no significant difference in sRAGE levels (pg/ml) between patients with and without cancer history (p=0.3). This indicates that having had cancer in the past does not result in aberrant sRAGE abundance. The whiskers on the box and whisker diagram indicate the range of the data with the median represented by the centre black line. Patient blood serum sources from patients recruited to the ovarian biomarker study.

Next an association between sRAGE levels and parity was evaluated (**Figure 7-4**). Parity is described as the number of times a woman has given birth to a foetus with a gestational age of 24 weeks or more, regardless of whether the child was born alive or still born (618). A large and consistent body of evidence indicates that increased parity and duration of oral contraceptive (OC) use are associated with reduced risk of OC (619). The box plot in **Figure 7-4** shows that there is no significant correlation between parity and sRAGE levels. A Kruskal Wallis Test did not report any significant differences between the groups with a p value of 0.565. This suggests that parity is not correlated with sRAGE serum levels in this dataset.

Box plot showing no significant difference in sRAGE levels with parity
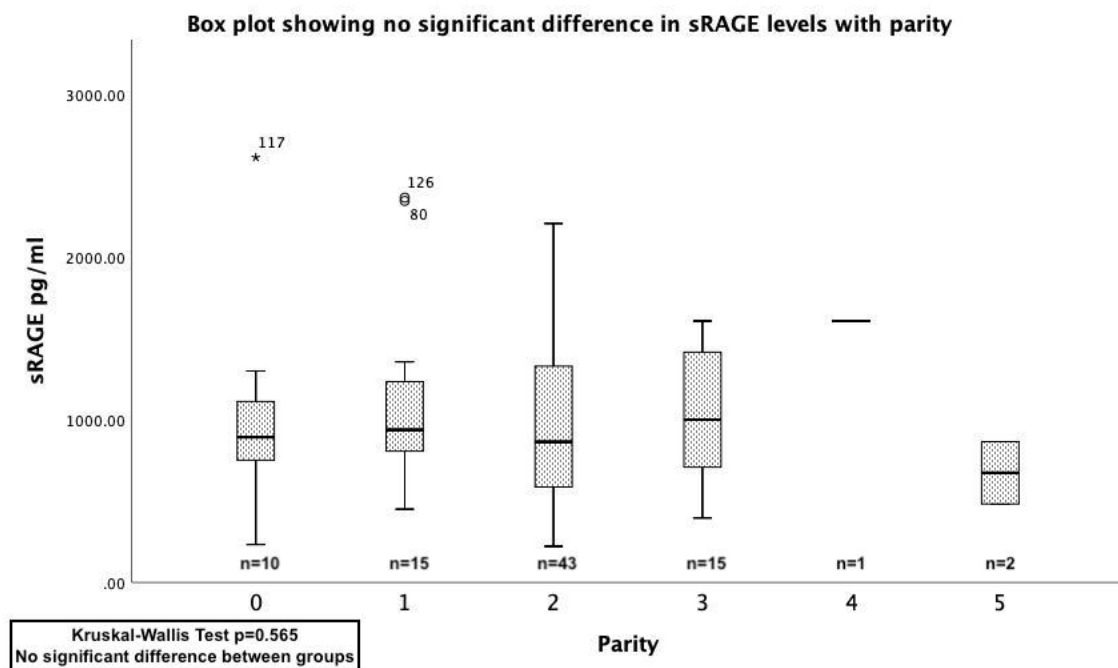
Figure 7-4 – Box plot showing sRAGE levels in the cohort grouped by parity
The boxplot above shows there is no altered abundance of sRAGE with parity. A Kruskal Wallis test did not report any significant differences between the groups with a p value of 0.565. Patients in this dataset most commonly had 1-3 children and the most common number of children was 2. This suggests that sRAGE was not correlated with parity in this dataset.

Figure 7-5 shows the levels of sRAGE in patients who smoke compared to patients that do not smoke. Smoking is reported to have an inflammatory effect (620) and with RAGE linked to inflammation it is important to understand if smoking alters the abundance of sRAGE in patients who smoke. In addition, smoking can increase the risk of certain types of ovarian cancer with approximately 3% of some types of OC seem to be linked to exposure to tobacco smoke (621). Out of the 130 patients 13 reported to be a smoker. Out of 130 people this number does seem quite low, however, some people reported to have smoked in the past and had since given up. The number 13 represents the number of people who were current smokers at the time of biopsy retrieval. **Figure 7-5** shows that there is no significant difference in sRAGE levels between the patients in this study who were current smokers and those who were not. A Mann Whitney test reported a p value of 0.173 indicating no statistically significant difference between the two groups. This suggests that sRAGE serum levels are not correlated with smoking status.

251

Box plot showing no significant difference in sRAGE levels depending on smoking status

Mann Whitney U Test p= 0.173
No significant difference
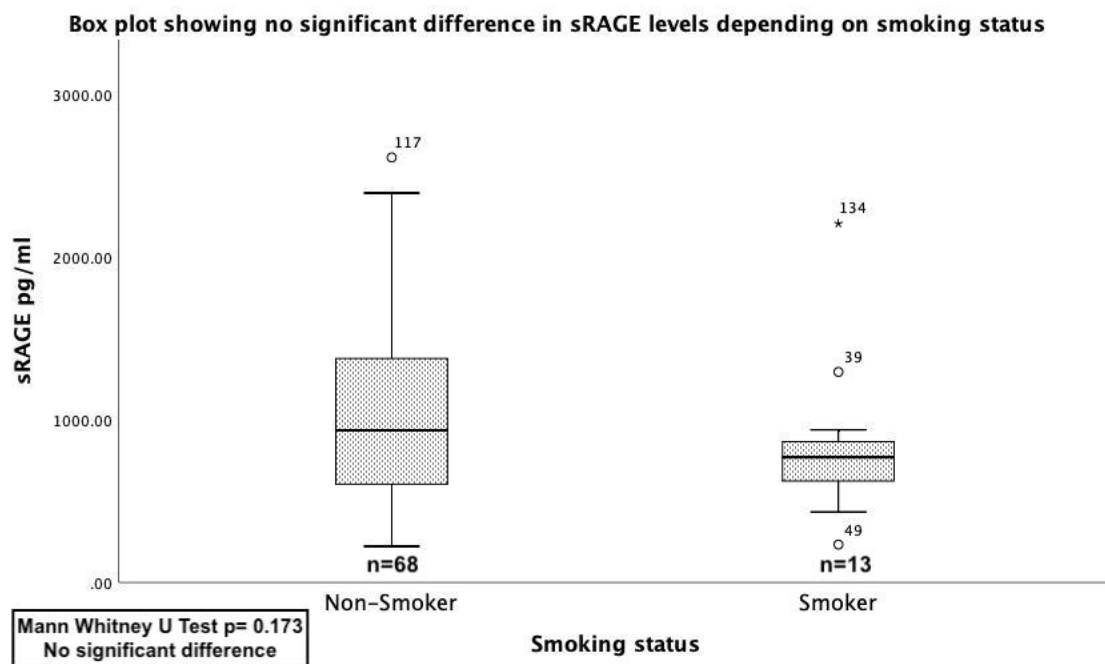
Figure 7-5 – Comparison of sRAGE levels in the cohort grouped according to smoking status
The box plot above shows the abundance of sRAGE in patients who smoke versus those who are non-smokers. There was no statistically significant difference between the two groups by Mann Whitney test (p=0.173). This suggests that sRAGE serum levels are not correlated with smoking status.

Endometriosis is an inflammatory gynaecological disorder that is characterised by the presence of endometrial tissue growing outside of the endometrium leading to chronic inflammation, pain and in some cases infertility (622). Although endometriosis is considered a benign gynaecological disease, the association with OC has been frequently described in literature since 1925. In 1925, Sampson produced the first histopathological criteria for the identification of malignant tumours arising from endometriosis (623). A systematic literature review by Ahmad Sayasneh reviewed all research publications up till 2010 and 7 out of the 8 papers reviewed showed an increased risk of OC from endometriosis (624). With endometriosis being linked to an increased risk of OC, both conditions having links to inflammation and RAGE being involved in inflammatory pathways it is important to assess sRAGE levels in the patients in this dataset who are diagnosed with endometriosis. **Figure 7-6** displays a box plot of the levels of sRAGE in the 6 endometriosis patients verses the 12 patients who were confirmed to not have endometriosis. The remaining patients in the dataset were not described as having or not having endometriosis either way. **Figure 7-6** shows a slightly higher level of sRAGE in the 6 endometriosis patients compared to the non-endometriosis patients. However, this increase is not considered statistically significantly different (Mann Whitney U t-test p value 0.151. This

could be due to a relatively small dataset, and future work is needed to determine if a statistical difference exists when assessing a larger sample size.
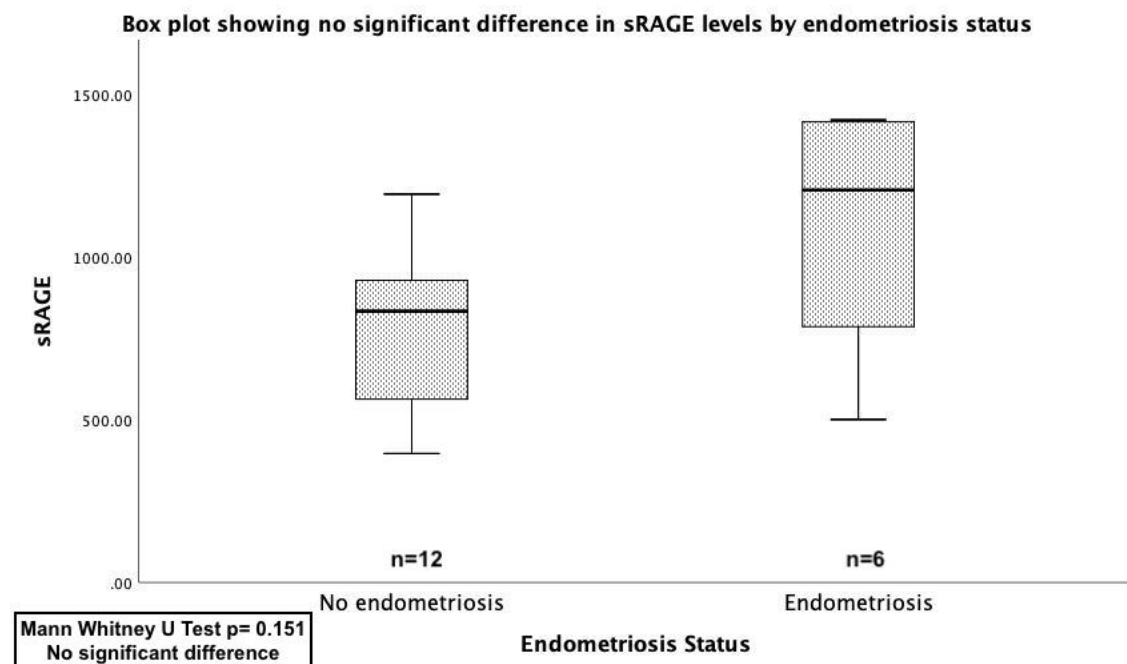
Figure 7-6 – Comparison of sRAGE levels between endometriosis and non-endometriosis samples
The box plot above shows the levels of sRAGE in patients with and without an endometriosis diagnosis. Levels of sRAGE are higher in the 6 endometriosis patients but not statistically significantly higher with a p value of 0.151 by Mann Whitney U test. The whiskers on the box and whisker diagram indicate the range of the data with the median represented by the centre black line. Patient blood serum sources from patients recruited to the ovarian biomarker study.

Over 75% of the patients recruited for the ovarian biomarker study are post-menopausal. This supports the statistic that women are most commonly diagnosed with OC later in their life (625). Only 9% of women recruited to the study were pre-menopausal and 17% were not described either way and were under 60 years of age and subsequently, were excluded from pre/post-menopausal analysis of sRAGE. **Figure 7-7** shows no statistically significant difference in the levels of sRAGE in post-menopausal women compared to pre-menopausal women in this dataset. A Mann Whitney test returned a p value of 0.780 indicating no statistically significant difference. Therefore, in this dataset menopausal status did not correlate with sRAGE serum abundance.
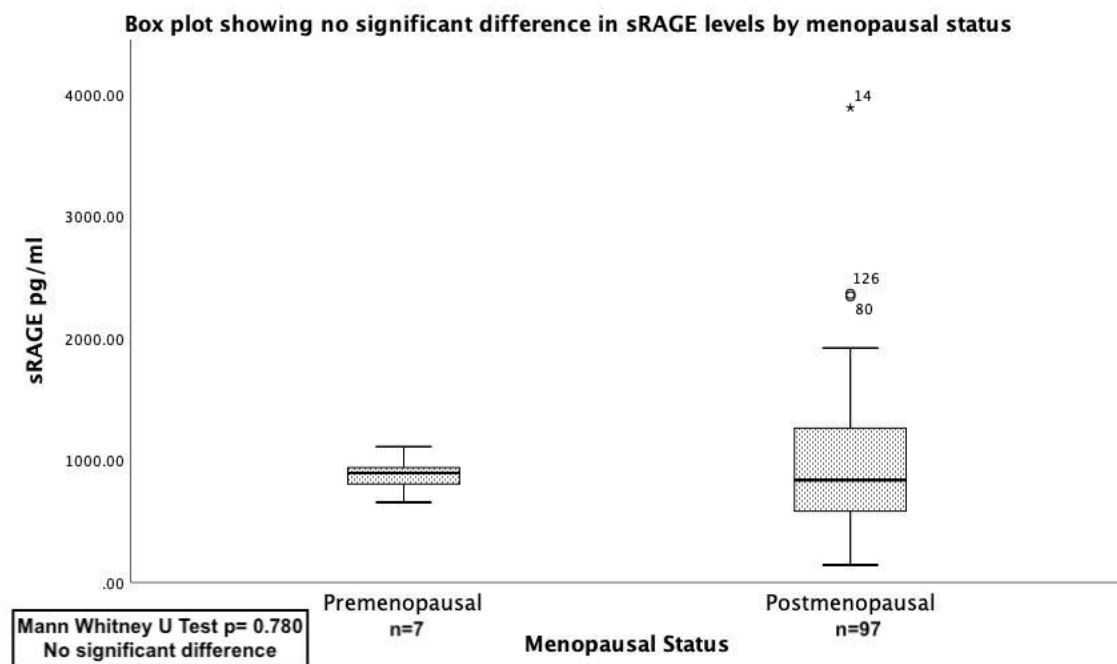
Figure 7-7 – Comparison of sRAGE levels according to the menopausal status
The box plot above shows the levels of sRAGE in post-menopausal patients compared to pre-menopausal patients. Over 75% of the patients were post-menopausal which is consistent with the literature where women are most commonly diagnosed with OC at 60-65 years of age. The analysis reports no statistically significant difference in sRAGE serum levels between the two groups. A Mann Whitney U test p value 0.780.

Menopause is diagnosed when a woman over 45 stops having a monthly menstrual cycle for 1 year or longer (626). Post-menopausal bleeding (PMB) is any vaginal bleeding that occurs after this diagnosis (627). It has been reported (628, 629) that the increased abdominal adiposity that generally occurs after menopause can contribute to increased inflammatory markers such as CRP. Additionally, the process of shedding the uterine lining is an inflammatory process, suggesting patients experiencing PMB may have aberrant sRAGE abundance. **Figure 7-8** assesses the abundance of sRAGE in patients experiencing PMB compared to patients not experiencing PMB. Only 10% of patients reported PMB, 50% reported specifically no PMB and 40% of patients were not reported as experiencing PMB either way. **Figure 7-8** shows a box plot comparing the sRAGE levels of patients who experienced PMB compared to those who did not. A statistically significantly lower abundance of sRAGE was observed in patients reporting PMB regardless of their cancer diagnosis. A Mann Whitney test returned a p value of 0.02 indicating a significant difference. sRAGE has been reported to act as a decoy for flRAGE ligands (630). In the case of inflammation, flRAGE abundance increases and as a result, inflammatory pathways are upregulated. sRAGE has been known to block inflammation by binding flRAGE ligands, suggesting an inverse correlation between sRAGE and flRAGE. In the case of PMB, flRAGE could

254

be overexpressed due to inflammation and sRAGE downregulated in turn and therefore not having a protective effect against inflammation.
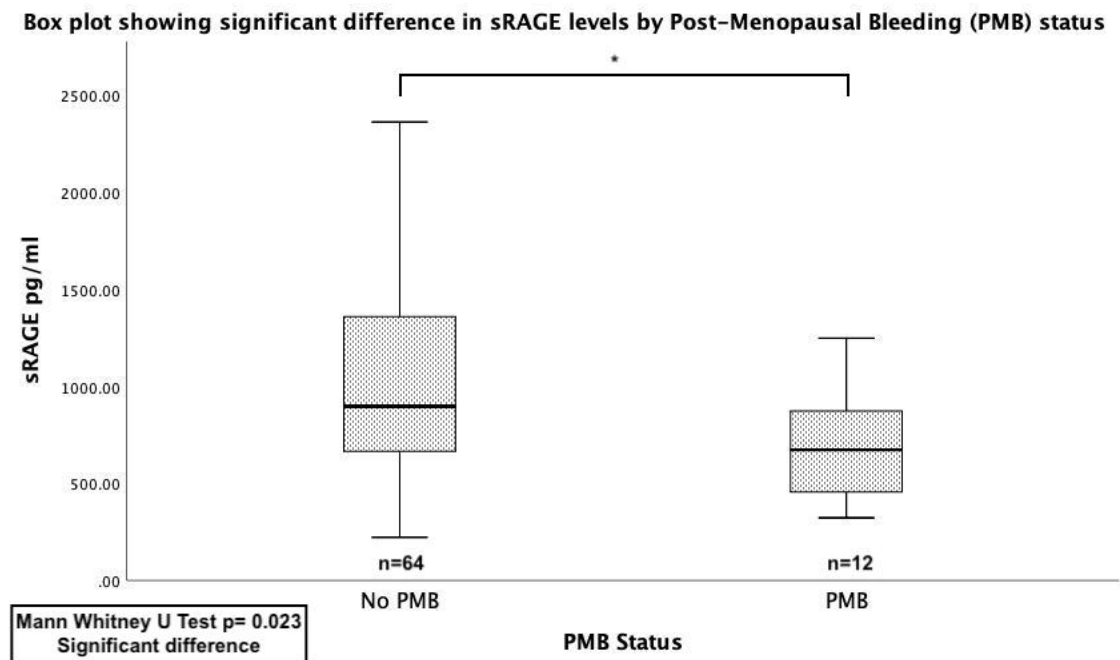
Figure 7-8 – Box plot showing a significant difference in sRAGE levels by Post-Menopausal Bleeding (PMB) status.
The above box plot shows a significantly lower expression of sRAGE in those patients reporting PMB. In inflammatory conditions, flRAGE is upregulated with RAGE inflammatory pathways. As sRAGE has been reported to act as a decoy for flRAGE ligands, it is possible that flRAGE and sRAGE inversely correlate with each other in inflammatory conditions. This data suggests that sRAGE is correlated with PMB status.

Due to this correlation between PMB and sRAGE, the previous Mann Whitney U tests (correlating sRAGE to menopausal status, endometriosis, smoking status, parity, cancer history) were repeated for the various patient metrics with the 12 PMB patients removed. This did not alter the significance result of any of the previous results.

Hormone Replacement Therapy (HRT) is a treatment administered to relieve the symptoms of menopause such as hot flushes, night sweats, mood swings, vaginal dryness and reduced sex drive. It replaces hormones that are present at a lower level as the menopause is approached. Many symptoms pass after a few years but taking HRT can provide relief for many women. HRT has been reported in a small number of cases to increase the risk of breast cancer depending on other patient factors such as race, weight and breast density (631). A Meta-Analysis study on the association between HRT and OC was carried out in 2019 (57). The study concluded that menopausal HRT may increase the risk of OC, particularly for serous and endometrioid tumours. Due to this association, the abundance of sRAGE was assessed in patients who had reported

undergoing HRT. No significant difference in sRAGE abundance was observed between patients who had undergone HRT and those who had not. A Mann Whitney test reported a p value of 0.579 suggesting no statistically significant difference between the two groups. In this dataset, sRAGE was not shown to correlate with HRT.
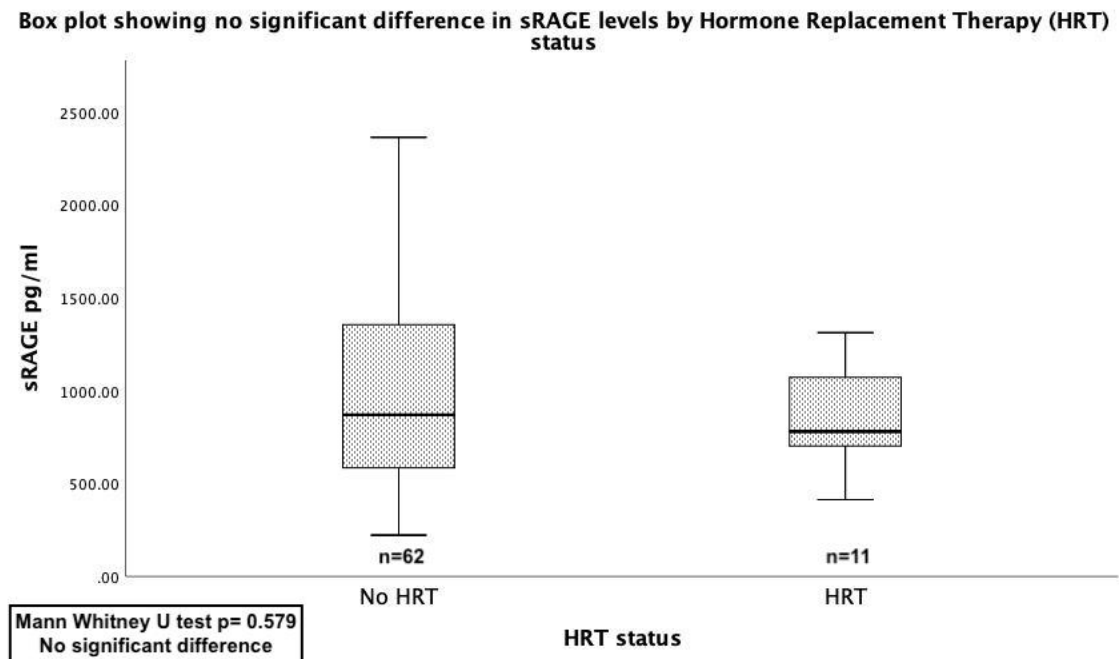
Figure 7-9 – Box plot showing no significant difference in sRAGE levels by Hormone Replacement Therapy (HRT) status
The box plot above compares the abundance of sRAGE in the blood serum of patients who had undergone HRT compared to those who had not. Only 11 patients out of 130 had reported having undergone HRT and no statistically significant difference in sRAGE levels was observed between those who had HRT and those who did not. A Mann Whitney returned a p value of 0.579, indicating no statistically significant difference between the two groups. In this dataset, sRAGE was not shown to correlate with HRT status.

The results above show that sRAGE serum abundance is not correlated to any of the patient metrics apart from PMB. sRAGE is more specific as a biomarker and therefore more useful if it is not aberrantly expressed in other conditions and patient metrics. The results show so far, that except PMB, sRAGE is not correlated to any of the patient metrics indicating sRAGE is a promising biomarker to explore in OC.

7.2.4 Using CA125 serum levels and RMI values to stratify patients in this dataset

Patients with and without OC in this dataset were analysed to see if they could be stratified using the existing methods of OC diagnosis - CA125 serum levels and RMI. This way, the

abundance of sRAGE in patient stratification can be directly compared to the current standard. The CA125 serum levels and the RMI values were obtained directly from the patient data forms and not obtained experimentally as part of this project.

Figure 7-10 shows the levels of serum CA125 in patients with any OC diagnosis compared to patients who were confirmed to have no diagnosis of OC. Patients diagnosed with OC had a statistically significantly higher CA125 serum level when compared to the patients who were confirmed to have no cancer diagnosis. A Mann Whitney U test revealed an extremely low p value of 0.0000000817. This shows that the current method to preliminarily indicate OC is capable of highly significantly stratifying the patients in this dataset.
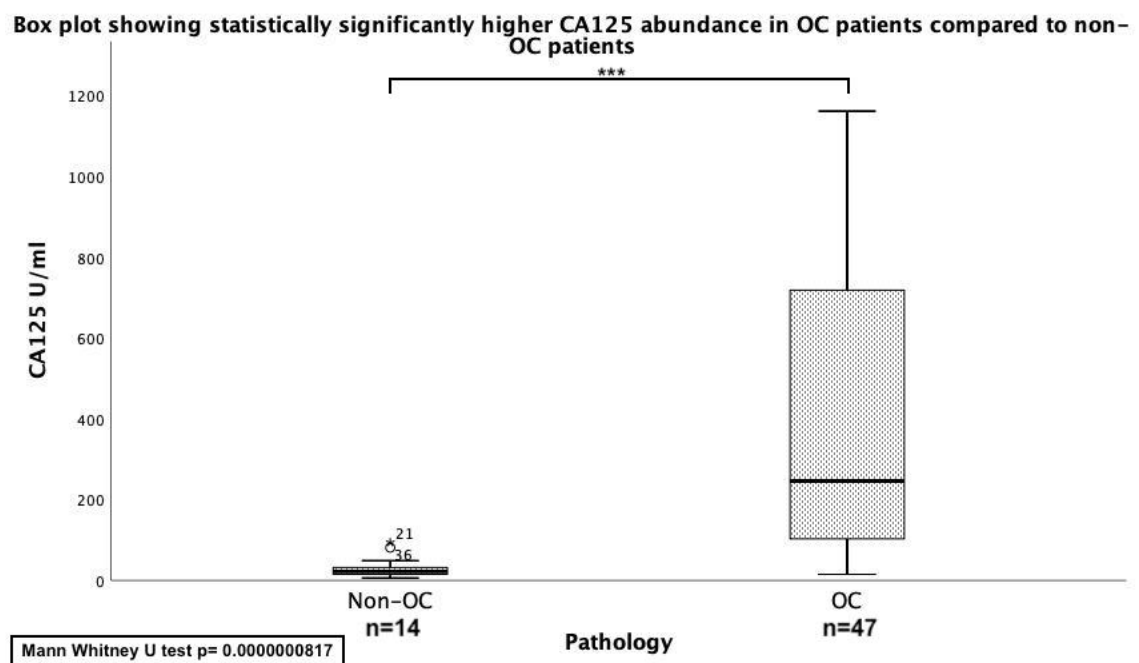
Figure 7-10 – Box plot showing statistically significantly higher CA125 abundance in OC patients compared to non-OC patients

The boxplot above shows that the levels of CA125 as recorded on the patient data sheet, are statistically significantly higher in confirmed OC patients than in confirmed non-OC patients. A Mann Whitney test revealed an extremely low p value of 0.000000817. This shows that the current CA125 metric is capable of stratifying OC from non-OC patients in this dataset.

Figure 7-11 shows the CA125 levels, recorded on the patient data forms, in the same non-cancer group but this time compared to patients specifically of a HGSOC subtype. HGSOC is the most common subtype of OC. Out of the 47 OC patients, 25 specifically had HGSOC. **Figure 7-11** shows that, when considering HGSOC patients only, the level of CA125 in the blood serum is still able to stratify patients by confirmed non-cancer and HGSOC. A Mann Whitney test returned a p value of 0.0000001 suggesting a highly statistically significant difference between the two

patient groups. This confirms that, in this dataset, CA125 levels can stratify patients by non-cancer and HGSOC.
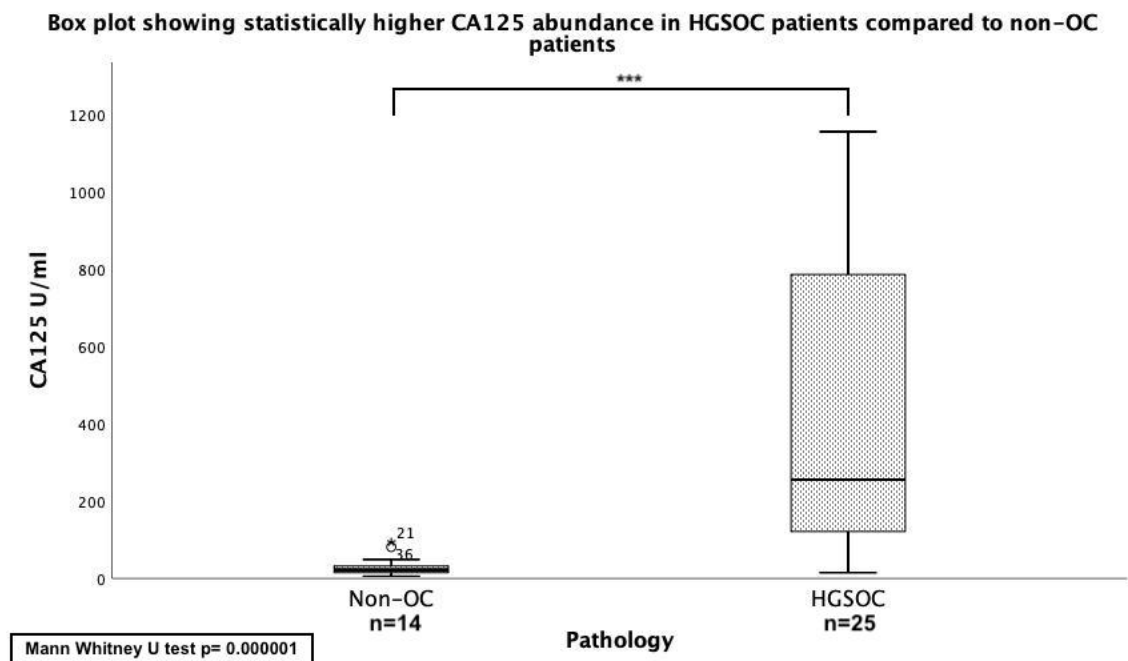
Figure 7-11 – Box plot showing statistically higher CA125 abundance in HGSOC patients compared to non-OC patients

The boxplot above shows that the levels of CA125 as recorded on the patient data sheet, are statistically significantly higher in confirmed HGSOC patients than in confirmed non-OC patients. A Mann Whitney test revealed an extremely low p value of 0.0000001. This shows that the current CA125 metric is capable of stratifying HGSOC from non-OC patients in this dataset.

With CA125 serum levels being capable of stratifying OC patients from non-OC patients in this dataset, **Figure 7-12** shows if there is any correlation between CA125 and sRAGE. No statistically significant correlation is observed between CA125 and sRAGE levels in this dataset. A Spearman Rho test for correlation returned a p value of 0.909, indicating no statistically significant correlation. This suggests sRAGE may not be capable of stratifying OC patients from non-OC patients in this dataset.
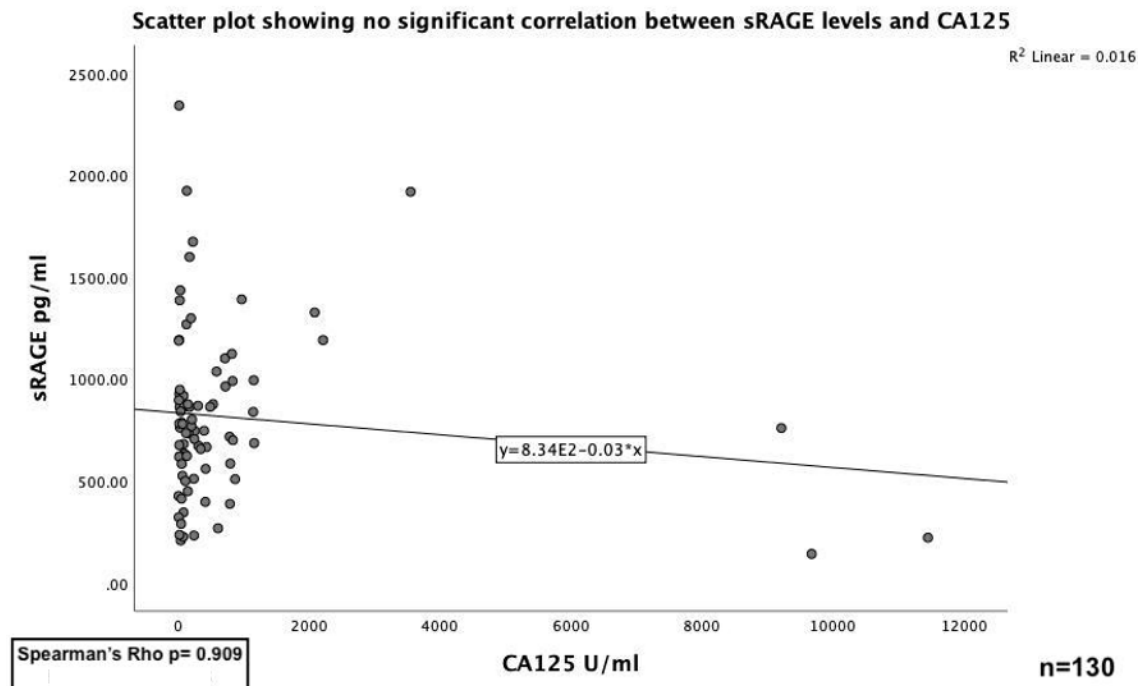
Figure 7-12 – Scatter plot showing no significant correlation between sRAGE levels and CA125

The scatter plot above assesses for correlation between levels of sRAGE and the levels of CA125 recorded on the patient data sheets. A Spearman Rho test for correlation shows no statistically significant difference with a p value of 0.909 between serum CA125 and sRAGE. A Pearson's test returned a p value of 0.258, also suggesting no significant difference. This suggests sRAGE may not be capable of stratifying OC patients from non-OC patients in this dataset.

The Risk of Malignancy Index (RMI) values of the individual patients are another patient metric recorded on the patient data forms. RMI is currently used in the clinic, along with other methods, to indicate the presence of OC. The data analysis shown below aims to establish if the RMI values of the patients presented in this dataset can successfully stratify these patients by OC and non-cancer. Out of 130 patients included in this analysis, 45 patients had their RMI calculated. Out of this 45, 12 were confirmed to have no cancer and 17 were confirmed have OC and the remaining patients were not included. Out of the patients not included, 2 were excluded from the graphs due to being dramatically higher than the other values. One outlier was 79049 and another was 18522. With all the other RMI values being under 4000 these two data points skewed the graphs. Both of these outliers were a part of the OC group therefore the significant difference seen would still have been observed but on a larger scale if these data points had been included. The other patients who had an RMI value recorded but were not included in the analysis were in the 'pelvic mass' group. This is a group where a mass has been identified but a confirmatory diagnosis was not described on the patient data forms. Therefore, these patients could not be assigned to the cancer or non-cancer group.

Figure 7-13 shows a boxplot comparing RMI values of 12 non-cancer patients to the RMI values of 17 confirmed OC patients. The analysis revealed a high statistically significant difference in the RMI values between the OC and non-cancer patients. A Mann Whitney test reports a p value of 0.000000732 suggesting a statistically significant difference. This shows that the RMI values recorded on the patient data forms are capable of stratifying patients by OC or non-cancer.
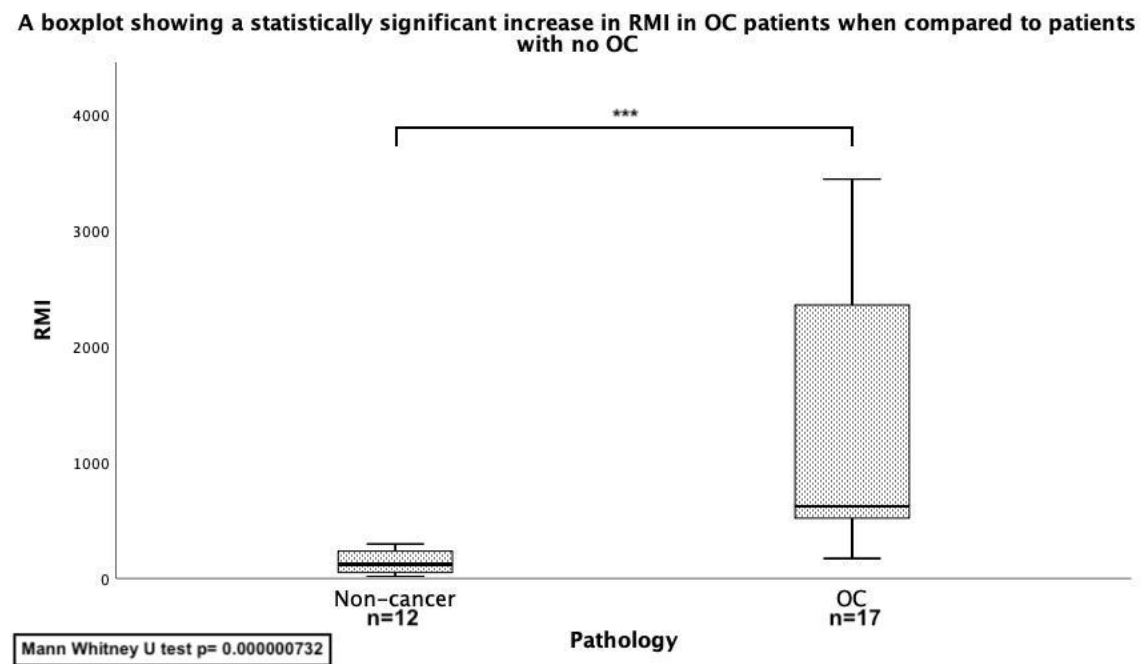
Figure 7-13 – A boxplot showing a statistically significant increase in RMI in OC patients when compared to patients with no OC

The boxplot box above shows that the RMI values recorded on the patient data forms are capable of stratifying patients by OC or non-cancer. A Mann Whitney test reports a p value of 0.000000732 suggesting a statistically significant difference between the two groups.

Figure 7-14 narrows down the 17 OC patients described in **Figure 7-13** to 9 patients who were specifically confirmed as a HGSOC subtype. HGSOC is the most common subtype of OC. **Figure 7-14** aims to uncover if the RMI values reported on the patient data forms can also stratify the 12 non-cancer patients from the 8 HGSOC patients. A Mann Whitney test reports a p value of 0.000016 suggesting a high statistically significant difference. This shows that in addition to the RMI values, recorded on the patient data forms, being able to stratify patients with OC from those with no cancer – RMI can also stratify patients with a specific HGSOC subtype from those with no cancer in this dataset.
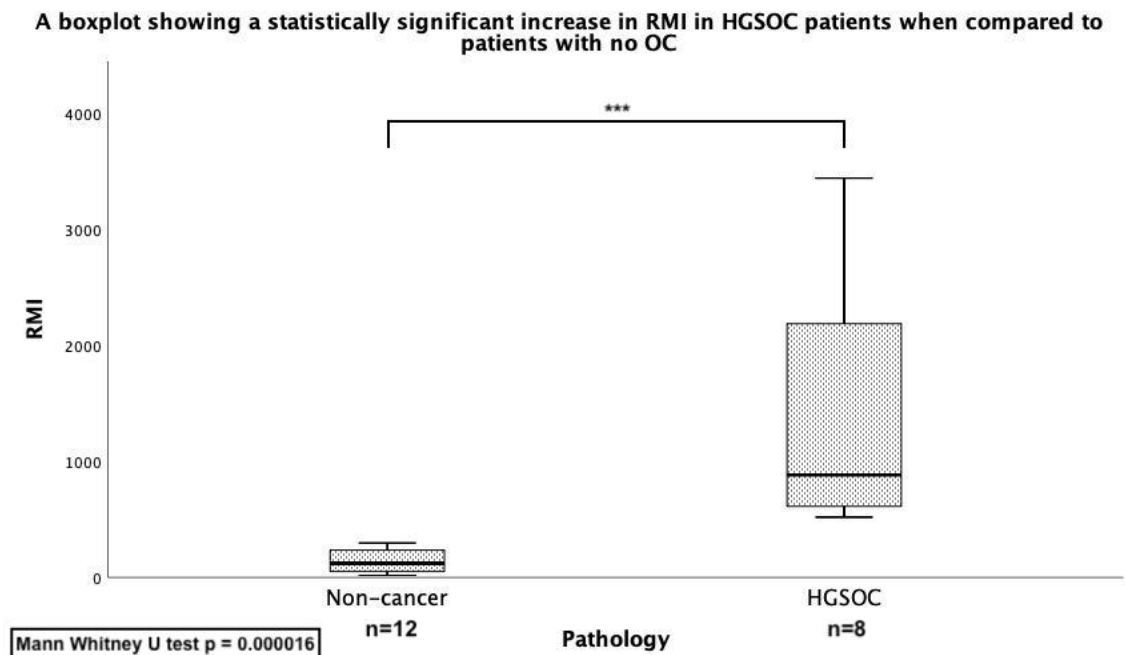
Figure 7-14 A boxplot showing a statistically significant increase in RMI in HGSOC patients when compared to patients with no OC

The boxplot box above shows that the RMI values recorded on the patient data forms are capable of stratifying patients by HGSOC or non-cancer. A Mann Whitney test reports a p value of 0.0000016 suggesting a statistically significant difference between the two groups.

Figure 7-15 aims to uncover if there is any correlation between the RMI values recorded on the patient data forms and sRAGE. A Spearman Rho test for correlation reports a p value of 0.049, suggesting a very small statistically significant correlation. This suggests that sRAGE may not be capable of stratifying patients in the way RMI has been shown to in **Figure 7-13** and **Figure 7-14**, but if it is capable, that sRAGE expression might be downregulated in OC.
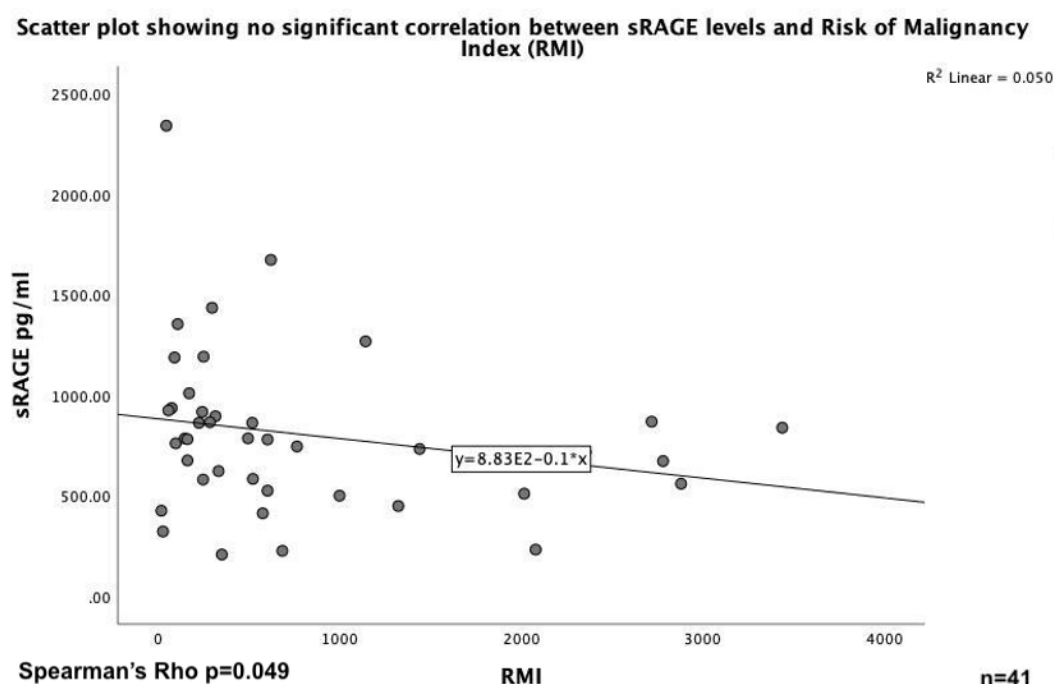
Figure 7-15 - Scatter plot showing a significant negative correlation between sRAGE levels and Risk of Malignancy Index (RMI)

The scatter plot above shows no statistically significant correlation between the levels of sRAGE and the RMI values recorded on the patient data forms. A Spearman Rho test for correlation reports a p value of 0.049, suggesting a very small statistically significant correlation. This suggests that sRAGE may not be capable of stratifying patients in the way that RMI can, but if it can then the expression of sRAGE might be downregulated in the serum of OC patients.

The data above confirms that CA125 serum levels and RMI values can statistically significantly stratify OC and HGSOC patients from those with no cancer diagnosis. In addition, there is no correlation between sRAGE serum levels and RMI CA125 serum levels and a very minor correlation between sRAGE and RMI. The data so far indicates that serum levels of sRAGE may not be capable of stratifying OC patients from non-cancer patients, but the minor correlation between sRAGE and RMI indicates that if it can stratify patients then sRAGE abundance might be lower in OC patients due to the trend seen in **Figure 7-15**.

7.2.5 Serum levels of sRAGE in ovarian cancer

The analysis here uncovers if patients with different OC pathologies, OC, HGSOC and non-cancer can be stratified by levels of sRAGE in their blood serum.

Figure 7-16 shows a box plot of the levels of sRAGE in the serum of patients with various ovarian pathologies as described in section 7.2.1. Initially, it can be seen that the levels of sRAGE does vary between groups. A Kruskal Wallis H test was carried out to assess if there is any statistically significant difference in the levels of sRAGE between the groups. A p value of 0.707 was

returned, indicating no statistically significant difference between any of the groups. This suggests that patients in these groups cannot be stratified using serum sRAGE levels.
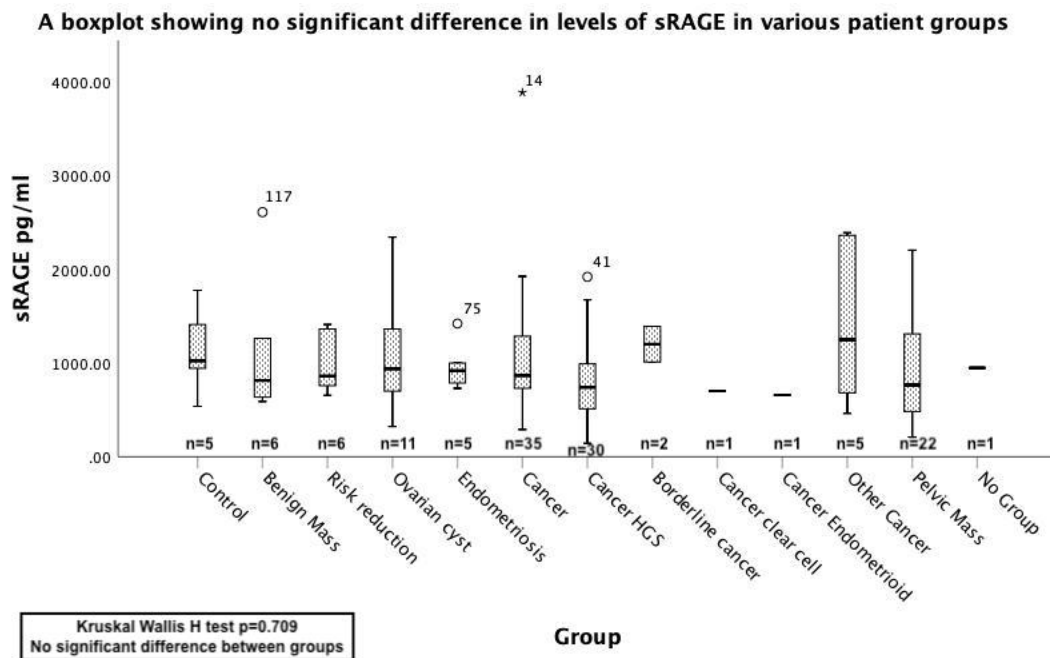
Figure 7-16 – A boxplot showing no significant difference in levels of sRAGE in various patient groups

The above boxplot shows the varying levels of sRAGE in the blood serum of patients grouped by ovarian pathology. A Kruskal Wallis H test reports no statistically significant difference between any of the groups with a P value of 0.709. This suggests that levels of sRAGE in the blood serum is not capable of stratifying patients by these groups.

Figure 7-17 shows the levels of sRAGE detected in the blood serum in patients with a confirmed diagnosis of OC (n=69) compared to those with a confirmed no cancer diagnosis (n=33). No statistically significant difference was found between the two groups. A Mann Whitney reported a p value of 0.176. This confirms that, in this dataset, the abundance of sRAGE detected in the blood serum cannot statistically significantly stratify patients with OC from those with no-OC.

Box plot showing no significant difference in sRAGE levels between patients diagnosed with OC and those with no cancer diagnosis

Mann Whitney U Test p = 0.176
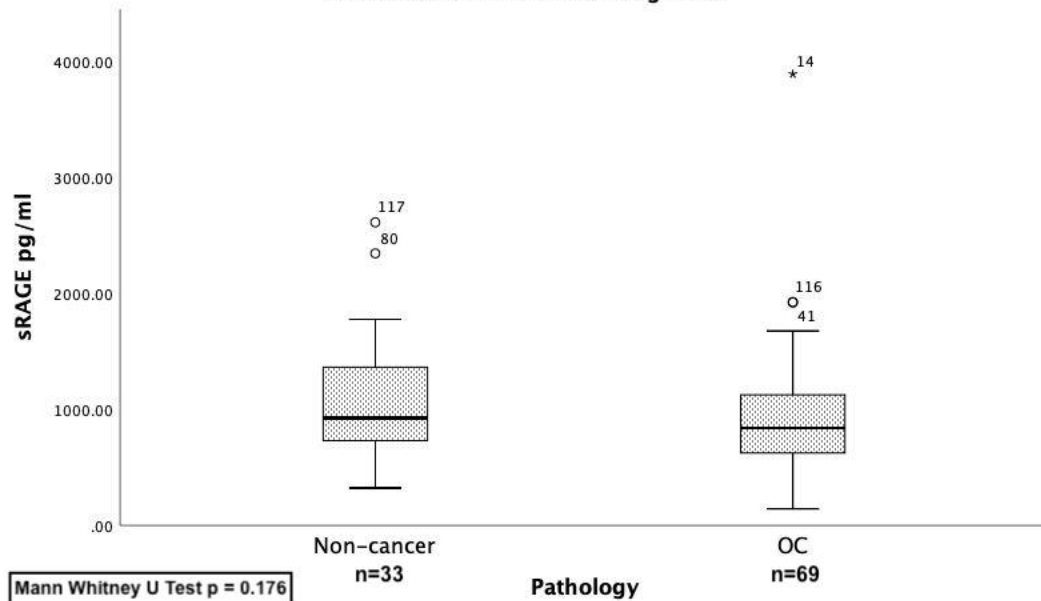
Figure 7-17 - Box plot showing no significant difference in sRAGE levels between patients diagnosed with OC and those with no OC diagnosis

The above boxplot shows no statistically significant difference in the levels of sRAGE detected in the serum in patients diagnosed with OC compared to those patients with no cancer diagnosis. A Mann Whitney test retuned a p value of 0.176, indicating no statistically significant difference. This confirms that levels of sRAGE detected in the blood serum is not capable of stratifying OC patients from non-OC patients in this dataset.

HGSOC is the most common type of OC diagnosed and is also one of the most aggressive subtypes**. Figure 7-18** compares the levels of sRAGE in HGSOC patients specifically to non-cancer patients. Due to being more aggressive, it is possible any significant differences in sRAGE levels may be more apparent when considering only HGSOC patients. A Mann Whitney U Test returned a p value of 0.03, indicating a statistically significant difference between the two groups. This confirms that, in this dataset, levels of sRAGE in the blood can stratify HGSOC patients from non-cancer patients.
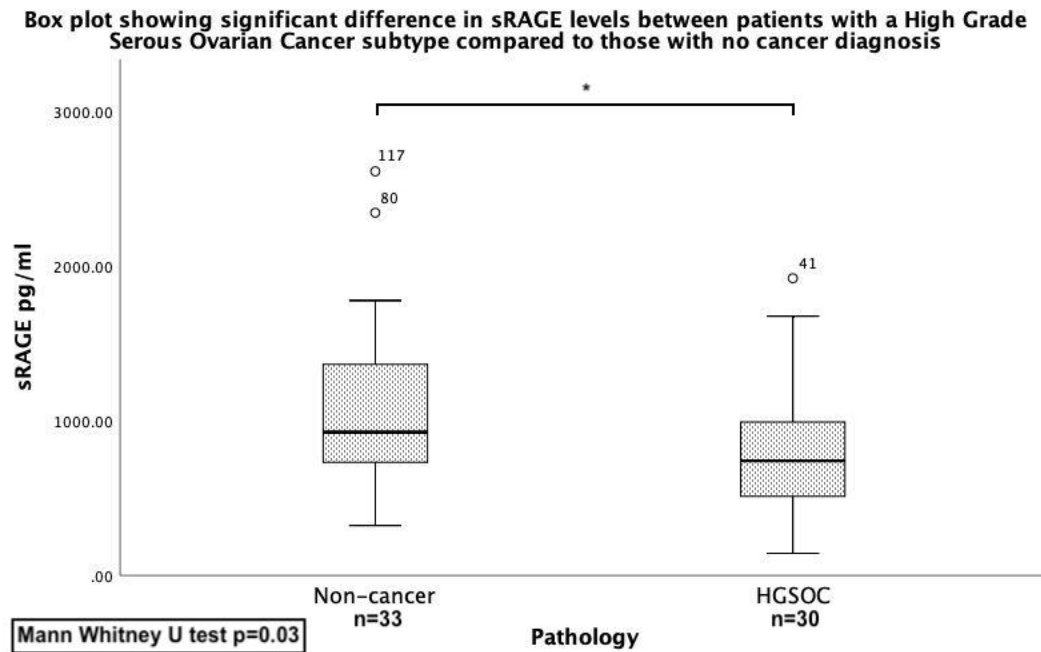
Figure 7-18 - Box plot showing significant difference in sRAGE levels between patients with a High Grade Serous Ovarian Cancer subtype compared to those with no cancer diagnosis

The boxplot above shows levels of sRAGE in patient serum to be statistically significantly lower in HGSOC patients when compared to non-cancer patients. A Mann Whitney U Test returned a p value of 0.03, indicating a statistically significant difference between the two groups. This confirms that, in this dataset, levels of sRAGE in the blood can stratify HGSOC patients from non-cancer patients.

This does contradict what would be expected given that ADAM10 protease cleaves full length RAGE to produce sRAGE and the matrix metalloproteinase function is usually higher in advance disease. A larger sample size and analysis of additional independent datasets would be beneficial to validate findings. It would be interesting for future work to address if sRAGE levels are higher in samples with metastatic disease.

7.3 Conclusions

Significantly lower abundances of sRAGE in the serum of OC patients could be advantageous for diagnosis and treatment. Patients could be diagnosed and stratified by detecting sRAGE in the blood serum. sRAGE abundance in the serum could also be used alongside existing methods for a more accurate and sensitive diagnosis and response to treatment monitoring. Additionally, a lower abundance of sRAGE in the serum will be advantageous if an ADC targeting flRAGE is used. sRAGE is reported to act as a decoy in the serum, where RAGE ligands bind sRAGE instead of flRAGE. This action prevents ligands from binding to flRAGE and therefore downregulated the signalling pathways as a result of this flRAGE-ligand binding. A lower abundance of sRAGE in the serum of OC patients means that the ADC targeting RAGE has more chance of binding to flRAGE

and delivering its cytotoxic payload to the malignant cell. A lower abundance of sRAGE in the serum of OC patients means less sRAGE decoy action and an upregulation of the flRAGE/RAGE-ADC binding and action. Additionally, sRAGE could be used to stratify patients for treatment using a RAGE targeting ADC. If an OC patient has a higher sRAGE abundance in the serum then this could be an indication that the RAGE targeting ADC will not work for them as effectively if they had a lower serum sRAGE abundance. This could be tested preclinically by a blood test.

Overall, levels of sRAGE detected in patient serum were not statistically significantly altered in any of the patient metrics reported on the patient data form, apart from PMB where there was a small but statistically significant difference. This meant that sRAGE abundance in the serum remains stable across common differing conditions between patients. This causes the correlation of sRAGE to HGSOC to be more specific to HGSOC when considering other common patient metrics.

The patients recruited for the ovarian biomarker study had their CA125 serum levels and RMI recorded as part of their recruitment and monitoring. When grouped into OC and non-cancer, CA125 and RMI could statistically significantly stratify patients. In addition, when grouped by specifically HGSOC and non-cancer, CA125 and RMI could still stratify patients. This confirms that the current standard of OC diagnosis in the clinic is capable of determining OC or non-cancer in this dataset. This is a baseline to compare sRAGE levels to in the final analysis.

In the final analysis, sRAGE did not correlate with either CA125 serum levels and had a very minor correlation to RMI. The abundance of sRAGE in the serum was also not significantly different in any of the ovarian pathology groups as shown in Figure 7-16. sRAGE was not capable of statistically significantly stratifying OC patients from non-cancer patients. However, when restricted to only the HGSOC patients, sRAGE was capable of statistically significantly stratifying patients in each group. This has implications for a more effective treatment with a RAGE-ADC and the potential to stratify patients for HGSOC diagnosis, treatment plan and monitoring the response to treatment.

Overall, while sRAGE can stratify the patients in this dataset by HGSOC and non-cancer, sRAGE does not appear to be as accurate or as sensitive as RMI and CA125 serum was in this dataset. The levels of significance were $x10^2$ higher for RMI and CA125 indicating sRAGE is not as good, or better, than the current standard. This could be due to a weak sampling of healthy participants. Only 5 out of 130 patients were recruited specifically as non-cancer controls with no described ovarian pathology. The other non-cancer patients were recruited for anything from a cyst, a benign mass to risk reduction surgery and were later confirmed to be non-cancer. This means the healthy controls may not have been 100% healthy – highlighting the challenge in

obtaining a truly healthy patient sample. However, sRAGE could be used to stratify patients who are to receive treatment using a RAGE ADC and a lower abundance of sRAGE in the serum of HGSOC patients suggests a greater effect with a RAGE ADC due to less of the decoy effect from circulating sRAGE.

It appears that sRAGE, from what is seen in this dataset, is not a suitable alone as a diagnostic tool for OC when compared to the current standards. It is possible that sRAGE could be used in conjunction with the current standards for a more accurate and specific diagnosis. The dataset is constantly becoming bigger as more patients are recruited for the study. In the future, this hypothesis can be tested again with the larger dataset. Additionally, serum could be requested from patients who have received treatment to measure their sRAGE in response to their treatment. Consideration can be given to increasing the non-cancer control samples to further strengthen the dataset.

Chapter 8: General Discussion

8.1 Identification of overexpressed proteins in OC with potential therapeutic value as ADC targets.

This thesis addresses the urgent need for a more effective therapeutic treatment method and a specific, high throughput liquid biopsy method for the early diagnosis of OC. Approximately 4100 women die from OC each year in the UK and OC accounts for 5% of all cancer deaths in females in the UK. This suggests the need for a more effective strategy to combat the high number of deaths associated with OC. OC survival is significantly associated with a diagnosis under the age of 40. Almost 9 in 10 women in England diagnosed between the ages of 15-39 survive OC for more than 5 years compared with only 1 in 5 women when diagnosed over 80 years old (28). This highlights the desperate need for a high throughput diagnostic test capable of confidently indicating OC at an early stage for increased survival probability.

Diagnosis is complicated by the absence of early pathognomonic symptoms, leading to late recognition of the disease and a high mortality rate. In an effort to stimulate drug development, OC, which has a prevalence of approximately 3 in 10,000, has been designated orphan disease status. Companies developing drugs for diseases designated orphan indication status to provide incentives, such as exclusive licensing rights. As a result, several putative modes of action are being explored to develop therapeutics for ovarian and other gynaecological cancers (632).

Of the different approaches being investigated, monoclonal antibodies targeting cancer specific cell-surface markers have shown promise. Bevacizumab (Avastin, Genentech/Roche), a humanised antibody targeting vascular endothelial growth factor-A, was first licensed in 2004 for colorectal cancer, and later for other metastatic cancers including breast, although this latter indication was removed by the FDA in 2010 (633). In 2012, Bevacizumab was licensed for OC, the first new drug for this indication in fifteen years; but due to the serious side effects, the costs and the short extension of life, Bevacizumab is approved only for OC in advanced stages and platinum therapy-resistant types (634). There is therefore an unmet demand for a targeted, safe, and effective treatment for OCs.

Antibody-Drug Conjugates (ADCs) are a new class of biologic therapeutics comprising a cancer-targeting antibody attached through a linker to a cancer-killing payload. Since ADCs selectively target specific tumour antigens, higher concentrations of the cytotoxic drug reach the malignant tissue and there is less collateral damage within healthy tissues, reducing unwanted side effects and expanding the therapeutic window compared to traditional chemotherapy (585).

This thesis explores the potential of six proteins as suitable targets for ADC development against OC. The focus of this study is on the identification process and characterisation prior to pre-clinical. The development of a successful ADC hinges on the identification of a novel target which

is present exclusively on the surface of malignant OC cells and minimally express in healthy tissue, while , capable of internalising antibody ligands.

The data of this thesis showed:

1. Identification of 6 potential targets using in silico database, Human protein Atlas and published observations. Specific expression of TSPAN6 in 8 OC cell lines by immunoblot and the clear localisation of TSPAN6, PCSK4 and PIEZO2 to the plasma membrane by immunofluorescence (Chapter 3)

2. Cell surface localisation of TSPAN6, PCSK4 and PIEZO2 on primary cells derived from ovarian cancer biopsies by immunofluorescence. Identification of a novel immunoreactive band (60 kDa) in TSPAN6 immunoblots which was statistically significantly elevated in protein extracts from OC biopsy collected from patients (Chapter 4)

3. TSPAN6 and RAGE proteins expressed at the cell surface are able to internalise antibody-dye conjugates into primary ovarian cells isolated from HGSOC biopsies at a statistically significant higher rate than non-cancer ovarian cells (Chapter 5).

4. High genetic stability (>95%) in the antibody epitope DNA coding region for RAGE and TSPAN6 by Next Generation Sequencing (Chapter 6)

5. sRAGE levels are statistically significantly higher in the serum of non-cancer patients compared to serum of HGSOC patients by ELISA (Chapter 7)

Overall, this thesis successfully screened for novel ADC targets, confirmed the expression and cellular location of these targets in protein and 2D cells derived from OC cell lines and patient biopsies and confirmed the internalisation and genetic stability of the most promising targets. In addition, this thesis explored a successful pipeline for the identification of novel biomarkers for the early detection of OC.

The presence of a target in any healthy organ can provoke on-target toxicity promoted by the ADC treatment that could be dose limiting, potentially resulting in failure of the ADC on clinical trials (635). TSPAN6 is typically expressed at low levels under normal physiological conditions in most tissues (434). This was further confirmed in this study by evaluating TSANP6 expression in protein extracts from healthy tissues corresponding to different organs.

Interestingly, TSPAN6 is not essential to life with data from knockout mouse models suggesting loss of TSPAN6 expression is associated with epilepsy and cognitive defects (636). Similarly, PIEZO2 is not essential to life with partial or incomplete knockdown of *Piezo2* reported to significantly reduce touch sensation (637). In the case of PCSK4, inactivation of this gene in mice causes male infertility in males and subfertility in females (446). Expression of these 3 targets have been previously associated with cancer. TSPAN6 expression has been studied in breast

cancer where it has been found that its mRNA levels were not prognostic in patients with ER-HER2- and ER-HER2+ tumours. In addition, a significant association of TSPAN6 expression with metastases-free survival in patients diagnosed with ER+HER2- breast cancer was reported by these authors (638). PIEZO channels have been identified as major transducers of mechanical stress into Ca^{2+} dependent signals and are overexpressed in several cancers such as breast, gastric and bladder whereas their downregulation has been reported in other cancers. PIEZO channels have been shown to have important roles in human homeostasis and pathophysiological conditions and studies have shown that the activation of PIEZO channels can deliver local Ca^{2+} influx which modulates key signalling pathways associated with cancer cell migration, proliferation and angiogenesis (639). PCSK4 is a favourable prognostic marker in endometrial cancer where it is significantly upregulated in endometrial cancer tissue on The Human Protein Atlas by IHC (301). In lung cancer, the targeting of Proprotein Convertases, such as PCSK4, decreases *in vitro* and *in vivo* growth (640).

In chapter 4, the abundance of the 60 KDa band by western blot was statistically significantly higher in protein extracted from 2D cultured cells derived from HGSOC patient biopsies when compared to non-cancer patients which was in agreement with a recent report that identified TSPAN6 gene expression as a biomarker and included it in a panel of 5 biomarkers that, when combined, indicated a favourable outcome in OC (641).

There are several biomarkers of OC that have been explored as ADC targets due to their differential expression including mesothelin, folate receptor 1, ephrin type-A1 receptor and mucin1 (421, 642, 643). Like TSPAN6, all these proteins are attractive targets for cancer therapy because of their cell surface location and differential expression between normal tissue and cancer. Mesothelin was originally identified as a cancer biomarker by the characterisation of an antibody targeting OC cells. Like TSPAN6 it is a cell surface receptor that is largely membrane bound. Mesothelin binds to MUC16 antigen which is also overexpressed in OCs. Compared to mesothelin, TSPAN6 is under researched whilst being similar in terms of cellular location and overexpression in OC. Folate receptor 1 is overexpressed in multiple epithelial-derived tumours such as ovarian, breast, renal, lung, colorectal and brain. Similar to TSPAN6, folate receptor 1 is a membrane bound protein and has been linked to neurological diseases (642). Ephrin-A1 is a cell surface protein belonging to a family receptor tyrosine kinases crucial for cell migration, repulsion and adhesion during neuronal, vascular and epithelial development (644). Like TSPAN6, Ephrin-A1 is upregulated in several cancers including colorectal cancer and breast cancer and is minimally expressed in healthy tissues throughout the body (301, 434). Mucin1 is an extensively researched cell membrane and secreted protein that is well documented to be

involved in promoting tumour progression (645). Compared to TSPAN6, Mucin1 is much more extensively researched and a considerably larger protein at 122 kDa compared to the 27 kDa TSPAN6 protein but has similarities in terms of cellular location, links to cancer progression and cellular signalling. Thus, our data gives confidence that TSPAN6 expression profile fulfils the desire properties of ADC target expression profile.

Data presented here demonstrate that TSPAN6, PCSK4 and RAGE antibodies can be found within the lysosomal compartment after 4hrs, demonstrating increased accumulation in lysosomes over time. Overall, this data provides further evidence that these antibodies can internalize into the cell and traffic to the appropriate subcellular location (late endosome, lysosome) where the potential ADC would release the drug payload. This receptor-mediated endocytosis capability is key given that it has been reported that non- internalized ADCs can induce significant systemic toxicity including a 'bystander effect'. The enhanced lysosomal accumulation of antibodies targeting these proteins is a desirable property of therapeutic targets of ADCs that require payload delivery to the intracellular environment. Compared to the optimal time point here of 4 hours, HER2 has been shown to internalise up to 12 hours before plateauing (646). The comparatively earlier internalisation time displayed here with these 3 targets can be advantageous by reducing toxicity and a faster mode of action. Therefore, these results suggest these targets are suitable for the production of ADCs.

Interestingly, it was observed that the coincubation of the cells with antibodies against TSPAN6 or RAGE did not inhibit the internalisation capacity of these receptors. This could be exploited for the development of a TSPAN6/RAGE bispecific ADC to enhance the binding specificity of an ADC to malignant cells. Binding multiple targets results in a greater likelihood of toxic payload delivery specifically to malignant cells. Bispecific antibodies have an advantage over monoclonals due to their higher binding avidity to targets, which can interact with more than one surface antigen; higher cytotoxic effects because of the direct recruitment of effector cells to the site of the disease; and in tumorigenic conditions, have less resistance to development due to the targeting of two different antibodies.

Genetic stability of the DNA coding region of the ADC epitope is paramount to the success of an ADC and the antibody epitope DNA coding region of TSPAN6 and RAGE was highly genetically stable with 95-99% of the reads matching the reference sequence in all 96 samples. Mutations in the DNA coding region of the epitope could result in reduced binding efficiency and therefore reduced efficacy as a therapeutic. This is exemplified by the identification of an activating mutation in the extracellular domain of HER2 which results in resistance to monoclonal antibody

therapy Pertuzumab (647). This highlights the necessity of confirming the genetic stability of the DNA coding region of the ADC target epitope as demonstrated in chapter 6.

Chapter 7 uses sRAGE as a preliminary biomarker to explore a blood serum liquid biopsy pipeline using an ELISA for the diagnosis of OC. The lower abundance of sRAGE in the serum of OC patients will confer an advantage for ADC development, due to the low quenching activity of the circulated target on the concentration of ADC in the bloodstream (318). In addition, given that RAGE target could be shredded from the cell membrane the low levels of circulating RAGE could indicate this process is not enhanced in OC patients. Thus, decreasing the probability of resistance to RAGE ADC therapies due to low target expression. In this context it has been reported that breast tumours expressing a truncated form of HER2 (p95HER2) are resistant to trastuzumab therefore other therapies and additional anti-HER2–targeting strategies are needed for these patients (648).

8.2 Novel ADC pipelines

High throughput screening for novel ADC targets rather than the in-depth characterisation of a new target is a highly under researched area (649). Many new targets are being investigated for their implications in various cancers, but little research is put into the large-scale screening of proteins for their anomalous expression in various cancers. Recently, a study (650) focused on identifying novel ADC targets in a broad range of tumours. In this study, PubMed and ClinicalTrials.gov were used to search for ADCs that are or were evaluated in clinical trials. Gene expression profiles of patient-derived tumour samples were collected, and Functional Genomic mRNA profiling was applied to predict per tumour type, the overexpression rate at the protein level of ADC targets. The approach described in this thesis instead used a mathematical algorithm to identify cell surface receptors that were overexpressed in OC while being minimally expressed in a healthy ovary. Both the approaches used patient-derived samples whereas this thesis did not use Functional Genomic mRNA profiling but instead chose to focus on protein expression assays and NGS.

It is clear that there is no consensus on the 'best' molecular target for OC. Out of the antibody therapies listed in Table 8-1 and Table 8-2 below, 8 of which are ADCs, there are distinct molecular targets, just 3 of which are common to more than one product; mesothelin, folate receptor 1 and CA125 currently in development . These targets are 'classical' tumour markers. Folate receptor 1 is also a target for small molecule development programmes, including Merck/Endocyte's vintafolide, which recently failed in Phase III. Farletuzumab, Eisai's anti folate receptor 1 antibody has also recently failed in Phase III.

Other targets include more recently discovered markers, such as sodium-dependent phosphate transporter protein 2b, the target for MedImmune's most recent ADC development programme in OC (419). This is not an exhaustive list, and it is likely that many more antibodies and ADCs are being developed in academic and industrial laboratories for which public domain information is not yet available. Furthermore, a subset of the many antibodies in development for 'solid tumours' may be positioned as OC drugs as they are developed, where the target shows tumour selectivity in this indication. For example, MedImmune/AstraZeneca and Genentech/Roche's pipelines show several antibodies in development for 'solid tumours' in Phase I, with specific cancer indications being investigated in later trials.

Table 8-1 Antibody drug conjugates in development (recently terminated) for OC

Drug	Company	Alternative names	Mode of action	Current stage of development in OC
Humanized IgG1 anti-MSLN conjugated to MMAE	Roche/Genentech	DMOT4039A	ADC targeting mesothelin	Phase I/IIa 19 OC patients (some efficacy)[i]
Anti-CA6-DM4 conjugate	ImmunoGen/Sanofi	SAR566658	ADC Targeting CA6	Phase I in 2010 (current status unknown)
Maytansinoid conjugated humanized monoclonal antibody against FOLRI	ImmunoGen	IMGN853	ADC targeting folate receptor 1	Phase 3 clinical trial FORWARD1 results announced on 2019.
Antibody drug conjugate consisting of a humanized IgG1 anti-NaPi2b monoclonal antibody and monomethyl auristatin E	MedImmune		ADC targeting sodium-dependent phosphate transporter protein 2b	Phase 1 data reported in 2019 (current status unknown)
Humanized IgG antibody against TROP2	Immunomedics	Sacituzumab govetican	ADC targeting Trop2, an antitrophoblastic cell surface antigen.	A phase I trial data reported for OC, approved as treatment for metastatic triple-

274

conjugated to SN-38, a camptothecin				negative breast cancer (2016)
Calicheamicin	MedImmune		ADC targeting ephrin type-A4 receptor	Terminated after phase I clinical trials due to limited response to adequate exposure of the ADC in patients
Thiomab ADC made up of a humanized anti-MUC16 IgG1 linked by a protease labile linker through engineered cysteine to the antimitotic payload, MMAE.	Roche	DMUC4064A	ADC targeting MUC16	The phase I trial completed enrolment of 35 patients in 2018, but results are not yet reported (NCT02146313)
Humanized IgG1 antibody targeting protein tyrosine kinase 7 (PTK7) conjugated by a cleavable valine-citrulline linker to MMAE	Pfizer Stemcentrx (now AbbVie) In collaboration with Indiana University	PF-06647020	ADC targeting protein tyrosine kinase 7 (PTK7)	Phase I evaluation of this drug is ongoing, with a planned expansion in patients with platinum-resistant OC combining PF-00647020 with Avelumab, a PD-1 inhibitor.

Table 8-2 - Unconjugated antibodies approved for use in OC

Drug	Company	Alternative names	EU/US Orphan drug register OC	Mode of action	Current stage of development in OC
Bevacizumab	Roche/Genentech	Avastin	EU and US	Antibody targeting VEGF	Approved in 2011 for recurrent disease. In various combination therapy trials.
Catumaxomab: Anti-epithelial cell adhesion molecule / anti-CD3 monoclonal antibody	Neovii Biotech GmbH/ Fresenius	Removab	EU and US	Rat/mouse hybrid trifunctional antibody targeting tumour cells, T-cells and accessory cells.	Phase II/III completed[ii]. Approved in EU (2009) in the European Union for the IP treatment of patients with malignant ascites (including OC)

Of the ADCs listed in Table 8-1, the Roche/Genentech's ADC DMOT4039A is an ADC targeted to mesothelin linked to monomethyl auristatin E (MMAE) with a lysosomal protease-cleavable valine-citrulline linker (421). A Phase I clinical trial was conducted in ovarian and prostate cancer patients (NCT01469793) and preliminary data was presented at the 2014 ASCO Annual Meeting. Primarily a safety study, the drug was found to be well tolerated at doses of 2.4 mg/kg. Adverse side effects were reported as fatigue, nausea, vomiting, decreased appetite, diarrhoea, and peripheral neuropathy. Of 10 OC patients treated at this dose, 3 showed a partial response based on RECIST (Response Evaluation Criteria in Solid Tumours: a set of published rules that define when cancer patients improve (respond), stay the same (stable) or worsen (progression) during treatments). A reduction in CA125 of more than 50% was observed in seven patients. They concluded from this trial data that the drug showed encouraging anti-tumour activity in

non-resectable pancreatic and OC, supporting further evaluation in these diseases (651). This is probably the most advanced ADC in development for OC currently. Bayer is also developing an ADC targeting mesothelin for OC, linked to the maytansinoid tubulin inhibitor DM4. Preclinical results were published in 2014 (652).

Sanofi Aventis/ImmunoGen has not published 2010 Phase I data from the ADC targeting CA6, SAR566658. In 2013 a new immunoassay was published to support the development of this drug, and it appears in the pipelines of both companies. The reason for the hiatus in its development is not known.

ImmunoGen's ADC targeting folate receptor 1, is the most promising of all ADCs included in Table 8-1. Mirvetuximab soravtansine showed impressive results in efficacy and tolerability in OC patients, particularly in those with a high folate receptor 1 expression. The randomised phase 3 trial will see 366 randomised patients receiving either Mirvetuximab soravtansine or a single agent chemotherapy. The response rate was documented to be higher for Mirvetuximab soravtansine when compared to chemotherapy. Mirvetuximab soravtansine was shown to be well tolerated with fewer patients experiencing grade 3 or greater adverse events, fewer dose reductions and fewer discontinuations due to drug-related adverse events when compared to chemotherapy (653).

A Phase I/II trial of MedImmune's ADC, MEDI-547 was started in 2008 (NCT00796055), but terminated in 2011 with no published data. This drug, targeting ephrin type-A2 receptor had been tested extensively in preclinical studies and showed much promise. MedImmune has also withdrawn its orphan drug application for an ADC, targeting ephrin type-A4 (654). MedImmune's most recent addition to its orphan drug portfolio, ADC targeting sodium-dependent phosphate transporter protein 2b has not yet entered clinical trials, but the detailed immunohistochemical analysis was published in 2012 to validate the target prior to its orphan drug registration in 2014.

However, there are two unconjugated antibodies that have achieved market approval for a subset of OC patients. Bevacizumab is approved in the US and EU for platinum-resistant recurrent disease (but not sanctioned for use in the NHS by NICE). It is still being tested in the clinic in combination with other small molecules and biological agents (655). Catumaxomab has recently been approved in the EU for the treatment of cancer patients with malignant ascites (656).

These data demonstrate how difficult and challenging the ADC landscape is when even targets showing desirable properties *in vitro*, later failed through the development pipeline.

New research regarding proteins involved in various cancers is published at a rapid rate (657, 658). The ability to regularly screen this cohort of proteins increases the likelihood of finding a highly selective ADC target that can specifically stratify malignant cells from non-cancer cells. This thesis found the algorithm screening to be effective with 3 out of the 6 initial targets showing significant promise.

A screening and initial characterisation process, such as the one displayed in this thesis, also has significance for the development of treatments for other cancers not discussed here. This clinical development pipeline focused on the identification of targets suitable for the stratification of malignant cells in gynaecological malignancies, however, the same pipeline can also be used to identify targets with aberrant expression in many other types of cancer.

The approval of ADCs to the market has increased rapidly in the last 5 years and with the ability to screen, narrow down and characterise more novel ADC targets, this number is expected to increase within the next 10 years. To increase the identification of efficacious targets in the future further research must be carried out to further understand the roles of various proteins in cancers. Further high-throughput screening to identify novel targets based on membrane expression and over expression in malignant cells would quickly identify efficacious targets.

8.3 TSPAN6 as a therapeutic target for the development of novel Antibody-Drug Conjugates

TSPAN6 is a novel membrane bound protein that was identified only 23 short years ago (499), with scarce information available in the form of publications. Its novelty and lack of research data, coupled with its aberrant expression in OC subtypes (301), mark it as significant for investigation as a potential ADC target. TSPAN6 is a small, 245 amino acids long protein, which could provide an advantage for use as an ADC as smaller targets are shown to internalise more effectively (450).

TSPAN6 was shown to internalise into various OC cells which supports the literature that reports that TSPAN6, acting as part of the tetraspanin web, to be involved in the clathrin and caveolin internalisation rout for viruses such as HPV16 (509). This supported and confirmed the ability of TSPAN6 to internalise itself and its ligand into the cell *via* receptor mediated endocytosis.

A high conservation of TSPAN6 between species homologues suggested genetic stability and biological importance (533). This has significance for future *in vivo* experiments as all common species conservatively express TSPAN6. Additionally, an ADC directed against TSPAN6 using this antibody epitope is highly likely to successfully bind to a very high number of patients, and a

very high number of TSPAN6 positive cells within the same patient. This suggests that the vast majority of patients could benefit from the effect of a TSPAN6 ADC. TSPAN6 is shown to be upregulated in the malignant tissues of patients with breast cancer, cervical cancer, endometrial cancer and colorectal cancer (301). This suggests that an ADC targeting TSPAN6 could be extended to benefit patients with these additional cancers as well.

Exosomes are small extracellular vesicles that have been reported to be involved in the progression of cancer (537, 659, 660). TSPAN6 has been linked to exosomes in a number of studies where TSPAN6 negatively regulates exosome production (534) and where it determines exosome release and lysosomal degradation of amyloid precursor protein fragments in Alzheimer's disease (661). With TSPAN6 being involved in exosome production and release and exosomes being linked to cancer it is possible that TSPAN6 could be aberrantly expressed in cancers due to its association with exosomes and has been linked to cancer progression in a number of studies (662, 663).

RAGE has been used as an example of a well-established ADC target within the group that has already been through this pipeline for characterisation (200, 201). TSPAN6, like RAGE, has reported association with inflammation and Alzheimer's Disease. TSPAN6 is reported to be involved with Alzheimer's disease, where the downregulation of TSPAN6 in primary neuronal cultures reduced amyloid beta production significantly (540). TSPAN6 is also associated with inflammation (527) , a known hall mark of cancer (529), which promotes the significance of its investigation. It has been reported that TSPAN6 negatively regulates immune signalling and an impaired immune response results in IFNs and inflammatory cytokines not being produced causing autoimmune and inflammatory related diseases. There is a possibility that TSPAN6 ADC treatment could impact the immune system. By reducing TSPAN6 expression it could increase IFNs/cytokines and could promote cancer development. This could be assessed by long term studies and toxicity evaluation. ELISAs could also be used to determine if IFNs/cytokine activity has changed due to treatment with a TSPAN6 ADC.

A limitation of the 2D cell data from TSPAN6, and the other novel targets, is that the lack of regular mycoplasma testing and no cell verification protocol. Cell validation is particularly important for patient-derived cell lines which are notoriously difficult to generate as there is a strong likelihood for stromal cells to take over. This will need to be considered if the data is to move towards the publication stage. Finally, as with all clinical studies, a larger sample size would increase statistical power.

8.4 The significance of developing a pipeline for detection of OC

The significance of developing a pipeline for the detection of OC is invaluably high when it comes to the increased chance of survival for OC patients. It is common for blood biomarkers to be non-specific and aberrantly expressed in other pathologies (664). The task of finding the protein that is specifically aberrantly expressed in the cancer of interest can be described as challenging due to the sheer vast number of proteins that are expressed in the blood (665).

This thesis followed a pipeline from the identification of possible targets to their characterisation and finally through to their potential as a diagnostic biomarker for the early detection of OC. The significance of this in terms of patient benefits is invaluable. The possibility of having a blood test for OC could simplify the current diagnostic pathway and could serve as a screening tool. The faster a unique blood biomarker indicative of OC can be found; the more lives will be saved. A unique blood biomarker is more likely to be discovered if a fast-screening process to identify these targets is developed.

Presently, CA125 serum levels are the current first line screening test for OC. A recent study (666) used the blood serum of 49 women who went onto develop OC and 31 control women, who were cancer free, and used proteomics-based biomarker discovery to identify novel biomarkers. Multimarker longitudinal models were derived and tested against CA125. The best performing models incorporate CA125, HE4. CHI3L1, PEBP4 and AGR2. In comparison to the pipeline developed in this thesis, this study used proteomics-based biomarker discovery whereas here a mathematical algorithm was used to identify suitable targets.

It is agreed that whilst much research has been carried out, little progress has been made in the identification of novel biomarkers for OC. More recently, in 2019, Russell *et al* (667) explored using four biomarkers, (CA125, phosphatidylcholine-sterol acyltransferase, vitamin K-dependent protein Z and C-reactive protein) in the early detection of OC. They concluded that the biomarker panel has the potential to diagnose OC 1-2 years earlier than the current standard. The studies described in the advancement of early diagnosis of OC all have in common that they identify a panel of multiple biomarkers. In relation to the preliminary data described here, the ELISA is a sensitive and high throughput method of testing any biomarker found in the serum in the cohort of patients recruited to the Ovarian Biomarker Study. This approach could lead to the discovery of a panel of novel biomarkers to be used in combination with a simple blood test that could significantly aid and speed the diagnosis pathway for OC.

These results are the beginning of a much broader application to OC diagnosis and treatment. The data shown here is the preliminary data before animal models and is an essential requirement before the progression to clinical trials. The crucial preclinical studies that will need

to be carried out include antibody validation using a knockout cell line to enable and strengthen a more in-depth target investigation, the production of a monoclonal antibody, the production of an ADC and finally the testing of the ADC in animal models. This data has great implications for OC but also has potential to expand to how targets for treatment are discovered in other cancers and human diseases.

8.5 Soluble RAGE in the blood serum as a diagnostic indicator of OC

The majority of research carried out by members of the RBGO group at Swansea University is pertaining to full-length membrane bound RAGE. This thesis explored RAGE in more depth, by investigating its soluble isoform in the blood serum of patients recruited to the Ovarian Biomarker study.

RAGE is a multiligand protein of the immunoglobulin super family and is expressed on the membrane of multiple cell types and is implicated in the inflammatory response, diabetes, Alzheimer's Disease and various cancers (200-202). Any correlation between full length RAGE and soluble RAGE in the blood is not yet fully understood. It is theorised that they are inversely correlated due to a reduction in sRAGE in pathologies where full-length RAGE is overexpressed (217).

This is supported by the RAGE ELISA data in chapter 7 where sRAGE was statistically significantly reduced in the blood serum of HGSOC patients when compared to non-cancer patients. The identification of a protein blood biomarker suitable for the early detection of OC has a high significance for the improved survival rate of OC patients because of faster treatment. The identification of such a biomarker would not have been possible if the full-length isoform of RAGE had not been identified by members of the RBGO group as a promising ADC target (200, 201). This suggests that the pipeline for identifying novel ADC targets could incorporate the screening of any soluble isomers for their use as diagnostic indicators.

The decreased expression of soluble RAGE shown in the ELISA results can have significant implications for subsequent treatment with a RAGE directed ADC. A reduced abundance of sRAGE in the blood serum can result in more ADC molecules binding to the full-length membrane bound RAGE and having its desired therapeutic effect, rather than binding to decoy sRAGE isoform in the blood serum which could reduce the therapeutic effect of the ADC treatment.

Soluble RAGE abundance in the blood serum also can become part of a panel of biomarkers for the early diagnosis of OC. Used alone, in the dataset investigated here, soluble RAGE can only stratify HGSOC patients from non-cancer ones. If used in conjunction with other known

biomarkers such as CA125 and HE4 then sRAGE could contribute to the development of a more reliable diagnostic test for the early detection of OC.

Soluble RAGE is only capable of stratifying HGSOC patients from non-cancer ones. Interestingly, He and colleagues examined the association of circulating sRAGE in multiple types of cancer by conducting a comprehensive meta-analysis using the ELISA technique to assess the abundance of sRAGE in the blood of various cancer patients (668). The potential role of transmembrane full RAGE protein and its ligands in cancer have been widely investigated and supported the notion of targeting RAGE directly as part of an effective therapeutic regime against cancer using ADCs (200, 669). An effective means to antagonize RAGE is to use its soluble form (sRAGE), with sRAGE levels potentially reflecting the activity of the ligand-RAGE axis. Several studies have stressed the importance of circulating sRAGE as a protective factor against cancer development by inhibiting the unfavourable influence of RAGE–ligand axis in angiogenesis, fibroblasts and macrophage activation (277). The sRAGE has been documented as an anti-angiogenic and tumour regressive molecular and a low level of circulating sRAGE was reported to be a significant risk factor for many types of cancer, such as breast cancer (670) and lung cancer (312). In this context data shown in this thesis supports the effect of sRAGE as a protective factor with non-cancer patients exhibiting high levels of sRAGE in circulation compared to patients suffering from aggressive HGSOC. However, in our study levels of sRAGE alone were not able to stratify OC in general. However, several possible limitations of our study should be considered. First, despite a panel of subgroup analyses had been undertaken, significant heterogeneity persisted in some subgroups, limiting the interpretation of the data. Moreover, considering the relatively small sample sizes in subgroups, more studies are warranted to quantify the effect reliably. Additionally, our study had circulating sRAGE measured only once and did not reflect the long-term level of sRAGE in the progression of cancer. This data came from only one data set, which needs to be acknowledged as a limitation. Independent analysis from multiple larger datasets would verify the findings.

8.6 Study limitations

Despite the volume of data, many of the results presented here are negative results therefore the limitations will be discussed here in the context of improving future experiments. Firstly, across all the experiments, as with many clinical based studies, the overall sample size would benefit from being larger to increase result validation and add statistical power. This is true of the sRAGE ELISA experiments, the western blots, the fluorescent microscopy, and the sequencing data. Further to this, a limited number of cell lines were used in preliminary

experiments such as initial western blots and the internalisation time point analysis. In future work, it would be very beneficial to include as many cell lines as time and cost allow to deepen the understanding, particularly around internalisation time points and fully optimise the main experiment. Furthermore, the antibody specificity for some targets is not definitive and could use further exploration to strengthen them as an ADC target. For example, all the targets apart from TSPAN6 had a negative western blot. Its likely that the issue was with the antibody chosen rather than the target protein or samples themselves. Therefore, it would be beneficial in a more focused analysis to acquire and test different antibodies against the same target due to different antibodies behaving differently in different applications. Antibody validation could be strengthened here by the production of a knockout cell line which would act as a true negative control. In terms of the western blot, a true negative and positive control protein sample should be obtained to validate the use of the antibodies in western blots where proteins are in a linear conformation. This would strengthen all the immunofluorescent work and in particular, further validate the internalisation work.

The whole project is highly focussed on one single data set. All the 2D cells derived from patient biopsies, the protein extracted from 2D cells derived from patient biopsies and the serum used in the sRAGE ELISA experiments are all from the single data set from the ovarian biomarker study. To strengthen, validate and add statistical power to results, the sample size should be increased, and other data sets included.

Finally, cell validation and mycoplasma testing of 2D cells derived from patient biopsies should be carried out as routine with all samples obtained. Cell validation is important, especially in cancer cells extracted from a tissue source which could easily not be the expected cell. Short Tandem Repeat profiling is the test that most journals require, where PCR amplicons are generated using primers for that region and visualised using capillary electrophoresis. This can be done in house, if the right kit is obtained providing a well-known Short Tandem Repeat is available. This avoids the need to buy primers and optimise PCR experiments. Alternatively, the cell lines could be sent away and the cell validation outsourced to a different lab. Cancer cell lines can have many mutations and deletions which would require careful analysis and data interpretation, which may again need to be outsourced if researchers are not experiences with this type of molecular biology data analysis.

Mycoplasma testing is a simple PCR that can be done in house to detect any contamination. Mycoplasma is a surprisingly frequent, invisible, contaminant present in around 15-35% of cell cultures. Mycoplasma can affect cell metabolism, increase sensitivity to inducers of apoptosis

or inhibit cell growth. Mycoplasma can be easily tested for using an in-house PCR. In the future, this should be carried out as standard for all cell lines.

8.7 Future Work

Two pipelines were explored in this thesis, and these pipelines could be used again to identify additional targets of interest. The algorithm could be improved and used again to scan the human proteome, which has been updated since 2016 when the spreadsheet list of targets was first generated. This can identify new targets for consideration. Many more publications have been made available since 2016, shedding light on the functions and pathways these proteins are involved in, to further help narrow down and identify promising targets (433).

One of the biggest advantages of this thesis is the access to the samples from the ovarian biomarker study. Having the opportunity to perform analysis in samples derived from patient biopsies is an invaluable resource for the characterisation of novel ADC targets. The bank of samples only grows larger as the years progress, which brings the advantage to future projects of a larger more diverse sample size. The ELISA can be repeated with an increased number of samples to uncover more representative results. The number of less common subtypes will also increase, allowing for the sample size in experiments involving these samples to increase again. The ELISA can quickly and easily be repeated to screen different targets as the algorithm generates more possibilities.

The six targets already identified here can be explored in more detail. The three targets eliminated in chapter 3 could be given more time and consideration. Different antibodies with different epitope regions targeting these proteins could be tested to identify and optimise an antibody that gives a clear specific western blot and clear membrane localisation with a good ability to internalise.

TSPAN6 and RAGE can be characterised in more depth by increasing the sample size and diversity in all experiments. TSPAN6 and RAGE can also be further analysed using Illumina NGS techniques. Alternative antibodies with different epitope regions may be tested against these targets and the DNA coding region of these epitopes could also undergo deep amplicon sequence variant analysis to confirm the genetic stability of these targets. The whole TSPAN6 or RAGE gene could also can be sequenced to further reveal polymorphisms and genetic stability. Once characterised in more depth, any of the promising targets identified here, such as TSPAN6, could be moved into an animal model for *in vivo* toxicity analysis.

Validation of multiple antibodies against a lead target molecule could be quickly determined with the generation of a target knockout cell line. One of the biggest challenges of this project was the lack of a true negative control. Validation of the antibody was difficult due to IOC

immortalised cell line not truly representing healthy cells coupled with the uncertainty that the healthy control patients with no described ovarian pathology had no other undiagnosed pathologies. The best agreed way to truly validate the binding specificity of an antibody is to use a knockout cell line to identify any non-specific binding. This process however was unsuccessful when tried in the past and can be very costly to outsource.

The identification of the distinct '60 KDa' band in the western blots undertaken with TSPAN6 in protein derived from a 3D source would be of great interest to follow up. This can stratify patients using this previously undocumented isomer. There are doors open to exploring this band in a larger number of samples derived from a 3D source and from 3D spheroids grown *in vitro*. Post-translational modification of proteins can be experimentally detected by a variety of techniques, including mass spectrometry, Eastern blotting, and Western blotting. This would determine if the 60 KDa band was a result of post-translational modifications determine the potential predictive value of the 60 KDa band.

Different antibodies against the targets can be screened for binding affinity and kinetics using a Biacore. The difficulty of the pipeline reported here is that it is a balancing act when choosing to screen more targets or screen more antibodies against the targets already identified. The Biacore could offer a quick screening method for various antibodies purchased against the chosen targets. However, this can become expensive as multiple antibodies are purchased against several targets.

There is a potential for preclinical trials to validate the efficacy of the candidate ADCs for the treatment of OCs. This can be carried out as tolerability and toxicity studies in 2D and 3D models *in vitro* before further expansion to *in vivo* animal models. There is a need for further exploration on the utility of ADCs against different OC subtypes. The functional consequence of targeting the proteins identified needs to be considered as this could affect cancer growth by stimulating an inflammatory response. Additionally, the route of delivery needs to be considered. The ADC could be administered locally to the affected area or systemically depending on several factors including the type of cancer being treated. The bystander effect needs to be considered if the ADC is to be administered systemically to avoid off target toxicity. Furthermore, any anticipated side effects need to be identified and addressed as the ADC moves through initial animal model analysis and eventually human clinical trials.

To better identify novel ADC targets in the future, the process needs to be comprehensive, easily repeatable as new data is released and high throughput. The method using a mathematical algorithm to search data bases for appropriate targets should be refined and made user friendly to be used by other group members as well as being expanded to include more databases as

they become available. The narrowing down of this list is what takes quite some time and manual effort on behalf of an individual researcher. Potentially, another algorithm could be designed to check for patents and commercially available antibodies to further narrow the list. To quickly check both expression and localisation, immuno-fluorescent experiments could be done using a high throughput machine such as an in-cell analyser in 96 well plate format on a confirmed positive and negative control cell line. Once expression and localisation to the membrane has been confirmed using an antibody validated in immuno-fluorescence, more focused work can begin on lead candidate targets. Different antibodies should also be considered against the selected targets. However, this process would still be long and costly. Future work should focus on shortening the time it takes to go through the identification pipeline to assess more targets. The focus should be on the over expression of the targets on the plasma membrane of OC cells whilst showing minimal expression on the plasma of the healthy ovary cells.

8.8 Conclusions

This thesis demonstrated the ability to identify, screen and characterise six novel ADC targets for the treatment of OC. In addition, this thesis took sRAGE and determined it can statistically significantly stratify HGSOC patients from non-cancer patients, however sRAGE could not confidently diagnose OC in earlier less aggressive stages.

This thesis identified TSPAN6 as the most promising target due to its confirmed plasma membrane location in 2D cell lines and 2D cells derived from patient biopsies. TSPAN6 was also shown to have more internalisation in 2D cells derived from HGSOC patients when compared to non-cancer patients. TSPAN6 was also the only target to produce a clear specific band in western blot which identified its aberrant expression in various proteins derived from 2D OC cell lines, patient biopsies and commercially purchased protein lysates. The identification of a previously undocumented 60 KDa band was identified when analysing TSPAN6 expression in protein derived directly from patient tissue biopsies. Finally, for TSPAN6, the epitope DNA coding region was reported to be genetically conserved in over 95% of reads in all 96 patients.

The results reported in this thesis, from the confirmation of vital ADC characteristics to the genetic stability of these targets and the preliminary exploration of a liquid biopsy method for the diagnosis and stratification of OC patients has the potential to initiate a programme of research with significant impact on the health, quality of life and survival of women with ovarian cancer worldwide.

Chapter 9: Bibliography

1. Mara JN, Zhou LT, Larmore M, Johnson B, Ayiku R, Amargant F, et al. Ovulation and ovarian wound healing are impaired with advanced reproductive age. Aging (Albany NY). 2020;12(10):9686-713.
2. Richards JS, Pangas SA. The ovary: basic biology and clinical implications. J Clin Invest. 2010;120(4):963-72.
3. Piprek RP, Kloc M, Kubiak JZ. Early Development of the Gonads: Origin and Differentiation of the Somatic Cells of the Genital Ridges. Results Probl Cell Differ. 2016;58:1-22.
4. Keith L. Moore AFDaAMRA. Clinically Oriented Anatomy. 8th ed: Wolters Kluwer; 2018.
5. Dubeau L, Drapkin R. Coming into focus: the nonovarian origins of ovarian cancer. Ann Oncol. 2013;24 Suppl 8:viii28-viii35. 10.1093/annonc/mdt308
6. Labidi-Galy SI, Papp E, Hallberg D, Niknafs N, Adleff V, Noe M, et al. High grade serous ovarian carcinomas originate in the fallopian tube. Nat Commun. 2017;8(1):1093.
7. Dubeau L. The cell of origin of ovarian epithelial tumours. Lancet Oncol. 2008;9(12):1191-7.
8. Lakshmanan M, Gupta S, Kumar V, Akhtar N, Chaturvedi A, Misra S, et al. Germ Cell Tumor Ovary: an Institutional Experience of Treatment and Survival Outcomes. Indian J Surg Oncol. 2018;9(2):215-9.
9. Quirk JT, Natarajan N. Ovarian cancer incidence in the United States, 1992-1999. Gynecol Oncol. 2005;97(2):519-23.
10. Smith HO, Berwick M, Verschraegen CF, Wiggins C, Lansing L, Muller CY, et al. Incidence and survival rates for female malignant germ cell tumors. Obstet Gynecol. 2006;107(5):1075-85.
11. Coffman LG, Pearson AT, Frisbie LG, Freeman Z, Christie E, Bowtell DD, et al. Ovarian Carcinoma-Associated Mesenchymal Stem Cells Arise from Tissue-Specific Normal Stroma. Stem Cells. 2019;37(2):257-69.
12. Khan AT, Shehmar M, Gupta JK. Uterine fibroids: current perspectives. Int J Womens Health. 2014;6:95-114.
13. Wood BJCaDL. The Human Body in Health and Disease 9th ed: Lippincott Williams and Wilkins; 2000.
14. Bowtell DD. The genesis and evolution of high-grade serous ovarian cancer. Nature reviews Cancer. 2010;10(11):803-8.
15. Momenimovahed Z, Salehiniya H. Epidemiological characteristics of and risk factors for breast cancer in the world. Breast Cancer (Dove Med Press). 2019;11:151-64.
16. Deng S, Lin Z, Li W. Recent Advances in Antibody-Drug Conjugates for Breast Cancer Treatment. Curr Med Chem. 2017;24(23):2505-27.
17. Torre LA, Trabert B, DeSantis CE, Miller KD, Samimi G, Runowicz CD, et al. Ovarian cancer statistics, 2018. CA Cancer J Clin. 2018;68(4):284-96.
18. Babaier A, Ghatage P. Mucinous Cancer of the Ovary: Overview and Current Status. Diagnostics (Basel). 2020;10(1).
19. Network CGAR. Integrated genomic analyses of ovarian carcinoma. Nature. 2011;474(7353):609-15.
20. Pierson WE, Peters PN, Chang MT, Chen LM, Quigley DA, Ashworth A, et al. An integrated molecular profile of endometrioid ovarian cancer. Gynecol Oncol. 2020;157(1):55-61.
21. Salcedo-Hernández RA, Lino-Silva LS, Cantú de León D, Pérez-Montiel MD, Luna-Ortiz K. Ovarian undifferentiated carcinoma with voluminous mesenteric presentation. Int J Surg Case Rep. 2012;3(11):551-4.
22. Shu CA, Zhou Q, Jotwani AR, Iasonos A, Leitao MM, Konner JA, et al. Ovarian clear cell carcinoma, outcomes by stage: the MSK experience. Gynecol Oncol. 2015;139(2):236-41.
23. Koshiyama M, Matsumura N, Konishi I. Subtypes of Ovarian Cancer and Ovarian Cancer Screening. Diagnostics (Basel). 2017;7(1). 10.3390/diagnostics7010012
24. Kaku T, Ogawa S, Kawano Y, Ohishi Y, Kobayashi H, Hirakawa T, et al. Histological classification of ovarian cancer. 10.1007/s007950300002
25. Rojas V, Hirshfield KM, Ganesan S, Rodriguez-Rodriguez L. Molecular Characterization of Epithelial Ovarian Cancer: Implications for Diagnosis and Treatment. Int J Mol Sci. 2016;17(12).
26. Web Pathology, Ovary (2018) [Online] Available from: https://www.webpathology.com/category.asp?category=114 Accessed: July 2021.

27.   Cancer Research UK, Ovarian cancer statistics, 2017, Accessed: 2020, [Online], Available from: https://www.cancerresearchuk.org/health-professional/cancer-statistics/statistics-by-cancer-type/ovarian-cancer#heading-Three.

28.   Cancer Research UK, Ovarian cancer statistics, 2017, Accessed 2020, [Online] Available from: https://www.cancerresearchuk.org/health-professional/cancer-statistics/statistics-by-cancer-type/ovarian-cancer#heading-Three.

29.   CancerReseachUK.   Ovarian   cancer   statistics   2017   [Available   from: https://www.cancerresearchuk.org/health-professional/cancer-statistics/statistics-by-cancer-type/ovarian-cancer#heading-Three.

30.   Klotz DM, Wimberger P. Cells of origin of ovarian cancer: ovarian surface epithelium or fallopian tube? Arch Gynecol Obstet. 2017 Dec;296(6):1055-1062. doi: 10.1007/s00404-017-4529-z. Epub 2017 Sep 23. PMID: 28940023.

31.   Testa U, Petrucci E, Pasquini L, Castelli G, Pelosi E. Ovarian Cancers: Genetic Abnormalities, Tumor Heterogeneity and Progression, Clonal Evolution and Cancer Stem Cells. Medicines (Basel). 2018;5(1). 10.3390/medicines5010016

32.   Karnezis AN, Cho KR, Gilks CB, Pearce CL, Huntsman DG. The disparate origins of ovarian cancers: pathogenesis   and   prevention   strategies.   Nat   Rev   Cancer.   2017   Jan;17(1):65-74.   doi: 10.1038/nrc.2016.113. Epub 2016 Nov 25. PMID: 27885265.

33.   Lengyel E. Ovarian cancer development and metastasis. Am J Pathol. 2010;177(3):1053-64.

34.   Karnezis AN, Cho KR. Preclinical Models of Ovarian Cancer: Pathogenesis, Problems, and Implications   for   Prevention.   Clin   Obstet   Gynecol.   2017   Dec;60(4):789-800.   doi: 10.1097/GRF.0000000000000312. PMID: 28719396; PMCID: PMC5843373.

35.   Jones PM, Drapkin R. Modeling High-Grade Serous Carcinoma: How Converging Insights into Pathogenesis and Genetics are Driving Better Experimental Platforms. Front Oncol. 2013;3:217. 10.3389/fonc.2013.00217

36.   Singh N, Gilks CB, Wilkinson N, McCluggage WG. The secondary Müllerian system, field effect, BRCA, and tubal fimbria: our evolving understanding of the origin of tubo-ovarian high-grade serous carcinoma and why assignment of primary site matters. Pathology. 2015 Aug;47(5):423-31. doi: 10.1097/PAT.0000000000000291. PMID: 26126051.

37.   Kurman RJ, Shih IeM. Molecular pathogenesis and extraovarian origin of epithelial ovarian cancer--shifting the paradigm. Hum Pathol. 2011 Jul;42(7):918-31. doi: 10.1016/j.humpath.2011.03.003. PMID: 21683865; PMCID: PMC3148026.

38.   Burney RO, Giudice LC. Pathogenesis and pathophysiology of endometriosis. Fertil Steril. 2012;98(3):511-9.

39.   Nezhat F, Datta MS, Hanson V, Pejovic T, Nezhat C, Nezhat C. The relationship of endometriosis and   ovarian   malignancy: a   review.   Fertil   Steril.   2008   Nov;90(5):1559-70.   doi: 10.1016/j.fertnstert.2008.08.007. PMID: 18993168.

40.   Ahn SH, Monsanto SP, Miller C, Singh SS, Thomas R, Tayade C. Pathophysiology and Immune Dysfunction in Endometriosis. Biomed Res Int. 2015;2015:795976.

41.   McConechy MK, Ding J, Senz J, Yang W, Melnyk N, Tone AA, Prentice LM, Wiegand KC, McAlpine JN, Shah SP, Lee CH, Goodfellow PJ, Gilks CB, Huntsman DG. Ovarian and endometrial endometrioid carcinomas have distinct CTNNB1 and PTEN mutation profiles. Mod Pathol. 2014 Jan;27(1):128-34. doi: 10.1038/modpathol.2013.107. Epub 2013 Jun 14. PMID: 23765252; PMCID: PMC3915240.

42.   Koshiyama M, Matsumura N, Konishi I. Recent concepts of ovarian carcinogenesis: type I and type II. Biomed Res Int. 2014;2014:934261. doi: 10.1155/2014/934261. Epub 2014 Apr 23. PMID: 24868556; PMCID: PMC4017729.

43.   Tanwar PS, Kaneko-Tarui T, Lee HJ, Zhang L, Teixeira JM. PTEN loss and HOXA10 expression are associated with ovarian endometrioid adenocarcinoma differentiation and progression. Carcinogenesis. 2013;34(4):893-901.

44.   Mandai M, Yamaguchi K, Matsumura N, Baba T, Konishi I. Ovarian cancer in endometriosis: molecular biology, pathology, and clinical management. Int J Clin Oncol. 2009 Oct;14(5):383-91. doi: 10.1007/s10147-009-0935-y. Epub 2009 Oct 25. PMID: 19856044.

45.   TheAmericanCancerSociety. Ovarian Cancer Risk Factors. 2020. [Online] Accessed: September 2021. Availble from: https://www.cancer.org/cancer/ovarian-cancer/about/key-statistics.html

46.   NHS. Causes of Ovarian Cancer. 2020. [Online] Accessed: September 2021. Availble from: https://www.nhs.uk/conditions/ovarian-cancer/causes/

47.   CDC. What are the risk factors for Ovarian Cancer? 2019. [Online] Accessed: September 2021. Available from: https://www.cdc.gov/cancer/ovarian/basic_info/risk_factors.htm

48.   Zhang M, Yang ZY, Binns CW, Lee AH. Diet and ovarian cancer risk: a case-control study in China. Br J Cancer. 2002;86(5):712-7.

49.   Crane TE, Khulpateea BR, Alberts DS, Basen-Engquist K, Thomson CA. Dietary intake and ovarian cancer risk: a systematic review. Cancer Epidemiol Biomarkers Prev. 2014;23(2):255-73.

50.   Tworoger SS, Huang T. Obesity and Ovarian Cancer. Recent Results Cancer Res. 2016;208:155-76.

51.   Olsen CM, Nagle CM, Whiteman DC, Ness R, Pearce CL, Pike MC, et al. Obesity and risk of ovarian cancer subtypes: evidence from the Ovarian Cancer Association Consortium. Endocr Relat Cancer. 2013;20(2):251-62.

52.   Leitzmann MF, Koebnick C, Danforth KN, Brinton LA, Moore SC, Hollenbeck AR, et al. Body mass index and risk of ovarian cancer. Cancer. 2009;115(4):812-22.

53.   Foong KW, Bolton H. Obesity and ovarian cancer risk: A systematic review. Post Reprod Health. 2017;23(4):183-98.

54.   La Vecchia C, Decarli A, Franceschi S, Regallo M, Tognoni G. Age at first birth and the risk of epithelial ovarian cancer. J Natl Cancer Inst. 1984;73(3):663-6.

55.   Troisi R, Bjørge T, Gissler M, Grotmol T, Kitahara CM, Myrtveit Saether SM, et al. The role of pregnancy, perinatal factors and hormones in maternal cancer risk: a review of the evidence. J Intern Med. 2018;283(5):430-45.

56.   Li DP, Du C, Zhang ZM, Li GX, Yu ZF, Wang X, et al. Breastfeeding and ovarian cancer risk: a systematic review and meta-analysis of 40 epidemiological studies. Asian Pac J Cancer Prev. 2014;15(12):4829-37.

57.   Liu Y, Ma L, Yang X, Bie J, Li D, Sun C, et al. Menopausal Hormone Replacement Therapy and the Risk of Ovarian Cancer: A Meta-Analysis. Front Endocrinol (Lausanne). 2019;10:801.

58.   Zhou B, Sun Q, Cong R, Gu H, Tang N, Yang L, et al. Hormone replacement therapy and ovarian cancer risk: a meta-analysis. Gynecol Oncol. 2008;108(3):641-51.

59.   Cook LS, Kamb ML, Weiss NS. Perineal powder exposure and the risk of ovarian cancer. Am J Epidemiol. 1997;145(5):459-65.

60.   Houghton SC, Reeves KW, Hankinson SE, Crawford L, Lane D, Wactawski-Wende J, et al. Perineal powder use and risk of ovarian cancer. J Natl Cancer Inst. 2014;106(9). DOI: 10.1093/jnci/dju208

61.   Rosenblatt KA, Weiss NS, Cushing-Haugen KL, Wicklund KG, Rossing MA. Genital powder exposure and the risk of epithelial ovarian cancer. Cancer Causes Control. 2011;22(5):737-42.

62.   Terry KL, Karageorgi S, Shvetsov YB, Merritt MA, Lurie G, Thompson PJ, et al. Genital powder use and risk of ovarian cancer: a pooled analysis of 8,525 cases and 9,859 controls. Cancer Prev Res (Phila). 2013;6(8):811-21.

63.   Kurta ML, Moysich KB, Weissfeld JL, Youk AO, Bunker CH, Edwards RP, et al. Use of fertility drugs and risk of ovarian cancer: results from a U.S.-based case-control study. Cancer Epidemiol Biomarkers Prev. 2012;21(8):1282-92.

64.   Diergaarde B, Kurta ML. Use of fertility drugs and risk of ovarian cancer. Curr Opin Obstet Gynecol. 2014;26(3):125-9.

65.   Brilhante AV, Augusto KL, Portela MC, Sucupira LC, Oliveira LA, Pouchaim AJ, et al. Endometriosis and Ovarian Cancer: an Integrative Review (Endometriosis and Ovarian Cancer). Asian Pac J Cancer Prev. 2017;18(1):11-6.

66.   Dawson A, Fernandez ML, Anglesio M, Yong PJ, Carey MS. Endometriosis and endometriosis-associated cancers: new insights into the molecular mechanisms of ovarian cancer development. Ecancermedicalscience. 2018;12:803.

67.   Pearce CL, Templeman C, Rossing MA, Lee A, Near AM, Webb PM, et al. Association between endometriosis and risk of histological subtypes of ovarian cancer: a pooled analysis of case-control studies. Lancet Oncol. 2012;13(4):385-94.

68.   Cibula D, Zikan M, Dusek L, Majek O. Oral contraceptives and risk of ovarian and breast cancers in BRCA mutation carriers: a meta-analysis. Expert Rev Anticancer Ther. 2011;11(8):1197-207.

69.   The reduction in risk of ovarian cancer associated with oral-contraceptive use. N Engl J Med. 1987;316(11):650-5.

70.   Zheng G, Yu H, Kanerva A, Försti A, Sundquist K, Hemminki K. Familial Ovarian Cancer Clusters with Other Cancers. Sci Rep. 2018;8(1):11561.

71.   Toss A, Tomasello C, Razzaboni E, Contu G, Grandi G, Cagnacci A, et al. Hereditary ovarian cancer: not only BRCA 1 and 2 genes. Biomed Res Int. 2015;2015:341723.

72.   Petrucelli N, Daly MB, Pal T. BRCA1- and BRCA2-Associated Hereditary Breast and Ovarian Cancer. 1998 Sep 4 [Updated 2016 Dec 15]. In: Adam MP, Ardinger HH, Pagon RA, et al., editors. GeneReviews® [Internet]. Seattle (WA): University of Washington, Seattle; 1993-2021.   Available from: https://www.ncbi.nlm.nih.gov/books/NBK1247/.

73.   Yarden RI, Pardo-Reoyo S, Sgagias M, Cowan KH, Brody LC. BRCA1 regulates the G2/M checkpoint by activating Chk1 kinase upon DNA damage. Nat Genet. 2002;30(3):285-9.

74.   Zhang J. The role of BRCA1 in homologous recombination repair in response to replication stress: significance in tumorigenesis and cancer therapy. Cell Biosci. 2013;3(1):11. DOI: 10.1186/2045-3701-3-11

75.   Roy R, Chun J, Powell SN. BRCA1 and BRCA2: different roles in a common pathway of genome protection. Nat Rev Cancer. 2011;12(1):68-78.DOI: 10.1038/nrc3181

76.   Meaney-Delman D, Bellcross CA. Hereditary breast/ovarian cancer syndrome: a primer for obstetricians/gynecologists. Obstet Gynecol Clin North Am. 2013;40(3):475-512.

77.   Steinke V, Engel C, Büttner R, Schackert HK, Schmiegel WH, Propping P. Hereditary nonpolyposis colorectal cancer (HNPCC)/Lynch syndrome. Dtsch Arztebl Int. 2013;110(3):32-8.

78.   Nakamura K, Banno K, Yanokura M, Iida M, Adachi M, Masuda K, et al. Features of ovarian cancer in Lynch syndrome (Review). Mol Clin Oncol. 2014;2(6):909-16.

79.   Dozois RR, Kempers RD, Dahlin DC, Bartholomeew LG. Ovarian tumors associated with the Peutz-Jeghers syndrome. Ann Surg. 1970;172(2):233-8.

80.   Win AK, Reece JC, Dowty JG, Buchanan DD, Clendenning M, Rosty C, et al. Risk of extracolonic cancers for people with biallelic and monoallelic mutations in MUTYH. Int J Cancer. 2016;139(7):1557-63.

81.   Yoneda A, Lendorf ME, Couchman JR, Multhaupt HA. Breast and ovarian cancers: a survey and possible roles for the cell surface heparan sulfate proteoglycans. J Histochem Cytochem. 2012;60(1):9-21.

82.   Gajjar K, Ogden G, Mujahid MI, Razvi K. Symptoms and risk factors of ovarian cancer: a survey in primary care. ISRN Obstet Gynecol. 2012;2012:754197.

83.   Committee on the State of the Science in Ovarian Cancer Research; Board on Health Care Services; Institute of Medicine; National Academies of Sciences, Engineering, and Medicine. Ovarian Cancers: Evolving Paradigms in Research and Care. Washington (DC): National Academies Press (US); 2016 Apr 25. 4, Diagnosis and Treatment.   Available from: https://www.ncbi.nlm.nih.gov/books/NBK367619/.

84.   NHS U. New test could improve diagnosis of ovarian cancer 2015 [Online] Accessed: September 2021. [Available from: https://www.nhs.uk/news/cancer/new-test-could-improve-diagnosis-of-ovarian-cancer/#where-did-the-story-come-from.

85.   Menon U, Skates SJ, Lewis S, Rosenthal AN, Rufford B, Sibley K, et al. Prospective study using the risk of ovarian cancer algorithm to screen for ovarian cancer. Journal of clinical oncology : official journal of the American Society of Clinical Oncology. 2005;23(31):7919-26.

86.   Skates SJ. OCS: Development of the Risk of Ovarian Cancer Algorithm (ROCA) and ROCA screening trials. International journal of gynecological cancer : official journal of the International Gynecological Cancer Society. 2012;22(Suppl 1):S24-S6.

87.   Menon U, Ryan A, Kalsi J, Gentry-Maharaj A, Dawnay A, Habib M, et al. Risk Algorithm Using Serial Biomarker Measurements Doubles the Number of Screen-Detected Cancers Compared With a Single-Threshold Rule in the United Kingdom Collaborative Trial of Ovarian Cancer Screening. Journal of clinical oncology : official journal of the American Society of Clinical Oncology. 2015;33(18):2062-71.

88.   Menon U, McGuire AJ, Raikou M, Ryan A, Davies SK, Burnell M, et al. The cost-effectiveness of screening for ovarian cancer: results from the UK Collaborative Trial of Ovarian Cancer Screening (UKCTOCS). British journal of cancer. 2017;117(5):619-27.

89.   Jacobs I, Oram D, Fairbanks J, Turner J, Frost C, Grudzinskas JG. A risk of malignancy index incorporating CA 125, ultrasound and menopausal status for the accurate preoperative diagnosis of ovarian cancer. Br J Obstet Gynaecol. 1990;97(10):922-9.

90.   Bouzari Z, Yazdani S, Shirkhani Kelagar Z, Abbaszadeh N. Risk of malignancy index as an evaluation of preoperative pelvic mass. Caspian J Intern Med. 2011;2(4):331-5.

91.   Van Holsbeke C, Van Calster B, Bourne T, Ajossa S, Testa AC, Guerriero S, et al. External validation of diagnostic models to estimate the risk of malignancy in adnexal masses. Clin Cancer Res. 2012;18(3):815-25.

92.   Meys EM, Kaijser J, Kruitwagen RF, Slangen BF, Van Calster B, Aertgeerts B, et al. Subjective assessment versus ultrasound models to diagnose ovarian cancer: A systematic review and meta-analysis. Eur J Cancer. 2016;58:17-29.

93. Chopra S, Vaishya R, Kaur J. An Evaluation of the Applicability of the Risk of Malignancy Index for Adnexal Masses to Patients Seen at a Tertiary Hospital in Chandigarh, India. J Obstet Gynaecol India. 2015;65(6):405-10.

94. Dochez V, Caillon H, Vaucel E, Dimet J, Winer N, Ducarme G. Biomarkers and algorithms for diagnosis of ovarian cancer: CA125, HE4, RMI and ROMA, a review. J Ovarian Res. 2019;12(1):28.

95. Moore RG, McMeekin DS, Brown AK, DiSilvestro P, Miller MC, Allard WJ, et al. A novel multiple marker bioassay utilizing HE4 and CA125 for the prediction of ovarian cancer in patients with a pelvic mass. Gynecol Oncol. 2009;112(1):40-6.

96. Li F, Tie R, Chang K, Wang F, Deng S, Lu W, et al. Does risk for ovarian malignancy algorithm excel human epididymis protein 4 and CA125 in predicting epithelial ovarian cancer: a meta-analysis. BMC Cancer. 2012;12:258.

97. Kaijser J, Van Belle V, Van Gorp T, Sayasneh A, Vergote I, Bourne T, et al. Prognostic value of serum HE4 levels and risk of ovarian malignancy algorithm scores at the time of ovarian cancer diagnosis. Int J Gynecol Cancer. 2014;24(7):1173-80.

98. Chen X, Zhou H, Chen R, He J, Wang Y, Huang L, et al. Development of a multimarker assay for differential diagnosis of benign and malignant pelvic masses. Clin Chim Acta. 2015;440:57-63.

99. Plebani M, Group HS. HE4 in gynecological cancers: report of a European investigators and experts meeting. Clin Chem Lab Med. 2012;50(12):2127-36.

100. Chandra A, Pius C, Nabeel M, Nair M, Vishwanatha JK, Ahmad S, et al. Ovarian cancer: Current status and strategies for improving therapeutic outcomes. Cancer Med. 2019;8(16):7018-31.

101. Schorge JO, McCann C, Del Carmen MG. Surgical debulking of ovarian cancer: what difference does it make? Rev Obstet Gynecol. 2010;3(3):111-7.

102. Dominguez-Valentin M, Crosbie EJ, Engel C, Aretz S, Macrae F, Winship I, et al. Risk-reducing hysterectomy and bilateral salpingo-oophorectomy in female heterozygotes of pathogenic mismatch repair variants: a Prospective Lynch Syndrome Database report. Genet Med. 2021;23(4):705-12.

103. Erekson EA, Martin DK, Ratner ES. Oophorectomy: the debate between ovarian conservation and elective oophorectomy. Menopause. 2013;20(1):110-4.

104. Arie AB, McNally L, Kapp DS, Teng NN. The omentum and omentectomy in epithelial ovarian cancer: a reappraisal: part II--The role of omentectomy in the staging and treatment of apparent early stage epithelial ovarian cancer. Gynecol Oncol. 2013;131(3):784-90.

105. Chiyoda T, Sakurai M, Satoh T, Nagase S, Mikami M, Katabuchi H, et al. Lymphadenectomy for primary ovarian cancer: a systematic review and meta-analysis. J Gynecol Oncol. 2020;31(5):e67.

106. Soper JT, Couchman G, Berchuck A, Clarke-Pearson D. The role of partial sigmoid colectomy for debulking epithelial ovarian carcinoma. Gynecol Oncol. 1991;41(3):239-44.

107. CancerCouncilVictoria. Ovarian Cancer Treatment. [Online] Accessed: September 2021. [Available from: https://www.cancervic.org.au/cancer-information/types-of-cancer/ovarian_cancer/treatment_for_ovarian_cancer.html.

108. TheAmericanCancerSociety. How Chemotherapy Drugs Work 2019. [Online] Accessed: September 2021. [Available from: https://www.cancer.org/treatment/treatments-and-side-effects/treatment-types/chemotherapy/how-chemotherapy-drugs-work.html.

109. BreastCancer. How Chemotherapy Works 2018. [Online] Accessed: September 2021. [Available from: https://www.breastcancer.org/treatment/chemotherapy/how_it_works.

110. MacmillanCancerCare. Chemotherapy for ovarian, Fallopian tube or primary peritoneal cancer 2020. [Online] Accessed: September 2021. [Available from: https://www.macmillan.org.uk/cancer-information-and-support/treatments-and-drugs/chemotherapy-for-ovarian-cancer.

111. Fields EC, McGuire WP, Lin L, Temkin SM. Radiation Treatment in Women with Ovarian Cancer: Past, Present, and Future. Front Oncol. 2017;7:177.

112. Montemorano L, Lightfoot MD, Bixel K. Role of Olaparib as Maintenance Treatment for Ovarian Cancer: The Evidence to Date. Onco Targets Ther. 2019;12:11497-506.

113. MacmillanCancerSupport. Olaparib (Lynparza ®) 2020. [Online] Accessed: September 2021. [Available from: https://www.macmillan.org.uk/cancer-information-and-support/treatments-and-drugs/olaparib.

114. The Royal Marsden, NICE approves olaparib in Cancer Drugs Fund (2019) [Online] Available from:https://www.royalmarsden.nhs.uk/nice-approves-olaparib-cancer-drugs-fund-royal-marsden-experts-react Accessed: July 2021.

115.	Ranieri G, Patruno R, Ruggieri E, Montemurro S, Valerio P, Ribatti D. Vascular endothelial growth factor (VEGF) as a target of bevacizumab in cancer: from the biology to the clinic. Curr Med Chem. 2006;13(16):1845-57.

116.	MacmillanCancerSupport. Bevacizumab (Avastin®) 2020. [Online] Accessed: September 2021. [Available from: https://www.macmillan.org.uk/cancer-information-and-support/treatments-and-drugs/bevacizumab.

117.	Canevari S, Raspagliesi F, Lorusso D. Bevacizumab treatment and quality of life in advanced ovarian cancer. Future Oncol. 2013;9(7):951-4.

118.	AmericanJointCommitteeonCancer. Ovary, Fallopian Tube, and Primary Peritoneal Carcinoma. In: Amin MB, Edge S, Greene F, Byrd DR, Brookland RK, et al, eds. A*JCC Cancer Staging Manual*. 8th ed. Chicago, IL2017.

119.	[Guideline]. Prat J, FIGO Committee on Gynecologic Oncology. FIGO Guidelines. Staging classification for cancer of the ovary, fallopian tube, and peritoneum. I*nt J Gynaecol Obstet* . 2014 Jan. 124 (1):1-5.

120.	[Guideline]. National Comprehensive Cancer Network. NCCN Clinical Practice Guidelines in Oncology: (NCCN Guidelines®) Ovarian Cancer Including Fallopian Tube Cancer and Primary Peritoneal Cancer. Available at http://www.nccn.org/professionals/physician_gls/pdf/ovarian.pdf. Version 1.2019 — March 8, 2019; Accessed: August 27, 2019.

121.	[Guideline]. Berek JS, Kehoe ST, Kumar L, Friedlander M. Cancer of the ovary, fallopian tube, and peritoneum. I*nt J Gynaecol Obstet* . 2018 Oct. 143 Suppl 2:59-78.

122.	Grabosch SM. Ovarian Cancer Staging 2019 [Available from: https://emedicine.medscape.com/article/2007140-overview.

123.	CRUK. Uterine cancer statistics 2019 [06.01.2020] [Online] Available from: https://www.cancerresearchuk.org/health-professional/cancer-statistics/statistics-by-cancer-type/uterine-cancer#heading-Four.

124.	Siegel RL, Miller KD, Jemal A. Cancer statistics, 2019. CA Cancer J Clin. 2019;69(1):7-34.

125.	Siegel RL, Miller KD, Jemal A. Cancer statistics, 2018. CA Cancer J Clin. 2018;68(1):7-30.

126.	Ali AT. Risk factors for endometrial cancer. Ceska Gynekol. 2013;78(5):448-59.

127.	Syeda S, Chen L, Hou JY, Tergas AI, Khoury-Collado F, Melamed A, et al. Chemotherapy, Radiation, or Combination Therapy for Stage III Uterine Cancer. Obstet Gynecol. 2019;134(1):17-29.

128.	De Boer SM, Nout RA, Bosse T, Creutzberg CL. Adjuvant therapy for high-risk endometrial cancer: recent evidence and future directions. Expert Rev Anticancer Ther. 2019;19(1):51-60.

129.	Latif NA, Haggerty A, Jean S, Lin L, Ko E. Adjuvant therapy in early-stage endometrial cancer: a systematic review of the evidence, guidelines, and clinical practice in the U.S. Oncologist. 2014;19(6):645-53.

130.	Hogberg T. Adjuvant chemotherapy in endometrial cancer. Int J Gynecol Cancer. 2010;20(11 Suppl 2):S57-9.

131.	Charo LM, Plaxe SC. Recent advances in endometrial cancer: a review of key clinical trials from 2015 to 2019. F1000Res. 2019;8. DOI: 10.12688/f1000research.17408.1

132.	Kang S, Nam JH, Bae DS, Kim JW, Kim MH, Chen X, et al. Preoperative assessment of lymph node metastasis in endometrial cancer: A Korean Gynecologic Oncology Group study. Cancer. 2017;123(2):263-72.

133.	Randall ME, Filiaci V, McMeekin DS, von Gruenigen V, Huang H, Yashar CM, et al. Phase III Trial: Adjuvant Pelvic Radiation Therapy Versus Vaginal Brachytherapy Plus Paclitaxel/Carboplatin in High-Intermediate and High-Risk Early Stage Endometrial Cancer. J Clin Oncol. 2019;37(21):1810-8.

134.	Creasman WT, Morrow CP, Bundy BN, Homesley HD, Graham JE, Heller PB. Surgical pathologic spread patterns of endometrial cancer. A Gynecologic Oncology Group Study. Cancer. 1987;60(8 Suppl):2035-41.

135.	J. WL. Diagnosis of uterine cancer by the vaginal smear. By George N. Papanicolaou and Herbert F. Traut. The Commonwealth Fund, New York. vii + 46 pp. 1943 ($5.00). The Anatomical Record. 1943;86(4):591-2.

136.	A. BD. The value of a pap smear program and suggestions for its implementation. Cancer. 1981;48(S1):613-21.

137.	CancerResearchUK. London Cervical Cancer Mortality Statistics 2014. [Online] Accessed: September 2021. [Available from: http://www.cancerresearchuk.org/healthprofessional/cancer-statistics/statistics-by-cancer-type/cervical-cancer.

138.   Cancer Research UK, *Breast Cancer statistics*, 2017. [Online] Accessed: September 2021. Available from: https://www.cancerresearchuk.org/health-professional/cancer-statistics/statistics-by-cancer-type/breast-cancer#heading-Two [Online] Accessed: 2020 [

139.   Yersal O, Barutca S. Biological subtypes of breast cancer: Prognostic and therapeutic implications. World J Clin Oncol. 2014;5(3):412-24.

140.   Onitilo AA, Engel JM, Greenlee RT, Mukesh BN. Breast cancer subtypes based on ER/PR and Her2 expression: comparison of clinicopathologic features and survival. Clin Med Res. 2009;7(1-2):4-13.

141.   Yao H, He G, Yan S, Chen C, Song L, Rosol TJ, et al. Triple-negative breast cancer: is there a treatment on the horizon? Oncotarget. 2017;8(1):1913-24.

142.   Tzikas AK, Nemes S, Linderholm BK. A comparison between young and old patients with triple-negative breast cancer: biology, survival and metastatic patterns. Breast Cancer Res Treat. 2020;182(3):643-54.

143.   Geyer FC, Pareja F, Weigelt B, Rakha E, Ellis IO, Schnitt SJ, et al. The Spectrum of Triple-Negative Breast Disease: High- and Low-Grade Lesions. Am J Pathol. 2017;187(10):2139-51.

144.   Bick U, Trimboli RM, Athanasiou A, Balleyguier C, Baltzer PAT, Bernathova M, et al. Image-guided breast biopsy and localisation: recommendations for information to women and referring physicians by the European Society of Breast Imaging. Insights Imaging. 2020;11(1):12.

145.   PDQ Adult Treatment Editorial Board. Breast Cancer Treatment (Adult) (PDQ®): Patient Version. 2021 Apr 8. In: PDQ Cancer Information Summaries [Internet]. Bethesda (MD): National Cancer Institute (US); 2002-. [Online] Accessed: September 2021. Available from: https://www.ncbi.nlm.nih.gov/books/NBK65969/.

146.   Watkins, Elyse J. DHSc, PA-C, DFAAPA   Overview of breast cancer, Journal of the American Academy of Physician Assistants: October 2019 - Volume 32 - Issue 10 - p 13-17 doi: 10.1097/01.JAA.0000580524.95733.3d.

147.   Witchel SF, Oberfield SE, Peña AS. Polycystic Ovary Syndrome: Pathophysiology, Presentation, and Treatment With Emphasis on Adolescent Girls. J Endocr Soc. 2019;3(8):1545-73.

148.   Khan MJ, Ullah A, Basit S. Genetic Basis of Polycystic Ovary Syndrome (PCOS): Current Perspectives. Appl Clin Genet. 2019;12:249-60.

149.   Bani Mohammad M, Majdi Seghinsara A. Polycystic Ovary Syndrome (PCOS), Diagnostic Criteria, and AMH. Asian Pac J Cancer Prev. 2017;18(1):17-21.

150.   Escobar-Morreale HF. Polycystic ovary syndrome: definition, aetiology, diagnosis and treatment. Nature Reviews Endocrinology. 2018;14:270. DOI: 10.1038/nrendo.2018.24

151.   Jiao J, Sagnelli M, Shi B, Fang Y, Shen Z, Tang T, et al. Genetic and epigenetic characteristics in ovarian tissues from polycystic ovary syndrome patients with irregular menstruation resemble those of ovarian cancer. BMC endocrine disorders. 2019;19(1):30.

152.   Ding DC, Chen W, Wang JH, Lin SZ. Association between polycystic ovarian syndrome and endometrial, ovarian, and breast cancer: A population-based cohort study in Taiwan. Medicine. 2018;97(39):e12608.

153.   Harris HR, Babic A, Webb PM, Nagle CM, Jordan SJ, Risch HA, et al. Polycystic Ovary Syndrome, Oligomenorrhea, and Risk of Ovarian Cancer Histotypes: Evidence from the Ovarian Cancer Association Consortium. Cancer epidemiology, biomarkers & prevention : a publication of the American Association for Cancer Research, cosponsored by the American Society of Preventive Oncology. 2018;27(2):174-82.

154.   Parasar P, Ozcan P, Terry KL. Endometriosis: Epidemiology, Diagnosis and Clinical Management. Curr Obstet Gynecol Rep. 2017;6(1):34-41.

155.   Sinaii N, Plumb K, Cotton L, Lambert A, Kennedy S, Zondervan K, et al. Differences in characteristics among 1,000 women with endometriosis based on extent of disease. Fertil Steril. 2008;89(3):538-45.

156.   Signorello LB, Harlow BL, Cramer DW, Spiegelman D, Hill JA. Epidemiologic determinants of endometriosis: a hospital-based case-control study. Ann Epidemiol. 1997;7(4):267-741.

157.   Missmer SA, Hankinson SE, Spiegelman D, Barbieri RL, Marshall LM, Hunter DJ. Incidence of laparoscopically confirmed endometriosis by demographic, anthropometric, and lifestyle factors. Am J Epidemiol. 2004;160(8):784-96.

158.   Darrow SL, Vena JE, Batt RE, Zielezny MA, Michalek AM, Selman S. Menstrual cycle characteristics and the risk of endometriosis. Epidemiology. 1993;4(2):135-42.

159.   Matalliotakis IM, Cakmak H, Fragouli YG, Goumenou AG, Mahutte NG, Arici A. Epidemiological characteristics in women with and without endometriosis in the Yale series. Arch Gynecol Obstet. 2008;277(5):389-93.

160.   Missmer SA, Hankinson SE, Spiegelman D, Barbieri RL, Malspeis S, Willett WC, et al. Reproductive history and endometriosis among premenopausal women. Obstet Gynecol. 2004;104(5 Pt 1):965-74.

161.   Sangi-Haghpeykar H, Poindexter AN, 3rd. Epidemiology of endometriosis among parous women. Obstet Gynecol. 1995;85(6):983-92.

162.   Cramer DW, Wilson E, Stillman RJ, Berger MJ, Belisle S, Schiff I, et al. The relation of endometriosis to menstrual characteristics, smoking, and exercise. Jama. 1986;255(14):1904-8.

163.   Moen MH, Schei B. Epidemiology of endometriosis in a Norwegian county. Acta Obstet Gynecol Scand. 1997;76(6):559-62.

164.   Hediger ML, Hartnett HJ, Louis GM. Association of endometriosis with body size and figure. Fertil Steril. 2005;84(5):1366-74.

165.   Parazzini F, Chiaffarino F, Surace M, Chatenoud L, Cipriani S, Chiantera V, et al. Selected food intake and risk of endometriosis. Hum Reprod. 2004;19(8):1755-9.

166.   Grodstein F, Goldman MB, Cramer DW. Infertility in women and moderate alcohol use. Am J Public Health. 1994;84(9):1429-32.

167.   Heilier JF, Donnez J, Nackers F, Rousseau R, Verougstraete V, Rosenkranz K, et al. Environmental and host-associated risk factors in endometriosis and deep endometriotic nodules: a matched case-control study. Environ Res. 2007;103(1):121-9.

168.   Chene G, Ouellet V, Rahimi K, Barres V, Provencher D, Mes-Masson AM. The ARID1A pathway in ovarian clear cell and endometrioid carcinoma, contiguous endometriosis, and benign endometriosis. Int J Gynaecol Obstet. 2015;130(1):27-30.

169.   Matsumoto T, Yamazaki M, Takahashi H, Kajita S, Suzuki E, Tsuruta T, et al. Distinct β-catenin and PIK3CA mutation profiles in endometriosis-associated ovarian endometrioid and clear cell carcinomas. Am J Clin Pathol. 2015;144(3):452-63.

170.   Scarfone G, Bergamini A, Noli S, Villa A, Cipriani S, Taccagni G, et al. Characteristics of clear cell ovarian cancer arising from endometriosis: a two center cohort study. Gynecol Oncol. 2014;133(3):480-4.

171.   Kumar S, Munkarah A, Arabi H, Bandyopadhyay S, Semaan A, Hayek K, et al. Prognostic analysis of ovarian cancer associated with endometriosis. Am J Obstet Gynecol. 2011;204(1):63.e1-7.

172.   Savaris RF, Fuhrich DG, Duarte RV, Franik S, Ross J. Antibiotic therapy for pelvic inflammatory disease. Cochrane Database Syst Rev. 2017;4:CD010285.

173.   Jennings LK, Krywko DM. Pelvic Inflammatory Disease. [Updated 2021 May 13]. In: StatPearls [Internet]. Treasure Island (FL): StatPearls Publishing; 2021 Jan-. Available from: https://www.ncbi.nlm.nih.gov/books/NBK499959/.

174.   Das BB, Ronda J, Trent M. Pelvic inflammatory disease: improving awareness, prevention, and treatment. Infect Drug Resist. 2016;9:191-7. doi: 10.2147/IDR.S91260

175.   Rasmussen CB, Kjaer SK, Albieri V, Bandera EV, Doherty JA, Høgdall E, et al. Pelvic Inflammatory Disease and the Risk of Ovarian Cancer and Borderline Ovarian Tumors: A Pooled Analysis of 13 Case-Control Studies. Am J Epidemiol. 2017;185(1):8-20.

176.   Chen L, Deng H, Cui H, Fang J, Zuo Z, Deng J, et al. Inflammatory responses and inflammation-associated diseases in organs. Oncotarget. 2018;9(6):7204-18.

177.   Hendrayani SF, Al-Harbi B, Al-Ansari MM, Silva G, Aboussekhra A. The inflammatory/cancer-related IL-6/STAT3/NF-κB positive feedback loop includes AUF1 and maintains the active state of breast myofibroblasts. Oncotarget. 2016;7(27):41974-85.

178.   Henríquez-Olguín C, Altamirano F, Valladares D, López JR, Allen PD, Jaimovich E. Altered ROS production, NF-κB activation and interleukin-6 gene expression induced by electrical stimulation in dystrophic mdx skeletal muscle cells. Biochim Biophys Acta. 2015;1852(7):1410-9.

179.   Newton K, Dixit VM. Signaling in innate immunity and inflammation. Cold Spring Harb Perspect Biol. 2012;4(3). DOI: 10.1101/cshperspect.a006049

180.   Singh N, Baby D, Rajguru JP, Patil PB, Thakkannavar SS, Pujari VB. Inflammation and cancer. Ann Afr Med. 2019;18(3):121-6.

181.   Todoric J, Antonucci L, Karin M. Targeting Inflammation in Cancer Prevention and Therapy. Cancer Prev Res (Phila). 2016;9(12):895-905.

182.   Tang F, Tang G, Xiang J, Dai Q, Rosner MR, Lin A. The absence of NF-kappaB-mediated inhibition of c-Jun N-terminal kinase activation contributes to tumor necrosis factor alpha-induced apoptosis. Mol Cell Biol. 2002;22(24):8571-9.

183.   Wang X, Lin Y. Tumor necrosis factor and cancer, buddies or foes? Acta Pharmacol Sin. 2008;29(11):1275-88.

184. Bona E, Andersson AL, Blomgren K, Gilland E, Puka-Sundvall M, Gustafson K, et al. Chemokine and inflammatory cell response to hypoxia-ischemia in immature rats. Pediatr Res. 1999;45(4 Pt 1):500-9.

185. Naylor MS, Stamp GW, Foulkes WD, Eccles D, Balkwill FR. Tumor necrosis factor and its receptors in human ovarian cancer. Potential role in disease progression. J Clin Invest. 1993;91(5):2194-206.

186. Hassuneh MR, Nagarkatti M, Nagarkatti PS. Role of interleukin-10 in the regulation of tumorigenicity of a T cell lymphoma. Leuk Lymphoma. 2013;54(4):827-34.

187. Ahmad N, Ammar A, Storr SJ, Green AR, Rakha E, Ellis IO, et al. IL-6 and IL-10 are associated with good prognosis in early stage invasive breast cancer patients. Cancer Immunol Immunother. 2018;67(4):537-49.

188. Mantovani A, Bottazzi B, Colotta F, Sozzani S, Ruco L. The origin and function of tumor-associated macrophages. Immunol Today. 1992;13(7):265-70.

189. Allavena P, Sica A, Vecchi A, Locati M, Sozzani S, Mantovani A. The chemokine receptor switch paradigm and dendritic cell migration: its significance in tumor tissues. Immunol Rev. 2000;177:141-9.

190. Turner MD, Nedjai B, Hurst T, Pennington DJ. Cytokines and chemokines: At the crossroads of cell signalling and inflammatory disease. Biochim Biophys Acta. 2014;1843(11):2563-82.

191. Mantovani A, Allavena P, Sica A, Balkwill F. Cancer-related inflammation. Nature. 2008;454(7203):436-44.

192. Grivennikov SI, Greten FR, Karin M. Immunity, inflammation, and cancer. Cell. 2010;140(6):883-99.

193. Hanahan D, Weinberg RA. The hallmarks of cancer. Cell. 2000;100(1):57-70.

194. Schmidt AM, Vianna M, Gerlach M, Brett J, Ryan J, Kao J, et al. Isolation and characterization of two binding proteins for advanced glycosylation end products from bovine lung which are present on the endothelial cell surface. J Biol Chem. 1992;267(21):14987-97.

195. Gkogkolou P, Böhm M. Advanced glycation end products: Key players in skin aging? Dermatoendocrinol. 2012;4(3):259-70.

196. Ramasamy R, Yan SF, Schmidt AM. Receptor for AGE (RAGE): signaling mechanisms in the pathogenesis of diabetes and its complications. Ann N Y Acad Sci. 2011;1243:88-102.

197. Devangelio E, Santilli F, Formoso G, Ferroni P, Bucciarelli L, Michetti N, et al. Soluble RAGE in type 2 diabetes: association with oxidative stress. Free Radic Biol Med. 2007;43(4):511-8.

198. Hofmann MA, Drury S, Fu C, Qu W, Taguchi A, Lu Y, et al. RAGE mediates a novel proinflammatory axis: a central cell surface receptor for S100/calgranulin polypeptides. Cell. 1999;97(7):889-901.

199. UniProt. UniProt: a worldwide hub of protein knowledge. Nucleic Acids Res. 2019;47(D1):D506-D15. Available from: https://www.uniprot.org

200. Healey GD, Frostell A, Fagge T, Gonzalez D, Conlan RS. A RAGE-Targeted Antibody-Drug Conjugate: Surface Plasmon Resonance as a Platform for Accelerating Effective ADC Design and Development. Antibodies (Basel). 2019;8(1). doi: 10.3390/antib8010007

201. Healey GD, Pan-Castillo B, Garcia-Parra J, Davies J, Roberts S, Jones E, et al. Antibody drug conjugates against the receptor for advanced glycation end products (RAGE), a novel therapeutic target in endometrial cancer. J Immunother Cancer. 2019;7(1):280. DOI: 10.1186/s40425-019-0765-z

202. Howard D, Garcia-Parra J, Healey GD, Amakiri C, Margarit L, Francis LW, et al. Antibody-drug conjugates and other nanomedicines: the frontier of gynaecological cancer treatment. Interface Focus. 2016;6(6):20160054.

203. Hudson BI, Stickland MH, Futers TS, Grant PJ. Effects of novel polymorphisms in the RAGE gene on transcriptional regulation and their association with diabetic retinopathy. Diabetes. 2001;50(6):1505-11.

204. UniProt, *Pre-B-cell leukemia transcription factor 2 (PBX2)* (Gene) (2018) [Online] Available from: https://www.uniprot.org/uniprot/P40425 Accessed: July 2021.

205. Schroeder HW, Cavacini L. Structure and function of immunoglobulins. J Allergy Clin Immunol. 2010;125(2 Suppl 2):S41-52.

206. Sparvero LJ, Asafu-Adjei D, Kang R, Tang D, Amin N, Im J, et al. RAGE (Receptor for Advanced Glycation Endproducts), RAGE ligands, and their role in cancer and inflammation. J Transl Med. 2009;7:17.

207. Ding Q, Keller JN. Evaluation of rage isoforms, ligands, and signaling in the brain. Biochim Biophys Acta. 2005;1746(1):18-27.

208. Scavello F, Zeni F, Tedesco CC, Mensà E, Veglia F, Procopio AD, et al. Modulation of soluble receptor for advanced glycation end-products (RAGE) isoforms and their ligands in healthy aging. Aging (Albany NY). 2019;11(6):1648-63.

209.   Tekabe Y, Li Q, Rosario R, Sedlar M, Majewski S, Hudson BI, et al. Development of receptor for advanced glycation end products-directed imaging of atherosclerotic plaque in a murine model of spontaneous atherosclerosis. Circ Cardiovasc Imaging. 2008;1(3):212-9.
210.   Caughey B, Lansbury PT. Protofibrils, pores, fibrils, and neurodegeneration: separating the responsible protein aggregates from the innocent bystanders. Annu Rev Neurosci. 2003;26:267-98.
211.   Mattson MP. Pathways towards and away from Alzheimer's disease. Nature. 2004;430(7000):631-9.
212.   Martin KC, Ephrussi A. mRNA localization: gene expression in the spatial dimension. Cell. 2009;136(4):719-30.
213.   Ding Q, Keller JN. Splice variants of the receptor for advanced glycosylation end products (RAGE) in human brain. Neurosci Lett. 2005;373(1):67-72.
214.   Cheng C, Tsuneyama K, Kominami R, Shinohara H, Sakurai S, Yonekura H, et al. Expression profiling of endogenous secretory receptor for advanced glycation end products in human organs. Mod Pathol. 2005;18(10):1385-96.
215.   Yan SD, Chen X, Fu J, Chen M, Zhu H, Roher A, et al. RAGE and amyloid-beta peptide neurotoxicity in Alzheimer's disease. Nature. 1996;382(6593):685-91.
216.   Du Yan S, Zhu H, Fu J, Yan SF, Roher A, Tourtellotte WW, et al. Amyloid-beta peptide-receptor for advanced glycation endproduct interaction elicits neuronal expression of macrophage-colony stimulating factor: a proinflammatory pathway in Alzheimer disease. Proc Natl Acad Sci U S A. 1997;94(10):5296-301.
217.   Koyama H, Yamamoto H, Nishizawa Y. RAGE and soluble RAGE: potential therapeutic targets for cardiovascular diseases. Mol Med. 2007;13(11-12):625-35.
218.   Bierhaus A, Humpert PM, Morcos M, Wendt T, Chavakis T, Arnold B, et al. Understanding RAGE, the receptor for advanced glycation end products. J Mol Med (Berl). 2005;83(11):876-86.
219.   González I, Romero J, Rodríguez BL, Pérez-Castro R, Rojas A. The immunobiology of the receptor of advanced glycation end-products: trends and challenges. Immunobiology. 2013;218(5):790-7.
220.   Karki R, Pandya D, Elston RC, Ferlini C. Defining "mutation" and "polymorphism" in the era of personal genomics. BMC Med Genomics. 2015;8:37.
221.   Hofmann MA, Drury S, Hudson BI, Gleason MR, Qu W, Lu Y, et al. RAGE and arthritis: the G82S polymorphism amplifies the inflammatory response. Genes Immun. 2002;3(3):123-35.
222.   Zhang S, Hou X, Zi S, Wang Y, Chen L, Kong B. Polymorphisms of receptor for advanced glycation end products and risk of epithelial ovarian cancer in Chinese patients. Cell Physiol Biochem. 2013;31(4-5):525-31.
223.   Tóth EK, Kocsis J, Madaras B, Bíró A, Pocsai Z, Fust G, et al. The 8.1 ancestral MHC haplotype is strongly associated with colorectal cancer risk. Int J Cancer. 2007;121(8):1744-8.
224.   Heizmann, C.W., 2013a. Chapter 15: RAGE-Mediated Cell Signaling. Methods in Molecular Biology , 963(1), p.588.
225.   Turovskaya O, Foell D, Sinha P, Vogl T, Newlin R, Nayak J, et al. RAGE, carboxylated glycans and S100A8/A9 play essential roles in colitis-associated carcinogenesis. Carcinogenesis. 2008;29(10):2035-43.
226.   Wei W, Lampe L, Park S, Vangara BS, Waldo GS, Cabantous S, et al. Disulfide bonds within the C2 domain of RAGE play key roles in its dimerization and biogenesis. PLoS One. 2012;7(12):e50736.
227.   Hudson BI, Carter AM, Harja E, Kalea AZ, Arriero M, Yang H, et al. Identification, classification, and expression of RAGE gene splice variants. Faseb j. 2008;22(5):1572-80.
228.   Kopan R, Ilagan MX. Gamma-secretase: proteasome of the membrane? Nat Rev Mol Cell Biol. 5. England2004. p. 499-504.
229.   Galichet A, Weibel M, Heizmann CW. Calcium-regulated intramembrane proteolysis of the RAGE receptor. Biochem Biophys Res Commun. 2008;370(1):1-5.
230.   Raucci A, Cugusi S, Antonelli A, Barabino SM, Monti L, Bierhaus A, et al. A soluble form of the receptor for advanced glycation endproducts (RAGE) is produced by proteolytic cleavage of the membrane-bound form by the sheddase a disintegrin and metalloprotease 10 (ADAM10). Faseb j. 2008;22(10):3716-27.
231.   Scharfenberg F, Helbig A, Sammel M, Benzel J, Schlomann U, Peters F, et al. Degradome of soluble ADAM10 and ADAM17 metalloproteases. Cell Mol Life Sci. 2020;77(2):331-50.
232.   Braley A, Kwak T, Jules J, Harja E, Landgraf R, Hudson BI. Regulation of Receptor for Advanced Glycation End Products (RAGE) Ectodomain Shedding and Its Role in Cell Function. J Biol Chem. 291: © 2016 by The American Society for Biochemistry and Molecular Biology, Inc.; 2016. p. 12057-73.
233.   Schmidt AM, Yan SD, Yan SF, Stern DM. The multiligand receptor RAGE as a progression factor amplifying immune and inflammatory responses. J Clin Invest. 2001;108(7):949-55.

234.	Lee HB, Yu MR, Yang Y, Jiang Z, Ha H. Reactive oxygen species-regulated signaling pathways in diabetic nephropathy. J Am Soc Nephrol. 2003;14(8 Suppl 3):S241-5.
235.	Chavakis T, Bierhaus A, Nawroth PP. RAGE (receptor for advanced glycation end products): a central player in the inflammatory response. Microbes Infect. 2004;6(13):1219-25.
236.	Rojas A, Delgado-López F, González I, Pérez-Castro R, Romero J, Rojas I. The receptor for advanced glycation end-products: a complex signaling scenario for a promiscuous receptor. Cell Signal. 2013;25(3):609-14.
237.	Xie J, Méndez JD, Méndez-Valenzuela V, Aguilar-Hernández MM. Cellular signalling of the receptor for advanced glycation end products (RAGE). Cell Signal. 2013;25(11):2185-97.
238.	Chavakis T, Bierhaus A, Al-Fakhri N, Schneider D, Witte S, Linn T, et al. The pattern recognition receptor (RAGE) is a counterreceptor for leukocyte integrins: a novel pathway for inflammatory cell recruitment. J Exp Med. 2003;198(10):1507-15.
239.	Neeper M, Schmidt AM, Brett J, Yan SD, Wang F, Pan YC, et al. Cloning and expression of a cell surface receptor for advanced glycosylation end products of proteins. J Biol Chem. 1992;267(21):14998-5004.
240.	Garlick RL, Mazer JS, Chylack LT, Jr., Tung WH, Bunn HF. Nonenzymatic glycation of human lens crystallin. Effect of aging and diabetes mellitus. J Clin Invest. 1984;74(5):1742-9.
241.	Toth C, Schmidt AM, Tuor UI, Francis G, Foniok T, Brussee V, et al. Diabetes, leukoencephalopathy and rage. Neurobiol Dis. 2006;23(2):445-61.
242.	Ansari NA, Dash D. Amadori glycated proteins: role in production of autoantibodies in diabetes mellitus and effect of inhibitors on non-enzymatic glycation. Aging Dis. 2013;4(1):50-6.
243.	Fritz G. RAGE: a single receptor fits multiple ligands. Trends Biochem Sci. 2011;36(12):625-32.
244.	Xue J, Rai V, Singer D, Chabierski S, Xie J, Reverdatto S, et al. Advanced glycation end product recognition by the receptor for AGEs. Structure. 2011;19(5):722-32.
245.	Cepas V, Collino M, Mayo JC, Sainz RM. Redox Signaling and Advanced Glycation Endproducts (AGEs) in Diet-Related Diseases. Antioxidants (Basel). 2020;9(2).
246.	Ostendorp T, Leclerc E, Galichet A, Koch M, Demling N, Weigle B, et al. Structural and functional insights into RAGE activation by multimeric S100B. Embo j. 2007;26(16):3868-78.
247.	Marenholz I, Heizmann CW, Fritz G. S100 proteins in mouse and man: from evolution to function and pathology (including an update of the nomenclature). Biochem Biophys Res Commun. 2004;322(4):1111-22.
248.	Fritz G, Botelho HM, Morozova-Roche LA, Gomes CM. Natural and amyloid self-assembly of S100 proteins: structural basis of functional diversity. Febs j. 2010;277(22):4578-90.
249.	Donato R, Cannon BR, Sorci G, Riuzzi F, Hsu K, Weber DJ, et al. Functions of S100 proteins. Curr Mol Med. 2013;13(1):24-57.
250.	Xia C, Braunstein Z, Toomey AC, Zhong J, Rao X. S100 Proteins As an Important Regulator of Macrophage Inflammation. Front Immunol. 2017;8:1908.
251.	Donato R. Functional roles of S100 proteins, calcium-binding proteins of the EF-hand type. Biochim Biophys Acta. 1999;1450(3):191-231.
252.	Leclerc E, Fritz G, Vetter SW, Heizmann CW. Binding of S100 proteins to RAGE: an update. Biochim Biophys Acta. 2009;1793(6):993-1007.
253.	Kuberappa PH, Bagalad BS, Ananthaneni A, Kiresur MA, Srinivas GV. Certainty of S100 from Physiology to Pathology. J Clin Diagn Res. 2016;10(6):Ze10-5.
254.	Weinstein D, Leininger J, Hamby C, Safai B. Diagnostic and prognostic biomarkers in melanoma. J Clin Aesthet Dermatol. 2014;7(6):13-24.
255.	Olaoba OT, Kadasah S, Vetter SW, Leclerc E. RAGE Signaling in Melanoma Tumors. Int J Mol Sci. 2020;21(23).
256.	Bresnick AR, Weber DJ, Zimmer DB. S100 proteins in cancer. Nat Rev Cancer. 2015;15(2):96-109.
257.	Yang H, Wang H, Chavan SS, Andersson U. High Mobility Group Box Protein 1 (HMGB1): The Prototypical Endogenous Danger Molecule. Mol Med. 2015;21 Suppl 1:S6-S12.
258.	Bianchi ME, Manfredi AA. High-mobility group box 1 (HMGB1) protein at the crossroads between innate and adaptive immunity. Immunol Rev. 2007;220:35-46.
259.	Tian J, Avalos AM, Mao SY, Chen B, Senthil K, Wu H, et al. Toll-like receptor 9-dependent activation by DNA-containing immune complexes is mediated by HMGB1 and RAGE. Nat Immunol. 2007;8(5):487-96.
260.	Banerjee S, Friggeri A, Liu G, Abraham E. The C-terminal acidic tail is responsible for the inhibitory effects of HMGB1 on efferocytosis. J Leukoc Biol. 2010;88(5):973-9.

261.   Tesarova P, Kalousova M, Zima T, Tesar V. HMGB1, S100 proteins and other RAGE ligands in cancer - markers, mediators and putative therapeutic targets. Biomed Pap Med Fac Univ Palacky Olomouc Czech Repub. 2016;160(1):1-10.

262.   Deane R, Du Yan S, Submamaryan RK, LaRue B, Jovanovic S, Hogg E, et al. RAGE mediates amyloid-beta peptide transport across the blood-brain barrier and accumulation in brain. Nat Med. 2003;9(7):907-13.

263.   Yan SS, Chen D, Yan S, Guo L, Du H, Chen JX. RAGE is a key cellular target for Abeta-induced perturbation in Alzheimer's disease. Front Biosci (Schol Ed). 2012;4:240-50.

264.   Daborg J, von Otter M, Sjölander A, Nilsson S, Minthon L, Gustafson DR, et al. Association of the RAGE G82S polymorphism with Alzheimer's disease. J Neural Transm (Vienna). 2010;117(7):861-7.

265.   Alexiou P, Chatzopoulou M, Pegklidou K, Demopoulos VJ. RAGE: a multi-ligand receptor unveiling novel insights in health and disease. Curr Med Chem. 2010;17(21):2232-52.

266.   Fineschi S, De Cunto G, Facchinetti F, Civelli M, Imbimbo BP, Carnini C, et al. Receptor for advanced glycation end products contributes to postnatal pulmonary development and adult lung maintenance program in mice. Am J Respir Cell Mol Biol. 2013;48(2):164-71.

267.   Englert JM, Hanford LE, Kaminski N, Tobolewski JM, Tan RJ, Fattman CL, et al. A role for the receptor for advanced glycation end products in idiopathic pulmonary fibrosis. Am J Pathol. 2008;172(3):583-91.

268.   Hori O, Brett J, Slattery T, Cao R, Zhang J, Chen JX, et al. The receptor for advanced glycation end products (RAGE) is a cellular binding site for amphoterin. Mediation of neurite outgrowth and co-expression of rage and amphoterin in the developing nervous system. J Biol Chem. 1995;270(43):25752-61.

269.   Rong LL, Yan SF, Wendt T, Hans D, Pachydaki S, Bucciarelli LG, et al. RAGE modulates peripheral nerve regeneration via recruitment of both inflammatory and axonal outgrowth pathways. Faseb j. 2004;18(15):1818-25.

270.   Weller J, Budson A. Current understanding of Alzheimer's disease diagnosis and treatment. F1000Res. 2018;7.

271.   Han SH, Kim YH, Mook-Jung I. RAGE: the beneficial and deleterious effects by diverse mechanisms of actions. Mol Cells. 2011;31(2):91-7.

272.   Cho HJ, Son SM, Jin SM, Hong HS, Shin DH, Kim SJ, et al. RAGE regulates BACE1 and Abeta generation via NFAT1 activation in Alzheimer's disease animal model. Faseb j. 2009;23(8):2639-49.

273.   Ruan Y, Guo Y, Zheng Y, Huang Z, Sun S, Kowal P, et al. Cardiovascular disease (CVD) and associated risk factors among older adults in six low-and middle-income countries: results from SAGE Wave 1. BMC Public Health. 2018;18(1):778.

274.   Yan SF, Ramasamy R, Schmidt AM. The receptor for advanced glycation endproducts (RAGE) and cardiovascular disease. Expert Rev Mol Med. 2009;11:e9.

275.   American Diabetes Association, Diagnosis and classification of diabetes mellitus. Diabetes Care. 2010;33 Suppl 1(Suppl 1):S62-9.

276.   Tanaka N, Yonekura H, Yamagishi S, Fujimori H, Yamamoto Y, Yamamoto H. The receptor for advanced glycation end products is induced by the glycation products themselves and tumor necrosis factor-alpha through nuclear factor-kappa B, and by 17beta-estradiol through Sp-1 in human vascular endothelial cells. J Biol Chem. 2000;275(33):25781-90.

277.   Logsdon CD, Fuentes MK, Huang EH, Arumugam T. RAGE and RAGE ligands in cancer. Curr Mol Med. 2007;7(8):777-89.

278.   Kang R, Tang D, Livesey KM, Schapiro NE, Lotze MT, Zeh HJ, 3rd. The Receptor for Advanced Glycation End-products (RAGE) protects pancreatic tumor cells against oxidative injury. Antioxid Redox Signal. 2011;15(8):2175-84.

279.   Riehl A, Németh J, Angel P, Hess J. The receptor RAGE: Bridging inflammation and cancer. Cell Commun Signal. 2009;7:12.

280.   Rojas A, González I, Morales E, Pérez-Castro R, Romero J, Figueroa H. Diabetes and cancer: Looking at the multiligand/RAGE axis. World J Diabetes. 2011;2(7):108-13.

281.   Brett J, Schmidt AM, Yan SD, Zou YS, Weidman E, Pinsky D, et al. Survey of the distribution of a newly characterized receptor for advanced glycation end products in tissues. Am J Pathol. 1993;143(6):1699-712.

282.   Chuah YK, Basir R, Talib H, Tie TH, Nordin N. Receptor for advanced glycation end products and its involvement in inflammatory diseases. Int J Inflam. 2013;2013:403460.

283.   Morbini P, Villa C, Campo I, Zorzetto M, Inghilleri S, Luisetti M. The receptor for advanced glycation end products and its ligands: a new inflammatory pathway in lung disease? Mod Pathol. 2006;19(11):1437-45.

284.   Oczypok EA, Perkins TN, Oury TD. All the "RAGE" in lung disease: The receptor for advanced glycation endproducts (RAGE) is a major mediator of pulmonary inflammatory responses. Paediatr Respir Rev. 2017;23:40-9.

285.   Riuzzi F, Sorci G, Sagheddu R, Chiappalupi S, Salvadori L, Donato R. RAGE in the pathophysiology of skeletal muscle. J Cachexia Sarcopenia Muscle. 2018;9(7):1213-34.

286.   Marinakis E, Bagkos G, Piperi C, Roussou P, Diamanti-Kandarakis E. Critical role of RAGE in lung physiology and tumorigenesis: a potential target of therapeutic intervention? Clin Chem Lab Med. 2014;52(2):189-200.

287.   Rojas A, GonzÁlez I, Araya P. RAGE in Cancer Lung: the End of a Long and Winding Road is in Sight. Zhongguo Fei Ai Za Zhi. 2018;21(9):655-7.

288.   Goldkorn T, Filosto S, Chung S. Lung injury and lung cancer caused by cigarette smoke-induced oxidative stress: Molecular mechanisms and therapeutic opportunities involving the ceramide-generating machinery and epidermal growth factor receptor. Antioxid Redox Signal. 2014;21(15):2149-74.

289.   Sabharwal SS, Schumacker PT. Mitochondrial ROS in cancer: initiators, amplifiers or an Achilles' heel? Nat Rev Cancer. 2014;14(11):709-21.

290.   Liu X, Chen Z. The pathophysiological role of mitochondrial oxidative stress in lung diseases. J Transl Med. 2017;15(1):207.

291.   Downs CA, Johnson NM, Tsaprailis G, Helms MN. RAGE-induced changes in the proteome of alveolar epithelial cells. J Proteomics. 2018;177:11-20.

292.   Chen MC, Chen KC, Chang GC, Lin H, Wu CC, Kao WH, et al. RAGE acts as an oncogenic role and promotes the metastasis of human lung cancer. Cell Death Dis. 2020;11(4):265.

293.   Bartling B, Hofmann HS, Weigle B, Silber RE, Simm A. Down-regulation of the receptor for advanced glycation end-products (RAGE) supports non-small cell lung carcinoma. Carcinogenesis. 2005;26(2):293-301.

294.   Hsieh HL, Schäfer BW, Sasaki N, Heizmann CW. Expression analysis of S100 proteins and RAGE in human tumors using tissue microarrays. Biochem Biophys Res Commun. 2003;307(2):375-81.

295.   Taguchi A, Blood DC, del Toro G, Canet A, Lee DC, Qu W, et al. Blockade of RAGE-amphoterin signalling suppresses tumour growth and metastases. Nature. 2000;405(6784):354-60.

296.   Rahimi F, Karimi J, Goodarzi MT, Saidijam M, Khodadadi I, Razavi AN, et al. Overexpression of receptor for advanced glycation end products (RAGE) in ovarian cancer. Cancer Biomark. 2017;18(1):61-8.

297.   Yang T, Cheng J, Yang Y, Qi W, Zhao Y, Long H, et al. S100B Mediates Stemness of Ovarian Cancer Stem-Like Cells Through Inhibiting p53. Stem Cells. 2017;35(2):325-36.

298.   Poljicanin A, Filipovic N, Vukusic Pusic T, Soljic V, Caric A, Saraga-Babic M, et al. Expression pattern of RAGE and IGF-1 in the human fetal ovary and ovarian serous carcinoma. Acta Histochem. 2015;117(4-5):468-76.

299.   Bonetti TC, Borges E, Jr., Braga DP, Iaconelli A, Jr., Kleine JP, Silva ID. Intrafollicular soluble receptor for advanced glycation end products (sRAGE) and embryo quality in assisted reproduction. Reprod Biomed Online. 2013;26(1):62-7.

300.   Rai V, Touré F, Chitayat S, Pei R, Song F, Li Q, et al. Lysophosphatidic acid targets vascular and oncogenic pathways via RAGE signaling. J Exp Med. 2012;209(13):2339-50.

301.   Uhlen M, Zhang C, Lee S, Sjostedt E, Fagerberg L, Bidkhori G, et al. A pathology atlas of the human cancer transcriptome. Science. 2017;357(6352).

302.   Uhlen M, Fagerberg L, Hallstrom BM, Lindskog C, Oksvold P, Mardinoglu A, et al. Proteomics. Tissue-based map of the human proteome. Science (New York, NY). 2015;347(6220):1260419.

303.   Leitao MM, Jr., Boyd J, Hummer A, Olvera N, Arroyo CD, Venkatraman E, et al. Clinicopathologic analysis of early-stage sporadic ovarian carcinoma. The American journal of surgical pathology. 2004;28(2):147-59.

304.   CancerResearchUk. Ovarian cancer incidence statistics. 2019. [Online] Accessed: September 2021. Available from: https://www.cancerresearchuk.org/health-professional/cancer-statistics/statistics-by-cancer-type/ovarian-cancer

305.   Zhang L, Bukulin M, Kojro E, Roth A, Metz VV, Fahrenholz F, et al. Receptor for advanced glycation end products is subjected to protein ectodomain shedding by metalloproteinases. J Biol Chem. 2008;283(51):35507-16.

306. Wang D, Li T, Ye G, Shen Z, Hu Y, Mou T, et al. Overexpression of the Receptor for Advanced Glycation Endproducts (RAGE) is associated with poor prognosis in gastric cancer. PLoS One. 2015;10(4):e0122697.

307. Aglago EK, Rinaldi S, Freisling H, Jiao L, Hughes DJ, Fedirko V, et al. Soluble Receptor for Advanced Glycation End-products (sRAGE) and colorectal cancer risk: a case-control study nested within a European prospective cohort. Cancer Epidemiol Biomarkers Prev. 2020.

308. Chen L, Duan Z, Tinker L, Sangi-Haghpeykar H, Strickler H, Ho GY, et al. A prospective study of soluble receptor for advanced glycation end-products and colorectal cancer risk in postmenopausal women. Cancer Epidemiol. 2016;42:115-23.

309. Jiao L, Taylor PR, Weinstein SJ, Graubard BI, Virtamo J, Albanes D, et al. Advanced glycation end products, soluble receptor for advanced glycation end products, and risk of colorectal cancer. Cancer Epidemiol Biomarkers Prev. 2011;20(7):1430-8.

310. Cho CH, Cha J. Analysis of neutrophil gelatinase-associated lipocalin, vascular endothelial growth factor, and soluble receptor for advanced glycation end-products in bone marrow supernatant in hematologic malignancies. Clin Biochem. 2020;80:19-24.

311. Wang H, Li Y, Yu W, Ma L, Ji X, Xiao W. Expression of the receptor for advanced glycation end-products and frequency of polymorphism in lung cancer. Oncol Lett. 2015;10(1):51-60.

312. Jing R, Cui M, Wang J, Wang H. Receptor for advanced glycation end products (RAGE) soluble form (sRAGE): a new biomarker for lung cancer. Neoplasma. 2010;57(1):55-61.

313. Wagner NB, Weide B, Reith M, Tarnanidis K, Kehrel C, Lichtenberger R, et al. Diminished levels of the soluble form of RAGE are related to poor survival in malignant melanoma. Int J Cancer. 2015;137(11):2607-17.

314. Wittwer C, Boeck S, Heinemann V, Haas M, Stieber P, Nagel D, et al. Circulating nucleosomes and immunogenic cell death markers HMGB1, sRAGE and DNAse in patients with advanced pancreatic cancer undergoing chemotherapy. Int J Cancer. 2013;133(11):2619-30.

315. Wittwer C, Boeck S, Heinemann V, Haas M, Stieber P, Nagel D, et al. Soluble receptor of advanced glycation end products (sRAGE) indicates response to chemotherapy in pancreatic cancer patients. Int J Clin Pharmacol Ther. 2013;51(1):67-9.

316. Krechler T, Jáchymová M, Mestek O, Zák A, Zima T, Kalousová M. Soluble receptor for advanced glycation end-products (sRAGE) and polymorphisms of RAGE and glyoxalase I genes in patients with pancreas cancer. Clin Biochem. 2010;43(10-11):882-6.

317. Piperis M, Provatopoulou X, Sagkriotis A, Kalogera E, Ampatzoglou E, Zografos GC, et al. Effect of breast cancer adjuvant therapies on potential biomarkers of pulmonary inflammation. Anticancer Res. 2012;32(11):4993-5002.

318. Nejadmoghaddam MR, Minai-Tehrani A, Ghahremanzadeh R, Mahmoudi M, Dinarvand R, Zarnani AH. Antibody-Drug Conjugates: Possibilities and Challenges. Avicenna J Med Biotechnol. 2019;11(1):3-23.

319. Nurgali K, Jagoe RT, Abalo R. Editorial: Adverse Effects of Cancer Chemotherapy: Anything New to Improve Tolerance and Reduce Sequelae? Front Pharmacol. 2018;9:245. doi: 10.3389/fphar.2018.00245

320. Sengupta S, Kulkarni A. Design principles for clinical efficacy of cancer nanomedicine: a look into the basics. ACS Nano. 2013;7(4):2878-82.

321. Decarvalho S, Rand HJ, Lewis A. COUPLING OF CYCLIC CHEMOTHERAPEUTIC COMPOUNDS TO IMMUNE GAMMA-GLOBULINS. Nature. 1964;202:255-8.

322. Jain N, Smith SW, Ghone S, Tomczuk B. Current ADC Linker Chemistry. Pharm Res. 2015 Nov;32(11):3526-40. doi: 10.1007/s11095-015-1657-7. Epub 2015 Mar 11. PMID: 25759187; PMCID: PMC4596905.

323. Lu R-M, Hwang Y-C, Liu IJ, Lee C-C, Tsai H-Z, Li H-J, et al. Development of therapeutic antibodies for the treatment of diseases. *J Biomed Sci*. 2020. DOI: 10.1186/s12929-019-0592-z

324. Stone KD, Prussin C, Metcalfe DD. IgE, mast cells, basophils, and eosinophils. J Allergy Clin Immunol. 2010;125(2 Suppl 2):S73-80.

325. Bioatla, Educational Appendix - Antibody Structure [Online] [Accessed: Oct 2020] Available from: https://www.bioatla.com/appendix/antibody-structure/

326. Chiu ML, Goulet DR, Teplyakov A, Gilliland GL. Antibody Structure and Function: The Basis for Engineering Therapeutics. Antibodies (Basel). 2019;8(4). doi: 10.3390/antib8040055

327. Alberts B, Johnson A, Lewis J, et al. Molecular Biology of the Cell. 4th edition. New York: Garland Science; 2002. B Cells and Antibodies. Available from: https://www.ncbi.nlm.nih.gov/books/NBK26884/.

328.   Weiner LM, Dhodapkar MV, Ferrone S. Monoclonal antibodies for cancer immunotherapy. Lancet. 2009;373(9668):1033-40.

329.   Goldmacher VS, Kovtun YV. Antibody-drug conjugates: using monoclonal antibodies for delivery of cytotoxic payloads to cancer cells. Ther Deliv. 2011;2(3):397-416.

330.   Zhang R, Liu Q, Peng J, Wang M, Gao X, Liao Q, et al. Pancreatic cancer-educated macrophages protect cancer cells from complement-dependent cytotoxicity by up-regulation of CD59. Cell Death Dis. 2019;10(11):836.

331.   Reis ES, Mastellos DC, Ricklin D, Mantovani A, Lambris JD. Complement in cancer: untangling an intricate relationship. Nat Rev Immunol. 2018;18(1):5-18.

332.   Azvolinsky A. Conjugating antibodies to cytotoxic agents: getting the best of both worlds? J Natl Cancer Inst. 105. United States2013. p. 1765-6. DOI: 10.1093/jnci/djt354

333.   Chari RV. Targeted cancer therapy: conferring specificity to cytotoxic drugs. Acc Chem Res. 2008;41(1):98-107.

334.   Hughes B. Antibody-drug conjugates for cancer: poised to deliver? Nat Rev Drug Discov. 2010;9(9):665-7.

335.   Chari RJ, Goldmacher VS, Lambert JM, Blattler WA, inventors;   Google Patents, assignee. Cytotoxic agents comprising maytansinoids and their therapeutic use . United States patent US 5,416,064 A. 1995. May 16.

336.   Panowski S, Bhakta S, Raab H, Polakis P, Junutula JR. Site-specific antibody drug conjugates for cancer therapy. MAbs. 2014;6(1):34-45.

337.   Elgersma RC, Coumans RG, Huijbregts T, Menge WM, Joosten JA, Spijker HJ, et al. Design, Synthesis, and Evaluation of Linker-Duocarmycin Payloads: Toward Selection of HER2-Targeting Antibody-Drug Conjugate SYD985. Mol Pharm. 2015;12(6):1813-35.

338.   Khandelwal A, Saber H, Shapiro MA, Zhao H. Antibody-drug conjugate development . In: Phillips GL, editor. Antibody-drug conjugates and immunotoxins . New York: Human Press; 2013. p. 23–38.

339.   Gerber HP, Kung-Sutherland M, Stone I, Morris-Tilden C, Miyamoto J, McCormick R, et al. Potent antitumor activity of the anti-CD19 auristatin antibody drug conjugate hBU12-vcMMAE against rituximab-sensitive and -resistant lymphomas. Blood. 2009;113(18):4352-61.

340.   Widdison WC, Chari RVJ. Factors involved in the design of cytotoxic payloads for antibody-drug conjugates . In: Phillips G, editor. Antibody-Drug Conjugates and Immunotoxins . New York: Human Press; 2013. p. 93–115.

341.   Govindan SV, Goldenberg DM. Designing immunoconjugates for cancer therapy. Expert Opin Biol Ther. 2012;12(7):873-90.

342.   Lazar AC, Wang L, Blättler WA, Amphlett G, Lambert JM, Zhang W. Analysis of the composition of immunoconjugates using size-exclusion chromatography coupled to mass spectrometry. Rapid Commun Mass Spectrom. 2005;19(13):1806-14.

343.   Acchione M, Kwon H, Jochheim CM, Atkins WM. Impact of linker and conjugation chemistry on antigen binding, Fc receptor binding and thermal stability of model antibody-drug conjugates. MAbs. 2012;4(3):362-72.

344.   Sievers EL, Senter PD. Antibody-drug conjugates in cancer therapy. Annu Rev Med. 2013;64:15-29.

345.   Kovtun YV, Audette CA, Ye Y, Xie H, Ruberti MF, Phinney SJ, et al. Antibody-drug conjugates designed to eradicate tumors with homogeneous and heterogeneous expression of the target antigen. Cancer Res. 2006;66(6):3214-21.

346.   Wang L, Amphlett G, Blättler WA, Lambert JM, Zhang W. Structural characterization of the maytansinoid-monoclonal antibody immunoconjugate, huN901-DM1, by mass spectrometry. Protein Sci. 2005;14(9):2436-46.

347.   Junutula JR, Raab H, Clark S, Bhakta S, Leipold DD, Weir S, et al. Site-specific conjugation of a cytotoxic drug to an antibody improves the therapeutic index. Nat Biotechnol. 2008;26(8):925-32.

348.   McPherson A, Gavira JA. Introduction to protein crystallization. Acta Crystallogr F Struct Biol Commun. 2014;70(Pt 1):2-20.

349.   Bordeaux J, Welsh A, Agarwal S, Killiam E, Baquero M, Hanna J, et al. Antibody validation. Biotechniques. 2010;48(3):197-209.

350.   ADC Review, *BLENTAMAB MAFODOTIN | GSK2857916 | J6M0-MCMMAF*, 2020, Acessed: October 2020, Available from:https://www.adcreview.com/drugmap/gsk2857916-j6m0-mcmmaf/

351.   Syed YY. Sacituzumab Govitecan: First Approval. Drugs. 2020;80(10):1019-25.

352.   ADC Review, *Trastuzumab Deruxtecan | Drug Description*, 2020, Accessed: October 2020, Available from:https://www.adcreview.com/trastuzumab-deruxtecan-drug-description/

353.   Rosenberg JE, O'Donnell PH, Balar AV, McGregor BA, Heath EI, Yu EY, et al. Pivotal Trial of Enfortumab Vedotin in Urothelial Carcinoma After Platinum and Anti-Programmed Death 1/Programmed Death Ligand 1 Therapy. J Clin Oncol. 2019;37(29):2592-600.

354.   ADC Review, *Polatuzumab Vedotin (Drug Description)*, 2019, Acessed: October 2020, Available from:https://www.adcreview.com/polatuzumab-vedotin-drug-description/

355.   ADC Review, Gemtuzumab Ozogamicin (Mylotarg) Drug Description, 2017, Accessed: October 2020, Available from: https://www.adcreview.com/gemtuzumab-ozogamicin-mylotarg/

356.   ADC Review, Inotuzumab ozogamicin (CMC-544) Drug Description, Accessed: October 2020, Available from: https://www.adcreview.com/inotuzumab-ozogamicin-cmc-544-drug-description/.

357.   Chen L, Wang L, Shion H, Yu C, Yu YQ, Zhu L, et al. In-depth structural characterization of Kadcyla® (ado-trastuzumab emtansine) and its biosimilar candidate. MAbs. 2016;8(7):1210-23.

358.   van de Donk NW, Dhimolea E. Brentuximab vedotin. MAbs. 2012;4(4):458-65.

359.   Ritchie M, Tchistiakova L, Scott N. Implications of receptor-mediated endocytosis and intracellular trafficking dynamics in the development of antibody drug conjugates. MAbs. 2013;5(1):13-21.

360.   Beck A, Haeuw JF, Wurch T, Goetsch L, Bailly C, Corvaïa N. The next generation of antibody-drug conjugates comes of age. Discov Med. 2010;10(53):329-39.

361.   Le Roy C, Wrana JL. Clathrin- and non-clathrin-mediated endocytic regulation of cell signalling. Nat Rev Mol Cell Biol. 2005;6(2):112-26.

362.   Mayor S, Pagano RE. Pathways of clathrin-independent endocytosis. Nat Rev Mol Cell Biol. 2007;8(8):603-12.

363.   Thermo Fisher Scientific, *Phagocytosis, Endocytosis, and Receptor Internalisation* [Online] Accessed: September 2021. Available from: https://www.thermofisher.com/uk/en/home/life-science/cell-analysis/cell-viability-and-regulation/endocytosis-exocytosis-and-phagocytosis.html.

364.   Kalim M, Chen J, Wang S, Lin C, Ullah S, Liang K, et al. Intracellular trafficking of new anticancer therapeutics: antibody-drug conjugates. Drug Des Devel Ther. 2017;11:2265-76.

365.   Höning S, Ricotta D, Krauss M, Späte K, Spolaore B, Motley A, et al. Phosphatidylinositol-(4,5)-bisphosphate regulates sorting signal recognition by the clathrin-associated adaptor complex AP2. Mol Cell. 2005;18(5):519-31.

366.   McMahon HT, Boucrot E. Molecular mechanism and physiological functions of clathrin-mediated endocytosis. Nat Rev Mol Cell Biol. 2011;12(8):517-33.

367.   Stenmark H. Rab GTPases as coordinators of vesicle traffic. Nat Rev Mol Cell Biol. 2009;10(8):513-25.

368.   Cao J, Zhong MB, Toro CA, Zhang L, Cai D. Endo-lysosomal pathway and ubiquitin-proteasome system dysfunction in Alzheimer's disease pathogenesis. Neurosci Lett. 2019;703:68-78.

369.   Huotari J, Helenius A. Endosome maturation. Embo j. 2011;30(17):3481-500.

370.   Roederer M, Bowser R, Murphy RF. Kinetics and temperature dependence of exposure of endocytosed material to proteolytic enzymes and low pH: evidence for a maturation model for the formation of lysosomes. J Cell Physiol. 1987;131(2):200-9.

371.   Russell MR, Nickerson DP, Odorizzi G. Molecular mechanisms of late endosome morphology, identity and sorting. Curr Opin Cell Biol. 2006;18(4):422-8.

372.   Mayor S, Parton RG, Donaldson JG. Clathrin-independent pathways of endocytosis. Cold Spring Harb Perspect Biol. 2014;6(6).

373.   Boucrot E, Howes MT, Kirchhausen T, Parton RG. Redistribution of caveolae during mitosis. J Cell Sci. 2011;124(Pt 12):1965-72.

374.   Morén B, Shah C, Howes MT, Schieber NL, McMahon HT, Parton RG, et al. EHD2 regulates caveolar dynamics via ATP-driven targeting and oligomerization. Mol Biol Cell. 2012;23(7):1316-29.

375.   Henley JR, Krueger EW, Oswald BJ, McNiven MA. Dynamin-mediated internalization of caveolae. J Cell Biol. 1998;141(1):85-99.

376.   Besterman JM, Airhart JA, Low RB, Rannels DE. Pinocytosis and intracellular degradation of exogenous protein: modulation by amino acids. J Cell Biol. 1983;96(6):1586-91.

377.   de Goeij BE, Lambert JM. New developments for antibody-drug conjugate-based therapeutic approaches. Curr Opin Immunol. 2016;40:14-23.

378.   Jackson D, Stover D. Using the Lessons Learned From the Clinic to Improve the Preclinical Development of Antibody Drug Conjugates. Pharm Res. 2015;32(11):3458-69.

379.	The Antibody Society, 2020, [Online] Accessed: October 2020, Available from: https://www.antibodysociety.org.

380.	The Antibody Society, Antibody therapeutics approved or in regulatory review in the EU or US, 2020, Acessed: October 2020, Available from: https://www.antibodysociety.org/resources/approved-antibodies/.

381.	Leslie LA, Younes A. Antibody-drug conjugates in hematologic malignancies. Am Soc Clin Oncol Educ Book. 2013.

382.	Iqbal N. Human Epidermal Growth Factor Receptor 2 (HER2) in Cancers: Overexpression and Therapeutic Implications. Mol Biol Int. 2014;2014:852748.

383.	Gbadamosi M, Meshinchi S, Lamba JK. Gemtuzumab ozogamicin for treatment of newly diagnosed CD33-positive acute myeloid leukemia. Future Oncol. 2018;14(30):3199-213.

384.	Döhner K, Döhner H. Molecular characterization of acute myeloid leukemia. [Book] Haematologica. 93. Italy2008. p. 976-82.

385.	Dombret H, Gardin C. An update of current treatments for adult acute myeloid leukemia. Blood. 2016;127(1):53-61.

386.	Thein MS, Ershler WB, Jemal A, Yates JW, Baer MR. Outcome of older patients with acute myeloid leukemia: an analysis of SEER data over 3 decades. Cancer. 2013;119(15):2720-7.

387.	Hamann PR, Hinman LM, Hollander I, Beyer CF, Lindh D, Holcomb R, et al. Gemtuzumab ozogamicin, a potent and selective anti-CD33 antibody-calicheamicin conjugate for treatment of acute myeloid leukemia. Bioconjug Chem. 2002;13(1):47-58.

388.	Paul SP, Taylor LS, Stansbury EK, McVicar DW. Myeloid specific human CD33 is an inhibitory receptor with differential ITIM function in recruiting the phosphatases SHP-1 and SHP-2. Blood. 2000;96(2):483-90.

389.	Crocker PR, Varki A. Siglecs, sialic acids and innate immunity. Trends Immunol. 2001;22(6):337-42.

390.	Appelbaum FR, Bernstein ID. Gemtuzumab ozogamicin for acute myeloid leukemia. Blood. 2017;130(22):2373-6.

391.	Ali S, Dunmore HM, Karres D, Hay JL, Salmonsson T, Gisselbrecht C, et al. The EMA Review of Mylotarg (Gemtuzumab Ozogamicin) for the Treatment of Acute Myeloid Leukemia. Oncologist. 2019;24(5):e171-e9.

392.	Zein N, Sinha AM, McGahren WJ, Ellestad GA. Calicheamicin gamma 1I: an antitumor antibiotic that cleaves double-stranded DNA site specifically. Science. 1988;240(4856):1198-201.

393.	Doronina SO, Toki BE, Torgov MY, Mendelsohn BA, Cerveny CG, Chace DF, et al. Development of potent monoclonal antibody auristatin conjugates for cancer therapy. Nat Biotechnol. 2003;21(7):778-84.

394.	Okeley NM, Miyamoto JB, Zhang X, Sanderson RJ, Benjamin DR, Sievers EL, et al. Intracellular activation of SGN-35, a potent anti-CD30 antibody-drug conjugate. Clin Cancer Res. 2010;16(3):888-97.

395.	Francisco JA, Cerveny CG, Meyer DL, Mixan BJ, Klussman K, Chace DF, et al. cAC10-vcMMAE, an anti-CD30-monomethyl auristatin E conjugate with potent and selective antitumor activity. Blood. 2003;102(4):1458-65.

396.	Oflazoglu E, Kissler KM, Sievers EL, Grewal IS, Gerber HP. Combination of the anti-CD30-auristatin-E antibody-drug conjugate (SGN-35) with chemotherapy improves antitumour activity in Hodgkin lymphoma. Br J Haematol. 2008;142(1):69-73.

397.	Fanale MA, Forero-Torres A, Rosenblatt JD, Advani RH, Franklin AR, Kennedy DA, et al. A phase I weekly dosing study of brentuximab vedotin in patients with relapsed/refractory CD30-positive hematologic malignancies. Clin Cancer Res. 2012;18(1):248-55.

398.	Younes A, Bartlett NL, Leonard JP, Kennedy DA, Lynch CM, Sievers EL, et al. Brentuximab vedotin (SGN-35) for relapsed CD30-positive lymphomas. N Engl J Med. 2010;363(19):1812-21.

399.	Peddi PF, Hurvitz SA. Ado-trastuzumab emtansine (T-DM1) in human epidermal growth factor receptor 2 (HER2)-positive metastatic breast cancer: latest evidence and clinical potential. Ther Adv Med Oncol. 2014;6(5):202-9.

400.	Slamon DJ, Clark GM, Wong SG, Levin WJ, Ullrich A, McGuire WL. Human breast cancer: correlation of relapse and survival with amplification of the HER-2/neu oncogene. Science. 1987;235(4785):177-82.

401.	Nahta R, Yu D, Hung MC, Hortobagyi GN, Esteva FJ. Mechanisms of disease: understanding resistance to HER2-targeted therapy in human breast cancer. Nat Clin Pract Oncol. 2006;3(5):269-80.

402.   Vogel CL, Cobleigh MA, Tripathy D, Gutheil JC, Harris LN, Fehrenbacher L, et al. Efficacy and safety of trastuzumab as a single agent in first-line treatment of HER2-overexpressing metastatic breast cancer. J Clin Oncol. 2002;20(3):719-26.

403.   Lewis Phillips GD, Li G, Dugger DL, Crocker LM, Parsons KL, Mai E, et al. Targeting HER2-positive breast cancer with trastuzumab-DM1, an antibody-cytotoxic drug conjugate. Cancer Res. 2008;68(22):9280-90.

404.   Remillard S, Rebhun LI, Howie GA, Kupchan SM. Antimitotic activity of the potent tumor inhibitor maytansine. Science. 1975;189(4207):1002-5.

405.   Shor B, Gerber HP, Sapra P. Preclinical and clinical development of inotuzumab-ozogamicin in hematological malignancies. Mol Immunol. 2015;67(2 Pt A):107-16.

406.   DiJoseph JF, Armellino DC, Boghaert ER, Khandke K, Dougher MM, Sridharan L, et al. Antibody-targeted chemotherapy with CMC-544: a CD22-targeted immunoconjugate of calicheamicin for the treatment of B-lymphoid malignancies. Blood. 2004;103(5):1807-14.

407.   DeAngelo DJ, Stock W, Stein AS, Shustov A, Liedtke M, Schiffer CA, et al. Inotuzumab ozogamicin in adults with relapsed or refractory CD22-positive acute lymphoblastic leukemia: a phase 1/2 study. Blood Adv. 2017;1(15):1167-80.

408.   Yurkiewicz IR, Muffly L, Liedtke M. Inotuzumab ozogamicin: a CD22 mAb-drug conjugate for adult relapsed or refractory B-cell precursor acute lymphoblastic leukemia. Drug Des Devel Ther. 2018;12:2293-300.

409.   Boué DR, LeBien TW. Expression and structure of CD22 in acute leukemia. Blood. 1988;71(5):1480-6.

410.   Haso W, Lee DW, Shah NN, Stetler-Stevenson M, Yuan CM, Pastan IH, et al. Anti-CD22-chimeric antigen receptors targeting B-cell precursor acute lymphoblastic leukemia. Blood. 2013;121(7):1165-74.

411.   ADC Review, Enfortumab Vedotin Drug Description, 2020, Accessed: October 2020, Available from: https://www.adcreview.com/enfortumab-vedotin-drug-description/

412.   ADC Review (Peter Hofland), Loncastuximab Tesirine Demonstrates an Overall High Response Rate in Pivotal Phase II Single-agent Trial, June 2020, Accessed: October 2020, Available from: https://www.adcreview.com/news/loncastuximab-tesirine-demonstrates-an-high-response-rates-in-pivotal-phase-ii-single-agent-trial/

413.   Stewart D, Cristea M. Antibody-drug conjugates for ovarian cancer: current clinical development. Curr Opin Obstet Gynecol. 2019;31(1):18-23.

414.   Zaman S, Jadid H, Denson AC, Gray JE. Targeting Trop-2 in solid tumors: future prospects. Onco Targets Ther. 2019;12:1781-90.

415.   Yang P, Cao X, Cai H, Feng P, Chen X, Zhu Y, et al. The exosomes derived from CAR-T cell efficiently target mesothelin and reduce triple-negative breast cancer growth. Cell Immunol. 2021;360:104262.

416.   Giamougiannis P, Martin-Hirsch PL, Martin FL. The evolving role of MUC16 (CA125) in the transformation of ovarian cells and the progression of neoplasia. Carcinogenesis. 2021;42(3):327-43.

417.   Banerjee S, Oza AM, Birrer MJ, Hamilton EP, Hasan J, Leary A, et al. Anti-NaPi2b antibody-drug conjugate lifastuzumab vedotin (DNIB0600A) compared with pegylated liposomal doxorubicin in patients with platinum-resistant ovarian cancer in a randomized, open-label, phase II study. Ann Oncol. 2018;29(4):917-23.

418.   Moore KN, Birrer MJ, Marsters J, Wang Y, Choi Y, Royer-Joo S, et al. Phase 1b study of anti-NaPi2b antibody-drug conjugate lifastuzumab vedotin (DNIB0600A) in patients with platinum-sensitive recurrent ovarian cancer. Gynecol Oncol. 2020;158(3):631-9.

419.   Gerber DE, Infante JR, Gordon MS, Goldberg SB, Martín M, Felip E, et al. Phase Ia Study of Anti-NaPi2b Antibody-Drug Conjugate Lifastuzumab Vedotin DNIB0600A in Patients with Non-Small Cell Lung Cancer and Platinum-Resistant Ovarian Cancer. Clin Cancer Res. 2020;26(2):364-72.

420.   Wan YL, Sapra P, Bolton J, Chua JX, Durrant LG, Stern PL. Combination Treatment with an Antibody-Drug Conjugate (A1mcMMAF) Targeting the Oncofetal Glycoprotein 5T4 and Carboplatin Improves Survival in a Xenograft Model of Ovarian Cancer. Target Oncol. 2019;14(4):465-77.

421.   Weekes CD, Lamberts LE, Borad MJ, Voortman J, McWilliams RR, Diamond JR, et al. Phase I Study of DMOT4039A, an Antibody-Drug Conjugate Targeting Mesothelin, in Patients with Unresectable Pancreatic or Platinum-Resistant Ovarian Cancer. Mol Cancer Ther. 2016;15(3):439-47.

422.   Orr B, Edwards RP. Diagnosis and Treatment of Ovarian Cancer. Hematol Oncol Clin North Am. 2018;32(6):943-64.

423.   Fader AN, Rose PG. Role of surgery in ovarian carcinoma. J Clin Oncol. 2007;25(20):2873-83.

424.   Ramus SJ, Gayther SA. The contribution of BRCA1 and BRCA2 to ovarian cancer. Mol Oncol. 2009;3(2):138-50.

425.   Li R, Yu G, Azarin SM, Hubel A. Freezing Responses in DMSO-Based Cryopreservation of Human iPS Cells: Aggregates Versus Single Cells. Tissue engineering Part C, Methods. 2018;24(5):289-99.

426.   Beaufort CM, Helmijr JC, Piskorz AM, Hoogstraat M, Ruigrok-Ritstier K, Besselink N, et al. Ovarian cancer cell line panel (OCCP): clinical importance of in vitro morphological subtypes. PLoS One. 2014;9(9):e103988.

427.   Nitta M, Katabuchi H, Ohtake H, Tashiro H, Yamaizumi M, Okamura H. Characterization and tumorigenicity of human ovarian surface epithelial cells immortalized by SV40 large T antigen. Gynecol Oncol. 2001;81(1):10-7.

428.   Kim M, Rhee JK, Choi H, Kwon A, Kim J, Lee GD, et al. Passage-dependent accumulation of somatic mutations in mesenchymal stromal cells during in vitro culture revealed by whole genome sequencing. Sci Rep. 2017;7(1):14508.

429.   Ye J, Coulouris G, Zaretskaya I, Cutcutache I, Rozen S, Madden TL. Primer-BLAST: a tool to design target-specific primers for polymerase chain reaction. BMC Bioinformatics. 2012;13:134.

430.   Cox KL, Devanarayan V, Kriauciunas A, et al. Immunoassay Methods. 2012 May 1 [Updated 2019 Jul 8]. In: Markossian S, Grossman A, Brimacombe K, et al., editors. Assay Guidance Manual [Internet]. Bethesda (MD): Eli Lilly & Company and the National Center for Advancing Translational Sciences; 2004-. Figure 1: [Diagram of a sandwich ELISA...]. Available from: https://www.ncbi.nlm.nih.gov/books/NBK92434/figure/immunometh.F1/.

431.   SPSS: Outliers [Online] 2020, Accessed December 2020, Available from: http://www.unige.ch/ses/sococ/cl/spss/concepts/outliers.html.

432.   SPSS, *Outliers* [Online] 2020, Acessed December 2020, Availble from:http://www.unige.ch/ses/sococ/cl//stat/concepts/outliers.html?

433.   Thul PJ, Åkesson L, Wiking M, Mahdessian D, Geladaki A, Ait Blal H, et al. A subcellular map of the human proteome. Science. 2017;356(6340).

434.   Uhlén M, Fagerberg L, Hallström BM, Lindskog C, Oksvold P, Mardinoglu A, et al. Proteomics. Tissue-based map of the human proteome. Science. 2015;347(6220):1260419.

435.   Tsirigos KD, Peters C, Shu N, Kall L, Elofsson A. The TOPCONS web server for consensus prediction of membrane protein topology and signal peptides. Nucleic Acids Res. 2015;43(W1):W401-7.

436.   Stelzer G, Rosen N, Plaschkes I, Zimmerman S, Twik M, Fishilevich S, et al. The GeneCards Suite: From Gene Data Mining to Disease Genome Sequence Analyses. Curr Protoc Bioinformatics. 2016;54:1 30 1-1 3.

437.   Gyamera-Acheampong C, Tantibhedhyangkul J, Weerachatyanukul W, Tadros H, Xu H, van de Loo JW, et al. Sperm from mice genetically deficient for the PCSK4 proteinase exhibit accelerated capacitation, precocious acrosome reaction, reduced binding to egg zona pellucida, and impaired fertilizing ability. Biol Reprod. 2006;74(4):666-73.

438.   Singh V, Bala R, Chakraborty A, Rajender S, Trivedi S, Singh K. Duplications in 19p13.3 are associated with male infertility. J Assist Reprod Genet. 2019;36(10):2171-9.

439.   Tardif S, Guyonnet B, Cormier N, Cornwall GA. Alteration in the processing of the ACRBP/sp32 protein and sperm head/acrosome malformations in proprotein convertase 4 (PCSK4) null mice. Mol Hum Reprod. 2012;18(6):298-307.

440.   Gyamera-Acheampong C, Mbikay M. Proprotein convertase subtilisin/kexin type 4 in mammalian fertility: a review. Hum Reprod Update. 2009;15(2):237-47.

441.   Freyer C, Kilpatrick LM, Salamonsen LA, Nie G. Pro-protein convertases (PCs) other than PC6 are not tightly regulated for implantation in the human endometrium. Reproduction. 2007;133(6):1189-97.

442.   Wang Y, Ren F, Chen P, Liu S, Song Z, Ma X. Identification of a six-gene signature with prognostic value for patients with endometrial carcinoma. Cancer Med. 2018;7(11):5632-42.

443.   Qiu Q, Basak A, Mbikay M, Tsang BK, Gruslin A. Role of pro-IGF-II processing by proprotein convertase 4 in human placental development. Proc Natl Acad Sci U S A. 2005;102(31):11047-52.

444.   Turpeinen H, Ortutay Z, Pesu M. Genetics of the first seven proprotein convertase enzymes in health and disease. Curr Genomics. 2013;14(7):453-67.

445.   Golias C, Batistatou A, Bablekos G, Charalabopoulos A, Peschos D, Mitsopoulos P, et al. Physiology and pathophysiology of selectins, integrins, and IgSF cell adhesion molecules focusing on inflammation. A paradigm model on infectious endocarditis. Cell Commun Adhes. 2011;18(3):19-32.

446.   Mbikay M, Tadros H, Ishida N, Lerner CP, De Lamirande E, Chen A, et al. Impaired fertility in mice deficient for the testicular germ-cell protease PC4. Proc Natl Acad Sci U S A. 1997;94(13):6842-6.

447.	Seidah NG, Day R, Hamelin J, Gaspar A, Collard MW, Chretien M. Testicular expression of PC4 in the rat: molecular diversity of a novel germ cell-specific Kex2/subtilisin-like proprotein convertase. Mol Endocrinol. 1992;6(10):1559-70.

448.	Nakayama K, Kim WS, Torii S, Hosaka M, Nakagawa T, Ikemizu J, et al. Identification of the fourth member of the mammalian endoprotease family homologous to the yeast Kex2 protease. Its testis-specific expression. J Biol Chem. 1992;267(9):5897-900.

449.	Tadros H, Chretien M, Mbikay M. The testicular germ-cell protease PC4 is also expressed in macrophage-like cells of the ovary. J Reprod Immunol. 2001;49(2):133-52.

450.	Kenworthy AK. Bigger Isn't Always Better: Bulking Up Impedes Receptor Internalization. Biophys J. 2018;114(6):1255-6.

451.	Ranade SS, Woo SH, Dubin AE, Moshourab RA, Wetzel C, Petrus M, et al. Piezo2 is the major transducer of mechanical forces for touch sensation in mice. Nature. 2014;516(7529):121-5.

452.	Bamshad M, Van Heest AE, Pleasure D. Arthrogryposis: a review and update. J Bone Joint Surg Am. 2009;91 Suppl 4(Suppl 4):40-6.

453.	Okubo M, Fujita A, Saito Y, Komaki H, Ishiyama A, Takeshita E, et al. A family of distal arthrogryposis type 5 due to a novel PIEZO2 mutation. Am J Med Genet A. 2015;167a(5):1100-6.

454.	Nonomura K, Woo SH, Chang RB, Gillich A, Qiu Z, Francisco AG, et al. Piezo2 senses airway stretch and mediates lung inflation-induced apnoea. Nature. 2017;541(7636):176-81.

455.	Delle Vedove A, Storbeck M, Heller R, Hölker I, Hebbar M, Shukla A, et al. Biallelic Loss of Proprioception-Related PIEZO2 Causes Muscular Atrophy with Perinatal Respiratory Distress, Arthrogryposis, and Scoliosis. Am J Hum Genet. 2016;99(5):1206-16.

456.	Huang Z, Sun Z, Zhang X, Niu K, Wang Y, Zheng J, et al. Loss of stretch-activated channels, PIEZOs, accelerates non-small cell lung cancer progression and cell migration. Biosci Rep. 2019;39(3).

457.	Yang H, Liu C, Zhou RM, Yao J, Li XM, Shen Y, et al. Piezo2 protein: A novel regulator of tumor angiogenesis and hyperpermeability. Oncotarget. 2016;7(28):44630-43.

458.	Cheng L, Shen Z, Zhou C. Promoter hypermethylation of PIEZO2 is a risk factor and potential clinical biomarker for laryngeal squamous cell carcinoma. Int J Clin Exp Pathol. 2017;10(12):11635-43.

459.	Etem EO, Ceylan GG, Ozaydin S, Ceylan C, Ozercan I, Kuloglu T. The increased expression of Piezo1 and Piezo2 ion channels in human and mouse bladder carcinoma. Adv Clin Exp Med. 2018;27(8):1025-31.

460.	Lou W, Liu J, Ding B, Jin L, Xu L, Li X, et al. Five miRNAs-mediated PIEZO2 downregulation, accompanied with activation of Hedgehog signaling pathway, predicts poor prognosis of breast cancer. Aging (Albany NY). 2019;11(9):2628-52.

461.	Edlich RF, Winters KL, Lin KY. Breast cancer and ovarian cancer genetics. J Long Term Eff Med Implants. 2005;15(5):533-45.

462.	Kinoshita T. Glycosylphosphatidylinositol (GPI) Anchors: Biochemistry and Cell Biology: Introduction to a Thematic Review Series. J Lipid Res. 2016;57(1):4-5.

463.	Paulick MG, Bertozzi CR. The glycosylphosphatidylinositol anchor: a complex membrane-anchoring structure for proteins. Biochemistry. 2008;47(27):6991-7000.

464.	Okda TM, Abd-Elghaffar SK, Katary MA, Abd-Alhaseeb MM. Chemopreventive and anticancer activities of indomethacin and vitamin D combination on colorectal cancer induced by 1,2-dimethylhydrazine in rats. Biomed Rep. 2021;14(2):27.

465.	VeryWellHealth. Neutrophils Function and Abnormal Results 2019 [Online] [Available from: https://www.verywellhealth.com/what-are-neutrophils-p2-2249134.

466.	Tchoupa AK, Schuhmacher T, Hauck CR. Signaling by epithelial members of the CEACAM family - mucosal docking sites for pathogenic bacteria. Cell Commun Signal. 2014;12:27.

467.	Ribon M, Mussard J, Semerano L, Singer BB, Decker P. Extracellular Chromatin Triggers Release of Soluble CEACAM8 Upon Activation of Neutrophils. Front Immunol. 2019;10:1346.

468.	Singer BB, Opp L, Heinrich A, Schreiber F, Binding-Liermann R, Berrocal-Almanza LC, et al. Soluble CEACAM8 interacts with CEACAM1 inhibiting TLR2-triggered immune responses. PLoS One. 2014;9(4):e94106.

469.	Lasa A, Serrano E, Carricondo M, Carnicer MJ, Brunet S, Badell I, et al. High expression of CEACAM6 and CEACAM8 mRNA in acute lymphoblastic leukemias.

470.	Kuroki M, Abe H, Imakiirei T, Liao S, Uchida H, Yamauchi Y, et al. Identification and comparison of residues critical for cell-adhesion activities of two neutrophil CD66 antigens, CEACAM6 and CEACAM8. J Leukoc Biol. 2001;70(4):543-50.

471.	Hauck CR, Meyer TF. 'Small' talk: Opa proteins as mediators of Neisseria-host-cell communication. Curr Opin Microbiol. 2003;6(1):43-9.

472.   Oikawa S, Sugiyama M, Kuroki M, Nakazato H. Extracellular N-domain alone can mediate specific heterophilic adhesion between members of the carcinoembryonic antigen family, CEACAM6 and CEACAM8. Biochem Biophys Res Commun. 2000;278(3):564-8.

473.   Pan W, Cheng Y, Zhang H, Liu B, Mo X, Li T, et al. CSBF/C10orf99, a novel potential cytokine, inhibits colon cancer cell growth through inducing G1 arrest. Sci Rep. 2014;4:6812.

474.   Yang M, Tang M, Ma X, Yang L, He J, Peng X, et al. AP-57/C10orf99 is a new type of multifunctional antimicrobial peptide. Biochem Biophys Res Commun. 2015;457(3):347-52.

475.   Watson AP, Evans RL, Egland KA. Multiple functions of sushi domain containing 2 (SUSD2) in breast tumorigenesis. Mol Cancer Res. 2013;11(1):74-85.

476.   Guo W, Shao F, Sun S, Song P, Guo L, Xue X, et al. Loss of SUSD2 expression correlates with poor prognosis in patients with surgically resected lung adenocarcinoma. J Cancer. 2020;11(7):1648-56.

477.   Patrick ME, Egland KA. SUSD2 Proteolytic Cleavage Requires the GDPH Sequence and Inter-Fragment Disulfide Bonds for Surface Presentation of Galectin-1 on Breast Cancer Cells. Int J Mol Sci. 2019;20(15).

478.   Hultgren EM, Patrick ME, Evans RL, Stoos CT, Egland KA. SUSD2 promotes tumor-associated macrophage recruitment by increasing levels of MCP-1 in breast cancer. PLoS One. 2017;12(5):e0177089.

479.   Lager TW, Roetman JJ, Kunkel J, Thacker M, Sheets JN, Egland KA, et al. Sushi Domain Containing 2 (SUSD2) inhibits platelet activation and binding to high-grade serous ovarian carcinoma cells. Platelets. 2018;29(8):834-7.

480.   Xu Y, Miao C, Jin C, Qiu C, Li Y, Sun X, et al. SUSD2 promotes cancer metastasis and confers cisplatin resistance in high grade serous ovarian cancer. Exp Cell Res. 2018;363(2):160-70.

481.   Sheets JN, Iwanicki M, Liu JF, Howitt BE, Hirsch MS, Gubbels JA, et al. SUSD2 expression in high-grade serous ovarian cancer correlates with increased patient survival and defective mesothelial clearance. Oncogenesis. 2016;5(10):e264.

482.   Zhang S, Zeng N, Alowayed N, Singh Y, Cheng A, Lang F, et al. Downregulation of endometrial mesenchymal marker SUSD2 causes cell senescence and cell death in endometrial carcinoma cells. PLoS One. 2017;12(8):e0183681.

483.   Sheets JN, Patrick ME, Egland KA. expression correlates with decreased metastasis and increased survival in a high-grade serous ovarian cancer xenograft murine model. Oncotarget. 2020;11(24):2290-301.

484.   Kagara N, Tanaka N, Noguchi S, Hirano T. Zinc and its transporter ZIP10 are involved in invasive behavior of breast cancer cells. Cancer Sci. 2007;98(5):692-7.

485.   Roohani N, Hurrell R, Kelishadi R, Schulin R. Zinc and its importance for human health: An integrative review. J Res Med Sci. 2013;18(2):144-57.

486.   Bin BH, Lee SH, Bhin J, Irié T, Kim S, Seo J, et al. The epithelial zinc transporter ZIP10 epigenetically regulates human epidermal homeostasis by modulating histone acetyltransferase activity. Br J Dermatol. 2019;180(4):869-80.

487.   Nakajima K, Lee MG, Bin BH, Hara T, Takagishi T, Chae S, et al. Possible involvement of zinc transporter ZIP10 in atopic dermatitis. J Dermatol. 2020;47(2):e51-e3.

488.   Brethour D, Mehrabian M, Williams D, Wang X, Ghodrati F, Ehsani S, et al. A ZIP6-ZIP10 heteromer controls NCAM1 phosphorylation and integration into focal adhesion complexes during epithelial-to-mesenchymal transition. Sci Rep. 2017;7:40313.

489.   Pal D, Sharma U, Singh SK, Prasad R. Association between ZIP10 gene expression and tumor aggressiveness in renal cell carcinoma. Gene. 2014;552(1):195-8.

490.   Kong BY, Duncan FE, Que EL, Kim AM, O'Halloran TV, Woodruff TK. Maternally-derived zinc transporters ZIP6 and ZIP10 drive the mammalian oocyte-to-egg transition. Mol Hum Reprod. 2014;20(11):1077-89.

491.   Croxford TP, McCormick NH, Kelleher SL. Moderate zinc deficiency reduces testicular Zip6 and Zip10 abundance and impairs spermatogenesis in mice. J Nutr. 2011;141(3):359-65.

492.   Vallee BL, Falchuk KH. The biochemical basis of zinc physiology. Physiol Rev. 1993;73(1):79-118.

493.   Vallee BL, Auld DS. Zinc coordination, function, and structure of zinc enzymes and other proteins. Biochemistry. 1990;29(24):5647-59.

494.   Chakravarty PK, Ghosh A, Chowdhury JR. Zinc in human malignancies. Neoplasma. 1986;33(1):85-90.

495.   Costello LC, Franklin RB. The clinical relevance of the metabolism of prostate cancer; zinc and tumor suppression: connecting the dots. Mol Cancer. 2006;5:17.

496.   Gupta SK, Singh SP, Shukla VK. Copper, zinc, and Cu/Zn ratio in carcinoma of the gallbladder. J Surg Oncol. 2005;91(3):204-8.

497.   Margalioth EJ, Schenker JG, Chevion M. Copper and zinc levels in normal and malignant tissues. Cancer. 1983;52(5):868-72.

498.   Tashiro H, Kawamoto T, Okubo T, Koide O. Variation in the distribution of trace elements in hepatoma. Biol Trace Elem Res. 2003;95(1):49-63.

499.   Maeda K, Matsuhashi S, Hori K, Xin Z, Mukai T, Tabuchi K, et al. Cloning and Characterization of a Novel Human Gene, TM4SF6, Encoding a Protein Belonging to the Transmembrane 4 Superfamily, and Mapped to Xq22. Genomics. 1998;52(2):240-2.

500.   Huang S, Yuan S, Dong M, Su J, Yu C, Shen Y, et al. The phylogenetic analysis of tetraspanins projects the evolution of cell-cell interactions from unicellular to multicellular organisms. Genomics. 2005;86(6):674-84.

501.   Hantak MP, Qing E, Earnest JT, Gallagher T. Tetraspanins: Architects of viral entry and exit platforms. Journal of Virology. 2018:JVI.01429-17.

502.   Detchokul S, Williams ED, Parker MW, Frauman AG. Tetraspanins as regulators of the tumour microenvironment: implications for metastasis and therapeutic strategies. Br J Pharmacol. 2014;171(24):5462-90.

503.   Jiang X, Zhang J, Huang Y. Tetraspanins in cell migration. Cell Adh Migr. 2015;9(5):406-15.

504.   Schaper F, van Spriel AB. Antitumor Immunity Is Controlled by Tetraspanin Proteins. Front Immunol. 2018;9:1185.

505.   Vences-Catalán F, Levy S. Immune Targeting of Tetraspanins Involved in Cell Invasion and Metastasis. Front Immunol. 2018;9:1277.

506.   Kashef J, Diana T, Oelgeschläger M, Nazarenko I. Expression of the tetraspanin family members Tspan3, Tspan4, Tspan5 and Tspan7 during Xenopus laevis embryonic development. Gene Expr Patterns. 2013;13(1-2):1-11.

507.   Zuidscherwoude M, Göttfert F, Dunlock VM, Figdor CG, van den Bogaart G, van Spriel AB. The tetraspanin web revisited by super-resolution microscopy. Sci Rep. 2015;5:12201.

508.   Florin L, Lang T. Tetraspanin Assemblies in Virus Infection. Front Immunol. 2018;9:1140.

509.   Spoden G, Freitag K, Husmann M, Boller K, Sapp M, Lambert C, et al. Clathrin- and caveolin-independent entry of human papillomavirus type 16--involvement of tetraspanin-enriched microdomains (TEMs). PloS one. 2008;3(10):e3313-e.

510.   Hemler ME. Tetraspanin proteins promote multiple cancer stages. Nature Reviews Cancer. 2013;14:49.

511.   Stipp CS. Laminin-binding integrins and their tetraspanin partners as potential antimetastatic targets. Expert reviews in molecular medicine. 2010;12:e3.

512.   Tsai YC, Weissman AM. Dissecting the diverse functions of the metastasis suppressor CD82/KAI1. FEBS letters. 2011;585(20):3166-73.

513.   Zöller M. Tetraspanins: push and pull in suppressing and promoting metastasis. Nature Reviews Cancer. 2008;9:40.

514.   Romanska HM, Berditchevski F. Tetraspanins in human epithelial malignancies. The Journal of pathology. 2011;223(1):4-14.

515.   Veenbergen S, van Spriel AB. Tetraspanins in the immune response against cancer. Immunology letters. 2011;138(2):129-36.

516.   Richardson MM, Jennings LK, Zhang XA. Tetraspanins and tumor progression. Clinical & experimental metastasis. 2011;28(3):261-70.

517.   Sala-Valdes M, Ailane N, Greco C, Rubinstein E, Boucheix C. Targeting tetraspanins in cancer. Expert opinion on therapeutic targets. 2012;16(10):985-97.

518.   Hemler ME. Targeting of tetraspanin proteins — potential benefits and strategies. Nature Reviews Drug Discovery. 2008;7:747.

519.   Haeuw J-F, Goetsch L, Bailly C, Corvaia N. Tetraspanin CD151 as a target for antibody-based cancer immunotherapy. Biochemical Society Transactions. 2011;39(2):553.

520.   Hwang JR, Jo K, Lee Y, Sung BJ, Park YW, Lee JH. Upregulation of CD9 in ovarian cancer is related to the induction of TNF-alpha gene expression and constitutive NF-kappaB activation. Carcinogenesis. 2012;33(1):77-83.

521.   Park CS, Kim TK, Kim HG, Kim YJ, Jeoung MH, Lee WR, et al. Therapeutic targeting of tetraspanin8 in epithelial ovarian cancer invasion and metastasis. Oncogene. 2016;35(34):4540-8.

522.   Holters S, Anacker J, Jansen L, Beer-Grondke K, Durst M, Rubio I. Tetraspanin 1 promotes invasiveness of cervical cancer cells. International journal of oncology. 2013;43(2):503-12.

523.   Takeda Y, Kazarov AR, Butterfield CE, Hopkins BD, Benjamin LE, Kaipainen A, et al. Deletion of tetraspanin Cd151 results in decreased pathologic angiogenesis in vivo and in vitro. Blood. 2007;109(4):1524-32.

524.   Bethesda MD. Gene [Internet] Gene ID: 7105 Homo sapiens (human) TSPAN6 tetraspanin 6. National Library of Medicine (US), National Center for Biotechnology Information (NCBI). 1988.

525.   The UniProt C. UniProt: a worldwide hub of protein knowledge. Nucleic Acids Research. 2018;47(D1):D506-D15.

526.   Madeira F, Park YM, Lee J, Buso N, Gur T, Madhusoodanan N, et al. The EMBL-EBI search and sequence analysis tools APIs in 2019. Nucleic acids research. 2019;47(W1):W636-W41.

527.   Wang Y, Tong X, Omoregie ES, Liu W, Meng S, Ye X. Tetraspanin 6 (TSPAN6) negatively regulates retinoic acid-inducible gene I-like receptor-mediated immune signaling in a ubiquitination-dependent manner. J Biol Chem. 2012;287(41):34626-34.

528.   Yoneyama M, Fujita T. RNA recognition and signal transduction by RIG-I-like receptors. Immunological reviews. 2009;227(1):54-65.

529.   Coussens LM, Werb Z. Inflammation and cancer. Nature. 2002;420(6917):860-7.

530.   Vinayagam A, Stelzl U, Foulle R, Plassmann S, Zenkner M, Timm J, et al. A directed protein interaction network for investigating intracellular signal transduction. Sci Signal. 2011;4(189):rs8.

531.   Huttlin EL, Bruckner RJ, Paulo JA, Cannon JR, Ting L, Baltier K, et al. Architecture of the human interactome defines protein communities and disease networks. Nature. 2017;545(7655):505-9.

532.   Stelzl U, Worm U, Lalowski M, Haenig C, Brembeck FH, Goehler H, et al. A human protein-protein interaction network: a resource for annotating the proteome. Cell. 2005;122(6):957-68.

533.   Nguyen Ba AN, Yeh BJ, van Dyk D, Davidson AR, Andrews BJ, Weiss EL, et al. Proteome-wide discovery of evolutionary conserved sequences in disordered regions. Science signaling. 2012;5(215):rs1-rs.

534.   Ghossoub R, Chéry M, Audebert S, Leblanc R, Egea-Jimenez AL, Lembo F, et al. Tetraspanin-6 negatively regulates exosome production. Proc Natl Acad Sci U S A. 2020;117(11):5913-22.

535.   Brzozowski JS, Bond DR, Jankowski H, Goldie BJ, Burchell R, Naudin C, et al. Extracellular vesicles with altered tetraspanin CD9 and CD151 levels confer increased prostate cell motility and invasion. Sci Rep. 2018;8(1):8822.

536.   Andreu Z, Yáñez-Mó M. Tetraspanins in extracellular vesicle formation and function. Front Immunol. 2014;5:442.

537.   Osaki M, Okada F. Exosomes and Their Role in Cancer Progression. Yonago Acta Med. 2019;62(2):182-90.

538.   Quicke KM, Diamond MS, Suthar MS. Negative regulators of the RIG-I-like receptor signaling pathway. Eur J Immunol. 2017;47(4):615-28.

539.   De-Strooper B. Means and method for diagnosis and treatment of alzheimer's disease. Patent application WO2013113696A1 THE PATENT COOPERATION TREATY (PCT) World Intellectual Property Organization International Bureau. 2013.

540.   Guix FX, Sannerud R, Berditchevski F, Arranz AM, Horre K, Snellinx A, et al. Tetraspanin 6: a pivotal protein of the multiple vesicular body determining exosome release and lysosomal degradation of amyloid precursor protein fragments. Mol Neurodegener. 2017;12(1):25.

541.   Salas IH, Callaerts-Vegh Z, Arranz AM, Guix FX, D'Hooge R, Esteban JA, et al. Tetraspanin 6: A novel regulator of hippocampal synaptic transmission and long term plasticity. PLoS One. 2017;12(2):e0171968.

542.   Abcam. Why is the actual band size different from the predicted? 2020 [Online] Available from: https://www.abcam.com/assets/popups/popup_bandhelp.htm.

543.   Shin KC, Park HJ, Kim JG, Lee IH, Cho H, Park C, et al. The Piezo2 ion channel is mechanically activated by low-threshold positive pressure. Sci Rep. 2019;9(1):6446.

544.   Bonsor DA, Günther S, Beadenkopf R, Beckett D, Sundberg EJ. Diverse oligomeric states of CEACAM IgV domains. Proc Natl Acad Sci U S A. 2015;112(44):13561-6.

545.   Sigrist CJ, De Castro E, Langendijk-Genevaux PS, Le Saux V, Bairoch A, Hulo N. ProRule: a new database containing functional and structural information on PROSITE profiles. Bioinformatics. 2005;21(21):4060-6.

546.   Kornfeld R, Kornfeld S. Assembly of asparagine-linked oligosaccharides. Annu Rev Biochem. 1985;54:631-64.

547. Kovalenko OV, Metcalf DG, DeGrado WF, Hemler ME. Structural organization and interactions of transmembrane domains in tetraspanin proteins. BMC Struct Biol. 2005;5:11.

548. Kovalenko OV, Yang X, Kolesnikova TV, Hemler ME. Evidence for specific tetraspanin homodimers: inhibition of palmitoylation makes cysteine residues available for cross-linking. Biochem J. 2004;377(Pt 2):407-17.

549. Seigneuret M, Delaguillaumie A, Lagaudrière-Gesbert C, Conjeaud H. Structure of the tetraspanin main extracellular domain. A partially conserved fold with a structurally variable domain insertion. J Biol Chem. 2001;276(43):40055-64.

550. Perez HL, Cardarelli PM, Deshpande S, Gangwar S, Schroeder GM, Vite GD, et al. Antibody-drug conjugates: current status and future directions. Drug Discov Today. 2014;19(7):869-81.

551. Press MF, Cordon-Cardo C, Slamon DJ. Expression of the HER-2/neu proto-oncogene in normal human adult and fetal tissues. Oncogene. 1990;5(7):953-62.

552. Chari RV, Miller ML, Widdison WC. Antibody-drug conjugates: an emerging concept in cancer therapy. Angew Chem Int Ed Engl. 2014;53(15):3796-827.

553. Shoelson SE, Lee J, Goldfine AB. Inflammation and insulin resistance. J Clin Invest. 2006;116(7):1793-801.

554. Tsalamandris S, Antonopoulos AS, Oikonomou E, Papamikroulis GA, Vogiatzi G, Papaioannou S, et al. The Role of Inflammation in Diabetes: Current Concepts and Future Perspectives. Eur Cardiol. 2019;14(1):50-9.

555. Peltomäki P, Vasen H. Mutations associated with HNPCC predisposition -- Update of ICG-HNPCC/INSiGHT mutation database. Dis Markers. 2004;20(4-5):269-76.

556. Banno K, Yanokura M, Kobayashi Y, Kawaguchi M, Nomura H, Hirasawa A, et al. Endometrial cancer as a familial tumor: pathology and molecular carcinogenesis (review). Curr Genomics. 2009;10(2):127-32.

557. Ardito F, Giuliani M, Perrone D, Troiano G, Lo Muzio L. The crucial role of protein phosphorylation in cell signaling and its use as targeted therapy (Review). Int J Mol Med. 2017;40(2):271-80.

558. Rachmilewitz J. Glycosylation: An intrinsic sign of "danger". Self Nonself. 2010;1(3):250-4.

559. Lee HS, Qi Y, Im W. Effects of N-glycosylation on protein conformation and dynamics: Protein Data Bank analysis and molecular dynamics simulation study.

560. PubChem 2019 update: improved access to chemical data: Phosphate [Internet]. *Nucleic Acids Res*. 2019. Available from: https://pubchem.ncbi.nlm.nih.gov/compound/Phosphate.

561. Shoham T, Rajapaksa R, Kuo CC, Haimovich J, Levy S. Building of the tetraspanin web: distinct structural domains of CD81 function in different cellular compartments. Mol Cell Biol. 2006;26(4):1373-85.

562. Bekešová S, Komis G, Křenek P, Vyplelová P, Ovečka M, Luptovčiak I, et al. Monitoring protein phosphorylation by acrylamide pendant Phos-Tag™ in various plants. Front Plant Sci. 2015;6:336.

563. Bass JJ, Wilkinson DJ, Rankin D, Phillips BE, Szewczyk NJ, Smith K, et al. An overview of technical considerations for Western blotting applications to physiological research. Scand J Med Sci Sports. 2017;27(1):4-25.

564. Bauer J, Wehland M, Infanger M, Grimm D, Gombocz E. Semantic Analysis of Posttranslational Modification of Proteins Accumulated in Thyroid Cancer Cells Exposed to Simulated Microgravity. Int J Mol Sci. 2018;19(8).

565. Ghahremani M, Stigter KA, Plaxton W. Extraction and Characterization of Extracellular Proteins and Their Post-Translational Modifications from Arabidopsis thaliana Suspension Cell Cultures and Seedlings: A Critical Review. Proteomes. 2016;4(3).

566. ThermoFisherScientific. Overview of Post-Translational Modifications (PTMs) 2020 [Online] [Available from: https://www.thermofisher.com/uk/en/home/life-science/protein-biology/protein-biology-learning-center/protein-biology-resource-library/pierce-protein-methods/overview-post-translational-modification.html.

567. Poeck H, Besch R, Maihoefer C, Renn M, Tormo D, Morskaya SS, et al. 5'-Triphosphate-siRNA: turning gene silencing and Rig-I activation against melanoma. Nat Med. 2008;14(11):1256-63.

568. Ellermeier J, Wei J, Duewell P, Hoves S, Stieg MR, Adunka T, et al. Therapeutic efficacy of bifunctional siRNA combining TGF-β1 silencing with RIG-I activation in pancreatic cancer. Cancer Res. 2013;73(6):1709-20.

569. Cooper GM. The Cell: A Molecular Approach. 2nd edition. Sunderland (MA): Sinauer Associates; 2000. Endocytosis. Available from: https://www.ncbi.nlm.nih.gov/books/NBK9831/.

570.   Lodish H, Berk A, Zipursky SL, et al. Molecular Cell Biology. 4th edition. New York: W. H. Freeman; 2000. Section 17.9, Receptor-Mediated Endocytosis and the Sorting of Internalized Proteins.   Available from: https://www.ncbi.nlm.nih.gov/books/NBK21639/.

571.   Dautry-Varsat A. Receptor-mediated endocytosis: the intracellular journey of transferrin and its receptor. Biochimie. 1986 Mar;68(3):375-81. doi: 10.1016/s0300-9084(86)80004-9. PMID: 2874839.

572.   Wileman T, Harding C, Stahl P. Receptor-mediated endocytosis. Biochem J. 1985;232(1):1-14.

573.   Kataoka K, Harada A, Nagasaki Y. Block copolymer micelles for drug delivery: design, characterization and biological significance. Adv Drug Deliv Rev. 2001;47(1):113-31.

574.   D L, WG M. Case Study: An Antibody–Drug Conjugate Targeting MUC16 for Ovarian Cancer. Phillips GL, editor   Antibody-Drug Conjugates and Immunotoxins: From Pre-Clinical Development to Therapeutic Applications   New York, NY: Springer New York. 2013:p. 221–39.

575.   Xu S. Internalization, Trafficking, Intracellular Processing and Actions of Antibody-Drug Conjugates. Pharm Res. 2015;32(11):3577-83.

576.   Santini F, Marks MS, Keen JH. Endocytic clathrin-coated pit formation is independent of receptor internalization signal levels. Mol Biol Cell. 1998;9(5):1177-94.

577.   Nath N, Godat B, Zimprich C, Dwight SJ, Corona C, McDougall M, et al. Homogeneous plate based antibody internalization assay using pH sensor fluorescent dye. J Immunol Methods. 2016;431:11-21.

578.   Promega. Technical manual: pHAb Amine and Thiol Reactive Dyes. 2017.

579.   Asokan A, Cho MJ. Exploitation of intracellular pH gradients in the cellular delivery of macromolecules. J Pharm Sci. 2002;91(4):903-13.

580.   Chalouni, C., Doll, S. Fate of Antibody-Drug Conjugates in Cancer Cells. J *Exp Clin Cancer Res*   37,   20 (2018). https://doi.org/10.1186/s13046-017-0667-1.

581.   Sutherland MS, Sanderson RJ, Gordon KA, Andreyka J, Cerveny CG, Yu C, Lewis TS, Meyer DL, Zabinski RF, Doronina SO, Senter PD, Law CL, Wahl AF. Lysosomal trafficking and cysteine protease metabolism confer target-specific cytotoxicity by peptide-linked anti-CD30-auristatin conjugates. J Biol Chem. 2006 Apr 14;281(15):10540-7. doi: 10.1074/jbc.M510026200. Epub 2006 Feb 16. PMID: 16484228.

582.   Yao Y, Dai W. Genomic Instability and Cancer. J Carcinog Mutagen. 2014;5:1000165. doi: 10.4172/2157-2518.1000165. PMID: 25541596; PMCID: PMC4274643.

583.   Vigneron N. Human Tumor Antigens and Cancer Immunotherapy. Biomed Res Int. 2015;2015:948501. doi: 10.1155/2015/948501. Epub 2015 Jun 16. PMID: 26161423; PMCID: PMC4487697.

584.   Dahlgren D, Lennernäs H. Antibody-Drug Conjugates and Targeted Treatment Strategies for Hepatocellular Carcinoma: A Drug-Delivery Perspective. Molecules. 2020 Jun 21;25(12):2861. doi: 10.3390/molecules25122861. PMID: 32575828; PMCID: PMC7356544.

585.   Chau CH, Steeg PS, Figg WD. Antibody-drug conjugates for cancer. Lancet. 2019 Aug 31;394(10200):793-804. doi: 10.1016/S0140-6736(19)31774-X. PMID: 31478503.

586.   Hunt SE, McLaren W, Gil L, Thormann A, Schuilenburg H, Sheppard D, et al. Ensembl variation resources. Database (Oxford). 2018;2018.

587.   Karczewski KJ, Francioli LC, Tiao G, Cummings BB, Alföldi J, Wang Q, et al. The mutational constraint spectrum quantified from variation in 141,456 humans.

588.   Qiagen. What is the error rate of HotStar HiFidelity DNA Polymerase? 2020 [Online] Accessed: September 2021. [Available from: https://www.qiagen.com/us/resources/faq?id=e06109a1-5943-4f1e-af93-f8f6d2d8d037(=en.

589.   Pfeiffer F, Gröber C, Blank M, Händler K, Beyer M, Schultze JL, et al. Systematic evaluation of error rates and causes in short samples in next-generation sequencing. doi: 10.1038/s41598-018-29325-6

590.   Ikram A, Anjum S, Tahir M. In Silico Identification and Conservation Analysis of B-cell and T-Cell Epitopes of Hepatitis C Virus 3a Genotype Enveloped Glycoprotein 2 From Pakistan: A Step Towards Heterologous Vaccine Design. Hepat Mon. 2014 Jun 1;14(6):e9832. doi: 10.5812/hepatmon.9832. PMID: 24976845; PMCID: PMC4071360.

591.   Li BT, Shen R, Buonocore D, Olah ZT, Ni A, Ginsberg MS, et al. Ado-Trastuzumab Emtansine for Patients With HER2-Mutant Lung Cancers: Results From a Phase II Basket Trial. Journal of clinical oncology : official journal of the American Society of Clinical Oncology. 2018;36(24):2532-7.

592.   Fultang L, Panetti S, Ng M, Collins P, Graef S, Rizkalla N, et al. MDSC targeting with Gemtuzumab ozogamicin restores T cell immunity and immunotherapy against cancers. EBioMedicine. 2019. DOI: 10.1016/j.ebiom.2019.08.025

593.   Domina M, Lanza Cariccio V, Benfatto S, Venza M, Venza I, Borgogni E, et al. Functional characterization of a monoclonal antibody epitope using a lambda phage display-deep sequencing platform. Scientific reports. 2016;6:31458.

594.   Mondaca S, Razavi P, Xu C, Offin M, Myers M, Scaltriti M, et al. Genomic Characterization of ERBB2-Driven Biliary Cancer and a Case of Response to Ado-Trastuzumab Emtansine. JCO Precis Oncol. 2019;3. DOI: 10.1200/PO.19.00223

595.   Kim K, Hu W, Audenet F, Almassi N, Hanrahan AJ, Murray K, et al. Modeling biological and genetic diversity in upper tract urothelial carcinoma with patient derived xenografts. Nat Commun. 2020;11(1):1975.

596.   Layton CJ, McMahon PL, Greenleaf WJ. Large-Scale, Quantitative Protein Assays on a High-Throughput DNA Sequencing Chip. Mol Cell. 2019;73(5):1075-82.e4.

597.   Domina M, Lanza Cariccio V, Benfatto S, D'Aliberti D, Venza M, Borgogni E, et al. Rapid profiling of the antigen regions recognized by serum antibodies using massively parallel sequencing of antigen-specific libraries. PLoS One. 2014;9(12):e114159.

598.   Nakamura A, Ohwada C, Takeuchi M, Takeda Y, Tsukamoto S, Mimura N, et al. Detection of MYD88 L265P mutation by next-generation deep sequencing in peripheral blood mononuclear cells of Waldenstrom's macroglobulinemia and IgM monoclonal gammopathy of undetermined significance. PLoS One. 2019;14(9):e0221941.

599.   Ong PY, Poon SL, Tan KT, Putti TC, Ow SGW, Chen SJ, et al. Using next-generation sequencing (NGS) platform to diagnose pathogenic germline BRCA1/2 mutations from archival tumor specimens. Gynecologic oncology. 2019. DOI: 10.1016/j.ygyno.2019.08.027

600.   NCRAS. Routs to diagnosis of cancer by stage 2012-2013 workbook 2016 Available from: http://www.ncin.org.uk/publications/routes_to_diagnosis.

601.   Suh-Burgmann EJ, Alavi M. Detection of early stage ovarian cancer in a large community cohort. Cancer Med. 2019;8(16):7133-40.

602.   Burges A, Schmalfeldt B. Ovarian cancer: diagnosis and treatment. Dtsch Arztebl Int. 2011 Sep;108(38):635-41. doi: 10.3238/arztebl.2011.0635. Epub 2011 Sep 23. PMID: 22025930; PMCID: PMC3198226.

603.   Donach M, Yu Y, Artioli G, Banna G, Feng W, Bast RC Jr, Zhang Z, Nicoletto MO. Combined use of biomarkers for detection of ovarian cancer in high-risk women. Tumour Biol. 2010 Jun;31(3):209-15. doi: 10.1007/s13277-010-0032-x. PMID: 20393825.

604.   Malkasian GD Jr, Knapp RC, Lavin PT, Zurawski VR Jr, Podratz KC, Stanhope CR, Mortel R, Berek JS, Bast RC Jr, Ritts RE. Preoperative evaluation of serum CA 125 levels in premenopausal and postmenopausal patients with pelvic masses: discrimination of benign from malignant disease. Am J Obstet Gynecol. 1988 Aug;159(2):341-6. doi: 10.1016/s0002-9378(88)80081-4. PMID: 2457318.

605.   Patsner B, Mann WJ. The value of preoperative serum CA 125 levels in patients with a pelvic mass. Am J Obstet Gynecol. 1988 Oct;159(4):873-6. doi: 10.1016/s0002-9378(88)80158-3. PMID: 3052078.

606.   Vasilev SA, Schlaerth JB, Campeau J, Morrow CP. Serum CA 125 levels in preoperative evaluation of pelvic masses. Obstet Gynecol. 1988 May;71(5):751-6. PMID: 3162763.

607.   Bangert A, Andrassy M, Müller AM, Bockstahler M, Fischer A, Volz CH, et al. Critical role of RAGE and HMGB1 in inflammatory heart disease. Proc Natl Acad Sci U S A. 2016;113(2):E155-64.

608.   Durning SP, Preston-Hurlburt P, Clark PR, Xu D, Herold KC, Group TDTS. The Receptor for Advanced Glycation Endproducts Drives T Cell Survival and Inflammation in Type 1 Diabetes Mellitus. J Immunol. 2016;197(8):3076-85.

609.   Yu YX, Pan WC, Cheng YF. Silencing of advanced glycosylation and glycosylation and product-specific receptor (RAGE) inhibits the metastasis and growth of non-small cell lung cancer. Am J Transl Res. 2017;9(6):2760-74.

610.   Nasser MW, Wani NA, Ahirwar DK, Powell CA, Ravi J, Elbaz M, et al. RAGE mediates S100A7-induced breast cancer growth and metastasis by modulating the tumor microenvironment. Cancer Res. 2015;75(6):974-85.

611.   El-Far AH, Sroga G, Jaouni SKA, Mousa SA. Role and Mechanisms of RAGE-Ligand Complexes and RAGE-Inhibitors in Cancer Progression. Int J Mol Sci. 2020;21(10).

612.   Nakamura K, Yamagishi S, Adachi H, Kurita-Nakamura Y, Matsui T, Yoshida T, et al. Serum levels of sRAGE, the soluble form of receptor for advanced glycation end products, are associated with inflammatory markers in patients with type 2 diabetes. Mol Med. 2007;13(3-4):185-9.

613.	CancerResearchUK. Epithelial ovarian cancer 2019 [Online] Accessed: September 2021 [Available from: https://www.cancerresearchuk.org/about-cancer/ovarian-cancer/types/epithelial-ovarian-cancers/epithelial.

614.	CancerResearchUK. Borderline ovarian tumours 2019 [Online] Accessed: September 2021 [Available from: https://www.cancerresearchuk.org/about-cancer/ovarian-cancer/types/borderline.

615.	NHS. Endometriosis 2019 [Online] Accessed: September 2021 [Available from: https://www.nhs.uk/conditions/endometriosis/.

616.	Poorolajal J, Jenabi E, Masoumi SZ. Body mass index effects on risk of ovarian cancer: a meta-analysis. Asian Pac J Cancer Prev. 2014;15(18):7665-71. doi: 10.7314/apjcp.2014.15.18.7665. PMID: 25292044.

617.	NHS. What is the body mass index (BMI)? 2019 [Online] Accessed: September 2021 [Available from: https://www.nhs.uk/common-health-questions/lifestyle/what-is-the-body-mass-index-bmi/.

618.	Opara EI, Zaidi J. The interpretation and clinical application of the word 'parity': a survey. BJOG. 2007;114(10):1295-7.

619.	McGuire V, Hartge P, Liao LM, Sinha R, Bernstein L, Canchola AJ, Anderson GL, Stefanick ML, Whittemore AS. Parity and Oral Contraceptive Use in Relation to Ovarian Cancer Risk in Older Women. Cancer Epidemiol Biomarkers Prev. 2016 Jul;25(7):1059-63. doi: 10.1158/1055-9965.EPI-16-0011. Epub 2016 Apr 12. PMID: 27197274; PMCID: PMC4930714.

620.	Smoking and Inflammation. PLoS Med. 2005;2(6). https://doi.org/10.1371/journal.pmed.0020198

621.	General Medical, *Ovarian Cancer: Know the symptoms*,[Online] Accessed: December 2020, Available from:https://www.generalandmedical.com/live-healthy/posts/2020/march/ovarian-cancer-know-the-symptoms/.

622.	Patel BG, Lenk EE, Lebovic DI, Shu Y, Yu J, Taylor RN. Pathogenesis of endometriosis: Interaction between Endocrine and inflammatory pathways. Best Pract Res Clin Obstet Gynaecol. 2018;50:50-60.

623.	Sampson JA. ENDOMETRIAL CARCINOMA OF THE OVARY, ARISING IN ENDOMETRIAL TISSUE IN THAT ORGAN. *Arch Surg*. 1925.

624.	Sayasneh A, Tsivos D, Crawford R. Endometriosis and ovarian cancer: a systematic review. ISRN Obstet Gynecol. 2011;2011:140310.

625.	Shen F, Chen S, Gao Y, Dai X, Chen Q. The prevalence of malignant and borderline ovarian cancer in pre- and post-menopausal Chinese women. Oncotarget. 2017;8(46):80589-94.

626.	Peacock K, Ketvertis KM. Menopause. [Updated 2020 Nov 21]. In: StatPearls [Internet]. Treasure Island (FL): StatPearls Publishing; 2020 Jan-. Available from: https://www.ncbi.nlm.nih.gov/books/NBK507826/.

627.	NHS. Postmenopausal bleeding 2017 [Online] Accessed: September 2021 [Available from: https://www.nhs.uk/conditions/post-menopausal-bleeding/.

628.	Lee CG, Carr MC, Murdoch SJ, Mitchell E, Woods NF, Wener MH, et al. Adipokines, inflammation, and visceral adiposity across the menopausal transition: a prospective study. J Clin Endocrinol Metab. 2009;94(4):1104-10.

629.	Neilson HK, Conroy SM, Friedenreich CM. The Influence of Energetic Factors on Biomarkers of Postmenopausal Breast Cancer Risk. Curr Nutr Rep. 2014;3:22-34.

630.	Zhang F, Su X, Huang G, Xin XF, Cao EH, Shi Y, et al. sRAGE alleviates neutrophilic asthma by blocking HMGB1/RAGE signalling in airway dendritic cells. Sci Rep. 2017;7(1):14268.

631.	Hou N, Hong S, Wang W, Olopade OI, Dignam JJ, Huo D. Hormone replacement therapy and breast cancer: heterogeneous risks by race, weight, and breast density. J Natl Cancer Inst. 2013;105(18):1365-72.

632.	European Medicines Agency, EU/3/20/2266, 2020 [Online] Acessed: December 2020, Available from:https://www.ema.europa.eu/en/medicines/human/orphan-designations/eu3202266.

633.	Sasich LD, Sukkari SR. The US FDAs withdrawal of the breast cancer indication for Avastin (bevacizumab). Saudi Pharm J. 2012 Oct;20(4):381-5. doi: 10.1016/j.jsps.2011.12.001. Epub 2011 Dec 28. PMID: 23960813; PMCID: PMC3744967.

634.	Garcia A, Singh H. Bevacizumab and ovarian cancer. Ther Adv Med Oncol. 2013 Mar;5(2):133-41. doi: 10.1177/1758834012467661. PMID: 23450196; PMCID: PMC3556875.

635.	Hinrichs MJ, Dixit R. Antibody Drug Conjugates: Nonclinical Safety Considerations. AAPS J. 2015 Sep;17(5):1055-64. doi: 10.1208/s12248-015-9790-0. Epub 2015 May 30. PMID: 26024656; PMCID: PMC4540738.

636.   Salas IH, Callaerts-Vegh Z, Arranz AM, Guix FX, D'Hooge R, Esteban JA, De Strooper B, Dotti CG. Tetraspanin 6: A novel regulator of hippocampal synaptic transmission and long term plasticity. PLoS One. 2017 Feb 16;12(2):e0171968. doi: 10.1371/journal.pone.0171968. Erratum in: PLoS One. 2017 Jul 7;12 (7):e0178016. Erratum in: PLoS One. 2017 Oct 24;12 (10):e0187179. PMID: 28207852; PMCID: PMC5312877.

637.   Murthy SE, Loud MC, Daou I, Marshall KL, Schwaller F, Kühnemund J, Francisco AG, Keenan WT, Dubin AE, Lewin GR, Patapoutian A. The mechanosensitive ion channel Piezo2 mediates sensitivity to mechanical pain in mice. Sci Transl Med. 2018 Oct 10;10(462):eaat9897. doi: 10.1126/scitranslmed.aat9897. PMID: 30305457; PMCID: PMC6709986.

638.   Penninger J, Novel Approaches to Breast Cancer Prevention and Inhibition of Metastases, 2014, [Online]   Accessed: September   2021.   Available from:https://apps.dtic.mil/dtic/tr/fulltext/u2/a620323.pdf.

639.   De Felice D, Alaimo A. Mechanosensitive Piezo Channels in Cancer: Focus on altered Calcium Signaling in Cancer Cells and in Tumor Progression. Cancers (Basel). 2020 Jul 3;12(7):1780. doi: 10.3390/cancers12071780. PMID: 32635333; PMCID: PMC7407875.

640.   Bassi DE, Zhang J, Renner C, Klein-Szanto AJ. Targeting proprotein convertases in furin-rich lung cancer cells results in decreased in vitro and in vivo growth. Mol Carcinog. 2017 Mar;56(3):1182-1188. doi: 10.1002/mc.22550. Epub 2016 Sep 22. PMID: 27584082; PMCID: PMC6166887.

641.   Sabatier, R., Finetti, P., Bonensea, J. e*t al.* A seven-gene prognostic model for platinum-treated ovarian carcinomas. B*r J Cancer* 105, 304–311 (2011). https://doi.org/10.1038/bjc.2011.219.

642.   Ott MG, Marmé F, Moldenhauer G, Lindhofer H, Hennig M, Spannagl R, Essing MM, Linke R, Seimetz D. Humoral response to catumaxomab correlates with clinical outcome: results of the pivotal phase II/III study in patients with malignant ascites. Int J Cancer. 2012 May 1;130(9):2195-203. doi: 10.1002/ijc.26258. Epub 2011 Sep 27. PMID: 21702044; PMCID: PMC3415680.

643.   Pascual MH, Verdier P, Malette P, Mnich J, Ozoux ML. Validation of an immunoassay to selectively quantify the naked antibody of a new Antibody Drug Conjugate--SAR566658--for pharmacokinetic interpretation improvement. J Immunol Methods. 2013 Oct 31;396(1-2):140-6. doi: 10.1016/j.jim.2013.06.012. Epub 2013 Jul 24. PMID: 23892158.

644.   Ogawa, K., Pasqualini, R., Lindberg, R. e*t al.* The ephrin-A1 ligand and its receptor, EphA2, are expressed during tumor neovascularization. O*ncogene* 19, 6043–6052 (2000). https://doi.org/10.1038/sj.onc.1204004.

645.   Nath S, Mukherjee P. MUC1: a multifaceted oncoprotein with a key role in cancer progression. Trends Mol Med. 2014 Jun;20(6):332-42. doi: 10.1016/j.molmed.2014.02.007. Epub 2014 Mar 22. PMID: 24667139; PMCID: PMC5500204.

646.   Shilova ON, Proshkina GM, Lebedenko EN, Deyev SM. Internalization and Recycling of the HER2 Receptor on Human Breast Adenocarcinoma Cells Treated with Targeted Phototoxic Protein DARPinminiSOG. Acta Naturae. 2015 Jul-Sep;7(3):126-32. PMID: 26483969; PMCID: PMC4610174.

647.   Zhang Y, Wu S, Zhuang X, Weng G, Fan J, Yang X, Xu Y, Pan L, Hou T, Zhou Z, Chen S. Identification of an Activating Mutation in the Extracellular Domain of HER2 Conferring Resistance to Pertuzumab. Onco Targets Ther. 2019 Dec 30;12:11597-11608. doi: 10.2147/OTT.S232912. PMID: 31920346; PMCID: PMC6941612.

648.   Maurizio Scaltriti, Federico Rojo, Alberto Ocaña, Judit Anido, Marta Guzman, Javier Cortes, Serena Di Cosimo, Xavier Matias-Guiu, Santiago Ramon y Cajal, Joaquin Arribas, José Baselga, Expression of p95HER2, a Truncated Form of the HER2 Receptor, and Response to Anti-HER2 Therapies in Breast Cancer, JNCI: Journal of the National Cancer Institute , Volume 99, Issue 8, 18 April 2007, Pages 628–638, https://doi.org/10.1093/jnci/djk134.

649.   Martineau P, Watier H, Pèlegrin A, Turtoi A. Targets for MAbs: innovative approaches for their discovery & validation, LabEx MAbImprove 6 th antibody industrial symposium, June 25-26, 2018, Montpellier, France. MAbs. 2019 Jul;11(5):812-825. doi: 10.1080/19420862.2019.1612691. Epub 2019 May 16. PMID: 31043141; PMCID: PMC6601567.

650.   Moek KL, de Groot DJA, de Vries EGE, Fehrmann RSN. The antibody-drug conjugate target landscape across a broad range of tumour types. Ann Oncol. 2017 Dec 1;28(12):3083-3091. doi: 10.1093/annonc/mdx541. PMID: 29045509.

651.   Genentech, A study of DMOT4039A in participants with unresectable pancreatic or platinum-resistant ovarian cancer, 2017 [Online] Available from:https://clinicaltrials.gov/ct2/show/NCT01469793.

652.   Zhao XY, Subramanyam B, Sarapa N, Golfier S, Dinter H. Novel Antibody Therapeutics Targeting Mesothelin In Solid Tumors. Clin Cancer Drugs. 2016 Oct;3(2):76-86. doi: 10.2174/2212697X03666160218215744. PMID: 27853672; PMCID: PMC5080863.

653.   Immunogen, ImmunoGen announces top-line results from phase 3 FORWARD I study of Mirvetuximab Soravtansine in Ovarian Cancer, 2019 [Online] Accessed: December 2020, Available from:https://investor.immunogen.com/news-releases/news-release-details/immunogen-announces-top-line-results-phase-3-forward-i-study.

654.   MedImmune LLC, Study of MEDI-547 to evaluate the safety, tolerability and biological activity of IV administration in subjects with relapsed or refractory solid tumours (MEDI-547) 2008 [Online] Accessed: December 2020, Available from:https://clinicaltrials.gov/ct2/show/NCT00796055.

655.   Keating GM. Bevacizumab: a review of its use in advanced cancer. Drugs. 2014 Oct;74(16):1891-1925. doi: 10.1007/s40265-014-0302-9. PMID: 25315029.

656.   Linke R, Klein A, Seimetz D. Catumaxomab: clinical development and future directions. MAbs. 2010 Mar-Apr;2(2):129-36. doi: 10.4161/mabs.2.2.11221. PMID: 20190561; PMCID: PMC2840231.

657.   Goossens N, Nakagawa S, Sun X, Hoshida Y. Cancer biomarker discovery and validation. Transl Cancer Res. 2015 Jun;4(3):256-269. doi: 10.3978/j.issn.2218-676X.2015.06.04. PMID: 26213686; PMCID: PMC4511498.

658.   Bhatt AN, Mathur R, Farooque A, Verma A, Dwarakanath BS. Cancer biomarkers - current perspectives. Indian J Med Res. 2010 Aug;132:129-49. PMID: 20716813.

659.   Kalluri R. The biology and function of exosomes in cancer. J Clin Invest. 2016;126(4):1208-15.

660.   Zhang L, Yu D. Exosomes in cancer development, metastasis, and immunity. Biochim Biophys Acta Rev Cancer. 2019;1871(2):455-68.

661.   Guix FX, Sannerud R, Berditchevski F, Arranz AM, Horré K, Snellinx A, et al. Tetraspanin 6: a pivotal protein of the multiple vesicular body determining exosome release and lysosomal degradation of amyloid precursor protein fragments. Mol Neurodegener. 2017;12(1):25.

662.   Perot BP, Ménager MM. Tetraspanin 7 and its closest paralog tetraspanin 6: membrane organizers with key functions in brain development, viral infection, innate immunity, diabetes and cancer. Med Microbiol Immunol. 2020;209(4):427-36.

663.   Qi Y, Li H, Lv J, Qi W, Shen L, Liu S, et al. Expression and function of transmembrane 4 superfamily proteins in digestive system cancers. Cancer Cell Int. 2020;20:314.

664.   Sansone A, Lauretta R, Vottari S, Chiefari A, Barnabei A, Romanelli F, Appetecchia M. Specific and Non-Specific Biomarkers in Neuroendocrine Gastroenteropancreatic Tumors. Cancers (Basel). 2019 Aug 4;11(8):1113. doi: 10.3390/cancers11081113. PMID: 31382663; PMCID: PMC6721814.

665.   Leeman M, Choi J, Hansson S, Storm MU, Nilsson L. Proteins and antibodies in serum, plasma, and whole blood-size characterization using asymmetrical flow field-flow fractionation (AF4). Anal Bioanal Chem. 2018 Aug;410(20):4867-4873. doi: 10.1007/s00216-018-1127-2. Epub 2018 May 29. PMID: 29808297; PMCID: PMC6061777.

666.   Whitwell, H.J., Worthington, J., Blyuss, O. e*t al.* Improved early detection of ovarian cancer using longitudinal multimarker models. B*r J Cancer* 122, 847–856 (2020). https://doi.org/10.1038/s41416-019-0718-9.

667.   Russell, M.R., Graham, C., D'Amato, A. e*t al.* Diagnosis of epithelial ovarian cancer using a combined protein biomarker panel. B*r J Cancer* 121, 483–489 (2019). https://doi.org/10.1038/s41416-019-0544-0.

668.   He, L., Bao, H., Xue, J. e*t al.* Circulating soluble advanced glycation end product is inversely associated with the significant risk of developing cancer: evidence from a meta-analysis. T*umor Biol.* 35, 8749–8755 (2014). https://doi.org/10.1007/s13277-014-2122-7.

669.   Sims GP, Rowe DC, Rietdijk ST, Herbst R, Coyle AJ. HMGB1 and RAGE in inflammation and cancer. Annu Rev Immunol. 2010;28:367-88. doi: 10.1146/annurev.immunol.021908.132603. PMID: 20192808.

670.   Tesarová P, Kalousová M, Jáchymová M, Mestek O, Petruzelka L, Zima T. Receptor for advanced glycation end products (RAGE)--soluble form (sRAGE) and gene polymorphisms in patients with breast cancer. Cancer Invest. 2007 Dec;25(8):720-5. doi: 10.1080/07357900701560521. PMID: 18058469.
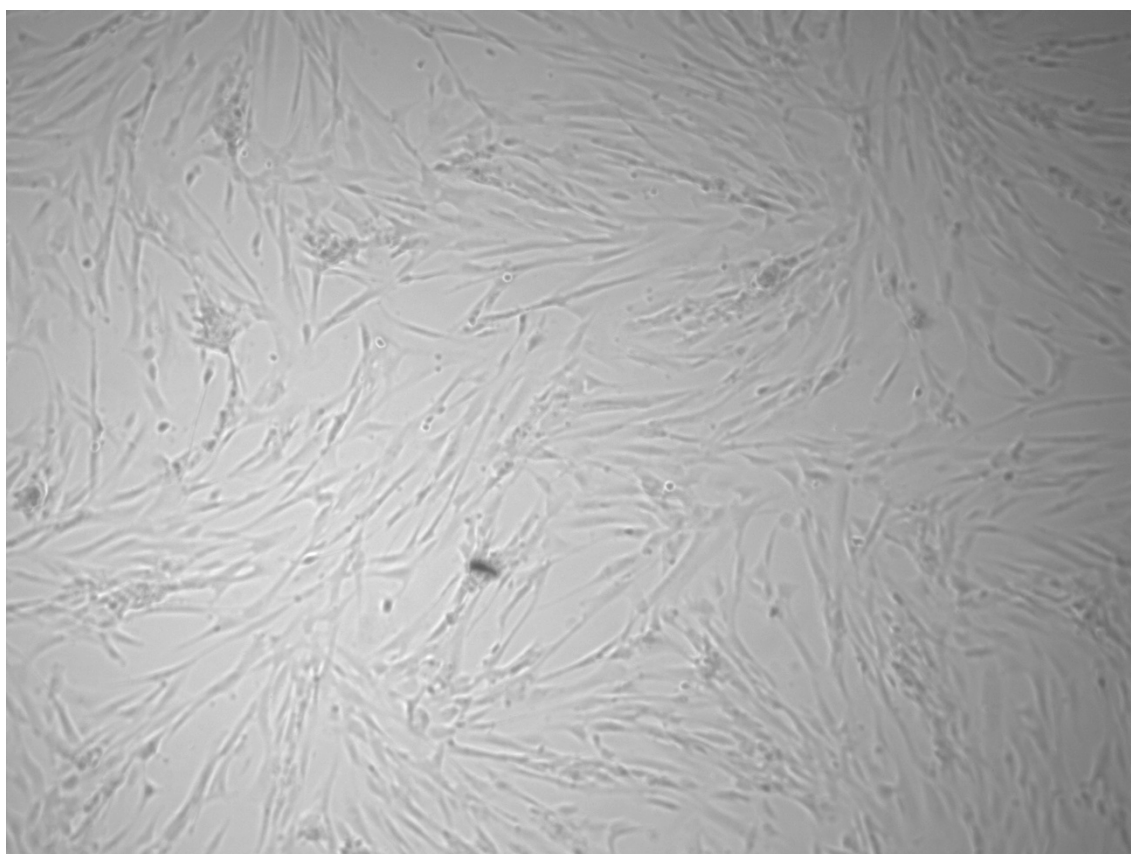
Appendix
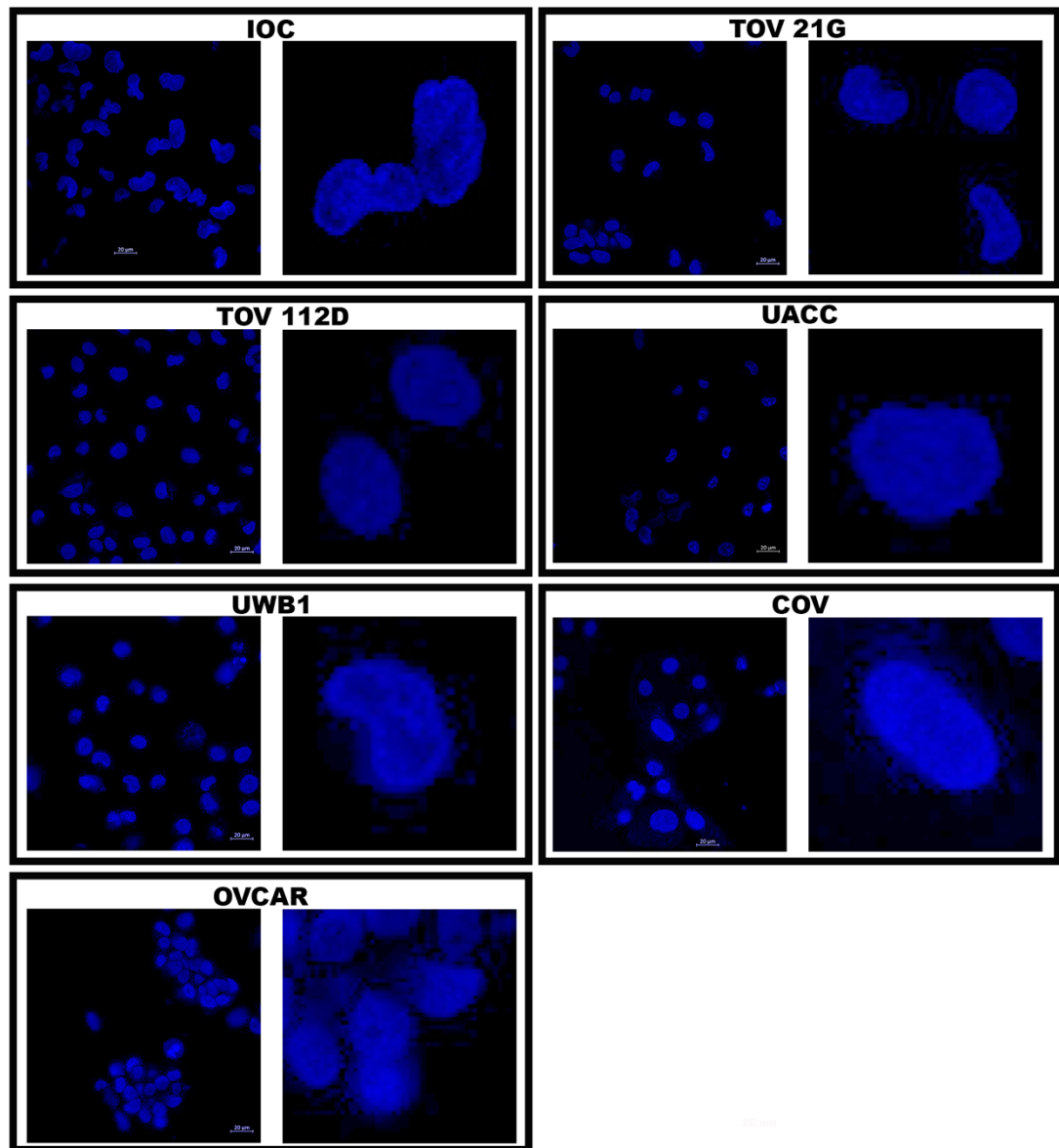
Appendix Figure 1 – No visible internalisation of IgG isotype antibody into various OC cell lines

Fluorescent intensity of IgG isotype antibody–dye conjugate into 2D cultured immortalised cell lines of various OC subtypes
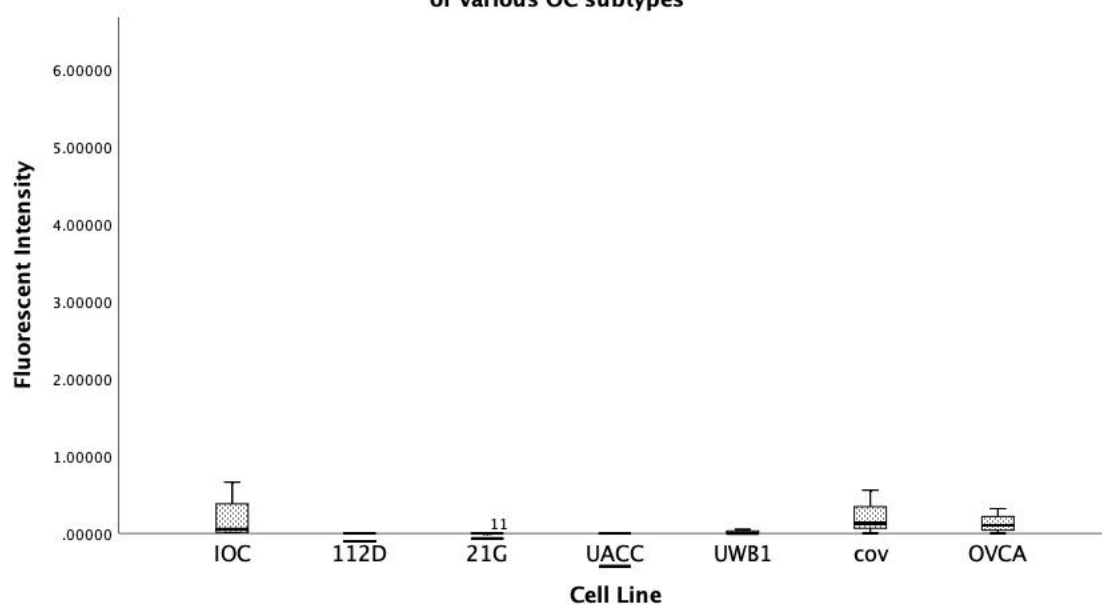
Appendix Figure 2 – Quantification of fluorescent intensity of IgG isotype antibody-dye conjugates into 2D cultured immortalised cell lines of various OC subtypes

Appendix Figure 3 – Representative image of 2D cells derived from patient biopsies (x40 magnification)